Identification and Characterisation of the Cellular and Molecular Changes in Intestinal Metaplasia Associated with Progression to Gastric Cancer

Athanasios Koulis

BSc, MRes

ORCID: 0000-0003-0939-8839

A thesis submitted in total fulfilment of the requirements of the degree of Doctor of Philosophy

July 2020

Sir Peter MacCallum Department of Oncology

And

Department of Medicine

The University of Melbourne

Thesis abstract

Gastric cancer (GC) patients are mainly asymptomatic and present at an advanced stage with a 5-year survival rate of only 20-30% in most countries. It is crucial to gain greater insight into the process of gastric carcinogenesis in order to develop tools that will allow improved patient stratification and targeted surveillance.

The relationship between intestinal metaplasia (IM), a key premalignant lesion in gastric carcinogenesis, and the diffuse type of gastric cancer (DGC) was investigated using data mining of GC patient pathology reports and existing gene expression data. IM and DGC were shown to be associated both histologically and molecularly in a proportion of cases suggesting that IM might be a precursor lesion to a subset of DGC cases.

Complete and incomplete IM subtypes, the latter being associated with a greater risk of progression, were characterised at the molecular level using gene expression data acquired from macro-dissected IM tissue. Complete IM was associated with genes highly expressed in the small intestine whereas incomplete IM was associated with genes expressed both in the colon and in GC suggesting it is molecularly closer to a state of malignancy.

Using OPAL™ multiplex immunohistochemistry, the macrophage and T cell landscape in IM was investigated. In addition to traditional “M1-like” (IRF8) and “M2-like” (CD163, CD206) macrophage populations, a novel hybrid subgroup “M1/2” containing macrophages expressing both M1 and M2 markers in different combinations was identified. Overall, complete IM was characterised by M2 macrophages and greater levels of T cell infiltration whereas incomplete IM was characterised by M1/2 macrophages and fewer CD8 and double negative (DN) T cells. Spatial cell analysis showed significantly fewer CD8 and DN T cells in the vicinity of incomplete IM epithelial cells suggesting reduced immune-surveillance may play a key role in progression to dysplasia.

IM subtyping is affected by intra-observer and inter-observer variation. To address this, the potential of CD10 and Das1 as biomarkers for subtyping complete and incomplete IM was investigated. Overall CD10 was shown to be an outstanding biomarker for complete IM and Das1 was shown to have potential as an additional risk associated biomarker.

GC animal models are associated with long duration and high cost. Optimised protocols for growing and characterising gastrointestinal organoids from gastroscopy biopsies were

developed. IM organoid cultures were successfully established and characterised. Additionally a human gastrointestinal organoid biobank was created.

In conclusion this thesis offers potential evidence of IM as a precursor lesion to DGC, characterises the molecular differences between complete and incomplete IM and shows key differences in the innate and adaptive immune system between IM subtypes and how these may play a role in progression to GC. It also identifies two biomarkers with potential clinical utility for subtyping IM and describes the methodology for growing IM organoids with future potential as a model for studying gastric carcinogenesis. Finally future studies are required to gain further insight into the cellular and molecular evolution of gastric carcinogenesis which should lead to better management of patients with premalignant lesions and ultimately to the prevention of GC.

Declaration

This is to certify that

i. the thesis comprises only my original work towards the PhD except where indicated in the preface,
ii. due acknowledgement has been made in the text to all other material used
iii. the thesis is fewer than 100,000 words in length, exclusive of tables, maps, bibliographies and appendices

Athanasios Koulis

Preface

All experiments and data analyses presented in this thesis were performed by Athanasios Koulis with the following exceptions:

Chapters 5 & 6: The OPAL™ multiplex immunohistochemistry panels used for the macrophage and T cell studies were initially optimised for use on gastric tumour tissue by Dr Yu-Kuan Huang and Dr Minyu Wang during their PhD studies, and further optimised for gastric premalignant tissue by myself.

Chapter 8: The optimisation of protocols for setting up and characterising organoid cultures was done in collaboration with Dr Rita Busuttil. Dr Rita Busuttil assisted with maintaining the large number of concurrently growing organoid cultures at any given time point.

Acknowledgements

I would like to thank all the people that have contributed to this work, either directly or indirectly. Although this thesis describes the work I did during the last four years, it would not have been possible if I had not received the support of so many highly talented individuals at the Peter MacCallum Cancer Centre and the University of Melbourne.

First I would like to thank my supervisors, Professor Alex Boussioutas, Dr Rita Busuttil and Dr David Goode and my mentor Associate Professor Nick Clemons. I still remember the Skype video call I had with Alex and Rita, one evening in October 2015, to discuss the possibility of doing a PhD with them. I was still living in London at the time and got really excited by the possibility of travelling to the other side of the planet to work with them. I managed to get my application in on time and by mid-December I was offered the Melbourne Research Scholarship that would allow me to commence. In July 2016, Ana and I arrived in Melbourne, Australia to start this epic journey that has lasted four whole years.

Thank you Alex for your continuous support throughout my PhD. Your enthusiasm and incredible knowledge of the gastric premalignant field have really kept me going. You have given me the time and space to develop my own ideas and to try out new things.

Thank you Rita for the remarkable effort you have put into helping me improve both my lab skills and my written skills. When I first arrived at the Peter Mac, I had grown cell lines before but only to a limited extent. Now I know how to grow and characterise human organoid cultures from upper endoscopy biopsies.

Thank you David for sharing your enthusiasm and knowledge in bioinformatics with me. I have really appreciated your willingness to explain even simple concepts to me when I was struggling to grasp them.

Thank you Nick for listening to me in difficult times and always guiding me to see things from a positive perspective. Thank you also for all the coffees during our meetings at Super 8!!

I would like to thank all the members in the Gastric Group and in particular Natasha who is incredible at what she does as a research assistant and very supportive as a colleague (also bakes delicious cakes and does home delivery too!), Tony (Yu-Kuan) who was willing to share details of his OPAL™ multiplex immunohistochemistry macrophage panel with me as described in this thesis and answer an incredibly large number of macrophage related questions without losing his temper once, Minyu who shared details of her OPAL™ multiplex immunohistochemistry T

cell panel with me as described in this thesis, Andrew for his great sense of humour and his willingness to write a review paper with me on intestinal metaplasia and finally Todd for his patience and excellent support during this last year of my PhD.

I would like to thank Dr Catherine Mitchell and Dr Stephen Lade for their help with the pathological assessment of tissues including the subtyping of a large number of intestinal metaplasia samples. Thank you also Catherine for willing to sit with me and subtype individual intestinal metaplasia glands. Really appreciate it.

For the bioinformatics part of my thesis, I would like to thank Dr Anna Trigos who opened my eyes to the joys of single sample gene set enrichment analysis, Dr Maria Doyle for always being there to discuss even the smallest issues regarding R and Dr Alan Hershtal for introducing me to generalised linear models in R and how to apply these for my work.

For all work involving immunohistochemistry, I would like to thank Associate Professor Sarah Ellis and all the staff at the Centre for Advanced Histology and Microscopy without whose help, this thesis would not exist. Thank you Marné for all your support with optimising the OPAL™ method and Metta for your incredible support in microscopy! Everyone in histology has been amazing in satisfying my incessant need to know and understand details about everything, and always with a smile.

For the organoid part of my thesis, I would like to thank Elhadi Iich and Dr Camilla Mitchell who were always willing to help me with reagents and advice. Thank you also to Dr Maree Faux and Dr Yumiko Hirokawa from the WEHI, Dr Rosie Millen and Dr Dustin Flanagan for all your support in helping me set up the project and supplying the required reagents at the beginning. I would also like to thank Dr Benjamin Blyth for his support on developing immunofluorescent methods for staining organoids. Additionally I would like to thank Viki Milovac and her support staff for helping me carry out the FACS part of the organoid project and for taking the time to explain to me the different aspects of what we were doing.

I would like to thank Associate Professor Caroline Owen for her phenomenal administrative support throughout these last four years. You are always there, paying attention to detail and helping students find their way forward. Also thank you to Niranga and Erica without whose support I would have struggled to complete my PhD.

All the projects described in this thesis are based on samples from patients that have been courageous enough to participate and share a part of themselves for the benefit of the rest.

Thank you! Also I would like to thank the University of Melbourne as a whole for providing me with this opportunity to do a PhD.

Finally I would like to thank Ana, my wife, who was willing to give up an excellent job in London and travel with me to Australia for a new adventure. Ana, thank you for your incredible patience and support throughout all these four years. I owe you more than just a coffee! Thank you also to all my family who have supported me and in particular my mother Irini, my father Athanasios, my sister Christina and my brother Nikos! Thank you also to my aunts Erato, Eleni and Sophia for their lifelong support. Also thank you to my niece Paraskevi who was willing to travel to Melbourne to come and visit us and to my cousin Joseph. Thank you to Andreas, Andrea and Guilherme for your support. Thank you also to my mother- and father-in-law Angela and Jorge and my brother-in-law Romulo. My last thank you goes to the Newport Baptist church and the wonderful people we have met there and who have now become our friends. These include the den Elzen family (Luna, David, Alex and Ashley), Kim and Jed, Bernie and Catherine, and Linda, our wedding celebrant among others.

Publications and Presentations

The following is a publication arising as a result of work in this thesis:

Koulis A, Buckle A, Boussioutas, A. Premalignant lesions and gastric cancer: Current understanding. World J Gastrointest Oncol. 2019;11(9):665-678. (Appendix A)

The following are presentations at national and international meetings as a result of work in this thesis:

May 2019 **Porto Cancer Meeting 2019** in Porto, Portugal. “Reduced immune-surveillance in intestinal metaplasia leads to increased risk of progression to gastric cancer” (oral presentation).

Nov 2018 **Biomed Link Conference 2018** in Melbourne. “Reduced immune-surveillance in intestinal metaplasia leads to increased risk of progression to gastric cancer” (oral presentation).

Aug 2018 **Comprehensive Student Cancer Symposium 2018** at the Peter MacCallum Cancer Centre, Melbourne. “Investigating the immune microenvironment in gastric intestinal metaplasia” (oral presentation).

Aug 2017 **Comprehensive Student Cancer Symposium 2017** at the Peter MacCallum Cancer Centre, Melbourne. “Identifying key genes and pathways dysregulated in the progression to gastric cancer” (poster presentation).

List of Abbreviations

ACRG	Asian Cancer Research Group
AG	Atrophic gastritis
AJCC	American Joint Committee on Cancer
AUROC	Area Under the Receiver Operating Characteristic
bcIM-GC	Bioinformatically subtyped complete intestinal metaplasia in patients without GC
biIM-GC	Bioinformatically subtyped incomplete intestinal metaplasia in patients without GC
BM	Basal medium
bmIM-GC	Bioinformatically subtyped mixed intestinal metaplasia in patients without GC
CD4 T cell	CD3+CD4+FOXP3-CD8- cell
CD8 T cell	CD3+CD4-FOXP3-CD8+ cell
CG	Chronic gastritis
CG+GC	Chronic gastritis in patients with concurrent GC
CG-GC	Chronic gastritis in patients without GC
CI	Confidence interval
CIBERSORT	Cell-type Identification By Estimating Relative Subsets Of RNA Transcripts
cIM	Complete intestinal metaplasia
cIM+GC	Complete intestinal metaplasia in patients with concurrent GC
cIM-GC	Complete intestinal metaplasia in patients without GC
CIN	Chromosomally instability
DAB	3,3'-Diaminobenzidine
DGC	Diffuse gastric cancer
DGC+IM	Diffuse gastric tumour with adjacent intestinal metaplasia
DGC-IM	Diffuse gastric tumour without adjacent intestinal metaplasia
DN T cell	Double negative T cell CD3+CD4-FOXP3-CD8- cell
EBV	Epstein Barr virus
ECM	Extracellular matrix
EGC	Early gastric cancer
EGF	Epidermal Growth Factor
EMR	Endoscopic mucosal resection
EMT	Epithelial Mesenchymal Transition
ESD	Endoscopic submucosal dissection
FCS	Foetal calf serum
FFPE	Formalin-fixed paraffin embedded
FGF	Fibroblast growth factor
GC	Gastric cancer
GEO	Gene Expression Omnibus
GI	Gastrointestinal
glm	Generalised linear model
GO	Gene Ontology
GOJ	Gastro-oesophageal junction
GS	Genomically stable
H&E	Haematoxylin and eosin
H. felis	*Helicobacter felis*
H. pylori	*Helicobacter pylori*
HGD	High grade dysplasia
HR	Hazard Ratio
HRP	Horseradish peroxidase
IARC	International Agency for Research and Cancer
IC	IntestiCult™
IFNγ	Interferon gamma
IGC	Intestinal gastric cancer
IGC+IM	Intestinal gastric tumour with adjacent intestinal metaplasia
IGC-IM	Intestinal gastric tumour without adjacent intestinal metaplasia
IHC	Immunohistochemistry

iIM	Incomplete intestinal metaplasia
iIM+GC	Incomplete intestinal metaplasia in patients with concurrent GC
iIM-GC	Incomplete intestinal metaplasia in patients without GC
IM	Intestinal metaplasia
IM+GC	intestinal metaplasia in patients with concurrent GC
IM-GC	intestinal metaplasia in patients without GC
IRF8	Interferon Regulatory Factor 8
KEGG	Kyoto Encyclopedia of Genes and Genomes
LGD	Low grade dysplasia
MAIT cell	Mucosal Associated Invariant T cell
MAUGIC	Molecular Analysis of Upper Gastrointestinal Cancer
MGC	Mixed gastric cancer
MHC	Major Histocompatibility Complex
mIHC	Multiplex immunohistochemistry
M-MLV	Moloney murine leukaemia virus
MNNG	*N*-methyl-*N*-nitro-*N*-nitrosoguanidine
MNU	*N*-methyl-*N*-nitrosourea
MSI	Microsatellite instability
MSigDB	The Molecular Signatures Database
NK cell	Natural Killer cell
NN	Normal gastric
OGM	Organoid growth medium
OLGA	Operative Link for Gastritis Assessment
OLGIM	Operative Link for Intestinal Metaplasia Assessment
OR	Odds Ratio
PDL1	Programmed death-ligand 1
Progressors	Patients that have progressed to high grade dysplasia
qRT-PCR	Quantitative Real Time Polymerase Chain Reaction
ROI	Region of interest
ROS	Reactive oxygen species
RR	Relative Risk
SD	Standard deviation
SPEM	Spasmolytic peptide expressing metaplasia
ssGSEA	Single sample gene set enrichment analysis
TAM	Tumour associated macrophage
TCGA	The Cancer Genome Atlas
TCR	T cell receptor
Th	Helper T cell
Treg	Regulatory T cell
WHO	World Health Organisation
κ	Kappa statistic

List of Figures

Figure 1.1 World map showing the estimated age-standardized incidence rates for gastric cancer in 2018 (obtained from http://globocan.iarc.fr/, accessed 01/06/2020) 1

Figure 1.2 Dual bar chart showing age-standardised incidence rates for gastric (stomach) cancer for each sex separately in 2018 (obtained from http://globocan.iarc.fr/) 3

Figure 1.3 The histology based Lauren classification system groups gastric adenocarcinomas into two main types: the intestinal type and the diffuse type 4

Figure 1.4 Schematic representation of molecular subtypes of gastric cancer by The Cancer Genome Atlas Research Network (adapted from TCGA 2014, [42]) 5

Figure 1.5 Visual representation of the histologically defined Correa model leading up to the intestinal type of gastric cancer (IGC) [65] 7

Figure 1.6 Schematic representation of the stomach and an oxyntic (body/corpus) gland 8

Figure 1.7 Forest plot showing gastric cancer risk among patients with intestinal metaplasia (IM) from multiple studies (adapted from Shao et al 2018 [94], random-effects model used) 10

Figure 1.8 Schematic representation showing the recommended biopsy sites from the updated Sydney protocol [102] and the Operative Link for Gastritis Assessment (OLGA) staging system 11

Figure 1.9 Forest plot showing individual and pooled risk ratios and 95% confidence intervals in studies comparing gastric cancer risk in patients with H. pylori eradication and controls (adapted from [112]) 12

Figure 1.10 Forest plot of subgroup of studies reporting gastric cancer after H. pylori eradication treatment in patients with differing baseline histology (adapted from [124]) 13

Figure 1.11 Figure and table showing relative improvements in patients with IM following H. pylori eradication treatment (adapted from [121]) 14

Figure 1.12 Examples of complete and incomplete intestinal metaplasia (IM) 15

Figure 1.13 Schematic and tabular representation of CD4+ T cell function including regulatory T cells (Tregs) following *Helicobacter pylori* infection (adapted from [188]) 22

Figure 1.14 Cross-talk communication between tumour cells and immune cells (adapted from [250]) 24

Figure 1.15 Diagram showing multiple roles of tumour-associated macrophages (TAMs) in supporting tumour cell biology (adapted from [196]) 25

Figure 1.16 Schematic representation of the general workflow from tissue or embryonic/induced pluripotent stem cells to organoid culture (adapted from [362]) 32

Figure 1.17 Schematic representation showing the use of tumour tissue derived organoids grown in the presence of stromal and immune cells using an air-liquid interface method (adapted from [374]) 33

Figure 2.1 Patients from the Molecular Analysis for Upper Gastro Intestinal Cancer (MAUGIC), the IM-GC, the Progressors and the Normal gastric cohorts were used for this thesis 39

Figure 2.2 Schematic representation of the Siewert classification system (adapted from [378]) 40

Figure 2.3 Subtyping of intestinal metaplasia samples 43

Figure 2.4 Spatial location analyses showing the nearest neighbour, number of cells within a specific radius (distance) and touch cell pairs..... 47

Figure 3.1 Diagram showing the sources of information available to characterise the histological association of premalignant lesions with gastric cancer Lauren subtypes..... 56

Figure 3.2 Schematic representation showing the presence of premalignant lesions adjacent and distant from gastric cancer..... 56

Figure 3.3 Chronic gastritis and intestinal metaplasia adjacent and distant (at least 2cm away) of Lauren gastric cancer types..... 59

Figure 3.4 Clinico-epidemiological details of patients with intestinal and diffuse gastric cancer without (-IM) and with (+IM) intestinal metaplasia adjacent to tumour..... 62

Figure 3.5 Pathology details of patients with intestinal and diffuse gastric cancer without (-IM) and with (+IM) intestinal metaplasia adjacent to tumour..... 63

Figure 4.1 Top 10 over-represented GO terms for (a) Biological Process and (b) Cellular Component in intestinal metaplasia (IM+GC; n=23) samples compared to normal gastric (NN; n=7) samples..... 72

Figure 4.2 Relative abundance of immune cells in chronic gastritis (CG+GC) and intestinal metaplasia (IM+GC) determined using CIBERSORT..... 74

Figure 4.3 Four way differential expressed gene analysis between premalignant tissues (chronic gastritis and intestinal metaplasia) and malignant tissues (intestinal and diffuse gastric cancer)..... 76

Figure 4.4 Gene set over-representation analysis with GO Biological Process comparing premalignant tissues (chronic gastritis and intestinal metaplasia) and malignant tissues (intestinal and diffuse gastric cancer)..... 77

Figure 4.5 Top 5 most significantly enriched Hallmark gene sets using ssGSEA in intestinal (IGC) and diffuse gastric cancer (DGC) when compared to intestinal metaplasia (IM+GC)..... 79

Figure 4.6 Trends in enriched chromosomal location and frequency of chromosomal copy number variations in tissues representing the Correa model..... 81

Figure 4.7 Expression of MYC and SOX9 in IM-GC and in rIM+GC samples..... 83

Figure 4.8 Gene set over-representation analysis with GO Biological Process using differentially overexpressed genes in rIM+GC compared to IM-GC samples..... 84

Figure 4.9 Gene expression correlation heatmap using Pearson's correlation coefficient (r) to identify possible targets for subtyping intestinal metaplasia in IM-GC..... 86

Figure 4.10 Hierarchically clustered heatmap (unsupervised) using gene expression of six key intestinal genes on IM-GC samples (n=14)..... 86

Figure 4.11 Hierarchical clustering (unsupervised) of all IM-GC samples using differentially expressed gene list..... 90

Figure 4.12 Expression of gastric cancer associated biomarkers CEACAM5 and CEACAM6 in bcIM-GC and biIM-GC samples..... 91

Figure 4.13 Gene expression of key T cell markers in bcIM-GC and biIM-GC samples..... 92

Figure 4.14 Correlation network showing T cell activity groups from bcIM-GC and biIM-GC samples..... 94

Figure 4.15 Relationship shown between gene expression of CD8α with MME and CDX1 genes and between KLRB1 gene signature and GO Cellular Component term Brush border (GO0005903) 95

Figure 4.16 Unsupervised hierarchical clustering of IM-GC samples from the Companioni et al 2017 study [388] 97

Figure 4.17 Gene expression of key T cell markers in the IM-GC samples from the Companioni 2017 study [388] 98

Figure 4.18 Single sample GSEA using ImmPort immune related gene sets with the IM-GC samples from the Companioni et al 2017 study [388]) 99

Figure 5.1 Use of inForm software to acquire multi-parameter single cell data from target tissue previously stained with OPAL™ reagents 109

Figure 5.2 Spectrally unmixed image and 3D scatter plot showing multiple macrophage subsets (CD68+ cells) present in gastric premalignant lesions based on cellular co-localisation of markers 111

Figure 5.3 Normalised mean expression of key markers on macrophage subsets 112

Figure 5.4 PDL1 staining on gastric epithelial cells but not on intestinal metaplastic glands .. 113

Figure 5.5 Total macrophage (CD68+) density differs between complete and incomplete intestinal metaplasia 114

Figure 5.6 Macrophage subset density in premalignant tissues from the IM-GC cohort 115

Figure 5.7 Macrophage subset density in premalignant tissues from the IM+GC cohort 117

Figure 5.8 Differences in total macrophage density between IM-GC and IM+GC samples 118

Figure 5.9 Differences in macrophage subset content between IM-GC and IM+GC samples .. 119

Figure 5.10 Total, M1, M1/2 and M2 macrophage density in samples with intestinal metaplasia and matched adjacent chronic gastritis tissue from the IM-GC cohort 120

Figure 5.11 Macrophage subset density in samples with intestinal metaplasia and matched adjacent chronic gastritis tissue from the IM-GC cohort 121

Figure 5.12 Total, M1, M1/2 and M2 macrophage density in samples with intestinal metaplasia and matched adjacent chronic gastritis tissue in IM+GC cohort 122

Figure 5.13 Macrophage subset density in samples with intestinal metaplasia and matched adjacent chronic gastritis tissue from the IM+GC cohort 123

Figure 5.14 M2 to M1/2 macrophage ratio in the IM-GC and IM+GC cohorts 124

Figure 5.15 Mean number of total macrophages within a distance of 40µm from epithelial cells in the IM-GC and IM+GC cohorts 126

Figure 5.16 Mean number of M2 and M1/2 macrophages within a distance of 40µm from epithelial cells in the IM-GC and IM+GC cohorts 126

Figure 5.17 Significant reduction of touching cell pair density in incomplete IM+GC between epithelial cells and total macrophages 127

Figure 5.18 Touch pair cell density between epithelial cells, CD68+CD163+CD206+ and CD68+CD163+CD206+IRF8+ macrophages in the IM-GC and IM+GC cohorts 129

Figure 5.19 Touch cell pair density between CD68+CD163+CD206+ and CD68+CD163+CD206+IRF8+ macrophages in the IM-GC and IM+GC cohorts 130

Figure 5.20 Diagram and images with insets showing high grade dysplasia (HGD) with adjacent chronic gastritis where present at different sites and time points in patient P1 133

Figure 5.21 Diagram and images with insets showing low grade (LGD) and high grade dysplasia (HGD) present at adjacent sites (A2a and A2b) in patient P2 133

Figure 5.22 Pooled and single site/time point macrophage density in patient P1 135

Figure 5.23 Pooled and single site/time point macrophage subset density in patient P1 136

Figure 5.24 Macrophage content in complete and incomplete IM differs by site and time point 137

Figure 5.25 High grade dysplasia at t3 shows large numbers of cells with high levels of expression for CD68, CD163 and IRF8 compared to matched adjacent chronic gastritis tissue 138

Figure 5.26 Pooled and single site/time point macrophage density in patient P2 140

Figure 5.27 Pooled and single site/time point macrophage subset density in patient P2 141

Figure 5.28 Macrophage profile in low grade and high grade dysplasia varies considerably in patient P2 142

Figure 5.29 M1-M2 macrophage spectrum including M1/2 macrophage subsets..... 144

Figure 6.1 OPAL™ multiplexed fluorescent immunohistochemistry staining using the T cell panel on human gastric intestinal metaplasia 152

Figure 6.2 T cell subsets based on the co-localisation of specific T cell markers..... 153

Figure 6.3 Total T cell density in chronic gastritis, in complete and in incomplete intestinal metaplasia in the IM-GC and IM+GC cohorts 153

Figure 6.4 Total T cell density increases in complete intestinal metaplasia and decreases in incomplete intestinal metaplasia with temporal progression 154

Figure 6.5 T cell subset density in the IM-GC and IM+GC cohorts..... 155

Figure 6.6 T cell subset densities plotted by tissue type comparing IM-GC (“early”) and IM+GC (“late”) gastric premalignant lesions..... 156

Figure 6.7 Total, CD4 and CD8 T cell density of matched chronic gastritis adjacent to intestinal metaplasia in IM-GC and IM+GC samples for individual patients 158

Figure 6.8 T cell subset and epithelial cell ratios in IM-GC and IM+GC samples 160

Figure 6.9 Mean number of T cells within a 40µm radius and touch cell pair density between T cell subsets in the IM-GC and IM+GC cohorts..... 162

Figure 6.10 Mean number of T cells within a 40µm radius and touch cell pair density between epithelial cells and T cell subsets in the IM-GC and IM+GC cohorts..... 164

Figure 6.11 Lymphoid aggregate adjacent to complete IM glands but absent in incomplete IM 166

Figure 6.12 Matched regions of interest rich in intestinal metaplastic glands showing the presence of both T cells and macrophages..... 167

Figure 6.13 Correlation analysis between total T cell (CD3+) and macrophage (CD68+) populations in matched regions of interest of the IM-GC and IM+GC cohorts 168

Figure 6.14 Quantitative relationships between T cell (CD3+) and macrophage (CD68+) subsets shown using correlation heatmaps in the IM-GC and IM+GC cohorts 171

Figure 6.15 Correlation networks of normalised touch cell pair densities in IM-GC and IM+GC cohorts show changing landscape of T cell and macrophage interaction and their relationship with the epithelium 173

Figure 6.16 Pooled and single site/time point T cell subset density in patient P1 175

Figure 6.17 T cell infiltration in high grade dysplasia and adjacent chronic gastritis in patient P1 at time point t3 including nearest neighbour spatial analysis 177

Figure 6.18 Multiplexed images showing the distance (length of intercellular lines) between each CD8 T cell and its nearest FOXP3 T cell in high grade dysplasia and adjacent chronic gastritis in patient P1 in site A3 at time point t3 178

Figure 6.19 Pooled and single site/time point T cell subset density in patient P2 180

Figure 6.20 How reduced immune-surveillance in incomplete intestinal metaplasia may lead to dysplasia 183

Figure 7.1 Representative staining of anti-CD10 and Das1 staining on small intestine and colon positive control tissues 191

Figure 7.2 Serial sections of biopsy tissue stained with haematoxylin and eosin and with the OPAL™ multiplex IHC T cell panel showing complete intestinal metaplasia with brush border and the presence of CD10 192

Figure 7.3 Serial sections of biopsy tissue stained with haematoxylin and eosin and with Das1 antibody showing incomplete intestinal metaplasia 193

Figure 7.4 Receiver Operating Characteristic (ROC) curve and Area Under Receiver Operating Characteristic (AUROC) for CD10 and CD10 combined with Das1 staining using logistic regression 196

Figure 7.5 Das1 staining in the lower part of incomplete intestinal metaplasia glands 197

Figure 7.6 Digital quantification of Das1 staining on intestinal metaplasia glands using an overlay 197

Figure 7.7 Das1 staining by region of interest in the IM-GC samples 198

Figure 7.8 Das1 stains positive a case of intestinal metaplasia with differing diagnosis 199

Figure 7.9 Analysis of Das1 staining across whole section in IM-GC samples 200

Figure 7.10 Das1 staining by region of interest in the IM+GC samples 201

Figure 7.11 Analysis of Das1 staining across whole section in IM+GC samples 201

Figure 7.12 Comparison of Das1 staining per section between IM-GC and IM+GC cohorts 202

Figure 7.13 The relationship between Das1 staining and macrophage subset density in incomplete intestinal metaplasia of IM-GC samples 203

Figure 8.1 Schematic representation including tissue details of workflow for establishing, growing and characterising gastrointestinal organoids 212

Figure 8.2 Human tissue samples used to set up organoid cultures 213

Figure 8.3 Human organoids grow successfully from a single gastric biopsy but have limited longevity 213

Figure 8.4 Gastric, small intestine and colon organoids grow from porcine tissue 214

Figure 8.5 Early porcine organoid cultures (day 6) grown from gastric and small intestinal tissue using both the enzyme digestion and the chelation buffer isolation methods 215

Figure 8.6 Early porcine organoid cultures (day 4) derived from gastric and small intestinal tissue in the presence and absence of FGF10 in the growth medium 216

Figure 8.7 Effect of starting amount of tissue in organoid colony formation and growth (day 6) 217

Figure 8.8 Porcine organoids grow from previously frozen small intestinal organoid cultures 217

Figure 8.9 Chelation buffer method for organoid derivation from human pooled gastric biopsies 219

Figure 8.10 RNA yield is proportional to the starting number of actively growing porcine organoids 219

Figure 8.11 Porcine small intestinal organoids stain positive with anti-CDX2 and anti-CD10 antibodies 220

Figure 8.12 Morphology does not allow differentiation between human gastric and small intestinal organoids 221

Figure 8.13 Optimised staining for MUC5C, MUC6, CDX2, TFF3 and CD10 antibodies on gastric and small intestinal tissue 223

Figure 8.14 MUC5AC and CDX2 staining of gastric and small intestinal organoids 224

Figure 8.15 Identification of gastric derived intestinal metaplasia organoids using CDX2 staining 224

Figure 8.16 Intestinal metaplastic organoids do not fully replicate expression pattern for MUC5AC, TFF3 and CD10 markers on tissue of origin in patient G25 225

Figure 8.17 Antral, body and small intestinal (SI) organoids characterised for expression of TFF1, TFF2 and VIL1 using qRT-PCR 226

Figure 8.18 Characterisation of clonal body, antral and small intestinal (SI) organoids for expression of TFF1, TFF2, VIL1 and CDX2 226

Figure 8.19 Experiment 1: Investigating the effect of removing the niche factors Wnt3A, nicotinamide and p38 MAPK inhibitor SB202190 on antral and small intestinal organoid cultures (Table 8.3) 229

Figure 8.20 Experiment 2: The contribution of different niche factors on antral, body and small intestine organoids (Table 8.3) 230

Figure 8.21 Experiment 2: The effect of niche factors on gene expression of antral, body and small intestinal organoids 233

Figure 8.22 Experiment 3: The effect of IntestiCult™ with and without human component B on antral and small intestinal organoids 234

Figure 8.23 OLFM4 staining of gastric, intestinal metaplastic and small intestinal tissue 236

Figure 8.24 FACS plots showing gating strategy to obtain single OLM4- and OLFM4+ cells from gastrointestinal organoids 237

Figure 8.25 Fluorescence-activated cell sorting of gastrointestinal organoids using stem cell marker OLFM4 results in organoid formation mainly in the negatively sorted fraction 238

Figure 8.26 Intestinal metaplastic organoids from patients G10 and G25 show differing OLFM4 staining 239

Figure 9.1 Histo-temporal model of increasing risk of progression using Correa premalignant lesions from patients with (IM+GC) and without concurrent gastric cancer (IM-GC) 254

Figure 9.2 Schematic summary of the key findings described in this thesis with respect to intestinal metaplasia and progression to gastric cancer..... 269

List of Tables

Table 1.1 Hazard Ratios (HR) and 95% confidence intervals (95% CI) for GC among patients with different premalignant lesions compared with the normal group (adapted from [85]) 9

Table 1.2 The Operative Link for Gastric Intestinal Metaplasia Assessment (OLGIM) staging system 11

Table 1.3 Combined use of chemical carcinogen and *H. pylori* to induce gastric cancer in rodent models (adapted from [291]) 28

Table 1.4 A summary of key genetic mouse models used to study gastric cancer (adapted from [289]) 29

Table 1.5 Mouse models of gastric premalignant lesions (adapted from [320]) 30

Table 2.1 General materials and reagents 35

Table 2.2 Antibodies 36

Table 2.3 OPAL™ 7-color manual IHC kit 36

Table 2.4 Primers used for quantitative Real Time PCR 37

Table 2.5 Cell lines used to produce conditioned media 37

Table 2.6 Equipment 37

Table 2.7 Software 37

Table 2.8 R packages (R version 3.5.3 and online server R version 3.5.1) 38

Table 2.9 OPAL panel staining details and fluorophores used 44

Table 2.10 Organoid growth media details 50

Table 2.11 Staining conditions of primary antibodies used with immunohistochemistry to characterise gastrointestinal organoids 53

Table 3.1 Description of patient cohort used in this study 57

Table 3.2 Frequency of premalignant lesions adjacent and distant (at least ≥ 2cm away) from Lauren gastric cancer subtypes 60

Table 3.3 Frequency of premalignant lesions adjacent and distant (at least ≥ 2cm away) from Lauren gastric cancer subtypes focusing on “true gastric cancers” only (GOJ excluded) 60

Table 4.1 Description of cohorts with Affymetrix microarray data (HG-U133 Plus 2.0) used in this study 70

Table 4.2 Top 10 differentially expressed genes ranked by log2 fold change between normal (NN) and intestinal metaplasia (IM+GC) tissue 71

Table 4.3 Top genes by log2 fold change overexpressed in macro-dissected IM-GC and rIM+GC samples 83

Table 4.4 Top 5 enriched Hallmark and Transcription Factor Target gene sets in rIM+GC 84

Table 4.5 Top enriched pathways/GO terms comparing bcIM-GC and biIM-GC using single sample gene set enrichment analysis 88

Table 4.6 Differentially expressed genes in bcIM-GC and biIM-GC samples 89

Table 4.7 Significantly enriched cytokines and chemokines in bcIM-GC and biIM-GC samples. 92

Table 4.8 Differentially expressed genes in cIM-GC[1] and iIM-GC[1] samples from Companioni et al 2017 [388] using GEO2R online tool 96

Table 4.9 Top 10 genes by adjusted p value[1] over-expressed in bcIM-GC compared to biIM-GC samples (Companioni et al 2017 study, [388])..... 97

Table 4.10 Significantly enriched cytokines, chemokines and their associated receptors using the IM-GC samples from the Companioni et al 2017 study [388]..... 98

Table 5.1 Clinical details of patients used for the OPAL™ multiplex immunohistochemistry macrophage study from the IM-GC, the Progressors and the IM+GC (MAUGIC) cohorts..... 108

Table 5.2 Normalised[1] touch cell pair analysis showing targeted changes across tissues representing histological progression in the IM-GC and IM+GC cohorts 131

Table 6.1 Normalised[1] touch pair analysis showing changes in T cell targeting across tissues representing histological progression in the IM-GC and the IM+GC cohorts..... 165

Table 6.2 Clinical parameters of patients with matched T cell and macrophage data..... 168

Table 7.1 Clinical details of IM-GC, Progressors and IM+GC patients with intestinal metaplastic tissue used to characterise CD10 and Das1 staining..... 190

Table 7.2 Sensitivity and specificity of CD10 for individual complete intestinal metaplastic glands 194

Table 7.3 Sensitivity and specificity of Das1 for individual incomplete intestinal metaplastic glands 195

Table 7.4 Logistic regression models comparing CD10 with combined CD10 + Das1 staining for complete intestinal metaplastic glands 196

Table 8.1 Clinical details of patient cohort used for gastrointestinal organoid study..... 211

Table 8.2 Isolation methods and growth media used to identify optimal conditions for establishing and growing porcine organoids 214

Table 8.3 Experimental plan to investigate the effect of niche factors on the proliferation and differentiation of gastrointestinal organoids..... 227

Table 8.4 Immunohistochemistry using MUC5AC and CDX2 to characterise differentiation of gastrointestinal organoids grown in customised growth media (Experiment 2)..... 231

Table of Contents

Thesis abstract ii
Declaration iv
Preface v
Acknowledgments vi
Publications and Presentations ix
List of Abbreviations x
List of Figures xii
List of Tables xix
Table of Contents xxi

Chapter 1 Literature review 1
1.1 Gastric cancer 1
1.1.1 Epidemiology 1
1.1.2 Risk factors 2
1.1.3 Histological classification of gastric cancer 3
1.1.4 Molecular classification of gastric cancer 4
1.1.5 Treatment options for patients with gastric cancer 6
1.2 Premalignant lesions and gastric cancer 6
1.2.1 The Correa model of progression 6
1.2.2 Clinical association between gastric premalignant lesions and gastric cancer 9
1.2.3 The Operative Link for Gastritis Assessment (OLGA) and the Operative Link for Intestinal Metaplasia Assessment (OLGIM) 10
1.3 Intestinal metaplasia 12
1.3.1 A point of no return? 12
1.3.2 Intestinal metaplasia subtypes 14
1.3.3 Why and how does intestinal metaplasia occur? 16
1.3.4 Risk factors in intestinal metaplasia 17
1.3.5 Spasmolytic peptide expressing metaplasia 18
1.4 The role of the immune system in gastric carcinogenesis 18
1.4.1 The innate immune system in gastric premalignant lesions 19
1.4.2 The adaptive immune system in gastric premalignant lesions 21
1.4.3 Gastric cancer and the immune system 24
1.5 Biomarkers of gastric carcinogenesis 26
1.5.1 Serum biomarkers 26
1.5.2 Tissue biomarkers based on intestinal metaplasia 27
1.6. Models of gastric carcinogenesis 27

1.6.1 Animal models of gastric cancer 27
1.6.2 Animal models of gastric precancerous lesions 29
1.6.3 The lack of cell lines to model gastric carcinogenesis 31
1.6.4 Organoid models in carcinogenesis 31
1.7 Goals of this thesis 34
Chapter 2 Materials & Methods 35
2.1 Materials 35
2.2 Patient cohorts 38
2.2.1 The Molecular Analysis for Upper Gastro Intestinal Cancer cohort 38
2.2.2 Screening and surveillance (S2P) cohorts 39
2.3 Histological association of intestinal metaplasia with Lauren gastric cancer subtypes (Chapter 3) 40
2.3.1 Patient selection criteria 40
2.3.2 Statistical analysis 41
2.4 Gene expression profiling (Chapter 4) 41
2.4.1 Differential gene expression 41
2.4.2 Gene set over-representation and single sample gene set enrichment analysis 41
2.4.3 Gene expression validation 42
2.4.4 Cell-type Identification By Estimating Relative Subsets Of RNA Transcripts (CIBERSORT) 42
2.5 OPAL™ multiplex immunohistochemistry (Chapters 5-7) 42
2.5.1 Sample selection and subtyping of intestinal metaplasia 42
2.5.1 Single slide library creation 43
2.5.2 Multiplex immunohistochemistry staining 45
2.5.3 Slide scanning and imaging using VECTRA microscope 45
2.5.4 inForm multispectral unmixing and cell phenotyping 45
2.5.5 Spatial location analysis of cell types 46
2.5.6 Statistical analysis 47
2.6 Biomarkers (Chapter 7) 48
2.6.1 Determining the presence of CD10 on individual IM glands 48
2.6.2 Determining the presence of Das1 on individual IM glands 48
2.6.3 Quantification of Das1 staining across whole section 48
2.6.4 Statistical analysis 48
2.7 Organoid model (Chapter 8) 49
2.7.1 Tissue processing and establishing human gastrointestinal organoid cultures 49
2.7.2 Organoid growth media 50

2.7.3 Establishing organoid cultures from fresh porcine tissue 50
2.7.4 Establishing porcine organoid cultures from previously cryopreserved tissue 51
2.7.5 Passaging/reseeding of organoid cultures 51
2.7.6 Freezing down organoid cultures 51
2.7.7 Reanimating cryopreserved organoid cultures 51
2.7.8 RNA isolation from organoid cultures 52
2.7.9 Reverse transcription 52
2.7.10 Quantitative Real Time PCR (qRT-PCR) 52
2.7.11 Fixing and embedding of organoids 52
2.7.12 Single stain immunohistochemistry 53
2.7.13 Production of conditioned media 53
2.7.14 Fluorescence-Activated Cell Sorting (FACS) 54
Chapter 3 Investigating the relationship between intestinal metaplasia and Lauren gastric cancer subtypes 55
3.1 Introduction 55
3.2 Hypothesis and aims 55
3.3 Results 55
3.3.1 Description of the study cohort 55
3.3.2 Prevalence of premalignant lesions adjacent and distant to tumour 58
3.3.3 Clinico-epidemiological details of gastric cancer patients without and with adjacent intestinal metaplasia 61
3.3.4 Pathology details of gastric cancer patients without and with adjacent intestinal metaplasia 61
3.4 Summary and discussion 64
3.4.1 Discussion 64
3.4.2 Study limitations 67
Chapter 4 Characterising the gene expression profile of tissues associated with gastric carcinogenesis 68
4.1 Introduction 68
4.2 Aims 68
4.3 Results 69
4.3.1 Samples profiled using Affymetrix microarrays 69
4.3.2 Intestinal metaplasia characterised using differential gene expression and gene set over-representation analysis 69
4.3.3 Characterising the immune landscape in chronic gastritis and intestinal metaplasia using CIBERSORT 73

4.3.4 Identifying shared differentially expressed genes between premalignant and malignant lesions 75
4.3.5 Single sample gene set enrichment analysis identifies shared enrichment in cancer hallmark pathways between intestinal metaplasia and gastric cancer subtypes 78
4.3.6 Trends in enriched chromosomal bands by gene expression correspond to copy number gains in gastric cancer 80
4.3.7 Molecular characterisation of intestinal metaplasia without and with concurrent gastric cancer reveals differences in levels of inflammation and transcription factors associated with gastric cancer 82
4.3.8 Subtyping of intestinal metaplasia using gene expression profiles 85
4.3.9 Single sample GSEA confirms metabolic and small intestinal character of bcIM-GC samples and suggests enriched immune activity 87
4.3.10 Differential gene expression allows further characterisation of intestinal metaplasia subtypes 88
4.3.11 Higher expression of gastric cancer associated biomarkers CEACAM5 and CEACAM6 in biIM-GC samples 91
4.3.12 Single gene analysis of immune related genes identifies distinct immune profiles in intestinal metaplasia subtypes 91
4.3.13 Immune gene correlation matrix suggests the presence of three main types of T cell activity 93
4.3.14 T cell immune gene signature associated with complete intestinal metaplasia 94
4.3.15 Gene expression profiling of intestinal metaplasia validation cohort from Companioni et al 2017 study [388] 95
4.3.16 Subtyping and characterisation of intestinal metaplasia samples from the Companioni cohort using 28 gene signature 96
4.4 Summary and discussion 99
4.4.1 Discussion 100
4.4.2 Study limitations 105
Chapter 5 Characterising the macrophage landscape in intestinal metaplasia 106
5.1 Introduction 106
5.2 Hypothesis and aims 107
5.3 Results 107
5.3.1 Description of cohorts used in this study 107
5.3.2 OPAL™ multiplex immunohistochemistry for macrophage panel 108
5.3.3 Macrophage immune profile in gastric premalignant lesions consists of six main subsets 110
5.3.4 Level of expression of key markers differs between macrophage subsets 110
5.3.5 Total macrophage cell density highest in complete and lowest in incomplete intestinal metaplasia with differing subset distribution 113

5.3.6 M2 macrophages dominate the macrophage profile of the microenvironment in intestinal metaplasia 114
5.3.7 Evolution of macrophage populations with time 117
5.3.8 Matched chronic gastritis has similar macrophage content compared to adjacent intestinal metaplasia 120
5.3.9 Reduced M2 to M1/2 macrophage ratio along histological and temporal progression 124
5.3.10 The macrophage landscape within a distance of 40µm from the epithelium changes with histo-temporal progression 125
5.3.11 Histo-temporal progression characterised by higher CD68+CD163+CD206+IRF8+ and lower CD68+CD163+CD206+ touch cell pair density with epithelial cells 127
5.3.12 Temporal progression in intestinal metaplasia characterised by lower touch cell pair density between CD68+CD163+CD206+ and CD68+CD163+CD206+IRF8+ macrophages 130
5.3.13 Decreased macrophage targeting of the epithelium in complete IM 131
5.3.14 Description of multi-site and time point tissue samples available from two case studies that have progressed to high grade dysplasia 132
5.3.15 Macrophage profiling of patient P1 shows high M1 and M1/2 macrophage density in high grade dysplasia 133
5.3.16 Macrophage profile of patient P2 shows high M2 macrophage density in high grade dysplasia 139
5.4 Summary and discussion 143
5.4.1 Discussion 143
5.4.2 Technical limitations 147
Chapter 6 Characterising the T cell landscape in intestinal metaplasia 150
6.1 Introduction 150
6.2 Hypothesis and aims 151
6.3 Results 151
6.3.1 Description of cohorts and OPAL™ multiplex immunohistochemistry used with the T cell panel 151
6.3.2 T cell immune profile in gastric premalignant lesions consists of four main subsets 152
6.3.3. Higher total T cell density in the complete subtype of intestinal metaplasia in both the IM-GC and IM+GC cohorts 153
6.3.4 Total T cell density increases in complete IM and decreases in incomplete IM with temporal progression 154
6.3.5 Complete intestinal metaplasia characterised by influx of CD4 and DN T cells whereas incomplete IM shows lower density of all T cell subsets except for FOXP3 T cells 154

6.3.6 Matched adjacent chronic gastritis has fewer CD4 T cells than complete intestinal metaplasia 157
6.3.7 T cell subset ratios show recurrent pattern across tissue types with time 159
6.3.8 Epithelial cell to T cell subset ratios differ between complete and incomplete intestinal metaplasia 159
6.3.9 Lower levels of T cell-T cell interaction in incomplete intestinal metaplasia 161
6.3.10 Lower levels of epithelial cell-T cell interaction in incomplete intestinal metaplasia 163
6.3.11 CD8 T cells target the epithelium in incomplete intestinal metaplasia 165
6.3.12 Investigating the relationship between T cells and macrophages 166
6.3.13 Quantitative relationships between T cell and macrophage subsets differ by tissue type and between cohorts 169
6.3.14 Integrating the spatial relationships of T cells, macrophage and epithelial cells .. 172
6.3.15 T cell profiling of Progressor patient P1 shows increased FOXP3 T cell density associated with progression to high grade dysplasia 174
6.3.16 T cell profile in patient P2 shows only minor differences 179
6.4. Summary and discussion 181
6.4.1 Discussion 181
6.4.2 Technical limitations 186
Chapter 7 Characterising the potential of CD10 and Das1 as biomarkers for the complete and incomplete subtypes of intestinal metaplasia 188
7.1 Introduction 188
7.2 Hypothesis and aims 189
7.3 Results 189
7.3.1 Validation of CD10 and Das1 as biomarkers of intestinal metaplasia subtypes 189
7.3.2 CD10 has very high sensitivity and specificity for identifying complete intestinal metaplasia glands 193
7.3.3 Das1 has low sensitivity but high specificity for identifying incomplete intestinal metaplasia glands 194
7.3.4 Logistic regression modelling of combined CD10 and Das1 staining 195
7.3.5 Das1 staining is associated with incomplete intestinal metaplasia in the IM-GC cohort 196
7.3.6 Whole section Das1 staining is higher in IM-GC patients with incomplete intestinal metaplasia 199
7.3.7 Das1 staining is associated with incomplete intestinal metaplasia tissue in the IM+GC cohort 200
7.3.8 Das1 staining is higher in complete intestinal metaplasia tissues of IM+GC patients 202

7.3.9 Das1 staining associated with CD68+IRF8+ and CD68+CD163+IRF8+ macrophages in incomplete intestinal metaplasia in IM-GC patients 202
7.4 Summary and discussion 204
7.4.1 Discussion 204
7.4.2 Technical limitations 207
Chapter 8 Developing an intestinal metaplasia organoid model 209
8.1 Introduction 209
8.2 Aims 210
8.3 Results 210
8.3.1 Clinical details of patient samples 210
8.3.2 Pilot study to determine feasibility of project 211
8.3.3 Establishing parameters for growing organoids using a porcine model 213
8.3.4 Growing human gastrointestinal organoids 218
8.3.5 Establishing parameters for characterising organoids using the porcine model 218
8.3.6 Characterising human gastrointestinal organoids by morphology and immunohistochemistry 220
8.3.7 Characterising gastrointestinal organoids using quantitative Real Time PCR 225
8.3.8 Investigating the role of niche factors in gastrointestinal organoid proliferation and differentiation 227
8.3.9 Growing organoids from cell sorted cells using the intestinal stem cell marker OLFM4 235
8.3.10 Creation of an organoid biobank 240
8.4 Summary and discussion 240
8.4.1 Discussion 240
8.4.2 Technical limitations 245
Chapter 9 Discussion and future directions 247
9.1 Intestinal metaplasia is associated with diffuse gastric cancer 247
9.2 The complete and incomplete subtypes of intestinal metaplasia differ at the molecular level 250
9.3 Macrophage and T cell landscapes differ between complete and incomplete intestinal metaplasia 253
9.4 Determining the biomarker potential of anti-CD10 and Das1 antibodies for subtyping complete and incomplete intestinal metaplasia 259
9.5 Intestinal metaplasia organoids can be grown from gastroscopy biopsies 262
9.6 Future directions 264
9.7 Conclusions 267

REFERENCES ……271
APPENDICES ……318

Chapter 1 Literature review

1.1 Gastric cancer

1.1.1 Epidemiology

The incidence of gastric cancer (GC) has been declining but it is still the fifth most common and third most lethal cancer in the world [1, 2]. Globocan data estimates that 1 034 000 new cases were diagnosed and 738 000 individuals died from this disease in 2018 (http://globocan.iarc.fr/ accessed 01/06/2020). Geographically, high risk areas include China (more than 40% of all new cases worldwide), Japan, South Korea, Eastern Europe, Central and South America [2] (Figure 1.1). Low incidence areas are Australia and New Zealand, North America, Western Europe, South Central Asia and most parts of Africa ([3], http://globocan.iarc.fr/ accessed 01/06/2020).

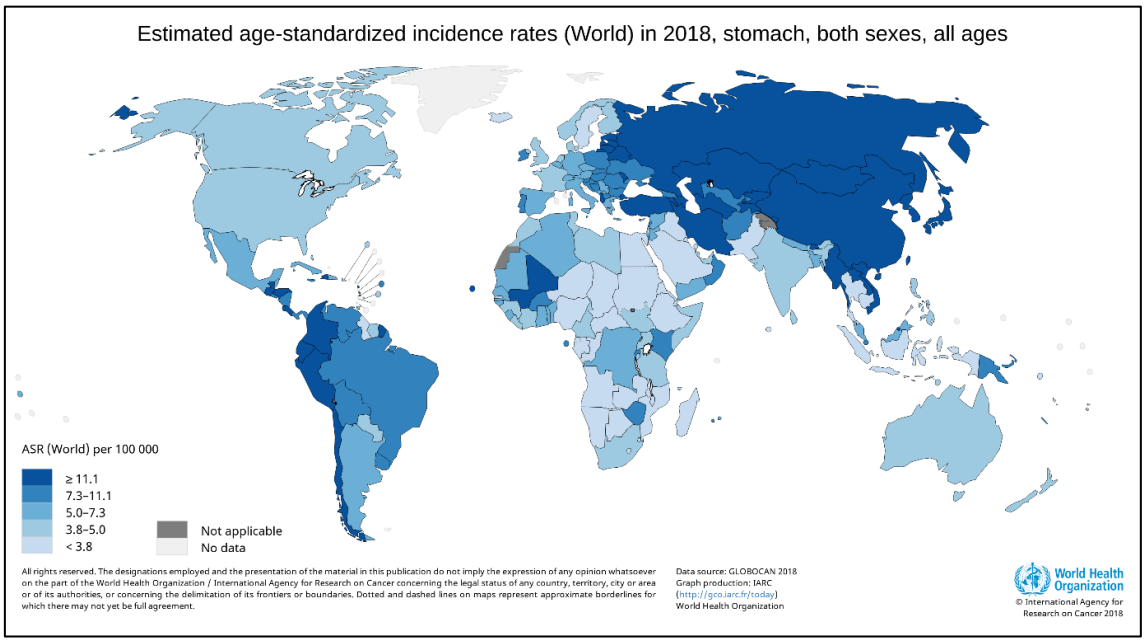


Figure 1.1 World map showing the estimated age-standardized incidence rates for gastric cancer in 2018 (obtained from http://globocan.iarc.fr/, accessed 01/06/2020)

Although the incidence and mortality in Australia for GC are much lower compared to those for the main five cancer types (prostate, breast, bowel, melanoma and lung cancer), more than 2200 new cases were diagnosed in 2015 and almost 1100 deaths occurred in 2016 due to this disease (https://www.cancer.org.au, accessed 05/06/2020). The five year survival rate is only 30%, much lower than that for prostate cancer (95%), breast cancer (91%) and bowel cancer (69%) but still higher than lung cancer (17%) (https://www.cancer.org.au, accessed 05/06/2020). GC tends to be asymptomatic and most GC patients present at an advanced stage of disease with no general population screening available [4, 5]. Given the low prevalence in this country it is difficult to make an economic argument for universal screening. However in high incidence

countries such as Japan and South Korea where population based screening is performed, the five year survival rate is much higher (61.6% and 76% respectively) [6, 7].

The vast majority of gastric cancers are sporadic gastric adenocarcinomas (>90%) and the premalignant conditions associated with these are the main focus of this thesis. Other less common types of GC include gastric lymphomas, hereditary diffuse gastric cancers or occur due to cancer predisposition syndromes such as Li-Fraumeni syndrome, Lynch syndrome and Peutz-Jegers syndrome [8-12] that will not be discussed further.

1.1.2 Risk factors

Infection with *Helicobacter pylori*, a Gram-negative spiral shaped microaerophilic bacterium [13], is the major cause of GC worldwide [14-17]. In 1994, *H. pylori* was categorised as a class I carcinogen by the International Agency for Research on Cancer [18]. The global systematic review by Hooi et al 2017 estimated that approximately 4.4 billion individuals were infected with *H. pylori* in 2015 (~60% of the total population in 2015) with infection rates varying widely between UN regions: from 24.4% in Oceania to 79.1% in Africa [19]. Australia had relatively low infection rates (overall 24.4%) but with regional wide variation and particularly high rates in Indigenous communities including the Martu remote rural communities in Western Australia reaching a prevalence of 91% [20].

In addition to regional differences, prevalence of *H. pylori* worldwide has also been shown to increase considerably with age [16, 21]. In the USA prevalence ranged from 20% in 18-29 year olds to 47% in 60-69 year olds [22] and in Japan it was less than 20% in 20 year olds increasing to 70-80% in 40 year olds [23]. Additionally the recent systematic review with meta-analysis by Zamani et al 2018 showed that prevalence overall was significantly higher in adults (>18 years) than in children across all continents with available data (no data for Oceania) [24].

Males are twice as likely to develop GC compared to females, particularly those of more advanced age (>50 years old) (http://globocan.iarc.fr/ accessed 01/06/2020, Figure 1.2). Environmental and lifestyle choices such as smoking and alcohol have also been shown to be associated with increased risk [25-27]. Other risk factors for GC include a high salt diet, smoked or dried meat and fish, pickled food, low intake of fresh fruit and vegetables, low exercise levels, obesity, low socioeconomic status and ionising radiation (studies summarised in [28]). Blood group is also a potential risk factor as individuals with blood group A or AB are at a higher risk of developing GC [29].

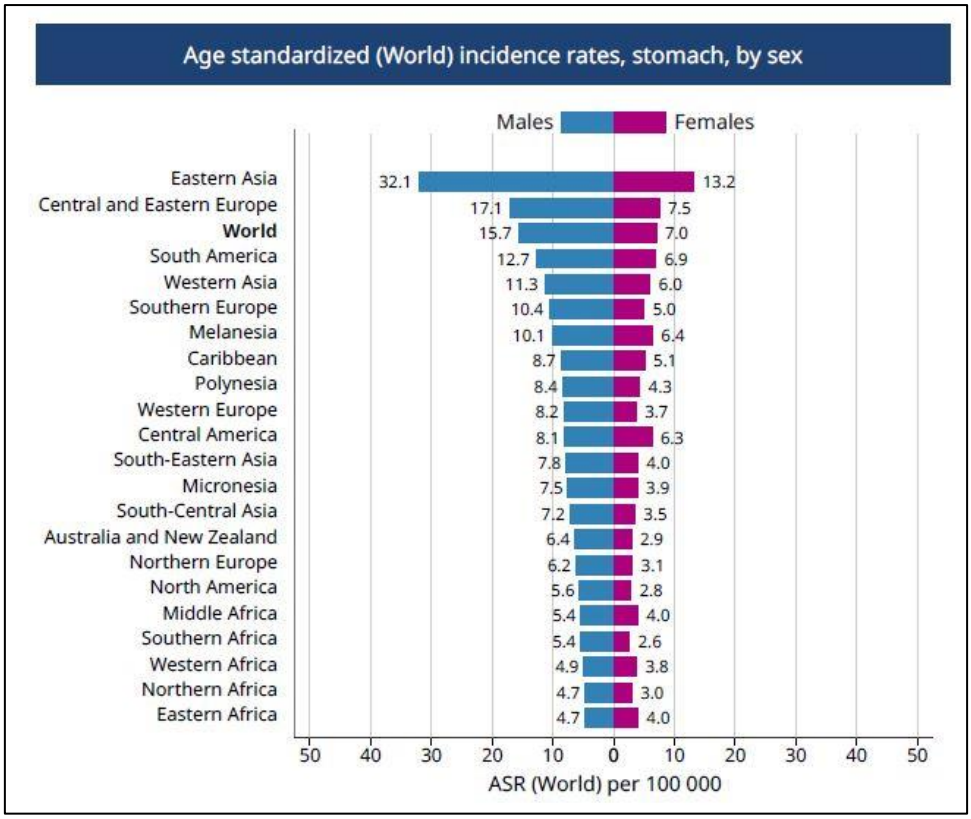


Figure 1.2 Dual bar chart showing age-standardised incidence rates for gastric (stomach) cancer for each sex separately in 2018 (obtained from http://globocan.iarc.fr/)

Race and ethnicity are also risk factors of developing GC. A US based study showed much higher rates of GC incidence in Hispanics/Asian/Pacific Islanders/American Indians/Alaskan Natives and African Americans compared to whites (multivariable-adjusted incidence rate ratios for non-cardia GC were from 1.7 to 3.9 compared to non-Hispanic whites, [30]). In this study increased risk of non-cardia GC was also observed with decreasing socio-economic status for Blacks and Hispanics [30].

1.1.3 Histological classification of gastric cancer

Several classification systems have been used to classify GC around the world including the Lauren, the Ming, the Goseki and the WHO classification systems [31-34]. The histology-based Lauren classification divides gastric adenocarcinoma into two main types: intestinal and diffuse [31]. Tumours that consist of both types are defined as mixed adenocarcinoma. The pathobiological Ming classification divides GC into the expanding and the infiltrative types with varying gross appearances and considerable overlap with the Lauren types (between intestinal and expanding and between diffuse and infiltrative, [32]). The histology based Goseki classification divides GC into four groups by combining the degree of glandular tubule differentiation (well and poor) and the intracellular mucus content (rich and poor): group I tubular differentiation – well, mucus in cytoplasm – poor; group II tubular differentiation – well,

mucus in cytoplasm – rich; group III tubular differentiation – poor, mucus in cytoplasm – poor; group IV tubular differentiation – poor, mucus in cytoplasm – rich [33]. Finally, the WHO classification divides GC into four major histology-based types (tubular, papillary, mucinous and poorly cohesive) with additional rare histological variants [35]. Although multiple studies have investigated the relationship between histopathological features in GC and patient characteristics, disease specific criteria and clinical outcome, the benefits of using one classification system over another remain disputed (as summarised and discussed in [34]).

Overall the Lauren system is the most commonly used and studied GC classification system [34]. Here, the intestinal type of GC (IGC, Figure 1.3) is characterised by tumours that tend to be more differentiated with glandular formation [31]. IGC occurs typically in older male patients, it is mostly found in the distal stomach and has better 5-year overall survival [36-39]. In contrast, the diffuse type of GC (DGC, Figure 1.3) is characterised by scattered single or small groups of tumour cells infiltrating the gastric wall where tumours are generally termed undifferentiated or poorly differentiated [38]. A subgroup of tumours may also have signet ring morphology. DGC occurs more frequently in younger patients and females, it is mostly found in the middle part (body/corpus) of the stomach and has worse 5 year overall survival rate [36-39]. Although the clinicopathological characteristics of patients with mixed GC (MGC) sit in between those of IGC and DGC, overall survival and disease free survival follow a similar pattern to DGC and not IGC [38].

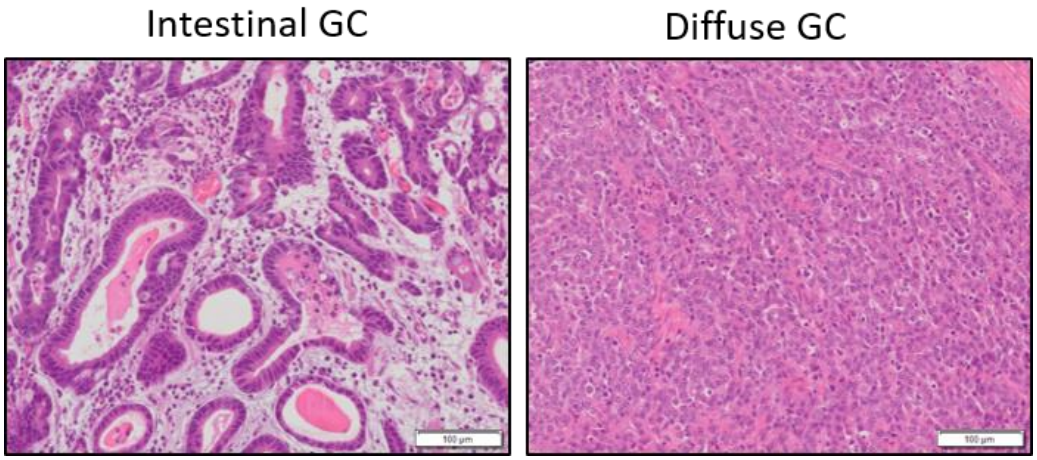


Figure 1.3 The histology based Lauren classification system groups gastric adenocarcinomas into two main types: the intestinal type and the diffuse type
Images of intestinal and diffuse gastric tumours from in-house tissue. Scale bar: 100µm.

1.1.4 Molecular classification of gastric cancer

Recent studies have classified GC into molecular subtypes based on their genomic characteristics [40-44]. The Cancer Genome Atlas Research Network (TCGA) [42] profiled samples from 295 GC

patients and integrated data obtained using six molecular platforms (DNA exome sequencing, RNA sequencing, microRNA sequencing, methylation, RPPA and chromosomal copy number analysis). This study identified four subtypes: the Epstein-Barr virus positive subtype (EBV, 8.8% of patients), the microsatellite unstable subtype (MSI, 21.7% of patients), the genomically stable subtype (GS, 19.7% of patients) and the chromosomal instability subtype (CIN, 49.8% of patients) (Figure 1.4). EBV tumours occurred more in male patients (81%) and were characterised by recurrent PIK3CA mutations, very high levels of DNA methylation, amplification of JAK2 and overexpression of PDL1 (CD274) and PDL2 (PDCD1LG2). The MSI tumours occurred mainly in older patients (median age 72 years), more in females (56%) and were characterised by frequent MLH1 silencing and TP53 mutations. The GS tumours occurred mainly in relatively younger patients (median age 59 years), were enriched for the diffuse histological type (73%) and had frequent CDH1 and RHOA mutations. Finally, CIN tumours were commonly found in the gastro-oesophageal junction/cardia of the stomach, were enriched for the intestinal histological type, with highly frequent chromosomal aberrations and TP53 mutations (highest). Overall having both a histological and a precise molecular description of GC subtypes has allowed greater insight into the possible evolution and different aspects of this disease.

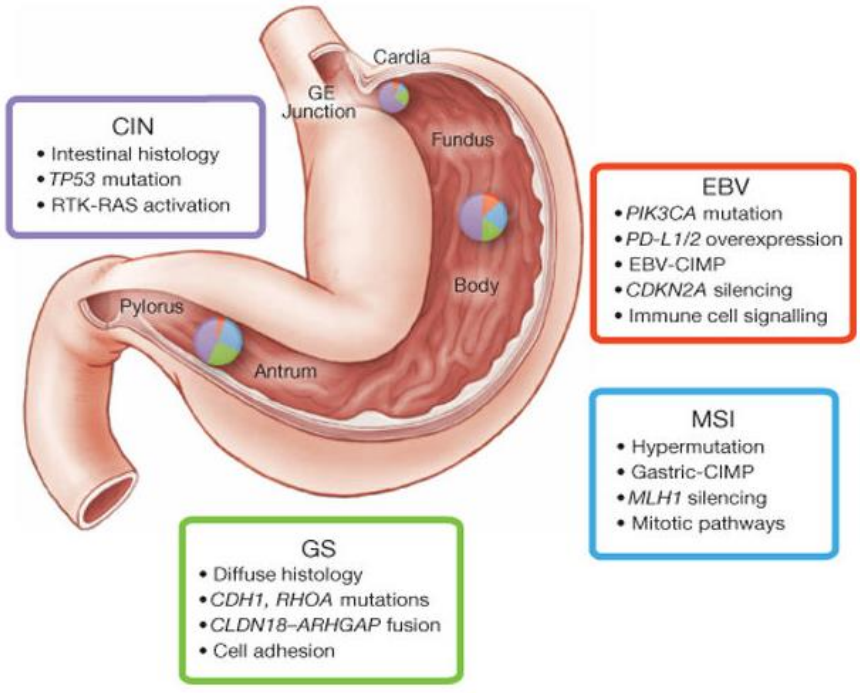


Figure 1.4 Schematic representation of molecular subtypes of gastric cancer by The Cancer Genome Atlas Research Network (adapted from TCGA 2014, [42])
Relative distribution of each molecular subtype shown by floating pie charts on stomach diagram. See text for more details of each molecular subtype.

1.1.5 Treatment options for patients with gastric cancer

Patients with GC may be treated with a combination of surgery, radiation therapy, chemotherapy, targeted therapy and more recently immunotherapy ([45-47], https://www.cancer.org.au/ accessed 11/06/2020). For early GC (EGC) i.e. carcinoma *in situ* and tumour invading the lamina propria (Tis and T1a respectively, TNM staging of gastric cancer as per AJCC 7th edition [48]), endoscopic mucosal resection (EMR) and submucosal dissection (ESD) is used instead of surgery [47, 49, 50]. For patients with more advanced GC (>T1a stage) and dependent on the extent of the tumour, partial or total gastrectomy is recommended together with a combination of other available treatments (Smyth et al 2016).

Radiation therapy may be used before surgery to reduce the size of the tumour and after surgery to kill any remaining tumour cells [45, 51, 52]. Neoadjuvant chemotherapy (prior to surgery) using a combination of drugs such as fluorouracil, cisplatin, capecitabine, oxaliplatine and epirubicin has been used to reduce tumour size and possibly local lymph node micrometastases [53-55]. Adjuvant chemotherapy (post-surgery) has also been used to eliminate remaining tumour cells, or at least slow down tumour growth [55, 56]. Targeted therapy is used to tackle specific cancers for example in the treatment of HER2-positive cancers with HER2-targeted therapy, and can be used in combination with chemotherapy agents as well (as reviewed in [57, 58]). For patients with high PDL1 and microsatellite instability (MSI-H) cancers, which have not responded to chemotherapy, immunotherapy with pembrolizumab (high affinity anti-PD1 monoclonal antibody) is currently being used [59, 60].

Although GC treatment has changed in recent years from a standard approach to a more individually tailored multimodal approach, overall outcome is still relatively poor for GC patients, particularly for those with advanced GC (T3 and T4 stages) [39, 61]. By contrast EGC has been shown to have >90% 5 year survival rate [62, 63]. Unlike high incidence countries such as South Korea and Japan, it is not cost effective to carry out general population screening in a low incidence country such as Australia. Thus, it is essential that patients are stratified in risk groups at the earliest possible time point and their surveillance program is personalised according to their risk profile.

1.2 Premalignant lesions and gastric cancer

1.2.1 The Correa model of progression

In 1975, Pelayo Correa described a histologically defined model with stepwise progression to GC [64]. This was further refined to include the key role that *H. pylori* has in gastric carcinogenesis

(Figure 1.5, [65]). Briefly *H. pylori* infection of the stomach leads to acute and then chronic gastritis (CG) [66, 67]. Persistent inflammation of the stomach can last several decades [68-70]) and although it is still unclear why, in some patients the chronic inflammation leads to atrophic gastritis (AG) [69, 71-73]. AG is characterised by the loss of the lower part of gastric glands, particularly in the fundus and the body (corpus) parts of the stomach, including the parietal (oxyntic) cells which normally generate hydrochloric acid and maintain the pH of gastric juice between 1.5 to 3.5 (Figures 1.5 and 1.6). The loss of parietal cells leads to an increase of gastric juice pH and long term AG is believed to progress to intestinal metaplasia (IM) in a subset of patients [74, 75].

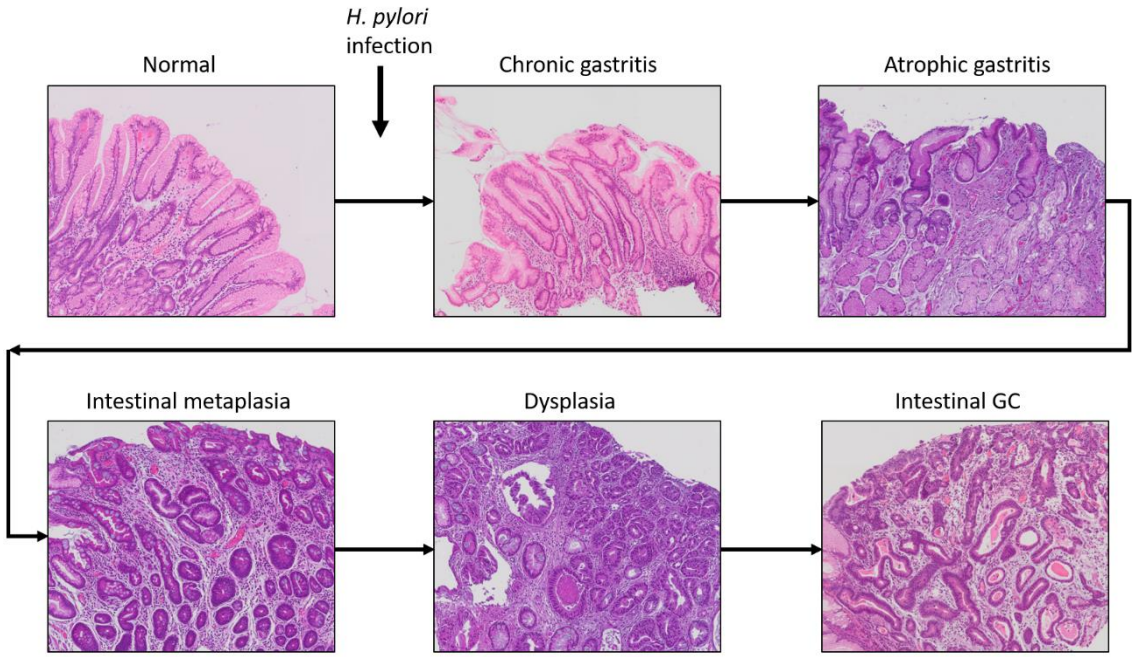


Figure 1.5 Visual representation of the histologically defined Correa model leading up to the intestinal type of gastric cancer (IGC) [65]
Images from available in-house tissue depicting the sequential steps described by the Correa model. Normal gastric tissue is infected by *H. pylori* which results in long term gastritis. Over time loss of the lower part of gastric glands leads to atrophic gastritis, followed by intestinal metaplasia and then dysplasia. Finally further genomic and epigenomic changes result in gastric cancer, particularly the intestinal type.

IM is characterised by the replacement of gastric epithelial cells by epithelial cell types found in the intestinal lining. The final precancerous stage in the Correa cascade is that of dysplasia, a neoplastic lesion which is characterised by abnormal looking cells and glandular structures. The international Padova classification system [76] divided dysplasia into five main categories: category 1, negative for dysplasia; category 2, indefinite for dysplasia; category 3, non-invasive neoplasia which includes both low grade and high grade neoplasia (LGD and HGD respectively); category 4, suspicious for invasive carcinoma; and category 5 for invasive adenocarcinoma. In a clinical setting, LGD and HGD are reported in particular as these have differing surveillance

follow up periods (12 months for LGD and 6 months for HGD) as described in the current Victorian upper gastrointestinal endoscopy categorisation guidelines for adults (https://www2.health.vic.gov.au/, accessed 08/06/2020).

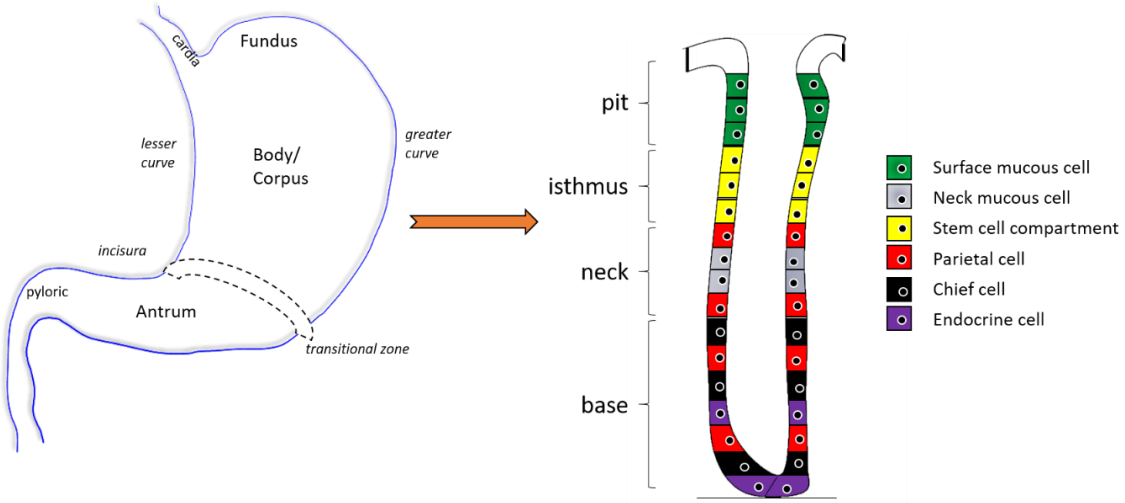


Figure 1.6 Schematic representation of the stomach and an oxyntic (body/corpus) gland
The stomach consists of at least four main areas. The proximal stomach is made up of the cardia, which neighbours the gastro-oesophageal junction. The upper part of the stomach or "pouch" is called the fundus and the middle part is the body or corpus. The distal or lower part of the stomach is known as the antrum, with the antral part neighbouring the duodenum of the small intestine known as the pyloric part. A gastric gland from the upper or middle part of the stomach is typically made up of surface mucous secreting cells, the stem cell compartment, neck mucous secreting cells, acid-producing parietal cells, chief cells and endocrine cells.

Generally the Correa model is thought to be particularly relevant in the development of the intestinal type of GC. However several studies have also shown an association between *H. pylori* infection and one or more premalignant lesions including IM with the diffuse subtype of GC [77-80]. Overall this is an area where the current thesis will attempt to add insight (all of Chapter 3 and Chapter 4 sections §4.3.3-6).

Each of the premalignant stages described in the Correa cascade are said to persist long term including IM which is believed to require a median time of 6.1 years to progress to GC, with the possible exception of low and high grade dysplasia [81]. LGD has been reported to progress to malignancy in 0% to 23% of cases, within a period of 12 to 48 months [82]. By contrast HGD cases progressed to a malignant stage in 60% to 85% over a median interval of 4 to 48 months (multiple studies summarised in [82, 83]), with almost 25% of cases receiving a diagnosis of GC within of 1 year of initial HGD diagnosis (reported by de Vries et al 2008 in the Netherlands, using the definition of severe dysplasia [84]). Overall the long period of time associated with progression from IM makes it an excellent candidate for intervention.

1.2.2 Clinical association between gastric premalignant lesions and gastric cancer

Numerous studies have investigated the relationship between gastric premalignant lesions and gastric cancer. A recent comprehensive population-based study was performed in Sweden using data from its national disease registers [85]. A total of 405 172 participants who were initially diagnosed with non-malignant pathologies were followed over a total period of 32 years (1979-2011). Patients with progressive premalignant lesions along the Correa model were shown to be associated with increasing Hazard Ratio for GC (HR, Table 1.1). The HR among patients was lower for cardia GC than for non-cardia GC for each lesion. The observed incidence rates predicted that within 20 years after gastroscopy, GC will develop in approximately 1 in 256 individuals with normal mucosa, 1 in 85 with gastritis, 1 in 50 with atrophic gastritis, 1 in 39 with intestinal metaplasia and in 1 in 19 with dysplasia overall. Similar associations between premalignant lesions and GC have been repeatedly shown in several studies in both low incidence and high incidence regions as well as meta-analysis studies [81, 84, 86-95] (Figure 1.7).

Table 1.1 Hazard Ratios (HR) and 95% confidence intervals (95% CI) for GC among patients with different premalignant lesions compared with the normal group (adapted from [85])

	Hazard Ratio (95% CI)[b]		
Mucosal status at baseline[a]	**Cardia gastric cancer**	**Non-cardia gastric cancer**	**All gastric cancer**
Normal	Reference	Reference	Reference
Minor mucosal change	1.1 (0.4-2.9)	1.9 (1.3-2.8)	1.8 (1.2-2.5)
Gastritis	1.8 (1.2-2.9)	2.8 (2.3-3.5)	2.6 (2.2-3.2)
Atrophic gastritis	2.4 (1.1-4.8)	5.0 (3.8-6.7)	4.5 (3.5-5.8)
Intestinal metaplasia	4.7 (2.3-9.5)	6.5 (4.8-8.9)	6.2 (4.7-8.2)
Dysplasia	6.0 (2.3-15.9)	12.1 (8.3-17.6)	10.9 (7.7-15.4)

[a]Initial biopsy identified in database. When multiple diagnoses were present, the most histologically progressed one was selected; [b]Using attained age as underlying time scale, estimated by Cox proportional hazards regression model and adjusted for sex.

An additional risk factor associated with progression to GC is pernicious anaemia which is particularly prevalent in older patients [96-98]. It occurs as a result of chronic atrophic autoimmune gastritis where self-antibodies target and then destroy the acid producing parietal cells in the oxyntic part (body) of the stomach [99, 100]. The long-term loss of parietal cells and the concomitant loss of gastric intrinsic factor (produced by the parietal cells) required for vitamin B12 absorption leads to vitamin B12 deficiency. A large US study comparing 1 138 390 cancer cases with 100 000 matched individuals without cancer (controls) showed that patients with pernicious anaemia were more than twice as likely to develop GC than those without (and more than eleven times to develop gastric carcinoids) [98].

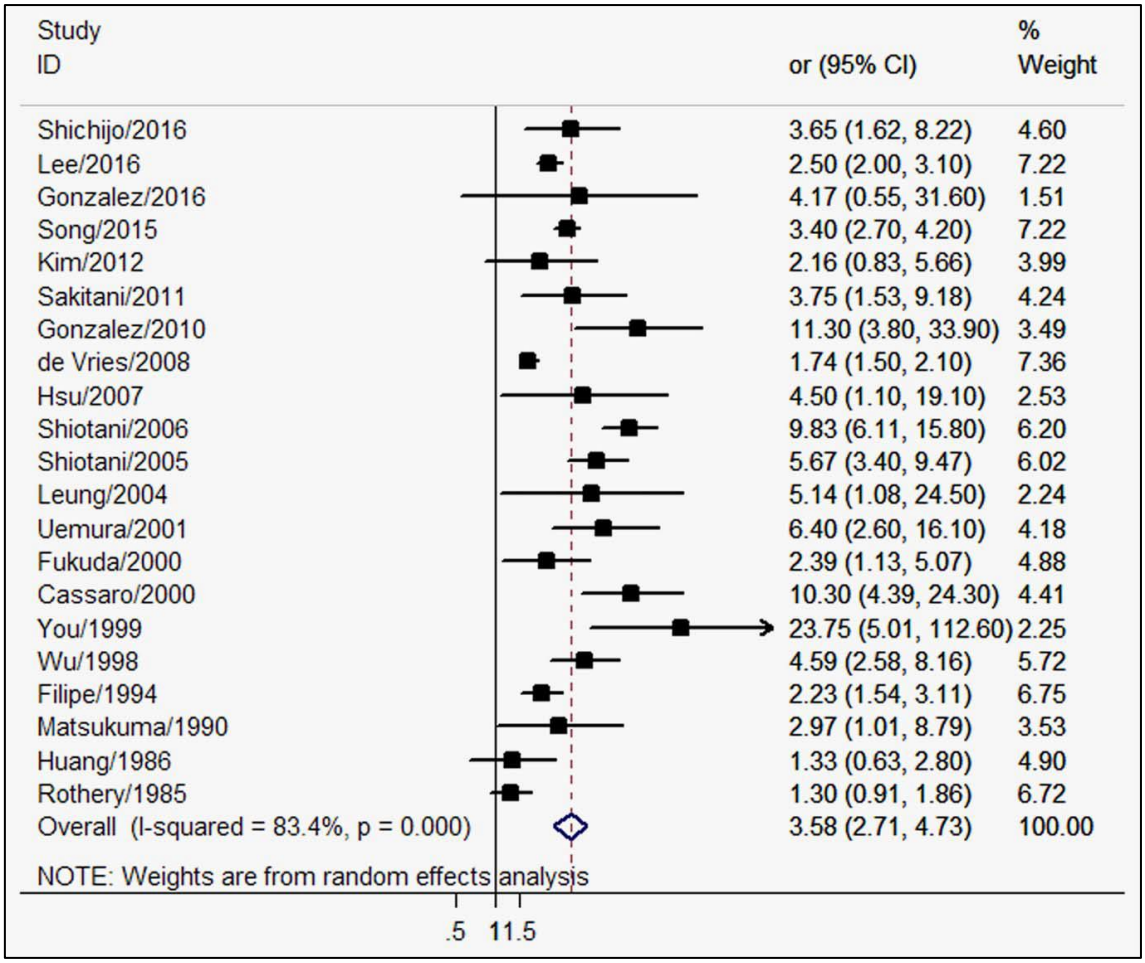
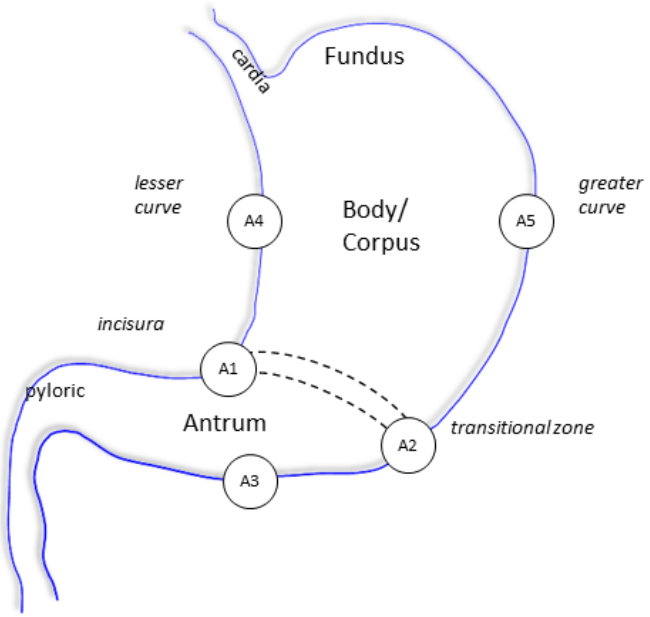


Figure 1.7 Forest plot showing gastric cancer risk among patients with intestinal metaplasia (IM) from multiple studies (adapted from Shao et al 2018 [94], random-effects model used)
Data shown from multiple studies comparing individuals without IM and those with IM for risk of gastric cancer (pooled overall Odds Ratio (OR) = 3.58, 95% confidence intervals (CI) 2.71-4.73). Total number of participants= 402 636 and 4535 gastric cancer patients.

1.2.3 The Operative Link for Gastritis Assessment (OLGA) and the Operative Link for Intestinal Metaplasia Assessment (OLGIM)

Together with the well-defined biopsy sampling protocol known as the Sydney protocol and its updated version from 1996 ([101, 102], Figure 1.8), a system for grading gastritis was developed in order to help assess patient risk of progression. This grading system became known as the Operative Link for Gastritis Assessment (OLGA). The integration of histological phenotypes (severity of atrophy) and topographical distribution (antrum versus body/corpus) allows an OLGA stage to be calculated with Stage 0 being equal to absence of atrophy, Stage I mild atrophy in the antrum or the body or both, Stage II moderate atrophy in the antrum or the body, or severe atrophy in the body in the absence of atrophy in the antrum, Stages III moderate atrophy in both the antrum and the body or at least severe atrophy in the antrum or the body separately and Stage IV severe atrophy in the antrum or body separately or together ([103], Figure 1.8).



Atrophy Score		Body (corpus)[2]			
		No atrophy (score 0)	Mild atrophy (score 1)	Moderate atrophy (score 2)	Severe atrophy (score 3)
Antrum[1]	No atrophy (score 0)	0	I	II	II
	Mild atrophy (score 1)	I	I	II	III
	Moderate atrophy (score 2)	II	II	III	IV
	Severe atrophy (score 3)	III	III	IV	IV

Figure 1.8 Schematic representation showing the recommended biopsy sites from the updated Sydney protocol [102] and the Operative Link for Gastritis Assessment (OLGA) staging system
Biopsy sites A1-A3 are categorised as antral (includes incisura) and sites A4-A5 as body (corpus); [1]Based on mean percentage of overall atrophy across all 3 antral biopsies; [2]Based on mean percentage of overall atrophy across both biopsies from the body (corpus).

Since the development of OLGA, a similar grading system was developed replacing AG with IM, the Operative Link for Intestinal Metaplasia Assessment (OLGIM) ([104], Table 1.2). The additional strength of OLGIM over OLGA was that IM is easier to detect and suffers from less inter-observer variability compared to AG (for AG, kappa value ranged from 0.41 to 0.57 and for IM from 0.80 to 0.82 among expert gastrointestinal pathologists in [105]).

Table 1.2 The Operative Link for Gastric Intestinal Metaplasia Assessment (OLGIM) staging system

IM Score		Body (corpus)[2]			
		No IM (score 0)	Mild IM (score 1)	Moderate IM (score 2)	Severe IM (score 3)
Antrum[1]	No IM (score 0)	0	I	II	II
	Mild IM (score 1)	I	I	II	III
	Moderate IM (score 2)	II	II	III	IV
	Severe IM(score 3)	III	III	IV	IV

[1]Based on mean percentage of overall intestinal metaplasia (IM) across all 3 antral biopsies as shown on Figure 1.8; [2]Based on mean percentage of overall IM across both biopsies from the body (corpus) as shown on Figure 1.8.

Both OLGA and OLGIM stages III-IV have been repeatedly shown to be more associated with progression to GC compared to stages I-II and thus have considerable potential in patient management and risk stratification [106-111]. Interestingly the OLGA/OLGIM staging systems have been shown to have predictive value for both the intestinal and the diffuse type of GC [80]. In a recent Korean study multivariable analysis showed that OLGA and OLGIM stages III/IV were independent risk factors for GC, irrespective of histological type [80].

1.3 Intestinal metaplasia

1.3.1 A point of no return?

Multiple studies in patients with gastric premalignant lesions have shown that *H. pylori* eradication treatment to eliminate *H. pylori* leads to overall reduced risk of progression to GC (see meta-analysis in [112], Figure 1.9). Eradication of *H. pylori* results in reduced inflammation, improved gastric acid secretion, normalisation of the microbiome and reduced *H. pylori*-induced DNA damage at least in a proportion of treated patients [113-122].

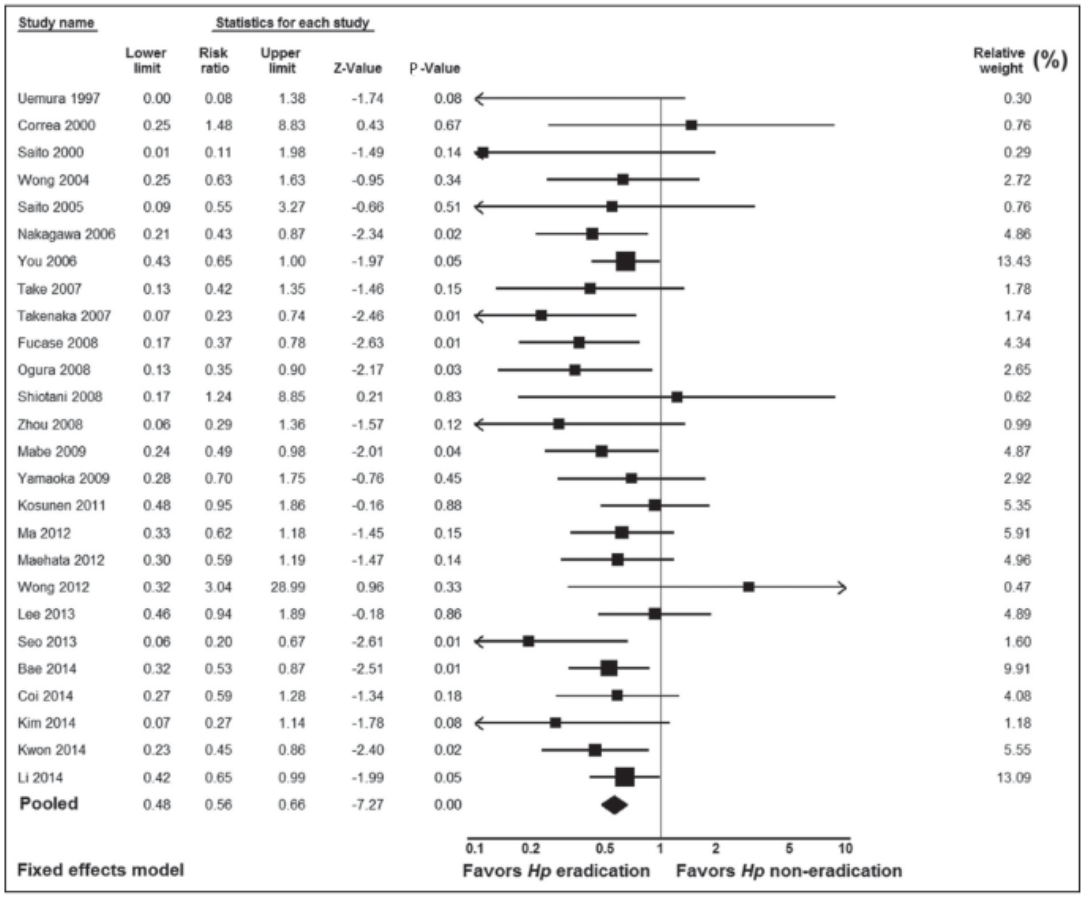


Figure 1.9 Forest plot showing individual and pooled risk ratios and 95% confidence intervals in studies comparing gastric cancer risk in patients with H. pylori eradication and controls (adapted from [112])

A total of 26 studies were used in this meta-analysis, with a total of 22619 patients and 29744 controls. Pooled RR = 0.56 and 95% CI = 0.48-0.66.

However baseline histology at which eradication treatment is commenced plays an important role with regards to progression risk [123, 124]. Further stratification on the data based on baseline histology stage has shown that treatment in IM and dysplasia may not necessarily benefit all patients from the point of view of risk reduction ([124, 125], Figure 1.10). In fact eradication treatment did not seem to protect patients with IM or dysplasia in a recent study which spanned 16 years. Here, an equal number of patients (n=5) progressed to GC as those that received placebo (out of 795 starting participants, randomised for intervention or placebo and with 456 final participants as described in [109]). Patients with non-atrophic gastritis or multifocal atrophic gastritis did not progress to GC over the same period of time [109]. In contrast a prospective study with up to 10 years follow up did show histological improvement for IM patients in both the antrum and the body after *H. pylori* eradication, suggesting that regression may occur in some IM patients ([121], Figure 1.11).

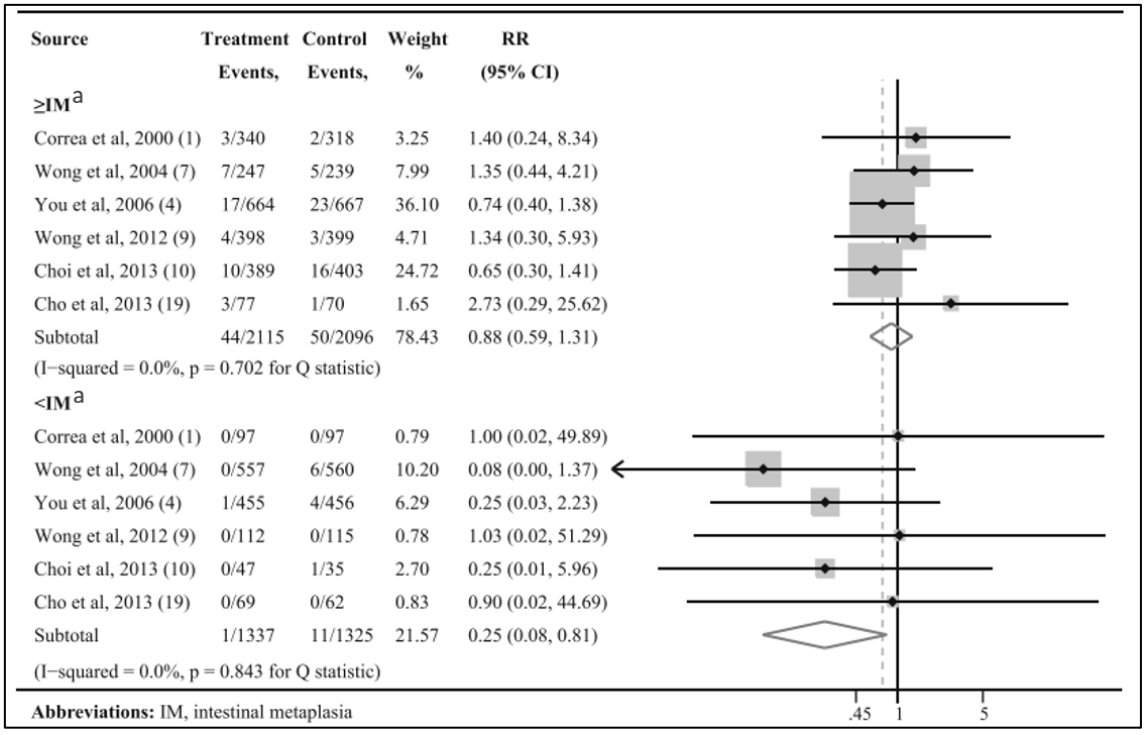
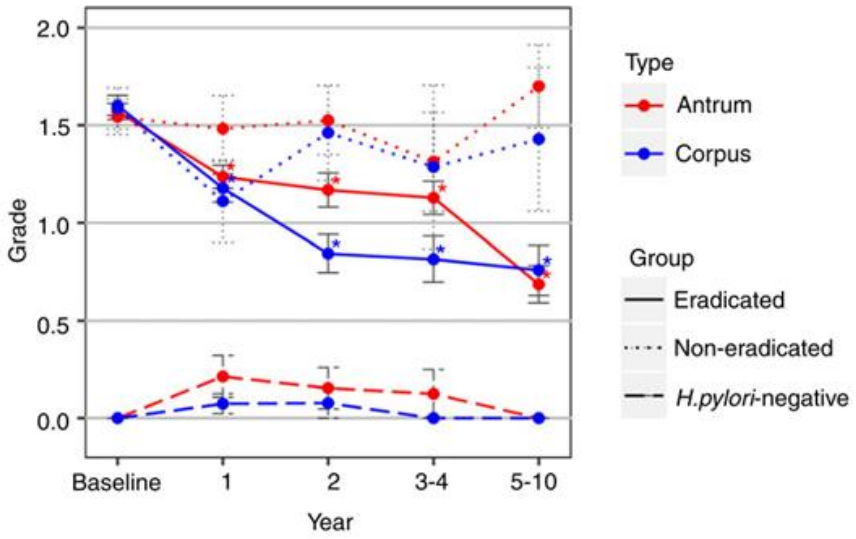


Figure 1.10 Forest plot of subgroup of studies reporting gastric cancer after H. pylori eradication treatment in patients with differing baseline histology (adapted from [124])

[a]Participants were subgrouped and analysed based on their baseline diagnoses into ≥IM (includes intestinal metaplasia and dysplasia) and <IM (includes non-atrophic gastritis and atrophic gastritis); Relative risk = RR, 95% confidence interval = 95% CI. Cochran's Q statistic and I^2 statistics used to assess heterogeneity among studies. Total participants = 6873, with 4211 participants in the ≥IM subgroup and 2662 participants in the <IM subgroup.

A)



B)

		Improvement	No improvement	P-value	OR (CI)
Antrum IM	*H. pylori*-eradicated	120 (54.3)	101 (45.7)	**0.001**	0.31 (0.15-0.62)
	H. pylori non-eradicated	12 (26.7)	33 (73.3)		
Corpus IM	*H. pylori*-eradicated	94 (66.2)	48 (33.8)	**0.001**	0.27 (0.12-0.62)
	H. pylori non-eradicated	10 (34.5)	19 (65.5)		

Figure 1.11 Figure and table showing relative improvements in patients with IM following H. pylori eradication treatment (adapted from [121])
A) Shows consecutive changes of grades for IM in the antrum and the corpus at baseline and after 1, 2, 3-4 and ≥5 years depending on *H. pylori* status and *H. pylori* eradication. Grading follows that of OLGIM (0 = none, 1 = mild, 2 = moderate, and 3 = severe) for both antrum and corpus (use of updated Sydney protocol). Grades of IM in both antrum and corpus continuously decreased from the 1-year follow up compared to those at baseline (both P <0.001 for all time periods). Grades of IM improved to levels that showed no significant difference with those of the *H. pylori*-negative group ≥3 years and ≥5 years in the corpus and the antrum respectively. B) Shows number of patients (%) with improvement and no improvement in the *H. pylori* eradicated and non-eradicated groups. Bold font style indicates statistical significance.

Overall these findings suggest that, for a subset of patients, the stage of IM represents a "point of no return", where certain epigenetic, mutational or chromosomal events or a combination of these are irreversible and ultimately lead to GC [126, 127]. Further investigation into the characteristics of IM which harbours these molecular, cellular and histological distortions is required to identify patients at higher risk of progression

1.3.2 Intestinal metaplasia subtypes

Intestinal metaplasia does not cause clinical symptoms and is usually identified in patients undergoing upper endoscopy (gastroscopy) for other reasons. IM is detected in almost a quarter of all patients undergoing upper endoscopy, its prevalence is associated with *H. pylori* infection and increases with age, IM prevalence is also higher in first degree relatives of GC patients and heavy smokers (>20 cigarettes/day) [128, 129]. IM is heterogeneous and the most widely used

histology based and clinically useful classification was developed by Jass and Filipe [130]. Complete IM resembles the small intestine epithelium with goblet cells, Paneth cells, enterocytes and a brush border (Figure 1.12). It is associated with the loss of gastric mucin markers (MUC1, MUC5AC, MUC6) and the gain of the intestinal mucin MUC2 [131-133]. Complete IM is also described as Type I IM, with cells expressing sialomucins. Incomplete IM more closely resembles colonic epithelium with goblet cells, enterocytes and irregular sized mucin droplets but no Paneth cells nor a brush border. It is associated with maintenance of gastric mucin markers MUC1, MUC5AC and MUC6 together with the gain of the intestinal mucin MUC2 [131-133]. Incomplete IM is further subdivided into Type II IM, with cells expressing a mixture of neutral mucins and intestinal sialomucins and Type III IM, with cells expressing sulfomucins.

In practice histological classification between complete and incomplete IM is often not mutually exclusive, with biopsy tissue containing features of both subtypes (mixed IM) [134, 135]. Also the differing patterns of mucin expression supports the hypothesis that IM subtypes are likely the result of two alternative pathways instead of a single pathway based on successive steps of phenotypic modification of the gastric mucosa [131, 136].

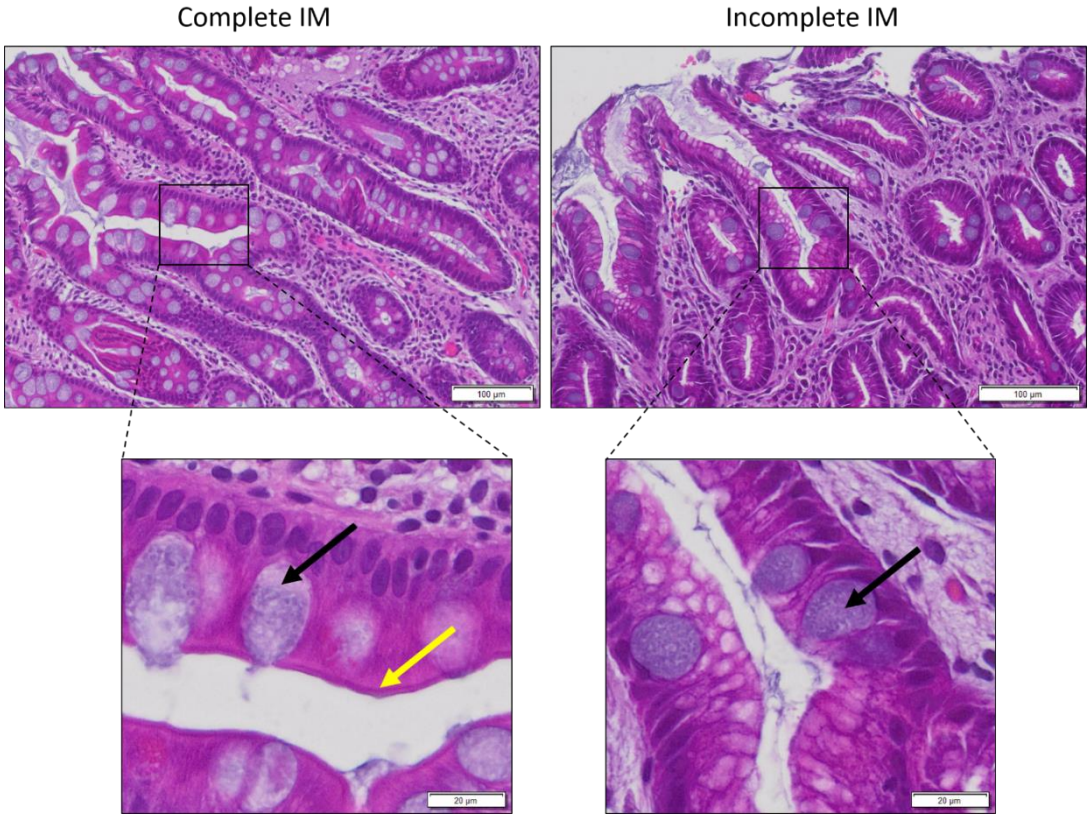


Figure 1.12 Examples of complete and incomplete intestinal metaplasia (IM)
Images of in-house H&E stained sections from gastroscopy biopsies showing complete IM and incomplete IM. Both IM subtypes have goblet cells (black arrows) but only complete IM has a brush border (yellow arrow). Scale bars: 100µm (top images) and 20µm (bottom images).

Clinically, incomplete IM has been shown to be associated with a greater risk of progression to GC in comparison to complete IM [89, 91, 94, 137, 138] thus subtyping IM has clearly potential value for patient stratification. In a Portuguese cohort, patients with incomplete IM had more than four times greater risk of progressing to dysplasia than those with complete IM [139]. However, guidelines for including incomplete IM as a factor for patient follow up differ between countries. In the United Kingdom, the British Society of Gastroenterology did not consider incorporating histological subtyping of IM into their guidelines as "the traditional diagnosis of 'complete IM' or 'incomplete IM' is made using enzyme-histochemical staining methods that are highly dependent on the person evaluating them and thus are not reproducible" [140]. By contrast the guidelines for the "management of epithelial precancerous conditions and lesions in the stomach (MAPS II)" produced by the European Society of Gastrointestinal Endoscopy (ESGE), the European Helicobacter and Microbiota Study Group (EHMSG), the European Society of Pathology (ESP) and the Sociedade Portuguesa de Endoscopia Digestiva (SPED) did recommend endoscopic surveillance within 3 years if incomplete IM was present in a single location as part of a multifactorial consideration that included family history of GC and persistent *H. pylori* infection [141]). In the local setting specific to this study (state of Victoria, Australia) the recommended surveillance period for extensive atrophic gastritis and/or multi-focal intestinal metaplasia (IM present in both the antrum and the body) is 2 years but IM subtype is not taken into consideration (Upper gastrointestinal endoscopy categorisation guidelines for adults 2018, https://www2.health.vic.gov.au/). Understanding the cellular and molecular pathways that lead to IM could add further insight into why IM subtypes vary with regards to progression risk and how this could be applied in a clinical setting.

1.3.3 Why and how does intestinal metaplasia occur?

IM develops in the context of long-term *H. pylori* infection possibly as an adaptive and protective lesion against epithelial trauma [136, 142]. On infection, *H. pylori* adheres on gastric epithelial cells through multiple adhesins (cell surface components that facilitate bacterial adhesion) such as BabA/B, SabA, OipA, HopZ and AlpA/B and forms a type IV secretion system (T4SS) pilus-like syringe which is part of the *cag* pathogenicity island (*cag*PAI) of approximately 30 genes [143, 144]. The injection of *cag*A together with peptidoglycans and bacterial DNA via the T4SS structure has the capacity to lead to multiple host cell consequences including the degradation and inactivation of key transcription factors p53 and RUNX3 (through interaction with ASPP2 and directly with RUNX3 respectively), deregulation of PI3K-AKT, Ras-ERK and Wnt pathways (through interaction with PI3K, SHP2 and c-Met respectively) as well as disruption of cell-cell

adherens junction (through interaction with E-cadherin). *H. pylori* has also been shown to lead to DNA hypermethylation in gastric epithelial cells [145, 146].

Long term gene dysregulation together with the toxic side effects of persistent inflammation, particularly of DNA damage-causing reactive oxygen and nitrogen free species (ROS and NOS respectively) results in oxyntic atrophy and consequently an increase in gastric pH but also reduction of *H. pylori* load. This environment seems to be perfect for duodeno-gastric reflux to induce the formation of IM similarly to gastroesophageal acid reflux in Barrett's oesophagus, an intestinal metaplastic lesion associated with oesophageal adenocarcinoma [147, 148]. IM develops first in the antrum and then over a period of time in the body of the stomach [149]. A large-scale study with a total of 2283 patients showed an association of exposure to bile acids with an increased incidence in IM [150]. It is possible that IM is part of a natural mechanism that offers greater resistance to the effects of bile compared to normal gastric mucosa.

An alternative, or more likely additional mechanism, to IM formation involves the inverse regulation by *H. pylori* of two key differentiation factors: SOX2 and CDX2 [151-153]. SOX2 is involved in gastric differentiation and negatively regulates intestinal differentiation whereas CDX2 plays an important role in intestinal differentiation as well as in establishing and maintaining IM [153-156]. *H. pylori* infection of gastric epithelial cells leads to decrease of SOX2 and increase of CDX2 expression, possibly via a NF-κB dependent pathway [151, 152, 157]. Expression of SOX2 between IM subtypes differs substantially as complete IM is predominantly SOX2 negative (93%) and incomplete IM is mainly SOX2 positive (85%) [158]. Taken together with the partial gastric mucin profile of incomplete IM, this suggests that the incomplete subtype is best described by a hybrid intestinal metaplastic phenotype, part colonic - part gastric.

1.3.4 Risk factors in intestinal metaplasia

In a study on IM genomic and epigenomic profiling, Huang et al 2018 showed shortened telomeres and chromosomal alterations, particularly gain of chromosome arm 8q, were associated with progression to dysplasia and GC [127]. FBXW7 mutations in a small fractions of gastric/IM patients (4.7%) were also shown to be a candidate for progression. The FBXW7 gene product is responsible for MYC degradation, whose gene is found on 8q and is strongly linked with GC [42, 159-162]. Interestingly, IM samples with the lowest levels of DNA methylation and mutation burden were linked with regression. Overall the Huang study did not report IM subtype, thus it was not possible to directly assess whether the increased risk of progression associated with incomplete IM is due to increased epi-/genomic instability.

The presence of genetic instability in IM has been investigated in several other studies by addressing microsatellite stability. Overall, IM was characterised by low level MSI (MSI-L) in 16%-39% cases and high level MSI (MSI-H) in 0%-9% cases [163-167]. IM patients with and without GC showed a similar percentage of MSI-L suggesting that MSI occurs at an early stage of IM development and in GC patients microsatellites had a higher frequency of alterations in IM coexisting with tumours that showed MSI [165]. In a single study where IM subtype was reported together with microsatellite status, only incomplete IM was positive for MSI (MSI-L in 4 out of six cases with incomplete IM and 0 out of 9 cases with complete IM) [163].

Thus far the following IM risk factors associated with progression to GC have been discussed: the extent and topography of IM including single and multifocal IM (OLGIM), family history of GC, histological subtype (complete and incomplete), alterations in chromosomal copy number, FBWX7 mutations, shortened telomere length and possibly levels of microsatellite instability. However other risk factors have also been shown to be associated with progression, including extensive IM in the corpus alone [94], IM located at the Maggenstrasse (a narrow area along the entire lesser curvature believed to represent the canal through which food passes from the oesophagus to the intestine along the lesser curve, Figure 1.8, [134]) but also precancerous gastric mucosal changes in first degree relatives [168] and ancestry, particularly East Asian as shown in a large US population study (as described in [169] with 810 821 unique participants).

1.3.5 Spasmolytic peptide expressing metaplasia

An alternative metaplastic lesion which has been associated with GC, but is not part of the Correa model, is known as spasmolytic peptide expressing metaplasia (SPEM) [134, 170, 171]. SPEM is only identified in the body of the stomach, in glands that stain positive for TFF2 [172, 173]. TFF2 is said to be normally expressed in antral and Brunner's glands (in the duodenum) but not normally at the base of body glands (reviewed in [174]). SPEM is believed to be a regenerative type of lesion and multiple studies in mice suggest it originates from the trans-differentiation of mature chief cells following the loss of parietal cells in the context of chronic inflammatory injury [175-178]. Alternatively SPEM may arise from Mist1+ stem cells located at the isthmus of the gastric gland [179, 180]. However the significance of SPEM in the sequence of human gastric carcinogenesis remains to be elucidated. Either as a concurrent or even as a precursor lesion to IM, it is not clear how SPEM contributes to progression risk in patients.

1.4 The role of the immune system in gastric carcinogenesis

The importance of long-term inflammation in the process of gastric carcinogenesis cannot be underestimated. Without chronic inflammation and the accompanying genetic/epigenetic

mutations that occur likely in the stem cell compartment of gastric and/or IM glands, GC would likely not develop [181]. Multiple studies have shown an association between single nucleotide polymorphisms (SNPs) in cytokine genes and GC risk as well as with gastric premalignant lesions [182-185]. SNPs are believed to be responsible for variations in cytokine expression and may have an effect on specific immune responses thus also influencing a patient's susceptibility to *H. pylori* infection and the development of GC. Generally cytokines are divided into pro-inflammatory and anti-inflammatory groups or belonging to both. Pro-inflammatory cytokines include IL1β, IL1α, IL6, IL8, IL12, IL17, IL18, TNFα and IFNγ whereas anti-inflammatory cytokines include IL4, IL10 and IL13 but some seem to have a dual character: IL10, IL22, and TGFβ1 [186-188]. Cytokines act both locally and systemically to initiate, maintain and then resolve an inflammatory response through the antagonistic role of members belonging to these groups. Dysregulation of this natural cycle can lead to autoimmune disease, chronic infection and inflammation as well as cancer [189, 190].

SNP association with GC has been shown for IFNγ, TNFα (only in a Chinese population), IL1β, IL1RN (also with IM), IL2, IL4, IL6, IL8 (also with AG and IM), IL10, IL17, IL18, IL22 (also with AG, IM and dysplasia) and IL32 [182-185]. Thus the host's immune response to *H. pylori* infection is highly critical in the development of acute and chronic gastritis and most likely plays a key role in progressive premalignant lesions that result in GC.

1.4.1 The innate immune system in gastric premalignant lesions

The immune system can be broadly divided into two categories, the innate and the adaptive. The innate immune system is involved in the immediate response to pathogen and tends to be activated by chemical properties of the pathogen. By contrast the adaptive immune system is characterised by an antigen specific response, occurs over time after first exposure to antigen and has both "memory" and "effector" aspects. Multiple immune cell types make up the innate immune system including neutrophils, macrophages, dendritic cells, basophils, mast cells, eosinophils and natural killer (NK) cells.

On infection of gastric tissues with *H. pylori*, there is a transient infiltration of neutrophils and macrophages within the first 2 days [191]. By day 10, neutrophil and macrophage numbers return back to baseline levels. However after 3 weeks of infection, an adaptive immune response is detected with increased local tissue infiltration of T cells, neutrophils and macrophages as well as increased numbers of T cells, macrophages and dendritic cells in the para-gastric lymph nodes [191]. The immune response is "initiated" by infected gastric epithelial cells which release multiple "danger signals" including interleukin 8 (IL8 or CXCL8) a powerful chemoattractant for

neutrophils [192]. Neutrophils enter the gastric tissues and can cross the epithelium to infiltrate the glandular lumen (both of gastric and IM glands). If infection is not resolved, their presence persists long term both in premalignant and GC lesions as up to 9 times more neutrophils were found in IM and 24 times more in GC compared to normal tissue [193].

Using the classic M1/M2 bipolar paradigm, macrophages are typically subdivided into "pro-inflammatory" (M1) macrophages with particular importance at the beginning of an acute response to pathogen invasion (just after neutrophils) and "tissue repair/wound healing" (M2) macrophages which become more abundant in tissues towards the end of an immune response [194]. Generally, in the context of cancer, M1 macrophages are thought to promote a Th1 T cell environment (IFNγ/IL12 high and IL10 low) and have tumour-cell killing activity whereas M2 macrophages are believed to promote a Th2 T cell environment (IL4/IL13 high and IL10 high) and have tumour-promoting properties [195, 196]. Recent studies into macrophage phenotype plasticity suggest that the M1/M2 paradigm is likely an over-simplification of a more complex reality (as discussed in [197], [198]).

During *H. pylori* infection of the gastric epithelium, macrophages are recruited to the site under attack and release multiple pro-inflammatory cytokines and chemokines [192, 199-201]. Together with neutrophils and dendritic cells, macrophages are vulnerable themselves to invasion by *H. pylori* which results in an altered cytokine secretion profile followed by apoptosis and bacterial release [202, 203]. Macrophages have been associated with severity of gastric immunopathology during *H. pylori* infection [204], their presence persists well into the chronic stage of inflammation and is characterised by mixed M1/M2 polarisation [202, 205, 206]. Interestingly AG was shown to be enriched in M1 macrophages whereas IM was shown to be enriched in M2 macrophages in another study using a single M2 marker (CD163) [205, 207].

Other innate immune cells such as dendritic cells have been shown to play an important role in the response against *H. pylori* infection by influencing the type of downstream polarised T cell immunity that develops (Th1 vs Th2 vs Th17) [208]. Prolonged exposure to antigen leading to dendritic cell exhaustion has also been suggested as a mechanism that contributes to the long term duration of gastritis [209]. Significant infiltration of basophils, eosinophils and mast cells in gastric tissues following *H. pylori* infection has also been reported but their possible role in acute and then chronic gastritis remains to be elucidated [210-215].

NK cells in *H. pylori* infected individuals exhibit higher levels of TNFα and IFNγ production, possibly driving the initial T cell response towards a Th1 phenotype together with dendritic cells

[216, 217], although their cytotoxic ability may be compromised [218, 219]. NK cell infiltration of intra-tumoural GC tissue was shown to be associated with reduced numbers and decreased cytotoxicity suggesting that this innate immune cell type plays a vital role in protection against carcinogenesis and in GC progression [220-222].

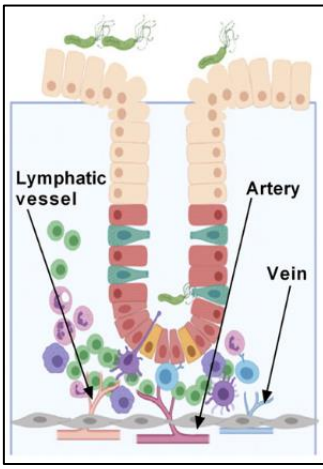
Overall the innate immune system responds quickly and aggressively upon *H. pylori* infection and continues to be relevant long term if resolution does not occur. It seems to play a critical role in setting up the phenotype of the ensuing adaptive immune response and to have both pro- and anti-carcinogenic aspects depending on context.

1.4.2 The adaptive immune system in gastric premalignant lesions

The adaptive immune system consists of two main cell types, T cells and B cells, each with a plethora of subsets with unique characteristics and function. T cells are lymphocytes that develop in the thymus and are unique compared to other lymphocytes in that they have a T-cell receptor (TCR) on the surface of the cell. All T cells express CD3 (cluster of differentiation 3) which is composed of the CD3γ, CD3δ and CD3ε chains (Alarcon 2003). All together these CD3 chains associate with the TCR and a zeta chain homodimer to initiate an activation signal in T cells [223]. Once T cells ("naïve") leave the thymus, they travel through the blood to secondary lymphoid organs where they differentiate after exposure to antigen by antigen presenting cells into memory and effector cells. Memory T cells are long-term antigen-experienced T cells that can quickly expand to large numbers of effector T cells upon re-exposure to the same antigen [224].

T cells play a crucial role in the response to *H. pylori* infection. CD4+ T cells including both helper T cells and regulatory T cells (Tregs) are the predominant infiltrate following infection (Figure 1.13) and likely drive gastritis through epithelial cell damage, as immunosuppressed (T cell deficient) RAG and SCID mice do not develop a response to *H. pylori* [188, 225-227]. The helper T cell response consists mainly of Th1 and Th17 cells with a smaller role for Th2 cells, strongly orchestrated by professional antigen presenting cells (macrophages, dendritic cells and B cells) through the release of various cytokines including IL1β, IL10, IL12, IL18, IL23 and TGFβ in response to *H. pylori* [188, 216, 227-230]. The wide range of cytokines produced by Th1 and Th17 cells and in particularly IFNγ and IL17 contribute to immunopathology observed during chronic gastritis. Indeed an increase in Tregs has been shown to be associated with reduced gastritis, although this may be Treg subset dependent [229, 231, 232]. Tregs seem to be able to immuno-regulate the highly inflammatory Th17 response both in adults and in children [233, 234]. Although the role of Th2 cells in *H. pylori* infection remains controversial, there is some

evidence to suggest gastritis-associated immunopathology is the result of an unbalanced Th1/Th2 response [235] that is Th1 weighted.



CD4+ Subset	Cytokines Produced	Epithelial Cell Response
Th1 Lymphocytes	IFNγ	• Activation of chemokines • Activates apoptosis
Th2 Lymphocytes	IL4, IL5, IL13	• Regulation of somatostatin • Potential impact on transdifferentiation
Th17 Lymphocytes	IL17a, IL17f, IL21, IL22	• Activation of antimicrobials • Induction of IL-8 • Impact on tissue remodeling
Treg Lymphocytes	IL10, TGFβ	• Antagonizes IFNγ • Impact on wound healing • Impact on tumorigenesis

Figure 1.13 Schematic and tabular representation of CD4+ T cell function including regulatory T cells (Tregs) following *Helicobacter pylori* infection (adapted from [188])
Helicobacter pylori represented by green spiral shape with flagella on the surface and within the gastric glands, CD4+ cells represented by green cells, B cells represented by blue cells, dendritic cells and macrophages represented by purple cells and neutrophils represented by pink cells. Different CD4+ T cells produce different types of cytokines which leads to various responses by gastric epithelial cells.

Only a limited number of studies have focussed on characterising more advanced premalignant lesions such as AG and IM. In one study, reduced numbers of CD4+ and FOXP3+ cells were observed in IM compared to gastritis suggesting lower levels of inflammation but also reduced immune-regulation in IM [236]. By contrast another study showed an association between high levels of IFNγ and IL12 with a higher degree of gastric inflammation and neutrophil activity but also the presence of IM [237]. In early premalignant lesions, CD8+ T cells were associated with severity of gastritis, however histological progression from chronic gastritis to atrophic gastritis to low grade then to high grade dysplasia and finally to GC was shown to be associated with a stepwise reduction of CD8+ cells [238, 239]. Interestingly the same study showed an inverse stepwise increase of negative costimulatory molecules PDL1, B7-H3 and B7-H4 on immune cells in the same tissues suggesting a possible role for checkpoint immune-regulation on CD8+ T cells in the process of gastric carcinogenesis [239]. A separate study investigating the relationship between CD8+ cells, FOXP3+ cells and PDL1 expression in gastric disease including normal gastric tissue and normal gastric tissue adjacent to tumour showed a highly significant decrease in both CD8+/FOXP3+ and CD8+/PDL1+ ratios between GC and normal adjacent tissues but only a decrease in CD8+/PDL1+ ratio compared to normal gastric tissue [240].

B cells have a wide range of immune functions from producing antibodies, modulating immune responses through cytokine secretion and presenting antigen [241]. They are characterised by

their remarkable ability to produce immunoglobulins/antibodies that remain on their cell surface or are secreted with an almost infinite type of antigen specificities aided through somatic hypermutation. B cell development begins in the foetal liver and continues in the bone marrow throughout adult life. Upon activation, B cells differentiate into plasmablasts, short lived proliferating and antibody secreting cells, then or concurrently into plasma cells, long lived non-proliferating antibody secreting cells. Memory B cells also rise from differentiation and circulate through the body, ready for a rapid antibody response if a previously detected antigen is recognised. Finally the isotype of secreted and/or membrane-bound immunoglobulins (IgA, IgD, IgE, IgG and IgM) plays a key role with regards to tissue location and B cell state. IgA is typically found in mucosal areas such as the gut and the respiratory tract, IgD is mainly found on antigen-unexperienced B cells but can also activate basophils and mast cells, IgE binds to allergen and induces histamine release from basophils and mast cells important in allergies and parasite response, IgG mainly provides antibody-based immunity against invading pathogens and IgM expressed both on the surface of B cells and in soluble form helps eliminate pathogens early on in an infection.

In gastric tissues, *H. pylori* infection leads to the formation of tertiary lymphoid structures rich in T cells and B cells in the *lamina propria* and their presence has been recently associated with tumourigenesis in a mouse model of GC [242]. An increase of IgA and IgG was initially described in gastritis, particularly in atrophic gastritis followed by a decrease in intestinal metaplastic tissue [243, 244]. *H. pylori* phagocytosis and killing by polymorphonuclear leukocytes (neutrophils, eosinophils and basophils) through IgG binding has also been described [245]. Additionally *H. pylori* infection is highly associated with mucosa-associated lymphoid tissue (MALT) B cell lymphoma. Although concurrent neoplasms of gastric lymphoma and carcinoma (GC) have been reported, the role of B cells in the development of GC is less well understood [246].

A key role for subverted CD4+ T cell helper function has been suggested in the inefficiency of B cell associated immunity to eliminate *H. pylori* and both T cells and B cells have been shown to be involved in the development of autoimmune gastritis, a response to self-antigens on parietal and chief cells with increased risk of GC progression [247]. Although most intracellular bacteria activate a Th1 response and extracellular bacteria a Th2 response, *H. pylori* which is mainly extracellular is able to induce a Th1/Th17 response resulting in a suboptimal B cell antibody (humoral) response with a consequent failure of the immune system to clear the infection.

Overall the adaptive immune system seems to be negatively influenced by *H. pylori* leading to persistent inflammation that includes a marked innate immunity aspect. This encourages a long term environment high in ROS and NOS which results in increased DNA damage and leads to gastric cancer. Thus it is crucial to gain further insight in the role of the immune microenvironment as a potential risk factor in progression.

1.4.3 Gastric cancer and the immune system

To better understand the possible role of the immune system in gastric carcinogenesis, it is useful to look at its overall role in cancer development and progression. Tumour promoting inflammation and avoiding immune destruction are two of the four "emerging hallmarks" of cancer [248, 249]. Thus for a neoplastic tumour to grow and invade tissues, it needs to first avoid attack and elimination by immune cells and then harness the immune system's capability to remodel its microenvironment to support tumour survival and progression ([250], Figure 1.14). So far, the role of the immune system in GC patients' prognostic outcome has been investigated in multiple studies [198, 251-258].

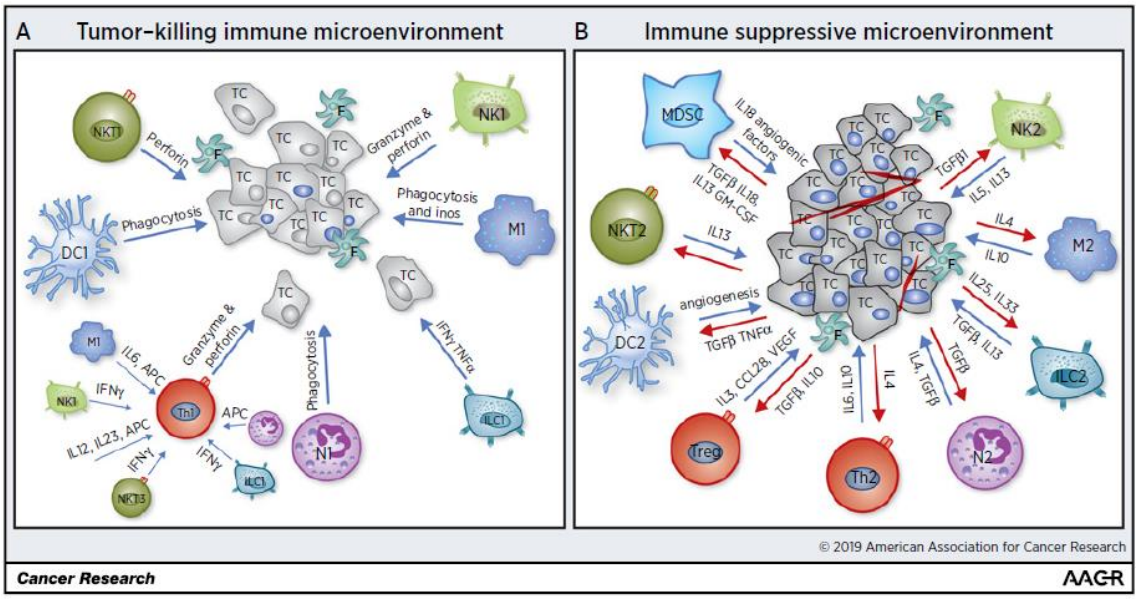


Figure 1.14 Cross-talk communication between tumour cells and immune cells (adapted from [250])

Different immune cell subsets are associated with either tumour-killing (A) or tumour-promoting activities (B), dependent on tumour type context. TC: tumour cells. In (A) NK1: Natural Killer cells type 1, M1: M1 macrophages ("classically activated"), ILC1: Innate Lymphoid Cell group 1, N1: N1 neutrophils; Th1: Helper T cells type 1, NKT1 and NKT3: Natural Killer T cells type 1 and type 3, APC: Antigen Presenting Cell, DC1: Dendritic cell type 1. In (B) NK2: Natural Killer cells type 2, M2: M2 macrophages ("alternatively activated"), ILC1: Innate Lymphoid Cell group 2, N2: N2 neutrophils; Th2: Helper T cells type 2, Treg: regulatory T cells, DC2: Dendritic cell type 2, NKT2: Natural Killer T cells type 2, MDSC: Myeloid-derived suppressor cells.

Tumour-associated macrophages (TAMs) have been shown to be one of the most abundant immune cells in the tumour microenvironment and to be associated with multiple tumour-promoting activities ([196], Figure 1.15). In GC there have been conflicting evidence on the pro- and anti- cancerous influence of TAMs in the tumour microenvironment. In Busuttil et al 2014 [259], a macrophage signature was associated with poor prognosis but in another study increased macrophage infiltration in the cancer cell nest had a beneficial impact on 5 year disease-free survival rate after curative resection [260] and a possible role for TAM distribution between cancer nest, invasive front and stroma has been suggested [261]. In a recent study by Huang et al [198], TAMs in GC were characterised both quantitatively and spatially and shown to consist of a highly heterogeneous population with up to seven predominant subsets.

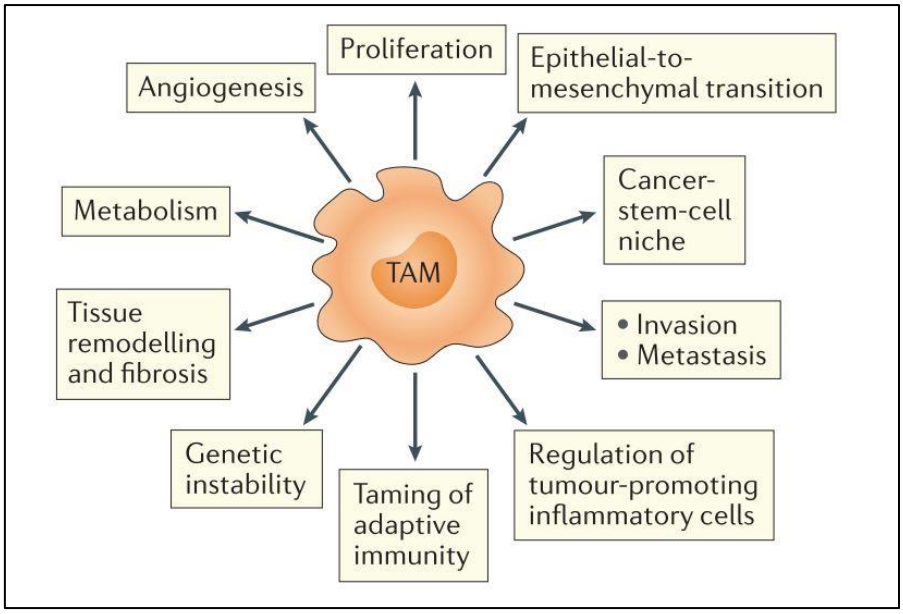


Figure 1.15 Diagram showing multiple roles of tumour-associated macrophages (TAMs) in supporting tumour cell biology (adapted from [196])

Tumour-infiltrating T cells (TILs) are another abundant immune cell type in the tumour micro-environment. Tumour cells express antigens and thus can become targets of T cell-mediated adaptive immunity. Experiments in mice showed that cytotoxic T cells (CD8+) could prevent tumour development and inhibit tumour progression ([262], summarised in [263]). More recent studies in humans have shown a positive association between cytotoxic T cells and improved patient survival across multiple cancer types including GC [264-267].

The role of Tregs, another type of TIL, has been shown to be associated with mixed outcomes in different cancer types [268-270]. Tregs are thought of suppressing anti-tumour cytotoxicity and thus promoting tumour survival [271]. Several studies have shown a negative association with

patient survival including GC patients but others have suggested that at least in a subgroup of patients, high Treg density may be beneficial [258, 269, 272].

Overall studies on the immune system in GC have produced valuable data with regards to the interaction between immune cells and tumour cells, as well as utility for patient prognosis and treatment. However they have provided only limited insight in its possible role in the process of gastric carcinogenesis. Investigating the immune microenvironment in gastric premalignant lesions could lead to improved patient stratification and possibly even help develop treatments that prevent the occurrence of this disease altogether.

1.5 Biomarkers of gastric carcinogenesis

In addition to furthering our understanding of the immune mechanisms involved in the process of gastric carcinogenesis, it is vital that reliable and accurate biomarkers are developed that will allow patient stratification based on personalised risk of progression. Such patient stratification is required to deliver targeted surveillance of patients at an increased risk of developing high grade dysplasia and/or EGC. The removal of neoplastic lesions and/or early malignant lesions using tools such as EMR and ESD will result in improved quality of life of patients and greatly reduce the costs associated with GC treatment, since the cost of an ESD to remove local HGD is less than 50% of that associated with a partial/total gastrectomy [273].

1.5.1 Serum biomarkers

So far in this chapter multiple factors have been discussed which are associated with an increased risk of progression including age, gender, family history, smoking, alcohol, diet and other lifestyle choices as well as histological, topograpical and molecular characteristics of IM. All of these can and should be used for assessing a patient's risk of progressing to GC. Additionally, pepsinogen levels have been shown to have potential utility in a clinical setting for patients with either AG or IM [274, 275]. Pepsinogens are proenzymes for pepsin with type I (PGI) secreted by chief and mucous neck cells in fundic glands, and type II (PGII) secreted by pyloric and Brunner's glands (duodenum). Increasing severity of chronic gastritis results in increasing serum levels of PGI and PGII but AG results in reduction of PGI. Thus the PGI/PGII ratio changes significantly. More severe AG and IM leads to a greater reduction of this ratio. Although shown to be reliable, the PGI/II test can only be used as an addition to gastroscopy tissue diagnosis but not a replacement as it does not provide any histological information.

Serum biomarkers for GC used in a clinical setting include carcinoembryonic antigens CEA, CA19-9 and CA72-4 but they lack the sensitivity and specificity necessary for reliable EGC diagnosis

[276-278]. Therefore it is crucial to identify additional risk biomarkers that are associated with premalignant lesions that can reliably guide a clinician's decision for surveillance on a patient by patient basis.

1.5.2 Tissue biomarkers based on intestinal metaplasia

Several studies have tried to identify markers in IM that are associated with greater progression risk but none have translated into clinical utility. Intestinal metaplastic biomarkers reported to be associated with progression include Schlafen 5 (SLFN5) and aquaporin 3 (AQP3) [279-281]. SLFN5 expression was inducible by IFNα and localised mainly in T cells in gastric mucosa with IM [279]. When compared to patients that did not progress to GC, IM in patients that progressed had significantly higher levels of SLFN5 ($p<0.0001$) and logistic regression analysis showed that stromal SLFN5 score was a significant risk factor for progression to GC (OR=18.1, 95% CI=4.14-79.1, p=0.0001). AQP3 was expressed in goblet cells of IM and was significantly associated with severity of IM in GC tissues [280]. A further study showed an association between AQP3 and incomplete IM (type III) [281]. A candidate cancer stem cell marker CD24 was also shown to be positively correlated with severity of IM and incomplete IM (Type II) [281, 282].

A fundamental absence in the Australian and in the UK recommendation guidelines is a patient surveillance strategy according to IM subtype, although this is clearly associated with differing risk of progression. Currently most pathologists in Australia do not report on the subtype of IM in biopsy sections. However if highly sensitive and specific biomarker tests were developed for IM subtypes, they could be added to the above guidelines leading to better risk management of IM patients overall.

1.6. Models of gastric carcinogenesis

To elucidate the fundamental mechanisms that lead to GC it is vital to have a truly representative model to test possible molecular and cellular hypotheses. Such carcinogenesis models are necessary universally for all cancer types to allow greater insight into the early steps of malignancy. This knowledge can then be applied in human patients to identify those at high risk of progression.

1.6.1 Animal models of gastric cancer

It is clear that GC develops in a microenvironment with continuous chronic inflammation triggered by *H. pylori* infection, as well as other environmental factors [42, 283-285]. Initiation and progression involves multiple steps and although several mouse models have been

developed, none have managed to fully recapitulate all of the human premalignant lesions described by the Correa model leading to the intestinal or the diffuse histological subtype of GC.

GC animal models can be broadly classified into three main types, chemically induced, infectious and genetic models, often combined to study different aspects of GC [286-289]. Both MNNG (*N*-methyl-*N*-nitro-*N*-nitrosoguanidine) and MNU (*N*-methyl-*N*-nitrosourea) are carcinogens used to create cancer models with a single dose of either enough to induce GC in rodents [286, 287, 290]. Combined models with various *H. pylori* strains have been used to study the role of *H. pylori* in carcinogenesis, both in Mongolian gerbils and mice (reviewed in [291], Table 1.3).

Table 1.3 Combined use of chemical carcinogen and *H. pylori* to induce gastric cancer in rodent models (adapted from [291])

***H. pylori* strain**	**Observation time**	**Rodent species**	**Chemical carcinogen**	**Implications**	**Refs**
H. pylori ATCC 43504	50 wks	Mongolian gerbils	MNNG[1]	MNNG promotes GC formation in a concentration-dependent manner. *H pylori* enhances the GC risk of gerbils treated with MNNG.	[292]
H. pylori SS1	54 wks	C57BL/6 mice	MNU[2]	The incidences of polypoid lesions, differentiated adenocarcinomas, and adenomatous hyperplasias in MUN-alone group were higher than in MNU + *H. pylori* group.	[293]
H. pylori ATCC 43504	50 wks	Mongolian gerbils	MNU/ MNNG	*H. pylori* promotes GC formation in gerbils treated with MNNG or MNU. Both MNNG and MNU promote gastric carcinogenesis in *H. pylori*-infected gerbils in a concentration-dependent manner.	[294]
H. pylori SS1	50 wks	C57BL/6 mice	MNU	*H. pylori* greatly increases the GC incidence of mice treated with MNU.	[295]
H. pylori SS1	24 wks	C57BL/6	MNNG	GC was developed at 6 months.	[296]

[1]MNNG (N-methyl-N-nitro-N-nitrosoguanidine); [2]MNU (N-methyl-N-nitrosourea)

Genetic models have focussed on investigating the role of a single or a small number of genes previously shown to be associated with GC including gastrin (ACT-GAS, $Gas^{-/-}$ and INS-GAS), CDH1 ($Cdh1^{+/-}$ + MNU), KRAS (K19:Kras-(V12D), LGR5 in combination with APC ($Lgr5^{CreERT2}$; APC^{Floxed}), SMAD4 ($Smad4^{+/-}$) and TFF1 ($Tff1^{-/-}$) (as reviewed in [288, 289], Table 1.4). The role of inflammation in GC has been particularly studied using the $gp130^{F/F}$ mouse model in which tumorigenesis is dependent on hyperactive STAT3 signalling through the common IL-6 family signalling receptor gp130 [297]. This model was recently used to identify an association between a chemokine gene signature linked with tertiary lymphoid structures in $gp130^{F/F}$ mice and advanced GC in human patients [242]. The role of inflammation has also been investigated using the $Nfkb1^{-/-}$ mouse model which develops intestinal type GC within 18 months [298].

Mongolian gerbils have been used in the study of gastric carcinogenesis as they have the added advantage of being readily infected by *H. pylori*. Infection of Mongolian gerbils lead to severe gastritis and intestinal metaplastic-like lesions after 26 weeks and the development of adenocarcinoma in over 33% of animals after 62 weeks [299]. However these findings were not

reproducible by another group who observed severe gastric inflammation but an absence of adenocarcinomas in long term *H. pylori*-infected Mongolian gerbils (up to 18 months) [300].

Table 1.4 A summary of key genetic mouse models used to study gastric cancer (adapted from [289])

Model	Onset	Incidence (%)	Location	Type	Inv.	Met.	Reference
ACT-GAS	20 mths	100	Body	WD	-	-	[301]
CA-AhR	12 mths	100	Body	WD	+	+	[302]
CEA-SV40	7 wks	100	Antrum	WD	+	-	[303]
AV4b-Cre; $Cdh1^{loxP/loxP}$; $p53^{loxP/loxP}$	12 mths	100	Body	PD	+	+	[304]
$Cdh1^{+/-}$ + MNU	10 mths	46	Antrum	PD	-	-	[305]
H/K-ATPase:Cdx2	3 mths	100	Body	WD	+	-	[306]
$Gas^{-/-}$	12 mths	60	Antrum	WD	-	-	[307]
GB-Cre; $Smad4^{Floxed}$	18 mths	100	Antrum	WD	-	-	[308]
$Gp130^{F/F}$	3 mths	100	Body/Antrum	WD	-	-	[297]
INS-GAS	20 mths	75	Body	WD	+	-	[309]
K19:Kras-(V12D)	16 mths	38	Body	WD	+	-	[310]
H/K-ATPase:1L1ß	18 mths	30	Antrum	WD	-	-	[284]
$Runx3^{-/-}$ + MNU	1 yr	60	Body/Antrum	WD	-	-	[311]
$Lgr5^{CreERT2}$; APC^{Floxed}	3 wks	100	Antrum	WD	-	-	[312]
MMTV-Ad12	4 mths	56	SCJ	WD	+	+	[313]
$Mth1^{-/-}$	18 mths	13	Antrum	WD	-	-	[314]
$Smad3^{-/-}$	10 mths	100	SCJ	WD	+	-	[315]
$Smad4^{+/-}$	18 mths	100	Body/Antrum	WD	+	-	[316]
$Tff1^{-/-}$	5 mths	30	Antrum	WD	+	-	[317]
K19-Wnt1:C2mE	5 mths	100	SCJ	WD	+	-	[318]
Villin-Cre; $KLF4^{Floxed}$	20 mths	29	Antrum	WD	-	-	[319]

SJC: squamocolumnar junction (mouse equivalent of gastro-oesophageal junction), WD: well differentiated, PD: poorly differentiated, Inv.: invasion, Met.: metastasis, +: present, -: absent,

1.6.2 Animal models of gastric precancerous lesions

Several animal models of gastric premalignant lesions have been developed (summarised in [176, 320], Table 1.5) and in particular the Cdx1 and Cdx2 transgenic models have managed to recapitulate human IM histologically [154, 306, 321, 322]. Both CDX1 and CDX2 are normally expressed in epithelial cells of the small intestine and the colon, but both are also expressed in IM [323-325]. Using transgenic mice (TG) the differing roles of Cdx1 and Cdx2 expression in the gastric mucosa were evaluated with the help of the H+/K+-ATPase β subunit gene promoter, a gene normally expressed in parietal cells. In the Cdx1 TG mice, normal parietal cells were fully replaced by IM within 120 days but no Cdx2 expression was detected. Overall IM glands stained blue with Alcian blue and black with high-iron diamine Alcian-blue (pH 2.5) confirming the presence of sulphomucins. They were positive for markers of goblet cells (Tff3), enterocytes (villin and sucrose-isomaltase, SI), enteroendocrine cells (secretin/serotonin) and Paneth cells (lysozyme) suggesting a mixed IM subtype. Cdx2 TG mice were characterised by the absence of Cdx1 expression and the lack of Paneth cells. In addition to IM, these mice also showed pseudopyloric gland metaplasia (antral type glands in the body of the stomach) [326]. After 100 weeks, all Cdx2 TG mice had developed gastric polyps, histopathologically similar to invasive gastric adenocarcinoma suggesting that gastric carcinogenesis in mice is a direct consequence of ectopic Cdx2 expression [306]. In the majority of mice, mutations were detected in the Apc

and p53 genes, both genes believed to play a key role in the process of human gastric carcinogenesis.

Table 1.5 Mouse models of gastric premalignant lesions (adapted from [320])

Model	Duration	Phenotype	Refs
GAS$^{-/-}$	4-5 mths	atrophy, metaplasia, dysplasia[1]	[327]
INS-GAS	20 mths	atrophy, metaplasia, dysplasia	[328]
H/K-ATPase-α$^{-/-}$	10 wks	atrophy, metaplasia, dysplasia	[329, 330]
H/K-ATPase-β$^{-/-}$	17 wks	atrophy	[331-333]
H/K-ATPase/DT	28-80 days	atrophy	[334]
Waved-2+DMP-777	1 wk	SPEM	[335]
Car9$^{-/-}$	4 wks	atrophy	[336]
CCK2R$^{-/-}$	18 wks	atrophy	[337, 338]
NHE2$^{-/-}$	17 days	atrophy	[339]
K-ras	1-4 mths	atrophy, metaplasia, dysplasia	[310, 340, 341]
IL-1β transgenic	12 mths	atrophy, metaplasia, dysplasia	[284, 342]
Cdx1 transgenic	120 days	IM	[322]
Cdx2 transgenic	12 wks	IM	[154, 306, 321, 322]
MNU	9 wks	atrophy, IM, dysplasia	[295, 343, 344]
MNU + *H. pylori*	12 mths	atrophy, metaplasia, dysplasia	[327]
DMP-777	7-14 days	atrophy, SPEM	[175, 345]
L-635	3-7 days	atrophy, SPEM	[175, 207]

[1]susceptible to MNU

The cellular and molecular aspects of metaplasia have been studied extensively using animal models of SPEM (Table 1.5, summarised in [176, 320]). Oral administration of the parietal cell specific protonophore drug DMP-777 leads to loss of parietal cells within 3 days followed by the appearance of SPEM if treatment is continued for 10-14 days [175]. This type of SPEM is reversible, occurs in a non-inflammatory environment and even long term drug administration (up to 2 years) does not lead to dysplasia or GC in mice or rats further confirming the vital role of inflammatory processes involved in gastric carcinogenesis. Oral administration of the L635 protonophore drug leads to loss of parietal cells and appearance of SPEM within 3 days in a highly inflammatory environment [175]. Interestingly M2 macrophages have been shown to drive SPEM formation in this model [207].

SPEM can also be induced in mice through infection with *Helicobacter felis*, commonly used in mouse models of gastric carcinogenesis instead of *H. pylori* which infects mice with difficulty [346]. In *H. felis*-infected mice, SPEM developed over a period of several weeks in the presence of inflammation (lymphocytes and neutrophils) which may be naturally more similar to *H. pylori*-induced human SPEM [172]. Interestingly *H. felis*, one of several non-pylori Helicobacter species that infect the human stomach [347], is estimated to be present in the stomach of approximately 9% of the human population [348].

H. pylori-infected Mongolian gerbils were shown to develop SPEM (20 weeks post-infection), which was followed by the formation of intestinal metaplasia (41 weeks post-infection) [349]. Although SPEM animal models have proven to be useful in gaining greater understanding of the

process of metaplasia, it remains to be validated how this knowledge can be used in the study of human IM and its role in gastric carcinogenesis.

1.6.3 The lack of cell lines to model gastric carcinogenesis

Two dimensional (2D) immortalised cell lines have been previously established and characterised from GC tumours [350-352] including the AGS, MKN28 and MKN45 cell lines which were recently used within our lab group [353] to develop an orthotopic mouse model. Up to four cell lines (CP-52731, CP-94251, CP-18821, and KR-42421) have also been developed from Barrett's epithelium (both of metaplastic and dysplastic origin) and used to study ploidy abnormalities and the role of telomerase [354, 355]. However so far 2D cell lines for IM have not been developed, possibly because 2D culture conditions generally do not support growth of untransformed non-neoplastic cells. Although attempts were made by Chen et al 2017 [356] to revert the MKN45 cell line (derived from a poorly differentiated carcinoma; [357]) to an intestinal metaplasia cell line by transfecting with p65 and p50 (NF-κB) eukaryotic plasmid constructs this was not a bona fide IM model and is unsuitable for use to study the process of gastric carcinogenesis.

1.6.4 Organoid models in carcinogenesis

While animal cancer models are useful, there is an ethical tendency to avoid use of animals as models of disease. Also they tend to have inherent biological limitations with regards to how accurately they represent the carcinogenic processes in humans as well as certain technical limitations such as cost, labour and duration of experiments [358, 359]. In an effort to reduce the use of animal models, three dimensional cell culture models called organoids have gained considerable popularity in the last decade. Organoids mimic tissue architecture of the organ of origin, are relatively easy to manipulate and have long-term growth capacity but are often poorly validated as models with reproducibility being a major issue in current organoid systems ([360-363], Figure 1.16).

Gastrointestinal organoids from normal tissue were first described by Sato et al 2009 (small intestine) [364] and Barker et al 2010 (gastric) [312] grown from single Lgr5+ stem cells in mice. Since then protocols for the establishment and maintenance of both normal and tumour human gastrointestinal organoids have been optimised and published [365, 366].

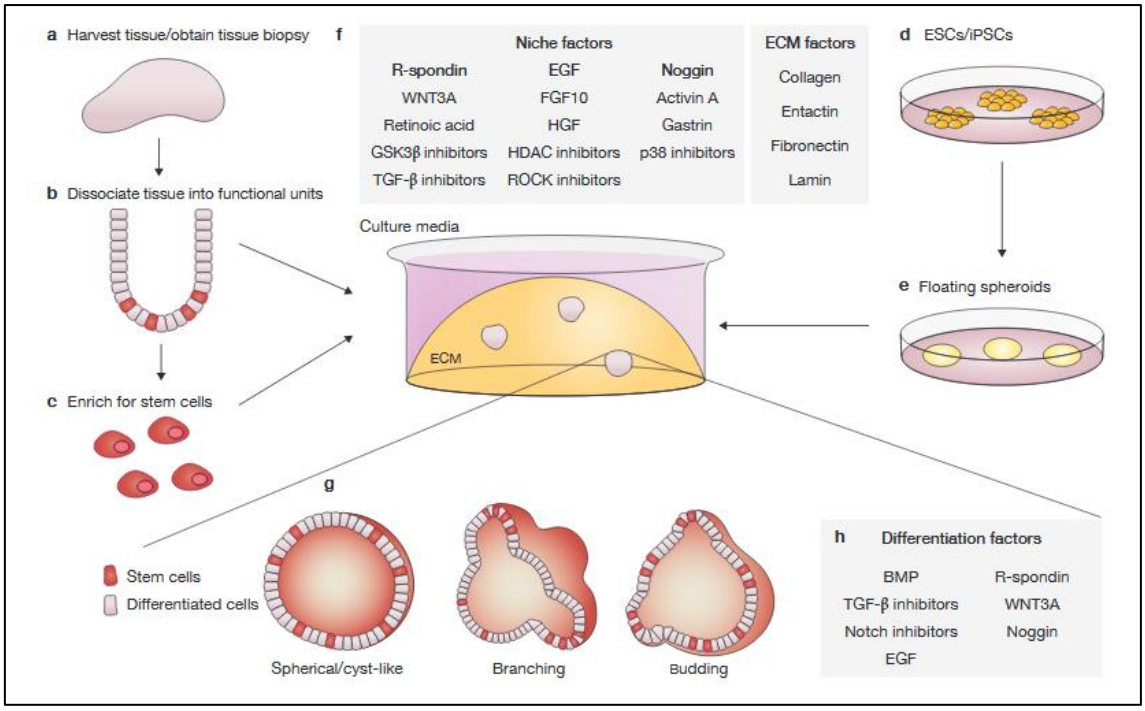


Figure 1.16 Schematic representation of the general workflow from tissue or embryonic/induced pluripotent stem cells to organoid culture (adapted from [362])
a) tissue obtained from surgery or endoscopy, b) tissue treated enzymatically and/or physically to release functional tissue subunits eg gastric glands, c) stem cell population enriched using FACS if required and either tissue subunits or single cells mixed with matrigel and cultured in growth media supplemented with niche factors dependent on tissue origin, d) organoids derived from embryonic stem cells (ESCs) or induced pluripotent stem cells (iPSCs), undergo directed differentiation, e) resulting floating organoids are mixed with matrigel and plated as before, f) and h) commonly used niche and differentiation factors each with a unique role in colony formation efficiency, proliferation, long term growth and differentiation and g) different conditions result in different cell types, levels of differentiation and organoid shapes

To study the process of carcinogenesis, sequential mutations were introduced in genes previously shown to be associated with colorectal cancer (APC, TP53, KRAS, PIK3CA, SMAD4) in human small intestinal [367] and colon [368] stem cell organoids by utilising CRISPR/Cas9-mediated genome editing. By modulating culture conditions they were able to grow the multi-mutant organoids without any of the niche factors required by normal intestinal organoids to grow. The tumourigenicity of these mutant organoids was then confirmed by transplantation into immune-deficient mice.

Engineered mouse gastric cancer organoids with $Kras^{G12D}$ mutation or with $p53^{flox/flox}$ (p53 null) or both were shown to exhibit dysplasia [369]. Also double engineered gastric organoids showed significant increase in proliferation and invasion (invasion assay). Dissociated cells from all three types of organoids exhibited tumourigenicity (high-grade invasive carcinomas) within 30 days of subcutaneous transplantation in immune-deficient NOG mice, with cells from the double mutant organoids producing less glandular and higher grade carcinomas.

In addition to modelling key mutational changes in carcinogenesis, gastric organoids have also been used to model and recapitulate the human gastric epithelial pathophysiological response to *H. pylori* infection *in vitro*. Both normal tissue [366, 370-372] and induced pluripotent stem cells [373] were used as starting material to achieve this objective. Finally modelling the tumour immune microenvironment using patient-derived organoids has also been described using the air-liquid interface (ALI) method from a wide range of tissues including the stomach ([374], Figure 1.17). Using this method, organoids are grown in a gel and exposed directly to air instead of being submerged underneath a nutrient medium [369, 374, 375]. However ALI organoids cultures tend to be shorter-lived (> 60 days) compared to "traditional" organoid cultures (> 1 year) but allow the integrative study of the relationship between stromal and immune cells and tissue derived-organoids [376, 377].

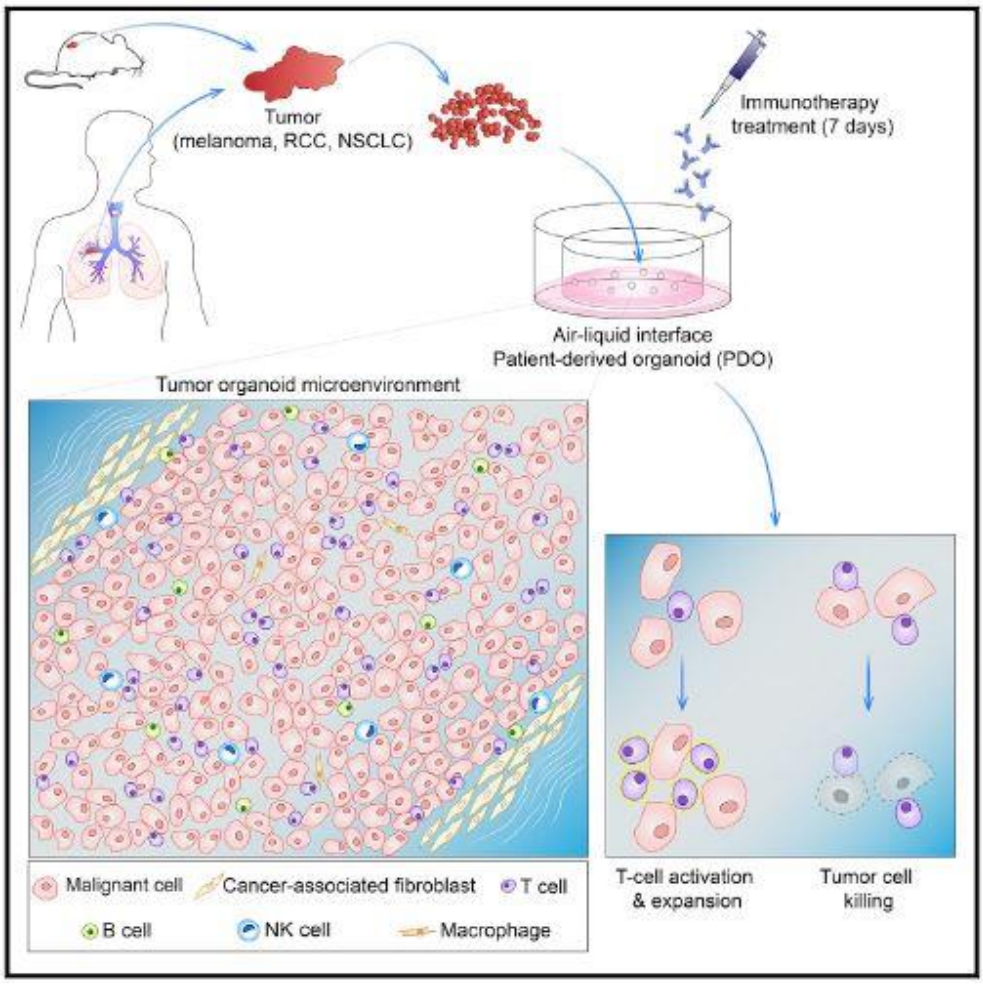


Figure 1.17 Schematic representation showing the use of tumour tissue derived organoids grown in the presence of stromal and immune cells using an air-liquid interface method (adapted from [374])

Human organoid cultures were established from a wide range of human tumour types together with cells from their natural microenvironment. Potential modelling of immunotherapy in human organoids + tumour infiltrating T cells was also investigated using anti-PD1 treatment *in vitro* over a period of 7 days.

Three dimensional organoids derived from intestinal metaplastic tissue have thus far not been described. Such an organoid model could be used to study the key genomic and epigenomic changes that cells undergo and progress to a dysplastic or a cancerous phenotype, gain further insight into the molecular differences between the complete and incomplete IM subtypes and characterise the role of immune cells in the overall process of gastric carcinogenesis.

1.7 Goals of this thesis

This literature review has highlighted the different aspects of gastric premalignant lesions, with particular emphasis on intestinal metaplasia, that are associated with progression to gastric cancer. Although a considerable volume of knowledge exists with regards to why certain patients with intestinal metaplasia progress to cancer, certain gaps still exist that need to be tackled in order to further improve patient stratification and targeted surveillance. This thesis set out to address five such gaps, and in particular:

1. The relationship between intestinal metaplasia and the diffuse type of gastric cancer

2. The molecular similarities and differences between the complete and the incomplete subtype of intestinal metaplasia

3. The macrophage and T cell landscape in intestinal metaplasia

4. The biomarker potential of CD10 and Das1 for subtyping complete and incomplete intestinal metaplasia

5. The development of an intestinal metaplasia organoid model from gastroscopy biopsies

Chapter 2 Materials & Methods

2.1 Materials

General materials and reagents used for this thesis and their suppliers can be found in Table 2.1. Antibodies used including clone type where appropriate, species of origin, control tissue and supplier can be found in Table 2.2. Specific details regarding the OPAL™ 7-color manual immunohistochemistry (IHC) kit used for Chapters 5, 6 and 7 can be found in Table 2.3. Primers for quantitative Real Time PCR (qRT-PCR) and cell lines used for Chapter 8 can be found in Tables 2.4 and 2.5. Finally equipment, software and specific R packages used can be found in Tables 2.6, 2.7 and 2.8 respectively.

Table 2.1 General materials and reagents

Reagent	Supplier
Advanced Dulbecco's Modified Eagle Medium	Life Technologies
Anti-Anti (penicillin, streptomycin, amphotericin B)	Life technologies
B27	Life Technologies
Bovine serum albumin	Sigma Aldrich
Cell Recovery Solution	Corning
Collagenase IV	Sigma Aldrich
Dispase	Gibco
DL-Dithiothreitol	Sigma Aldrich
DNAse I	Sigma Aldrich
dNTPs	Promega
D-sorbitol	Sigma Aldrich
EnVision+ System/HRP Mouse (DAB)	Dako
EnVision+ System/HRP Rabbit (DAB)	Dako
Foetal calf serum	Sigma-Aldrich
Gastrin	Sigma Aldrich
GlutaMAX	Life Technologies
HEPES	Life Technologies
Histogel	ThermoFisher Scientific
Hyaluronidase	Sigma Aldrich
IntestiCult™ Organoid Growth Medium (Human)	STEMCELL Technologies
Matrigel	Corning
M-MLV 5X reaction buffer	Promega
M-MLV reverse transcriptase	Promega
N-Acetylcysteine	Sigma Aldrich
Nicotinamide	Sigma Aldrich
p38 MAPK inhibitor SB202190	In Vitro Technologies
Potassium chloride	Merck
Potassium dihydrogen phosphate	Merck
Protein Block Serum-Free	Dako
Random Primers	Promega
Recombinant EGF	Life Technologies
Recombinant FGF10	Lonza Australia Pty
RNeasy Mini Kit	QIAGEN
ROCK inhibitor	Sigma Aldrich
Series 3 adhesive microscope slides	Trajan
Sodium chloride	Merck

Reagent	Supplier
Sodium phosphate dibasic	Astral Scientific
Sucrose	Merck
SYBR Green PCR master mix	Applied Biosystems
TGFβ inhibitor A-83-01	Tocris
TrypLE™	ThermoFisher Scientific
Tween 20®	Sigma-Aldrich

Table 2.2 Antibodies

Antibody (clone)	Species	Control tissue (human)	Supplier
AE1AE3 (AE1, AE3)	Mouse	Skin	Novocastra
APC-labelled anti-mouse IgG	Goat	na[1]	In Vitro Technologies
CD10 (56C6)	Mouse	Small intestine	Abcam
CD163 (MRQ-26)	Rabbit	Liver	Cell Marque
CD206 (ab64693)	Rabbit	Liver	Abcam
CD3 (SP7)	Rabbit	Tonsil	Spring Bioscience
CD4 (4B12)	Mouse	Tonsil/stomach	ThermoFisher Scientific
CD68 (514H12)	Rabbit	Liver	Leica
CD8 (4B11)	Mouse	Tonsil	ThermoFisher Scientific
CDX2 (EPR2764Y)	Rabbit	Small intestine	Cell marque
Das1 (7E12H12)	Mouse	Colon	Merck
FOXP3	Rabbit	Tonsil/stomach	BioSB
Intestinal Alkaline Phosphatase	Rabbit	Small intestine	Sapphire Bioscience
IRF8 (E-9)	Rabbit	Tonsil	Santa Cruz
MUC2	Rabbit	Small intestine	Santa Cruz
MUC5AC (MRQ-19)	Mouse	Stomach	Cell Marque
MUC6 (CLH5)	Mouse	Stomach	Novus Biologicals
OLFM4 (GW112)	Mouse	Small intestine	Sino Biological Inc.
PDL1 (SP142)	Rabbit	Placenta	Spring Bioscience
TFF3 (415909)	Mouse	Small intestine	BioScientific

[1]not applicable

Table 2.3 OPAL™ 7-color manual IHC kit

Reagent	Function
10X AR6 buffer	Antigen retrieval buffer
HRP Mouse secondary antibody	HRP labelled goat antibody, binds to mouse IgG primary antibodies
HRP Rabbit secondary antibody	HRP labelled goat antibody, binds to rabbit IgG primary antibodies
DMSO	Diluent for lyophilised fluorophores
Fluorophores (OPAL reagents) 520, 540, 570, 620, 650 and 690	React with HRP labelled anti-mouse and anti-rabbit secondary antibodies
1X Amplification diluent	To dilute fluorophores
Spectral DAPI	Fluorescent stain, binds DNA allowing nuclear cell segmentation

Table 2.4 Primers used for quantitative Real Time PCR

Gene	Primer 5'-----3'
GAPDH forward	AAGGTGAAGGTCGGAGTCAA
GAPDH reverse	AATGAAGGGGTCATTGATGG
TFF1 forward	GGAGAACAAGGTGATCTGCG
TFF1 reverse	AATTCTGTCTTTCACGGGGG
TFF2 forward	ATGGATGCTGTTTCGACTCC
TFF2 reverse	TCTGAGACCTCCATGACGC
CDX2 forward	GGAACCTGTGCGAGTGGAT
CDX2 reverse	TCCGTGTACACCACTCGATATT
VIL1 forward	CCTGGAGCAGCTAGTGAACA
VIL1 reverse	CCAAAGGCCTGAGTGAAATC

Table 2.5 Cell lines used to produce conditioned media

Reagent	Supplier
HEK293-mNoggin-Fc Noggin secreting cell line	Hubrecht Institute
HEK293T-hu-RSPO1-Fc R-Spondin 1 secreting cell line	Dr Camilla Mitchell (Peter MacCallum Cancer Centre)
L-cell Wnt3A secreting cell line	Dr Dustin Flanagan (Peter Doherty Institute)

Table 2.6 Equipment

Equipment	Company
BD FACSAria™ Fusion	BD Biosciences
Jung Autostainer XL	Leica
LightCycler 480	Roche
NanoDrop™ 1000 Spectrophotometer	ThermoFisher Scientific
Vectra® automated quantitative pathology imaging system	PerkinElmer
VS120 slide scanner	Olympus

Table 2.7 Software

Software	Version	Company
GraphPad Prism	8.1.0	GraphPad Software
cellSens Dimension	1.16	Olympus
Cytoscape	3.7.2	Open Source software provided by Cytoscape consortium
FlowLogic	7.2.1	Inivai Technologies
ImageJ	1.8.0_112	Open source
inForm	2.3	PerkinElmer
OlyVIA	3.12	Olympus
Phenochart	1.0.7	PerkinElmer
R	3.5.3	R Foundation
RStudio	1.2.1578	Rstudio

Table 2.8 R packages (R version 3.5.3 and online server R version 3.5.1)

Package	Version	Package	Version
affy	1.58.0	Limma	3.35.5
annotate	1.58.0	Magrittr	1.5
Biobase	2.40.0	pheatmap	1.0.12
Bioconductor	3.7	phenoptr	0.2.3
clinfun	1.0.15	phenoptrReports	0.2.4
corrplot	0.84	Plotly	4.9.0
corrr	0.4.0	RColorBrewer	1.1-2
dplyr	0.8.3	reshape2	1.4.3
ggplot2	3.2.1	ROCR	1.0-7
ggpubr	0.2.3	Stringi	1.4.3
ggrepel	0.8.1	tidyverse	1.2.1
GSVA	1.28.0	VennDiagram	1.6.20
hgu133plus2.db	3.2.3		

2.2 Patient cohorts

2.2.1 The Molecular Analysis for Upper Gastro Intestinal Cancer cohort

The Molecular Analysis for Upper Gastro Intestinal Cancer (MAUGIC) cohort consists of gastric and oesophageal cancer patients enrolled in an on-going tissue banking study from 1999-present. From each study participant, written informed consent was obtained and ethical approval was acquired from the Institutional Review Boards of the individual hospitals that took part in the study (HREC ref 12/25 for both St Vincent's Hospital and the Peter MacCallum Cancer Centre). Tissues and data from patients enrolled until 2009 were used for this thesis (Figure 2.1).

In addition at the time of gastric resection, tumour and non-malignant tissue samples (at least 2cm away from the tumour) were collected for research purposes and stored both as fresh frozen and as formalin-fixed paraffin embedded tissue (FFPE). Samples were reviewed and histologically characterised by the in-house research pathologist Dr Catherine Mitchell to evaluate tumour type and identify premalignant tissue changes. FFPE blocks containing non-malignant tissue with evidence of chronic gastritis (CG+GC) or intestinal metaplasia (IM+GC) were identified for use in the OPAL™ multiplex immunohistochemistry (IHC) and Biomarker studies (Chapters 5, 6 and 7).

Gene expression data (.CEL) was previously generated (GEO accession: GSE51105; [259]) using homogenised frozen tissue (both gastric cancer and premalignant tissue) and profiled with Affymetrix Human Genome U133 plus GeneChips™ (HG-U133 Plus 2.0). This data was used for gene expression profiling in Chapter 4. Gene expression data files were also available from a small group of samples with normal gastric histology (Normal gastric cohort) from pooled crushed frozen biopsy tissue acquired using Affymetrix HG-U133 Plus 2.0 arrays. All samples were validated for quality control at the time of the original experiments.

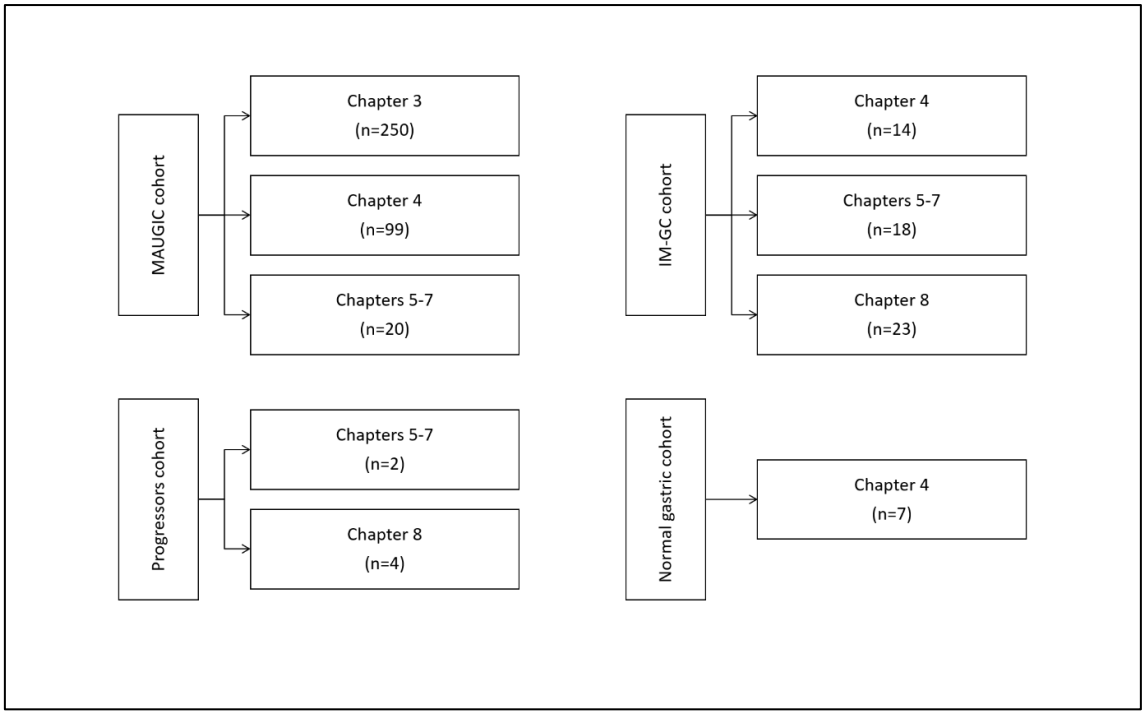


Figure 2.1 Patients from the Molecular Analysis for Upper Gastro Intestinal Cancer (MAUGIC), the IM-GC, the Progressors and the Normal gastric cohorts were used for this thesis
The MAUGIC cohort was used to investigate the histological association between intestinal metaplasia (IM) and gastric cancer (GC) subtypes as described in Chapter 3 (n=250). Gene expression profiling from Affymetrix Human Genome U133 plus GeneChips™ was performed using data from a) GC tissue, intestinal metaplasia (IM+GC) and chronic gastritis (CG+GC) at least 2cm away from tumour (all MAUGIC cohort), b) from patients with intestinal metaplasia tissue but without GC (IM-GC cohort, n=14) and c) normal gastric tissue from patients without IM nor GC (Normal gastric cohort, n=7) as described in Chapter 4. The immune microenvironment was characterised using OPAL™ multiplex immunohistochemistry in IM+GC (n=20), IM-GC (n=18) and patients that had progressed to high grade dysplasia/intramucosal GC (Progressors cohort, n=2) as described in Chapters 5 and 6. Tissue from the same patients were used to identify the biomarker potential of CD10 and Das1 for the complete and incomplete subtype of IM respectively as described in Chapter 7. Finally tissue samples from IM-GC patients (n=23) and Progressors patients (n=4) were used to set up gastrointestinal organoid cultures as described in Chapter 8.

2.2.2 Screening and surveillance (S2P) cohorts

A third cohort was collected as part of a screening and surveillance program which consisted of IM patients with no evidence of GC (IM-GC) (Figure 2.1). Gene expression data files from a representative group of samples was previously generated using Affymetrix arrays (HG-U133 Plus 2.0) with RNA extracted from fresh frozen tissue which was macrodissected to enrich for IM epithelium.

An additional cohort of patients, initially part of the screening and surveillance program but who ultimately progressed to dysplasia and/or intra-mucosal gastric cancer (“Progressors cohort”)

was utilised. For these patients samples were collected from multiple anatomical locations and at multiple time points/visits.

All samples including those from the Normal gastric cohort were collected following the Institutional Review Boards of the individual hospitals (HREC ref 12/25 for St Vincent's Hospital and the Peter MacCallum Cancer Centre and HREC ref 2005.075 for the Royal Melbourne Hospital).

2.3 Histological association of intestinal metaplasia with Lauren gastric cancer subtypes (Chapter 3)

2.3.1 Patient selection criteria

Patients were selected from the MAUGIC cohort if they met the following criteria: i) gastric adenocarcinoma or ii) gastro-oesophageal junction adenocarcinoma with Siewert classification Type II or III (Figure 2.2). For each patient, information regarding the presence of premalignant tissue directly adjacent to tumour was extracted from the patient's pathology report which included pre- and post-surgery detailed described pathology. Details regarding the characteristics of the premalignant tissue 2cm distant from the tumour were generated through review of the research FFPE blocks by in-house research pathologist Dr Catherine Mitchell.

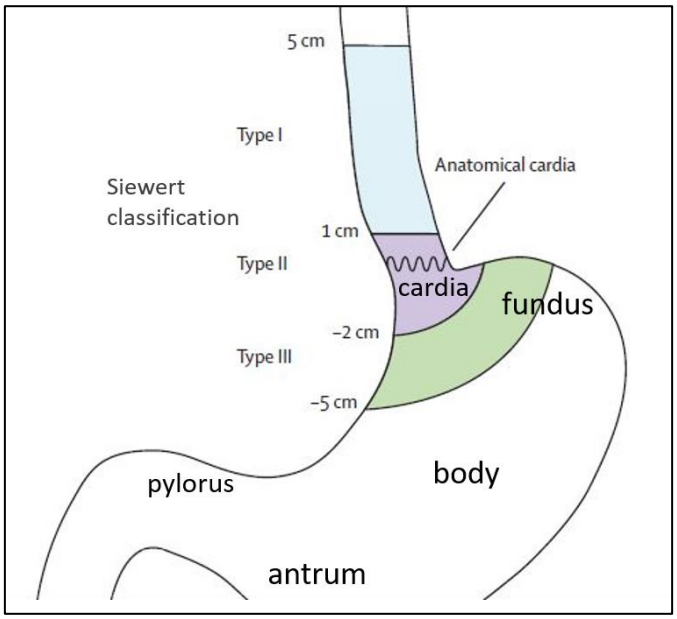


Figure 2.2 Schematic representation of the Siewert classification system (adapted from [378]) Tumours at the gastro-oesophageal junction (GOJ) are subdivided into three types: Type I which are lower oesophageal adenocarcinomas, Type II which are "true cardia" adenocarcinomas and Type III which are gastric subcardial adenocarcinomas. For this study only Types II and III were included.

2.3.2 Statistical analysis

Statistical analysis was carried out using GraphPad Prism. To determine possible significant associations between chronic gastritis (CG), intestinal metaplasia (IM) and Lauren GC types, a chi-squared test was used. To determine possible differences in CG/IM association between GC types, a Fisher's exact test was used. To test for differences in clinicopathological details between groups of patients with and without IM adjacent to tumour of either GC type, Fisher's exact test was used where two variables were present, and a chi-squared test where more than two variables were present. For all tests a p-value <0.05 was considered significant.

2.4 Gene expression profiling (Chapter 4)

2.4.1 Differential gene expression

Differential gene expression was carried out using R with the affy and the limma packages from Bioconductor. Normalisation used the robust multi-array average (RMA) algorithm and probes/genes were said to be differentially expressed if the log2 fold change was >1.2 (approximately equal to 2.3 fold change in real values) with a p-value <0.05 after Benjamini-Hochberg correction for multiple testing [379-381]. When individual genes were investigated, the probe with the maximum expression was analysed and statistical significance for differential expression was determined using the unpaired t test (normal distribution of data) or the Mann Whitney test (data not normally distributed). The Jonckheere-Terpstra test in R was used to determine trends in gene expression from tissues representing the Correa cascade (normal -> chronic gastritis (CG+GC) -> intestinal metaplasia (IM+GC) -> intestinal gastric cancer) [382]. For visualisation purposes heatmaps were created with the pheatmap package in R.

2.4.2 Gene set over-representation and single sample gene set enrichment analysis

Gene set over-representation analysis (ORA) was carried out using the Gene Ontology domains Biological Process, Cellular Component and Molecular Function to interpret the biological and cellular functions of the available differentially expressed gene lists between two conditions. To do this both the online tool g:Profiler and the Cytoscape plugin ClueGO were used [383-385]. To correct for multiple tests, the g:SCS algorithm was used with the former and the Bonferroni step down method with the latter [386].

Single sample gene set enrichment analysis (ssGSEA, [387]) was performed using the GSVA package in R in conjunction with gene sets downloaded from the MSigDB and ImmPort websites (gsea-msigdb.org and import.org). To test for statistical significance, the Wilcoxon test was used

together with the Benjamini-Hochberg correction for multiple tests. A p-value <0.05 was considered significant.

The gene sets used were:

- H: hallmark (MSigDB)
- C1: positional (MSigDB)
- C2: KEGG (MSigDB)
- C3: transcription factor targets (MSigDB)
- C5: GO Biological Process (MSigDB)
- C5: GO Cellular Component (MSigDB)
- C5: GO Molecular Function (MSigDB)
- GO Immune (ImmPort)

2.4.3 Gene expression validation

The Companioni et al 2017 data set was downloaded from the NCBI website (GEO accession: GSE78523; [388]). Differential gene expression was carried out online using the GEO2R tool and individual gene expression analysis was carried out on the normalised highest expressing probe data provided. Heatmaps were created with the pheatmap package in R.

2.4.4 Cell-type Identification By Estimating Relative Subsets Of RNA Transcripts (CIBERSORT)

CIBERSORT (cibersort.stanford.edu, [389]) allows the characterisation within a tissue of the relative numbers of immune cell subsets using gene expression data. In this study it was used to obtain an initial estimation of the main immune cells and cell subsets present in the CG+GC and the IM+GC samples. When comparing CG+GC with IM+GC immune cell subset values, the unpaired t test for normal distribution of data and the Mann Whitney test for data not normally distributed were used to test for possible differences, with a p-value <0.05 considered significant. These results together with the other gene expression data analyses laid the foundation for the types of immune cell subsets investigated in the OPAL™ multiplex IHC study that followed.

2.5 OPAL™ multiplex immunohistochemistry (Chapters 5-7)

2.5.1 Sample selection and subtyping of intestinal metaplasia

Samples for OPAL™ multiplex IHC were selected using the following criteria. IM samples were subtyped independently using a 4µm thick FFPE section stained with haematoxylin and eosin by two in-house research pathologists (Dr Catherine Mitchell and Dr Stephen Lade) and further

discussion was held to reach a consensus if required. IM containing 0% to 40% glands with a brush border was classified as “incomplete IM”, IM containing 40% to 60% glands with a brush border was classified as “mixed IM” and IM containing 60% to 100% glands with a brush border as “complete IM”. For the purpose of this study, and in the absence of published guidelines, any sample with ≤60% of complete IM was assigned to the “predominantly incomplete IM” group thus merging “mixed IM” and “incomplete IM” (Figure 2.3). In the interest of simplifying terminology throughout this thesis, the “predominantly incomplete IM” group will be referred to as incomplete IM (iIM).

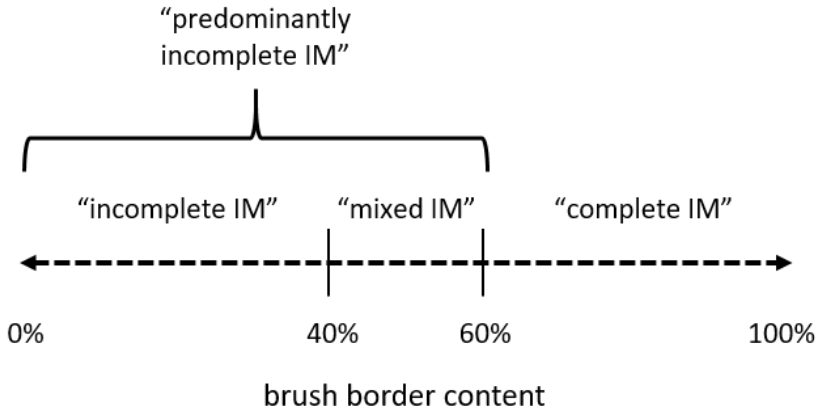


Figure 2.3 Subtyping of intestinal metaplasia samples
Samples were stratified into three groups based on the presence or absence of a brush border: “incomplete IM” with 0%-40% of glands having a brush border, “mixed IM” with 40%-60% of glands having a brush border and “complete IM” with 60%-100% of glands having a brush border. The incomplete and mixed groups were merged and defined as “predominantly incomplete IM”. In the interest of simplifying terminology throughout this thesis, the “predominantly incomplete IM” group will be referred to as incomplete IM (iIM).

2.5.1 Single slide library creation

OPAL™ multiplex IHC (PerkinElmer) is a cyclical process which uses several rounds of antibody-stripping steps and tyramide signal amplification fluorophores (OPAL™ reagents) to achieve multiplexing of antibodies even from the same species together with Dapi (4’,6-diamidino-2-phenylindole) as a nuclear marker [390]. In combination with the VECTRA Automated Quantitative Pathology Imaging System, the inForm software and R, high resolution images from multiplex IHC stained sections can be used to obtain quantitative and spatial information of multiple cell types based on the co-localisation of antibody markers. Specific tissue types can be targeted using tissue segmentation.

To spectrally unmixed a high resolution scanned image of a multiplex IHC stained section, a single stain library is required. Such single stain libraries were created for both the Macrophage and the T cell panel using 4µm FFPE sections of control tissue (Tables 2.2 and 2.9).

Table 2.9 OPAL panel staining details and fluorophores used

OPAL panel	1° Antibody	1° Ab dilution[1]	2° Ab dilution[1]	OPAL reagent[2]	Antigen retrieval buffer
Macrophage					
	CD206	1 : 6000	1 : 1000	620	EDTA buffer[3]
	CD68	1 :100	1 : 500	570	EDTA buffer
	IRF8	1 : 500	1 : 1000	650	EDTA buffer
	CD163	1 : 500	1 : 1000	540	EDTA buffer
	PD-L1	1 : 1000	1 : 1000	520	EDTA buffer
	AE1AE3	1 : 200	1 : 1000	690	EDTA buffer
	Dapi	2 drops in 1 ml 0.1% TBST		na[4]	EDTA buffer
T cell					
	CD4	1:50	1:500	520	EDTA buffer
	CD8	1:200	1:500	620	EDTA buffer
	FOXP3	1:100	1:1000	540	EDTA buffer
	CD3	1:500	1:1000	570	AR6[5]
	CD10	1:50	1:500	650	AR6
	AE1AE3	1:200	1:1000	690	EDTA buffer
	Dapi	2 drops in 1 ml 0.1% TBST		na[4]	EDTA buffer

[1]All antibody dilutions done in 0.1% BSA in 0.1% TBST; [2]All OPAL reagents diluted 1:50 in 1X Amplification diluent; [3]EDTA buffer= 1mM EDTA buffer, pH 8.0; [4]not applicable; all washing steps done with 0.1% TBST; [5]Antigen retrieval buffer from the OPAL™ 7-color manual IHC kit

Following an initial dewaxing step (overnight at 60°C) antigen retrieval was performed using either 1mM EDTA buffer solution (pH 8.0) or the AR6 buffer solution provided with the OPAL™ kit in a pressure cooker depending on the primary antibody to be used (see Tables 2.2 and 2.3). The slides were cooled on ice, washed with 0.1% TBST, and incubated with 3% (Macrophage panel, Table 2.9) or 0.3% (T cell panel, Table 2.9) hydrogen peroxide to block any endogenous peroxidase activity for 10min. Following washes with 0.1% TBST buffer, the slides were incubated with serum free protein blocking solution (Dako) for 10min to prevent non-specific binding of antibodies. After washing, the primary antibody (in 0.1% BSA solution/0.1% TBST buffer) was applied and incubated for 30min. Slides were washed with 0.1% TBST buffer and secondary HRP labelled antibody (Table 2.3) was applied for 10min. Slides were then washed, and incubated with the appropriate OPAL™ fluorophore (Table 2.3) prepared in amplification buffer for 10min. Following another round of washes, antigen retrieval was carried out using a microwave in 1mM EDTA buffer solution. Slides were mounted with VECTASHIELD, nail polish was applied to seal the cover slip and stored in the dark overnight prior to scanning on the VECTRA microscope. Single stains were visualised at x10 and x20 magnification and individual

fluorophore spectra were created from x20 images using inForm. The above protocol was also followed to create the Dapi stain spectrum but the primary/secondary antibody steps were replaced with incubations in 0.1% BSA solution/0.1% TBST buffer.

2.5.2 Multiplex immunohistochemistry staining

For each tissue to be characterised four FFPE serial sections (4µm thick each) were cut and mounted onto highly adhesive Trajan glass slides. Sections were used as follows: 1) haematoxylin and eosin staining (H&E), 2) the Macrophage panel, 3) the T cell panel and 4) Das1 biomarker (Chapter 7). H&E staining was carried out first and scanned at x20/x40 magnification using the VS120 slide scanner to document the exact location of IM on the section. The protocol used for OPAL IHC staining was as described for the single stain library with additional, sequential staining steps using all the markers in a panel (Table 2.9). Following the last round of antigen retrieval, the slides were washed and incubated with Dapi for 2min. As before slides were mounted with VECTASHIELD, nail polish was applied to seal the cover slip and stored in the dark overnight prior to scanning on the VECTRA microscope.

2.5.3 Slide scanning and imaging using VECTRA microscope

Optimal scanning exposure times and focus settings for each stained section were determined at both low (x10) and high (x20) resolution for each filter cube of the VECTRA microscope. This was followed by whole slide low resolution scanning and imaging with the Phenochart software. Regions rich in IM glands and rich in gastric glands were identified using a 1x1 rectangular shape (669µm x 500µm in real size, field resolution=0.5µm). Regions containing tertiary lymphoid structures were excluded to avoid bias due to higher T cell numbers compared to local glandular tissue. The regions of interest were then scanned at high resolution and analysed using inForm.

2.5.4 inForm multispectral unmixing and cell phenotyping

High resolution image files were imported into inForm, spectrally unmixed using the previously prepared single stain library (§2.5.1) and tissue segmented where necessary. At least 3 tissue categories were created: CG (chronic gastric tissue), IM (intestinal metaplastic tissue) and Other (tissue that contained tertiary lymphoid structures or a mixture of gastric and IM glands or only a small amount of tissue making it unlikely to produce a reliable result). For the Progressors cohort a fourth tissue category was created: IMD (dysplastic tissue). Next cell segmentation was carried out using the Dapi stain to identify the cell nucleus, the appropriate cell markers to identify the cell membrane (CD163 and CD206 for the Macrophage panel and CD3, CD4 and CD8 for the T cell panel) and the cytoplasm where possible (CD68 for Macrophage panel). Individual

cells were then phenotyped depending on the intensity and the co-localisation of fluorophores present. PDL1 expression was absent in the majority of premalignant tissues and was not used directly for phenotyping but analysed using fluorophore intensity values with R. Next, the classifier tool was trained to identify all cell types using 5-150 of positively phenotyped cells. This was further refined by repeated phenotyping and retraining of the cell classifier until a satisfactory level of cell classification was obtained. All image types including composite and pseudo-pathology views of each fluorophore as well as data files containing a full list of measured parameters (eg. cell type, x and y coordinates of each cell, fluorophore intensities on each cell segment for each cell including min, mean and max values) were exported and a summary file for each image was created that contained the total cell number and cell density of each cell type.

2.5.5 Spatial location analysis of cell types

To gain insight into the possible physical and paracrine interactions between the immune cells of interest but also with epithelial cells, the "phenoptr" package [391] in R was used to carry out three types of spatial location analyses: a) nearest neighbour which calculates the mean distance in microns between two different cell types, b) number of cells within a specified radius in microns which calculates the mean number of a specific cell type around a reference cell and c) touch cell pair density which uses morphological analysis of nuclear and membrane segmentation maps to find touching cells of paired phenotypes, and together with the area of each region of interest (ROI) characterised, a touching cell pair density is calculated representative of the possible physical interaction between two different cell types (Figure 2.4). Although useful in describing intercellular distances, nearest neighbour analysis was only used in the Progressors part of the study (Chapters 5 and 6). Most spatial work in this study focussed on short to medium range cellular interactions [392, 393] and included quantitative analyses of both cells within a specified distance and touching cell pairs.

Based on previous work by Feng et al 2017 [394] and Carstens et al 2017 [395], the mean number of cells within 40μm of a target cell population was chosen to be representative of both key physical and paracrine interactions, and this was termed the functional space around a specific reference cell type. In this analysis, if the mean number of cells was lower than 1 for example if the mean number of FOXP3 T cells in a radius of 40μm around CD8 T cells ($CD8^{40\mu m}FOXP3$) = 0.5, then that meant that half of the CD8 T cells had a single FOXP3 T cell within their surrounding functional space of r=40μm.

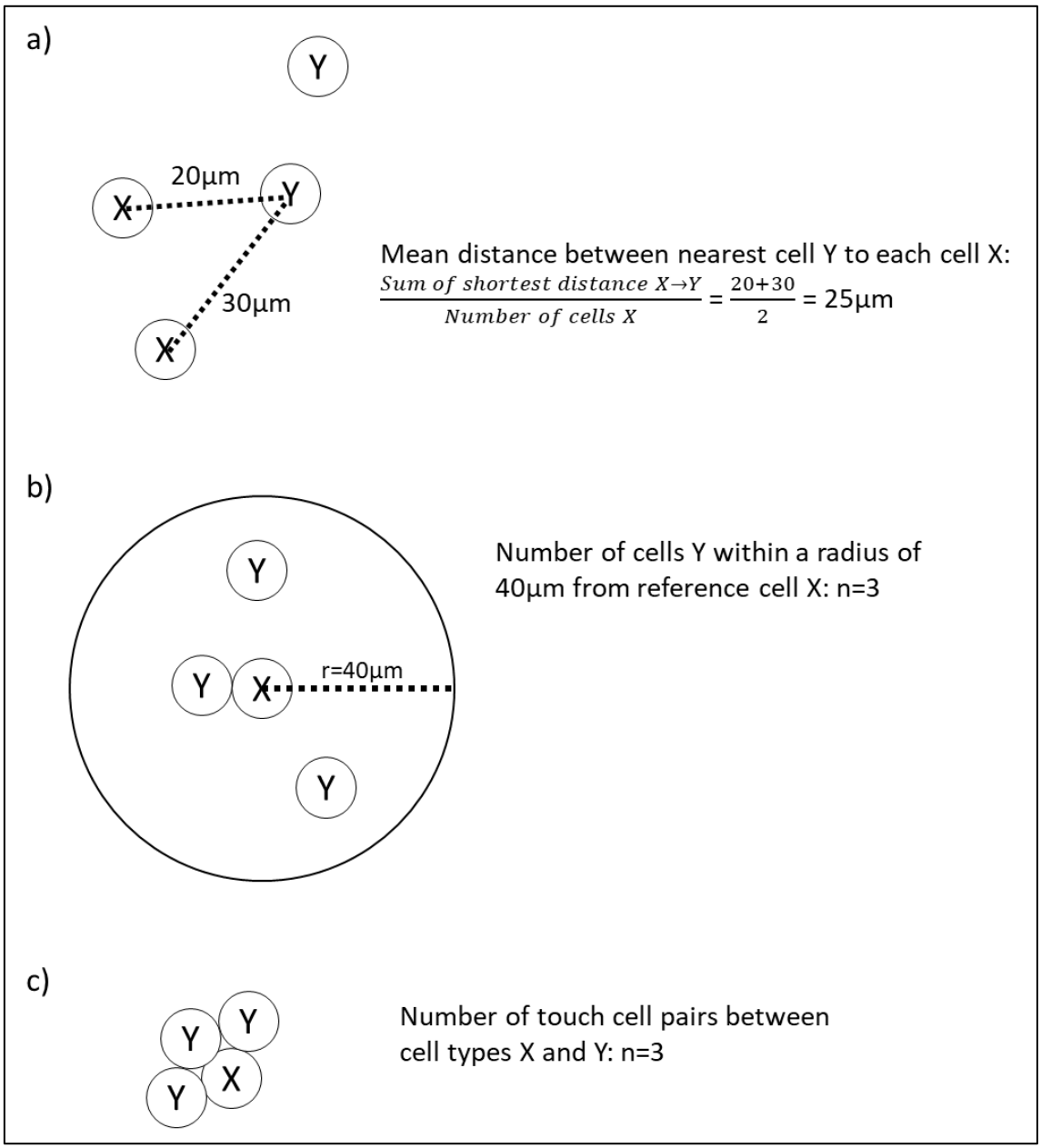


Figure 2.4 Spatial location analyses showing the nearest neighbour, number of cells within a specific radius (distance) and touch cell pairs

a) mean distance between cell type X and the nearest neighbouring cell type Y; b) number of cells type Y within a specific radius (=40µm) of reference cell X; c) number of touch cell pairs between a small group of X and Y cells. All analyses carried out with phenoptr package in R.

2.5.6 Statistical analysis

A generalised linear model (glm function in R) was used to analyse the data. This took into account the differing number of ROIs per sample and the varying distribution types of data. Generalised linear models were used in both the cell density and spatial location parts of the OPAL study to identify significant differences between tissues and cohorts, and data visualisation was done using GraphPad Prism and R. Spearman's rank correlation was used to

identify quantitative and spatial relationships between macrophage and T cell subsets. A p-value <0.05 was considered significant.

2.6 Biomarkers (Chapter 7)

2.6.1 Determining the presence of CD10 on individual IM glands

The OPAL™ 650 fluorophore was used together with the anti-CD10 antibody as part of the OPAL™ T cell panel to determine the presence of this marker on IM tissue (Table 2.9). The OPAL™ 650 pseudo-pathology view image files were produced with inForm by spectral unmixing the raw .im3 files obtained from scanning the multiplex stained sections as per section §2.5.4. These images were used to assess the CD10 status of individual IM glands.

2.6.2 Determining the presence of Das1 on individual IM glands

Das1 antibody staining was carried out on 4µm FFPE serial sections of IM-GC, Progressors and IM+GC tissue samples (§2.5.2). Briefly the primary antibody (1/200) was applied and incubated overnight at 4^0C, followed by an incubation step with the EnVision+ System/anti-mouse HRP reagent and visualised with DAB chromogen. Das1 stained slides were scanned on the VS120 slide scanner microscope at x20/x40 magnification and the resulting high resolution images (.vsi files) were used to assess the Das1 status of individual IM glands. Image files were opened with the cellSens Dimension software, and IM glands were marked using the previously annotated H&E images of the same tissue as guide and scored blindly as positive or negative by two researchers (Prof Alex Boussioutas and Dr Rita Busuttil).

2.6.3 Quantification of Das1 staining across whole section

Digital quantification of Das1 staining was carried out on high resolution .vsi files using the cellSens Dimension software. The same regions of interest characterised using the OPAL™ T cell panel were investigated for Das1 staining using equivalent tissue segmentation carried out with the polygon tool. Fraction area of each ROI positive for Das1 staining was measured by using first the “threshold tool” with R-G-B threshold detection parameters kept constant for all images and second with the “Count and Measure on ROI” tool. All result files were exported in csv format for further analysis.

2.6.4 Statistical analysis

Confidence intervals for sensitivity and specificity were obtained using the Clopper-Pearson interval [396]. Area under the receiver operating characteristic (AUROC) for each biomarker was calculated using the ROCR package in R. Logistic regression modelling in R was used to compare

subtyping of complete IM glands with CD10 on its own versus CD10 combined with Das1 staining. Regions positive for Das1 staining were compared between two conditions using a generalised linear model (glm function in R) with a quasibinomial distribution. Das1 staining of whole tissue sample comparing two conditions was carried out using an unpaired t test or a Mann Whitney test where appropriate. Pearson's correlation coefficient was calculated to determine the relationship between Das1 staining, T cell and macrophage subset densities (GraphPad Prism). A p-value of <0.05 was considered significant.

2.7 Organoid model (Chapter 8)

2.7.1 Tissue processing and establishing human gastrointestinal organoid cultures

Human gastroscopy biopsy samples were transferred directly from the patient into cold basal medium (BM; Advanced DMEM/F12, 1x Anti/Anti, 1x GlutaMAX, 10mM HEPES) and processed within 24 hours using the following techniques:

a) Enzyme digestion method (described in [366]): tissue samples were minced using 2 scalpel blades and incubated in 5ml of preheated enzymatic cocktail solution containing Penicillin/Streptomycin (0.02ml/ml), Collagenase IV (75U/ml), Dispase (125µg/ml), Hyaluronidase (20µg/ml) and DNAse I (0.1µg/ml) for 40min at 37°C. 10ml of cold basal medium (Advanced DMEM/F12, 1x Anti/Anti, 1x GlutaMAX, 10mM HEPES) was added, the solution filtered through a 70µm filter and the filter washed with 5ml of basal media and centrifuged (200g for 5min at 4°C). The pellet was resuspended in matrigel. 20µl matrigel domes/per well of a 48 well plate were seeded and allowed to polymerise at 37°C for 30min. 200 µl of growth medium preheated to 37°C was then added to each well.

b) Chelation buffer method (described in [366]): tissue samples were washed with chelating buffer (5.6mM Na2HPO4, 8.0mM KH2PO4, 96.2mM NaCl, 1.6mM KCl, 43.4mM sucrose, 54.9mM D-sorbitol, 0.5mM DL-dithiothreitol, pH 7) and minced into small pieces. These were transferred to a 50ml Falcon tube, washed with chelating buffer until the remaining supernatant was clear and then incubated in chelating buffer supplemented with 10mM EDTA for 30min at 4°C. The supernatant was removed and remaining tissue fragments were transferred to 10cm cell culture plate and gently squeezed upon using a sterile glass slide to release the glands. The glands were collected in cold BM, centrifuged (200g for 5min at 4°C), resuspended in matrigel and plated as before.

c) Vigorous pipetting method (as described in[397]): tissue samples were transferred onto a 10cm cell culture plate followed by 3-5 washes in cold PBS buffer. They were then incubated in

PBS supplemented with 2.5mM EDTA for 40min at 4°C, transferred to fresh PBS and the intestinal crypts were released using repeated vigorous pipetting (at least 10 times) with a 10ml pipette. The supernatant containing the crypts was transferred to a new Falcon tube, centrifuged (200g for 5min at 4°C), mixed with matrigel and plated as before.

2.7.2 Organoid growth media

Organoids were grown in either an in-house customised organoid growth medium (OGM: WRNEFGSTNi as described in [365] and [366]) or the commercially available IntestiCult™ Organoid Growth Medium (STEMCELL Technologies) (Table 2.10). Growth medium was changed 3x times per week.

Table 2.10 Organoid growth media details

Growth medium	Compound/ component	Amount/ conc^n	Comment
OGM	Wnt3A CM	50%	Induces canonical Wnt signalling
(WRNEFGSTNi)	R-Spondin 1 CM	20%	Stimulates Wnt signalling
	Noggin CM	10%	BMP antagonist
	Epidermal growth factor (EGF)	50ng/ml	Organoid regeneration/mitogenic
	Fibroblast growth factor 10 (FGF10)	200ng/ml	Organoid survival/mitogenic
	Gastrin	10nM	Produced in antrum/small intestine
	SB202190	10µM	p38 MAPK inhibitor
	A 83-01	500nM	ALK4/5/7 inhibitor
	Nicotinamide	10mM	Amide form of vitamin B3
	Y27632	10µM	ROCK inhibitor
	N-Acetylcysteine	1mM	Long term maintenance
	B-27 supplement	1x	Long term maintenance
	Basal medium (BM)[1]	1x	Base media
IntestiCult™			
(IC)	IntestiCult OGM Human Component A	50%	No data available
	IntestiCult OGM Human Component B	50%	No data available

[1]Basal medium: Advanced DMEM/F12, 1x Anti/Anti, 1x GlutaMAX, 10mM HEPES

2.7.3 Establishing organoid cultures from fresh porcine tissue

Whole pig stomach and parts of the small and the large intestine were obtained from the Diamond Valley Pork abattoir in Laverton. Organs were cut into 1-3cm^2 pieces and washed repeatedly in PBS supplemented with 1x Anti-Anti to reduce the possibility of infection. Tissue was then cut into 0.5-1 cm^2 pieces and washed 2x PBS with Anti-Anti in sterile conditions. Tissue pieces were either cryopreserved in freezing medium (FM: 90% foetal calf serum + 10% DMSO) or processed using both the Enzyme digestion and Chelation buffer methods.

2.7.4 Establishing porcine organoid cultures from previously cryopreserved tissue

Cryopreserved tissue was thawed at 37°C and washed in cold PBS with 1x Anti-Anti. Samples were then placed on a 10cm cell culture plate, washed with chelation buffer, cut into smaller pieces (2-5 mm^2) and transferred to a 50ml Falcon tube. Samples were washed again with chelation buffer until the supernatant was clear and then incubated in chelation buffer with either 10mM EDTA (stomach) or 2mM EDTA (small intestine) for 10min (stomach) or for 30min (small intestine) at room temperature (stomach) or 4°C (small intestine). Finally the supernatant was removed; the remaining tissue fragments were transferred to a new 10cm cell culture plate and squeezed using a sterile glass slide to release the glands as before (§2.7.1). The glands were collected in cold BM, centrifuged at 200g for 5min at 4°C and resuspended in the appropriate amount of matrigel. The rest of the protocol was the same as before (§2.7.1).

2.7.5 Passaging/reseeding of organoid cultures

During routine maintenance organoids were either reseeded to dilute high density cultures or passaged to propagate the organoid population. For both procedures organoids were released from the matrigel using 2x 0.5ml of cold BM and transferred into a 1.5ml Eppendorf tube or 15ml Falcon tube if several wells were pooled together. Tubes were centrifuged at 500g for 5min at 4°C and the supernatant removed. For reseeding the organoid pellet was resuspended in the appropriate amount of matrigel and plated. The rest of the protocol was the same as before (§2.7.1).

Passaging of organoids included an additional incubation step with TrypLE™ for 5min at 37°C after the centrifugation step. The reaction was stopped with the addition of 0.5ml cold BM and a second centrifugation step to retrieve the digested organoid fragments. The pellet was mixed with matrigel, plated and growth medium added as before (§2.7.1).

2.7.6 Freezing down organoid cultures

Starting with multiple wells of organoid cultures, organoids were released from the matrigel using cold BM and the resulting solutions were pooled together. They were centrifuged at 500g for 5min at 4°C, the supernatant was removed and 1ml of FM was added. The samples were transferred to cryovials, placed in an insulated container and frozen at -80°C.

2.7.7 Reanimating cryopreserved organoid cultures

A cryovial containing frozen organoids was quickly thawed in a 37°C water bath and its contents were transferred to a 15ml FT containing 10ml of pre-warmed BM. This was spun down at 500g

for 5min at 8°C, the supernatant was removed and the organoid pellet was mixed with matrigel and plated as before (§2.7.1).

2.7.8 RNA isolation from organoid cultures

Starting with at least 2 wells, organoids were released from the matrigel using cold BM or Cell Recovery Solution and the resulting solutions were pooled together and incubated on ice for 25-30min. The mixture was centrifuged at 500g for 5min at 4°C, the supernatant was removed and total RNA was isolated from the organoid pellet using the RNeasy Mini Kit (Qiagen) following the manufacturer's instructions. RNA concentration was determined using the NanoDrop™ 1000 spectrophotometer. Isolated RNA samples were stored at -80°C.

2.7.9 Reverse transcription

1µg of total RNA was diluted in 18µl sterile water and mixed with 1µg of random primers (Promega). Samples were denatured at 70°C for 5min. A master mix containing 5µl of 2.5mM dNTPs (Promega), 6 µl of 5x M-MLV reaction buffer (Promega) and 1µl of 200U/µl M-MLV reverse transcriptase (Promega) were added and incubated at 42°C for 90min, followed by a deactivation step at 95°C for 5min. Samples were diluted with sterile water to 10ng/µl.

2.7.10 Quantitative Real Time PCR (qRT-PCR)

Quantitative Real Time PCR was performed in triplicate in a total volume of 10 µl using the SYBR green assay on the LightCycler 480 (Roche): 5ng of cDNA (0.5µl), 5µl of SYBR Green (Applied Biosystems), 1µM forward and reverse primers (0.5µl) and 4µl of sterile water (Table 2.4). The amplification conditions were 50°C for 2 minutes, 95°C for 10 minutes, 40 cycles of 95°C for 15 seconds followed by 1 minute at 60°C. The threshold cycle numbers were exported from the LightCycler 480 software and relative gene expression levels calculated using the comparative threshold cycle method (ΔΔCT), normalised to GAPDH.

2.7.11 Fixing and embedding of organoids

Starting with at least two wells, organoids were released from the matrigel using cold BM and the resulting solutions were pooled together and incubated on ice for 10min. The organoids were then centrifuged at 500g for 5min at 4°C and the supernatant removed. A volume of 500 µl of freshly prepared cold 4% paraformaldehyde was added and incubated for 30 min on ice to fix the organoids. The organoids were then centrifuged at 500g for 5min at 4°C, the supernatant removed and the remaining pellet washed with 500µl of cold PBS. Following another spin at 500g for 5min at 4°C, the supernatant was removed and the remaining organoid pellet was

mixed with 20µl of pre-heated liquified histogel. The mixture was pipetted onto parafilm, allowed to cool, and then embedded into paraffin.

2.7.12 Single stain immunohistochemistry

Staining (H&E and immunohistochemistry) were performed on 4µm FFPE sections. Sections were first air dried, put in an oven at 60°C for at least 20min and dewaxing was completed using an automated stainer (Leica). Antigen retrieval was done using either with 1mM EDTA buffer or the AR6 buffer from the OPAL™ kit (see Table 2.3) at 121°C in a pressure cooker. The slides were cooled down at room temperature and washed with Milli-Q water. They were then incubated in 3% hydrogen peroxide solution for 20min, followed by washes with 0.05% TBST buffer and a blocking step of 30min in 10% BSA solution. Primary antibody prepared in 1% BSA solution (in 0.05% TBST buffer) was added (see Table 2.11 for specific conditions). Slides were washed in 0.05% TBST buffer and either the EnVision+ System/HRP Mouse or the EnVision+ System/HRP Rabbit together with DAB were used to visualise the staining.

Table 2.11 Staining conditions of primary antibodies used with immunohistochemistry to characterise gastrointestinal organoids

Primary antibody	Antigen retrieval[1]	Dilution[2]	Temperature	Incubation period
CD10	AR6	1/50	4°C	overnight
CDX2	AR6	1/200	4°C	overnight
IAP[3]	EDTA	1/100	4°C	overnight
MUC2	AR6	1/4000	4°C	overnight
MUC5AC	AR6	1/1000	4°C	overnight
MUC6	AR6	1/200	4°C	overnight
OLFM4	AR6	1/2000	4°C	overnight
TFF3	AR6	1/50	22°C	1hr

[1]Antigen retrieval buffers: AR6 buffer from the OPAL™ kit and 1mM EDTA buffer; [2]All antibody dilutions done in 1% BSA/0.05% TBST; [3]Intestinal alkaline phosphatase

2.7.13 Production of conditioned media

The HEK293-mNoggin-Fc Noggin secreting cell line (Table 2.5) was cultured in DMEM + 10% FCS + 1% Anti/Anti + G418 at 500 µg/ml). When confluent, cells were passaged 1:6 and placed in culture medium without G418. At day 4, harvest medium (ADMEM/F12 + 15 Anti-Anti + 10mM HEPES + 1x GlutaMAX) was added to the cells and the Noggin conditioned medium was harvested 8 days later centrifuged at 1200 rpm, filtered through a 0.22µm filter and stored at -20°C for up to 1 year.

R-Spondin 1 and Wnt3A conditioned media were produced in-house using the HEK293T-hu-RSPO1-Fc R-Spondin 1 and the L-cell Wnt3A secreting cell lines (Table 2.5) and the appropriate protocols as described in Appendix B.

2.7.14 Fluorescence-Activated Cell Sorting (FACS)

Starting with cultures from at least 8 wells, organoids were released from matrigel using cold BM and pooled together. The mixture was then spun down at 500g for 5min at 4°C, the supernatant was removed and the remaining organoid pellet was resuspended in previously pre-warmed TrypLE™ and incubated at 37°C for 45min to obtain single cells. Cold BM was added and the sample was placed on ice for 10min. It was then spun at 600g for 5min at 4°C, the resulting cell pellet was resuspended in 75µl of FACS buffer (PBS + 2% foetal calf serum + 1mM EDTA) with anti-OLFM4 antibody (1/75) and incubated for 30min on ice. The cells were then washed with 750µl of cold FACS buffer, spun at 600g for 5min at 4°C, the supernatant removed, and the cell pellet was resuspended in 75µl of FACS buffer containing a rat anti-Mouse IgG1 antibody conjugated with APC (1/20). This was then followed by a 15min incubation on ice. Finally the cells were washed with 750µl of cold FACS buffer, spun down at 600g for 5min at 4°C, the supernatant removed, and the cell pellet was resuspended in 500µl of FACS buffer ready for cell sorting. Fluorescent-activated cell sorting was carried out on the BD FACSAria™ Fusion (BD Biosciences) at the Advanced Centre for Cancer Cell Isolation and Flow Cytometry. Cells were sorted into OLFM4 negative and OLFM4 positive fractions, spun down at 600g for 5min at 4°C, resuspended in matrigel and cultures set up as before using IntestiCult™ as growth medium. Digested but unstained/unsorted cells were included as controls. Further data analysis was carried out using the FlowLogic software.

Chapter 3 Investigating the relationship between intestinal metaplasia and Lauren gastric cancer subtypes

3.1 Introduction

Using specimens from 1344 patients, Lauren published a seminal paper in 1965 describing two main histological types of gastric cancer (GC): the intestinal-type gastric adenocarcinoma (IGC) and the diffuse gastric adenocarcinoma (DGC) [31]. In the remaining cases the structure of the carcinoma was heterogeneous in composition and generally poorly differentiated. A model describing the histological progression to the intestinal type of GC, via a series of premalignant stages was described by Pelayo Correa in 1975 [64] and was further refined in 1992 [65]. Subsequent research has failed to address the possible role that these same lesions may play in the process of diffuse gastric carcinogenesis. Therefore this current study aimed to examine the association of intestinal metaplasia (IM) with these two distinct histological types of GC. Research into the physical location of these lesions in relation to tumour is necessary to gain greater understanding of how GC types arise and this could lead to improved patient stratification in clinic.

3.2 Hypothesis and aims

Hypothesis: “Intestinal metaplasia is associated with the diffuse subtype of gastric cancer”.
The main aims of this study were:

1. To investigate the prevalence of chronic gastritis and intestinal metaplasia adjacent and distant to Lauren histological gastric cancer types
2. To compare and contrast the clinicopathological features of intestinal and diffuse gastric cancer patients with and without adjacent intestinal metaplasia to tumour

3.3 Results

3.3.1 Description of the study cohort

Pathology reports based on pre- and post-surgery specimens of 250 patients in the MAUGIC cohort (§2.2.1) were examined to identify cases with chronic gastritis (CG) or IM located adjacent to tumour (Figures 3.1 and 3.2, Table 3.1). Details of the Lauren tumour type were extracted from the pathology report where available. Where information for tumour type was lacking from the pathology report, tumour blocks taken for research purposes were reviewed by the in-house research pathologist Dr Catherine Mitchell to establish GC type. Tissue sections from blocks taken at least 2cm away (defined as distant) from the tumour for research purposes were also characterised. A small subset of patients (n=21) were classified as adenocarcinomas

without determined Lauren classification (ANOS) by both the hospital pathologist and where tissue was available by the in-house research pathologist Dr Catherine Mitchell. Most of the cases characterised here have been previously described in [39].

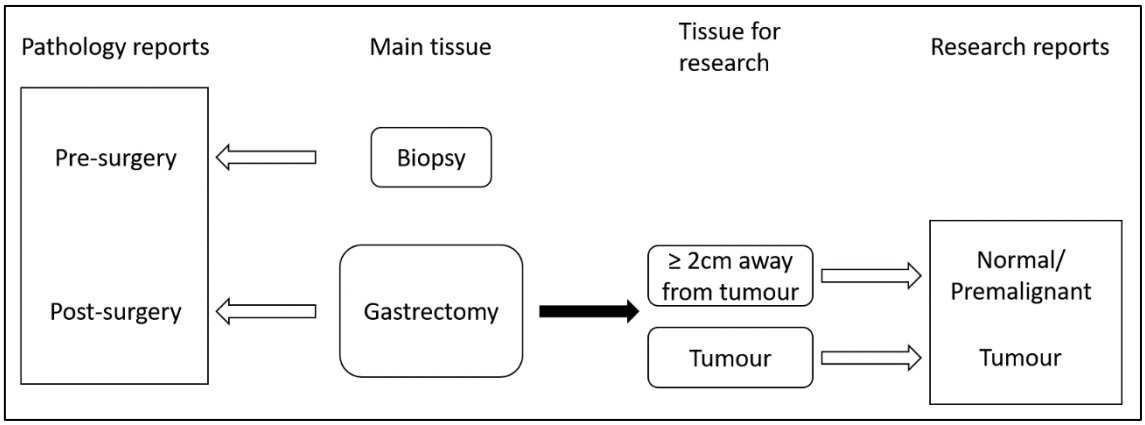


Figure 3.1 Diagram showing the sources of information available to characterise the histological association of premalignant lesions with gastric cancer Lauren subtypes
Pathology reports and where necessary research reports (tumour block) were used to subtype gastric cancers from the MAUGIC cohort (n=250 patients). The presence of premalignant lesions (chronic gastritis and intestinal metaplasia) adjacent to tumour was identified from pathology reports whereas their presence distant (at least 2cm away) from tumour was identified using research reports (in-house research pathologist Dr Catherine Mitchell).

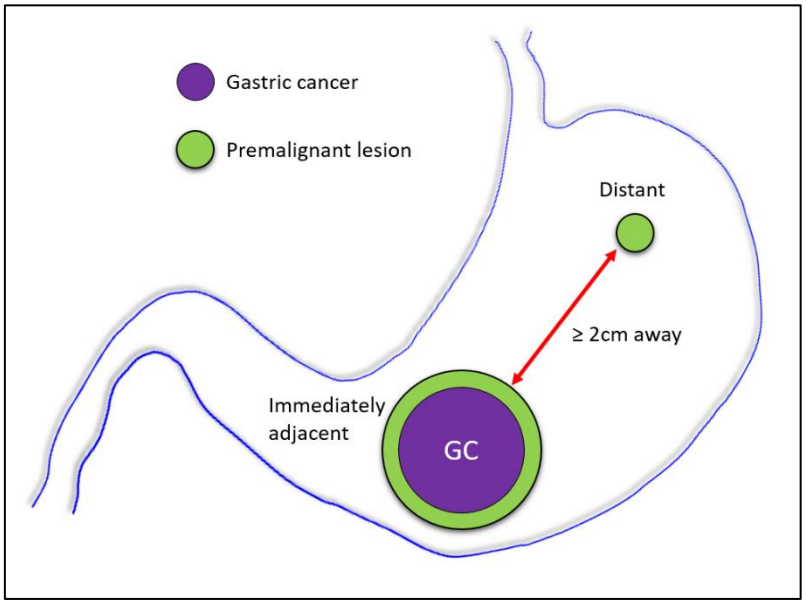


Figure 3.2 Schematic representation showing the presence of premalignant lesions adjacent and distant from gastric cancer
The presence of chronic gastritis and/or intestinal metaplasia adjacent and at least 2cm away from tumour (distant) was systematically documented using pre-/post-surgery and research reports.

Table 3.1 Description of patient cohort used in this study

Parameter	n
Gender	
Male	166
Female	84
Age	
Male	66 (25-95)[1]
Female	67 (20-86)[1]
Pathology	
Intestinal (IGC)	119
Diffuse (DGC)	74
Mixed (MGC)	36
Adenocarcinoma NOS[2] (AdNOS)	21
Tumour location (based on histology)	
Antrum (IGC/DGC/MGC/ AdNOS)	51 (28/11/8/4)
Body (IGC/DGC/MGC/ AdNOS)	130 (54/49/24/3)
GOJ/Cardia[3] (IGC/DGC/MGC/AdNOS)	69 (37/14/4/14)
Differentiation	
Undifferentiated	41
Poorly differentiated	135
Moderately differentiated	64
Well differentiated	6
Unspecified	4
T stage	
T0/Tis/Tx	1/4/2
T1	42
T2	48
T3	141
T4	9
Unspecified	3
Lymph node status	
N0/Nx	99/8
N1	89
N2	38
N3	13
Unspecified	3
AJCC stage	
0	5
I	60
II	65
III	93
IV	25
Unspecified	2

[1]Age median and range shown; [2]classified as adenocarcinomas without determined Lauren classification by both the hospital pathologist and the in-house research pathologist; [3]Included adenocarcinomas at the gastro-oesophageal junction with Siewert classification Type II (n=31) and Type III (n=38) (see section §2.3.1 and Figure 2.2).

Overall the majority of gastric cancers were found at the body of the stomach (130/250) (Table 3.1). With regards to the relationship between GC tumour type and location, DGC and MGC were mainly found at the body (49/74=66.2% and 24/36=66.7% respectively) whereas IGC showed relatively better distribution between antrum (28/119=23.5%), body (54/119=45.4%) and GOJ (34/119=31.1%). Interestingly AdNOS were mainly located at the GOJ (14/21=66.7%).

3.3.2 Prevalence of premalignant lesions adjacent and distant to tumour

Analysis of samples collected distant and adjacent to IGC and DGC tumours showed evidence of both CG and IM (Table 3.2, Figure 3.3). To determine whether CG and IM were significantly associated with the diffuse and intestinal types of GC, their frequency adjacent to tumour was compared to that distant from tumour. Although highly prevalent adjacent to both IGC and DGC tumours (>80%), CG was significantly more present distant to tumour (p=0.024 and p=0.0082 respectively, Chi-square test). In total more than 95% of GC patients had CG distant to tumour suggesting that pan-gastritis was highly prevalent in this cohort.

Although a trend was observed of IM adjacent to DGC tumours (>40% of cases), this did not reach significance when compared to distant IM (p=0.21, Chi-square test). In contrast, IM was found adjacent to the majority of IGC tumours (67%), compared to distant IM (p<0.0001, Chi-square test). The frequency of IM adjacent to IGC and MGC compared to DGC was significantly higher (p=0.0007 and p=0.0018 respectively, Fisher's exact test).

The same series of analyses were performed with "true gastric cancers" by excluding cases found at the GOJ (Table 3.3). Overall the results were similar with a couple of notable observations. The percentage of IGC cases with adjacent IM reached 88.5% suggesting an even tighter relationship between the presence of IM and the development of this Lauren GC type in the antrum and the body. Also IM distant to IGC was found in more than half of the cases and significantly more than in DGC and MGC cases (p=0.016 and p=0.031 respectively, Fisher's exact test), suggesting that IGC evolves in a permissive environment which is already highly enriched in IM.

Finally when analysed by location, both CG and IM adjacent to differing GC tumour type followed a similar distribution as described for the main tumour location (Table 3.1, Appendix C). CG and IM adjacent to both DGC and MGC were predominantly found in the body (for DGC, CG=73.2% and IM=71.4%; for MGC, CG=66.7% and IM=72.0%), whereas these two lesions adjacent to IGC followed a more equal distribution between antrum (CG=24.2% and IM=33.3%) and body

(CG=50.5% and IM=58.7%) but were marked by a reduced presence at the GOJ for IM lesions (CG=25.3% and IM=8.0%).

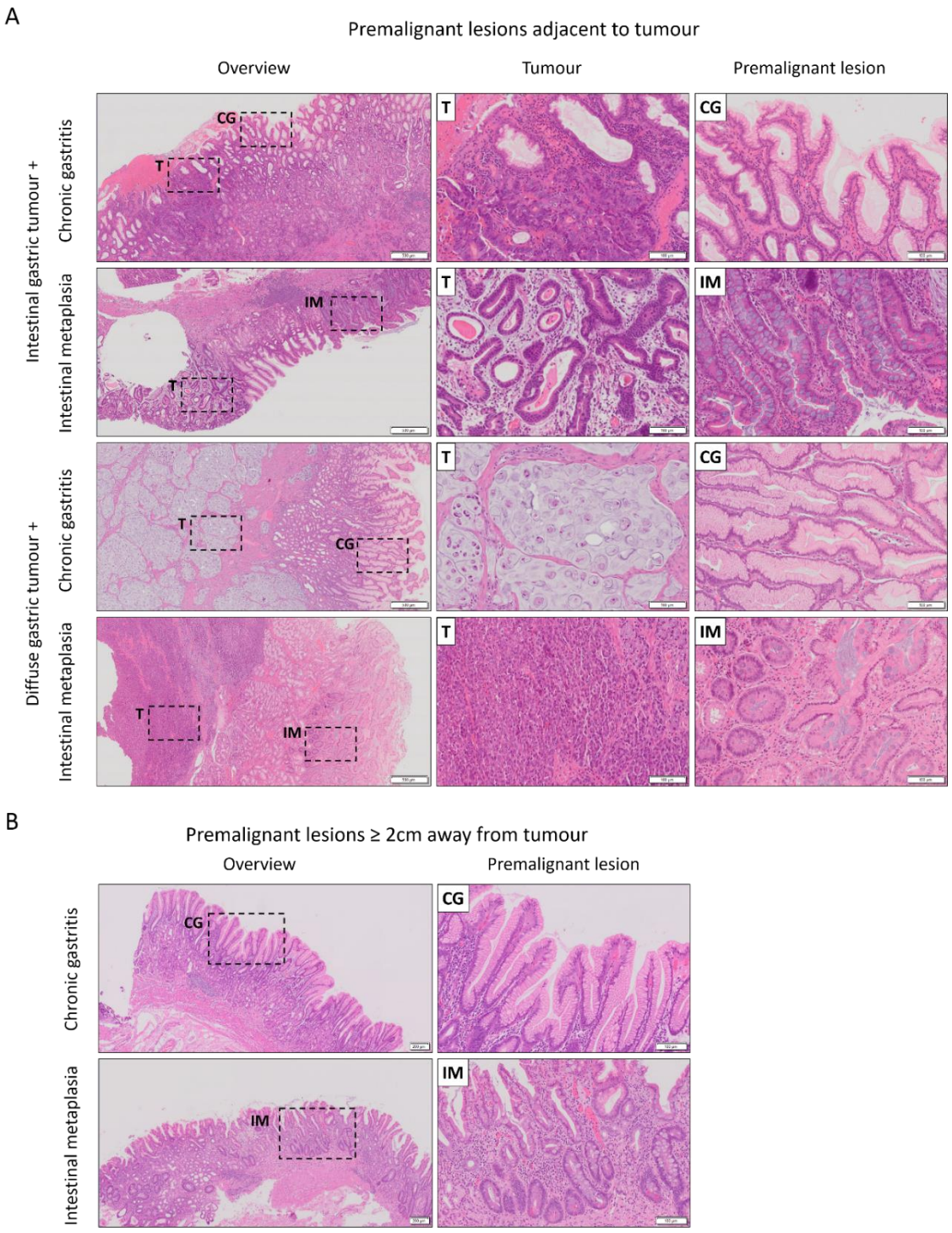


Figure 3.3 Chronic gastritis and intestinal metaplasia adjacent and distant (at least 2cm away) of Lauren gastric cancer types

In-house images showing A) overview and inset of tumour and adjacent premalignant lesions; scale bar for overview image: 500µm and for inset images: 100µm. B) overview and inset images of premalignant lesions at least 2cm away from tumour; scale bar for overview image: 200µm and for inset image: 100µm.

Table 3.2 Frequency of premalignant lesions adjacent and distant (at least ≥ 2cm away) from Lauren gastric cancer subtypes

Parameter	All GC n=250 (%)	Intestinal n=119 (%)	Diffuse n=74 (%)	Mixed n=36 (%)	AdNOS[1] n=21 (%)
Chronic gastritis					
Adjacent	197/233 (84.5)	95/112 (84.8)	56/69 (81.2)[a]	33/34 (97.1)[a]	13/18 (72.2)
Distant	192/201 (95.5)	99/105 (94.3)	55/57 (96.5)	33/34 (97.1)	5/5 (100.0)
p value[2]	**0.0002**	**0.024**	**0.0082**	>0.99	0.18
Intestinal metaplasia					
Adjacent	130/233 (55.8)	75/112 (67.0)[b]	28/69 (40.6)[b,c]	25/34 (73.5)[c]	2/18 (11.1)
Distant	68/201 (33.8)	41/105 (39.0)	17/57 (29.8)	10/34 (29.4)	0/5 (0.0)
p value[2]	**<0.0001**	**<0.0001**	0.21	**0.0003**	0.44
Unreported	17/49	7/14	5/17	2/2	3/16

[1]Adenocarcinoma without determined Lauren classification; [2]Chi-square test of independence. Fisher's exact test used to compare premalignant lesion frequency between Lauren GC subtypes: [a]Diffuse versus Mixed GC p=0.032; [b]Intestinal versus Diffuse GC p=0.0007; [c]Diffuse versus Mixed GC p=0.0018.

Table 3.3 Frequency of premalignant lesions adjacent and distant (at least ≥ 2cm away) from Lauren gastric cancer subtypes focusing on "true gastric cancers" only (GOJ excluded)

Parameter	All GC n=181 (%)	Intestinal n=82 (%)	Diffuse n=60 (%)	Mixed n=32 (%)	AdNOS[1] n=7 (%)
Chronic gastritis					
Adjacent	154/173 (89.0)	71/78 (91.0)	49/59 (83.1)	29/30 (96.7)	5/6 (83.3)
Distant	149/155 (96.1)	71/74 (95.9)	46/48 (95.8)	30/31 (96.8)	2/2 (100.0)
p value[2]	**0.015**	0.22	**0.037**	0.98	0.54
Intestinal metaplasia					
Adjacent	118/173 (68.2)	69/78 (88.5)[a]	24/59 (40.7)[a,b]	24/30 (80.0)[b]	1/6 (16.7)
Distant	64/155 (41.3)	40/74 (54.1)[c,d]	15/48 (31.3)[c]	9/30 (30.0)[d]	0/2 (0.0)
p value[2]	**<0.0001**	**<0.0001**	0.31	**<0.0001**	0.54
Unreported	8/26	4/8	1/12	2/2	1/5

[1]Adenocarcinoma without determined Lauren classification; [2]Chi-square test of independence. Fisher's exact test used to compare premalignant lesion frequency between Lauren GC subtypes: [a]Intestinal versus Diffuse GC p<0.0001; [b]Diffuse versus Mixed GC p=0.0006; [c]Intestinal versus Diffuse GC p=0.016;[d]Intestinal versus Mixed GC p=0.031.

3.3.3 Clinico-epidemiological details of gastric cancer patients without and with adjacent intestinal metaplasia

Clinico-epidemiological details of patients without and with IM adjacent to tumour for both intestinal and diffuse subtypes of GC (IGC-IM/IGC+IM and DGC-IM/DGC+IM) were collated to identify potential associations. Four key risk factors previously shown to be associated with IM and GC were studied including age, gender, smoking status (former and current) and *H. pylori* status (determined through histology and serology) (§1.1.2, §1.3.4, [169]). For both IGC and DGC patients, no significant difference was observed in gender nor in smoking status between patients without and with IM adjacent to tumour (Figure 3.4). However both IGC and DGC patients with adjacent IM were older in age (median age for IGC-IM versus IGC+IM: 61yrs vs 67yrs with $p=0.019$ and for DGC-IM vs DGC+IM: 54yrs vs 73yrs with $p<0.0001$, Mann-Whitney test). DGC+IM patients also showed a strong trend ($p=0.059$, Fisher's exact test) associated with *H. pylori* infection compared to DGC-IM patients which was absent when IGC+IM patients were compared to IGC-IM patients.

3.3.4 Pathology details of gastric cancer patients without and with adjacent intestinal metaplasia

Pathology details of GC patients including tumour location, T stage, N stage and AJCC stage were analysed to identify potential significant associations (Figure 3.5). IGC-IM tumours occurred predominantly in the GOJ whereas IGC+IM tumours were mainly found in the body and the antrum ($p<0.0001$, Chi-square test). More than 70% of IGC-IM tumours were of a N1 stage whereas more than 50% of IGC+IM tumours had no nodal involvement (N0) ($p=0.0008$, Chi-square test). T stage and AJCC stage did not differ between IGC-IM and IGC+IM patients. Interestingly DGC-IM and DGC+IM patients did not show any difference in tumour location, T stage, N stage and AJCC stage.

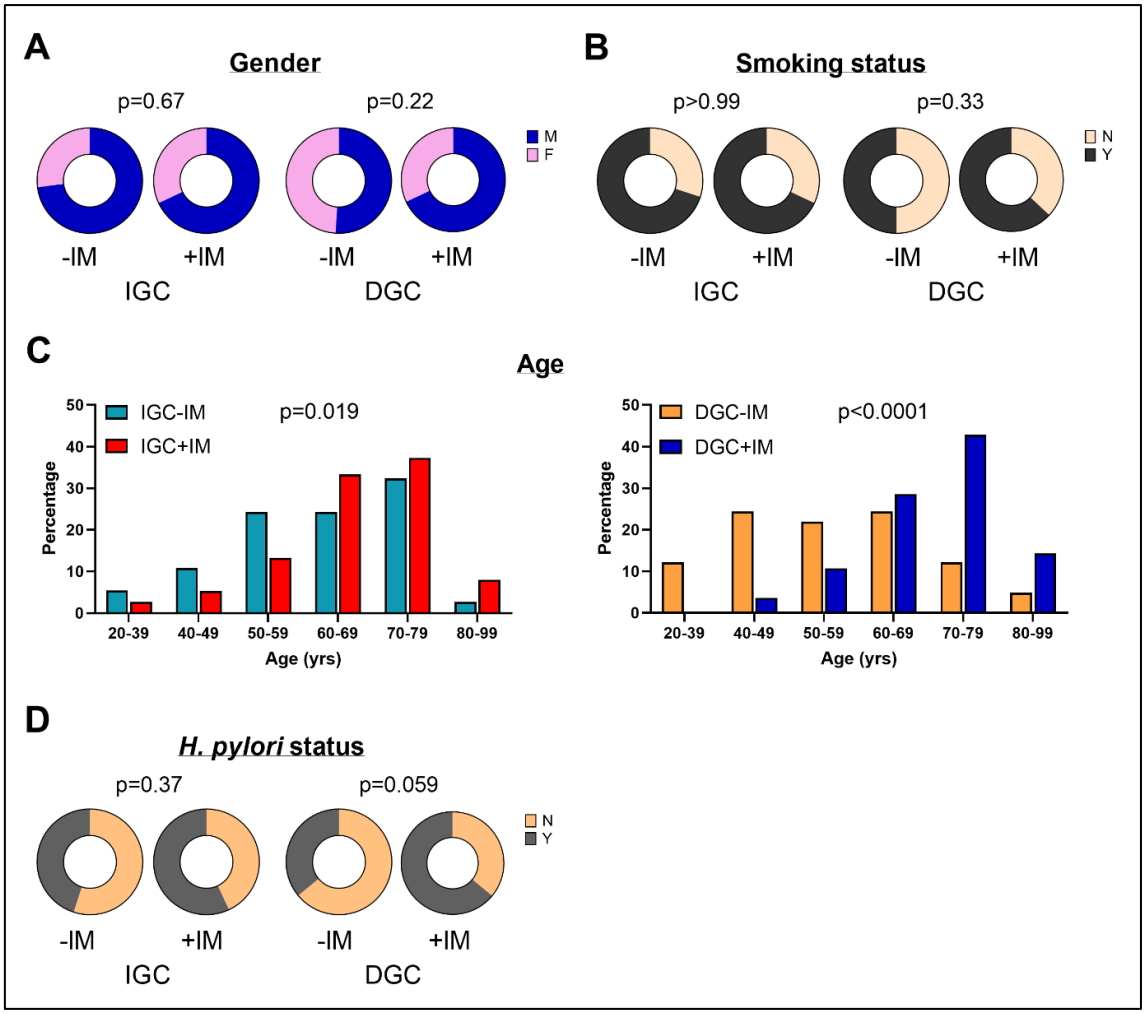


Figure 3.4 Clinico-epidemiological details of patients with intestinal and diffuse gastric cancer without (-IM) and with (+IM) intestinal metaplasia adjacent to tumour

A: gender distribution (intestinal GC: IGC-IM [n=37] and IGC+IM [n=75], and diffuse GC: DGC-IM [n=41] and DGC+IM [n=28]); B: smoking status of IGC-IM [n=37] and IGC+IM [n=73], and DGC-IM [n=40] and DGC+IM [n=20] patients; C: age distribution of IGC-IM [n=37] and IGC+IM [n=75], and DGC-IM [n=41] and DGC+IM [n=28] patients; D: *H. pylori* status of IGC-IM [n=29] and IGC+IM [n=67], and DGC-IM [n=33] and DGC+IM [n=22] patients. For A, B and D, statistical analysis carried out using Fisher's exact test and for C using Mann-Whitney test on continuous age data.

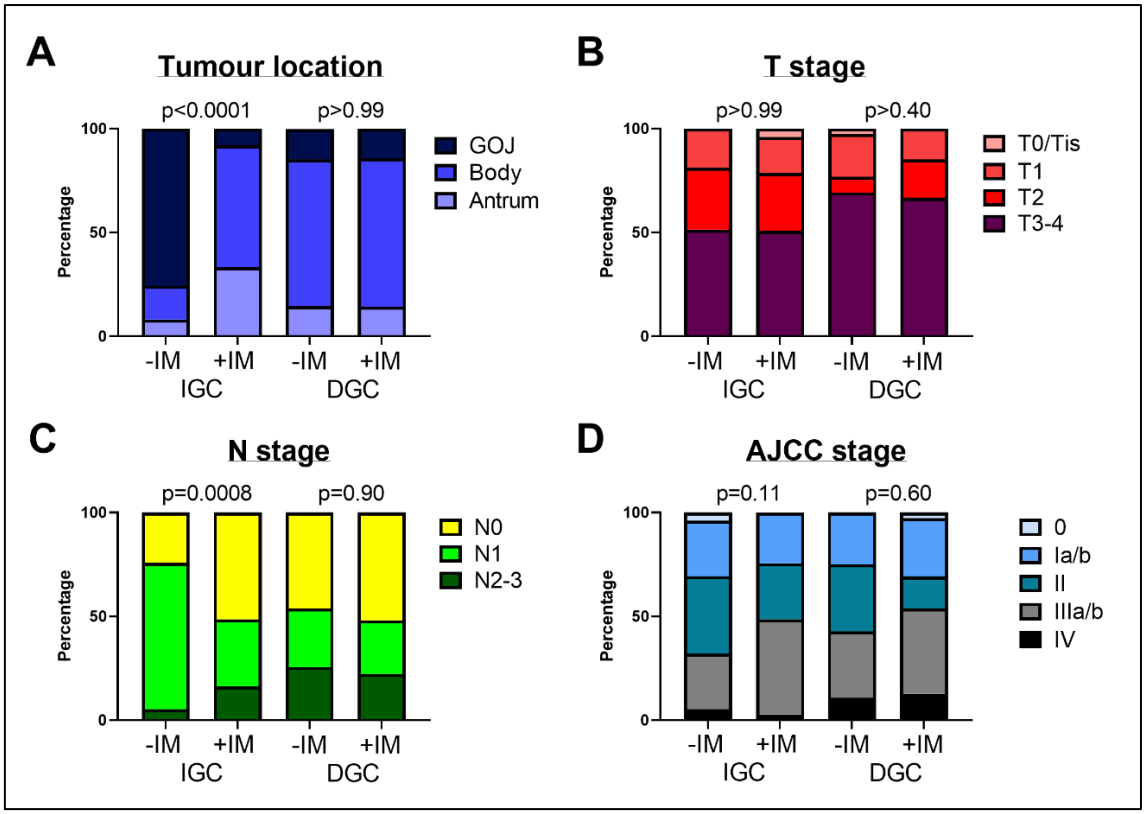


Figure 3.5 Pathology details of patients with intestinal and diffuse gastric cancer without (-IM) and with (+IM) intestinal metaplasia adjacent to tumour

A: Tumour location of gastric cancer (intestinal GC: IGC-IM [n=37] and IGC+IM [n=75], and diffuse GC: DGC-IM [n=41] and DGC+IM [n=28]); B: T stage of IGC-IM [n=37] and IGC+IM [n=75], and DGC-IM [n=39] and DGC+IM [n=27] patients; C: N stage of IGC-IM [n=37] and IGC+IM [n=74], and DGC-IM [n=39] and DGC+IM [n=27] patients; D: AJCC stage of IGC-IM [n=37] and IGC+IM [n=75], and DGC-IM [n=39] and DGC+IM [n=28] patients. For all statistical analyses a Chi-square test was used.

3.4 Summary and discussion

The following is a summary of the main outcomes of this study.

1. A trend was observed between IM and diffuse GC but this did not reach significance
2. IM was shown to be histologically associated with both intestinal and mixed GC
3. Chronic gastritis was present distant from tumour in over 90% of GC patients
4. Intestinal and diffuse GC patients with IM adjacent to tumour were older in age
5. Diffuse GC patients with adjacent IM showed an association with *H. pylori* infection that did not reach significance and intestinal GC patients with adjacent IM had a lower N stage
6. IM was less likely to be found associated with intestinal GC at the GOJ (Siewert type II/III)

3.4.1 Discussion

This study described the prevalence of CG and IM in the Australian based MAUGIC cohort. Clinicopathological details of patients with either Lauren GC subtype without and with IM adjacent to tumour were used to identify associations between tumour type, adjacent IM and patient characteristics.

Compared to Lauren's original observation in 1965, the current study showed a higher prevalence of CG in the mucosa surrounding DGC tumours but a very similar prevalence around IGC tumours: 81.2% (current study) vs 45% (Lauren) and 84.8% (current study) vs 88% (Lauren) respectively [31]. It is difficult to comment on why there is such a large difference in the percentage of DGC tumours with surrounding CG between the two studies, although it may be due to differences in cohort size (current study = 111 DGC patients, Lauren study = 271 DGC patients) and origin (multi-ethnic cohort from Australia versus Finland).

The current study showed a slightly lower prevalence of IM in the mucosa surrounding both DGC and IGC tumours compared to the Lauren [34] and the Matsukura [398] studies, with DGC showing 40.6% (current study) vs 55% (Lauren) vs 50% (Matsukura) and IGC 67.0% (current study) vs 91% (Lauren) vs 95% (Matsukura) respectively. In part this may be explained by Lauren's sub-grouping of the presence of IM into three groups: scanty, fairly profuse and profuse. As there are currently no guidelines in reporting the presence of IM adjacent to tumour in post-surgery pathology reports, it is most likely that tumour blocks in the current study with only very little IM were not regularly reported. The Matsukura study looked at the surrounding mucosa of minute GC (less than 5mm in largest diameter) and investigated a relatively small number of cases: 20 IGC and 6 DGC patients [398]. Interestingly of the patients positive for IM,

16/19 and 2/3 with minute IGC and DGC respectively were surrounded by the incomplete subtype of IM suggesting that this subtype most likely progresses to cancer, irrespective of Lauren subtype.

It has been suggested that IM develops as a protective lesion over time due to the cumulative effects of various "irritants" such as bile acid, *H. pylori* infection, exposure to N-nitroso–containing compounds and chronic inflammation by-products such as reactive oxygen and nitrogen free species [142, 150, 399]. It is likely that IM occurs more frequently with increasing age independently of intestinal or diffuse tumour development and that it acts as an indicator of local cellular and molecular damage [169]. However the observed trend of IM adjacent to DGC suggests that the origins of DGC tumours may follow at least two putative paths. One path may involve IM as a precancerous lesion and the other may be independent of IM. The high prevalence of IM adjacent to both IGC and MGC suggests that this premalignant lesion also plays a key role in intestinal/mixed gastric carcinogenesis.

IM adjacent to DGC and IGC occurred with highest prevalence in older patients, and showed similar patterns with respect to gender, smoking and *H. pylori* status. As DGC is known to occur generally in younger patients [36, 38], the substantial difference in median age observed between DGC-IM and DGC+IM patients (54yrs and 73yrs respectively) adds particular significance to this finding. When compared to a previous study that included a large number of DGC cases in a Taiwanese population (n=1000, [38]) and separated patients' age into two groups of <65yrs (56.9%) and ≥65yrs (43.1%), the current study's overall age findings were similar (<65yrs: 53.6% and ≥65yrs: 46.4%) but differed substantially when separated into DGC-IM (<65yrs: 70.7% and ≥65yrs: 29.3%) and DGC+IM (<65yrs: 28.6% and ≥65yrs: 71.4%) subgroups. The additional trend observed in DGC+IM cases with *H. pylori* infection further supports the potential of two separate paths to diffuse gastric carcinogenesis, one associated with *H. pylori* infection, IM and older age and the other independent of *H. pylori* and IM and occurring at younger age.

The analysis of clinicopathological details of IGC patients with and without adjacent IM showed that IGC-IM tumours were generally found in the gastro-oesophageal junction whereas IGC+IM tumours were mainly found in the body and the antrum suggesting that the process of carcinogenesis involved in the GOJ area may differ from that in the rest of the stomach. It is possible that IGC-IM tumours do not faithfully follow the Correa model and that *H. pylori* infection may not be the initiating step. Indeed previous studies in cardia GC, the area of the stomach near the oesophagus, have shown no or even a negative association with *H. pylori*

infection in Western countries [77, 78, 400]. In contrast, studies based on Eastern Asian populations including China and South Korea have shown a positive association between *H. pylori* infection and cardia GC [79, 401, 402]. The importance of geographic location and GC prevalence (low vs high) was further confirmed by a systematic review and meta-analysis of published studies addressing the association of *H. pylori* infection with cardia and non-cardia GC [403] which showed a strong positive association with cardia GC only in high risk settings (RR = 1.98, 95% CI 1.38–2.83; I^2 = 18.4%; data from China, Japan and South Korea included) but none in low risk settings (RR = 0.78, 95% CI 0.63–0.97; I^2 = 11.6%; including data from Australia). In contrast a strong positive *H. pylori* association with non-cardia GC was seen in both low and high incidence countries (RR = 2.56, 95% CI 1.99–3.29; I^2 = 46.6% and RR = 3.02, 95% CI 1.92–4.74; I^2 = 90.7%, respectively). For a subset of IGC at the GOJ/cardia area, it is possible that other processes such as gastro-oesophageal reflux may play a key additional role in the process of carcinogenesis, similar to oesophageal adenocarcinogenesis which has also been shown to be negatively associated with *H. pylori* infection [404].

The presence of IM adjacent to IGC was shown to be associated with a lower N stage in these patients. More than 50% of IGC+IM patients were N0 whereas more than 70% of IGC-IM patients had N1 stage disease. The extent of nodal resection is at the discretion of the surgeon and has been shown to be associated with patient survival in patients with T1 tumours [405]. However, other than differences in aetiology and location, the difference in N stage suggests that the presence of IM may play a role in tissue stability and act as a brake to tumour progression/metastasis towards the lymph nodes. Alternatively IM related IGC may be slower growing or were by chance discovered earlier.

Overall the findings of this study suggest that the process of gastric carcinogenesis towards each of the GC histological types may be heterogeneous. It is likely affected by a multitude of factors including age, gender, infection with *H. pylori*, host genetic factors and lifestyle choices such as smoking and diet (summarised in §1.1.2). The multiplicity of pathways in gastric carcinogenesis was clearly also suggested by the TCGA findings which classified GC into four molecular subtypes (§1.1.4, [42]). Approximately 73% of the GS molecular subtype were DGC tumours and the remaining DGC tumours consisted of the EBV, MSI and CIN subtypes. IGC tumours were mainly of the EBV, MSI and CIN molecular subtypes but also of the GS subtype. Interestingly CIN tumours occurred at a higher frequency in the GOJ/cardia area which correlates well with the high prevalence of IGC tumours without adjacent IM observed in the current study.

3.4.2 Study limitations

This study consisted of a comprehensive multiple pathological review of 250 GC cases. It included a systematic analysis of all available data, with particular emphasis on the relationship between IM and diffuse GC. However the study did have a small number of potential limitations. First it was carried out retrospectively and thus may have suffered from selection bias and information bias. Second the number of cases characterised was smaller compared to other studies that had access to clinicopathological details of >1000 patients [31, 38]. Third the description of CG and IM adjacent to GC was up to the discretion of the hospital pathologist reporting, thus not systematic and could result in an underestimation of the true frequency of premalignant lesions adjacent to tumour. Finally the tissue taken at least 2cm away from tumour for research purposes was randomly selected, thus the data obtained was possibly subject to sampling error and may not have accurately represented the prevalence of CG and IM distant to tumour.

Overall this study suggested a possible histological association between IM and the diffuse subtype of GC which supports the findings of previous studies into the relationship between *H. pylori* infection, atrophic gastritis and intestinal metaplasia with this subtype of GC [77-80, 107]. However the relatively low number of cases investigated does not allow a definitive conclusion. The current study also raises new questions with regards to the process of gastric carcinogenesis itself. Further insight into the four histological subgroups of GC described in this study (IGC-IM/+IM and DGC-/+IM) could be gained from molecular profiling these tumours and their adjacent premalignant/IM lesions where present.

Chapter 4 Characterising the gene expression profile of tissues associated with gastric carcinogenesis

4.1 Introduction

Several studies have investigated the molecular process of carcinogenesis by characterising the relationship between premalignant and malignant gastric lesions and between intestinal metaplasia subtypes associated with varying risk of progression to cancer [127, 388, 406, 407]. However, to date, no study has concurrently investigated the relationship between premalignant lesions with gastric cancer, the differences between intestinal metaplasia in patients with and without gastric cancer and between intestinal metaplasia subtypes using a histo-molecular approach with the ultimate aim of gaining further insight into gastric carcinogenesis. The overall objective of this chapter was to identify genes and pathways associated with this process by investigating all three cellular compartments: the epithelium, the stroma and the immune infiltrate.

4.2 Aims

The aim of this study was to perform an *in silico* analysis of existing expression array data representing multiple stages of the Correa cascade to discover genes and pathways involved in gastric carcinogenesis. Three main approaches were used: 1) differential gene expression followed by pathway over-representation analysis, 2) single sample gene set enrichment analysis and 3) hierarchical clustering of samples into bioinformatically defined IM subtypes to molecularly characterise gastric carcinogenesis. More specifically this study's aims were:

1. To characterise the gene expression profile of intestinal metaplasia and identify specific immune cell subsets enriched in chronic gastritis and intestinal metaplasia
2. To identify shared differentially expressed genes between premalignant lesions (chronic gastritis/intestinal metaplasia) and gastric cancer subtypes (intestinal/diffuse)
3. To characterise differences in gene expression profiles of macro-dissected intestinal metaplasia in patients with and without concurrent GC
4. To subtype intestinal metaplasia using bioinformatics and identify differences between complete and incomplete intestinal metaplasia with regards to epithelial and immune infiltrate

4.3 Results

4.3.1 Samples profiled using Affymetrix microarrays

To address these aims Affymetrix microarray expression data previously generated in our laboratory derived from the MAUGIC, the IM-GC and the normal gastric patient cohorts was utilised (§2.2.1, GEO accession: GSE51105, [259]). Gastric cancer (GC) and premalignant samples were selected from the MAUGIC cohort and consisted of homogenised gastric tumour or matched non-tumour tissue collected at the time of gastrectomy. Data was available from 50 intestinal gastric cancer (IGC), 38 diffuse gastric cancer (DGC) and 10 mixed gastric cancer (MGC) patients. In addition 22 matched chronic gastritis (CG+GC) and 23 matched intestinal metaplasia (IM+GC) tissues taken at least 2cm away from tumour mass were profiled. Clinical data for these patients is summarised in Table 4.1. Four of the IM+GC tissues were macro-dissected and the extracted RNA was rerun (rIM+GC) to allow for a technical comparison with the IM-GC cohort.

The second cohort comprised samples from 14 IM-GC patients. These samples were prepared by macro-dissection to minimise stromal contamination and enrich for regions of IM epithelium before RNA extraction (§2.2.2). Finally Affymetrix data available from homogenised normal gastric biopsies (NN; n=7) was used as control (§2.2.1). Clinical data for these patients is given in Table 4.1.

4.3.2 Intestinal metaplasia characterised using differential gene expression and gene set over-representation analysis

To characterise the gene expression and pathway profile of intestinal metaplasia samples derived from patients with concurrent GC (IM+GC), differential gene expression and gene set over-representation with GO Biological Processes and GO Cellular Component were carried out using the normal gastric samples (NN) as a comparator. Probes with log2 normalised expression of less than 5 were excluded as this was assumed to be the lower limit of detection for the Affymetrix Human Genome U133 plus GeneChip™ arrays used (and thus potentially background noise). In total 159 genes were overexpressed in the NN samples and 596 genes in the IM+GC samples. The top 10 genes overexpressed in the NN samples included, as expected, stomach related genes such as *GAST* which codes for gastrin (Table 4.2). Gastrin is produced by neuroendocrine G cells in the antrum and plays a crucial role in gastric acid secretion by parietal cells. By contrast the IM+GC samples were characterised by highly overexpressed genes associated not only with the intestine such as *DEFA5* as expressed by Paneth cells but also with inflammation such as *S100A8* (neutrophils and macrophages).

Table 4.1 Description of cohorts with Affymetrix microarray data (HG-U133 Plus 2.0) used in this study

Parameters	MAUGIC (n=99)	IM-GC[1] (n=14)	Normal (n=7)
Gender			
Male	66	12	3
Female	32	2	2
Unspecified	0	0	2
Age			
Male	66 (32-85)[2]	67 (32-84)[2]	72 (62-74)[2]
Female	69.5 (33-86)[2]	80.5 (79-82)[2]	58.5 (53-64)[2]
Pathology			
Intestinal	50	-	-
Diffuse	38	-	-
Mixed	10	-	-
Tumour location			
Antrum	22		
Body	58		
GOJ	18		-
Differentiation			
Undifferentiated	28	-	-
Poorly differentiated	36	-	-
Moderately differentiated	30	-	-
Well differentiated	3	-	-
Carcinoma *in situ*	1	-	-
T stage			
Tis	1	-	-
T1	7	-	-
T2	22	-	-
T3	67	-	-
T4	1	-	-
Lymph node status			
N0	31	-	-
N1	35	-	-
N2	25	-	-
N3	7	-	-
AJCC stage			
0	1	-	-
IA	2	-	-
IB	14	-	-
II	26	-	-
IIIA	24	-	-
IIIB	20	-	-
IV	10	-	-
Premalignant tissue[3]			
Chronic gastritis (CG+GC)	22	-	-
Intestinal metaplasia (IM+GC)[4]	23	14	-

[1]RNA extracted from macro-dissected intestinal metaplastic (IM) epithelial tissue; [2]Age median (range) [3]Matched premalignant tissue in MAUGIC cohort obtained at least 2cm away from tumour; [4]Four samples were rerun following macro-dissection of IM epithelial tissue (rIM+GC).

Table 4.2 Top 10 differentially expressed genes ranked by log2 fold change between normal (NN) and intestinal metaplasia (IM+GC) tissue

Symbol	Function	logFC	AveExpr	adj.P.Val
High in NN				
GAST	Gastric acid secretion	3.64	8.10	6.50E-03
PSD3	Guanine nucleotide exchange factor	2.67	6.66	6.77E-08
IL1R2	Inhibits IL1α/β activity	2.54	8.25	4.23E-04
UPK1B	Cell development and growth	2.41	7.28	3.54E-04
VSIG1	Maintenance of epithelium	2.41	7.76	2.87E-03
MUCL3	Cell growth	2.22	10.46	6.10E-03
CAPN9	Cysteine protease	2.19	7.86	1.79E-03
FA2H	Sphingolipid metabolism	2.18	6.24	2.26E-06
GALNT5	Glycotransferase	2.14	6.58	2.51E-06
ARHGEF28	Guanine nucleotide exchange factor	2.08	5.44	5.83E-05
High in IM+GC				
RGS1	Signal transduction	-5.28	7.98	2.67E-08
GREM1	BMP antagonist	-4.97	7.91	5.36E-09
SFRP2	Cell growth/differentiation	-4.85	7.57	1.01E-08
CYR61	Cell proliferation/adhesion	-4.58	8.53	1.65E-10
S100A8	Immune response	-4.11	7.77	1.25E-05
OGN	Bone formation	-4.11	7.05	1.96E-07
DEFA5	Antimicrobial activity (Paneth cells)	-3.85	8.49	1.22E-02
C7	Complement pathway	-3.83	7.75	1.01E-07
REG3A	Antimicrobial activity	-3.77	10.72	1.74E-03
GPNMB	Bone formation and cell adhesion	-3.76	8.49	7.76E-09

Affymetrix array data obtained from NN (n=7) and IM+GC (n=23) samples, normalised using the RMA algorithm and differential gene expression carried out using the limma package in R; differentially expressed genes were defined as log2 fold change >1.2 with adjusted p<0.05 using the Benjamini-Hochberg method for multiple test correction; genes with log2 normalised average expression of less than 5 were excluded.

Gene set over-representation analysis with GO Biological Process confirmed this initial observation as the list of over-represented GO terms (564 GO terms with adjusted p<0.05, §2.4.2) was mainly populated by immune related processes including both higher and lower level terms such as Immune system process (GO:0002376, adj. p=1.31E-42), Immune response (GO:0006955, adj. p= 2.11E-38) but also T cell activation (GO:0042110, adj. p=2.81E-16) (Figure 4.1). Over-representation analysis using GO Cellular Component (67 GO terms with adj. p<0.05) showed that IM+GC samples were particularly rich in extracellular matrix and other extracellular related activities including Collagen-containing extracellular matrix (GO:0062023, adj. p= 1.73E-33) and Extracellular region (GO:0005576, adj. p= 1.73E-24) (Figure 4.1).

Overall, this initial analysis comparing normal samples with intestinal metaplasia samples from GC patients showed that the latter were characterised not only by an intestinalisation of the gastric lining but also by an inflammation rich environment.

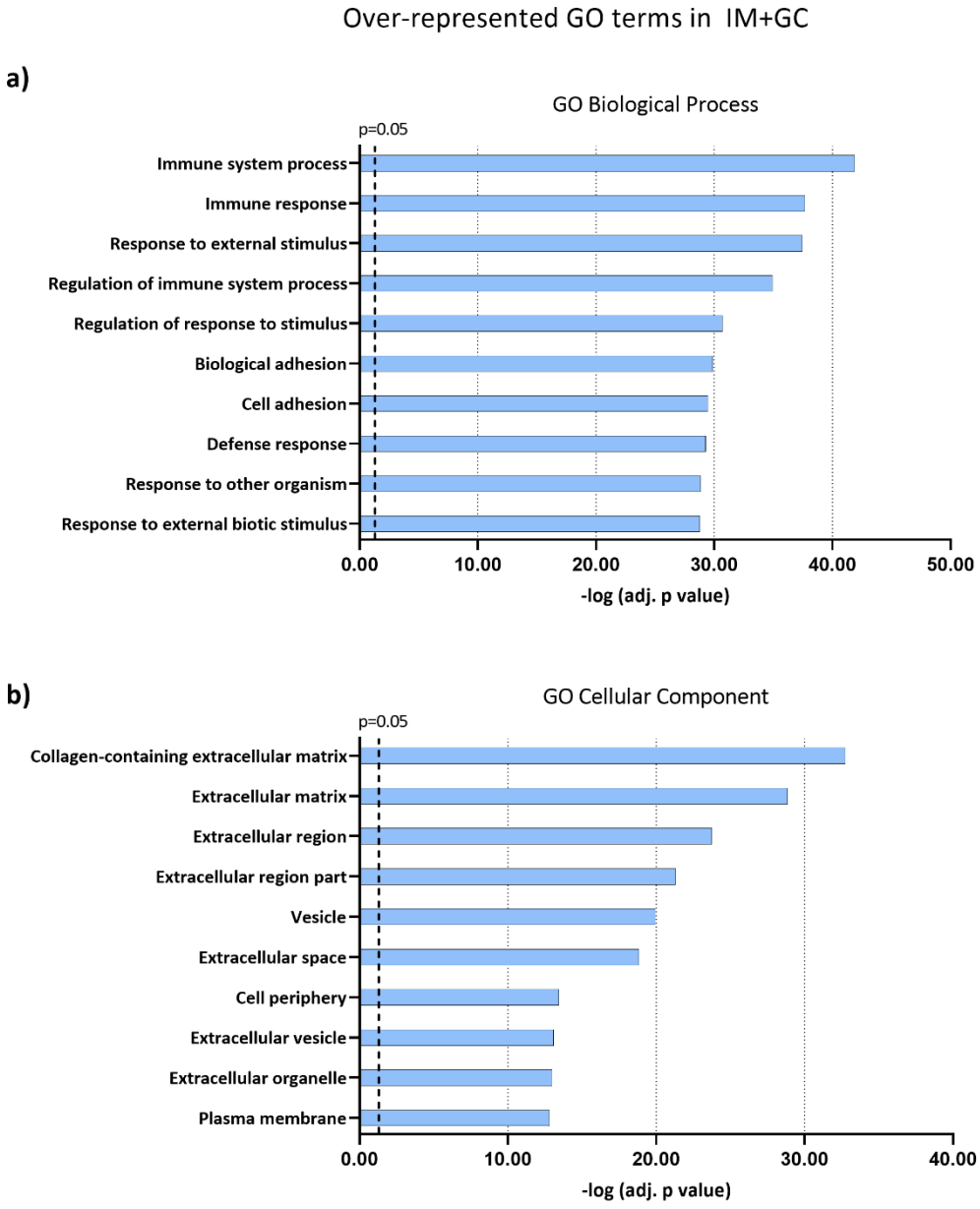


Figure 4.1 Top 10 over-represented GO terms for (a) Biological Process and (b) Cellular Component in intestinal metaplasia (IM+GC; n=23) samples compared to normal gastric (NN; n=7) samples

The g:Profiler tool was used to carry out gene set over-representation analysis from the differentially expressed genes in IM+GC samples compared to NN samples. All adjusted p values were obtained using the g:SCS method for multiple testing correction. A p value of 0.05 is equivalent to a negative log10 value of 1.30 (as shown by thick dashed line).

4.3.3 Characterising the immune landscape in chronic gastritis and intestinal metaplasia using CIBERSORT

Having established that intestinal metaplasia is likely characterised by a highly inflammatory environment, the relative abundance of immune cells in chronic gastritis and intestinal metaplasia was further investigated using the CG+GC (n=22) and IM+GC samples (n=23) using the CIBERSORT online tool (https://cibersort.stanford.edu/index.php). The main aim of this analysis was to identify the prominent immune subsets and their quantitative distribution in chronic gastritis and intestinal metaplasia and determine whether there are any fundamental differences between these two histologically different tissue types. The advantage of CIBERSORT is that it allows the characterisation of cell composition of complex tissues from their gene expression profiles ([389], §2.4.4).

Innate immune cell populations were mainly comprised of macrophages and mast cells (resting/activated) in both CG+GC and IM+GC samples (Figure 4.2). Interestingly M2 macrophages made up the majority of the macrophage population in both tissue types. Minor innate immune cell populations included neutrophils, NK cells (resting/activated), monocytes, eosinophils and dendritic cells (resting/activated). Although only present in low abundance, resting dendritic cells were significantly more present in IM+GC than CG+GC samples ($p=0.0033$, Mann-Whitney test).

Adaptive immune cell populations consisted mainly of plasma cells, resting CD4 memory T cells and CD8 T cells in both tissue types. Minor adaptive immune cell populations included B cells (naïve/memory), CD4 T cells (naïve/activated memory), follicular helper T cells, regulatory T cells and γδ T cells. For all adaptive immune cell subsets no statistical differences were observed between CG+GC and IM+GC samples.

Overall, the use of the established CIBERSORT method for determining immune cell composition from gene expression profiles [389, 408] showed that M2 macrophages, mast cells, plasma cells (largest population), resting CD4 memory T cells and CD8 T cells are the major immune cell subsets present in both CG+GC and IM+GC. It also showed that these two tissue types have very similar immune cell profiles.

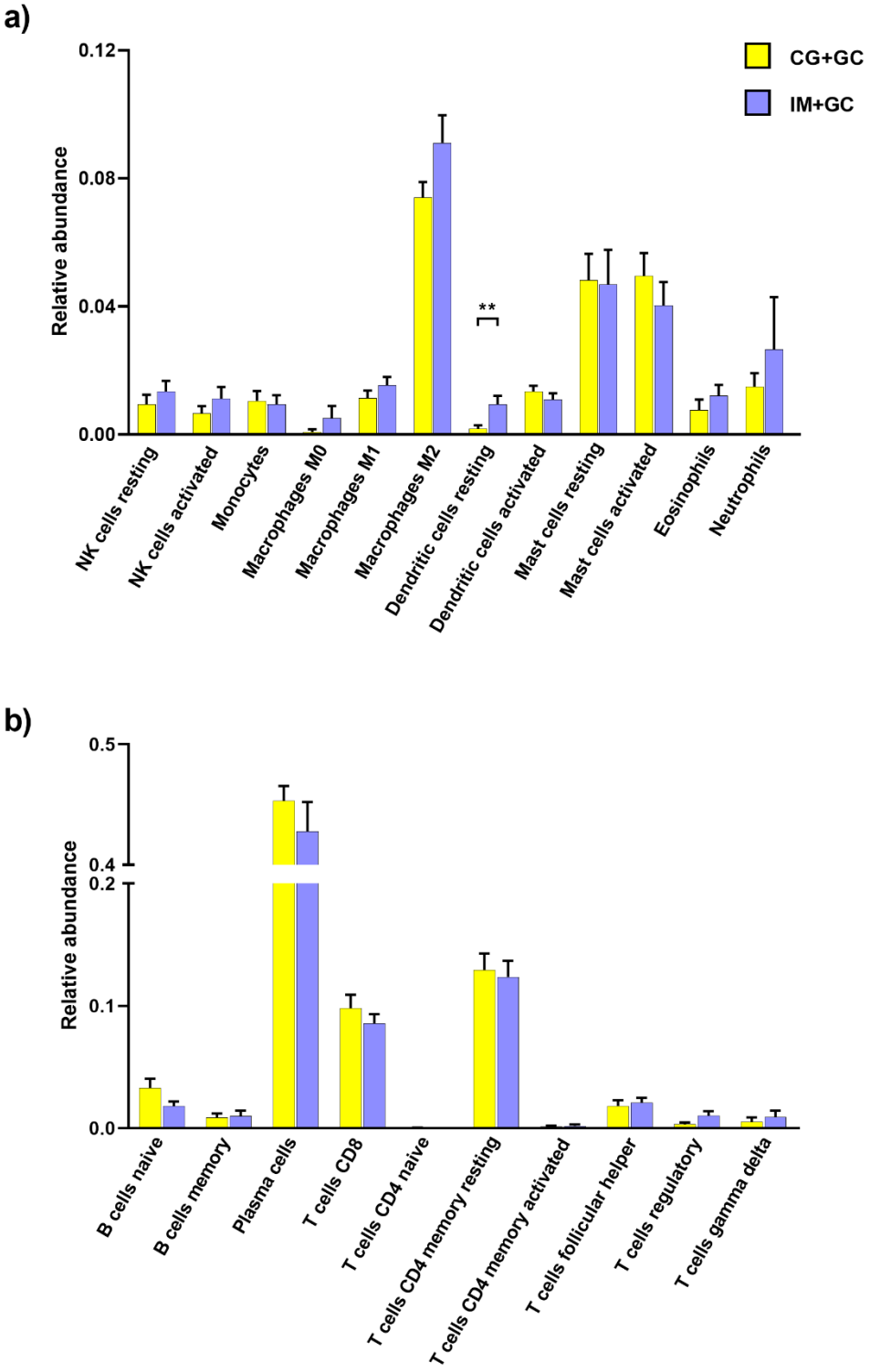


Figure 4.2 Relative abundance of immune cells in chronic gastritis (CG+GC) and intestinal metaplasia (IM+GC) determined using CIBERSORT

a) Mean relative abundance of innate immune cell subsets and b) mean relative abundance of adaptive immune cell subsets in CG+GC (n=22) and IM+GC (n=23) samples. Data presented as mean + SEM. Statistical analysis done using Mann Whitney test. ** is equal to $p<0.01$.

4.3.4 Identifying shared differentially expressed genes between premalignant and malignant lesions

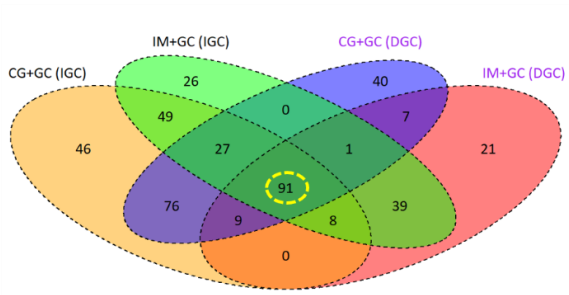
To investigate further the possible role of chronic gastritis and intestinal metaplasia in both intestinal and diffuse gastric carcinogenesis, a four way differential gene expression analysis was carried out (CG+GC vs IGC, IM+GC vs IGC, CG+GC vs DGC and IM+GC vs DGC). The aim of this analysis was to identify differentially expressed genes common in both premalignant lesions and those common in both subtypes of malignant tumours. In total there were 306 and 241 differentially overexpressed genes in CG+GC and IM+GC samples when compared to IGC respectively, with 175 genes shared (Figure 4.3). Highly overexpressed genes in premalignant lesions were mainly associated with normal gastrointestinal function such as *ATP4A/B*, *GIF*, *GKN1/2*, *DEFA5/6* and *SI* as expected (Appendix D). Compared to DGC, there were 251 and 176 genes differentially overexpressed in CG+GC and IM+GC samples respectively, with 108 genes shared. Overall the majority of overexpressed genes were similar to those obtained when compared to IGC (Appendix E) and in total 91 genes were commonly differentially overexpressed in both premalignant tissue types when compared to both malignant tissue types suggesting a possible common evolutionary process in intestinal and diffuse gastric carcinogenesis (Figure 4.3). Further investigation of these genes using gene set over-representation with GO Biological Process confirmed that they were mainly associated with digestion, maintenance of the gastrointestinal epithelium and tissue homeostasis (Figure 4.4).

A comparison of IGC samples with CG+GC and IM+GC samples showed 285 and 188 differentially overexpressed genes respectively of which 105 were shared (Figure 4.3). Top overexpressed genes included *INHBA*, *SPP1* (with both CG+GC and IM+GC), *OLFM4*, *CDH17* and *CLDN1/3/7* which have all been shown previously to be associated with GC (Appendix D). DGC samples showed differential overexpression of 349 and 154 genes compared to CG+GC and IM+GC samples respectively of which 145 genes were shared (Figure 4.3). As before, the top overexpressed genes showed similarity with those in IGC including *INHBA* and *SFRP4* (Appendix E), with a total of 45 genes commonly differentially overexpressed in both malignant tissue types when compared to both premalignant tissue types. Further analysis showed that these genes were mainly associated with extracellular matrix and structure organisation (GO Biological Process terms GO:0030198 and GO:0043062) as well as various high level developmental and morphogenetic processes (Figure 4.4).

Overall both chronic gastritis and intestinal metaplasia were shown to share sets of genes that were commonly differentially expressed with progression to either Lauren GC subtype suggesting a common path in gastric carcinogenesis. Activities lost with progression were mainly

associated with epithelial maintenance and function whereas those gained were associated with stromal changes.

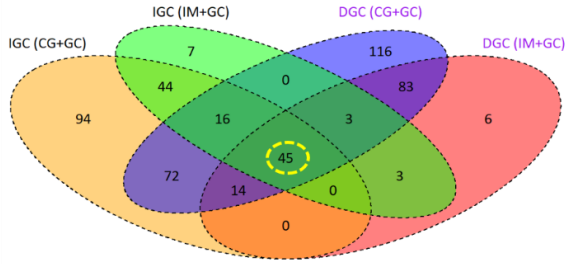
a)



List of genes commonly overexpressed in premalignant tissues

AADAC	CA2	FUT9	LINC01133	PSAPL1	TENT5C
ADGRG2	CAPN9	GHRL	LIPF	PSCA	TFF1
ADH1C	CCKBR	GIF	LTF	RASSF6	TFF2
ADTRP	CHGA	GKN1	MAL	REG1A	TMED6
AKR1B10	CPA2	GKN2	MAP7D2	REG3A	TMEM238L
AKR1C1	CXCL17	HPGD	MFSD4A	SCARA5	TNFRSF17
AKR1C2	CYP2C18	IGH	MSMB	SCGB2A1	TPCN2
AKR7A3	CYP3A5	JCHAIN	MT1F	SCNN1B	TRIM50
ALDH3A1	DPT	KCNE2	MT1G	SLC26A9	UGT2B15
ANKRD36BP2	EPN3	KCNJ15	MT1M	SLC2A12	VSIG1
ANXA10	ERO1B	KCNJ16	MUC5AC	SOSTDC1	VSIG2
ATP4A	ESRRG	KIAA1324	MUC6	SST	
ATP4B	FAM3B	KRT20	MUCL3	SSTR1	
AZGP1	FBP2	LIFR	PBLD	SULT1C2	
C16orf89	FCGBP	LINC00261	PGC	SYTL5	
C6orf58	FMO5	LINC00982	POU2AF1	TCN1	

b)



List of genes commonly overexpressed in malignant tissues

ADAMTS12	COL5A2	PLA2G7
ADAMTS2	COL8A1	PLAU
ANLN	CST1	PMEPA1
ANOS1	CTHRC1	RARRES1
APOC1	CXCL8	SERPINH1
APOE	DUXAP10	SFRP4
ASPN	FAP	SPARC
BGN	FCGR1B	SPP1
CEMIP	FNDC1	SULF1
CHI3L1	HOXC6	THBS2
CLDN1	INHBA	THY1
COL10A1	KLK10	TMEM158
COL12A1	MFAP2	WISP1
COL1A1	MMP3	
COL1A2	NID2	
COL4A1	OLFML2B	

Figure 4.3 Four way differential expressed gene analysis between premalignant tissues (chronic gastritis and intestinal metaplasia) and malignant tissues (intestinal and diffuse gastric cancer)

a) Venn diagram showing differentially overexpressed genes in chronic gastritis (CG+GC, n=22) and intestinal metaplasia (IM+GC, n=23) compared to intestinal and diffuse gastric samples (IGC, n=50 and DGC, n=38); The 91 genes listed in the table (dashed yellow circle in Venn diagram) were commonly overexpressed in both premalignant lesions compared to both malignant lesions; b) Venn diagram showing differentially overexpressed genes in IGC and DGC samples compared to CG+GC and IM+GC samples; The 45 genes listed in the table (dashed yellow circle in Venn diagram) were commonly overexpressed in both malignant lesions compared to both premalignant lesions. Differentially expressed gene lists were produced using log2 fold change >1.2 with adjusted p<0.05 (Benjamini-Hochberg method) with the affy and limma packages in R.

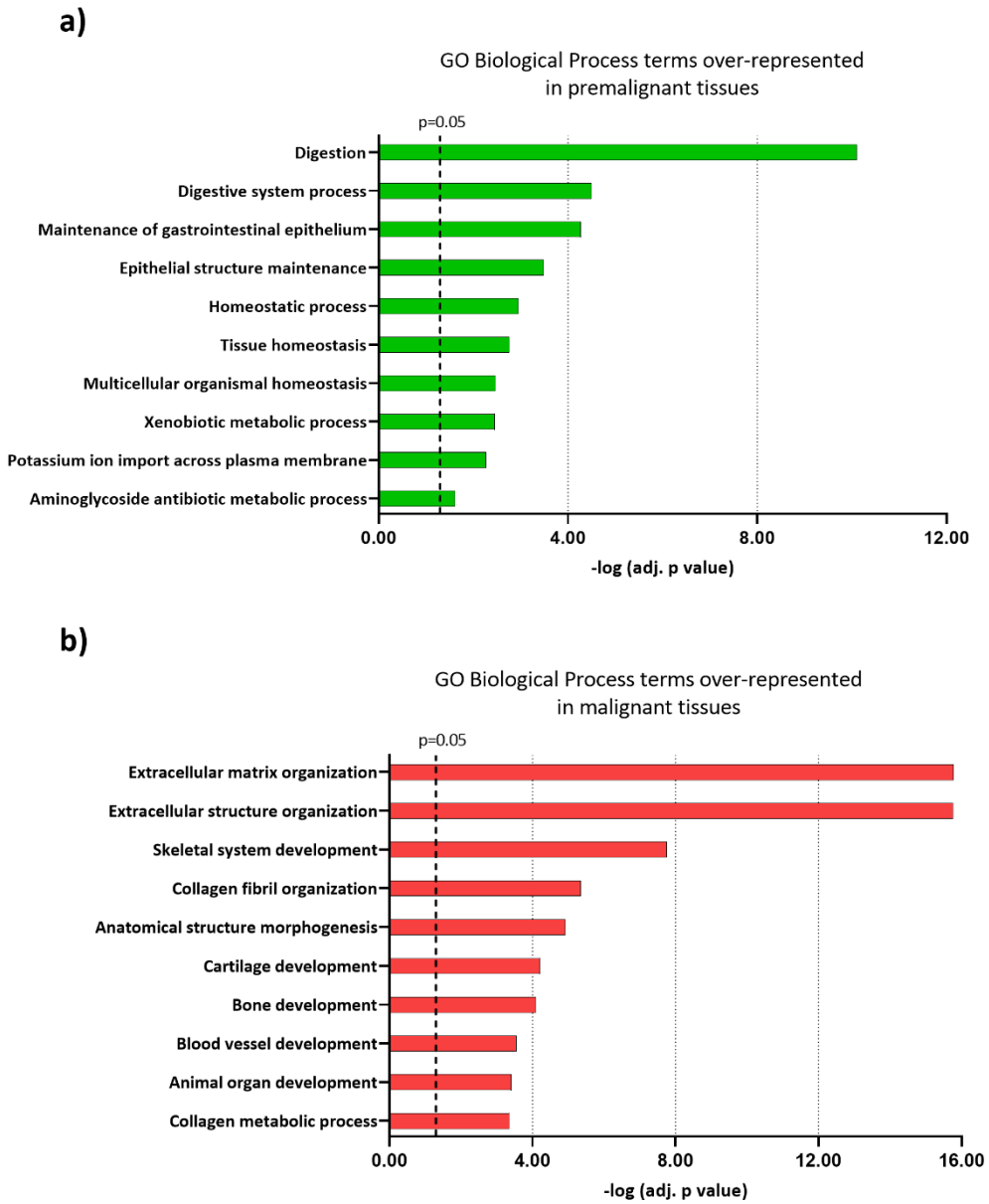


Figure 4.4 Gene set over-representation analysis with GO Biological Process comparing premalignant tissues (chronic gastritis and intestinal metaplasia) and malignant tissues (intestinal and diffuse gastric cancer)

a) Shared significantly over-represented GO Biological Process terms in both premalignant tissues obtained from gene list shown in Figure 4.3a; b) Shared significantly over-represented GO Biological Process terms in both malignant tissues obtained from gene list shown in Figure 4.3b. The g:Profiler tool was used to identify over-represented gene sets (terms) from GO Biological Process. Adjusted p values were obtained using the g:SCS method for multiple testing correction. A p value of 0.05 is equivalent to a negative log10 value of 1.30 as shown by thick dashed line in c) and d).

4.3.5 Single sample gene set enrichment analysis identifies shared enrichment in cancer hallmark pathways between intestinal metaplasia and gastric cancer subtypes

Having identified genes and general epithelial and stromal changes associated with progression to either GC subtype, single sample gene set enrichment analysis (ssGSEA) was carried out with the Hallmark gene sets (Molecular Signatures Database, https://www.gsea-msigdb.org, §2.4.2) to profile potential key shared pathways with the use of intestinal metaplasia (IM+GC) as a reference tissue. The ssGSEA method has an advantage over both gene set over-representation and gene set enrichment analysis as it transforms a single sample's gene expression profile into a gene set enrichment profile by calculating a separate enrichment score for each pairing of a sample and gene set ([387], GSVA package in R). Overall 25/50 and 22/50 gene sets were enriched in IGC (n=50) and DGC (n=38) samples respectively when compared to IM+GC (n=23) samples of which 18 sets were shared suggesting a considerable level of overlap in tumour hallmark pathway activity. As expected based on previous studies [406, 407], IGC was particularly enriched in DNA repair function, cell cycle and cell proliferation gene sets including DNA repair, E2F targets, G2M checkpoint, Mitotic spindle and MYC targets v1 (all at adjusted p=1.1E-05, Wilcoxon test with Benjamini-Hochberg multiple test correction) but these were also enriched in DGC samples, although at lower levels of significance (Figure 4.5). These latter samples were particularly enriched in gene sets associated with cell signalling and extracellular matrix remodelling including Notch signalling (at adj. p=1.0E-09), Epithelial Mesenchymal Transition (at adj. p=8.6E-09), TGFβ signalling (at adj. p=4.4E-09), Angiogenesis (at adj. p=8.6E-09) and Apical junction (at adj. p=7.7E-06), although these same gene sets were also enriched in IGC samples at lower levels of significance.

Overall the use of IM samples as a reference tissue showed there is considerable commonality in cancer-associated hallmark activities in Lauren GC subtypes. Levels of enrichment and not types of hallmark activities mainly separated IGC and DGC pointing towards a potential role of IM as a tissue of origin in the divergent process of gastric carcinogenesis that results in differing GC subtypes.

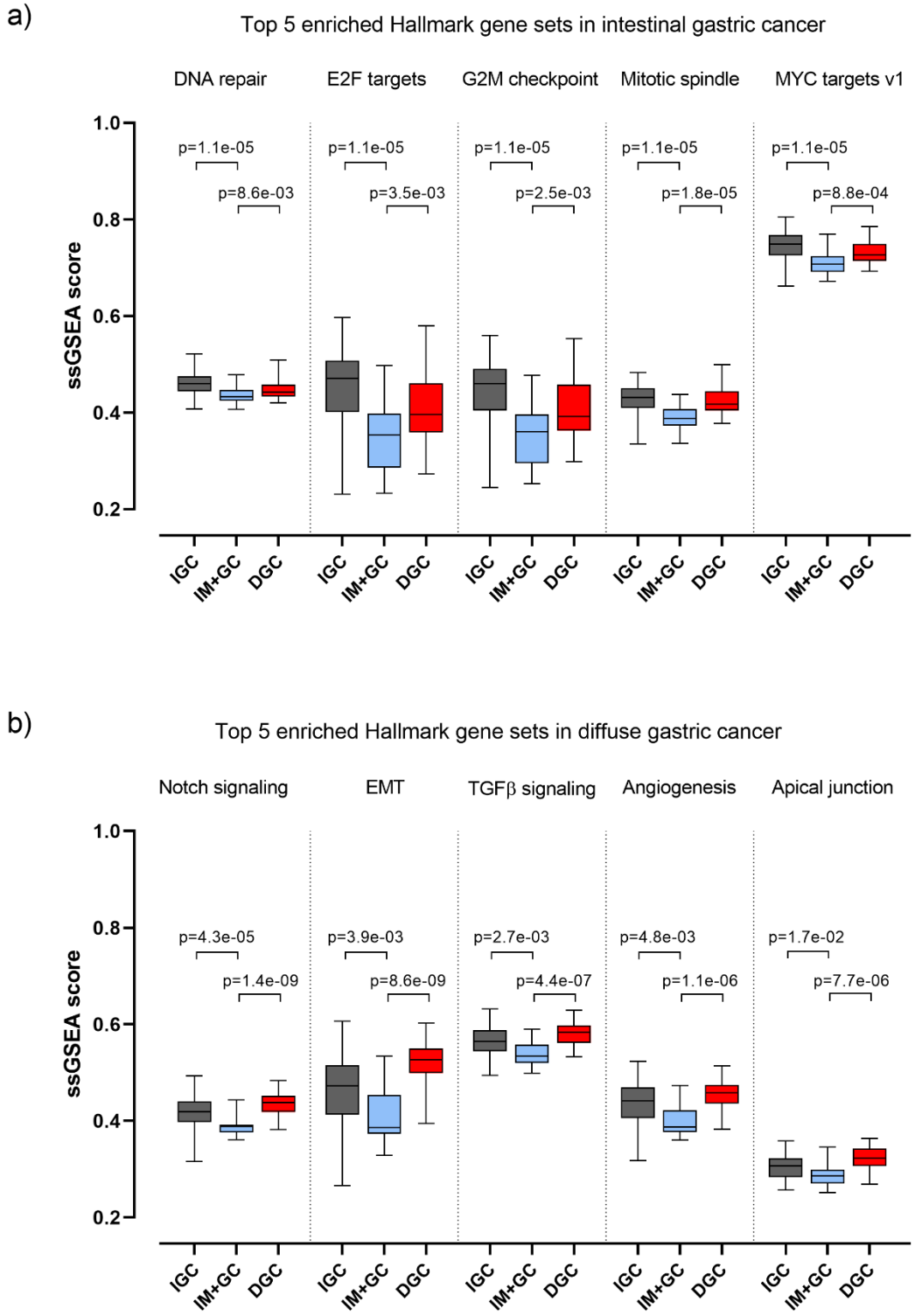


Figure 4.5 Top 5 most significantly enriched Hallmark gene sets using ssGSEA in intestinal (IGC) and diffuse gastric cancer (DGC) when compared to intestinal metaplasia (IM+GC)

a) Five most significantly enriched Hallmark gene sets in IGC samples (n=50) compared to IM+GC (n=23) with DGC scores (n=38) shown for comparison; b) Five most significantly enriched Hallmark gene sets in DGC compared to IM+GC with IGC scores shown for comparison. Hallmark gene sets downloaded from https://www.gsea-msigdb.org. Single sample gene set enrichment analysis carried out using the GSVA package in R. Wilcoxon test with Benjamini-Hochberg correction used to determine statistical significance.

4.3.6 Trends in enriched chromosomal bands by gene expression correspond to copy number gains in gastric cancer

The previous analysis showed a highly significant enrichment of MYC targets v1 gene set in both IGC and DGC samples suggesting that MYC may play a pivotal role in both tumour types. The *MYC* gene is located on chromosome band 8q24 and previous studies have shown a higher risk of progression in IM patients with 8q gain [127] as well as an association with GC [159, 409, 410]. To determine whether gene expression profiles in tissues along the Correa model reflect changes in chromosomal copy numbers, ssGSEA with the Positional gene sets (MSigDB, https://www.gsea-msigdb.org) and the Jonckheere-Terpstra test for trends was carried out using the normal (n=7), chronic gastritis (CG+GC, n=22), intestinal metaplasia (IM+GC, n=23) and unmatched (to premalignant samples) IGC (n=29) samples. The findings of this analysis were then compared to previously obtained chromosomal copy number data of 16 MAUGIC patients (12 IGC and 4 DGC) as part of an ongoing whole exome sequencing study in our laboratory (Busuttil et al 2020 [411]) (Figure 4.6).

Overall the three most significantly enriched chromosome arms/bands by gene expression were 8q24, 7p15 and 7p14. Chromosomal copy number data showed that chromosome arms 6p, 7p, 8p, 8q, 13q, 20p and 20q had a frequency of copy number gain of 0.5 or above. Except for chromosome arm 20p, all other high frequency gains were reflected in the gene expression positional analysis suggesting a strong correlation between increase in gene copy number in GC and gene expression.

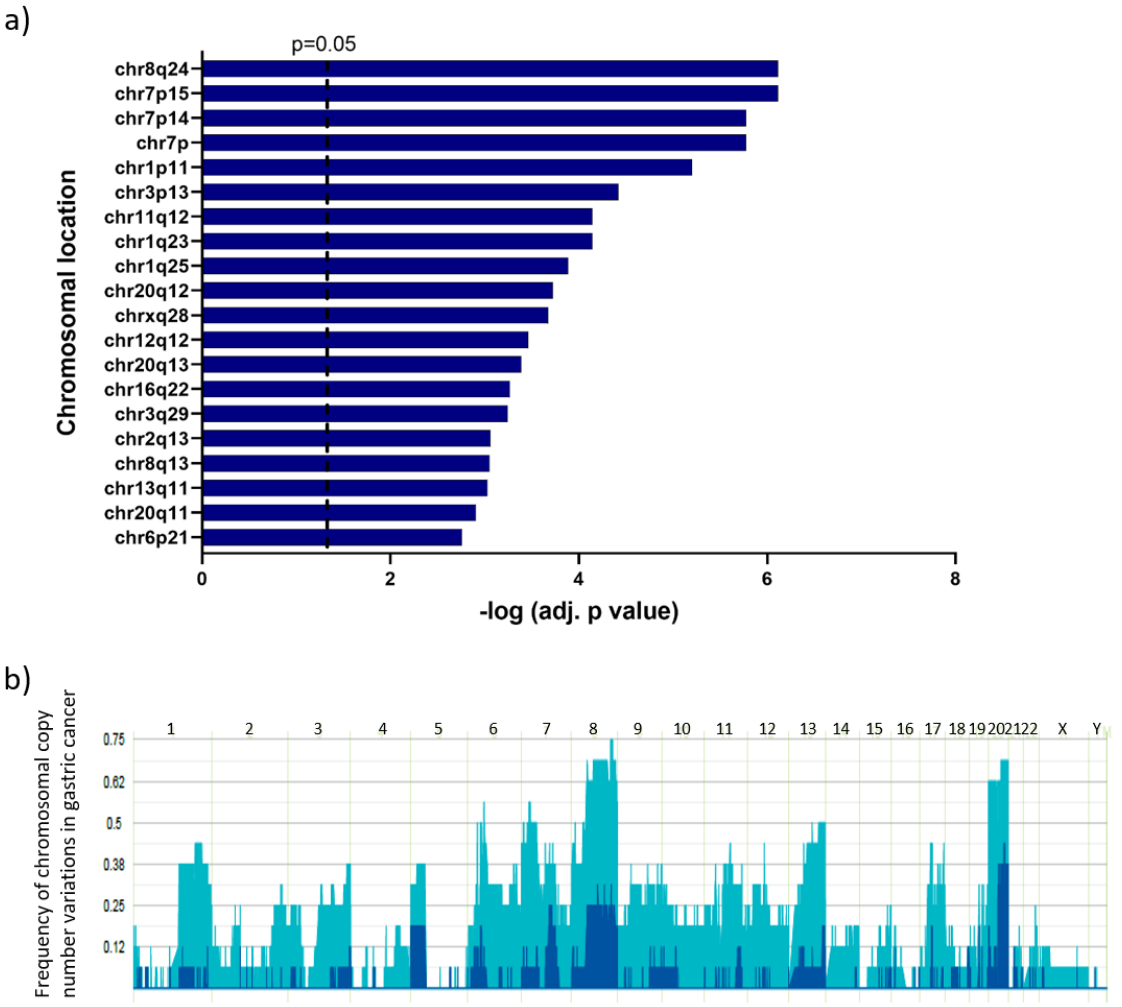


Figure 4.6 Trends in enriched chromosomal location and frequency of chromosomal copy number variations in tissues representing the Correa model

a) Bar chart showing trends in enriched Positional gene sets (MSigDB, https://www.gsea-msigdb.org) obtained using Affymetrix microarray data from normal (n=7), chronic gastritis (n=22), intestinal metaplasia (n=23) and unmatched IGC (n=29) samples. Trends calculated using the Jonckheere-Terpstra test and adjusted for multiple tests using the Benjamini-Hochberg method.

b) Frequency of chromosomal copy number variations from 16 MAUGIC patients (12 IGC and 4 DGC) obtained using whole exome sequencing (Busuttil et al 2020 [411]).

4.3.7 Molecular characterisation of intestinal metaplasia without and with concurrent gastric cancer reveals differences in levels of inflammation and transcription factors associated with gastric cancer

Having investigated the possible role of IM as a precursor lesion to both IGC and DGC, gene expression profiling was carried out on Affymetrix microarray data acquired using RNA extracted from macro-dissected intestinal metaplastic tissue from patients without (IM-GC, n=14) and with gastric cancer (rIM+GC, n=4). This analysis used tissue enriched in IM epithelium in order to study its role at a greater resolution but also to gain insight into immune cell activity in its direct proximity (local microenvironment). The ultimate aim was to identify whether rIM+GC samples differed to IM-GC samples due to a possible field cancerisation effect [412]. Due to the small number of samples available and in order to identify more subtle differentially expressed genes, differential expression criteria were reduced to log2 fold change >0.6 (overall value >1.5) but the adjusted p value after Benjamini-Hochberg correction was kept strictly at <0.05 to ensure only truly significant differentially expressed genes were filtered through.

IM-GC samples showed only 8 differentially over-expressed genes whereas the rIM+GC samples showed 135 genes differentially over-expressed genes (Table 4.3). Top genes overexpressed in IM-GC were mainly associated with fatty acid/lipid activity whereas in rIM+GC they were mainly inflammation, ECM and wound healing, including two genes (*SMOC2* and *PDZK1IP1*) associated with GC and other types of carcinomas. Two other genes closely associated with GC, *MYC* and *SOX9*, were also significantly overexpressed in rIM+GC (Figure 4.7).

Gene set over-representation analysis with GO Biological Process using the differentially overexpressed gene list in rIM+GC showed five key terms that were enriched in intestinal metaplasia in patients with concurrent gastric cancer: T cell homeostasis (GO:0043029), regulation of protein export from nucleus (GO:0046825), ATP generation from ADP (GO:0006757), histone demethylase activity (GO:0032452) and mRNA stabilisation (GO:0048255) (Figure 4.8). Further investigation using ssGSEA with the Hallmark gene sets showed at least two inflammation related gene sets with a trend towards enrichment in rIM+GC (TNFα signalling via NF-Kβ and Interferon-γ response both at adjusted p=0.088 with Benjamini-Hochberg correction) as well as higher KRAS signalling (adj. p=0.088) (Table 4.4). To identify potential subtle differences in activity of key transcription factors between IM-GC and rIM+GC, ssGSEA was carried out with the Transcription Factor Target gene sets (MSigDB, https://www.gsea-msigdb.org) which showed 5 gene sets that were enriched significantly in rIM+GC including “MYCMAX 03” and “E2F Q2” (both with adj. p=0.04) (Table 4.4).

Table 4.3 Top genes by log2 fold change overexpressed in macro-dissected IM-GC and rIM+GC samples

Symbol	Function	logFC	AveExpr	adj.P.Val
High in IM-GC				
LINC00520[1]	Long non-coding RNA	1.97	7.61	4.24E-02
GDPD3	Phosphatidylinositol metabolism	1.9	8.98	3.63E-02
SULT1C2	Sulfotransferase activity	1.64	10.75	1.77E-02
FABP5	Fatty acid uptake and transport	1.05	11.12	4.74E-02
ELOVL6	Fatty acid metabolism	1.01	10.19	4.45E-02
H3F3A	Histone/nucleosome structure	0.99	7.09	4.59E-02
MID1IP1	Lipid biosynthesis	0.82	8.23	4.03E-02
PDZD3	Response to bacterial toxins	0.61	5.81	2.78E-02
High in rIM+GC				
RGS1	Signal transduction	-3.43	5.79	1.61E-02
HLA-DQB1	MHC class II activity	-2.58	6.93	2.20E-04
C3	Complement activity	-2.12	6.77	1.89E-02
CYP4X1	Cytochrome P450 Family	-2.11	5.93	4.01E-02
TSC22D3	Anti-inflammatory/immunosuppressive	-2.03	8.91	9.33E-03
CTGF	ECM	-2.00	7.24	2.85E-02
SMOC2[2]	Wound healing	-1.86	6.60	2.85E-02
PDZK1IP1[3]	Inflammation	-1.80	7.79	3.66E-02
IL7R	Lymphocyte cell signalling	-1.77	6.04	4.79E-02
FCRL5	B cell differentiation	-1.71	6.25	4.22E-02

Differential gene expression carried out with Affymetrix microarray data obtained using mRNA extracted from macro-dissected intestinal metaplastic tissue from patients without (IM-GC, n=14) and with gastric cancer (rIM+GC, n=4); Differential expression set at log2 fold change >0.6 (overall value >1.5) and adjusted p value<0.05 after Benjamini-Hochberg correction; [1]Associated with breast cancer; [2]Associated with gastric cancer; [3]Overexpressed in most carcinomas.

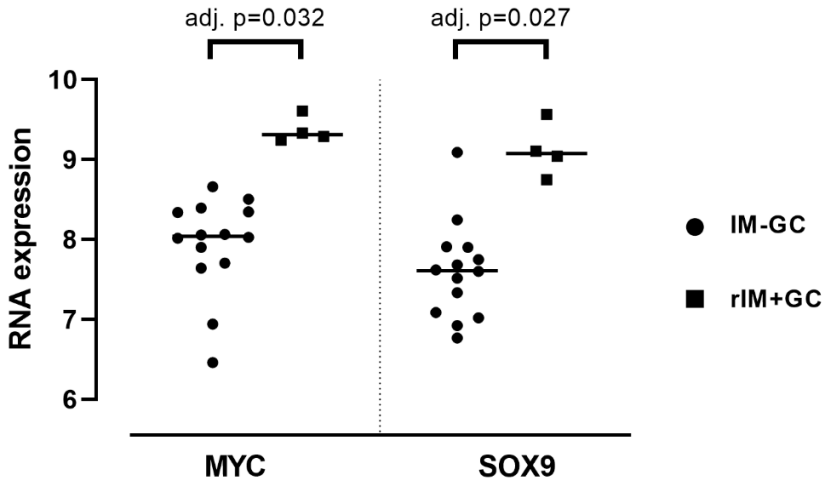


Figure 4.7 Expression of MYC and SOX9 in IM-GC and in rIM+GC samples
Gene expression of *MYC* and *SOX9* in IM-GC (n=14) and rIM+GC (n=4) samples. Line shows median value; adjusted p values calculated using Benjamini-Hochberg method.

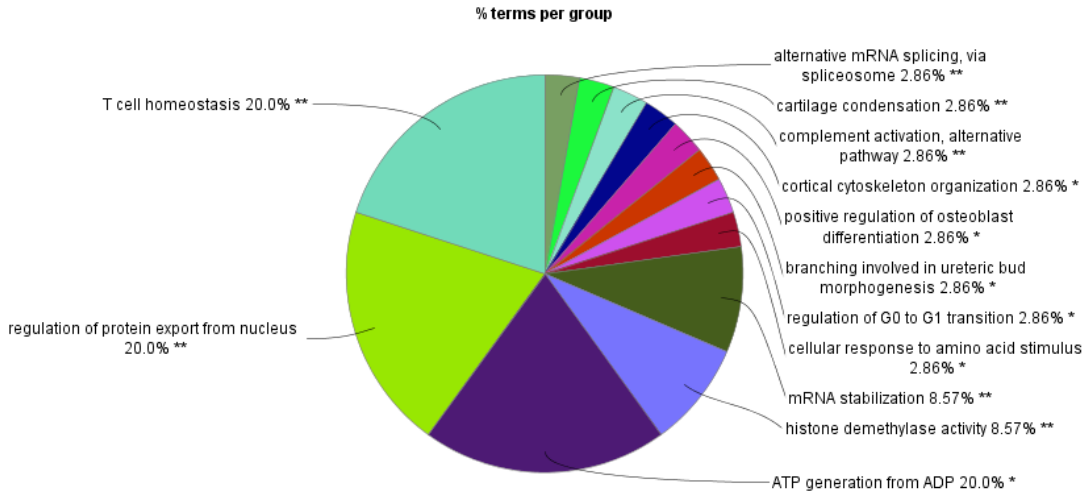


Figure 4.8 Gene set over-representation analysis with GO Biological Process using differentially overexpressed genes in rIM+GC compared to IM-GC samples
The differentially overexpressed gene list for rIM+GC was used to identify over-represented GO Biological Process terms with the ClueGO app in Cytoscape (§2.4.2). The Bonferroni step down was used to correct for multiple testing and a group term p<0.05 was considered significant.

Table 4.4 Top 5 enriched Hallmark and Transcription Factor Target gene sets in rIM+GC

Gene set	adj.P.Val
Hallmark	
TNFα signalling via NF-Kβ	8.80E-02
Interferon-γ response	8.80E-02
Complement	8.80E-02
KRAS signalling Up	8.80E-02
Pancreas beta cells	8.80E-02
Transcription Factor Target	
USF Q6	4.00E-02
MYCMAX 03	4.00E-02
HIF1 Q3	4.00E-02
E2F Q2	4.00E-02
YRTCANNRCGC unknown	4.00E-02

ssGSEA carried out on IM-GC (n=14) and rIM+GC (n=4) samples with the Hallmark and Transcription Factor Target gene sets (MSigDB, https://www.gsea-msigdb.org) using the GSVA package in R. Wilcoxon test with Benjamini-Hochberg correction used to determine statistical significance.

Overall gene expression profiles of targeted IM epithelium in patients with and without concurrent GC showed that the latter was enriched in inflammation and RNA/nuclear protein export regulatory associated processes as well as two key transcription factors, MYC and E2F, previously shown to be significantly enriched in both subtypes of GC. These findings suggest that IM tissue taken even 2cm or more away from tumour is under the influence of a possible field cancerisation effect and is of a “molecularly more advanced stage” than IM-GC tissue.

4.3.8 Subtyping of intestinal metaplasia using gene expression profiles

Based on previous literature on the complete and incomplete subtype of IM that had shown differences in brush border markers such as CD10 (*MME* gene), SI and VIL1 [133, 398, 399, 413-415] and a tissue enriched/specific search for colon markers on https://www.proteinatlas.org**,** a small set of genes (*CDX1*, *CDX2, MME*, *SI*, *VIL1*, *TFF3*, *MUC2*, and *MUC12*) was identified that could be tentatively used to subgroup the epithelium enriched macro-dissected IM-GC (n=14) samples into complete or incomplete subtypes using a bioinformatics approach. A key assumption for this exploratory phase was that complete IM would theoretically have higher expression of small intestine related genes and incomplete IM would have higher expression of colon related genes. *CDX1* and *CDX2* mRNA is expressed in epithelial cells in both the small intestine and the colon, with the former showing increasing and the latter decreasing expression from the duodenum to the distal colon [323, 416]. Higher CDX2 protein expression has been shown in complete IM compared to incomplete IM [417]. *MME*, *SI* and *VIL1* are genes expressed mainly in the brush border of the small intestine [418-420]. *TFF3* mRNA is expressed in goblet cells of both the small intestine and the colon [421], *MUC2* mRNA is differentially expressed in goblet cells of the small intestine (intermediate levels) and the colon (high levels) and *MUC12* mRNA is mainly expressed by enterocytes cells of the colon [422, 423].

An exploratory gene expression correlation map using Pearson's correlation coefficient (r) was created to identify potential relationships between these key intestinal genes in IM-GC (Figure 4.9). *SI* had a significant positive correlation with *CDX2* (r=0.57 at p=0.033) and *MME* (r=0.78 at p=0.001) as expected and a negative correlation with *TFF3* (r=-0.62 at p=0.019). *TFF3* also had a negative correlation with *MME* (r=-0.77 at p=0.0012) but positive correlations with *CDX1* (r=0.83 at p=0.0002) and *MUC12* (r=0.55 at p=0.041). *MUC12* had a negative correlation with *MME* (r=-0.57 at p=0.034) and *MUC2* showed a positive correlation with *CDX1* (r=0.58 at p=0.030). Interestingly *VIL1* did not show a significant correlation with any of the other genes.

Using expression levels of *SI*, *MME*, *CDX2*, *CDX1*, *TFF3* and *MUC12*, the IM-GC samples clustered (unsupervised) into two main clusters (Figure 4.10). The first cluster (C1) contained samples with high expression of the intestinal and brush border genes *CDX2*, *MME* and *SI* (samples S1, S12, S3, S9, S2, S4 and S6) whereas the second cluster (C2) contained samples with relatively higher expression of *MUC12*, *TFF3* and *CDX1* (samples S10, S5, S7, S8, S14, S11 and S14). C1 was selectively filtered by removing sample S12 as this had relatively high expression of all six target genes, and the remaining samples were defined as bioinformatically subtyped complete intestinal metaplasia (bcIM-GC: S1, S3, S9, S2, S4 and S6). C2 was also selectively filtered by

removing sample S8 as this had relatively high expression of *CDX2*, *MME* and *SI* and the remaining C2 samples were defined as bioinformatically subtyped incomplete intestinal metaplasia (biIM-GC: S10, S5, S7, S14, S11 and S14). Finally S8 and S12 were pooled together and defined as bioinformatically subtyped mixed intestinal metaplasia (bmIM-GC).

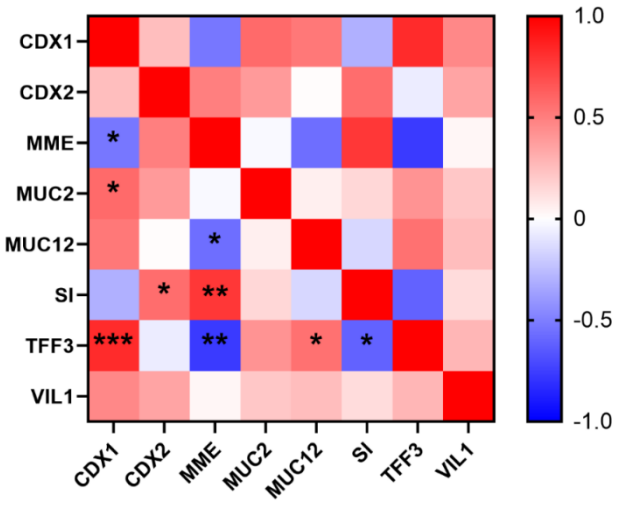


Figure 4.9 Gene expression correlation heatmap using Pearson's correlation coefficient (r) to identify possible targets for subtyping intestinal metaplasia in IM-GC
Colour legend shows size and direction of correlation between genes; * p<0.05, ** p<0.01 and *** p<0.001.

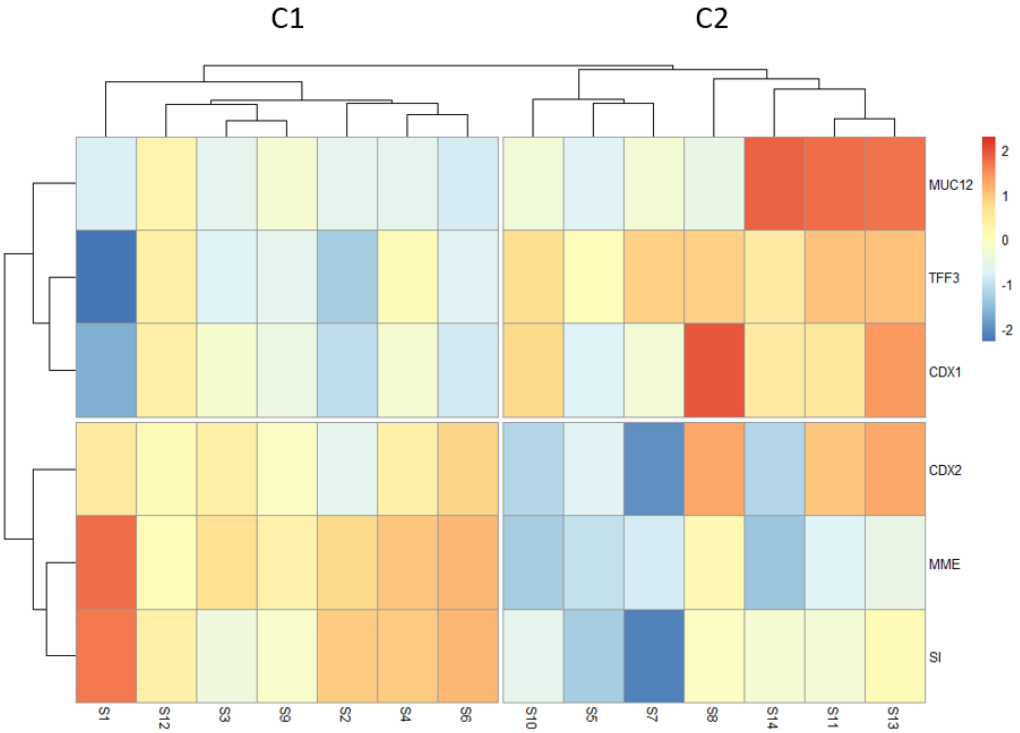


Figure 4.10 Hierarchically clustered heatmap (unsupervised) using gene expression of six key intestinal genes on IM-GC samples (n=14)
Pheatmap package in R used. Expression levels have been standardised (centered and scaled) within rows for visualization. Legend shows z score.

4.3.9 Single sample GSEA confirms metabolic and small intestinal character of bcIM-GC samples and suggests enriched immune activity

To establish potential pathway differences between bcIM-GC and biIM-GC samples, ssGSEA was carried out with KEGG, GO Biological Process and GO Cellular Component. For all three databases containing pathways/GO terms, no enrichment was detected in biIM-GC, even with adjusted p value at <0.1. For KEGG, significantly enriched pathways (adjusted p<0.05, Benjamini Hochberg method) in bcIM-GC (31/186) were mainly metabolism related with the top 5 consisting of "galactose metabolism", "glycine serine and threonine metabolism", "glycerolipid metabolism", "arachidonic acid metabolism" and "linoleic acid metabolism" all with adjusted p=0.015 (Table 4.5). For GO Biological Process, significantly enriched terms in bcIM-GC (201/4436) were also mainly metabolism related with "digestion" being in the top 5 with adjusted p=0.043 (Table 4.5). For GO Cellular Component, close to significantly enriched terms in bcIM-GC included "brush border", "brush border membrane" and "microvillus" all with adjusted p=0.063 (Table 4.5). Interestingly the terms "T cell receptor complex" and "MHC class II protein complex" showed a trend towards enrichment (both adj. p=0.063) suggesting an enriched immune cell response in bcIM-GC samples.

To gain further insight into potential immunological differences between bcIM-GC and biIM-GC, ssGSEA was carried out using a list of immunologically relevant genes curated with functions and Gene Ontology terms from https://www.immport.org/. Enriched terms were only found in bcIM-GC and included "chemokine", "cytokines" (both at p=0.0087) and "TCR signalling pathway" (p=0.04), further suggesting enriched immune activity in bcIM-GC (Table 4.5).

Overall the bioinformatically subtyped complete IM-GC samples were shown to be enriched in pathways and cellular components associated with the small intestine. In addition these samples were characterised by an enrichment in immune associated processes including TCR signalling suggesting increased T cell presence/activity compared to the biIM-GC samples.

Table 4.5 Top enriched pathways/GO terms comparing bcIM-GC and biIM-GC using single sample gene set enrichment analysis

Database	Pathway/Term/Category	Adj.P.Val
High in bcIM-GC		
KEGG	Galactose metabolism	1.50E-02
KEGG	Glycine serine and threonine metabolism	1.50E-02
KEGG	Glycerolipid metabolism	1.50E-02
KEGG	Arachidonic acid metabolism	1.50E-02
KEGG	Linoleic acid metabolism	1.50E-02
High in biIM-GC		
KEGG	None	
High in bcIM-GC		
GO:BP	Acylglycerol homeostasis	4.30E-02
GO:BP	Digestion	4.30E-02
GO:BP	Oligosaccharide metabolic process	4.30E-02
GO:BP	Carbohydrate transport	4.30E-02
GO:BP	Antimicrobial humoral response	4.30E-02
High in biIM-GC		
GO: BP	None	
High in bcIM-GC		
GO:CC	T cell receptor complex	6.30E-02
GO:CC	Brush border	6.30E-02
GO:CC	MHC class II protein complex	6.30E-02
GO:CC	Brush border membrane	6.30E-02
GO:CC	Microvillus	6.60E-02
High in biIM-GC		
GO: CC	None	
High in bcIM-GC		
IP[1]	Chemokine	8.70E-03
IP	Cytokines	8.70E-03
IP	TCR Signalling pathway	4.00E-02
IP	Cytokines receptors	8.20E-02
IP	Interleukin receptors	2.10E-01
High in biIM-GC		
IP	None	

[1]Curated immune related gene lists downloaded from https://www.immport.org; ssGSEA carried out on bcIM-GC and biIM-GC samples (both n=6) with KEGG, GO Biological Process, GO Cellular Component and ImmPort gene sets using the GSVA package in R. Wilcoxon test with Benjamini-Hochberg correction used to determine statistical significance.

4.3.10 Differential gene expression allows further characterisation of intestinal metaplasia subtypes

To gain further insight into how bcIM-GC and biIM-GC might differ at the gene expression level, differential gene expression analysis was carried out. There were a total of 18 and 10 over-expressed genes (inclusion criteria: average gene expression >5 and adj. p value<0.05 using Benjamini-Hochberg method) in bcIM-GC and biIM-GC respectively (Table 4.6). The bcIM-GC gene list was highly populated by small intestine specific genes (RBP2, MME, XPNPEP2) including many related to carbohydrate digestion (APOA4, SLC2A5, SLC2A2, MGAM and KHK) further confirming the strong small intestinal-like character of bcIM-GC. There was also a highly

enriched chemokine, CCL25 (logFC=3.88, adj. p=0.0092), which is normally selectively and constitutively expressed in the small intestine epithelium [424]. The biIM-GC gene list contained genes normally expressed in the colon (HOXA10 and HOXA13 at logFC=3.09 and 2.80 with adj. p=0.0025 and 0.015 respectively) and also a chemokine, CXCL5, known to be a powerful chemoattractant for neutrophils (logFC=2.49, adj. p=0.017) [425]. In addition to these three genes known to be associated with GC [426-428], two other GC associated genes were present in the biIM-GC list (CLDN1 and CDH3, [429, 430]) suggesting a higher level of oncogenic processes in the incomplete subtype of IM.

Table 4.6 Differentially expressed genes in bcIM-GC and biIM-GC samples

Symbol	Name	logFC	AveExpr	adj.P.Val
High in bcIM-GC				
RBP2	Retinol Binding Protein 2	5.36	10.73	1.70E-02
MME	Membrane Metalloendopeptidase	4.08	7.22	3.90E-03
APOA4	Apolipoprotein A4	3.96	9.34	4.60E-02
CCL25[1]	C-C Motif Chemokine Ligand 25	3.88	7.29	9.20E-03
SLC2A5[2]	Solute Carrier Family 2 Member 5	3.74	7.60	2.40E-02
SLC2A2[3]	Solute Carrier Family 2 Member 2	3.17	6.40	8.10E-03
XPNPEP2	X-Prolyl Aminopeptidase 2	3.05	7.29	1.70E-02
MGAM	Maltase-Glucoamylase	3.00	7.69	2.40E-02
SEMA6D	Semaphorin 6D	2.36	5.89	1.90E-02
SLC5A1	Solute Carrier Family 5 Member 1	2.16	8.87	3.70E-02
KHK	Ketohexokinase	1.98	8.93	4.70E-02
PCK2	Phosphoenolpyruvate Carboxykinase 2,	1.73	10.09	4.70E-02
KLK11	Kallikrein Related Peptidase 11	1.67	7.65	3.40E-02
TTTY14[4]	Testis-Specific Transcript, Y-Linked 14/CYorf14	1.49	5.55	4.60E-02
SFRP5	Secreted Frizzled Related Protein 5	1.34	6.10	1.70E-02
SLC37A4	Solute Carrier Family 37 Member 4	1.24	8.56	4.60E-02
ADRB2	Adrenoceptor Beta 2	0.90	6.04	3.20E-02
NUP210	Nucleoporin 210	0.85	7.12	1.70E-02
High in biIM-GC				
HOXA10	Homeobox A10	-3.09	6.60	2.50E-03
HOXA13	Homeobox A13	-2.80	5.74	1.50E-02
CXCL5[5]	C-X-C Motif Chemokine Ligand 5	-2.49	5.48	1.70E-02
CLDN1	Claudin 1	-2.09	7.28	1.90E-02
F5	Coagulation Factor V	-1.89	7.25	3.20E-02
CDH3	Cadherin 3	-1.69	7.62	5.60E-03
CTSV	Cathepsin V	-1.61	7.44	1.90E-02
CPD	Carboxypeptidase D	-1.26	8.01	4.50E-02
RSPH1	Radial Spoke Head Component 1	-1.11	7.17	2.00E-02
FAM3D	Family With Sequence Similarity 3 Member D	-0.69	10.16	3.00E-02

[1]Contributes to small intestinal (not colon) homing of T cells; [2]GLUT5; [3]GLUT2; [4]RNA gene; [5]Stimulates chemotaxis of neutrophils. Differentially expressed genes were defined as log2 fold change >0.6 (overall value >1.5) with adjusted p<0.05 using the Benjamini-Hochberg method for multiple test correction; genes with log2 normalised average expression of less than 5 were excluded.

Using hierarchical clustering (unsupervised), all IM-GC samples were analysed together with the 28 DEGs obtained to detect potential outliers and identify whether samples in bmIM-GC truly belonged to a separate group. All samples belonging to bcIM-GC and biIM-GC separated clearly from each other and there were no samples in either group with a "mixed" identity. The bmIM-GC samples clustered in a separate group on their own but closer to biIM-GC than bcIM-GC having high expression levels of biIM-GC associated genes but also relatively high expression levels of some bcIM-GC associated genes (Figure 4.11).

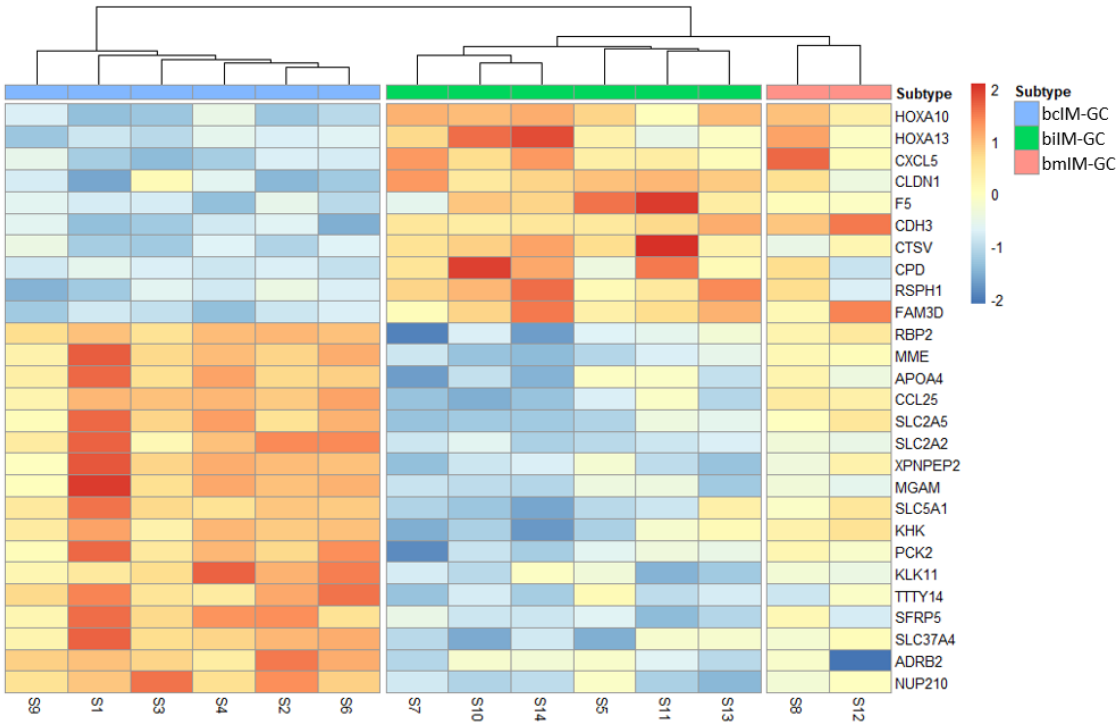


Figure 4.11 Hierarchical clustering (unsupervised) of all IM-GC samples using differentially expressed gene list

Gene expression heatmap showing unsupervised clustering of all IM-GC samples based on previously obtained differentially expressed gene list. Pheatmap package in R used. Expression levels have been standardised (centered and scaled) within rows for visualization. Legend shows z score**.**

Overall differential gene expression analysis showed that the bcIM-GC samples were highly enriched in genes associated with the small intestine whereas the biIM-GC samples showed differential overexpression of genes associated with the colon and gastric cancer.

4.3.11 Higher expression of gastric cancer associated biomarkers CEACAM5 and CEACAM6 in biIM-GC samples

To further investigate the relationship between biIM-GC and cancer associated markers, the expression levels of *CEACAM5* and *CEACAM6* in bcIM-GC and biIM-GC samples were analysed. Both of these genes are cell adhesion molecules that have been associated with gastric cancer with the former being currently used as a biomarker (*CEACAM5* encodes CEA, §1.5.1) for this disease [431-433]. Overall expression levels of both *CEACAM5* and *CEACAM6* were significantly higher in biIM-GC further suggesting that this subtype has a more oncogenic character and is more closely associated with GC than bcIM-GC (Figure 4.12).

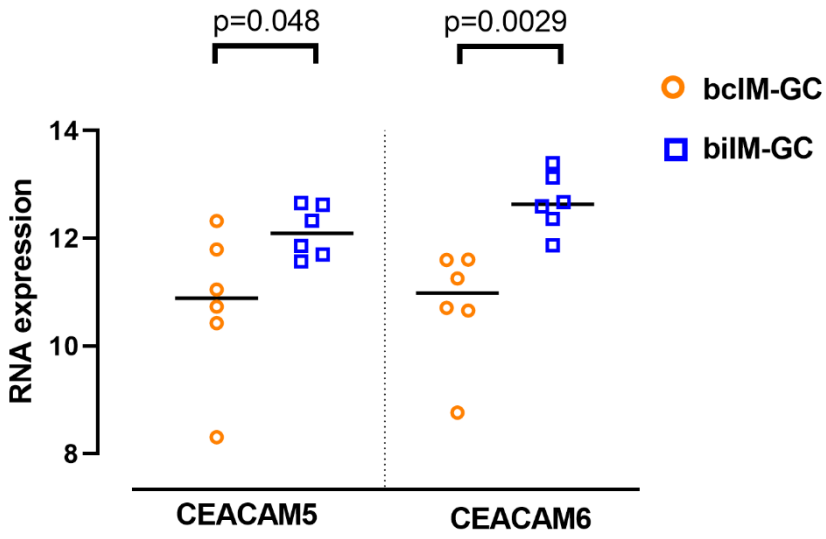


Figure 4.12 Expression of gastric cancer associated biomarkers CEACAM5 and CEACAM6 in bcIM-GC and biIM-GC samples
Mid line shows median value. Statistical analysis carried out using unpaired t test.

4.3.12 Single gene analysis of immune related genes identifies distinct immune profiles in intestinal metaplasia subtypes

Earlier findings within the current study showed that inflammation and immune cell associated processes were highly enriched in intestinal metaplasia (§4.3.2, §4.3.3, §4.3.7, §4.3.9). To gain insight into potential differences in immune profiles between the bcIM-GC and the biIM-GC samples and their possible role in progression to GC, an extensive bioinformatics based analysis was carried out on all genes of the cluster of differentiation family (CD), the interleukin family (IL), the interferon family (IFN), the transforming growth factor family (TGF) and all chemokine related genes (CCL, CCR and CXCL and CXCR) as well as FOXP3 and KLRB1 (CD161) (Appendix F). The T cell specific markers *CD2*, *CD3δ*, *CD3γ*, *CD8α* and *KLRB1* had significantly higher expression in bcIM-GC suggesting an increased T cell presence, particularly of CD8+ and CD161+ T cells (Figure 4.13). Significant differences were also observed in cytokine and chemokine profiles. For

cytokines, bcIM-GC was enriched in *IL11RA* (p=0.005), *IL18RAP* (p=0.049), *IL27RA* (p=0.036), *IL2RB* (p=0.026), *IL37* (p=0.038), *IL6R* (p=0.0038), *IL7R* (p=0.012) and *TGFBRAP1* (p=0.0029) (Table 4.7). In contrast only two cytokines had higher expression in biIM-GC, specifically *IL18* (p=0.031) and *IL20RA* (p=0.0087). In addition to high expression of *CCL25*, *CXCL17* (p=0.022), *CCL5* (p=0.00089), *CCL2* (p=0.015), *CXCL12* (p=0.015) and *CCR5* (p=0.0087) had significantly higher expression in bcIM-GC compared to biIM-GC. Except for *CXCL5*, there was no other chemokine gene with higher expression in iIM-GC (Table 4.7).

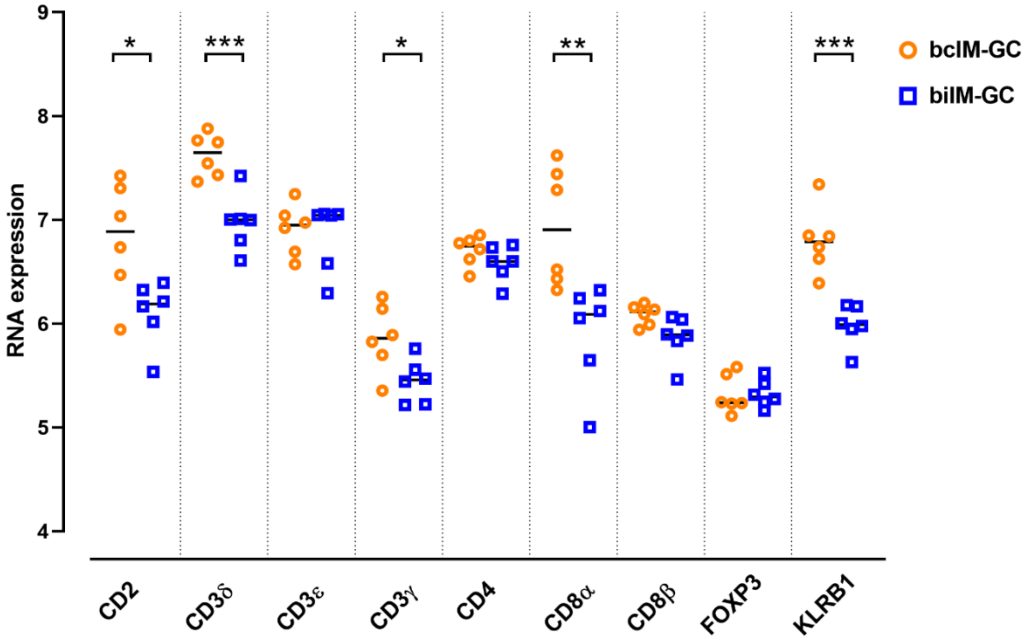


Figure 4.13 Gene expression of key T cell markers in bcIM-GC and biIM-GC samples
For statistical analysis, unpaired t-test and Mann-Whitney test used for data with and without normal distribution respectively; *, **, *** is equal to p<0.05, p<0.01 and p<0.001.

Table 4.7 Significantly enriched cytokines and chemokines in bcIM-GC and biIM-GC samples

Cytokine	logFC	AveExpr	p val.[1]	Chemokine	logFC	AveExpr	p val.[1]
High in bcIM-GC				High in bcIM-GC			
IL6R	0.96	7.21	3.80E-03	*CCL25*	3.82	7.29	2.02E-05
IL11RA	0.61	6.33	5.00E-03	*CXCL17*	1.68	9.24	2.20E-02
IL7R	0.56	6.17	1.20E-02	*CCL5*	1.43	7.76	8.90E-04
IL18RAP	0.44	5.93	4.90E-02	*CCL2*	1.06	5.39	1.50E-02
IL27RA	0.41	5.59	3.60E-02	*CXCL12*	0.86	5.89	1.50E-02
IL2RB	0.29	6.62	2.60E-02	*CCR5*	0.32	6.87	8.70E-03
IL37	0.29	5.44	3.80E-02				
TGFBRAP1	0.27	7.00	2.90E-03				
High in biIM-GC				High in biIM-GC			
IL18	-0.91	7.31	4.10E-02	*CXCL5*	-2.46	5.65	6.47E-05
IL20RA	-0.84	6.55	8.70E-03				

[1]Statistical significance calculated for each gene separately using either unpaired t-test or Mann-Whitney test depending on data distribution. All genes of the interleukin family (IL), the interferon family (IFN), the transforming growth factor family (TGF) and all chemokine related genes (CCL, CCR and CXCL and CXCR) analysed for significant difference in gene expression (Appendix F).

4.3.13 Immune gene correlation matrix suggests the presence of three main types of T cell activity

To further characterise the nature of differing T cell activity observed between bcIM-GC and biIM-GC samples, a correlation matrix was created using the five T cell associated genes previously shown to be enriched in bcIM-GC together with all the immune related genes investigated (Appendix F). Stringent inclusion criteria of Pearson's correlation coefficient r<-0.8 or r>0.8 with p<0.01 were used to create a network of highly correlated genes associated with these T cell markers (Figure 4.14). The overall result suggested there were three groups associated with T cell activity: TA1, TA2 and TA3. TA1 was primarily made up of *CD2* and *CD8α* with very high correlations (CD8α/CCL5 r=0.97, CD8α/CD2 r=0.95, CD2/CCL5 r=0.93, CD2/IL7R r=0.91 and CD8α/IL18RAP r=0.90). TA2 consisted primarily of *CD3δ* and *KLRB1*, (CD3δ/KLRB1 r=0.90 and CD3δ/CCL25 r=0.94), with *CCL5* connecting TA1 and TA2. TA3 had *CD3γ* as a central node with relatively lower correlations and shared *CD160* and *IL11RA* with *KLRB1*.

Both *CD2* and *CD8α* gene expression had a highly negative correlation with *IL18* expression (CD2/IL18 r=-0.87 and CD8α/IL18 r=-0.85) suggesting a possible regulatory role of this cytokine on TA1. Both *CD3δ* and *KLRB1* were highly negatively correlated with *CXCL5* (CD3δ/CXCL5 r=-0.85 and KLRB1/CXCL5 r=-0.87) suggesting also a possible regulatory of this chemokine in the function of TA2. Finally *CD3γ* had a highly negative correlation with *CD24*, *IL20RA*, *IL1RN* and *IL1R2* (r=-0.86, r=-0.83, r=-0.82 and r=-0.81 respectively).

Overall T cell activity in the bcIM-GC and biIM-GC samples was divided into three main groups by correlation: TA1 (CD2/CD8α), TA2 (CD3δ/KLRB1) and TA3 (CD3γ). Each T cell activity group was characterised by its own unique set of potential regulatory markers with the highly expressed *IL18*, *CXCL5* and *IL20RA* genes in biIM-GC samples negatively correlated with TA1, TA2 and TA3 respectively.

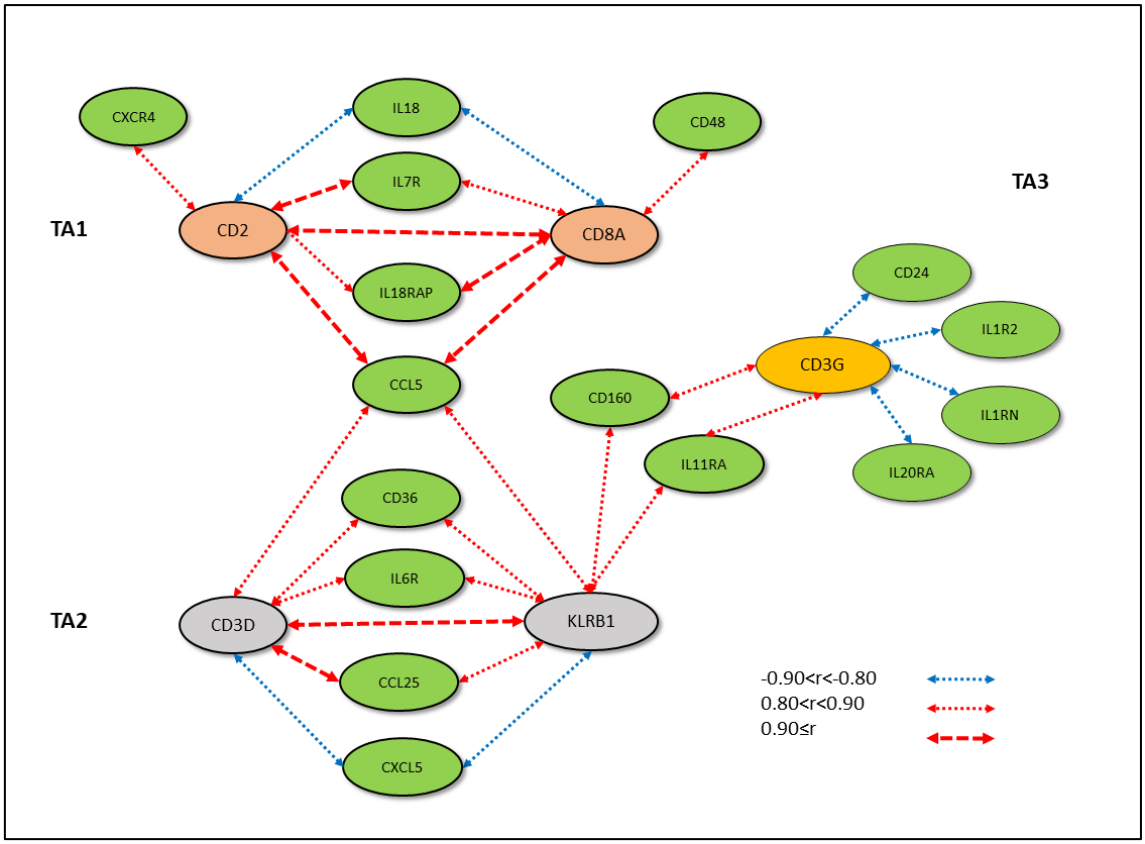


Figure 4.14 Correlation network showing T cell activity groups from bcIM-GC and biIM-GC samples

Genes highly correlated (r<-0.80 or r>0.8 with p<0.01) with the five enriched T cell markers in bcIM-GC (n=6) were used to create a correlation network from bcIM-GC and biIM-GC (n=6) expression data. Three main T cell activity groups were identified: TA1 (key nodes *CD2* and *CD8α*), TA2 (key nodes *CD3δ* and *KLRB1*) and TA3 (key node *CD3γ*). List of immune related genes used for correlation shown in Appendix F.

4.3.14 T cell immune gene signature associated with complete intestinal metaplasia

The relationship between T cell gene expression and intestinal metaplasia subtypes was further investigated a) by comparing gene expression levels of CD8α, MME (brush border, bcIM-GC epithelium) and CDX1 (mainly biIM-GC epithelium) and b) by comparing the ssGSEA scores of the KLRB1 gene signature first described by Fergusson et al 2014 [434] (Appendix G) with that of the GO Cellular Component Brush border term (GO:0005903). These authors showed that there is a core transcriptional signature enriched in KLRB1++ MAIT cells, which is also shared by other T cell lineages that express KLRB1 including CD8+, CD4+ and γδ T cells.

Overall *CD8α* had a positive correlation with *MME* (r=0.73, p=0.0069) and a negative correlation (r=-0.70, p=0.011) with *CDX1* (Figure 4.15) suggesting that bcIM-GC is enriched in CD8+ T cells of either αβ or γδ TCR origin. The KLRB1 gene signature was significantly enriched in bcIM-GC (p=0.049) and was highly positively correlated with the GO Cellular Component Brush border

term GO:0005903 (r=0.84, p=0.00068) suggesting that bcIM-GC is possibly enriched in innate like T cells (MAIT and γδ T cells) (Figure 4.15).

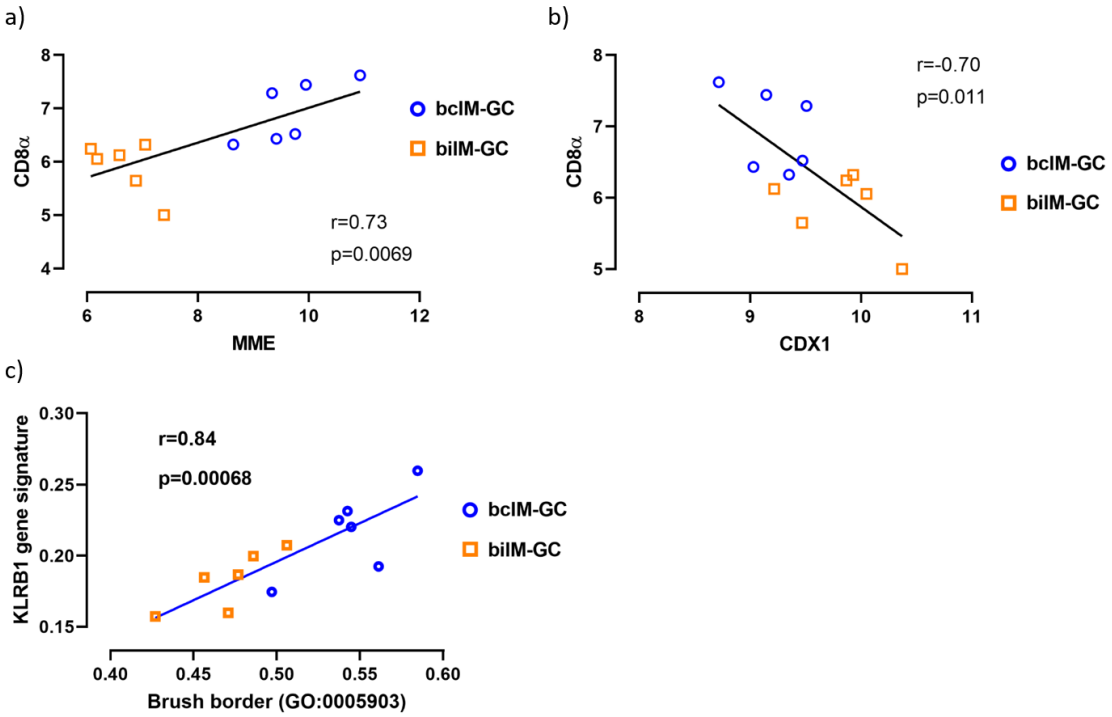


Figure 4.15 Relationship shown between gene expression of CD8α with MME and CDX1 genes and between KLRB1 gene signature and GO Cellular Component term Brush border (GO0005903)

Pearson's correlation (r) used to investigate the relationship in gene expression between (a) *CD8α* vs *MME* and (b) *CD8α vs CDX1*, and (c) between the ssGSEA scores of the KLRB1 gene signature described in Fergusson et al 2014 [434] (Appendix G) and the GO Cellular Component Brush border term. ssGSEA carried out using the GSVA package in R. Wilcoxon test used to determine statistical significance.

4.3.15 Gene expression profiling of intestinal metaplasia validation cohort from Companioni et al 2017 study [388]

In an attempt to validate the findings of the current study, the publically available data set (GSE78523) from Companioni et al 2017 was used [388]. In this study, Affymetrix Almac-Xcel arrays were used to profile total RNA from gastric mucosa. Normalised data was available from 9 histologically subtyped cases of complete and 7 cases of incomplete IM in patients without GC (cIM-GC and iIM-GC). Differential gene expression analysis was performed with the GEO2R online tool and identified 8 genes overexpressed in cIM-GC and 2 genes overexpressed in iIM-GC (inclusion criterium: adjusted p<0.05, Table 4.8). Interestingly 2 of the enriched genes in cIM-GC were the transcription factors EBF1 (logFC=7.5, adj. p=0.025) and TAF10 (logFC=1.52, adj. p=0.032). EBF1 plays a crucial role in regulating expression of SLAM1 co-stimulatory receptor in B cells [435], and TAF10 is a transcription initiation factor for RNA polymerase II. However, overall there was no overlap of differentially expressed genes between the bioinformatically

subtyped IM-GC samples from our lab and the histologically subtyped IM-GC samples from the Companioni study.

Table 4.8 Differentially expressed genes in cIM-GC[1] and iIM-GC[1] samples from Companioni et al 2017 [388] using GEO2R online tool

Symbol	Name	logFC	adj.P.Val
High in cIM-GC			
EBF1	Early B-Cell Factor 1	7.50	2.50E-02
ACTN4	Actinin Alpha 4	2.24	2.60E-02
PRKCSH	Protein Kinase C Substrate 80K-H	1.52	2.60E-02
TAF10	Transcription initiation factor TFIID subunit 10	1.52	3.20E-02
LINC00965	Long Intergenic Non-Protein Coding RNA 965	1.37	2.50E-02
METTL22	Methyltransferase Like 22	1.12	2.70E-02
UBE2G2	Ubiquitin-conjugating enzyme E2 G2	1.03	4.10E-02
High in iIM-GC			
GOLGA1	Golgi Autoantigen, Golgin Subfamily A, 1	-1.59	3.10E-02
C11orf57	NKAP Domain Containing 1	-1.41	4.10E-02

[1]Histologically subtyped complete (n=9) and incomplete (n=7) intestinal metaplasia samples in patients without gastric cancer.

4.3.16 Subtyping and characterisation of intestinal metaplasia samples from the Companioni cohort using 28 gene signature

Using unsupervised hierarchical clustering with the same 28 gene signature previously used to subtype IM-GC samples from our lab (§4.3.10, Table 4.6), the histologically subtyped IM-GC samples from the Companioni study divided into two main clusters (Figure 4.16). Cluster 1 (C1) contained the samples with high expression of small intestinal specific genes such as *MME*, *RBP2* and *MGAM* whereas Cluster 2 (C2) contained the samples with low expression of these genes. As before, C1 was termed bioinformatically subtyped complete intestinal metaplasia (bcIM-GC) and C2 was termed bioinformatically subtyped incomplete metaplasia (biIM-GC). Overall, the histological and the bioinformatic subtyping of the Companioni samples differed substantially with only 5/8 and 4/8 samples showing overlap between cIM-GC/bcIM-GC and iIM-GC/biIM-GC (Figure 4.16).

To further characterise the intestinal character of the bcIM-GC and biIM-GC samples, differential gene expression was carried out which showed over-expressed genes only in bcIM-GC (adjusted $p<0.05$, 61 genes), consisting mostly of small intestine specific genes (Table 4.9). Single gene analysis of T cell markers did not show significant differences between bcIM-GC and biIM-GC (Figure 4.17). However single gene analysis of cytokines and chemokines (§4.3.10, Appendix F) did show several overexpressed genes (IL32, IFNGR1, IL22RA, IFNAR1, IL18BP and TGFBR2) in bcIM-GC, with only IL36B overexpressed in biIM-GC (Table 4.10). Interestingly IL18BP which is an IL18 signalling inhibitor and downregulates Th1 responses was overexpressed in bcIM-GC

[436]. CCL25 was the only chemokine gene that overlapped with the findings from the IM-GC cohort in our lab further confirming the likely important role of this cytokine in complete IM. ssGSEA with the ImmPort gene sets showed significant enrichment of Interferon Receptors in bcIM-GC and also a trend towards enrichment in TCR Signalling Pathway (Figure 4.18).

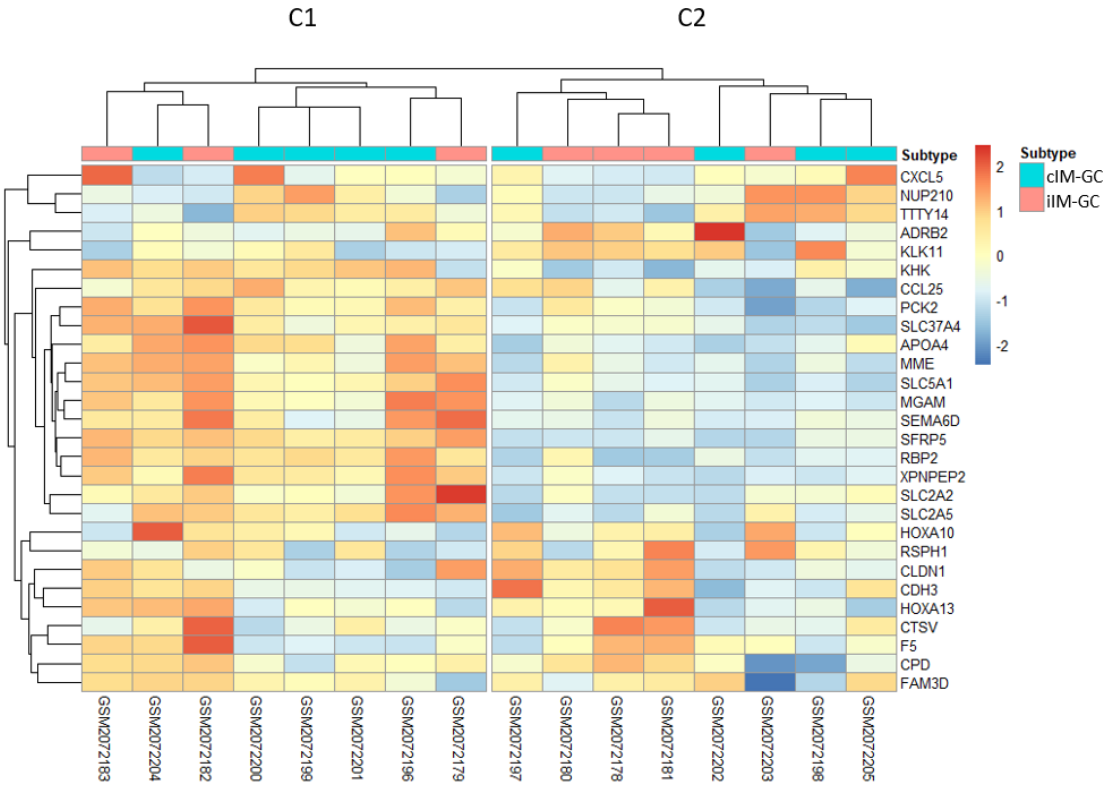


Figure 4.16 Unsupervised hierarchical clustering of IM-GC samples from the Companioni et al 2017 study [388]

Gene expression heatmap showing unsupervised clustering of histologically subtyped IM-GC samples from the Companioni et al 2017 study using 28 gene list from §4.3.10 and Table 4.6. Pheatmap package in R used. Expression levels have been standardised (centred and scaled) within rows for visualization. Legend shows z score.

Table 4.9 Top 10 genes by adjusted p value[1] over-expressed in bcIM-GC compared to biIM-GC samples (Companioni et al 2017 study, [388])

Symbol	adj.P.Val	logFC
High in bcIM-GC		
SFRP5	4.30E-05	-2.62
XPNPEP2	2.30E-03	-2.70
SLC15A1	2.30E-03	-2.40
RBP2	2.30E-03	-2.24
SLC5A1	2.30E-03	-2.01
SLC46A1	3.50E-03	-2.03
TMEM236	4.90E-03	-1.92
CEACAM20	5.80E-03	-2.92
MME	6.00E-03	-2.38
SLC6A19	6.00E-03	-2.17

[1]Sorted by adjusted p value and not logFC as several genes with high logFC did not reach significance (adjusted p value<0.05). Analysis carried out on bioinformatically subtyped samples of the Companioni et al 2017 study.

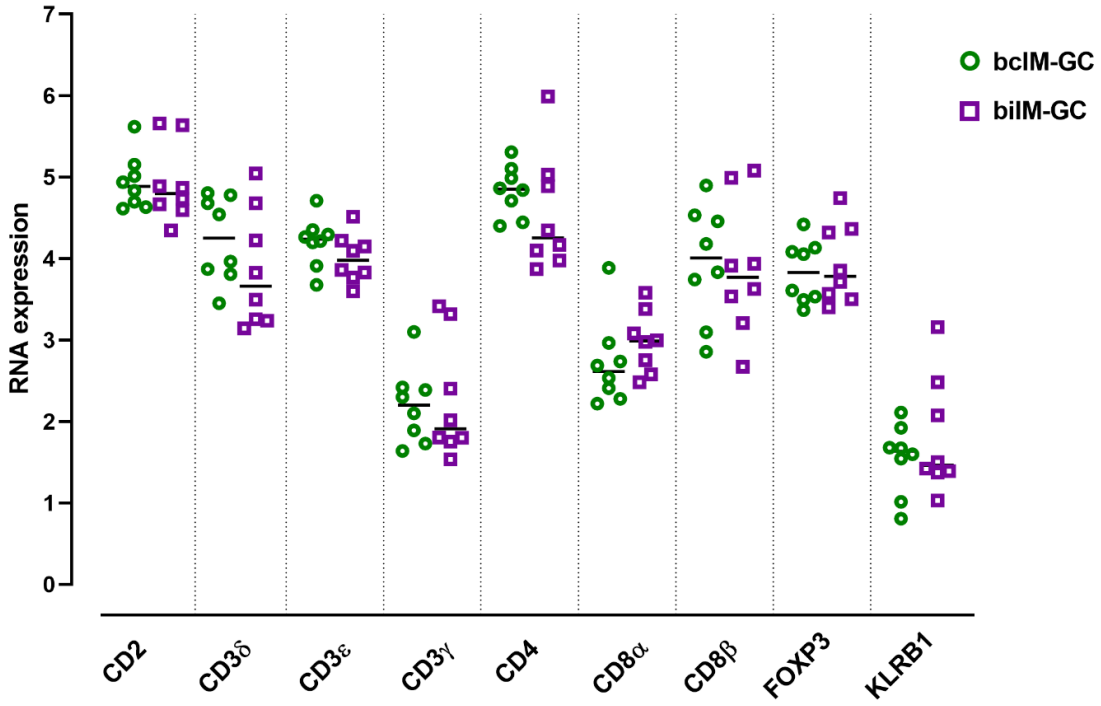


Figure 4.17 Gene expression of key T cell markers in the IM-GC samples from the Companioni 2017 study [388]

Unpaired t-test and Mann-Whitney test used for statistical analysis, dependent on data distribution. Analysis carried out on bioinformatically subtyped samples from the Companioni et al 2017 study.

Table 4.10 Significantly enriched cytokines, chemokines and their associated receptors using the IM-GC samples from the Companioni et al 2017 study [388]

Cytokine	logFC	p val.	Chemokine	logFC	p val.
High in bcIM-GC			High in bcIM-GC		
IL32	1.77	1.50E-03	*CCL25*	1.69	2.50E-02
IFNGR1	1.22	4.10E-02			
IL22RA	1.03	2.70E-03			
IFNAR1	0.63	2.00E-02			
IL18BP	0.97	3.40E-02			
TGFBR2	0.21	1.70E-03			
High in biIM-GC			High in biIM-GC		
IL36B	-0.18	4.20E-02	None		

All genes of the interleukin family (IL), the interferon family (IFN), the transforming growth factor family (TGF) and all chemokine related genes (CCL, CCR and CXCL and CXCR) were analysed for significant difference in gene expression (Appendix F). Analysis carried out on bioinformatically subtyped samples from the Companioni et al 2017 study.

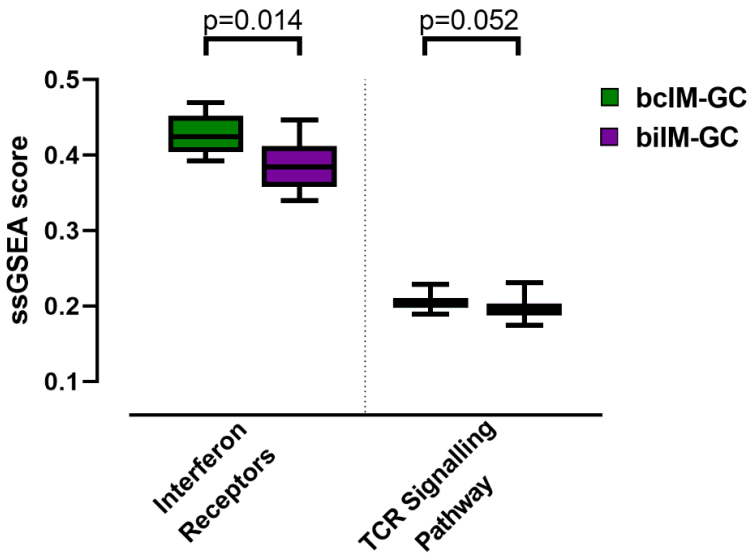


Figure 4.18 Single sample GSEA using ImmPort immune related gene sets with the IM-GC samples from the Companioni et al 2017 study [388])
ssGSEA carried out on bioinformatically subtyped samples from the Companioni et al 2017 study using the GSVA package in R. Wilcoxon test used to determine statistical significance. Curated immune related gene lists downloaded from https://www.immport.org.

4.4 Summary and discussion

The following is a summary of the main outcomes of this study.

1. Chronic gastritis and intestinal metaplasia share similar immune cell profiles and are predominantly rich in plasma cells, CD4+ resting memory and CD8+ T cells, M2 macrophages and mast cells.
2. Progression to both intestinal and diffuse gastric cancer subtypes is characterised by a shared loss of gastro-intestinal epithelial processes and gain of stromal associated activity when compared to chronic gastritis and intestinal metaplasia.
3. Intestinal and diffuse gastric cancer share common enriched cancer hallmark pathways but at differing levels of significance when compared to intestinal metaplasia as a potential unique precursor lesion.
4. Intestinal metaplasia in patients with gastric cancer is associated with greater levels of inflammation and enriched *MYC* and *E2F* transcription factor activity when compared to intestinal metaplasia in patients without gastric cancer.
5. Subtyping based on gene expression profiles shows high expression of small intestine associated genes in complete IM and of colon associated genes in incomplete IM. Several genes associated with gastric cancer were also upregulated in the latter.
6. Bioinformatically subtyped complete IM is highly enriched in gene expression and pathways associated with T cell function.

4.4.1 Discussion

In the current study, IM was initially shown to be enriched in immune system associated processes by comparison to normal tissue. Further investigation of the immune microenvironment in CG and IM using CIBERSORT showed not only an abundance of plasma cells but also CD4+ resting memory and CD8+ T cells confirming the chronic character of inflammation in these two lesion types. Interestingly both CG and IM had a high abundance of M2 macrophages and also equal amounts of resting and activated mast cells. M1 macrophage abundance was relatively low, suggesting a prevalent Th2 presence in these samples. A previous study by Quiding-Jarbrink et al 2010 [205] showed a mixed M1/M2 macrophage profile in CG with enhanced M1 polarisation in AG. Four of the six AG patients in that study also had local intestinal metaplasia but no IM data was provided. By contrast Petersen et al 2014 [207] showed the presence of CD163 positive macrophages in IM suggesting a predominant M2 response. Overall in the current study no significant differences were detected between CG and IM in the context of immune cells except for an increased abundance of resting dendritic cells in the latter.

Following on from the histology based findings in Chapter 3, the potential role of CG and IM as precursor lesions not only for the intestinal subtype but also for the diffuse subtype of GC was investigated by identifying a set of genes commonly differentially overexpressed in the premalignant lesions and a set of genes commonly differentially overexpressed in the malignant lesions. Overall the former was associated with digestion, loss of gastrointestinal epithelial function and tissue homeostasis. The latter was associated with ECM organisation and structural developmental processes.

The possible role of IM as a unique precursor lesion to both IGC and DGC was further investigated by characterising commonly enriched pathways. Overall IGC and DGC showed shared enrichment in several cancer hallmark pathways with the former more associated with cell proliferation including MYC and E2F targets and the latter more associated with Notch/TGFβ signalling and EMT as would be expected from poorly differentiated morphology of this tumour type, as reported in previous studies [160, 406, 437-441]. The possibility of a shared precursor for both intestinal and diffuse gastric carcinogenesis was recently suggested by a study which described two mouse models with alterations in pathways that characterise the CIN and the GS subtypes of human GC [442]. *Anxa10*-CreER^{T2};*Tp53*$^{R172H/+}$;*Kras*$^{G12D/+}$; *Smad4*$^{fl/fl}$ mice produced intestinal type tumours with glandular structures whereas *Anxa10*-CreER^{T2}; *Cdh1*$^{fl/fl}$;*Kras*$^{G12D/+}$; *Smad4*$^{fl/fl}$ mice produced poorly differentiated diffuse type tumours with signet ring cell

formation suggesting that mutations in just two key GC associated genes (TP53 and CDH1) may be enough for divergent carcinogenesis from a common precursor.

Using available expression data from normal, CG, IM and unmatched IGC trends of enriched chromosomal bands were identified and compared to available in-house chromosomal copy number data (Busuttil et al 2020 [411]). The chromosomal locations 8q24, 7p15, 7p14, 7p and 1p11 were the five most enriched by gene expression. Although a previous study showed that the correlation between copy number gains and upregulation of mRNA levels are gene-specific in GC [410], the chromosomal CN data in the current study showed good correlation with the expression data confirming that IGC is mainly a chromosomal instability disease, as shown in the TCGA study where ~49% of GC had CIN [42]. Although gene expression dysregulation through altered methylation levels has been shown to play an important role in gastric carcinogenesis, chromosomal instability is highly characteristic of many GC tumour cells [40, 42, 443, 444]. Chromosomal instability and in particular that of chromosome 8 seems to be one of the earliest destabilising events, as MYC (on 8q24) and chromosome arm 8q amplification both have been shown to occur in IM and are associated with increased risk of progression [127, 159]. MYC is a known oncogene with key roles in cell proliferation, cell growth, cell differentiation and apoptosis and MYC mRNA/protein expression levels have been previously shown to be significantly associated with chromosomal copy number in GC [160, 410, 445, 446]. Other chromosomal gains, particular of chromosome 7, 13 and 20 have also been shown to occur frequently in GC [447-450].

To characterise the role of IM as a premalignant lesion to GC, IM tissue from patients without (IM-GC) and with concurrent GC (IM+GC) were compared. Generally in cancer studies, histologically normal tissue adjacent to tumour is used as a control to identify aberrations. Although implied, histological normalcy does not equate to molecular normalcy. Indeed, normal tissue adjacent to tumour is reported to show allelic imbalance, altered telomere length, epigenetic and transcriptomic abnormalities [451, 452]. This may reflect an intermediate state between true healthy normal and tumour tissue, possibly until at least 1 cm away from tumour, with commonly over-expressed genes involved in inflammation and wound healing processes [451-453]. In the current study a small number of IM+GC samples taken at least 2cm away from tumour were macro-dissected to remove stromal contaminants and enrich for IM epithelium (rIM+GC) and their expression profiles compared to that of macro-dissected IM-GC samples. Interestingly the rIM+GC samples showed enrichment in gene expression and pathways associated with inflammation including T cell presence, ECM organisation and wound healing as

well as of two key GC associated genes, namely *MYC* and *SOX9*. Overall these results suggest that the "field cancerisation effect" persists even in tissue greater than 2cm away from tumour [412, 454]. The consequence of this is that molecular progression risk studies for IM patients are much more suitably carried out in IM patients without than in IM patients with concurrent GC. However IM samples from patients that have progressed to dysplasia and from patients with concurrent GC could still be used as comparators to study progressive intermediate IM stages towards malignancy.

Using gene expression profiles of a small number of key intestinal genes, IM-GC samples were separated into three groups representative of histological subtypes of intestinal metaplasia, the complete, the incomplete and the mixed subtype. One of the main assumptions was that complete IM is similar to the small intestine and will express high levels of brush border associated genes such as *MME* (CD10), *Villin* and *SI*, all three of which have been previously shown to be present in IM [133, 413, 414]. Another key assumption was that incomplete IM is similar to the colon thus it will express colon specific mucins such as *MUC12* and mixed IM samples will express a mixture of both types of intestinal markers. This is the first attempt to subtype intestinal metaplasia using a histo-molecular approach.

Overall the gene expression profile of complete IM was shown to be similar to that of the small intestine with overexpression of multiple mature enterocyte related genes and enrichment of brush border, digestion and metabolism related processes. By contrast the incomplete subtype was enriched in expression of colon but also GC associated genes including CLDN1, CDH3 and the GC biomarker *CEACAM5* [429, 430]. Of particular interest was the overexpression of the homeobox genes *HOXA10* and *HOXA13*, both found on enriched chromosome band 7p15. Given that both *HOXA10* and *HOXA13* have transcription target binding sites for MYC and E2F1 (gene located on highly amplified chromosome arm 20q in GC samples), it is possible that synergy between key transcription factors on amplified chromosomes plays an important role in early progression from incomplete IM to dysplasia/gastric cancer (https://www.genecards.org/, [455]).

As GC occurs in the context of long term chronic inflammation and considering little is known about the role of the immune microenvironment in progression, immune gene expression profiling was carried out using the bioinformatically subtyped IM-GC samples to identify potentially significant differences. Gene and pathway analysis showed higher expression of multiple T cell associated genes including CD3δ, CD3γ, CD8α and KLRB1 and overall enrichment in Chemokine, Cytokine and TCR signalling in complete IM. A biological explanation for increased

T cell gene expression and thus possibly of T cell infiltration was offered by the highly positive correlation with CCL5 and CCL25, two chemokines known to be chemotactic for T cells [456, 457]. Interestingly the latter is selectively secreted by small intestinal epithelial cells suggesting that complete IM reproduces at least in part small intestinal immune functions (Campbell and Butcher 2002). Single gene cytokine and chemokine analysis further showed overexpression of multiple pro-inflammation related markers including *IL6R* and *IL11RA* in complete IM suggesting the presence of an inflammation-rich microenvironment.

Incomplete IM had higher expression of *IL18* whereas complete IM had higher expression of *IL18RAP*, a receptor accessory protein associated with IL18 activity but also of *IL37*, an anti-inflammatory cytokine which inhibits IL18 signalling [458] suggesting that IL18 activity may form a fundamental immune difference between complete and incomplete IM. Gene correlation analysis showed that *IL18* was highly negatively correlated with *CD2* and also *CD8α* suggesting a possible immune-regulatory role for this cytokine. Generally IL18 is regarded as a pro-inflammatory cytokine with the capacity to activate established Th1 cells to produce IFNγ in the presence of IL12 [459]. However in the absence of IL12 and presence of IL2, IL18 stimulates NK cells, NKT cells and established Th1 cells to produce IL3, IL9 and IL13 thus facilitating a Th2 response [458]. In a mouse model with *Helicobacter felis* infection IL18 was shown to counteract excessive gastric immunopathology, possibly by regulating an excessive Th17 cell driven response [460]. In the intestine, intestinal epithelial cells were shown to produce large amounts of IL18 which regulated Th17 cell differentiation and was critical for FOXP3+ regulatory T cell-mediated control of intestinal inflammation [461]. Incomplete IM also showed differential overexpression of CXCL5, a powerful chemoattractant for neutrophils [462, 463] suggesting that this immune cell type may have higher levels of infiltration in this subtype of IM. Previously Fu and colleagues showed a 9-fold and 24-fold increase in neutrophils when comparing intestinal metaplasia and gastric cancer tissues with normal gastric tissue controls [193].

Finally the T cell immune microenvironment was further investigated using the KLRB1 gene signature from Fergusson et al [434] and shown to be not only enriched in complete IM but also to be highly positively correlated with brush border genes. KLRB1 is expressed on most NK cells, Th17 cells, γδ T cells and with particular high expression on MAIT cells [434]. Thus complete IM may be rich in Th17/innate like T cell populations.

Overall these data suggest that the immune response in intestinal metaplasia exists within a spectrum that has two distinct extremes. On the one side is a possible highly inflammatory environment rich in CD8+ and innate like T cells and most likely dependent on IL6 and IL11

signalling notably in complete IM; on the other side exists an IL18 immuno-regulatory environment with a reduced T cell immune response, possibly associated with neutrophil infiltration driven by CXCL5 recruitment, notably in incomplete IM.

To validate the current study's findings, gene expression profiling of a cohort [388] similar to the IM-GC cohort was carried out using the 28 differentially expressed gene list previously obtained (§4.3.8 and §4.3.14). Overall the validation cohort separated into two distinct clusters, one with high expression of small intestine specific genes such as SFRP5, RPB2, MME and also higher expression of CCL25 as observed in my study, and a second cluster with low expression of this type of genes. However these two clusters did not fully correlate with the histologically assigned subtypes in their study. Differences observed between the two data sets may be explained by the following:

1) The Companioni data set [388] was obtained using the Affymetrix Almac Xcel array specifically optimized for use with degraded paraffin embedded formalin fixed tissue. Although RNA integrity was checked at the time of extraction, it does not necessarily translate to the same RNA quality obtained within our lab from snap frozen tissue.

2) The Companioni study used RNA extracted from whole sections not from macro-dissected IM areas of sections, thus had possibly relatively lower IM epithelial content and was more likely contaminated with T cell rich tertiary lymphoid structures that occur near IM and can dilute potentially significant differences.

3) Complete and incomplete IM glands are intermixed three-dimensionally within most samples and a different subtype may be predominantly present at different depths of a biopsy. As a result the histologically defined section may not be truly representative of the entire biopsy.

4) The RNA extraction kits used differed between the Companioni study and our laboratory: Recover All Nucleic Acid for FFPE kit by Ambion versus mirVANA kit by Applied Biosystems. The microarray quantification platform used in our lab was the Affymetrix® Human Genome U133 Plus 2.0 Array, which is 98% cross-mapped to the Almac Xcel™ Array. Although this played an important role in choosing this dataset for validation, potential differences are still possible.

5) The ethnic origin of the patient cohorts used (multi-ethnic including eastern Asian patients living in Victoria for the Australian vs mainly Spanish patients in the Campanioni study) differed which may have contributed to different IM profiles.

4.4.2 Study limitations

This study included a systematic analysis of gene expression profiles to characterise both gastric premalignant and malignant tissues. Also macro-dissected IM samples with an enriched epithelial component were subtyped using a novel histo-molecular approach. However the current study did have a small number of potential limitations including:

a) The small number of normal and premalignant tissue samples from GC patients characterised; the effect of the latter was minimised by using pooled analysis of each premalignant lesion type (CG and IM) when comparing to malignant tissue types (IGC and DGC) instead of matched patient analysis.

b) The small number of macro-dissected rerun IM+GC samples and IM-GC samples thus producing results with limited statistical power.

c) The small number of samples available in the validation data set by Companioni et al 2014.

d) Although highly informative, this *in silico* study does not reveal the cell type of origin for specific genes; targeted validation of some of this study's key findings is described in Chapters 5-7 using single and multiplex immunohistochemistry.

Overall the current study investigated the immune microenvironment in CG and IM, provided possible gene expression evidence linking both these lesions with progression not only to the intestinal but also to the diffuse subtype of GC and showed that two molecular types of IM exist, one enriched in expression of small intestinal genes and pathways similar to histological complete IM and another type with high expression of colon related genes similar to histological incomplete IM. The bioinformatically subtyped complete IM seemed to have a T cell rich inflammatory signature whereas the incomplete IM was characterised by a relatively immuno-suppressive environment with possibly reduced T cell infiltration. The validation data set from Campanioni et al partially supported the findings from this bioinformatics approach to subtyping IM samples. Finally the difference in immune signatures between IM subtypes associated with differing risk of progression to GC may play a significant role and requires further characterisation using other methods such as immunohistochemistry.

Chapter 5 Characterising the macrophage landscape in intestinal metaplasia

5.1 Introduction

Gene expression analysis described in section §4.3.3 of this thesis suggested that M2 macrophages were the predominant macrophage population in both chronic gastritis and intestinal metaplasia. Macrophages with M2 characteristics ("alternatively activated", promote cell proliferation and tissue repair) are functionally highly heterogeneous and based on the applied stimuli and resulting transcriptional changes, M2 macrophages have been further subdivided into M2a, M2b and M2c states and in some instances into M2d as well [195, 464-466]. The M2a state is created in an environment rich in IL4 and IL13, the M2b state as a response to immune complexes and LPS, the M2c in the presence of glucocorticoids and TGFβ and the M2d state as a response to IL6 and leukemia inhibitory factor. It is not obvious whether these states are fixed or in flux depending on the local *in vivo* microenvironment. Activated by intracellular pathogens, LPS, IFNγ and TNFα the M1 macrophage phenotype ("classically activated", pro-inflammatory) seems to reside in a more stable state and is associated with the ability to secrete inflammatory cytokines and produce nitric oxide (NO) which is cytotoxic to target cells [195].

Studies of the immune microenvironment associated with premalignant gastric lesions have primarily focussed on identifying and characterising the key immune changes in chronic gastritis (CG) [205, 213, 467-470]. Some studies have combined chronic with atrophic gastritis (AG) to identify changes associated with progression but only a limited number of studies have attempted to characterise the immune microenvironment in intestinal metaplasia (IM) [207, 236, 471].

So far no other study has studied the macrophage landscape in the complete and incomplete subtypes of IM with the aim to identify differences that may explain their differing risk associated with progression to gastric cancer (GC). As described in section §4.3.7 using gene expression profiling, in addition to histological progression there is an element of temporal progression in IM samples from patients without (IM-GC) to patients with concurrent GC (IM+GC) due to a possible "field cancerisation effect" extending at least 2cm away from the tumour. Thus using tissues from both the IM-GC and the IM+GC cohorts a histo-temporal model of gastric carcinogenesis can be constructed based on IM subtype together with IM-GC samples representing "early IM" and IM+GC samples representing "late IM".

5.2 Hypothesis and aims

Hypothesis: “The macrophage landscape differs between intestinal metaplasia subtypes and is associated with differing risk of progression”.

The main aims of this study were:

1. To identify and characterise total macrophage and macrophage subset density in CG, complete and incomplete IM in the IM-GC and IM+GC cohorts in both histological and temporal order of progression.
2. To compare macrophage density in CG surrounding IM in the IM-GC and IM+GC cohorts and between cohorts.
3. To determine quantitative relationships between macrophage subset densities and between macrophage subsets and epithelial cells by investigating their ratios in the IM-GC and the IM+GC cohorts.
4. To characterise the spatial relationships between macrophage subsets and between macrophages and epithelial cells in the IM-GC and the IM+GC cohorts.
5. To characterise the macrophage landscape in two patients that have progressed to high grade dysplasia (“Progressors”).

5.3 Results

5.3.1 Description of cohorts used in this study

Samples representative of the IM-GC, IM+GC and Progressors cohorts were used as described in Table 5.1. Where available, CG areas surrounding IM and dysplastic areas on the same section were also characterised. For the IM-GC and the Progressors cohorts, tissue was obtained during gastroscopy and collected using the updated Sydney protocol as described in §1.2.3 and Figure 1.8. Subtyping of IM was carried out as described in §2.5.1 and Figure 2.3.

Table 5.1 Clinical details of patients used for the OPAL™ multiplex immunohistochemistry macrophage study from the IM-GC, the Progressors and the IM+GC (MAUGIC) cohorts

Parameters	IM-GC (n)[1]	Progressors (n)[2]	IM+GC (n)
Gender			
Male	12	2	13
Female	6	0	7
Age			
Male	69 (39-86)[3]	60-68 (64)[3]	68 (39-86)[3]
Female	71.5 (44-79)[3]	-	66 (49-83)[3]
Premalignant condition			
Chronic gastritis	12	15	15
Intestinal metaplasia subtype[4]			
complete	10	5	11
incomplete	12	11	9
Dysplasia	0	4[5]	0
Premalignant tissue site			
Antrum			
A1	10	6	nd
A2	1	4	nd
A3	7	6	nd
Body			
A4	3	3	nd
A5	2	1	nd
Matched tumour pathology			
Intestinal	-	-	14
Diffuse	-	-	6
Matched tumour location			
Antrum	-	-	11
Body	-	-	8
GOJ	-	-	1
T stage			
Tis	-	-	2
T1	-	-	3
T2	-	-	5
T3	-	-	9
Unspecified	-	-	1
Lymph node status			
N0	-	-	14
N1	-	-	4
N2	-	-	1
Unspecified	-	-	1

[1]For some patients, more than 1 sample was characterised differing in either the site or the time point taken; [2]Cohort consisted of two patients (P1 and P2) with tissue taken from multiple stomach sites across multiple time points; [3]Median age and range; [4]Subtyping of intestinal metaplasia described in §2.5 and Figure 2.3; [5]P1 had 2 samples from the same site taken at different time points with high grade dysplasia and P2 had 1 sample with high grade dysplasia;

5.3.2 OPAL™ multiplex immunohistochemistry for macrophage panel

The OPAL™ multiplex immunohistochemistry (IHC) macrophage panel consisted of primary antibodies against the following antigens/cell markers: AE1AE3, CD68, CD163, CD206, IRF8 and PDL1 (§2.5.2, Table 2.9) as previously published by our laboratory [198]. Each OPAL™ antibody was optimised independently before multiplexing. Multiplex IHC was followed by low and high

resolution scanning on the VECTRA microscope and multi-parameter data was obtained using spectral unmixing with the previously created spectral library (§2.5.2, Appendix H), tissue segmentation and then cell segmentation with the inForm software (Figure 5.1). The number of regions of interest (ROIs) per sample differed dependent on size and CG and IM tissue abundance and this was taken into account by using a generalised linear model in R for statistical analysis (§2.5.7).

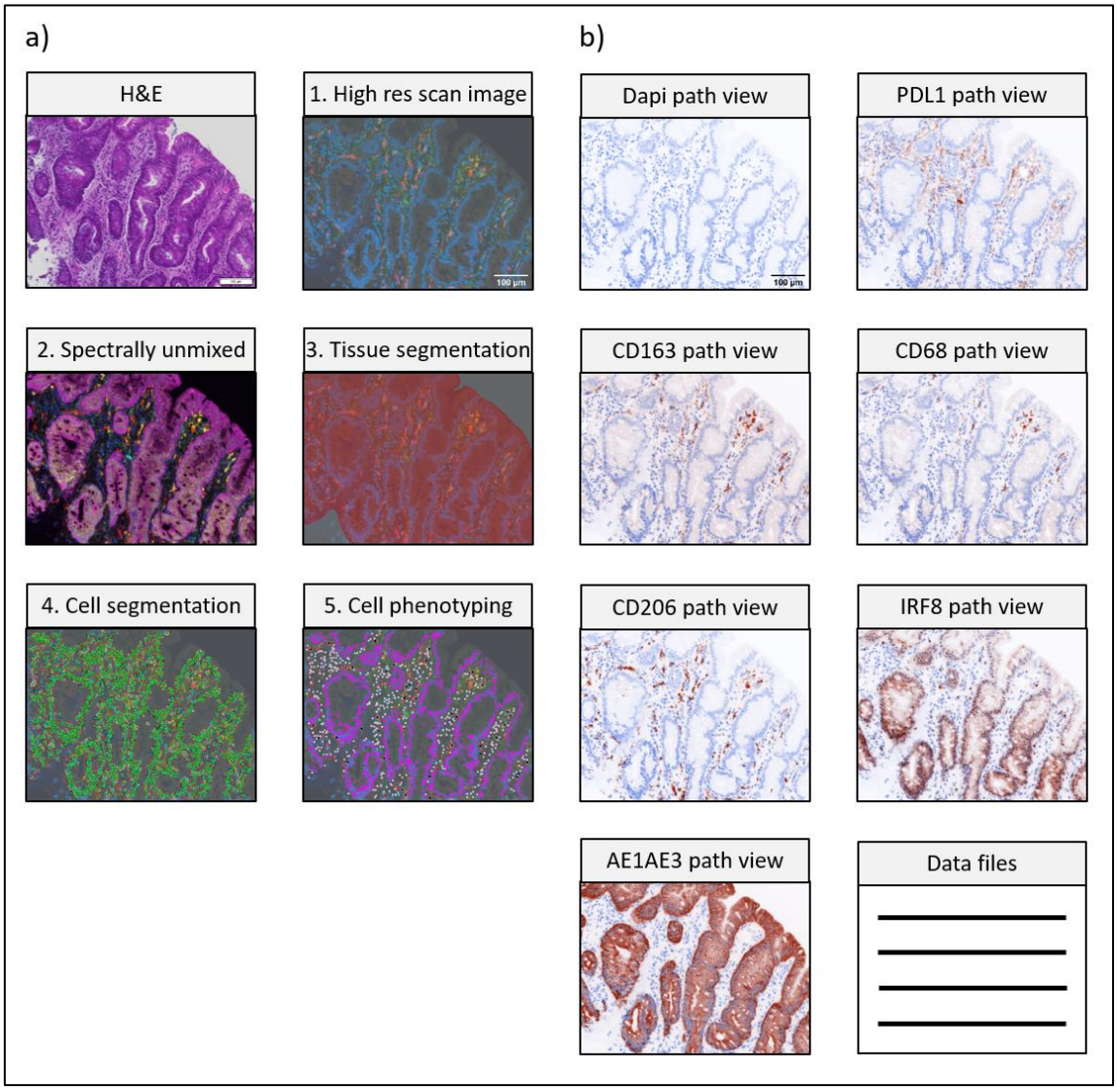


Figure 5.1 Use of inForm software to acquire multi-parameter single cell data from target tissue previously stained with OPAL™ reagents
a) High resolution images (x20) of target tissue were spectrally unmixed, tissue segmented, cell segmented and then cell phenotyped using the classifier tool in inForm; b) Pseudo-pathology images of each OPAL™ fluorophore (marker) shown. Scale bars: 100µm.

Dapi was used as a nuclear counterstain for cell visualisation and segmentation. All CD68+ cells were considered to be macrophages. CD163 (Haemoglobin-Haptoglobin Scavenger Receptor) and CD206 (C-Type Mannose Receptor 1) were considered M2 macrophage markers [472] and IRF8 (interferon regulatory factor 8) which is induced by IFNγ was considered an M1 marker

[473]. Epithelial cells (Ep) were identified as AE1AE3+ cells. Cells positive only for Dapi were assigned to a group named Other. PDL1, an immune checkpoint protein associated with T cell response regulation [474], was added to the panel to identify potential variations in its expression across premalignant lesions.

5.3.3 Macrophage immune profile in gastric premalignant lesions consists of six main subsets

Based on the cellular co-localisation of the markers used in the OPAL™ multiplex IHC macrophage panel (§2.5.2, Table 2.9), six main subsets (CD68+CD163+, CD68+CD163+IRF8+, CD68+CD163+CD206+, CD68+CD163+CD206+IRF8+, CD68+CD206+ and CD68+IRF8+) were identified in the gastric premalignant tissues characterised across all cohorts studied: (Figure 5.2). The majority of macrophages were located near the epithelium, usually as individual cells although macrophage aggregates were occasionally observed. Overall, most samples characterised were rich in macrophages.

The following became apparent while characterising the macrophage populations in these gastric premalignant tissues:

- M1 macrophages (CD68+IRF8+) were rarely seen and often completely absent.

-Three macrophage populations did not follow a strict M1/M2 paradigm as they displayed markers of both: CD68+CD163+CD206-IRF8+, CD68+CD163+CD206+IRF8+, and CD68+CD163-CD206+IRF8+. To adjust for this, these three subsets were used to create a novel macrophage subgroup: M1/2 macrophages that may have properties of both traditional M1 and M2 macrophages (M2 markers in the presence of IFNγ in the microenvironment as shown by IRF8 expression) and most likely lie functionally somewhere in the middle of the M1 and M2 bipolar spectrum.

5.3.4 Level of expression of key markers differs between macrophage subsets

To detect possible differences in levels of marker expression between macrophage subsets, all macrophages in tissues belonging to all three cohorts (IM-GC, IM+GC and Progressors) were analysed by normalised mean marker intensity (Figure 5.3). CD68 was expressed less in the CD68+CD163+CD206+ subset compared to the other subsets. CD163 expression in both CD68+CD163+ and CD68+CD163+CD206+ (both M2) subsets was lower than that observed in CD68+CD163+IRF8+ and CD68+CD163+CD206+IRF8+ macrophages (both M1/2). CD206 had lower expression in CD68+CD163+CD206+ macrophages (M2) compared to the CD68+CD163+CD206+IRF8+ and CD68+CD206+IRF8+ macrophages (both M1/2). Finally

CD68+IRF8+ macrophages (M1) had higher IRF9 expression than CD68+CD163+IRF8+, CD68+CD163+CD206+IRF8+ and CD68+CD206+IRF8+ macrophages (all M1/2).

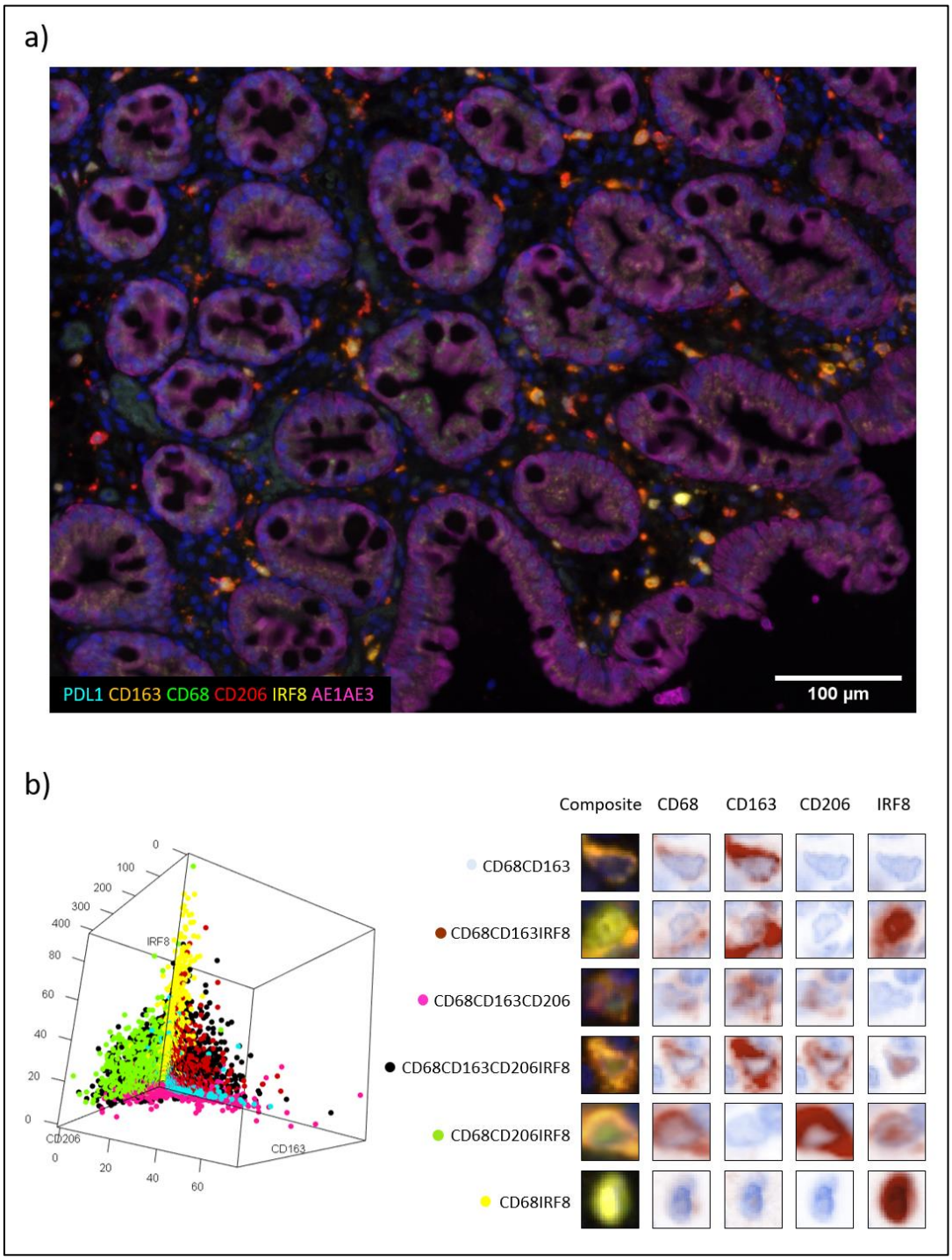


Figure 5.2 Spectrally unmixed image and 3D scatter plot showing multiple macrophage subsets (CD68+ cells) present in gastric premalignant lesions based on cellular co-localisation of markers

a) shows various macrophages between intestinal metaplastic glands as determined by the presence of goblet cells (black disks); b) shows the presence of six main types of macrophage subsets as shown by the combination of CD163, CD206 and IRF8 on CD68+ cells, first by normalised fluorophore intensity (bottom left, pooled total number of macrophages characterised=73250) and then on pseudo-pathology images produced by inForm from spectrally unmixed images (bottom right).

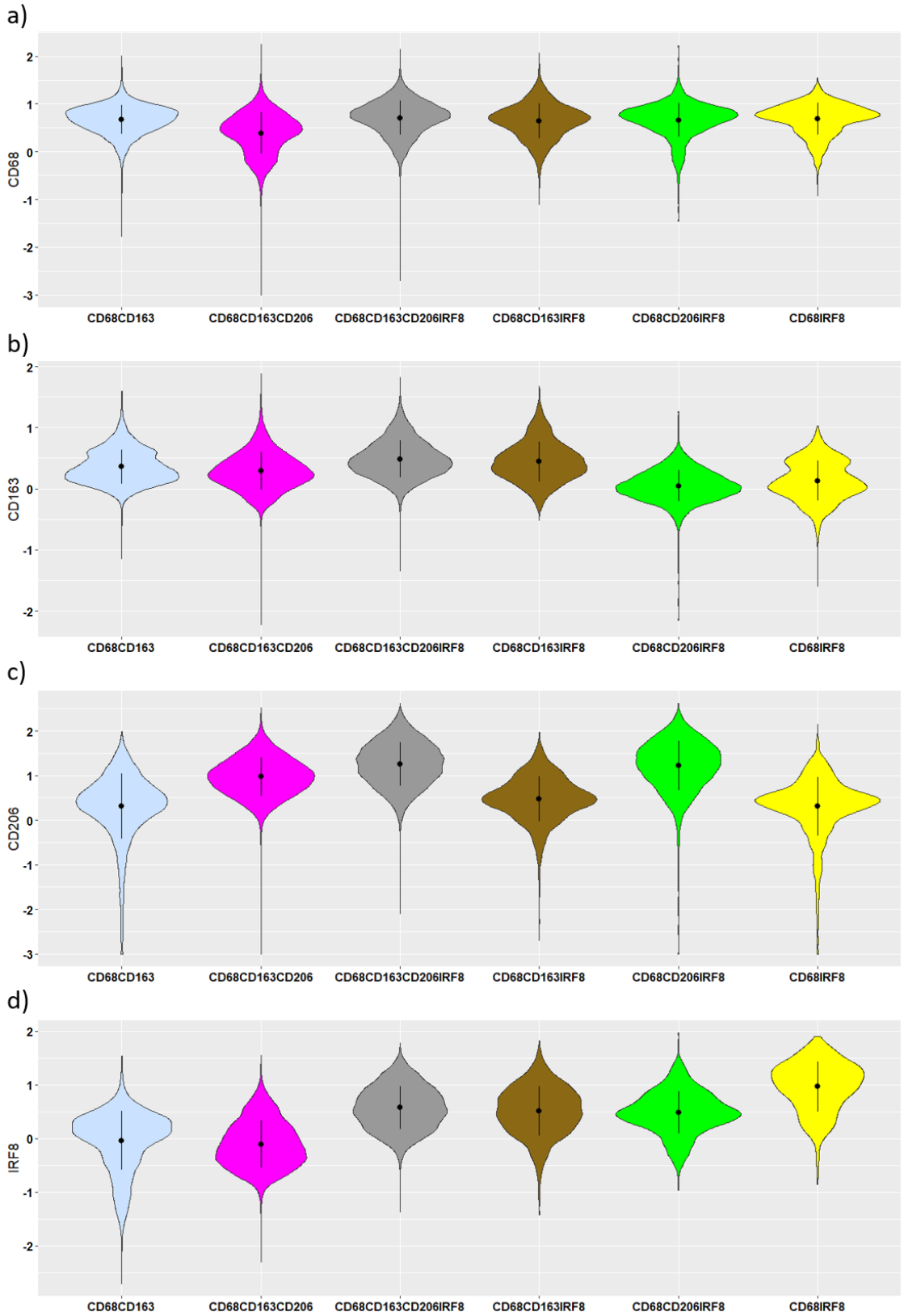


Figure 5.3 Normalised mean expression of key markers on macrophage subsets
Violin plots showing log transformed normalised mean intensity for key macrophage markers a) CD68, b) CD163, c) CD206 and d) IRF8. Mean with +/- SD shown. Data shown from pooled total number of macrophages in all tissues across IM-GC, Progressors and IM+GC cohorts (n=73250).

PDL1 expression on macrophages was rarely seen. PDL1 expression was occasionally observed on epithelial cells located in regions of chronic gastritis (Figure 5.4) but was not further investigated. IRF8 was expressed by other cells in addition to macrophages, including some intestinal metaplastic epithelial cells and other non-macrophage cells (CD68-ve cells).

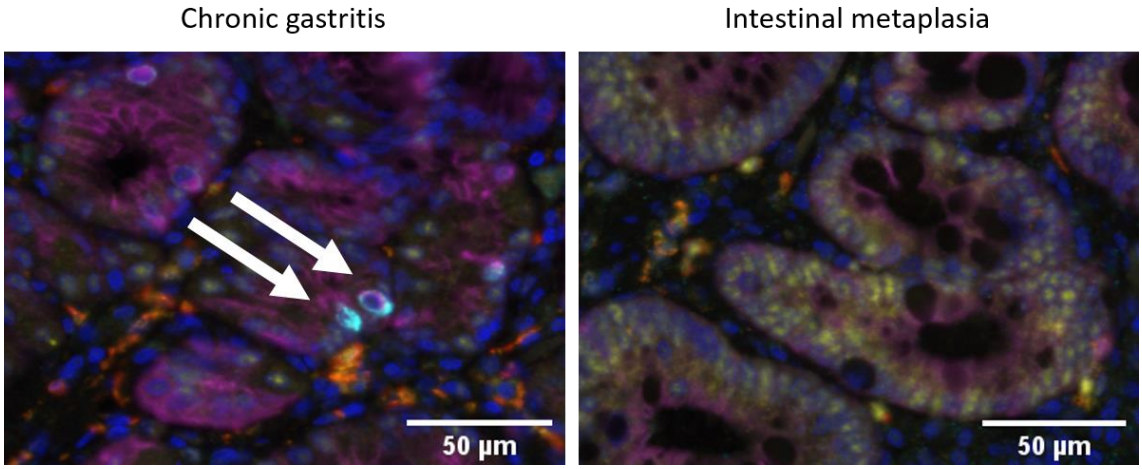


Figure 5.4 PDL1 staining on gastric epithelial cells but not on intestinal metaplastic glands
PDL1 staining (single light blue cells shown by white arrows, left image) was occasionally present on gastric epithelial cells in regions with chronic gastritis but was completely absent on intestinal metaplastic glands (right image).

5.3.5 Total macrophage cell density highest in complete and lowest in incomplete intestinal metaplasia with differing subset distribution

All macrophage (CD68+) subsets were quantified using inForm and combined to determine the total macrophage density for each tissue type studied in the IM-GC and IM+GC cohorts (Figure 5.5). Analysis of the IM-GC cohort showed total macrophage density was higher in complete IM (cIM-GC) than in CG (CG-GC; p=0.0072) and incomplete IM (iIM-GC; p=0.050) tissue. In all three tissue types, CD68+CD163+CD206+ and CD68+CD163+CD206+IRF8+ macrophages were the two predominant subsets, with a relatively larger component being CD68+CD163+CD206+IRF8+ in iIM-GC.

In the IM+GC cohort, a lower density of macrophages was detected in incomplete IM (iIM+GC) when compared to both CG (CG+GC, p=0.001) and complete IM (cIM+GC, p=1.6e-05) (Figure 5.5). Although the CD68+CD163+CD206+ and CD68+CD163+CD206+IRF8+ macrophage subsets were again the two largest across all three tissue types studied, a substantial component of the macrophage population in the IM+GC cohort was made up also of CD68+CD163+ and CD68+CD206+IRF8+ macrophages.

When comparing total macrophage density between IM-GC and IM+GC cohorts, relatively similar patterns and numbers were observed across the premalignant lesions studied but the distribution of the subsets differed substantially (Figure 5.5).

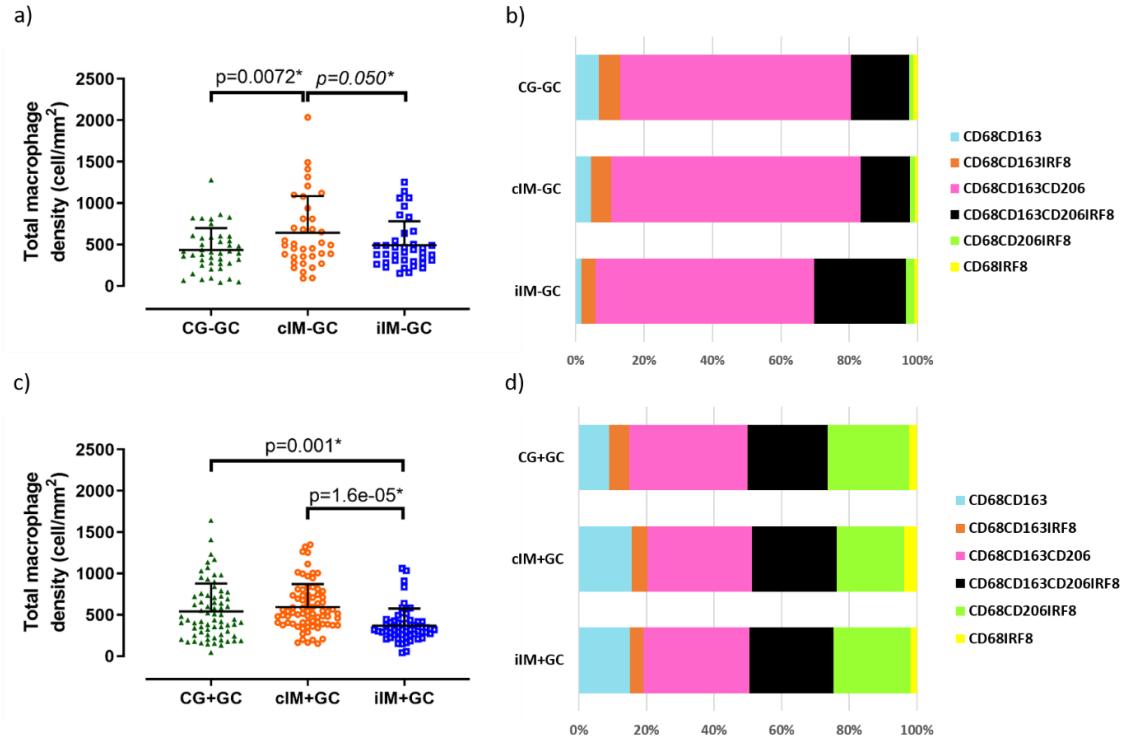


Figure 5.5 Total macrophage (CD68+) density differs between complete and incomplete intestinal metaplasia

a) Total macrophage density in samples with chronic gastritis (CG-GC, n=14), complete intestinal metaplasia (cIM-GC, n=10) and incomplete intestinal metaplasia (iIM-GC, n=11) from patients without gastric cancer; b) Distribution of macrophage subsets in CG-GC, cIM-GC and iIM-GC; c) Total macrophage density in samples with chronic gastritis (CG+GC, n=14), complete intestinal metaplasia (cIM+GC, n=9) and incomplete intestinal metaplasia (iIM+GC, n=7) from patients with gastric cancer (tissue samples taken at least 2cm away from tumour); d) Distribution of macrophage subsets in CG+GC, cIM+GC and iIM+GC. Each symbol represents data from a single region of interest (ROI). Multiple ROIs per sample. Data presented as mean + S.D. in a) and c) and as mean in b) and d). *All statistical analysis done using glm function in R.

5.3.6 M2 macrophages dominate the macrophage profile of the microenvironment in intestinal metaplasia

To accurately identify the quantitative distribution of M1, M1/2 and M2 macrophage subgroups in the IM-GC cohort, each subgroup was analysed separately by tissue type (Figure 5.6). There were very few M1 (CD68+IRF8+) macrophages in all three premalignant lesions investigated in this cohort. Most samples showed some infiltration of M1/2 macrophages (CD68+CD163+CD206+IRF8+, CD68+CD163+IRF8+ and CD68+CD206+IRF8+) with iIM-GC having a significant higher density than CG-GC (p=0.014). However M2 macrophages (CD68+CD163+CD206+ and CD68+CD163+) were the predominant macrophage population

across all three tissue types with cIM-GC having a significantly higher density than both CG-GC and iIM-GC (p=0.028 and p=0.0014 respectively).

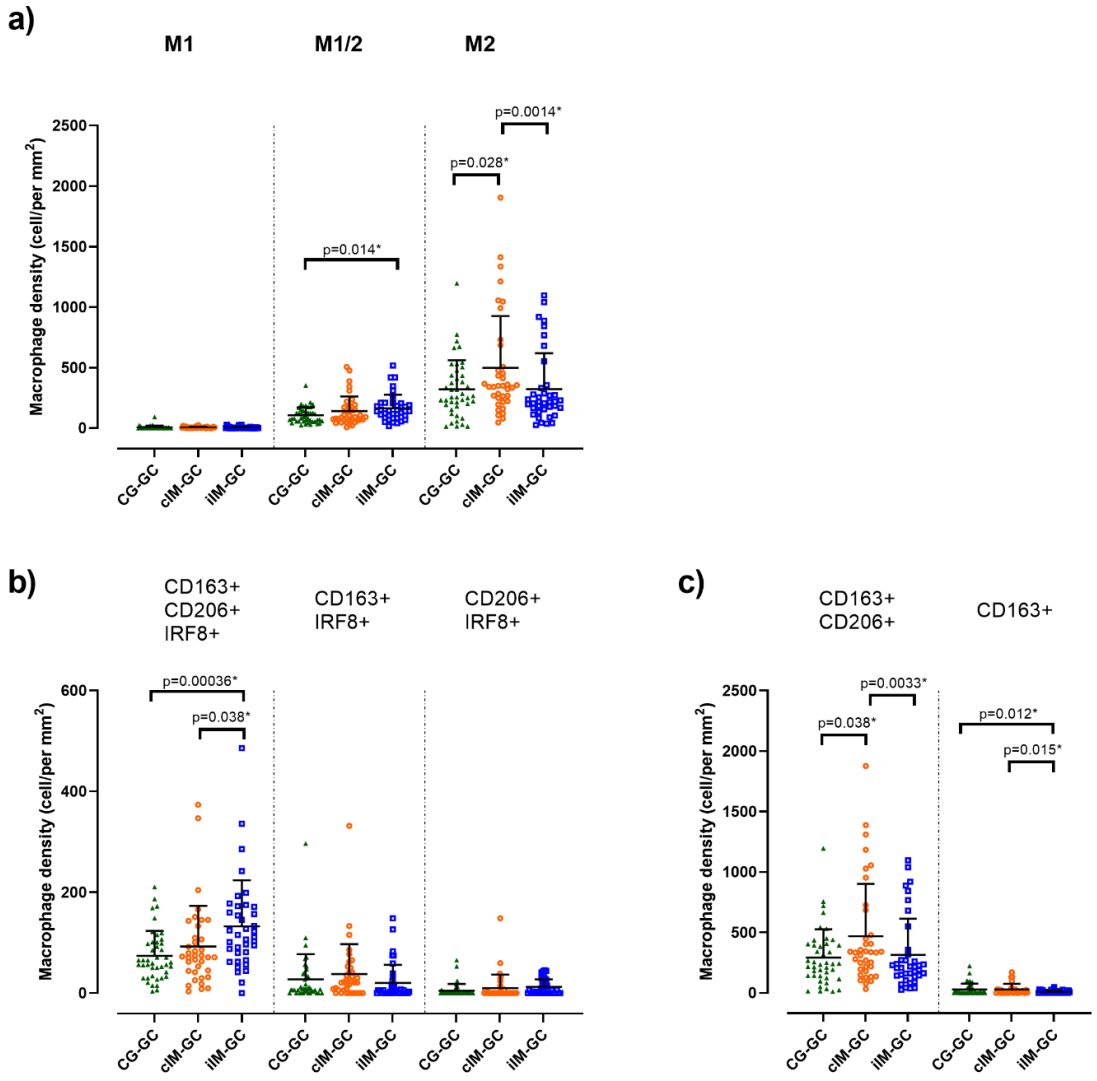


Figure 5.6 Macrophage subset density in premalignant tissues from the IM-GC cohort
a) Macrophage density of M1 (CD68+IRF8+), M1/2 (CD68+CD163+CD206+IRF8+, CD68+CD163+IRF8+ and CD68+CD206+IRF8+) and M2 (CD68+CD163+CD206+ and CD68+CD163+) macrophage subgroups, b) Macrophage density of M1/2 macrophage subsets and c) shows macrophage density of M2 subsets in CG-GC (n=14), cIM-GC (n=10) and iIM-GC (n=11) samples. Each symbol represents data from a single region of interest (ROI). Multiple ROIs per sample. Data presented as mean + S.D. *All statistical analysis done using glm function in R.

CD68+CD163+CD206+IRF8+ macrophages were the predominant M1/2 subset in all three tissue types with an incremental increase from CG-GC to cIM-GC and then to iIM-GC (CG-GC vs iIM-GC: p=0.00036 and cIM-GC vs iIM-GC: p=0.038). Although absent in several tissue samples, no significant difference was observed in CD68+CD163+IRF8+ and CD68+CD206+IRF8+ macrophage populations between IM-GC tissue types. CD68+CD163+CD206+ macrophages were the predominant M2 subset with cIM-GC having a significantly higher density than CG-GC and iIM-

GC (p=0.038 and p=0.0033 respectively). Although only a minor population, CD68+CD163+ macrophages were fewer in iIM-GC than in CG-GC and cIM-GC (CG-GC vs iIM-GC: p=0.012 and cIM-GC vs iIM-GC: p=0.015).

Analysis of the IM+GC cohort showed there were again very few M1 macrophages (CD68+IRF8+) (Figure 5.7). Interestingly M1/2 and M2 macrophages were present in roughly equal amounts between all three tissue types investigated with iIM+GC showing a significant reduction in both macrophage subgroups compared to cIM+GC (p=0.0043 and p=0.0001 respectively). In more detail, iIM+GC had significantly lower cell density of CD68+CD163+CD206+IRF8+, CD68+CD163+IRF8+ (both M1/2, p=0.0082 and p=0.012 respectively), CD68+CD163+CD206+ and CD68+CD163+ (both M2, p=0.0082 and p=0.0045 respectively) macrophages compared to cIM+GC.

Overall in the IM-GC cohort M2 macrophages were the main subgroup, with high density of CD68+CD163+CD206+ macrophages in cIM-GC suggesting a possible protective role for this subset. In contrast iIM-GC had relatively more CD68+CD163+CD206+IRF8+ macrophages suggesting an association between this subset and a higher risk of progression. In the IM+GC cohort, there was a general shift towards the M1/2 phenotype with approximately equal numbers of M1/2 and M2 macrophages. However iIM+GC was characterised by a reduction of the majority of macrophage subsets (5 out of 6) suggesting that both quantitative and qualitative differences may play a role in progression.

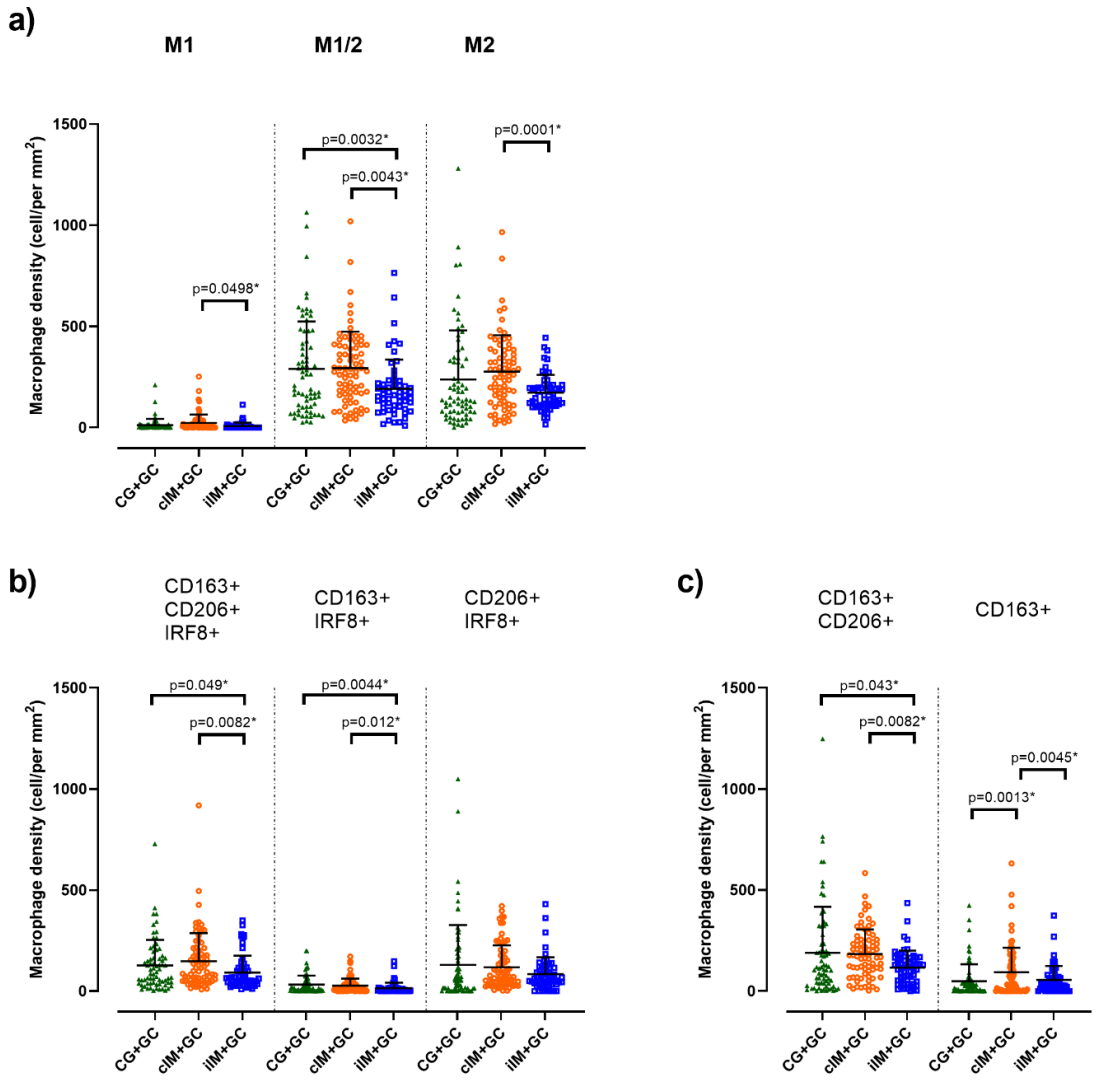


Figure 5.7 Macrophage subset density in premalignant tissues from the IM+GC cohort
a) Macrophage density of M1 (CD68+IRF8+), M1/2 (CD68+CD163+CD206+IRF8+, CD68+CD163+IRF8+ and CD68+CD206+IRF8+) and M2 (CD68+CD163+CD206+ and CD68+CD163+) macrophage subgroups, b) Macrophage density of M1/2 macrophage subsets and c) Macrophage density of M2 subsets in CG+GC (n=14), cIM+GC (n=9) and iIM+GC (n=7) samples. Each symbol represents data from a single region of interest (ROI). Multiple ROIs per sample. Data presented as mean + S.D. *All statistical analysis done using glm function in R.

5.3.7 Evolution of macrophage populations with time

To gain further insight into how changes in macrophage numbers and phenotype may play a role over time, total macrophage and subset densities were analysed across the IM-GC ("early premalignant lesions") and the IM+GC ("late premalignant lesions") cohorts. Total macrophage density in chronic gastritis increased with time (p=0.028) but decreased in incomplete IM (p=0.0056). No significance change was observed in complete IM (Figure 5.8).

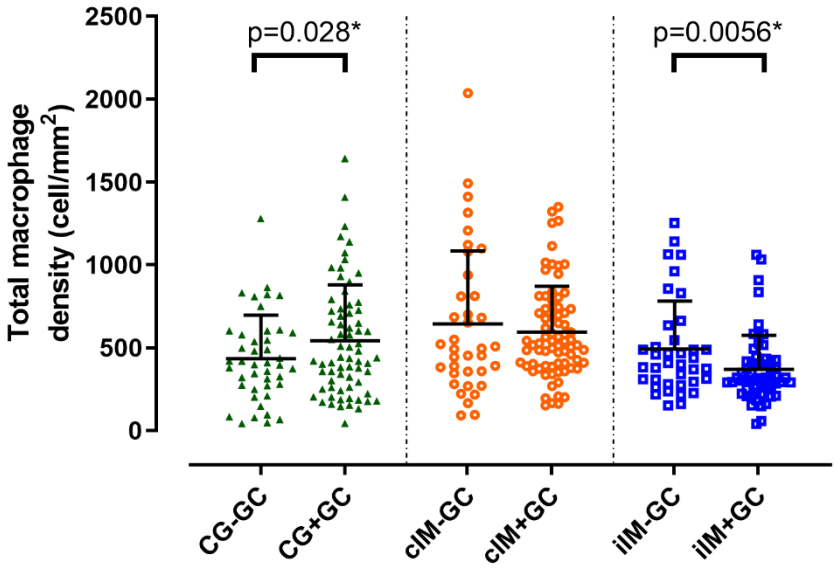


Figure 5.8 Differences in total macrophage density between IM-GC and IM+GC samples
Total macrophage cell density was compared between the IM-GC ("early premalignant lesions") and the IM+GC ("late premalignant lesions") cohorts to identify changes with time (temporal progression) within individual tissue types. Each symbol represents data from a single region of interest (ROI). Multiple ROIs per sample. Data presented as mean + S.D. *All statistical analysis done using glm function in R.

A more detailed analysis showed M1/2 macrophages were higher in CG+GC compared to CG-GC (p=6.1e-08). Both M1 and particularly M1/2 macrophages were significantly higher in cIM+GC compared to cIM-GC (p=0.043 and p=0.00018 respectively, Figure 5.9a). By contrast M2 macrophages were lower in both cIM+GC and iIM+GC compared to cIM-GC and iIM-GC respectively (p=0.027 and p=0.0004 respectively). The largest change in M1/2 subsets was observed in the CD68+CD206+IRF8+ subset which showed an increase across all three tissue types (for chronic gastritis p=0.001, for complete IM p=1.7e-06 and for incomplete IM p=2.6e-05, Figure 5.9b). Additionally an increase in CD68+CD163+CD206+IRF8+ was also detected in chronic gastritis (p=0.0028). M2 macrophage subsets showed opposing trends, with CD68+CD163+CD206+ macrophages decreasing (for chronic gastritis p=0.049, for complete IM p=3.0e-05 and for incomplete IM p=1.4e-05) and CD68+CD163+ macrophages increasing (for chronic gastritis p=0.045, for complete IM p=0.00012 and for incomplete IM p=0.00048) in density with time across all three tissues (Figure 5.9c).

Overall, temporal progression was characterised by a dynamic change in macrophage subset densities in all three premalignant lesions studied and was associated mainly with a lower total macrophage population (incomplete IM), an overall increase of M1/2 macrophages particularly of the CD68+CD206+IRF8+ subset and a decrease in M2 macrophages particularly of the CD68+CD163+CD206+ subset (Figure 5.9).

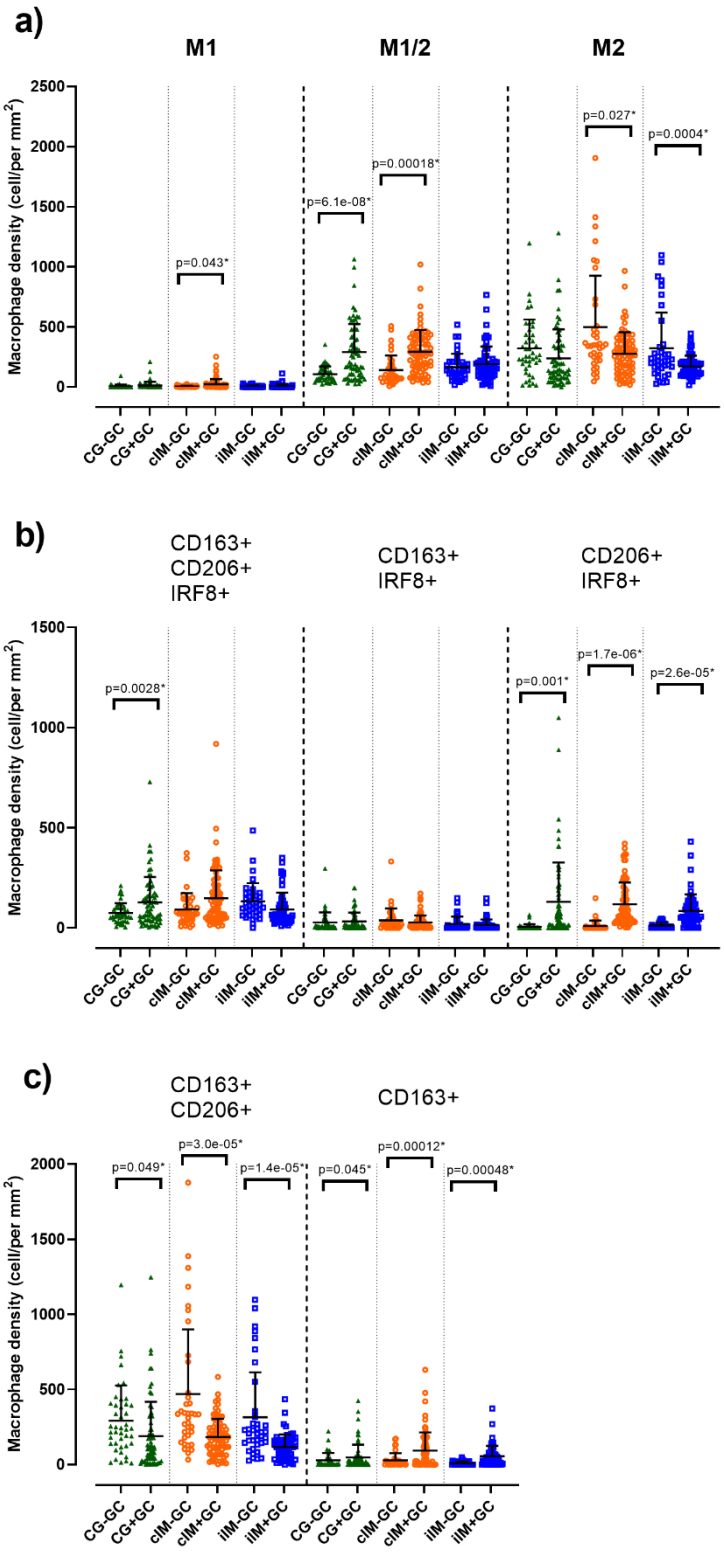


Figure 5.9 Differences in macrophage subset content between IM-GC and IM+GC samples
a) Macrophage subgroup (M1, M1/2 and M2), b) M1/2 subset and c) M2 subset densities were compared between IM-GC ("early premalignant lesions") and the IM+GC ("late premalignant lesions") samples to identify changes with time (temporal progression) within individual tissue types. Each symbol represents data from a single region of interest (ROI). Multiple ROIs per sample. Data presented as mean + S.D. *All statistical analysis done using glm function in R.

5.3.8 Matched chronic gastritis has similar macrophage content compared to adjacent intestinal metaplasia

To identify possible local differences in macrophage content between IM and adjacent CG, a paired analysis was performed using cases where IM samples with matched CG were available. In IM-GC, no differences in total macrophage density were observed between matched samples (CG vs IM) and between CG adjacent to differing IM subtypes (Figure 5.10a). Further stratification of the samples into M1, M1/2 and M2 macrophage subgroups also showed no change in macrophage density between CG and IM (Figure 5.10b-d). However CG adjacent to incomplete IM had a greater representation of CD68+CD163+CD206+IRF8+ macrophage subsets compared to CG adjacent to complete IM (p=0.023, Figure 5.11).

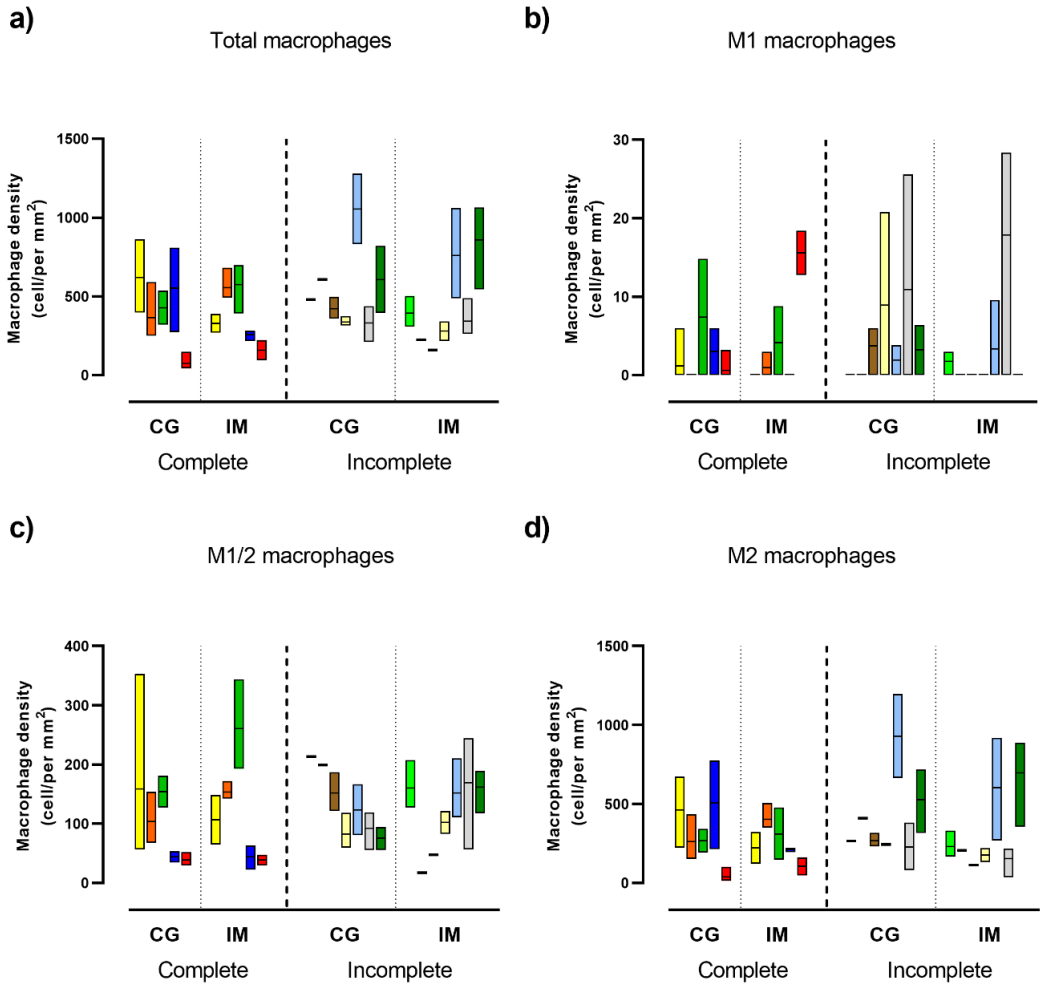


Figure 5.10 Total, M1, M1/2 and M2 macrophage density in samples with intestinal metaplasia and matched adjacent chronic gastritis tissue from the IM-GC cohort
Matched colour floating bars (min, mean, and max value) showing macrophage data from multiple ROIs per tissue type of matched CG adjacent to IM tissue. Data shown for CG with matched complete IM (n=5) and for CG with matched incomplete IM (n=7) from the IM-GC cohort; a) total macrophage density, b) M1 macrophage density, c) M1/2 macrophage density and d) M2 macrophage density Statistical analysis carried out using the Wilcoxon test and the paired and unpaired t-tests where appropriate in GraphPad Prism.

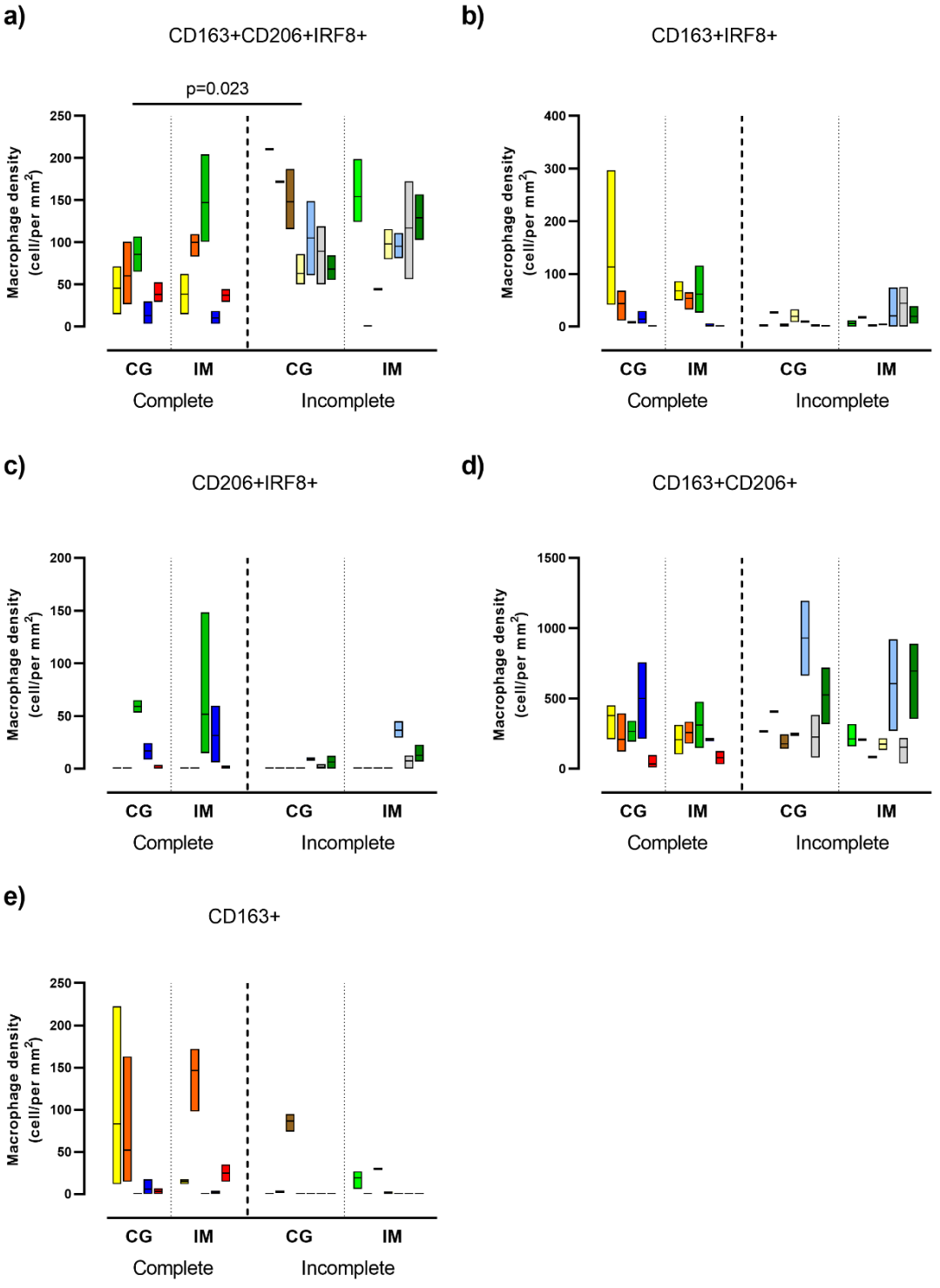


Figure 5.11 Macrophage subset density in samples with intestinal metaplasia and matched adjacent chronic gastritis tissue from the IM-GC cohort

Matched colour floating bars (min, mean, and max value) showing macrophage data from multiple ROIs per tissue type of matched CG adjacent to IM tissue samples. Data shown for CG with matched complete IM (n=5) and for CG with matched incomplete IM (n=7) from the IM-GC cohort; a) CD68+CD163+CD206+IRF8+, b) CD68+CD163+IRF8+, c) CD68+CD206+IRF8+, d) CD68+CD163+CD206+, and e) CD68+CD163+. Statistical analysis carried out using the Wilcoxon test and the paired and unpaired t-tests where appropriate in GraphPad Prism.

A similar comparison was made using the IM+GC cohort. Matched samples (CG vs IM) did not show any difference in macrophage density irrespective of IM subtype but CG adjacent to incomplete IM had fewer macrophages than CG adjacent to complete IM (p=0.014, Figure 5.12a). Further stratification of the samples showed that this lower macrophage density was mainly due to fewer M1 (CD68+IRF8+, p=0.0081, Figure 5.12b) and M1/2 macrophage subsets (p=0.028, Figure 5.12c) but not M2 macrophages (Figures 5.12 and 5.13). No significant differences in macrophage subset density were observed between matched CG and IM samples nor between CG adjacent to differing IM subtype (Figure 5.13).

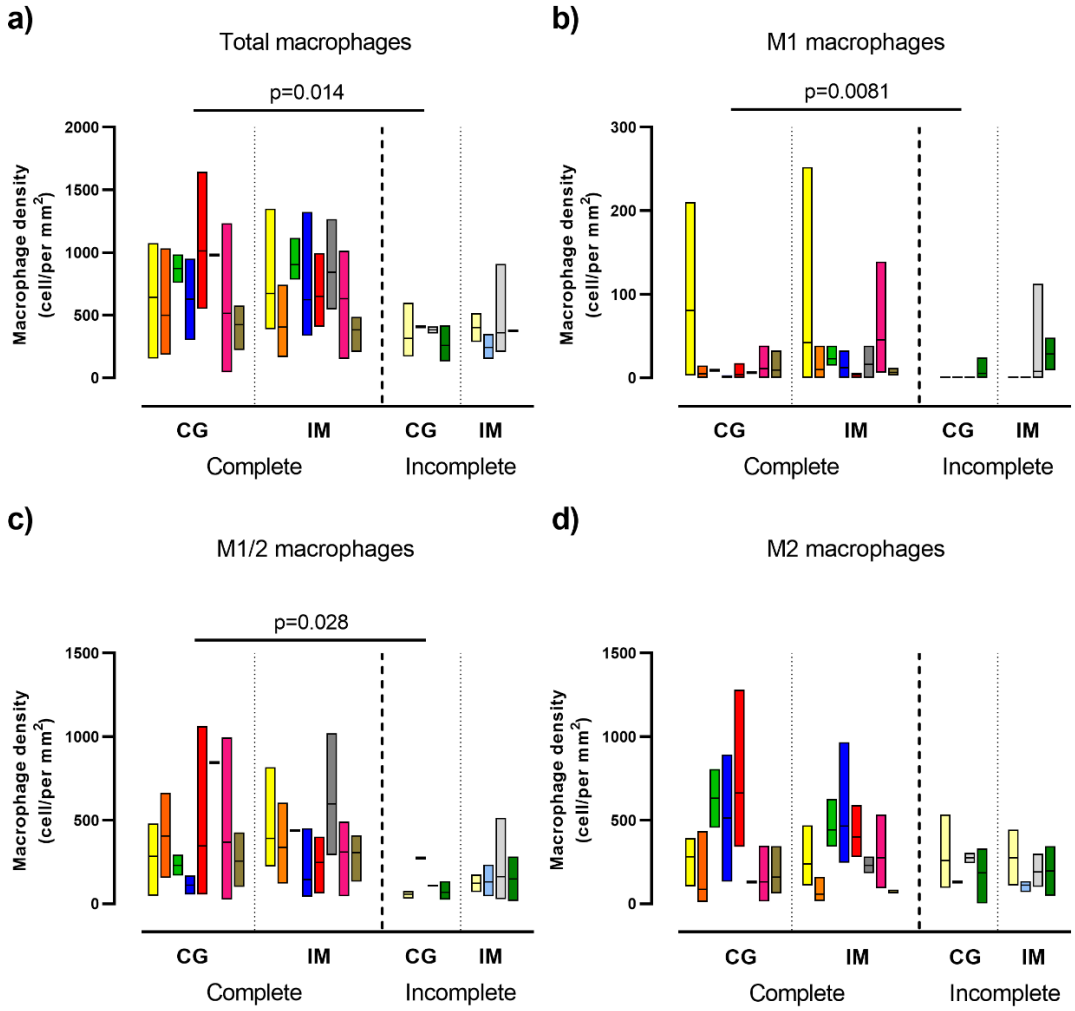


Figure 5.12 Total, M1, M1/2 and M2 macrophage density in samples with intestinal metaplasia and matched adjacent chronic gastritis tissue in IM+GC cohort

Matched colour floating bars (min, mean, and max value) showing macrophage data from multiple ROIs per tissue type of matched CG adjacent to IM tissue. Data shown for CG with matched complete IM (n=8) and for CG with matched incomplete IM (n=4) from the IM+GC cohort; a) total macrophage density, b) M1 macrophage density, c) M1/2 macrophage density and d) M2 macrophage density Statistical analysis carried out using the Wilcoxon test and the paired and unpaired t-tests where appropriate in GraphPad Prism.

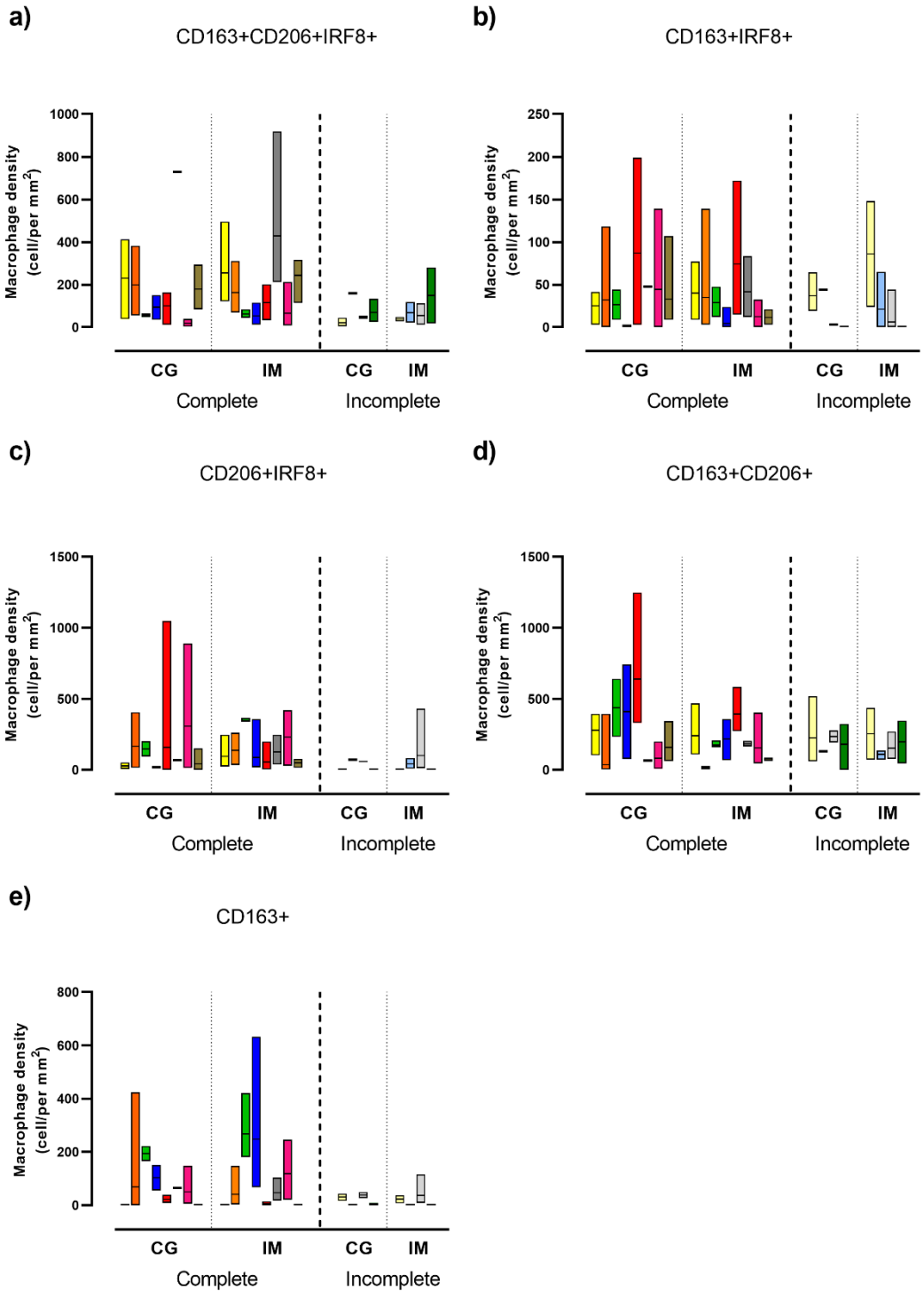


Figure 5.13 Macrophage subset density in samples with intestinal metaplasia and matched adjacent chronic gastritis tissue from the IM+GC cohort

Matched colour floating bars (min, mean, and max value) showing macrophage data from multiple ROIs per tissue type of matched CG adjacent to IM tissue samples. Data shown for CG with matched complete IM (n=8) and for CG with matched incomplete IM (n=4) from the IM+GC cohort; a) CD68+CD163+CD206+IRF8+, b) CD68+CD163+IRF8+, c) CD68+CD206+IRF8+, d) CD68+CD163+CD206+, and e) CD68+CD163+. Statistical analysis carried out using the Wilcoxon test and the paired and unpaired t-tests where appropriate in GraphPad Prism.

Overall this matched sample analysis showed that CG and adjacent IM had similar macrophage subset density profiles suggesting that the local macrophage landscape in adjacent tissues is relatively homogeneous. The differences observed between CG tissues adjacent to differing IM subtype suggest that CG next to incomplete IM is poorer in macrophages than CG next to complete IM, particularly in the IM+GC cohort.

5.3.9 Reduced M2 to M1/2 macrophage ratio along histological and temporal progression

Having characterised macrophage changes across histological and temporal progression, the next step was to determine whether there was a fundamental difference in quantitative relationships between M2 and M1/2 macrophages. In the IM-GC cohort, iIM-GC had significantly lower M2 to M1/2 ratio (median=1.8) compared to both CG-GC and cIM-GC (median=2.4; p=0.0496 and median=3.1; p=0.0027 respectively) (Figure 5.14). In the IM+GC cohort there were no significant differences in M2 to M1/2 ratios between CG+GC, cIM+GC and iIM+GC (median=0.76, 0.94 and 0.90 respectively). When comparing across cohorts from IM-GC to IM+GC, the M2 to M1/2 ratio was reduced in all three tissue types studied, with complete IM showing the most significant reduction (p=8.1e-07).

Overall both histological and temporal progression were associated with a reduction of the M2 to M1/2 macrophage ratio. This further suggested that M2 type macrophages may have a "protective" role in IM whereas M1/2 macrophages may be associated with "higher risk".

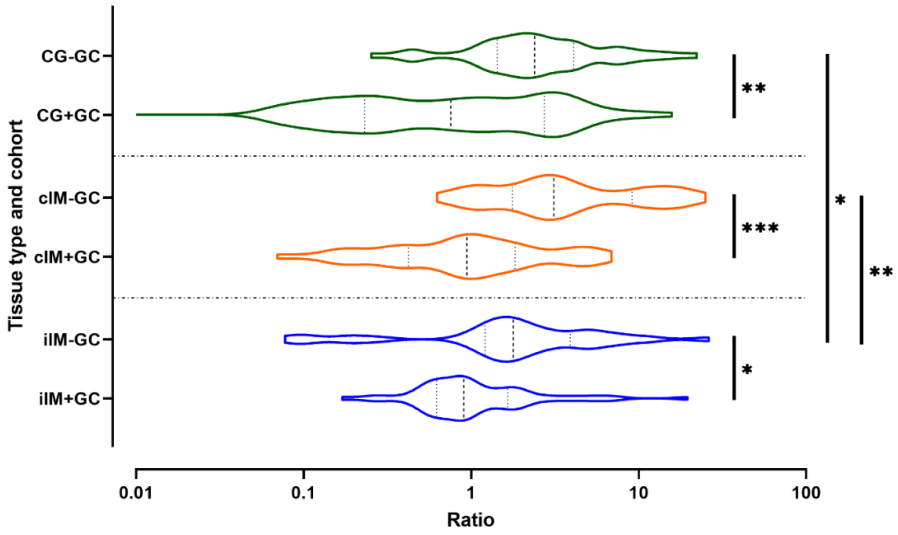


Figure 5.14 M2 to M1/2 macrophage ratio in the IM-GC and IM+GC cohorts
Macrophage subsets where grouped into M1/2 (CD68+CD163+CD206+IRF8+, CD68+CD163+IRF8+ and CD68+CD206+IRF8+) and M2 (CD68+CD163+CD206+ and CD68+CD163+) types to determine ratios per region of interest (ROI). Data presented as violin plot with 25% percentile, median and 75% percentile shown. All statistical analysis done using glm function in R. *, **, *** is equal to p<0.05, p<0.01 and p<0.001.

5.3.10 The macrophage landscape within a distance of 40µm from the epithelium changes with histo-temporal progression

Having quantitatively characterised the macrophage landscape in IM, the next step was to characterise the spatial relationship between macrophages and the epithelium. Macrophages are able to phagocytose *H. pylori* infected cells as well as tumour cells, dead cells and debris [475]. The level of possible physical and paracrine interaction between macrophages and epithelial cells was investigated using the touch cell pair density and number cells within a specific distance of a reference cell methodology described in §2.5.5 and Figure 2.4.

First the total number of macrophages within a functional space of 40µm around epithelial cells was analysed. In the IM-GC cohort, complete IM had significantly more macrophages located around epithelial cells compared to CG (CG-GC mean=1.8, cIM-GC mean 2.6, p=0.0064) (Figure 5.15). In the IM+GC cohort, incomplete IM had fewer macrophages around epithelial cells when compared to CG+GC (CG+GC mean=2.3, iIM+GC mean=1.6, p=0.0014) (Figure 5.15). Temporal progression was characterised by an increase of total macrophages in CG (p=0.0056) and a decrease in incomplete IM (iIM-GC mean=1.9, p=0.0089).

To gain further insight into how the relationship between the epithelium, M2 and M1/2 macrophages may play a role in progression, a separate analysis was performed and the results analysed and plotted along temporal progression (Figure 5.16). Overall, the mean number of M2 macrophages around epithelial cells was higher than that of M1/2 macrophages in the IM-GC cohort across tissues. This difference was not seen in the IM+GC cohort, with an M2:M1/2 ratio equal to ~1, similar to the ratios observed between M2 and M1/2 cell densities, suggesting that cell density is a key parameter with regards to M2 and M1/2 location around the epithelium. In CG, temporal progression was associated with an increase in M1/2 macrophages (from a mean of 0.5 to 1.2). In complete IM, temporal progression was associated with an increase in M1/2 macrophages (from 0.6 to 1.3) but a decrease in M2 macrophages (from 2 to 1.1). Finally in incomplete IM, temporal progression was associated with only a decrease in M2 macrophages (from 1.2 to 0.7).

Overall this data showed that histo-temporal progression is associated with a reduction in total macrophages within a distance of 40µm from epithelial cells. It is characterised by an increase of M1/2 macrophages and a decrease of M2 macrophages surrounding the epithelium.

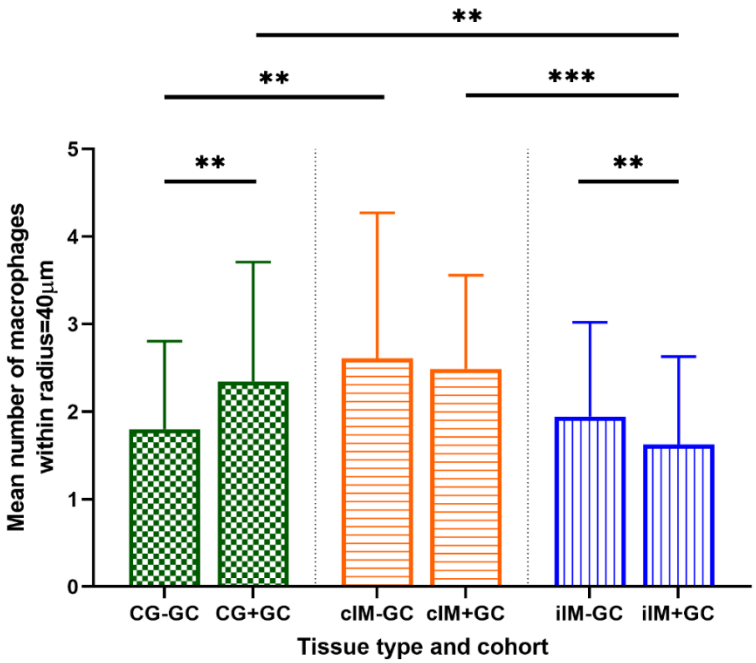


Figure 5.15 Mean number of total macrophages within a distance of 40µm from epithelial cells in the IM-GC and IM+GC cohorts

Mean number of all macrophages within a radius of 40µm around epithelial cells in the IM-GC and IM+GC cohorts. Mean + S.D. shown. All statistical analysis carried out in R using the glm function. *, **, *** is equal to p<0.05, p<0.01 and p<0.001.

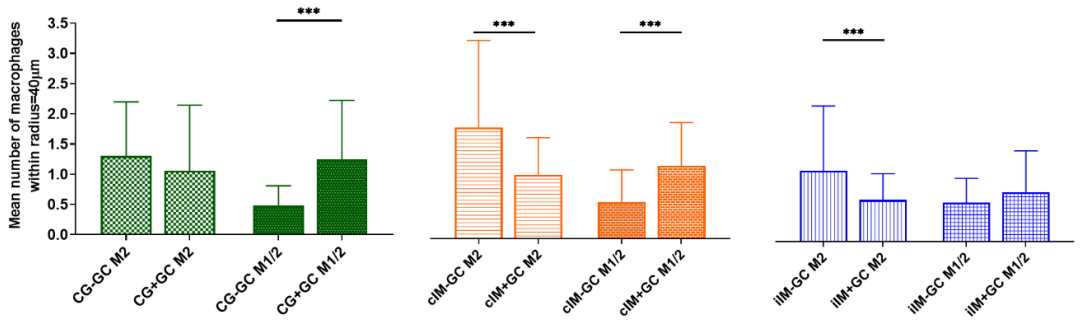


Figure 5.16 Mean number of M2 and M1/2 macrophages within a distance of 40µm from epithelial cells in the IM-GC and IM+GC cohorts

Mean number (+ S.D.) of M2 (CD68+CD163+ and CD68+CD163+CD206+) and M1/2 (CD68+CD163+CD206+IRF8+, CD68+CD163+IRF8+ and CD68+CD206+IRF8+) macrophages within a radius of 40µm around epithelial cells in the IM-GC and IM+GC cohorts. Mean + S.D. shown. All statistical analysis carried out in R using the glm function. *, **, *** is equal to p<0.05, p<0.01 and p<0.001.

5.3.11 Histo-temporal progression characterised by higher CD68+CD163+CD206+IRF8+ and lower CD68+CD163+CD206+ touch cell pair density with epithelial cells

Touch cell pair density analysis focussed on the relationship between epithelial cells and the two main macrophages subsets (CD68+CD163+CD206+ and CD68+CD163+CD206+IRF8+) that were abundantly present across all tissues in both the IM-GC and IM+GC cohorts. Although a macrophage may be deemed to be physically touching an epithelial cell by the method employed here, it is not possible to comment on whether macrophage pseudopodia actually extend through the epithelial basal membrane to carry out phagocytosis or other type of cell-cell interaction.

When comparing touch pair density between epithelial cells and all macrophages, no differences were observed between CG-GC, cIM-GC and iIM-GC suggesting that if macrophages do indeed play a role in progression it is likely to be qualitative rather than quantitative in these "early" lesions (Figure 5.17). In contrast in the IM+GC cohort, iIM+GC did show a reduced density of touching cell pairs compared to CG+GC (p=0.00065). When comparing across cohorts (temporal progression) there was a highly significant reduction in touch pair density only within the incomplete subtype of IM (p=1.1e-06) suggesting that a decrease in quantitative epithelial to macrophage physical interaction only becomes important at the most "advanced stage" of this premalignant lesion.

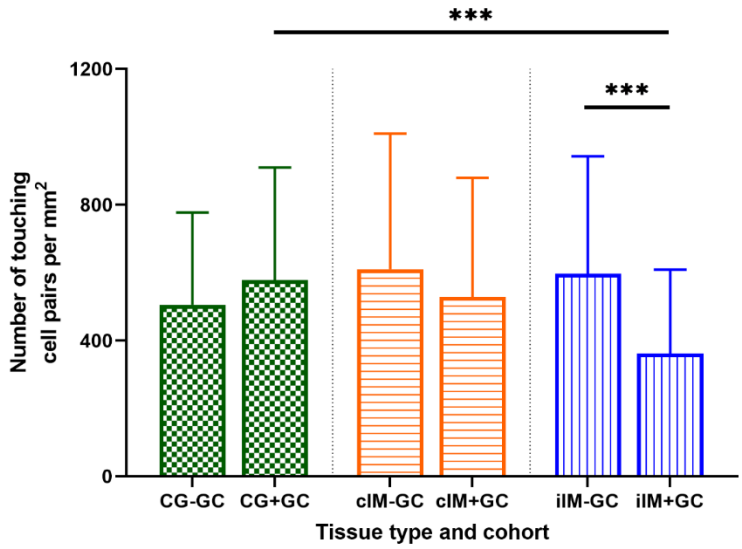


Figure 5.17 Significant reduction of touching cell pair density in incomplete IM+GC between epithelial cells and total macrophages
Touch cell pair density between epithelial cells and all macrophages was calculated by creating a single macrophage group consisting of all CD68+CD163+, CD68+CD163+IRF8+, CD68+CD163+CD206+, CD8+CD163+CD206+IRF8+, CD68+CD206+IRF8+ and CD68+IRF8+ macrophages per region of interest and using the phenoptr package in R. Mean + S.D. shown. All statistical analysis carried out in R using the glm function. *, **, *** is equal to p<0.05, p<0.01 and p<0.001.

To determine whether specific macrophage subsets may have a more “protective” role than others, the touch cell pair densities between CD68+CD163+CD206+ and CD68+CD163+CD206+IRF8+ macrophages with epithelial cells were investigated (Figure 5.18). In CG-GC and cIM-GC, CD68+CD163+CD206+ macrophages had a higher touch cell pair density with epithelial cells than CD68+CD163+CD206+IRF8+ macrophages (p=1.1e-06 and p=5.8e-07, respectively) (Figure 5.18a). No such difference was observed in iIM-GC suggesting that CD68+CD163+CD206+ macrophages may have a more benevolent role in these “early” lesions than CD68+CD163+CD206+IRF8+ macrophages. When comparing across tissue types, iIM-GC showed a higher touch cell pair density of CD68+CD163+CD206+IRF8+ macrophages with epithelial cells compared to CG-GC (p=0.001).

In the IM+GC cohort, no significant differences in touch cell pair density were observed between CD68+CD163+CD206+ and CD68+CD163+CD206+IRF8+ macrophages with epithelial cells in all tissues investigated (Figure 5.18b). However when comparing across tissue types, both cIM+GC and iIM+GC had a lower CD68+CD163+CD206+ macrophage touch cell pair density compared to CG+GC (p=0.044 and p=0.016, respectively). Additionally iIM+GC had lower CD68+CD163+CD206+IRF8+ macrophage touch cell pair density compared also to CG+GC (p=0.012).

Across cohorts, temporal progression was characterised by a lower touch cell pair density between CD68+CD163+CD206+ macrophages and epithelial cells across all three tissue types (for CG p=0.0057, for complete IM p=5.1e-07, and for incomplete IM p=2.4e-07). A reduction of touch pair cell density between CD68+CD163+CD206+IRF8+ macrophages and epithelial cells was only seen for incomplete IM (p=7.3e-05) with progression.

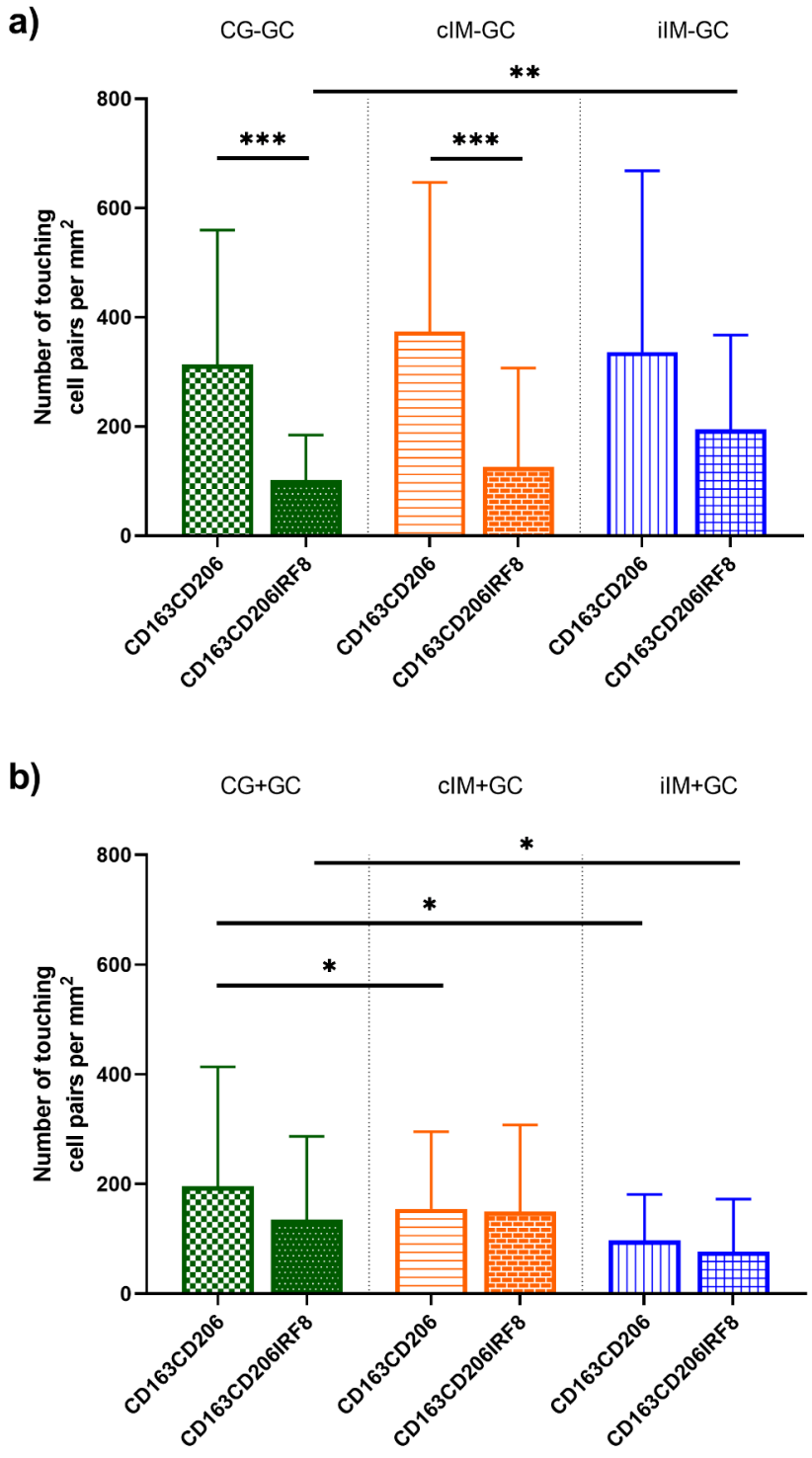


Figure 5.18 Touch pair cell density between epithelial cells, CD68+CD163+CD206+ and CD68+CD163+CD206+IRF8+ macrophages in the IM-GC and IM+GC cohorts

Touch cell pair density of epithelial cells with CD68+CD163+CD206+ and with CD68+CD163+CD206+IRF8+ macrophages in a) IM-GC cohort and b) IM+GC cohort. Mean touch cell pair density + S.D. shown. Statistical analysis carried out using i) paired Wilcoxon test in GraphPad Prism for within tissue differences and ii) using glm function in R to compare tissue types. *, **, *** is equal to $p<0.05$, $p<0.01$ and $p<0.001$.

5.3.12 Temporal progression in intestinal metaplasia characterised by lower touch cell pair density between CD68+CD163+CD206+ and CD68+CD163+CD206+IRF8+ macrophages

The two most abundant macrophage subsets across tissue types and cohorts (CD68+CD163+CD206+ and CD68+CD163+CD206+IRF8+) were analysed to describe their level of possible physical interaction (Figure 5.19). Histological progression in the IM-GC cohort showed a higher touch cell pair density in complete IM compared to CG, and in the IM+GC cohort a lower touch cell pair density in incomplete IM compared to complete IM. Temporal analysis across cohorts showed a lower touch cell pair density in both complete and incomplete IM going from the IM-GC to the IM+GC samples. Overall this data suggested that lower levels of physical interaction between the two main subsets of macrophages may be associated with a higher risk of progression.

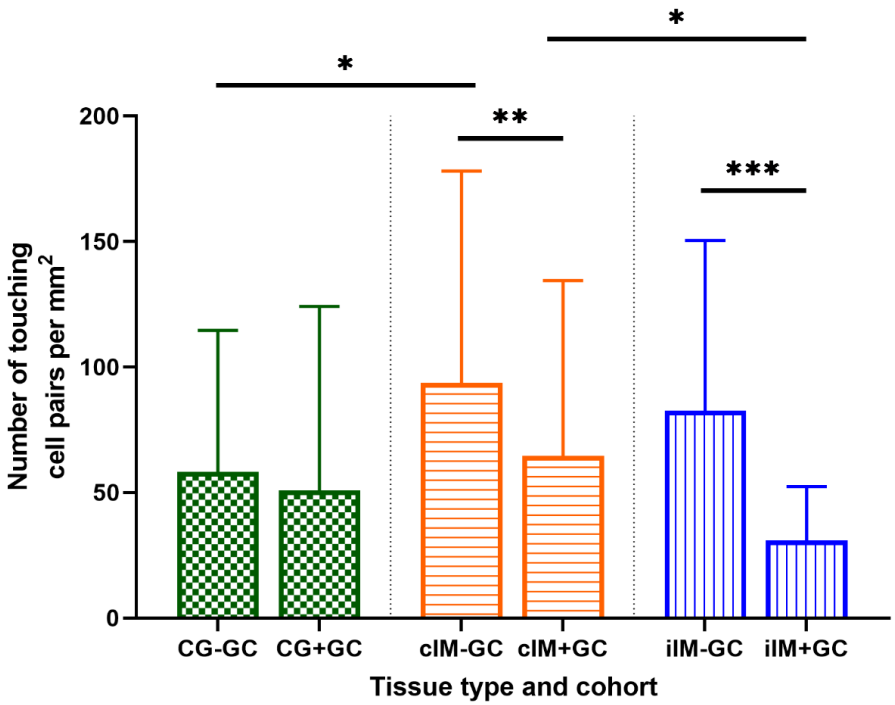


Figure 5.19 Touch cell pair density between CD68+CD163+CD206+ and CD68+CD163+CD206+IRF8+ macrophages in the IM-GC and IM+GC cohorts
Touch cell pair density between CD68+CD163+CD206+ and CD68+CD163+CD206+IRF8+ macrophages was compared across tissue types and cohorts. Mean + S.D. shown. All statistical analysis carried out in R using the glm function. *, **, *** is equal to $p<0.05$, $p<0.01$ and $p<0.001$.

5.3.13 Decreased macrophage targeting of the epithelium in complete IM

Having quantified the overall cell to cell spatial relationships, the next step was to characterise the pattern of individual macrophages targeting epithelial cells or other macrophages among tissues representing histological progression. By normalising touch cell pair density using cell density as a factor, a higher normalised touch cell pair density would suggest that a specific cell type e.g. cell type B was better at physically targeting a reference cell type e.g. cell type A, thus reducing the potential influence of random distribution [395].

Equation to calculate normalised touch cell pair density: $$\frac{\text{touch cell pair A//B density}}{\text{cell B density}}$$

Normalised spatial analysis was carried out to identify targeting patterns between total macrophages and epithelial cells and between the two main macrophage subsets (CD68+CD163+CD206+ and CD68+CD163+CD206+IRF8+ macrophages).

Progression from CG-GC to cIM-GC was characterised by a significant reduction of total macrophages (p=0.0024) including both CD68+CD163+CD206+IRF8+ and CD68+CD163+CD206+ subsets targeting epithelial cells (p=0.03 and p=0.0053 respectively) (Table 5.2). By contrast progression from cIM-GC to iIM-GC showed a complete reversal in macrophage targeting patterns (p=0.00013, p=0.03 and p=0.0048 respectively) as well as a decrease in CD68+CD163+CD206+IRF8+ macrophages targeting CD68+CD163+CD206+ macrophages (p=0.026).

Table 5.2 Normalised[1] touch cell pair analysis showing targeted changes across tissues representing histological progression in the IM-GC and IM+GC cohorts

Touch cell pairs		CG -> cIM		cIM -> iIM	
Cell A	**Cell B**	**Change[2]**	**pval[3]**	**Change[4]**	**pval[3]**
IM-GC cohort					
Epithelial	All macrophages	↓	**0.0024**	↑	**0.00013**
Epithelial	CD68+CD163+CD206+IRF8+	↓	**0.03**	↑	**0.03**
Epithelial	CD68+CD163+CD206+	↓	**0.0053**	↑	**0.0048**
CD68+CD163+CD206+	CD68+CD163+CD206+IRF8+	↑	ns	↓	**0.026**
IM+GC cohort					
Epithelial	All macrophages	↓	ns	↑	ns
Epithelial	CD68+CD163+CD206+IRF8+	↓	ns	↓	ns
Epithelial	CD68+CD163+CD206+	↓	**0.0017**	↑	ns
CD68+CD163+CD206+	CD68+CD163+CD206+IRF8+	↑	ns	↑	**0.045**

[1]Normalisation carried out by dividing touch pair cell density between cell A and cell B with the cell density of cell B; [2]Direction of change in median value of normalised data in complete IM (cIM) when compared to CG; [3]p value shown calculated using glm function in R; [4]Direction of change in median value of normalised data in incomplete IM (iIM) when compared to cIM.

Progression from CG+GC to cIM+GC was characterised by a significant reduction only of CD68+CD163+CD206+ macrophages targeting epithelial cells (p=0.0017, Table 5.2). Interestingly progression from cIM+GC to iIM+GC showed an increase in CD68+CD163+CD206+IRF8+ macrophages targeting CD68+CD163+CD206+ macrophages (p=0.045).

Overall this part of the macrophage study showed significant differences in the levels and type of macrophage targeting of epithelial cells in "early" premalignant lesions (IM-GC), most of which were absent in the more "advanced" lesions (IM+GC). Although present in much larger quantities, CD68+CD163+CD206+ macrophages do not target the epithelium in cIM-GC as effectively as they do in iIM-GC. This is in contrast with the CD68+CD163+CD206+IRF8+ subset which is more effective at targeting the epithelium in iIM-GC irrespective of numerical differences.

5.3.14 Description of multi-site and time point tissue samples available from two case studies that have progressed to high grade dysplasia

Samples from a small number of patients who comprised the Progressors cohort were analysed next. These patients had evidence of progressive disease with biopsies from multiple anatomical locations sampled at multiple time points thus allowing for a comprehensive temporal and topographical analysis. The use of these case studies could be particularly valuable in gaining insight into how the macrophage landscape varies by stomach site, across time and with progression from both complete and incomplete IM to dysplasia. Also characterising the IM tissue from these patients could be useful in understanding the immune landscape journey from "early" (IM-GC cohort) to "late" IM lesions (IM+GC cohort).

Tissue samples from patient P1 were collected using the updated Sydney protocol over a period of 416 days across five time points (t1=d0, t2=d178, t3=d254, t4=d360 and t5= d416) which presented with high grade dysplasia (HGD) in the antrum (site A3) at t1, t2 and t3 surrounded by chronic gastritis and/or intestinal metaplasia and in the body (site A4) at t1 (Figure 5.20). P1 received an endoscopic mucosal resection (EMR) during t3 to remove the HGD tissue. These samples shared common evolutionary genomic events but also unique ones that set them apart as identified from whole exome sequencing using fresh frozen tissue (Appendix I, Busuttil et al 2020 [411]). For the OPAL study, HGD FFPE samples were available from site A3 at t2 and t3 (Figure 5.20).

Tissue samples from multiple stomach sites were also obtained from patient P2 over a period of 249 days across four visits (t1=d0, t2=d62, t3=d164 and t4=d249). P2 presented with HGD in site A2 at t1 and t2 which was removed with an EMR at t2. Similarly to patient P1, IM and HGD in P2

showed common genomic evolutionary paths but also unique changes in each sample (Appendix J, Busuttil et al 2020 [411]). For the OPAL study, low grade dysplasia (LGD) and HGD FFPE samples were available from adjacent sites in A2 (A2a and A2b) at t2 (Figure 5.21).

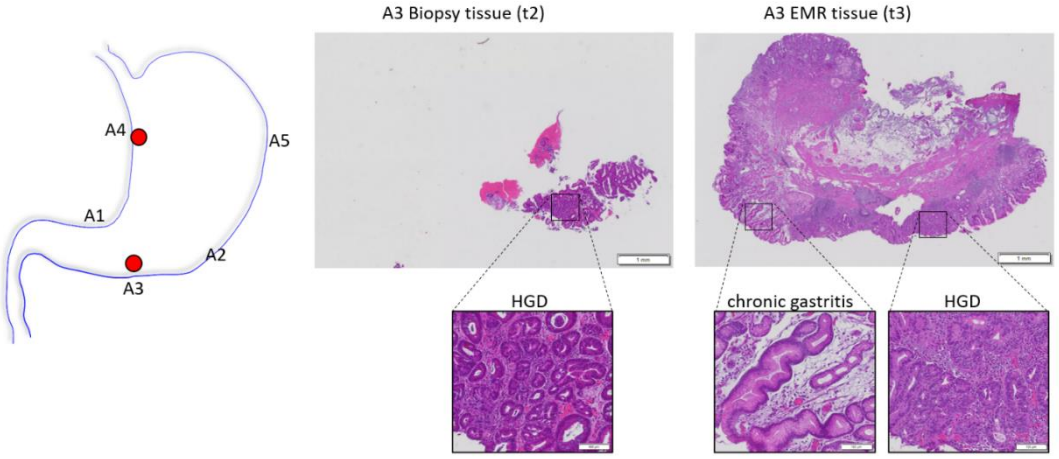


Figure 5.20 Diagram and images with insets showing high grade dysplasia (HGD) with adjacent chronic gastritis where present at different sites and time points in patient P1
High grade dysplasia (red disks) was diagnosed on frozen tissue at stomach sites A3 (time points t1/2/3) and A4 (time point t1). Formalin fixed paraffin embedded tissue (biopsy and endomucosal resection) was available from A3 at t2 and t3 for characterisation with the macrophage OPAL™ panel. Scale bars: 1mm and 100µm (inset).

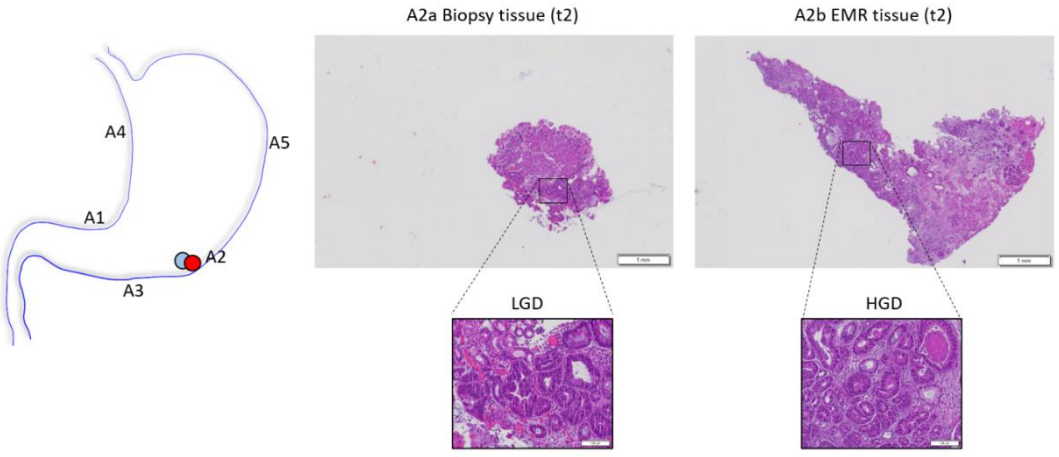


Figure 5.21 Diagram and images with insets showing low grade (LGD) and high grade dysplasia (HGD) present at adjacent sites (A2a and A2b) in patient P2
Low grade (light blue disk) and high grade dysplasia (red disk) were diagnosed in formalin fixed paraffin embedded tissue samples (biopsy and endomucosal resection) taken from adjacent sites (A2a and A2b) at time point t2 and made available for use with the macrophage OPAL™ panel. Scale bars: 1mm and 100µm (inset).

5.3.15 Macrophage profiling of patient P1 shows high M1 and M1/2 macrophage density in high grade dysplasia

To address the possible role of macrophages in progression to HGD, the macrophage OPAL™ panel was used on tissue samples from patient P1, selected to be rich in CG, complete and incomplete IM and HGD areas or a combination of these. Macrophage density was analysed first

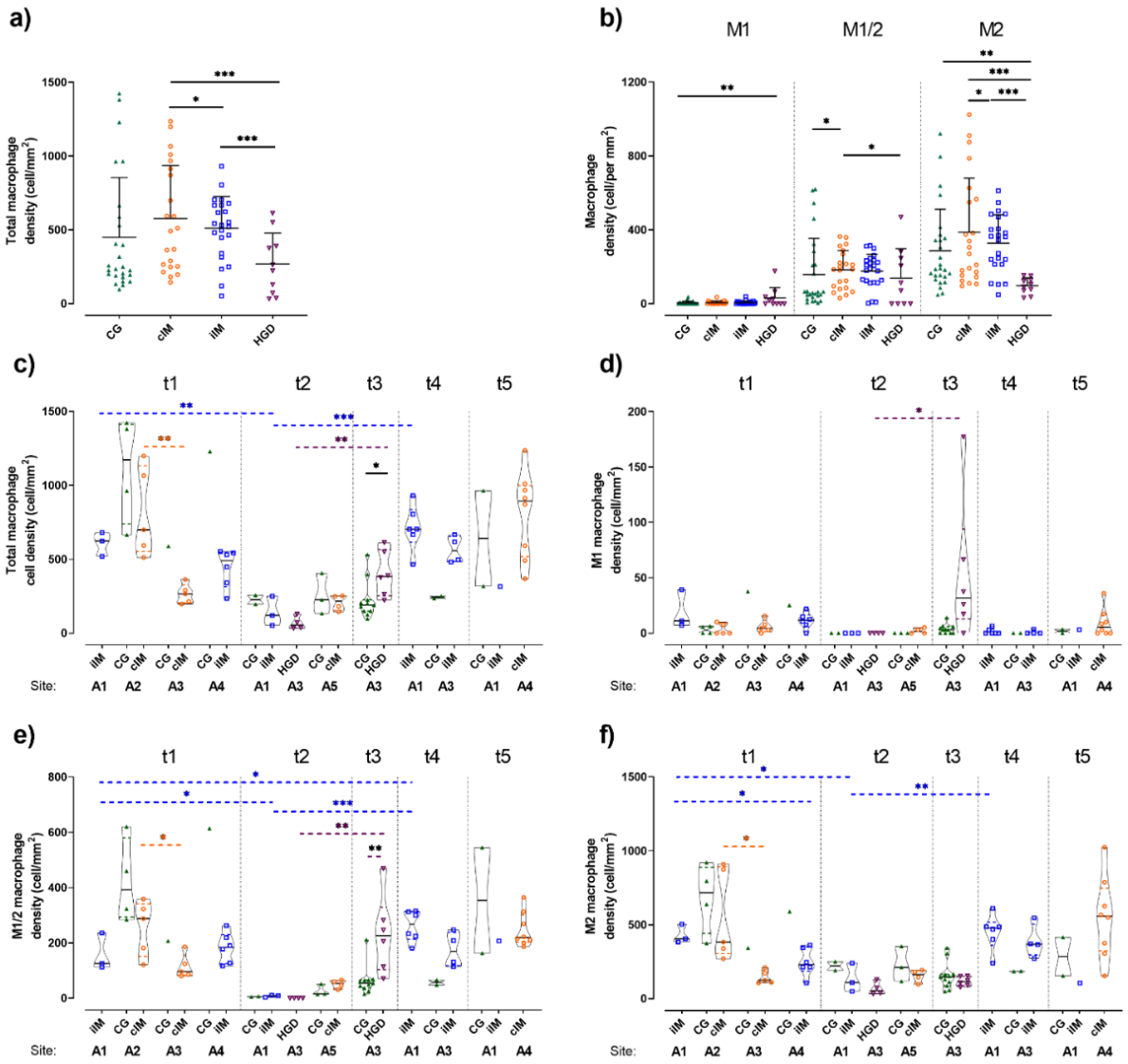
by pooling all same tissue type data together and then individually per site and time point (Figure 5.22).

Overall pooled total macrophage density was significantly lower in HGD compared to complete and incomplete IM (Figure 5.22a). Separating total macrophage density into its component subgroups showed that CG, complete and incomplete IM were predominantly characterised by M2 macrophages. In contrast, HGD was predominantly rich in M1/2 macrophages and had a low density of M2 macrophages (Figure 5.22b). Analysis by site and time point showed considerable variation in total macrophage density in incomplete IM tissues but also a significant increase in HGD at t3 compared to adjacent CG and HGD at t2 (Figure 5.22c). HGD at t3 had a particularly high density of M1 but was also rich in M1/2 macrophages (Figure 5.22d-e).

Pooled macrophage subset analysis showed that CD68+CD163+CD206+ macrophages were the predominant subset in CG, complete and incomplete IM but not in HGD (Figure 5.23a). HGD at t3 was particularly rich in CD68+CD163+IRF8+ macrophages, but also had more CD68+CD163+CD206+IRF8+ and CD68+CD206+IRF8+ macrophages than HGD at t2 (Figure 5.23b-d). The same pattern was observed with matched adjacent CG except for the latter subset. Interestingly complete IM tissue in site A2 had significantly more CD68+CD163+CD206+IRF8+ and CD68+CD163+CD206+ macrophages than in site A3 at the same time point (t1) (Figure 5.23c and 5.23f).

There were no differences in the main unique chromosomal and single nucleotide variants in this patient between the high grade dysplastic lesions at t2 and t3 in site A3 (Appendix I) suggesting that changes to the macrophage landscape in HGD from t2 to t3 were not likely associated with specific genomic events in the HGD glands. However such a conclusion could not be definite as the genomic data was obtained from whole exome sequencing of frozen tissue and the macrophage OPAL™ IHC was carried out on adjacent FFPE, thus the local dysplastic genomic profile might have differed.

Overall multi-site and multi-time point analysis in patient P1 showed that macrophage populations in gastric premalignant lesions within a single patient vary considerably suggesting a highly dynamic flux of localised macrophage trafficking (Figure 5.24). Also HGD at a later time point showed a relatively high density of M1 macrophages, a predominant M1/2 population and relatively few M2 macrophages strongly suggesting an association between macrophages expressing IRF8 and an increased risk of progression (Figure 5.25).



a) pooled total macrophage density and b) M1, M1/2 and M2 macrophage density shown by tissue type; macrophage density by site, tissue type and time point shown c) for all macrophages, d) for M1 macrophages, e) for M1/2 macrophages and f) for M2 macrophages. Each symbol represents data from a single ROI.

For pooled data (a, b) mean +S.D. shown and p values calculated using glm function in R and for individual samples (c, d, e, f) quartiles shown with t-test and Mann Whitney test used to calculate significance (minimum of 3 ROIs). *, **, *** is equal to $p<0.05$, $p<0.01$ and $p<0.001$.

For c), d), e) and f) coloured dashed lines show significant same tissue differences by site and time point (orange for complete IM, blue for incomplete IM, purple for HGD). Black lines show significant differences between matched CG and adjacent IM/HGD lesion

Figure 5.22 Pooled and single site/time point macrophage density in patient P1

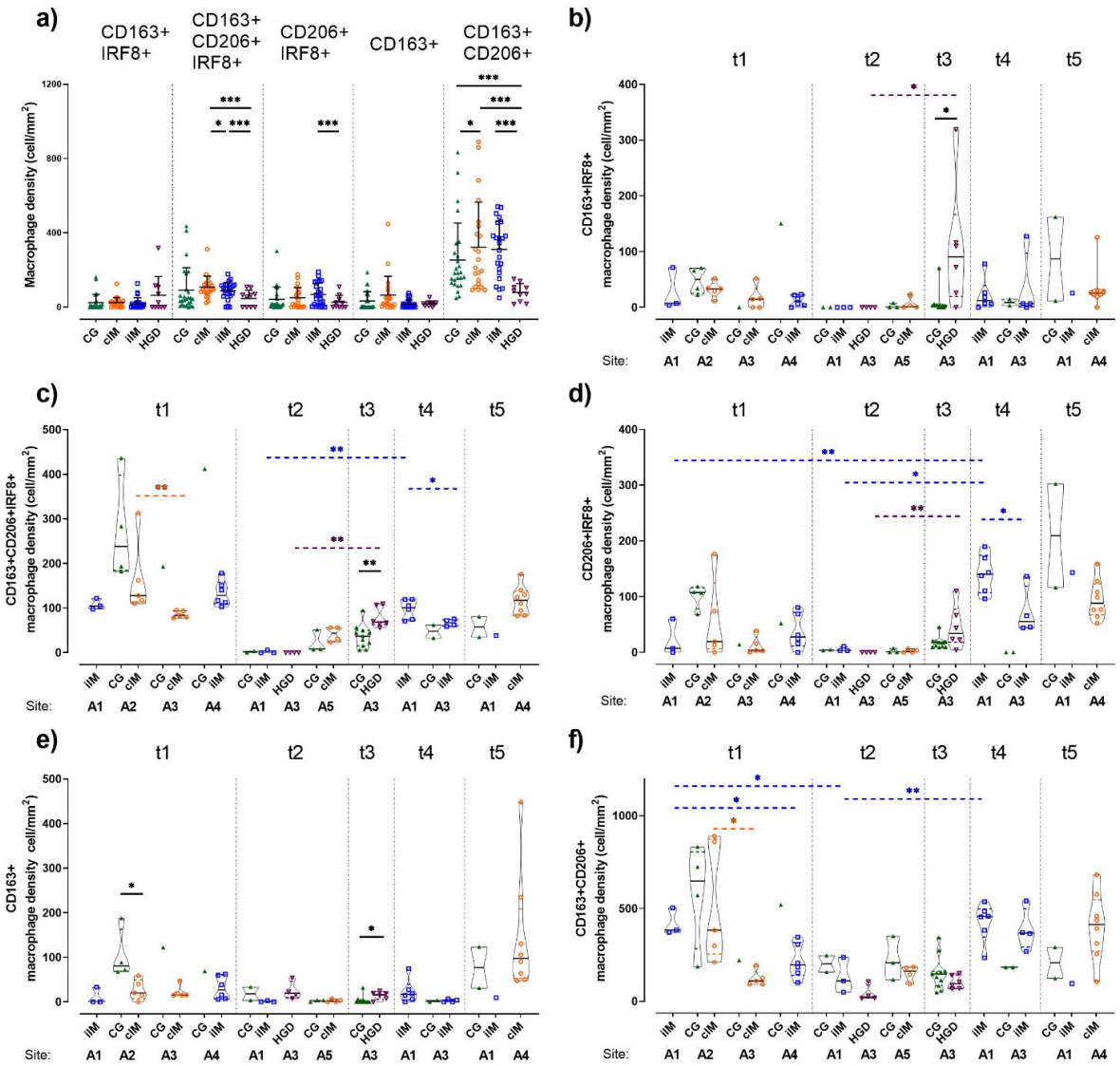


Figure 5.23 Pooled and single site/time point macrophage subset density in patient P1

a) Pooled macrophage subset density by tissue type; macrophage density by site, tissue type and time point shown for b) CD163+IRF8+ macrophages, c) CD163+CD206+IRF8+ macrophages, d) CD206+IRF8+ macrophages, e) CD163+ macrophages and f) CD163+CD206+.

Each symbol represents data from a single ROI. For pooled data (a) mean +S.D. shown and p values calculated using glm function in R and for individual samples (b, c, d, e, f) quartiles shown with t-test and Mann Whitney test used to calculate significance (minimum of 3 ROIs). *, **, *** is equal to $p<0.05$, $p<0.01$ and $p<0.001$.

For b), c), d), e) and f) coloured dashed lines show significant same tissue differences by site and time point (orange for complete IM, blue for incomplete IM, purple for HGD). Black lines show significant differences between matched CG and adjacent IM/HGD lesion.

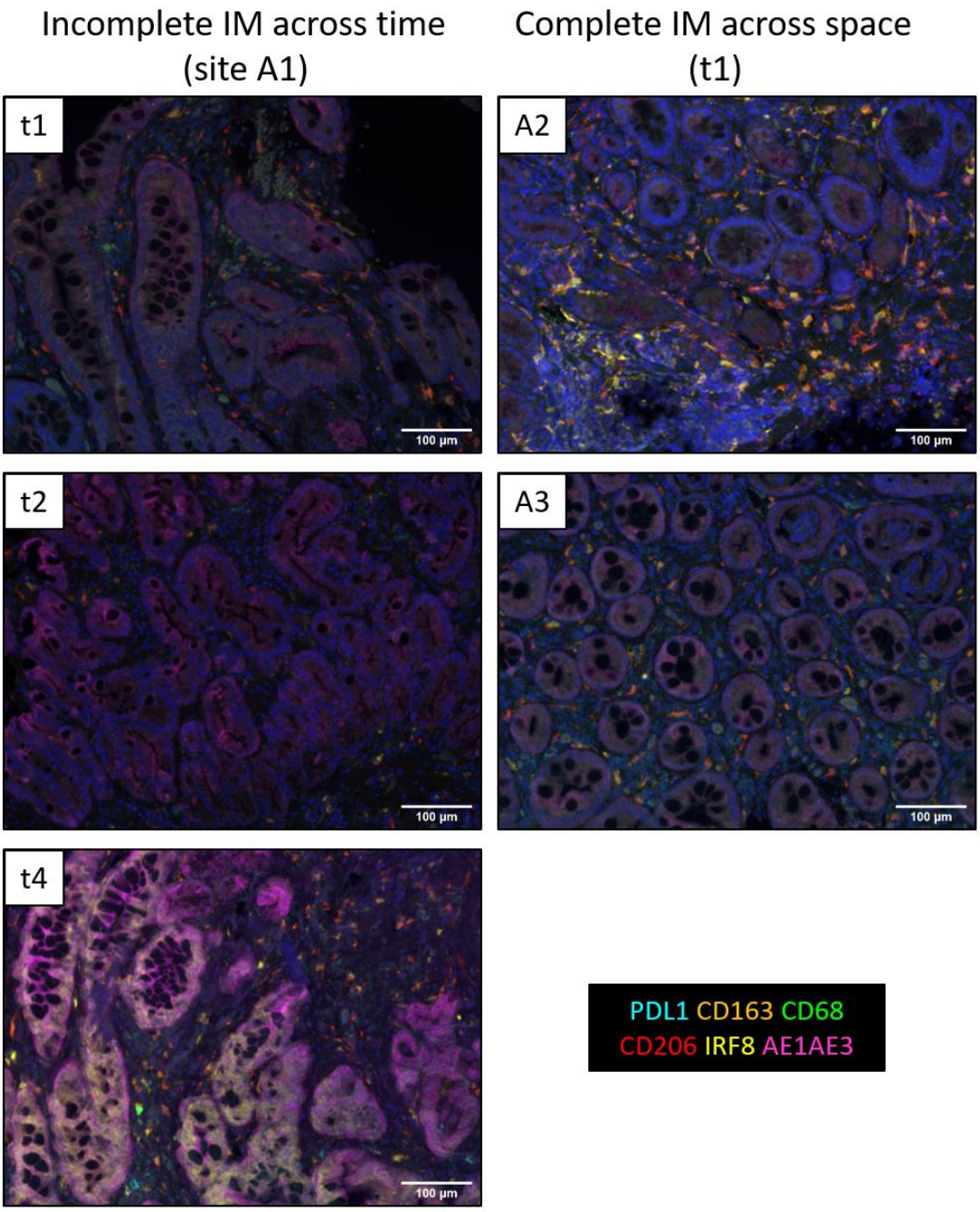


Figure 5.24 Macrophage content in complete and incomplete IM differs by site and time point
Spectrally unmixed composite images of incomplete IM at site A1 at three different time points (t1, t2 and t4) and of complete IM at time point t1 at two different sites (A2 and A3) show considerable variation in macrophage content. Scale bars: 100µm.

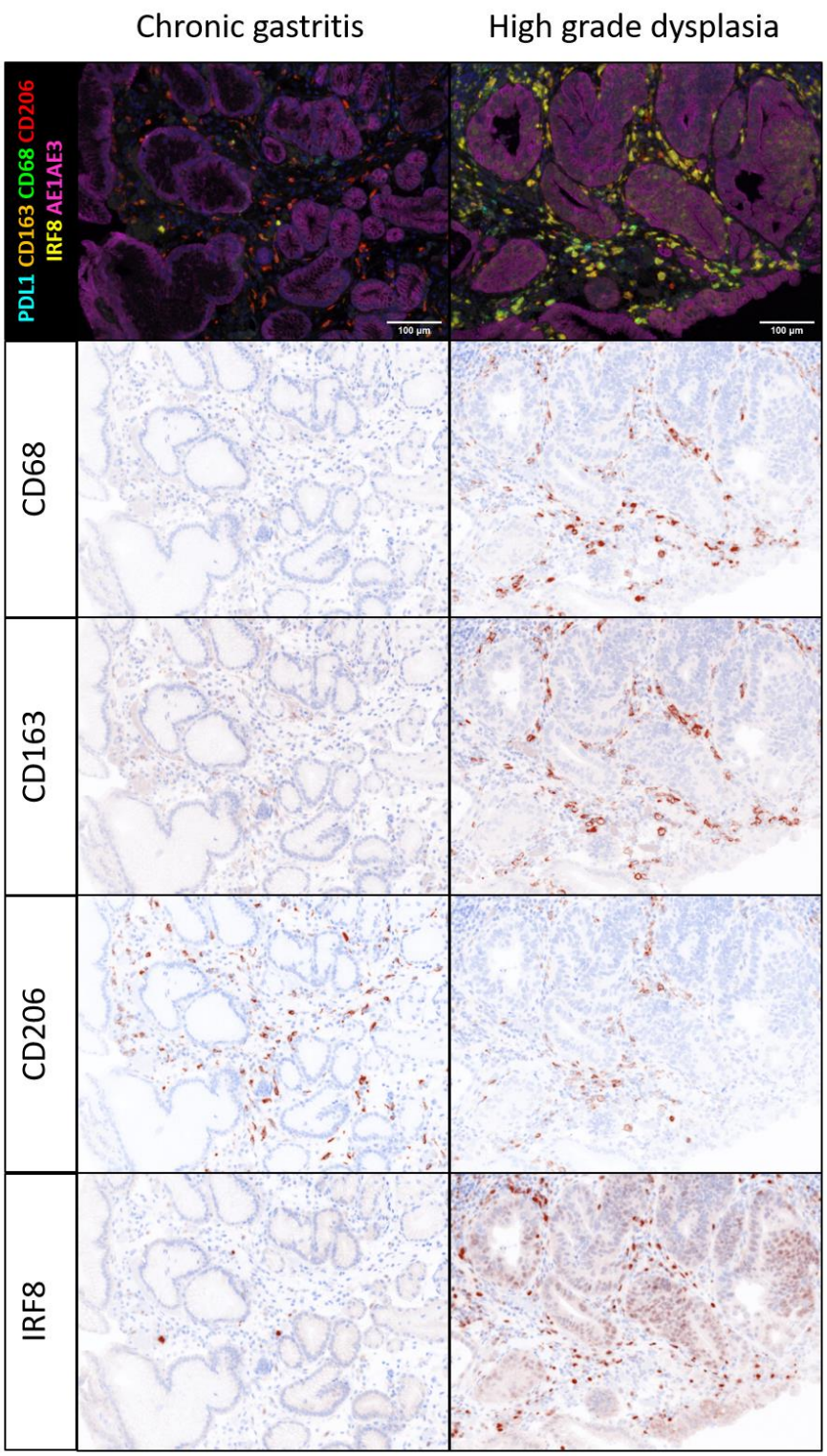


Figure 5.25 High grade dysplasia at t3 shows large numbers of cells with high levels of expression for CD68, CD163 and IRF8 compared to matched adjacent chronic gastritis tissue
Spectrally unmixed composite image together with pseudo-pathology images (inForm) shown of CD68, CD163, CD206 and IRF8 markers from HGD with matched adjacent CG. Scale bars: 100µm.

5.3.16 Macrophage profile of patient P2 shows high M2 macrophage density in high grade dysplasia

Multi-site and multi-time point tissue samples from patient P2 were also characterised using the macrophage OPAL™ panel. Overall total macrophage density was significantly higher in dysplasia (LGD and HGD combined) with particularly high density in HGD (Figure 5.26a). When separated into component subgroups, all three tissues investigated were infiltrated by a predominantly M2 macrophage population with dysplasia showing an almost absolute M2 phenotype (Figure 5.26b). There was no significant difference in M1 (CD68+IRF8+) macrophage content between CG, incomplete IM and dysplasia, although LGD did have significantly more M1 macrophages than HGD (Figure 5.26c-d). Overall dysplasia had fewer M1/2 macrophages than CG and incomplete IM, with LGD having again a greater density than HGD (Figure 5.26e).

When the M1/2 and M2 macrophage subgroups were analysed by single component subsets, dysplasia overall showed a decrease only in the CD68+CD163+CD206+IRF8+ subset (Figure 5.27a). However when comparing LGD with HGD, the latter had fewer CD68+CD163+CD206+IRF8+ as well as CD68+CD206+IRF8+ macrophages. In contrast, significantly more CD68+CD163+ macrophages were present around dysplastic regions when compared with CG and incomplete IM and also more CD68+CD163+CD206+ macrophages compared to the former. Although LGD had a higher density of CD68+CD163+ macrophages than adjacent CG tissue, this was still lower than HGD which had a remarkably high density of this macrophage subset. Interestingly incomplete IM had fewer CD68+CD163+CD206+IRF8+ macrophages than adjacent CG tissue in A3 (t4). Additionally CD68+CD206+IRF8+ macrophage density in CG fluctuated not only by site at t2 (A1 vs A4, higher in the latter) but also across time points in A1 (t2 vs t3, higher in the latter).

Although no genomic data was available for the LGD lesion, the genomic profile obtained from HGD frozen tissue in site A2 at t2 included gains of chromosomes 8, 10 and 13 but was mainly characterised by the large number of chromosomal losses including that of 1p, 4, 5, 7, 11, 12, 14, 15, 16, 17p, 19, 21 and 22 suggesting a possible relationship between multiple chromosomal loss and the highly M2 polarised macrophage landscape observed in this patient (Appendix J). Again the differing tissue of origin used for whole exome sequencing and OPAL™ multiplex IHC did not allow a definite conclusion to be made.

Overall, progression to HGD in patient P2 was characterised by an almost complete loss of the M1/2 macrophage population and a highly significant increase in M2 macrophages (Figure 5.28).

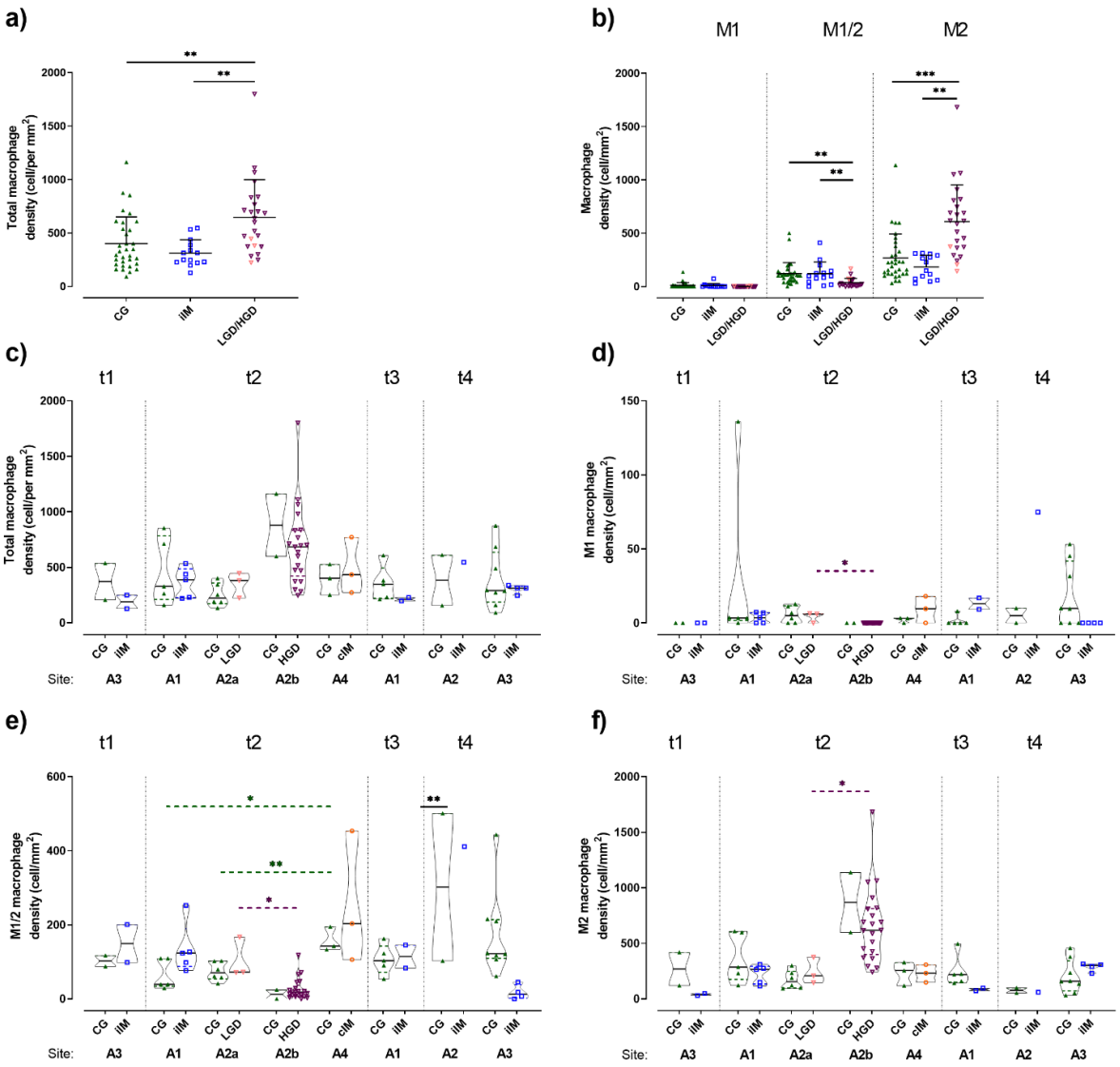


Figure 5.26 Pooled and single site/time point macrophage density in patient P2

a) pooled total macrophage density and b) M1, M1/2 and M2 macrophage density shown by tissue type; macrophage density by site, tissue type and time point shown c) for all macrophages, d) for M1 macrophages, e) for M1/2 macrophages and f) for M2 macrophages. Each symbol represents data from a single ROI.

For pooled data (a, b) mean +S.D. shown and p values calculated using glm function in R and for individual samples (c, d, e, f) quartiles shown with t-test and Mann Whitney test used to calculate significance (minimum of 3 ROIs). *, **, *** is equal to $p<0.05$, $p<0.01$ and $p<0.001$.

For c), d), e) and f) coloured dashed lines show significant same tissue differences by site (green for chronic gastritis, purple for LGD/HGD). Black lines show significant differences between matched CG and adjacent IM/LGD/HGD lesion.

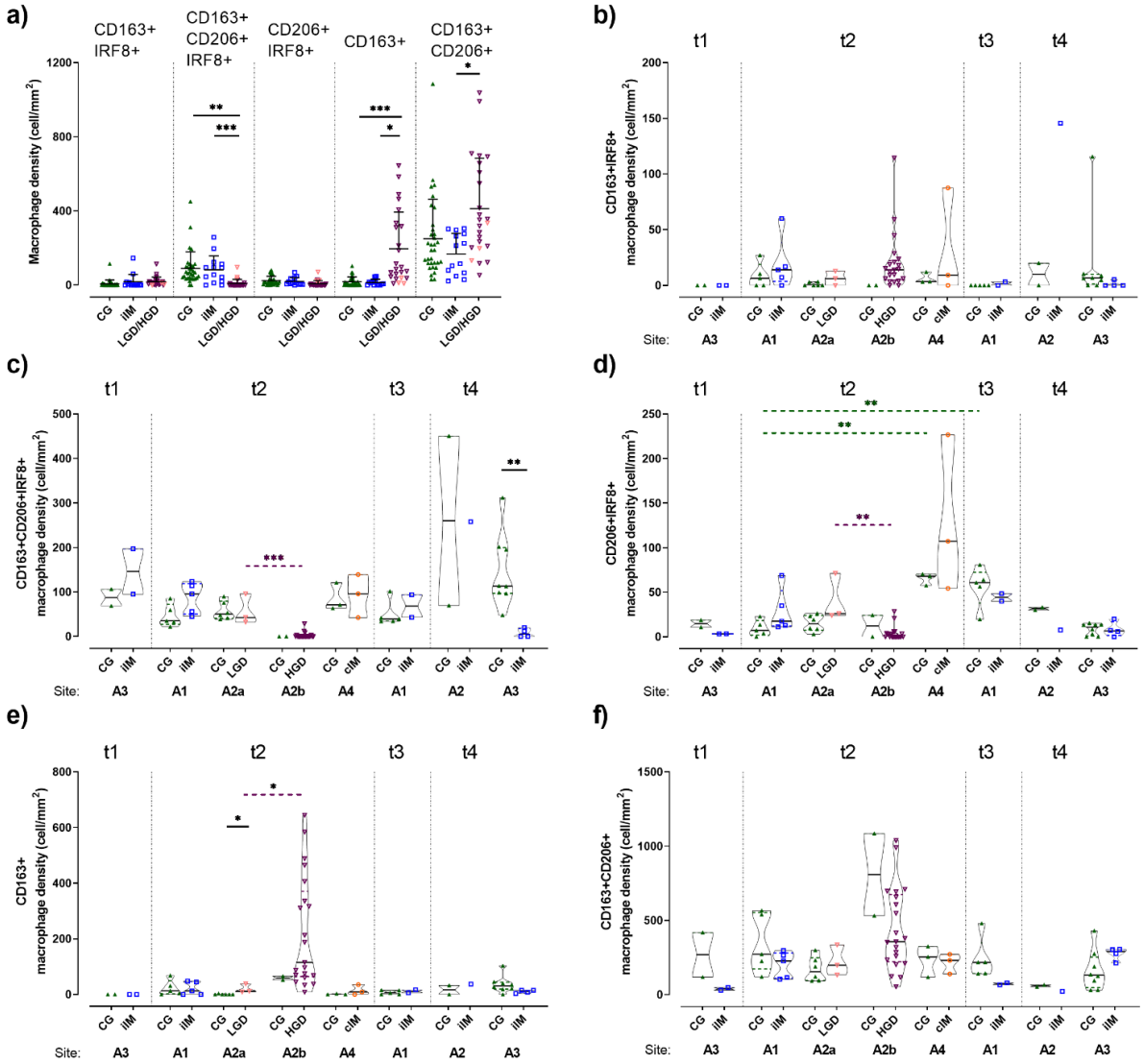


Figure 5.27 Pooled and single site/time point macrophage subset density in patient P2

a) Pooled macrophage subset density by tissue type; macrophage density by site, tissue type and time point shown for b) CD163+IRF8+ macrophages, c) CD163+CD206+IRF8+ macrophages, d) CD206+IRF8+ macrophages, e) CD163+ macrophages and f) CD163+CD206+.

Each symbol represents data from a single ROI. For pooled data (a) mean +S.D. shown and p values calculated using glm function in R and for individual samples (b, c, d, e, f) quartiles shown with t-test and Mann Whitney test used to calculate significance (minimum of 3 ROIs). *, **, *** is equal to $p<0.05$, $p<0.01$ and $p<0.001$.

For b), c), d), e) and f) coloured dashed lines show significant same tissue differences by site and time point (green for chronic gastritis, purple for LGD/HGD). Black lines show significant differences between matched CG and adjacent IM/LGD/HGD lesion.

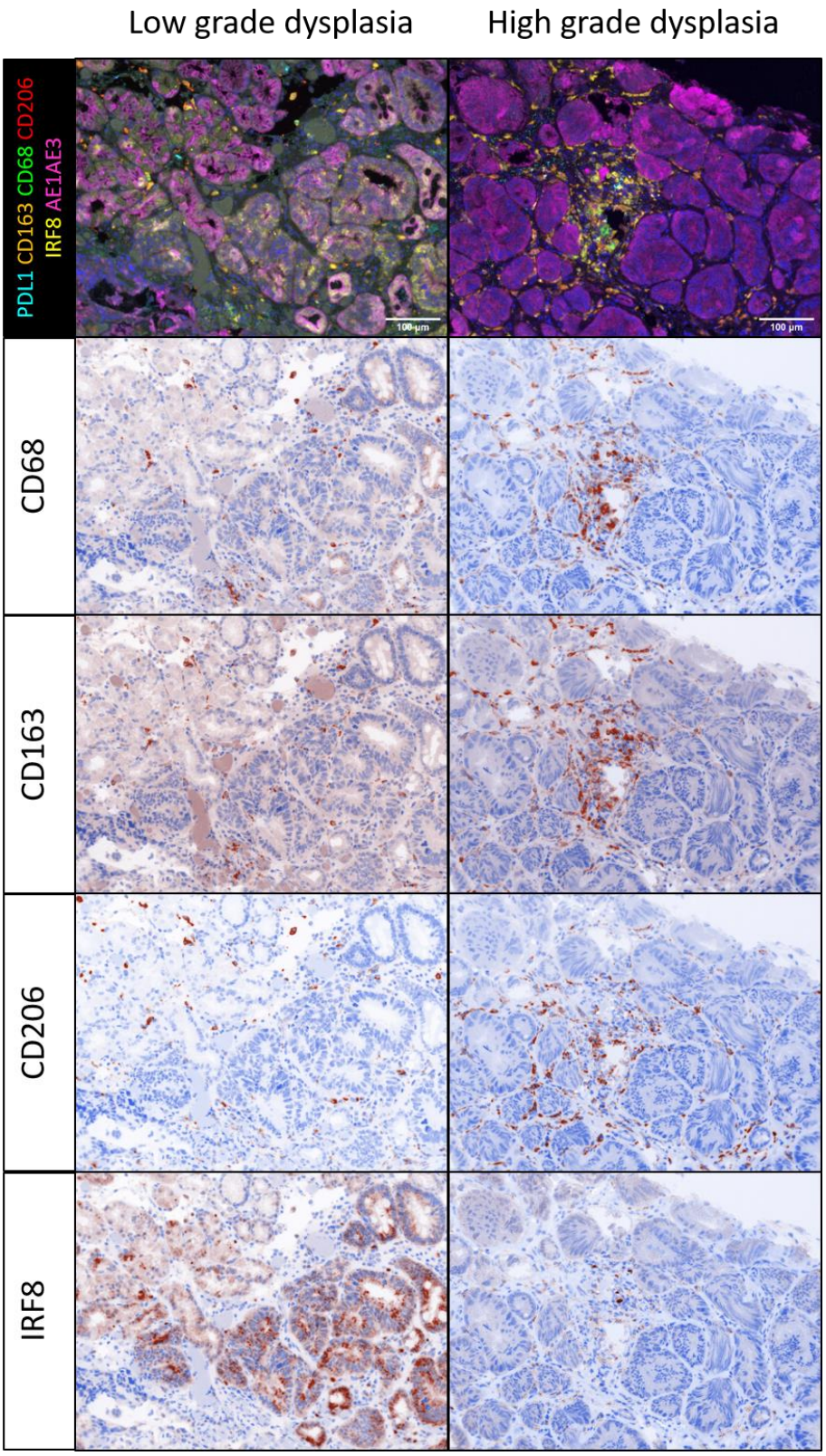


Figure 5.28 Macrophage profile in low grade and high grade dysplasia varies considerably in patient P2

Spectrally unmixed composite image together with pseudo-pathology images (inForm) shown of CD68, CD163, CD206 and IRF8 markers from low and high grade dysplasia. Scale bars: 100µm.

5.4 Summary and discussion

The following is a summary of the main outcomes of this study.

1. Gastric premalignant lesions contained six main subsets of macrophages that did not strictly adhere to the M1-M2 bipolar paradigm;
2. Complete intestinal metaplasia was characterised by greater total macrophage density compared to incomplete intestinal metaplasia. This was predominantly comprised of the M2 macrophage subtype
3. Patient matched intestinal metaplasia and adjacent chronic gastritis exhibited similar macrophage content
4. Temporal progression in chronic gastritis, complete and incomplete intestinal metaplasia was associated with an overall reduction of M2 to M1/2 ratio
5. Spatial relationship between the two main macrophage subsets (CD68+CD163+CD206+ and CD68+CD163+CD206+IRF8+) and epithelial cells reflected quantitative differences but macrophages in complete intestinal metaplasia targeted less the epithelium
6. Analysis of two case studies that had progressed to high grade dysplasia showed contrasting macrophage polarisation with considerable variation of macrophage content in intestinal metaplasia by site and by time point

5.4.1 Discussion

To characterise the macrophage landscape in IM four distinct macrophages markers were selected: CD68, CD163, CD206 and IRF8. CD68 was chosen as it is a pan monocyte-derived macrophage marker which localises mainly in lysosomes and endosomes with a smaller fraction on the cell surface [476, 477]. CD163 is an M2 macrophage marker whose expression is amplified by IL4, IL6, IL10 and macrophage colony stimulating factor (M-CSF) and downregulated in the presence of TNFα, IFNγ and bacterial lipopolysaccharides (LPS) [472, 478, 479]. It has particular relevance in tumour associated macrophages (TAMs), with likely a pro-tumoural role in GC [480, 481]. However it has been shown that on its own, it is not a reliable M2 marker [482]. CD206 is an M2 macrophage marker expressed by tissue resident macrophages and its expression can be amplified by IL4, granulocyte macrophage colony stimulating factor (GM-CSF) and TGFβ among others [472, 479, 483, 484]. IRF8 is an IFNγ–inducible transcription factor closely involved in the differentiation and function of myeloid populations including macrophages [473, 485]. It is an M1 macrophage marker and has been shown to control an anti-metastatic program in TAMs [486].

In this study IM was shown to contain six main macrophage populations based on marker co-localisation with varying staining intensity (and thus likely expression). These six subsets did not fully adhere to the M1-M2 bipolar paradigm, although they did show some degree of similarity to those identified recently in GC by Huang et al 2019 [198] on which the current macrophage OPAL™ panel was based on. Huang et al used high IRF8 expression on macrophages that were CD68+CD163-CD206- to define M1-like macrophages. However in the current study the macrophage panel was further optimised to allow the detection of IRF8 expression at lower levels. Of the six macrophage subsets, one had a clear M1 phenotype (CD68+CD163-CD206-IRF8+), two had a clear M2 phenotype (CD68+CD163+CD206-IRF8- and CD68+CD163+CD206+IRF8-) and three had a mixture of both (CD68+CD163+CD206+IRF8+, CD68+CD163+CD206-IRF8+ and CD68+CD163-CD206+IRF8+).

The three macrophage subsets that expressed a mixture of both M1 and M2 markers were used to create a novel macrophage subgroup termed M1/2 based on the key cell fate determining role of IRF8 in macrophages. This new subgroup contained macrophages whose functional role most likely lies between "pure" M1 and M2 macrophages (Figure 5.29).

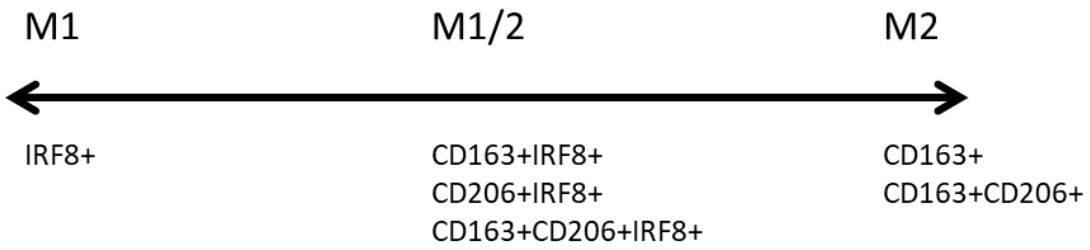


Figure 5.29 M1-M2 macrophage spectrum including M1/2 macrophage subsets
M1 macrophages: CD68+IRF8+, M1/2 macrophages: CD68+CD163+IRF8+, CD68+CD206+IRF8+ and CD68+CD163+CD206+IRF8+ and M2 macrophages: CD68+CD163+ and CD68+CD163+CD206+. Macrophages defined as being CD68+ cells.

Several studies have characterised the M1 and M2 phenotypes *in vitro* but these do not necessarily translate to *in vivo* microenvironments where macrophages with different polarization and different activation markers coexist in tissues [487-489]. Also the level of plasticity observed in macrophages does not necessarily exclude the possibility of an M1 macrophage transitioning to an M2 macrophage phenotype and vice versa. Nor does is it exclude the possibility of relatively stable macrophage phenotypes that have a mixture of M1 and M2 associated functions as the M1 and M2 phenotypes are likely the two extremes of a continuum. This could explain the M1/2 macrophage subsets observed in the current study.

Total macrophage cell density was shown to be highest in complete IM and lowest in incomplete IM. Overall M2 macrophages were the dominant subgroup in both IM subtypes in "early" IM

(IM-GC cohort) with very low numbers of M1 macrophages in most samples. However incomplete IM was relatively rich in M1/2 macrophages with the largest M1/2 subset consisting of CD68+CD163+CD206+IRF8+ macrophages and a significantly higher density compared to both CG and complete IM. The largest M2 subset consisted of CD68+CD163+CD206+ macrophages and these were significantly reduced in incomplete IM.

In “late” IM (IM+GC cohort), incomplete IM was characterised by fewer M1, M1/2 (including both CD68+CD163+CD206+IRF8+ and CD68+CD163+IRF8+ subsets), and M2 macrophages (including both CD68+CD163+CD206+ and CD68+CD163+ subsets) when compared to complete IM. When analysed across cohorts from “early” IM to “late” IM, there was an overall reduction in total macrophage content in incomplete IM, an increase in M1 and M1/2 macrophages in complete IM and a decrease of M2 macrophages (CD68+CD163+CD206+) in both IM subtypes. Although not universally present across all samples, the CD68+CD206+IRF8+ subset was significantly increased across all three tissue types in IM+GC patients.

Overall histo-temporal progression in IM was characterised by a progressively decreasing ratio of M2 to M1/2 macrophages and a lower macrophage density in the incomplete subtype suggesting that higher numbers of macrophages provided better protection against progression to dysplasia/cancer and that M1/2 macrophages are associated with higher risk. Fewer macrophages likely results in lower levels of antigen presentation to T cells in the local microenvironment.

It is difficult to speculate on why M1/2 macrophages may be associated with higher risk of progression although similarly to more defined M1 macrophages [195], they may also express iNOS and produce NO that could have an adverse effect on DNA stability of IM epithelial cells. Altered peptide presentation due to microsatellite instability in incomplete IM may also play an important role [163-165, 167].

Recent studies in GC have shown that local TAM populations do not adhere strictly to the M1/M2 paradigm [198, 490]. Additionally the spatial distribution of macrophage subsets was shown to differ between the tumour core, edge, margin and surrounding normal tissue suggesting that macrophage phenotype is likely to be significantly influenced by multiple local environmental stimuli [198]. This was also suggested in the current study as matched tissue analysis in a subset of the “early” and “late” IM patients showed that CG adjacent to IM tissue tended to have similar quantitative and qualitative macrophage populations.

Immune cells interact with target cells through both physical and paracrine communication via cytokine secretion. Cytokines are diffusible mediators and are responsible for promoting and regulating immune responses [491]. Spatial range of cytokine communication differs in scale considerably, ranging from very short range in narrow junctions between cells (the immunological synapse: ~15nm) to long range, equivalent to the diameter of multiple cells (up to or more than 50µm) in a dense multicellular environment [392]. Based on previous work by Feng et al 2017 [394] and Carstens et al 2017 [395], the mean number of cells within 40µm of a target cell population was chosen to be representative of both key physical and paracrine interactions. In the current study spatial analysis of macrophages within a distance of 40µm from epithelial cells showed histo-temporal progression was associated with an overall increase of M1/2 macrophages around the epithelium in CG and complete IM and a decrease of M2 macrophages in both subtypes of IM.

Overall the physical relationship of CD68+CD163+CD206+ and CD68+CD163+CD206+IRF8 macrophages with epithelial cells mirrored that of the quantitative differences observed between IM subtypes suggesting that their distribution was relatively uniform (homogeneous). However a more refined analysis showed that both macrophage subsets were actually much less efficient at targeting the epithelium in complete IM, particularly in “early” IM lesions, suggesting potential fundamental differences in macrophage movement adjacent to glands between IM subtypes.

Two patients who had progressed to HGD and had multi-site and multi-time point tissue available for whole exome sequencing and OPAL™ multiplex IHC showed that macrophage populations fluctuated considerably across space and time. In some instances, these fluctuations were observed within a distance of 200-300µm in the same tissue type in adjacent regions of interests. However using the current methodology it was not possible to assess why this occurred. It may be that immune cells were responding to a highly localised immunogenic insult through chemokine release of an epithelial cell “under attack” or a chemokine/cytokine gradient created by macrophages or other immune cells leading to the loose formation of multicellular immune cell aggregates.

In patient P1 two samples with HGD from the same site separated by only 78 days showed a significant influx of M1 and M1/2 macrophages and a reduction of M2 macrophages suggesting the rapid formation of a highly inflammatory IFNγ-driven microenvironment that may play a key role in at least a fraction of patients with HGD. In patient P2, LGD and HGD samples from the

same time point showed a difference in macrophage subgroups with the former having more M1 and M1/2 macrophages and the latter a much greater content of M2 macrophages.

Overall these two case studies suggested that progression to HGD may be associated with differing local immune response. Although both patients were characterised by multiple chromosomal aberrations in the sequenced adjacent HGD tissue, patient P2 had clearly more chromosomal losses which may have had an important impact on the type of "danger signals" produced by the neoplastic cells/glands due to an accompanying massive gene loss/reduced expression. This may explain the contrasting macrophage profiles, although possible differences in infiltration of other immune cell types in the local microenvironment may also contribute to this. Quantitative and qualitative changes in peptide antigen presentation by macrophages may play key differentiating roles in the immune response to HGD with differing genomic profiles, as similarly observed in the EBV and MSI subtypes of GC which have been shown to be more immunogenic compared to the GS and CIN subtypes [42, 492].

Previously Guo et al 2019 [239] showed a gradual increase of macrophages density during progression via the sequence from superficial chronic gastritis, atrophic gastritis, low and high grade dysplasia and then to GC. However this study lacked comprehensive macrophage phenotype data. A decrease of infiltrating CD8+ cells was however reported suggesting a possible link between macrophage and T cell function in the process of gastric carcinogenesis.

5.4.2 Technical limitations

The current study was a systematic and comprehensive characterisation of the main macrophage populations present in gastric premalignant lesions. It included both quantitative and spatial aspects of the macrophage landscape. However this study did have a small number of potential limitations including:

a) The number of tissue samples characterised from patients with (IM+GC) and without (IM-GC) concurrent gastric cancer was relatively small. The former tissue samples tended to be larger in size as they were obtained following a partial or full gastrectomy. By contrast IM-GC samples were biopsies specimens and thus smaller pieces of tissue. One of the main criteria for inclusion in this study was the content of IM in the target tissue. Samples of either cohort with only one or a small number of IM glands were excluded, creating a possible bias towards patients with extensive local IM. It is most likely that these IM glands were clonally related as previous work by Guttierez-Gonzalez et al 2011 demonstrated the clonal origins of IM glands [493].

b) The OPAL methodology which is based on tyramide signal amplification [390, 494] has certain inherent limitations. The 7 marker protocol used for the macrophage panel in this study had a duration of 3 days with multiple antigen retrieval steps which can give rise to tissue quality issues, although these were reduced by using the highly adhesive Trajan glass slides (Table 2.1, §2.5.2). Additional issues can arise because of fluorophore cross-interference.

c) A limitation of the inForm software used for acquiring data is a requirement for a minimum number of cells (≥5 cells) to "train" the classifier to distinguish user defined cell phenotypes, usually centred on the co-localisation of cell markers. In this study rare macrophage subsets including CD68+CD163-CD206-IRF8- and CD68+CD163-CD206+IRF8- macrophages did not match this criteria thus it was not possible to quantitate them. Although unlikely to play an important role with regards to the overall immune microenvironment in gastric premalignant lesions, it is important to reflect on the limitations of the method used for data acquisition.

d) The 20 tissue samples characterised from the Progressors' cohort originated from 2 patients due to limited case studies being available. This introduced patient bias into the analysis. More patients which have progressed to high grade dysplasia will need to be characterised in future studies to validate the current study's findings.

e) The genomic profile of each dysplastic tissue was obtained through whole exome sequencing of frozen tissue. Although the FFPE tissue used for macrophage characterisation was acquired exactly adjacent, it does not necessarily translate to dysplastic cells having the same chromosomal and mutational profile. Due to localised tissue heterogeneity, the areas sequenced and the areas immune profiled may differ substantially thus any conclusions cannot be definite.

Overall this study investigated the macrophage landscape in IM and showed the presence of six main macrophage subsets. Although both subtypes of IM were predominantly rich in M2 macrophages, the incomplete subtype showed a higher density of M1/2 macrophages, a novel hybrid subgroup of macrophages based on macrophage subsets expressing both strict M1 and M2 associated markers. Temporal progression in IM as described between IM-GC and IM+GC patients was also characterised by fewer M2 and more M1/2 macrophages.

In the majority of tissues investigated, irrespective of IM subtype, the two main subsets CD68+CD163+CD206+IRF8+ and CD68+CD163+CD206+ macrophages were found within relative proximity of each other and were most likely exposed to a similar mixture of chemokines, cytokines and other extracellular compounds present in the local intercellular spaces. In some

instances, these two macrophage subsets were physically touching. However only one of these two subsets expressed IRF8 most likely in response to IFNγ suggesting that they may differ in a fundamental way.

Spatial distribution of the main macrophage subsets reflected overall quantitative differences but a more refined analysis showed significant differences in macrophage targeting of epithelial cells and of each other between IM subtypes. Further investigation of the immune microenvironment in IM is required to define its possible role in gastric carcinogenesis.

Chapter 6 Characterising the T cell landscape in intestinal metaplasia

6.1 Introduction

Gene expression profiling carried out in section §4.3.3 of this thesis suggested that both chronic gastritis (CG) and intestinal metaplasia (IM) were rich in CD8 T cells and resting memory CD4 T cells. Additional profiling (§4.3.12-14) showed that the complete subtype of IM was rich in gene expression of T cell associated markers. Also OPAL™ multiplex immunohistochemistry (IHC) in chapter 5 showed that complete IM had higher macrophage infiltration than incomplete IM further suggesting a greater level of inflammation.

A limited number of previous T cell studies in IM have produced contrasting results. Using single IHC Cheng et al 2012 [236] showed IM had fewer CD4+ and FOXP3+ cells compared to surrounding gastritis and peptic ulcer but Liu et al 2017 [471] showed higher scores for both CD4 and CD8 IHC staining compared to gastric ulcer and gastric carcinoma without reaching statistical significance.

So far no other study has investigated the T cell landscape in the complete and incomplete subtypes of IM with the aim to identify differences that may explain their differing risk associated with progression to gastric cancer (GC). The main objective of this part of my thesis was to use multiplex IHC (OPAL™ platform) to identify and characterise the predominant T cell subsets in patients as they progress through the premalignant lesions of the Correa Cascade (§1.2.1, Figure 1.5). Additionally, I wanted to investigate the relationship between macrophages (Chapter 5) and T cells to examine their possible combined role in progression. These two immune cell types interact in a bidirectional way: 1) macrophages present antigen to T cells via MHC I (CD8) and MHC II (CD4) molecules [495] and 2) T cells direct macrophage differentiation within the M1 to M2 phenotype spectrum [496]. Thus, macrophages and T cells together are vital components of the innate and the adaptive immune response and likely an important role in eliminating virally/bacterially infected cells and early neoplastic cells. The same patient tissue samples previously described in chapter 5 were used for this chapter.

6.2 Hypothesis and aims

Hypothesis: “The T cell landscape differs between intestinal metaplasia subtypes and is associated with differing risk of progression”.

The main aims of this study were:

1. To identify and characterise total T cell and T cell subset density in CG, complete and incomplete IM in the IM-GC and IM+GC cohorts in both histological and temporal order of progression
2. To compare T cell density in CG surrounding IM in the IM-GC and IM+GC cohorts and across cohorts
3. To determine quantitative relationships between T cell subset densities and between T cell subsets and epithelial cells by investigating ratios in the IM-GC and the IM+GC cohorts
4. To characterise the spatial relationships between T cell subsets and between T cells and epithelial cells in the IM-GC and the IM+GC cohorts
5. To evaluate the quantitative and spatial relationships between macrophage and T cell subsets
6. To characterise the T cell landscape in two patients that have progressed to high grade dysplasia

6.3 Results

6.3.1 Description of cohorts and OPAL™ multiplex immunohistochemistry used with the T cell panel

For this study the same patient cohorts were used as in Chapter 5 (Table 5.1). The OPAL™ multiplex IHC T cell panel (§2.5.1-2, Tables 2.2 and 2.9) was based on that used on gastric cancer (GC) tissue in Wang et al 2020 [258] with changes to two of the antibodies selected. To prevent background staining the anti-CD4 rabbit monoclonal antibody SP35 (Spring Bioscience) was replaced by the mouse monoclonal antibody 4B12 (ThermoFisher Scientific) and the anti-CD56 mouse monoclonal antibody CD564 (Leica) was replaced by the anti-CD10 mouse monoclonal antibody 56C6 (Abcam). The remaining antibodies used were the anti-CD3 rabbit monoclonal antibody SP7 (Spring Bioscience), an anti-FOXP3 rabbit polyclonal antibody (Bio SB), the anti-CD8 mouse monoclonal antibody 4B11 (ThermoFisher Scientific) and the multi anti-cytokeratin mouse antibodies AE1/AE3 (Novocastra). Serial sections were used for multiplex IHC staining followed by digital data acquirement and statistical analysis as described in §2.5.3-6 and §5.3.2 (Appendix K, Figure 6.1, glm function in R). Anti-CD10 staining of the brush border in IM was not

quantified for this study but its findings will be discussed in Chapter 7. Subtyping of IM was carried out as described in detail in §2.5.1 and Figure 2.3.

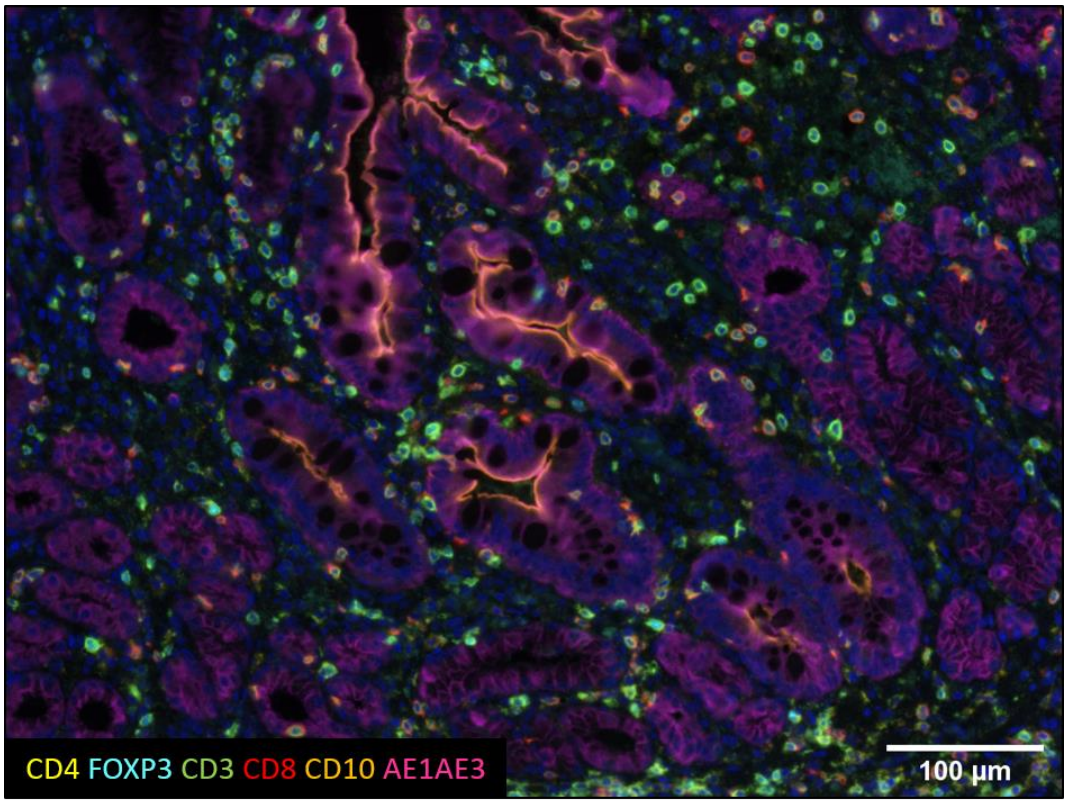


Figure 6.1 OPAL™ multiplexed fluorescent immunohistochemistry staining using the T cell panel on human gastric intestinal metaplasia
Intestinal metaplastic (complete) tissue stained with the OPAL™ multiplex IHC T cell panel and scanned at high resolution followed by spectral unmixing in inForm. This image represents a single region of interest (ROI).

6.3.2 T cell immune profile in gastric premalignant lesions consists of four main subsets

Analysis of all premalignant conditions across all three cohorts studied identified four T cell subsets (Figure 6.2).

1. CD3+CD4+FOXP3-CD8- (CD4 T cells)
2. CD3+CD4+FOXP3+CD8- (FOXP3 T cells)
3. CD3+CD4-FOXP3-CD8+ (CD8 T cells)
4. CD3+CD4-FOXP3-CD8- (double negative or DN T cells)

Subsets 1-3 were localised either (i) close to the epithelium or (ii) as small pockets highly rich in T cells containing a mixture of all three T cell subsets, defined as lymphoid aggregates. In some tissue samples, tertiary lymphoid structures were present in the *lamina propria* and these regions were excluded from the analysis to prevent inconsistencies with regards to overall T cell densities. Subset 4 (DN T cells) were distinct and were mainly found near epithelial cells and not in lymphoid aggregates.

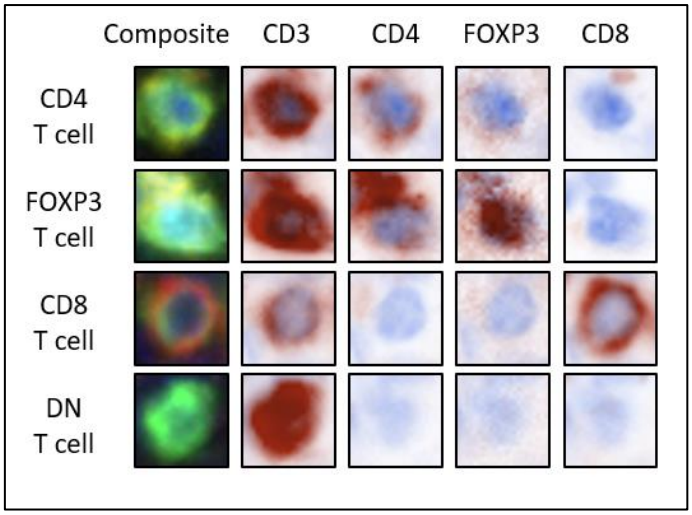


Figure 6.2 T cell subsets based on the co-localisation of specific T cell markers
T cell subsets were CD3+CD4+FOXP3-CD8- (CD4 T cells), CD3+CD4+FOXP3+CD8- (FOXP3 T cells), CD3+CD4-FOXP3-CD8+ (CD8 T cells) and CD3+CD4-FOXP3-CD8- (DN T cells).

6.3.3. Higher total T cell density in the complete subtype of intestinal metaplasia in both the IM-GC and IM+GC cohorts

The sum of all CD3 positive cells was calculated to determine the total T cell density in the IM-GC and IM+GC cohorts (Figure 6.3). Complete IM in both the IM-GC and the IM+GC cohorts (n=10 for both cIM-GC and cIM+GC) was characterised by a significantly higher total T cell density compared to CG (CG-GC, n=12 and CG+GC, n=14). Incomplete IM in both the IM-GC and the IM+GC cohorts (iIM-GC, n=12 and iIM+GC, n=8) had a lower total T cell density compared to both CG and complete IM.

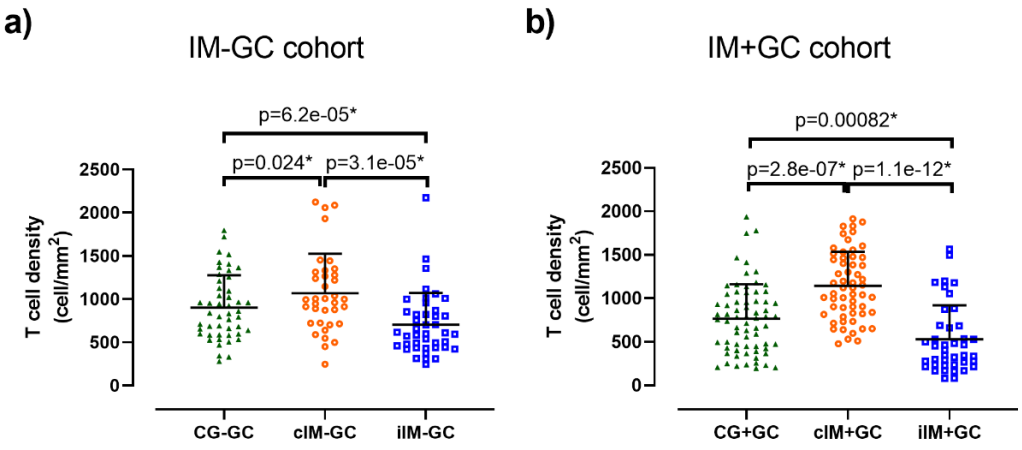


Figure 6.3 Total T cell density in chronic gastritis, in complete and in incomplete intestinal metaplasia in the IM-GC and IM+GC cohorts
a) data shown from chronic gastritis (CG-GC, n=12), complete IM (cIM-GC, n=10) and incomplete IM (iIM-GC, n=12) samples from the IM-GC cohort and b) data shown from chronic gastritis (CG+GC, n=14), complete IM (cIM+GC, n=10) and incomplete IM (iIM+GC, n=8) samples from the IM+GC cohort. Each symbol represents data from a single region of interest (ROI). Multiple ROIs per sample. Data presented as mean + S.D. *All statistical analysis done using glm function in R (see section §2.5.6).

6.3.4 Total T cell density increases in complete IM and decreases in incomplete IM with temporal progression

The same data was then analysed in a different way, this time looking at tissues of the same subtype and comparing the non-cancer (IM-GC, "early" lesions) and the cancer setting (IM+GC, "late" lesions). No significant difference was observed in in the CG tissues (Figure 6.4). However, for the complete IM tissues a significant increase in total T cell density was seen as this lesion type progressed temporally. By contrast a decrease in total T cell density was observed for incomplete IM as temporal progression occurred.

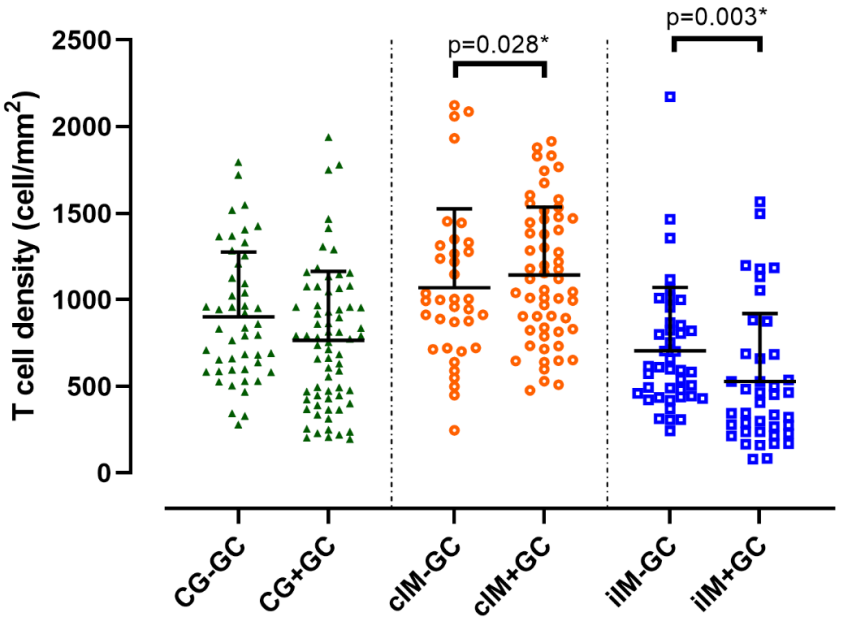


Figure 6.4 Total T cell density increases in complete intestinal metaplasia and decreases in incomplete intestinal metaplasia with temporal progression
Data shown from CG-GC (n=13) and CG+GC (n=14), cIM-GC and cIM+GC (both n=10) and iIM-GC (n=12) and iIM+GC (n=8) samples. Each symbol represents data from a single region of interest (ROI). Multiple ROIs per sample. Data presented as mean + S.D. *All statistical analysis done using glm function in R (see section §2.5.6).

6.3.5 Complete intestinal metaplasia characterised by influx of CD4 and DN T cells whereas incomplete IM shows lower density of all T cell subsets except for FOXP3 T cells

The abundance of T cells in different histological subtypes was further analysed by subset and setting. In the non-cancer setting (IM-GC cohort), CD4 and DN T cell densities were higher in cIM-GC compared to CG-GC. Also significantly lower CD8 and DN T cells densities were observed in iIM-GC compared to both CG-GC and cIM-GC (Figure 6.5a).

In the context of cancer (IM+GC cohort) similar findings were observed in that cIM+GC had significantly higher T cell density of CD4 and DN T cells but also of FOXP3 T cells compared to

CG+GC (Figure 6.5b). Again iIM+GC had significantly lower CD8 and DN T cell densities compared to CG+GC but also of CD4 T cells compared to cIM+GC.

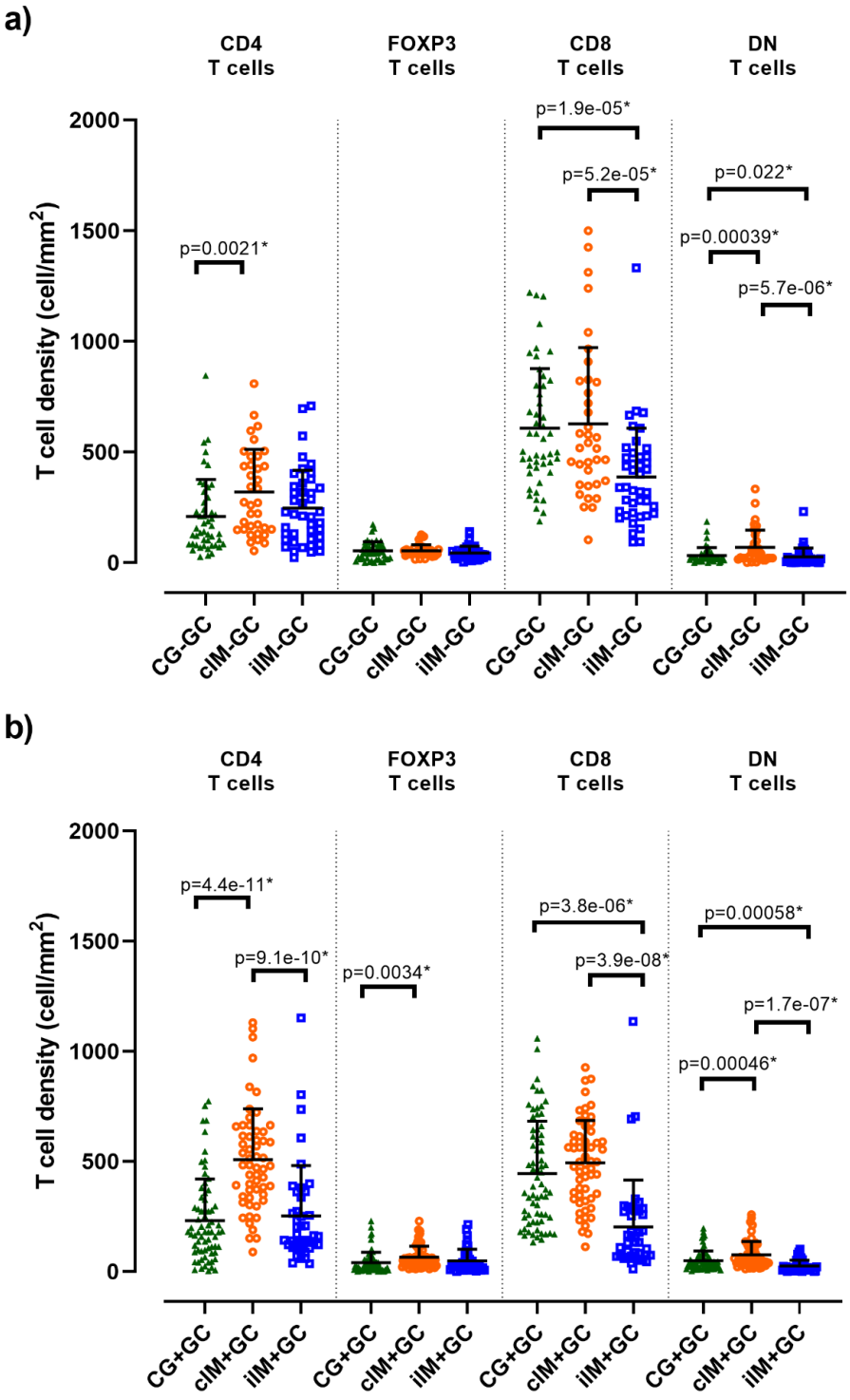


Figure 6.5 T cell subset density in the IM-GC and IM+GC cohorts
Individual T cell subset densities shown from samples described in Figures 6.3 and 6.4 with a) for the IM-GC cohort and b) for the IM+GC cohort. Each symbol represents data from a single ROI. Multiple ROIs per sample. Data presented as mean + S.D. *All statistical analysis done using glm function in R.

The same data was then reanalysed to compare T cell density by tissue type between the IM-GC ("early" lesions) and the IM+GC ("late" lesions) cohorts. Both CG and complete IM were characterised by a higher density of CD4 and DN T cells whereas incomplete IM was characterised by a lower density of CD8 T cells with temporal progression (Figure 6.6).

Overall, complete IM was characterised by higher levels of T cell infiltration, suggesting a higher intensity of chronic inflammation and incomplete IM was characterised by a particularly low density of CD8 and also DN T cells. In the IM+GC cohort the same differences as in IM-GC were observed but even more pronounced, with an additional lower density of CD4 T cells in incomplete IM.

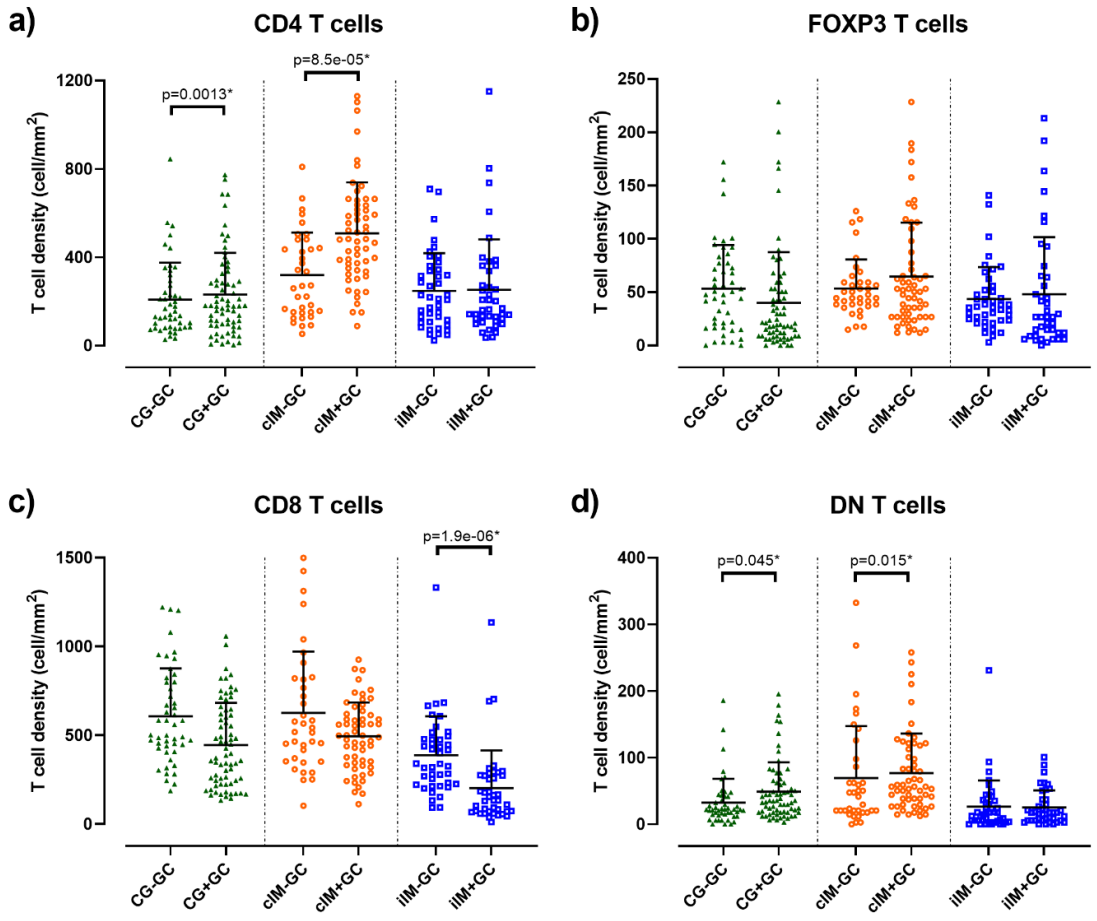


Figure 6.6 T cell subset densities plotted by tissue type comparing IM-GC ("early") and IM+GC ("late") gastric premalignant lesions
Reanalysis of data shown in Figure 6.5 to determine T cell subset density differences within the same tissue type between the IM-GC ("early" lesions) and the IM+GC ("late" lesions) cohorts. Each symbol represents data from a single region of interest (ROI). Multiple ROIs per sample. Data presented as mean + S.D. *All statistical analysis done using glm function in R.

6.3.6 Matched adjacent chronic gastritis has fewer CD4 T cells than complete intestinal metaplasia

To further understand the possible association of different T cell subsets on IM initiation/progression, a paired analysis of complete IM and incomplete IM samples together with their matched adjacent CG was performed. This was done independently for the IM-GC and IM+GC cohorts (Figure 6.7).

In IM-GC there were no significant differences observed in total T cell (Figure 6.7a) nor in CD4 T cell (Figure 6.7c) density between adjacent CG and matched IM tissue nor between CG adjacent to differing IM subtypes. However, a strong trend with respect to CD8 T cell density was observed with incomplete IM having a lower tissue infiltration than adjacent CG ($p=0.056$, Figure 6.7e). In the IM+GC samples, complete IM had a greater total T cell (Figure 6.7b) and CD4 T cell (Figure 6.7d) density compared to adjacent CG ($p=0.034$ and $p=0.0066$, respectively). No differences were detected between incomplete IM and adjacent CG.

Overall matched sample analysis showed that CG and adjacent IM tended to have similar T cell profiles irrespective of IM subtypes, although specific differences were detected particularly in the IM+GC samples. Additionally CG between differing IM subtypes seemed relatively similar with respect to T cell content.

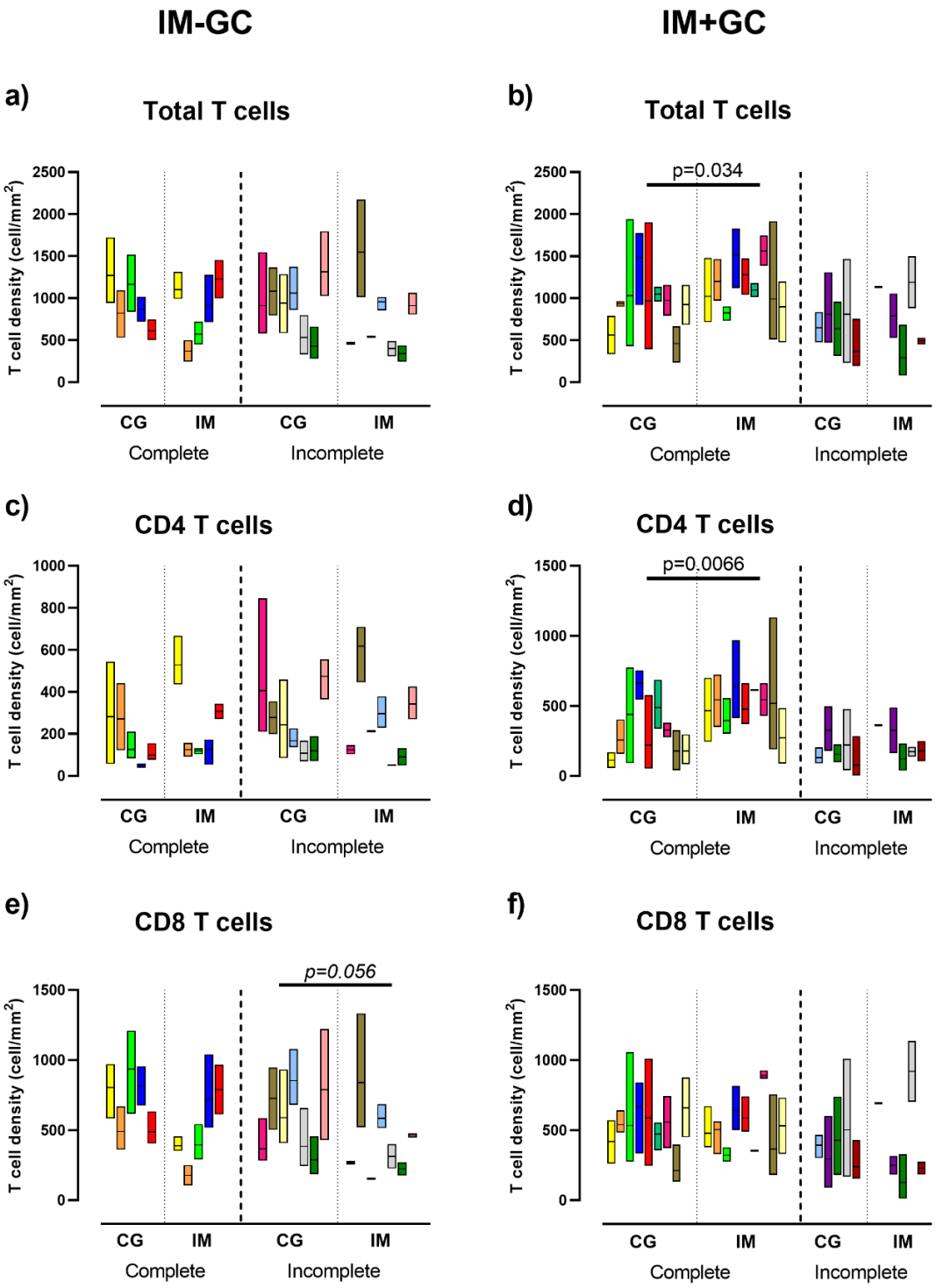


Figure 6.7 Total, CD4 and CD8 T cell density of matched chronic gastritis adjacent to intestinal metaplasia in IM-GC and IM+GC samples for individual patients

Matched colour floating bars (min/mean/max) showing T cell data from multiple ROIs per tissue type of matched CG adjacent to IM tissue. Data shown in a), c) and e) for CG with matched complete IM (n=5) and for CG with matched incomplete IM (n=7) from the IM-GC cohort and in b), d) and f) for CG with matched complete IM (n=9) and for CG with matched incomplete IM (n=5) from the IM+GC cohort. Statistical analysis carried out using Wilcoxon test and the paired and unpaired t-tests where appropriate in GraphPad Prism.

6.3.7 T cell subset ratios show recurrent pattern across tissue types with time

Having identified possible differences in relationships between T cell subsets in these premalignant tissues representing different stages of histological and temporal progression, cell density ratios of CD4, CD8 and FOXP3 T cells were quantified and compared (Figure 6.8). In the IM-GC cohort, a significant increase of CD4 to CD8 T cell ratio was observed along histological progression from CG to incomplete IM (Figure 6.8a). In the IM+GC cohort, both CD4 to FOXP3 and CD4 to CD8 T cell ratios were greater in cIM+GC compared to CG+GC (Figure 6.8c). Interestingly the CD8 to FOXP3 T cell ratio was characterised by a decrease along histological progression from CG to incomplete IM (Figure 6.8c).

Overall the differences observed in the IM+GC cohort were more pronounced than in the IM-GC cohort with a recurrent pattern of a higher CD4:CD8 T cell ratio in complete IM. A lower CD8:FOXP3 T cell ratio in incomplete IM suggested a greater potential for T cell immune-regulation in this tissue type.

6.3.8 Epithelial cell to T cell subset ratios differ between complete and incomplete intestinal metaplasia

T cells are capable of offering effective protection against virus/bacteria infected cells and early cancerous cells thus investigating the ratio between epithelial cell and T cell subsets could provide insight into the role of the latter in the battle between host and foreign agent invasion/cancer. In the IM-GC cohort, epithelial cell to total T cell ratios were characterised by a highly significant increase in iIM-GC thus the number of T cells involved in immune surveillance T cells in relation to the epithelium was much reduced in this tissue type. The difference was mainly due to the large number of epithelial cells per CD8 T cell present in this IM subtype. Interestingly although the epithelial to total T cell ratio did not differ between CG-GC and cIM-GC tissues, the epithelial to CD4 and FOXP3 T cell ratios were significantly smaller in the latter.

In the IM+GC cohort, the epithelial cell to total T cell ratio was lower in cIM+GC compared to CG+GC. This difference in quantitative relationship between epithelial cells and total T cell population was distributed among all three T cell subsets (CD4, FOXP3 and CD8 T cells) further confirming the highly T cell rich microenvironment in the complete subtype of IM. Epithelial cell to T cell subset ratios were higher in incomplete IM with the maximum difference observed in the epithelial to CD8 T cell ratio, further suggesting that this IM subtype is characterised by a relatively T cell poor microenvironment.

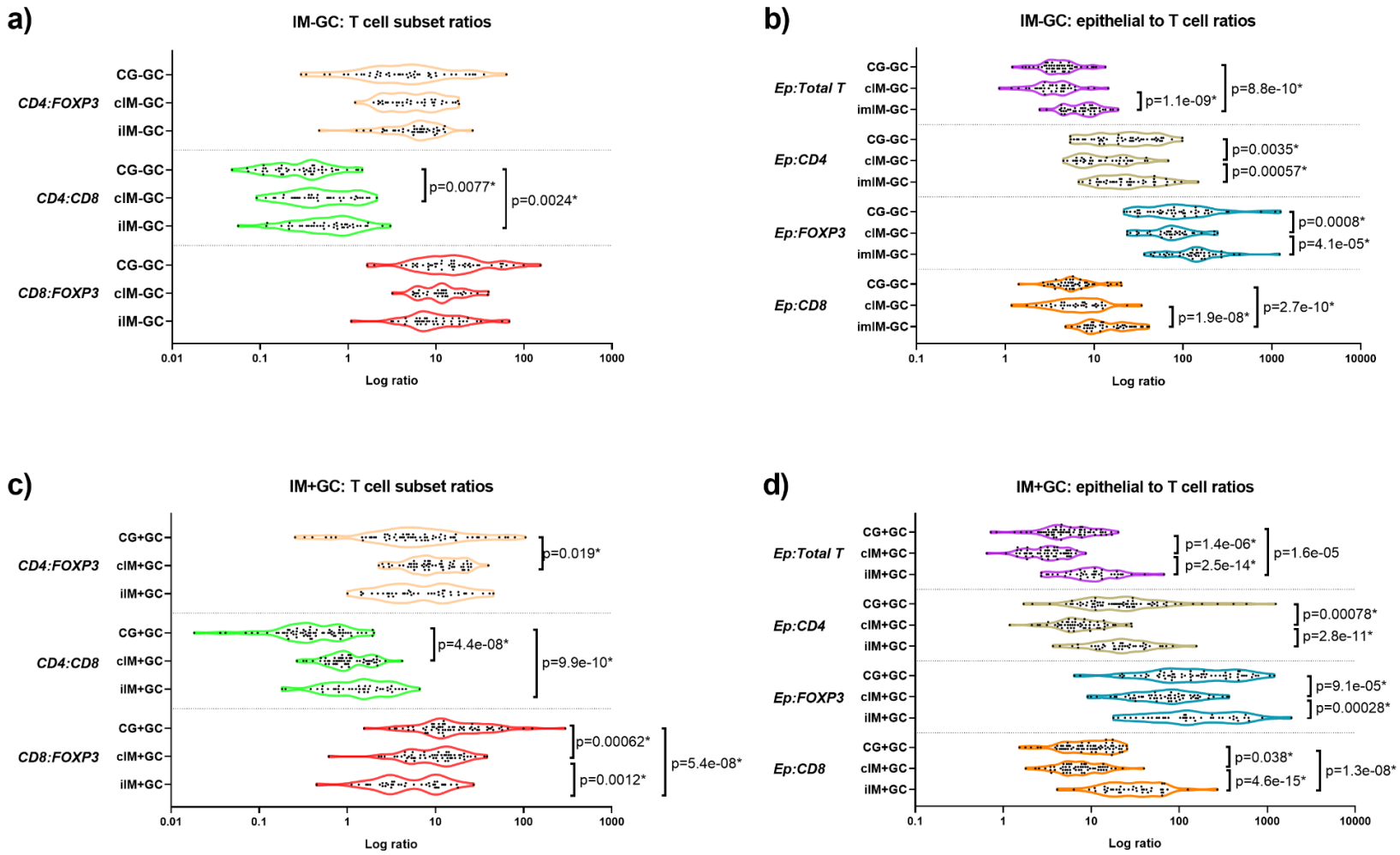


Figure 6.8 T cell subset and epithelial cell ratios in IM-GC and IM+GC samples

a) shows T cell subset ratios and b) epithelial cell to T cell subset ratios in the IM-GC samples (CG-GC=13, cIM-GC=10 and iIM-GC=12); c) shows T cell subset ratios and d) epithelial cell to T cell subset ratios in the IM+GC samples (CG+GC=14, cIM+GC=10 and iIM+GC=8). Ep: epithelial cell. Each symbol represents data from a single ROI. Multiple ROIs per sample. *All statistical analysis done using glm function in R.

6.3.9 Lower levels of T cell-T cell interaction in incomplete intestinal metaplasia

To gain insight into the spatial relationship between T cell subsets and how this may relate to risk of progression associated with tissue type, the mean number of T cells within a 40µm distance of a reference cell's was investigated. This would include both cells that are physically immediately adjacent (~10-15µm) thus possibly physically interacting and also cells with potential paracrine influence (~15-40µm) (§2.5.5 and Figure 2.4).

In both IM-GC and IM+GC samples, CD8 T cells were the most prevalent T cell subset within a 40µm radius of CD4 T cells and vice versa (Figure 6.9a-b). In IM-GC samples CD8 T cells were also the most prevalent T cell subset within a 40µm radius of FOXP3 T cells, whereas in IM+GC samples CD4 and CD8 T cells were roughly equal in abundance within a 40µm radius of this T cell subset. With respect to IM subtype, CD8 T cells were fewer around CD4 and FOXP3 T cells in incomplete IM of both cohorts. Incomplete IM was further characterised by a lower mean number of CD4 T cells around FOXP3 and CD8 T cells in IM+GC.

Levels of physically touching T cell pairs were directly investigated by touch cell pair analysis which showed that CD4//CD8 T cell touch pairs had the greatest touch cell pair density in both the IM-GC and the IM+GC samples. CG and complete IM showed a similar T cell touch pair profile in IM-GC, whereas incomplete IM was characterised by a lower T cell-T cell touch pair density of all T cell subsets investigated (CD4//FOXP3, CD4//CD8, CD4//DN, FOXP3//CD8, FOXP3//DN, CD8//DN) compared to the latter. In the IM+GC samples, complete IM showed a higher touch cell pair density of all T cell subsets except for FOXP3//DN compared to CG, suggestive of a microenvironment rich in T cell interaction. Compared to the complete subtype, incomplete IM had a lower touch cell pair density of all T cell subsets with the sole exception being again the FOXP3//DN touch cell pair.

Overall T cell-T cell spatial location analysis, which included both physically touching cell pairs and number of cells within a 40µm radius mirrored the previously observed quantitative differences with regards to T cell infiltration of IM subtypes. This analysis showed lower levels of physical/paracrine interaction between all three T cell subsets in incomplete IM, decreasing even further with temporal progression and suggestive of a reduced T cell immunity in this IM subtype.

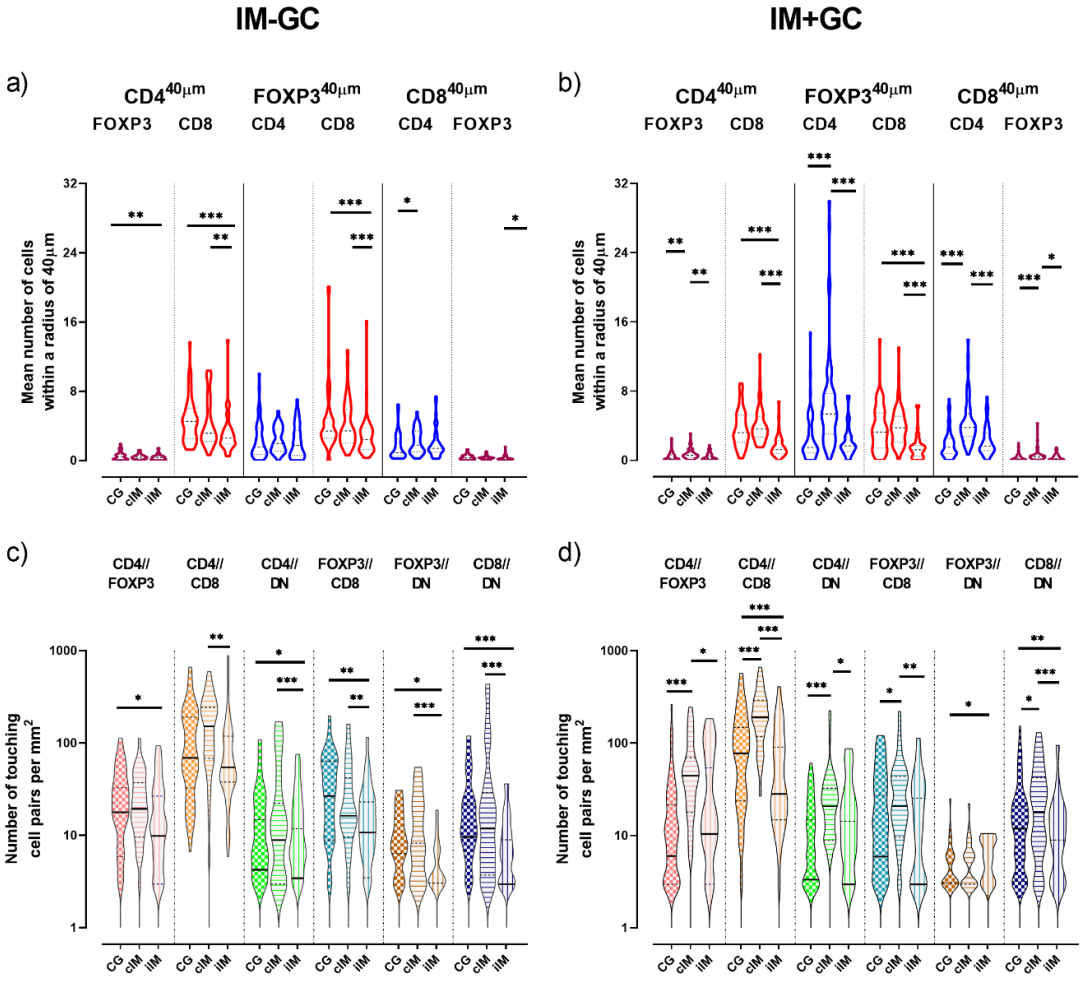


Figure 6.9 Mean number of T cells within a 40µm radius and touch cell pair density between T cell subsets in the IM-GC and IM+GC cohorts

Violin plots showing a) and b) the mean number of other T cells within a 40µm radius of individual CD4 ($^{40\mu m}$FOXP3 and $^{40\mu m}$CD8), FOXP3 ($^{40\mu m}$CD4 and $^{40\mu m}$CD8) and CD8 ($^{40\mu m}$CD4 and $^{40\mu m}$CD8) T cells for the IM-GC (CG-GC=13, cIM-GC=10, iIM-GC=12) and IM+GC (CG+GC=14, cIM+GC=10, iIM+GC=8) cohorts respectively, and c) and d) touch cell pair density between T cell subsets in IM-GC and IM+GC cohorts respectively. Median and quartile values shown. All statistical analysis done using glm function in R. *, **, *** is equal to $p<0.05$, $p<0.01$ and $p<0.001$.

6.3.10 Lower levels of epithelial cell-T cell interaction in incomplete intestinal metaplasia

Having characterised the functional space between T cell subsets, the next logical step was to investigate the spatial relationship between epithelial cells and T cells. Specific T cell subsets require physical or proximally close interactions with their target cell in order to be functional *eg* cytotoxic T cells induce target-cell apoptosis by releasing granzyme-containing granules across the immune synapse [497]. Keeping in mind that the epithelium is believed to be the source of an early dysplastic cell that eventually leads to a tumour if it is not cleared up effectively by the immune system, the amount of T cell to epithelial cell interaction could be representative of the effectiveness of T cells in removing abnormal cells [498].

Across both cohorts, the main T cell subsets within 40µm of epithelial cells were CD8 T cells, followed by CD4 T cells (Figure 6.10). The incomplete IM epithelium in both cohorts was characterised by a lower number of both CD8 and DN T cells within 40µm compared to the complete IM subtype. Additionally incomplete IM in the IM+GC samples had fewer CD4 T cells in the proximity of the epithelium.

The level of potential physical interaction between epithelial cells and T cells was directly quantitated by touch cell pair analysis. Again incomplete IM was characterised by lower touch cell pair density between epithelial cells and CD8 and DN T cells in both cohorts. Additionally a lower touch cell pair density was also detected with CD4 T cells in incomplete IM of the IM+GC samples.

Overall the spatial relationship between T cells and epithelial cells reflected the numerical differences observed previously (§6.3.5 and Figure 6.5) and showed incomplete IM had fewer T cells in the vicinity of the epithelium. In particular, lower levels of physical interaction with CD8 and DN T cells suggest that the incomplete IM epithelium is less surveilled by T cells with cytotoxic capacity including both cytotoxic and innate-like (MAIT and γδ T cells) T cells. This could result in incomplete IM having a more permissive microenvironment for the potential outgrowth of unstable stem cell clones.

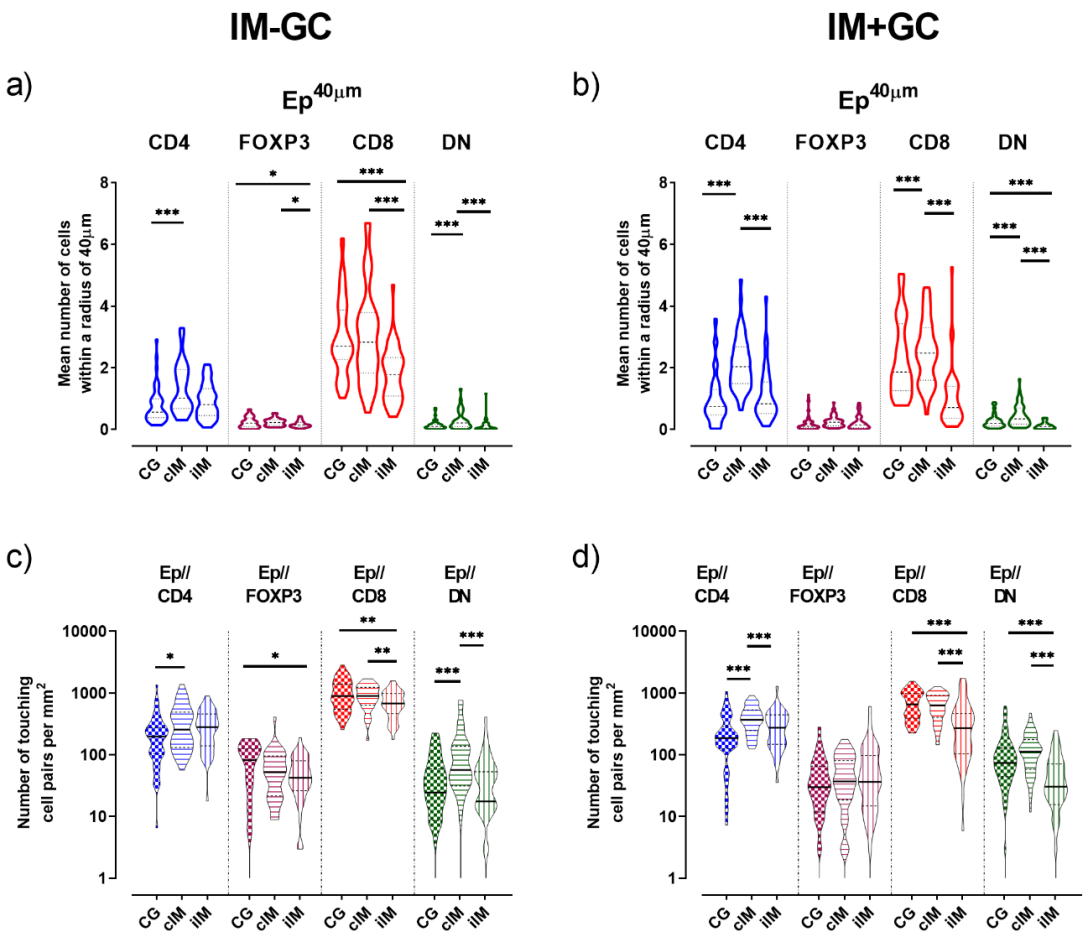


Figure 6.10 Mean number of T cells within a 40µm radius and touch cell pair density between epithelial cells and T cell subsets in the IM-GC and IM+GC cohorts

Violin plots showing a) and b) the mean number of T cells within a 40µm radius of epithelial cells for the IM-GC (CG-GC=13, cIM-GC=10, iIM-GC=12) and IM+GC (CG+GC=14, cIM+GC=10, iIM+GC=8) cohorts respectively, and c) and d) touch cell pair density between epithelial cells and T cell subsets in the IM-GC and IM+GC cohorts respectively. Median and quartile values shown. All statistical analysis done using glm function in R. *, **, *** is equal to $p<0.05$, $p<0.01$ and $p<0.001$.

6.3.11 CD8 T cells target the epithelium in incomplete intestinal metaplasia

Having quantified the overall cell to cell spatial relationships, the next step was to characterise the pattern of single T cells targeting epithelial cells or other T cells among tissues representing histological progression. The same normalisation method was used as described in §5.3.13 to identify whether T cell distribution was mainly random or more targeted towards specific cell types.

All pair combinations of CD4, CD8, FOXP3 and epithelial cells were investigated (Table 6.1). In the IM-GC cohort, individual CD8 T cells targeted more the CD4 T cells in complete IM than in CG (p=0.0495). By contrast individual CD4 and CD8 T cells in incomplete IM targeted more the epithelial cells when compared to the complete IM subtype (p=0.047 and p=0.00078, respectively).

Table 6.1 Normalised[1] touch pair analysis showing changes in T cell targeting across tissues representing histological progression in the IM-GC and the IM+GC cohorts

Touch cell pairs		CG -> cIM		cIM -> iIM	
Cell A	**Cell B**	**Change[2]**	**pval[3]**	**Change[4]**	**pval[3]**
IM-GC cohort					
Epithelial	CD4 T cell	↓	ns	↑	**0.047**
Epithelial	FOXP3 T cell	↓	ns	↑	ns
Epithelial	CD8 T cell	↓	ns	↑	**0.00078**
CD4 T cell	FOXP3 T cell	↑	ns	↓	ns
CD4 T cell	CD8 T cell	↑	**0.0495**	↓	ns
FOXP3 T cell	CD8 T cell	↓	ns	↑	ns
IM+GC cohort					
Epithelial	CD4 T cell	↓	**0.00015**	↑	**3.5e-09**
Epithelial	FOXP3 T cell	↓	**0.0033**	↑	**0.002**
Epithelial	CD8 T cell	↓	**0.00026**	↑	**2.7e-05**
CD4 T cell	FOXP3 T cell	↑	**1.5e-05**	↓	**0.0037**
CD4 T cell	CD8 T cell	↑	**2.6e-08**	↓	**0.0045**
FOXP3 T cell	CD8 T cell	↑	**0.021**	↓	ns

[1]Normalisation carried out by dividing touch pair cell density between cell A and cell B with the cell density of cell B; [2]Direction of change in median value of normalised data in complete IM (cIM) when compared to CG; [3]p value shown calculated using glm function in R; [4]Direction of change in median value of normalised data in incomplete IM (iIM) when compared to cIM.

In the IM+GC cohort, complete IM was characterised by a higher level of targeting of CD4 T cells by both FOXP3 and CD8 T cells (p=1.5e-05 and p=2.6e-08, respectively). The latter also targeted more FOXP3 T cells (p=0.021) suggesting overall a highly robust T cell-T cell interactive microenvironment in the complete subtype of IM. Interestingly targeting of epithelial cells by all three T cell subsets was reduced in this IM subtype compared not only to CG (CD4 T cells p=0.00015, FOXP3 T cells p=0.002 and CD8 T cells p=0.00026) but also to incomplete IM (CD4 T cells p=3.5e-09, FOXP3 T cells p=0.0033 and CD8 T cells p=2.7e-05), suggesting potential fundamental differences in the T cell response of these three premalignant lesions.

Having determined that T cell subsets targeted relatively less the epithelium but more each other in complete IM, ROIs were visually reassessed to identify possible cell spatial patterns that could explain this. Indeed what became apparent was that lymphoid aggregates, defined as an accumulation of lymphocytes (and plasma cells) without a fully formed germinal centre, tended to form in between IM glands in complete IM, but were relatively absent in incomplete IM (Figure 6.11). Thus the numerical advantage in T cell subsets other than FOXP3 T cells in complete IM compared to incomplete IM was shared between lymphoid aggregates and direct "epithelial surveillance", resulting in reduced direct epithelial targeting by CD8 T cells but still an overall larger touch cell pair density (level of possible physical interaction) between CD8 T cells and epithelial cells in this IM subtype.

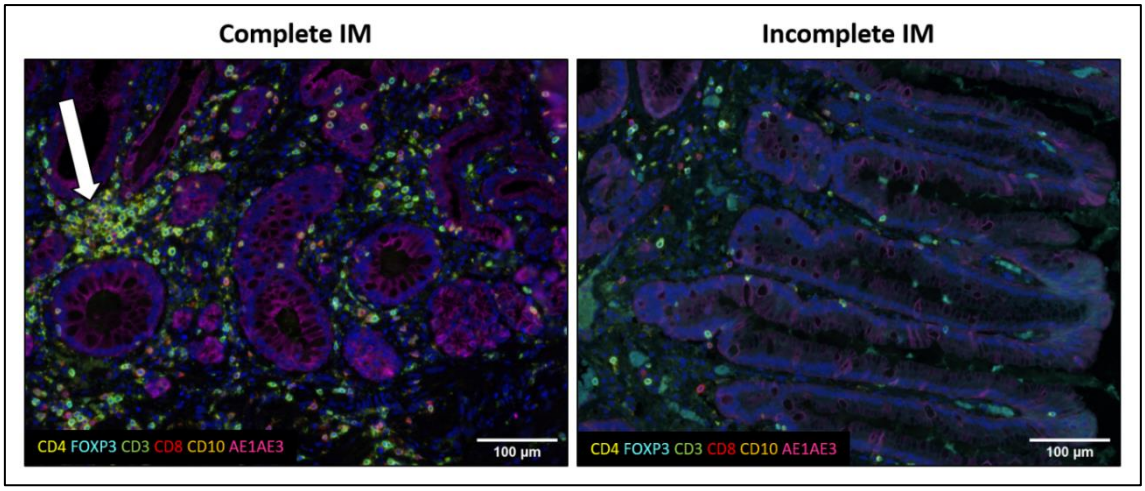


Figure 6.11 Lymphoid aggregate adjacent to complete IM glands but absent in incomplete IM
Lymphoid aggregates (white arrow) were present in complete IM and consisted mainly of CD4 T cells but were also rich in CD8 and FOXP3 T cells. Other non-CD3+ cells, possibly B cells/plasma were also present. Both images taken from samples belonging to the IM+GC cohort.

6.3.12 Investigating the relationship between T cells and macrophages

To investigate the relationship between T cells and macrophages within premalignant gastric lesions with variable risk of progression, a subset of available regions of interest from both the IM-GC and IM+GC T cell and macrophage (Chapter 5) studies were visually matched and analysed (Figure 6.12). Table 6.3 shows the clinical parameters of the patients and the details of the ROIs analysed for each tissue type.

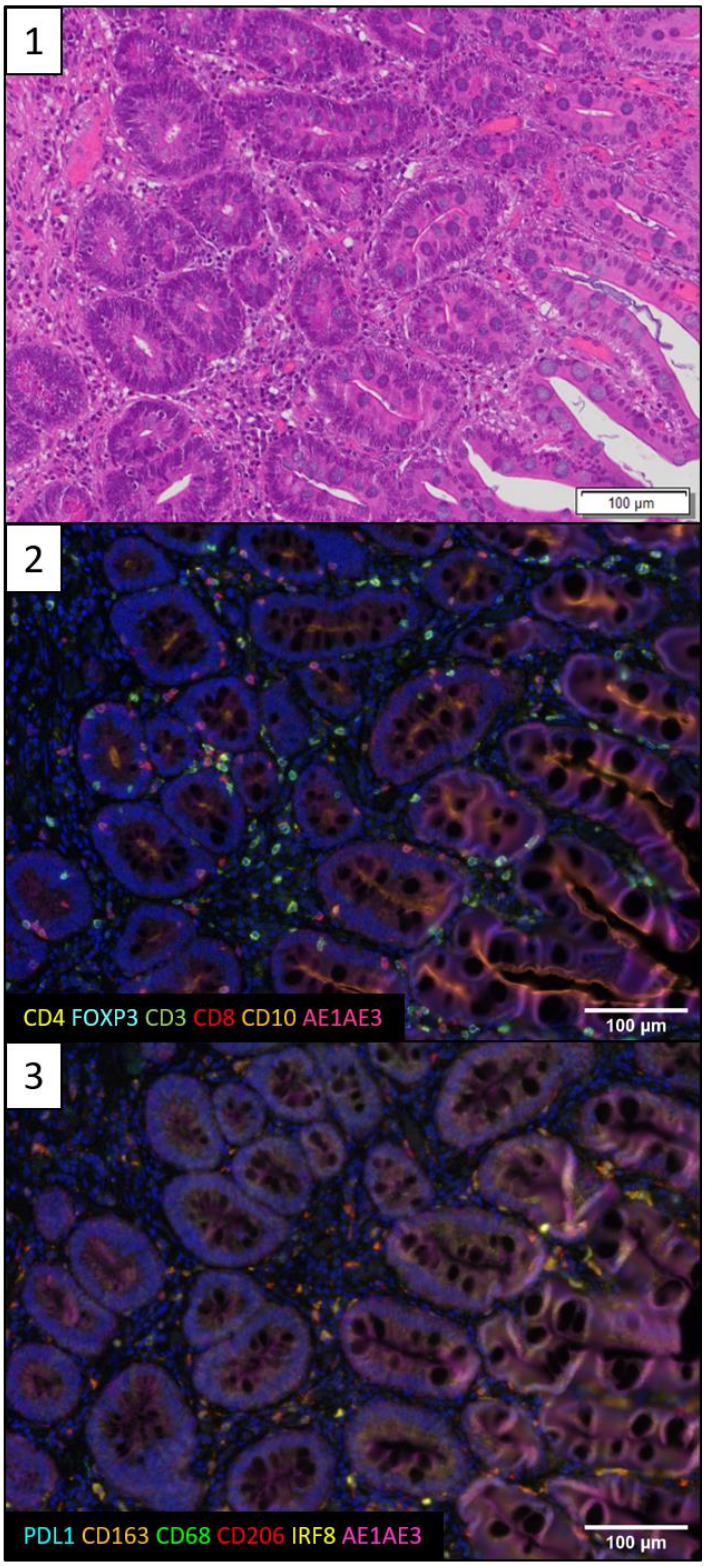


Figure 6.12 Matched regions of interest rich in intestinal metaplastic glands showing the presence of both T cells and macrophages

1) Haematoxylin and eosin stain with matched spectrally unmixed images obtained using 2) the T cell and 3) macrophage panels on tissue from a patient sample of the IM+GC cohort.

Table 6.2 Clinical parameters of patients with matched T cell and macrophage data

Parameter		IM-GC cohort	IM+GC cohort
Gender			
	Male	12	11
	Female	6	5
Age			
	Male	69 (39-86)[3]	74 (63-95)[3]
	Female	71.5 (44-79)[3]	68 (49-83)[3]
Tissue diagnosis			
	Chronic gastritis[1] (ROI)[2]	12 (36)	12 (32)
	Complete IM (ROI)[2]	10 (33)	9 (43)
	Incomplete IM (ROI)[2]	11 (36)	6 (28)

[1]Chronic gastritis tissue adjacent to IM rich areas; [2]Number of regions of interest with available data; [3]Median age value and range

Total T cell and macrophage densities were positively correlated in CG and incomplete IM in both IM-GC and IM+GC cohorts (Figure 6.13). However complete IM showed only a weak correlation in the IM-GC cohort and none in the IM+GC suggesting that tissue infiltration of T cells and macrophages was not tightly coordinated.

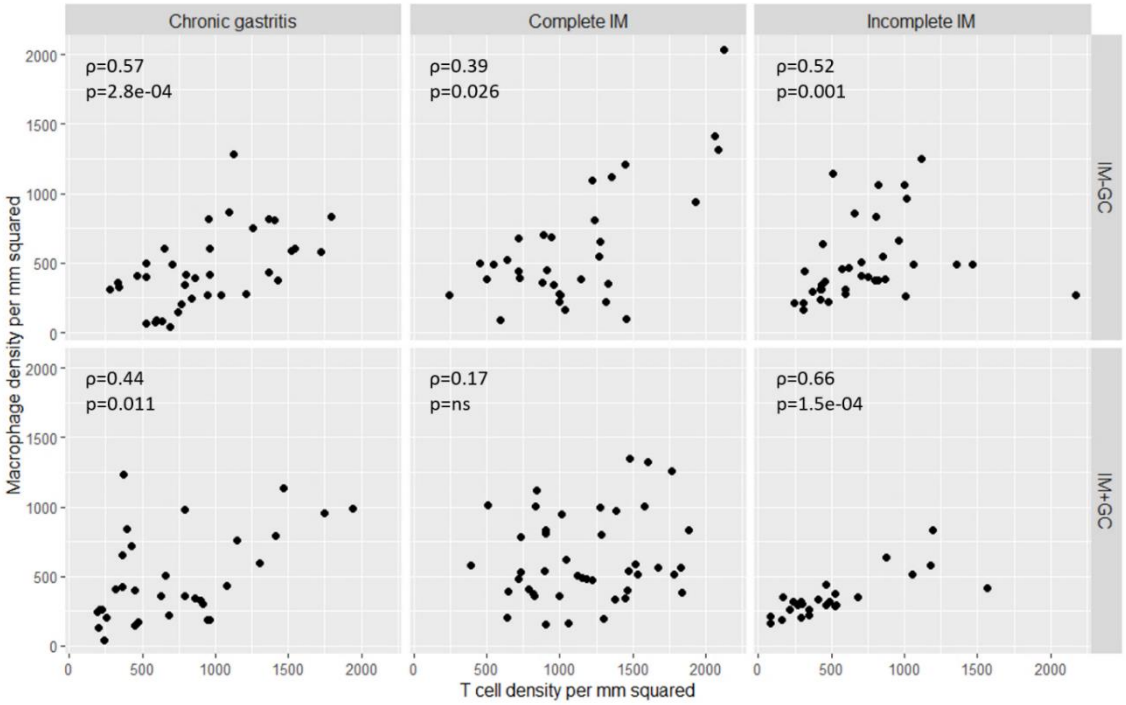


Figure 6.13 Correlation analysis between total T cell (CD3+) and macrophage (CD68+) populations in matched regions of interest of the IM-GC and IM+GC cohorts
Total T cell and macrophage densities from matched ROIs were correlated using Spearman's rank correlation. Each symbol represents data from a single ROI. Statistics done in GraphPad Prism and visualisation in R; p value <0.05 considered as significant.

6.3.13 Quantitative relationships between T cell and macrophage subsets differ by tissue type and between cohorts

Having established the overall relationship between T cells and macrophages, a correlation heatmap matrix was created using Spearman's rank correlation for each tissue type and cohort to evaluate the quantitative relationships among macrophage and T cell subsets and between these two immune cell types (Figure 6.14). Overall the pattern of correlations between subsets varied considerably across tissues and between cohorts.

In the IM-GC cohort, CG was characterised mainly by positive correlations between CD68+CD163+ and CD68+CD163+IRF8+ macrophages (ρ=0.46 with p=0.0044), between CD68+CD163+CD206+ macrophages and CD4 T cells (ρ=0.78 with p=2.7e-08) and between CD4 and CD8 T cells (ρ=0.46 with p=0.0047). A negative correlation between CD68+CD163+ macrophages and CD68+CD206+IRF8+ macrophages was also detected (ρ=-0.44 with p=0.0076).

Complete IM in the IM-GC cohort was characterised mainly by positive correlations between CD68+CD163+CD206+IRF8+ macrophages and CD68+CD163+IRF8+ macrophages (ρ=0.58 with p=4.2e-04), between CD68+CD163+CD206+ macrophages and CD8 T cells (ρ=0.56 with p=0.00067) and between CD68+IRF8+ and CD8 T cells (ρ=0.47 with p=0.0055). Negative correlations were mainly detected between CD68+CD163+IRF8+ and DN T cells (ρ=-0.45 with p=0.0087) and between CD68+CD206+IRF8+ and FOXP3 T cells (ρ=-0.54 with p=0.0011).

Incomplete IM in the IM-GC stood out compared to the two other premalignant lesions by the relatively large number of positive but also some negative correlations among macrophage and T cell subset populations. CD68+CD163+CD206+ macrophages had a positive correlation with DN T cells (ρ=0.60 with p=1.1e-04), CD68+CD163+CD206+IRF8+ macrophages had a positive correlation with both CD68+CD163+IRF8+ macrophages (ρ=0.58 with p=2.1e-04) and CD8 T cells (ρ=0.48 with p=0.0034), CD68+CD163+IRF8+ macrophages had a positive correlation with CD8 T cells (ρ=0.54 with p=0.00072) and CD68+CD206+IRF8+ macrophages had a positive correlation with CD4 (ρ=0.68 with p=4.1e-06), FOXP3 (ρ=0.66 with p=1.3e-05) and DN T cells (ρ=0.58 with p=2.3e-04). Finally CD4 T cells had a particularly strong correlation with FOXP3 T cells (ρ=0.80 with p=3.6e-09). Significant negative correlations were observed only between CD68+CD163+ macrophages and CD68+CD206+IRF8+ macrophages (ρ=-0.58 with p=2.2e-04), CD4 (ρ=-0.63 with p=4.1e-05) and FOXP3 T cells (ρ=-0.57 with p=3.1e-04).

In the IM+GC cohort, CG was characterised by an increased number of positive correlations including between CD68+CD163+ macrophages and both CD68+CD206+IRF8+ macrophages (ρ=0.61 with p=2.0e-04) and CD4 T cells (ρ=0.69 with p=1.3e-05), between CD68+CD206+IRF8+

macrophages and both CD68+IRF8+ macrophages (ρ=0.53 with p=0.0019) and CD4 T cells (ρ=0.47 with p=0.0067), between CD68+CD163+CD206+IRF8+ macrophages and FOXP3 T cells (ρ=0.55 with p=0.0011), and between CD8 T cells and both CD4 (ρ=0.66 with p=4.2e-05) and FOXP3 T cells (ρ=0.46 with p=0.0082).

Complete IM was again characterised by a mixture of positive and negative correlative subset relationships, with a positive correlation between CD68+CD163+ macrophages and CD4 T cells (ρ=0.47 with p=0.0015), between CD68+CD163+IRF8+ macrophages and both CD68+CD163+CD206+ (ρ=0.40 with p=0.0077) and CD68+CD163+CD206+IRF8+ (ρ=0.71 with p=1.1e-07) macrophages, between CD68+CD206+IRF8+ and CD68+IRF8+ macrophages (ρ=0.39 with p=0.0094), and between FOXP3 T cells and both CD4 (ρ=0.45 with p=0.0027) and CD8 (ρ=0.42 with p=0.0053) T cells. Negative correlations were detected mainly between CD68+CD163+ macrophages and both CD68+CD163+CD206+IRF8+ (ρ=-0.58 with p=4.7e-05) and CD68+CD163+IRF8+ (ρ=-0.41 with p=0.0057) macrophages.

As before, incomplete IM in the IM+GC cohort stood out by its large number of highly positive correlations between the majority of pairs of T cell subsets as well as between macrophage and T cell subsets. More specifically, a positive correlation was observed between CD68+CD163+ macrophages and CD68+CD163+CD206+IRF8+ macrophages (ρ=0.52 with p=0.0042), CD4 (ρ=0.53 with p=0.0036) and DN (ρ=0.52 with p=0.0049) T cells, between CD68+CD163+CD206+IRF8+ macrophages and CD4 T cells (ρ=0.60 with p=0.00072), between CD68+IRF8+ macrophages and DN T cells (ρ=0.53 with p=0.0034), between DN T cells and CD4 (ρ=0.80 with p=2.8e-07), FOXP3 (ρ=0.60 with p=0.00079) and CD8 (ρ=0.60 with p=0.00074) T cells and between CD8 T cells and both CD4 (ρ=0.67 with p=1.0e-04) and FOXP3 (ρ=0.62 with p=4.8e-04) T cells. A single negative correlation was observed between CD68+CD163+ and CD68+CD163+CD206+ macrophages (ρ=-057. with p=0.0017).

Overall macrophage and T cell subsets were mostly positively correlated in CG and incomplete IM tissues in both the IM-GC and IM+GC cohorts, whereas a mixture of positive and negative correlations were observed in complete IM, irrespective of cohort. These patterns were in line with the correlation values observed by comparing total T cell and macrophages populations. Incomplete IM seemed to have the most “organised” and complete IM the most “disorganised” T cell-macrophage immune landscape based on overall correlation patterns. Also incomplete IM was characterised by particularly strong positive correlations between T cell subset pairs.

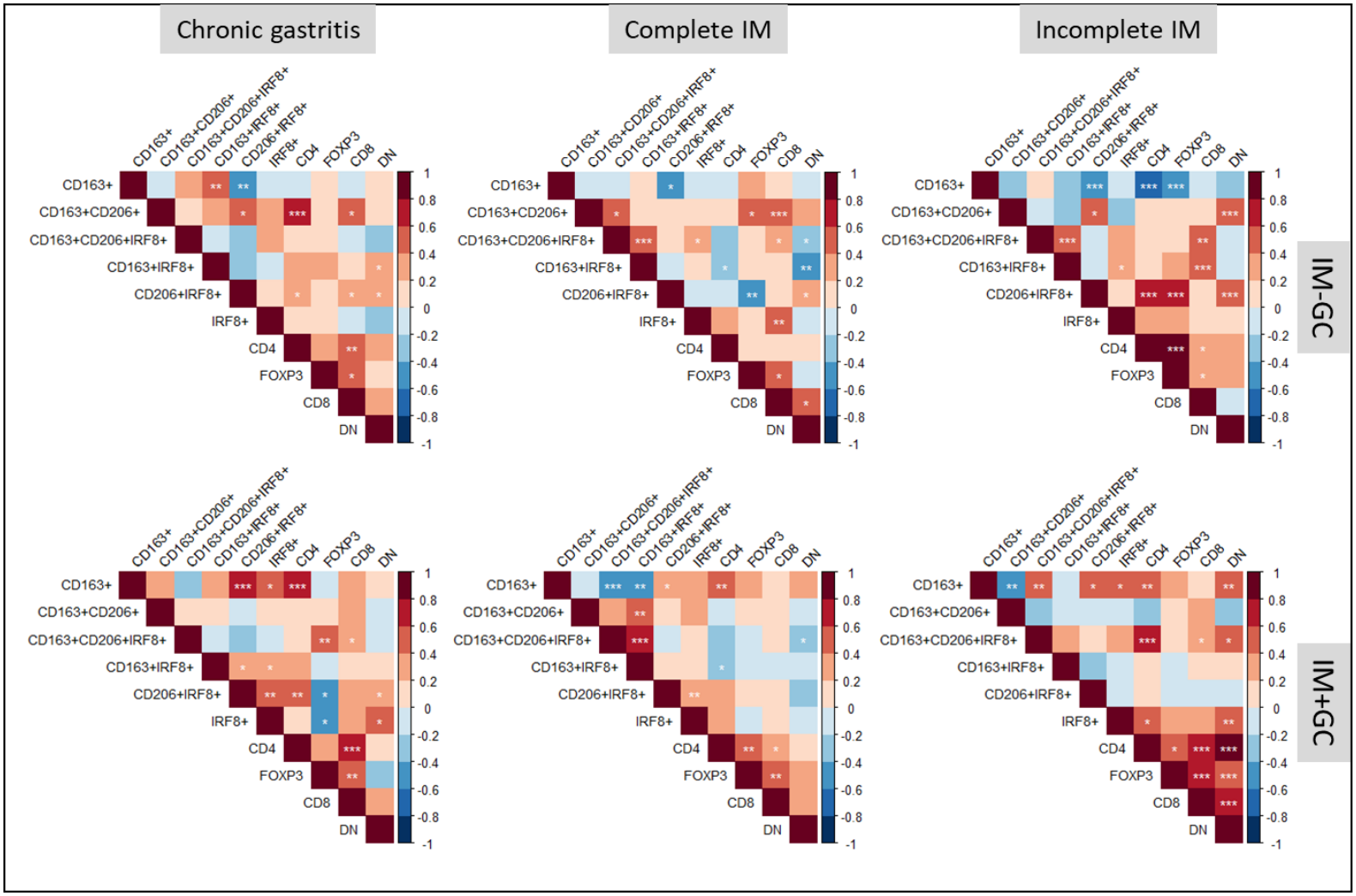


Figure 6.14 Quantitative relationships between T cell (CD3+) and macrophage (CD68+) subsets shown using correlation heatmaps in the IM-GC and IM+GC cohorts

Correlation heatmap matrices of T cell and macrophage subset densities from matched ROIs using Spearman's rank correlation. .*, **, *** is equal to $p<0.05$, $p<0.01$ and $p<0.001$.

6.3.14 Integrating the spatial relationships of T cells, macrophage and epithelial cells

Key aspects of macrophage and T cell function such as phagocytosis, antigen presentation, cytotoxic killing of a diseased cell depend on physical interaction between cells pairs. To obtain insight into the targeted spatial relationships between pairs of T cells, macrophages and epithelial cells, a correlation network was created using normalised touch cell pair density data between the most abundant T cell subsets (CD4, CD8 and FOXP3 T cells), the most consistent macrophage subsets (CD68+CD163+CD206+ and CD68+CD163+CD206+IRF8+) and the epithelial cells for all tissue types and cohorts studied (§5.3.13, §6.3.11, Figure 6.15). By placing highly correlated touch cell pairs closer together, the proximity of the points being determined using multidimensional clustering (corrr package in R) and joining them with stronger paths using colour coding to describe the sign (direction) of the correlation, it was possible to visually discover which touching cell pairs are more or less closely associated with one another.

In the CG and incomplete IM samples of the IM-GC cohort, epithelial//T cell touch pairs, including all three CD4, CD8 and FOXP3 T cell subsets, clustered closely together whereas in complete IM the epithelial cell//FOXP3 T cell touch pair was absent from this cluster. Negatively correlated with this cluster group was another cluster group composed of T cell-T cell touch pairs (CD4//FOXP3, CD4//CD8 and FOXP3//CD8), particularly in incomplete IM. This T cell-T cell pair cluster was more loosely present in the complete subtype of IM suggesting potential fundamental differences in the immune landscape away from the epithelium between IM subtypes in a non-cancer setting. Finally epithelial//macrophage touch pairs including both CD68+CD163+CD206+ and CD68+CD163+CD206+IRF8+ macrophages tended to cluster together across tissue types in this cohort.

In the CG and complete IM samples of the IM+GC cohort, the epithelial//T cell touch pair cluster did not contain the epithelial//FOXP3 T cell touch pair. In both tissue types, it was replaced by the epithelial//CD68+CD163+CD206+IRF8+ macrophage touch pair. However in complete IM additional tight clustering with the epithelial//CD68+CD163+CD206+ macrophage touch pair suggested that the vicinity of the epithelium in this tissue type is rich not only in T cell associated activity but also concurrent macrophage activity. The epithelial//CD68+CD163+CD206+ touch pair also clustered closely with the epithelial//T cell cluster in incomplete IM. Finally the T cell-T cell touch pair cluster was again negatively correlated with the epithelial//T cell touch pair cluster in incomplete IM whereas this was less so in CG and complete IM.

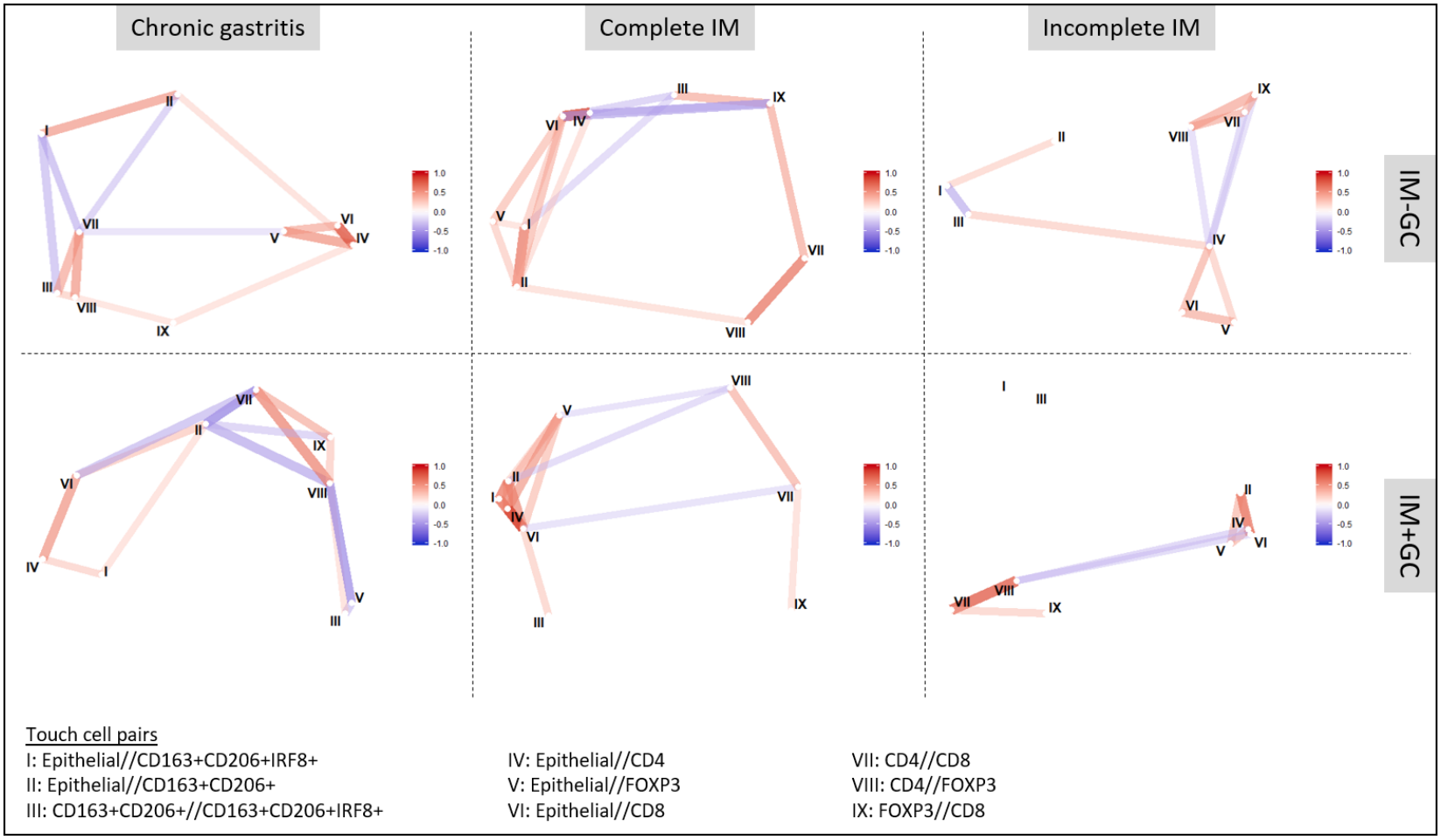


Figure 6.15 Correlation networks of normalised touch cell pair densities in IM-GC and IM+GC cohorts show changing landscape of T cell and macrophage interaction and their relationship with the epithelium

Correlation networks based on normalised touch cell pair densities of T cells, macrophages and epithelial cells. More highly correlated touch cell pairs appear closer together and are joined by stronger paths. Paths are also coloured by their sign (red for positive and blue for negative). The proximity of the points are determined using multidimensional clustering (corrr package in R). Correlations with $-0.3<\rho<0.3$ not plotted.

Overall the three types of tissues investigated showed similarities, but also some differences. All three tissues contained an epithelial cell//T cell touch pair and a separate T cell-T cell touch pair cluster which were mostly negatively correlated with each other. Incomplete IM showed the greatest level of polarisation with T cell-T cell activity occurring clearly away from epithelial-T cell activity. Temporal progression from the IM-GC to the IM+GC cohort was characterised by the introduction of macrophages in the epithelial-T cell touch pair cluster, first of the epithelial// CD68+CD163+CD206+IRF8+ touch pair and then by the epithelial// CD68+CD163CD206+ touch pair, suggesting a significant shift in the immune landscape immediately adjacent to the epithelium.

6.3.15 T cell profiling of Progressor patient P1 shows increased FOXP3 T cell density associated with progression to high grade dysplasia

To address the possible role of T cells in progression to high grade dysplasia, the OPAL™ IHC T cell panel was used on serial sections of those used to characterise the macrophage landscape in the two case studies of the Progressors cohort (Table 5.1, §5.3.14, Appendices H and I). Particular emphasis was given on characterising the CD8 and FOXP3 T cell subsets as these have previously been suggested to play key roles in GC [258, 499].

T cell density was analysed first by pooling all same tissue type data together and then individually per site and time point (Figure 6.16). Pooled T cell density showed a significant decrease in incomplete IM, similarly seen in the main part of the OPAL T cell study, but no significant change in HGD (Figure 6.16a). In more detail, IM samples tended to have similar T cell densities as the adjacent CG except at anatomical sites A2 (Transition zone) and A4 (Lesser curve) (both time point t1) where complete and incomplete IM had significantly lower T cell content respectively (Figure 6.16b). HGD showed an increased trend with temporal progression (t3 vs t2) but it did not reach significance.

Pooled FOXP3 T cell density showed a significant increase in HGD compared to all three other tissue types (Figure 6.16c). As before there was no separation between CG, complete and incomplete IM. Interestingly HGD in t3 had a significantly higher FOXP3 T cell density compared to adjacent CG and showed an increasing trend compared to HGD in t2 (Figure 6.16d). When comparing tissues of different sites in t1, complete IM had a higher FOXP3 T cell density in A3 than in A2 and CG had a higher FOXP3 T cell density in A4 than in A2.

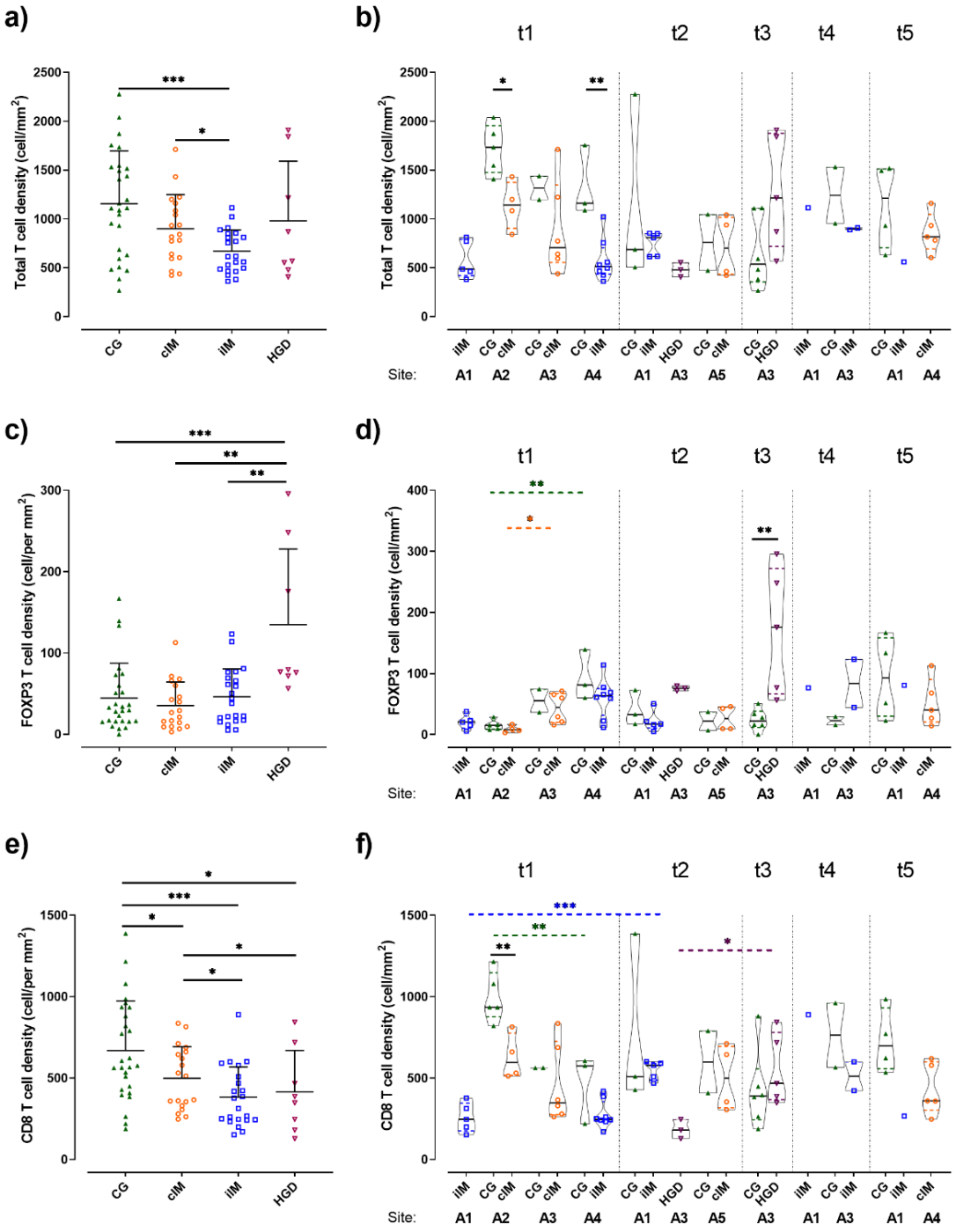


Figure 6.16 Pooled and single site/time point T cell subset density in patient P1

a) Pooled and b) individual total T cell density by sample, c) pooled and d) individual FOXP3 T cell density by sample and e) pooled and f) individual CD8 T cell density by sample. Each symbol represents data from a single ROI. For pooled data mean +S.D. shown with glm function in R used to calculate significance and for individual samples, quartiles shown with t-test and Mann Whitney test used to calculate significance (minimum of 3 ROIs). *, **, *** is equal to $p<0.05$, $p<0.01$ and $p<0.001$.

For b), d) and f) coloured dashed lines show significant same tissue differences by site (green for CG, orange for complete IM, blue for incomplete IM). Black lines show significant differences between matched CG and adjacent IM/HGD lesion.

Pooled CD8 T cell density showed a stepwise decrease from CG to complete IM and then to incomplete IM (Figure 6.16e). HGD was characterised by similar levels to incomplete IM and had lower CD8 T cell density than CG and complete IM. With the lowest density across all sites and time points, HGD in t2 had significantly fewer CD8 T cells than HGD at t3 with median values for t2 HGD equal to 181 CD8 T cells/mm^2 and for t3 HGD equal to 468 CD8 T cells/mm^2 (Figure 6.16f). When comparing matched samples, complete IM in A2 had fewer CD8 T cells than surrounding CG in t1, the latter having also a greater density than CG in A4. Interestingly incomplete IM showed a highly significant increase across time (t1 vs t2) in site A1.

Overall this part of the study showed that HGD at an early time point in patient 1 had a low CD8 T cell density which increased progressively with time and the same trend was observed in FOXP3 content suggesting that latter HGD was characterised by a highly active but also immuno-regulated T cell landscape (Figure 6.17a). Multi-site and multi-time point analysis showed that FOXP3 and CD8 T cell densities varied significantly a) between matched CG adjacent to IM/dysplasia, b) between the same tissue type across space from one site to another and c) across time in the same site and tissue subtype suggesting an overall highly dynamic flux of localised T cell trafficking.

To gain insight into the spatial effect of the increased FOXP3 T cell infiltration in the HGD sample in site A3 at time point t3, nearest neighbour analysis was carried out (§2.5.5) with adjacent CG as control tissue (Figure 6.17b). This sample was particularly valuable for further analysis as there were no contaminating IM glands in between the HGD glands and gastric glands in areas with CG were clearly separate away from the HGD glands. For both CG and HGD tissue the spatial relationship of FOXP3 and CD8 T cells with neighbouring epithelial cells was relatively similar (median values from FOXP3/CD8 T cells to nearest epithelial cell in CG: 21.7µm/8.5µm and in HGD: 15.3µm/11.5µm respectively) (Figure 6.17b). Also very similar were the spatial relationships of FOXP3 and CD8 T cells with neighbouring CD8 T cells (median values from FOXP3/CD8 T cells to nearest CD8 T cell in CG: 16.2µm/8.1µm and in HGD: 13.5µm/7.8µm respectively). However the median distance between CD8 T cells and neighbouring FOXP3 T cells differed greatly in HGD compared to CG: 28.6µm vs 90.3µm. Calculating the percentage of CD8 T cells with a neighbouring FOXP3 T cell within a range of 10-40µm further confirmed this difference between HGD and CG. In fact 66.2% of CD8 T cells in HGD had a neighbouring FOXP3 T cell within a distance of 40µm, whereas only 15.2% of CD8 T cells in CG had a neighbouring FOXP3 T cell within the same distance (Figure 6.17c and Figure 6.18).

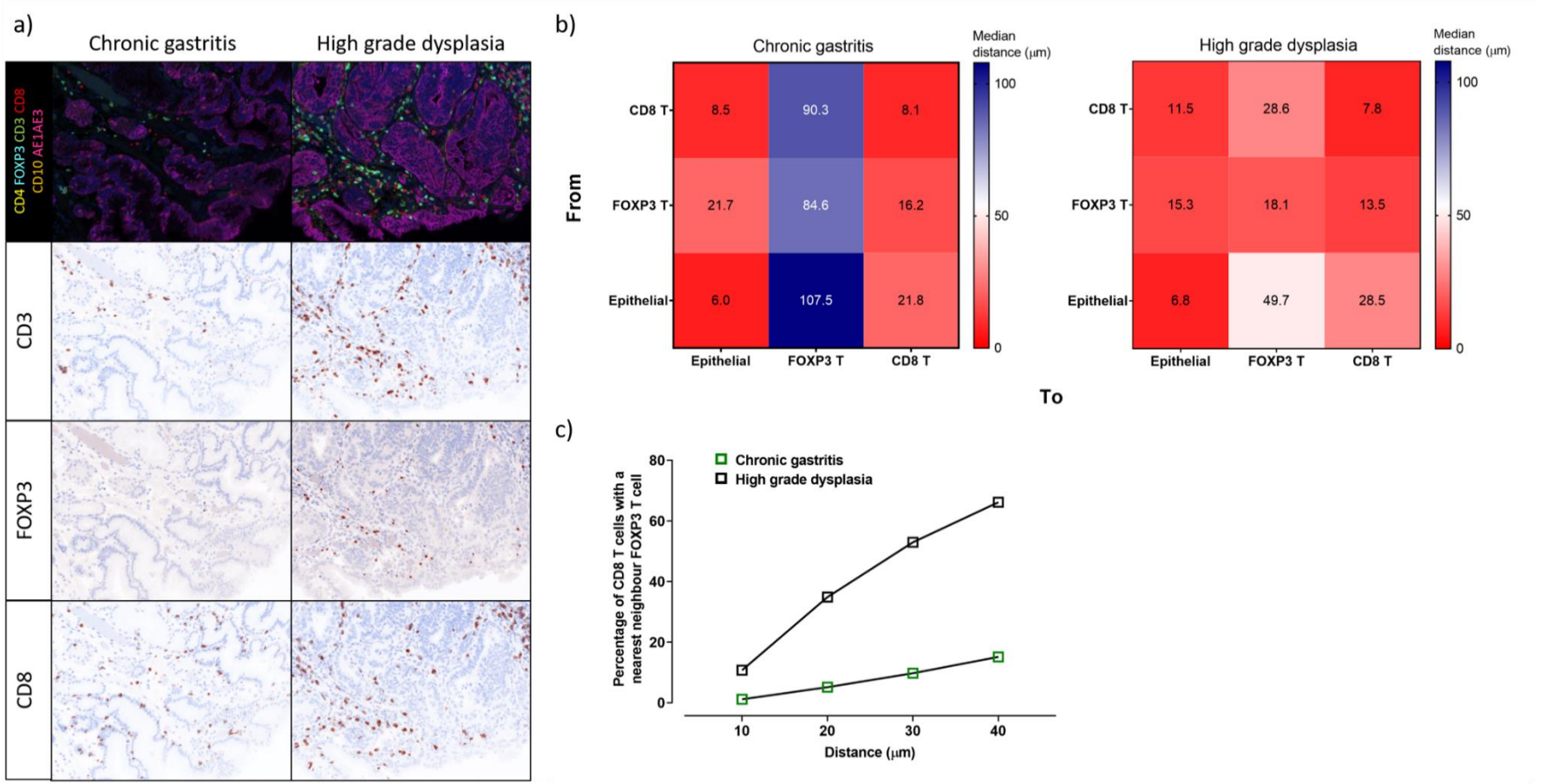


Figure 6.17 T cell infiltration in high grade dysplasia and adjacent chronic gastritis in patient P1 at time point t3 including nearest neighbour spatial analysis

a) Spectrally unmixed composite together with pseudo-pathology images (inForm software) CD3, FOXP3 and CD8 markers from high grade dysplasia and adjacent chronic gastritic tissue, b) Heatmaps showing median distance of nearest neighbouring cells (From cell A To cell B) in HGD and adjacent CG and c) Percentage of CD8 T cells with a nearest neighbour FOXP3 T cell at a distance of 10μm, 20μm, 30μm and 40μm in HGD and adjacent CG. Phenoptr and phenoptrReports in R used to calculate all intercellular distances.

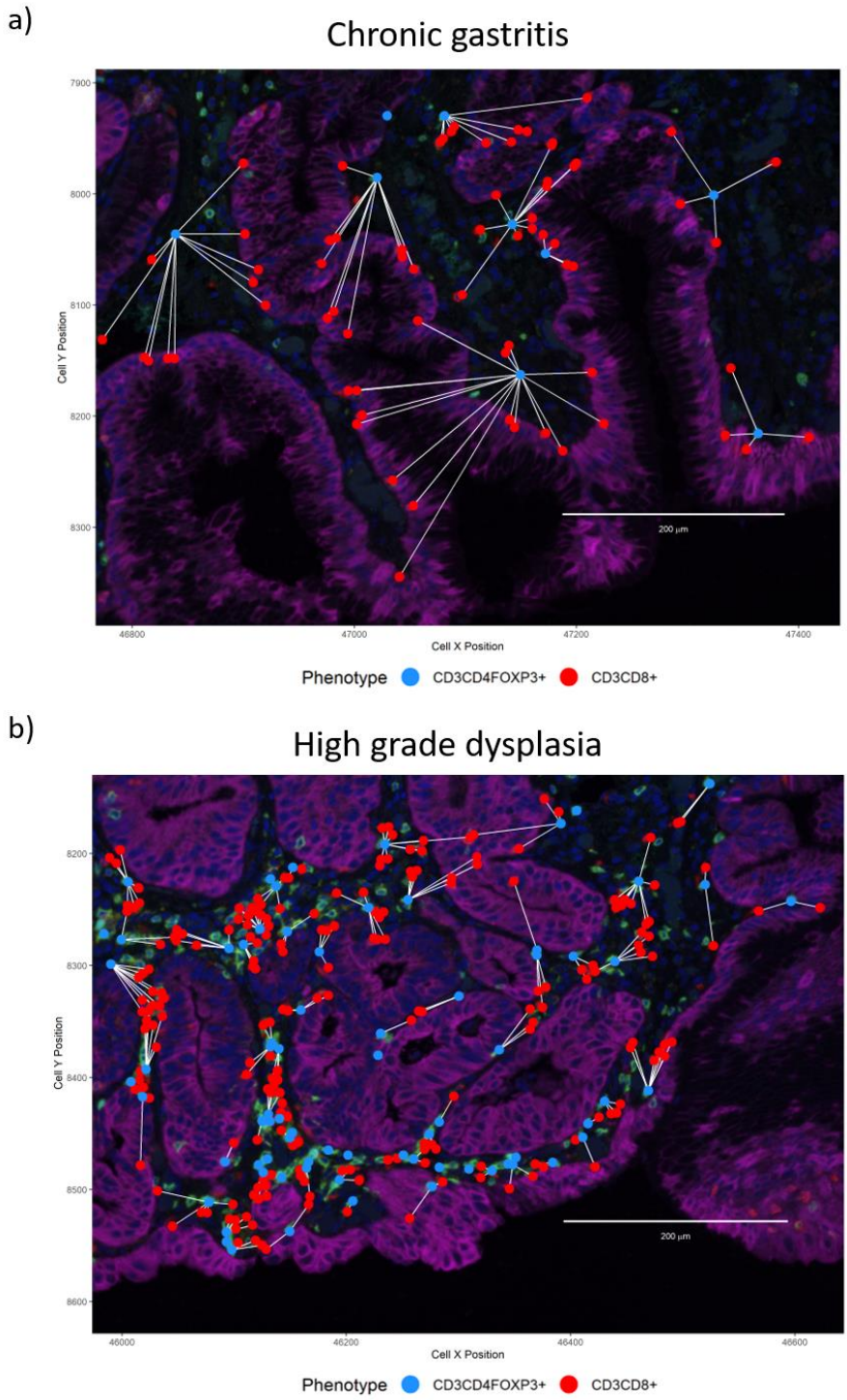


Figure 6.18 Multiplexed images showing the distance (length of intercellular lines) between each CD8 T cell and its nearest FOXP3 T cell in high grade dysplasia and adjacent chronic gastritis in patient P1 in site A3 at time point t3

a) Chronic gastritis and b) High grade dysplasia. The large influx of FOXP3 T cells in HGD results in much shorter distances between CD8 T cells (red) and neighbouring FOXP3 T cells (blue), represented by white lines connecting red and blue dots. Analysis done and images created using phenoptr and phenoptrReports packages in R. X and Y coordinates of region of interest on slide shown. Scale bar: 200µm.

Overall nearest neighbour analysis showed that the median distance from CD8 T cells to FOXP3 T cells in HGD was greatly reduced and that roughly two thirds of CD8 T cells had a neighbouring FOXP3 T cell within their functional space of 40µm suggesting that FOXP3 T cell mediated immune-regulation may play an important role in progression to gastric cancer. However given that whole exome sequencing of adjacent snap frozen tissue with HGD did not show major genomic alterations between t2 and t3 (Appendix I), it suggests that the observed changes to the T cell landscape in the HGD microenvironment are not likely associated with specific genomic events in the HGD glands.

6.3.16 T cell profile in patient P2 shows only minor differences

To establish the possible evolutionary trajectory of the T cell landscape between incomplete IM and HGD, a second patient with multi-site and multi-time point premalignant tissue available including LGD was characterised as before with the OPAL™ T cell panel. Unfortunately the anti-FOXP3 staining on the HGD tissue failed and no data for this marker was available from this sample.

Pooled total T cell, FOXP3 and CD8 T cell density did not show a significant difference between CG, incomplete IM and dysplasia (LGD+HGD) nor with HGD on its own (Figure 6.19). Single sample analysis showed total T cell content in incomplete IM varied by time point in A1 (t2 vs t3, lower in the latter), FOXP3 T cell content was greater in incomplete IM compared to adjacent CG in site A3 at t4 and CD8 T cell content was lower in incomplete IM compared to adjacent CG in site A1 at t3.

Overall this patient's T cell profile with respect to total T cell content, FOXP3 and CD8 T cells did not show any significant differences between all tissue types investigated. Also only a small number of site and time point variations were observed suggesting that the T cell landscape in this patient was relatively homogenous with few changes along histological progression. This is particularly interesting given that the HGD lesion sequenced from adjacent snap frozen tissue at time point t2 showed a large number of chromosomal aberrations (Appendix J) and that it is unlikely that all other FFPE tissues characterised in this case study would have similar genomic profiles. This would suggest that in this patient the genomic profile of the high grade dysplastic glands does not necessarily play a major role in the formation of the local T cell landscape.

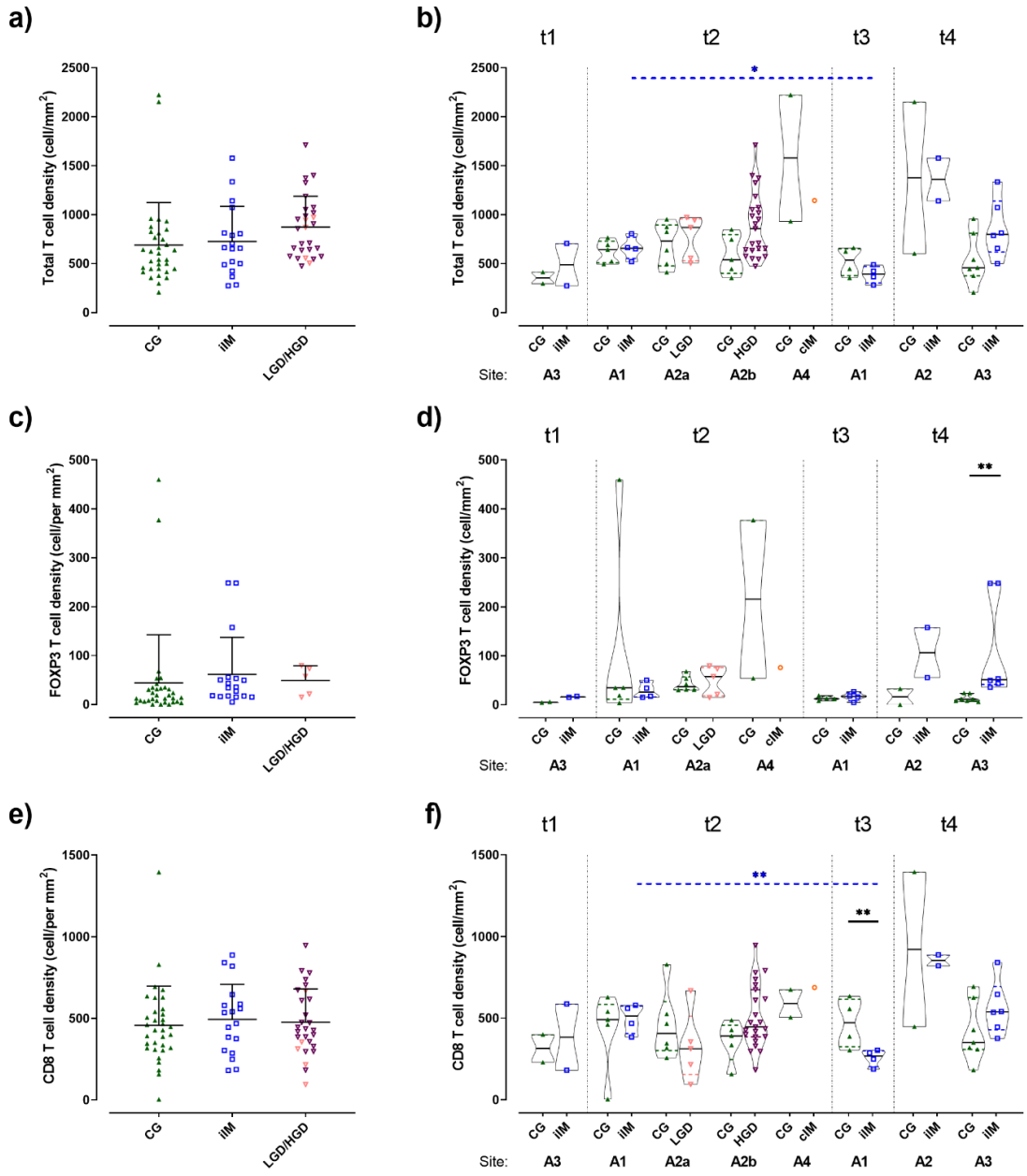


Figure 6.19 Pooled and single site/time point T cell subset density in patient P2

a) Pooled and b) individual total T cell density by sample, c) pooled and d) individual FOXP3 T cell density by sample and e) pooled and f) individual CD8 T cell density by sample. Each symbol represents data from a single ROI. For pooled data mean +S.D. shown with glm function in R used to calculate significance and for individual samples, quartiles shown with t-test and Mann Whitney test used to calculate significance (minimum of 3 ROIs). *, **, *** is equal to $p<0.05$, $p<0.01$ and $p<0.001$.

For b), d) and f) coloured dashed lines show significant same tissue differences by site (blue for incomplete IM). Black lines show significant differences between matched CG and adjacent IM/HGD lesion.

6.4. Summary and discussion

The following is a summary of the main outcomes of this study:

1. Gastric premalignant lesions contained four main T cell subsets, namely CD3+CD4+ (CD4 T cells), CD3+CD4+FOXP3+ (FOXP3 T cells), CD3+CD8+ (CD8 T cells) and CD3+CD4-CD8- (DN T cells).
2. Complete intestinal metaplasia was particularly rich in CD4 and DN T cells whereas the incomplete subtype was particularly poor in CD8 and DN T cells.
3. Chronic gastritis adjacent to intestinal metaplasia subtypes shared similar T cell profiles.
4. Spatial location analysis showed that complete intestinal metaplasia was rich in T cell pairs in close proximity as seen in lymphoid aggregates as well as in T cells in the vicinity of the epithelium; by contrast incomplete IM was characterised by a reduced T cell presence adjacent to epithelial cells but a greater level of individual CD8 T cells targeting the epithelium.
5. T cell and macrophage populations showed mainly positive correlations in chronic gastritis and in incomplete intestinal metaplasia but less so in complete intestinal metaplasia.
6. Correlation network analysis of normalised touch cell pair densities showed clustering of T cell subsets with epithelial cells, clustering of T cell subsets away from the epithelium and increasing presence of macrophages in the former cluster with temporal progression from IM-GC to IM+GC patients.
7. In one out of two multi-site and –time point case studies that had progressed to high grade dysplasia, a particularly large influx of FOXP3 T cells was detected with almost 66% of CD8 T cells having a neighbouring FOXP3 T cell within a distance of 40µm.

6.4.1 Discussion

The objective of this study was to characterise the T cell landscape in intestinal metaplasia and its possible role in progression. To achieve this, biopsy and gastrectomy tissue samples enriched for IM were selected from IM-GC and IM+GC cohorts. A third cohort of patients with progressive disease with multi-site and multi-time point samples were also used. These cohorts of patients were used to create a histo-temporal model of progression that could be used to identify step wise changes in T cell content. Using an optimised panel with key T cell markers on the OPAL™ platform, followed by digitalisation and then analysis with inForm, four main T cell subsets were identified. Additionally each cell within a region of interest was segmented and identified with

unique two dimensional attributes within a matrix that allowed cellular spatial location analysis using R.

The four T cell subsets detected across all tissue types investigated were defined as CD4, CD8, FOXP3 and DN (double negative) T cells based on the presence or absence of co-localised markers. It was not possible to define these T cell subsets in more detail because the T cell markers used were not absolute in their ability to specify cell type. “Conventional” helper T cells and cytotoxic T cells express CD4 and CD8 respectively. However mucosa-associated invariant T cells (MAIT) and γδ T cells can also express CD4 and CD8, and both have been shown to be enriched in the gut [500, 501]. Indeed CD8+ and also CD4-CD8- (double negative) MAIT cells as well as γδ T cells have been shown to be present in human gastric tissue infected by *H. pylori* [502, 503] and may have opposing roles, the former increasing immunopathology and the latter being more protective [470, 504]. Also although the majority of FOXP3+ T cells are αβ regulatory T cells (αβ Tregs), FOXP3+ γδ regulatory T cells (γδ Tregs) have also been described [505]. These γδ Tregs were shown to suppress proliferation of anti-CD3/anti-CD28 stimulated peripheral blood mononuclear cells and likely have a similar function as αβ Tregs. Even though the T cell markers used in this current study cannot be used to separate conventional and innate like T cell populations in absolute terms, they do likely mirror functionally similar T cell subsets within the tissues investigated.

In both IM-GC and IM+GC patients, complete IM was characterised by a T cell rich microenvironment which was reflected spatially in high levels of close proximity T cell-T cell pairs as described by the formation of lymphoid aggregates as well as T cell-epithelial cell pairs. By contrast the microenvironment in incomplete IM was particularly poor in CD8 and DN T cells, and was characterised by overall lower numbers of T cell-T cell pairs in close proximity as well as T cell-epithelial cell pairs. Thus this subtype of IM was shown to potentially have not only lower T cell-T cell immunity by quantitative and spatial analysis but also lower levels of T cell-epithelial cell immunity. T cells that express CD8 as well as T cells that are negative for both CD4 and CD8 have been shown to have cytotoxic capacity [502, 506-508] thus the ability to efficiently and effectively eliminate early abnormal cells within incomplete IM glands is likely compromised. Although the setting may differ, patients with overall T cell rich tumours have been associated with better prognosis [264], including CD4+ and CD8+ cells in GC [267]. It is possible that the complete and the incomplete subtype of IM share certain similarities with gastric tumours which are relatively rich and poor in T cell content with regards to outcome. High levels of T cell immunity in complete IM may provide protection against progression, similar

to patients with T cell rich gastric tumours where an effective T cell response provides protection against tumour growth and metastasis by eliminating efficiently tumour cells. By contrast, incomplete IM likely suffers from reduced immune-surveillance that results in a greater risk of progression to dysplasia through "immune escape" (Figure 6.20) similar to patients with T cell poor gastric tumours that suffer from greater tumour growth, metastasis and ultimately death due to an inability to effectively and efficiently remove tumour cells (loss of maintenance of "cancer-immune equilibrium" as described in [509]. Interestingly CD8 T cells in incomplete IM were shown to target individually the epithelium more than in complete IM but their overall lower numbers resulted in a reduced presence in the vicinity of epithelial cells which suggests a potentially suboptimal T cell immune response.

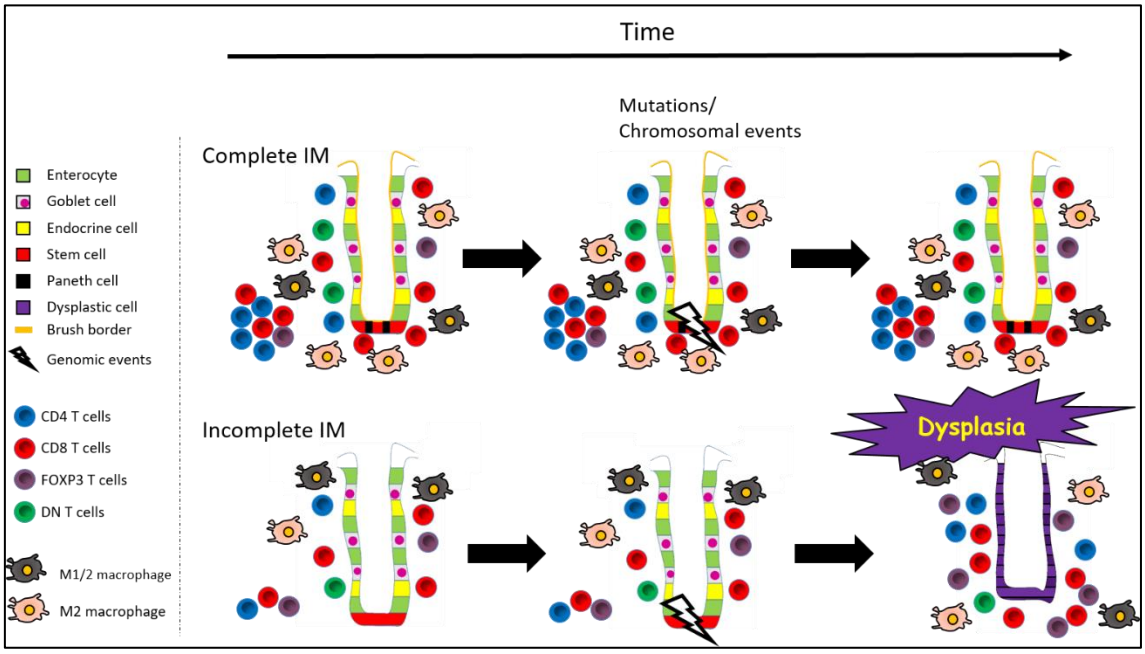


Figure 6.20 How reduced immune-surveillance in incomplete intestinal metaplasia may lead to dysplasia

The immune microenvironment in incomplete intestinal metaplasia (IM) is characterised by low numbers of macrophages and T cells. With time, genomic events such as mutations and chromosomal copy number changes occur in the stem cell compartment of IM glands leading to the formation of early abnormal cells [127]. In complete IM the robust presence of T cells and macrophages, particularly M2 macrophages, results in the rapid and efficient elimination of these early abnormal cells, mainly through cytotoxic activity of CD8 and DN T cells. In incomplete IM the lower levels of CD8 and DN T cells together with a predominant M1/2 macrophage presence results in a suboptimal capacity to eliminate early abnormal cells and ultimately leads to dysplasia which is associated with a greater risk of progression to gastric cancer.

Interestingly the relatively constant levels of FOXP3 T cells, a lineage specific transcription factor in regulatory T cells [270, 510] suggest that immune-regulation in IM subtypes with differing progression risk does not play a major role in this event. This is in contrast to GC and other types of cancer which have mainly shown a negative association with outcome in patients with high

levels of regulatory T cells [267, 269, 499]. However a recent study by Wang et al 2020 [258] did actually show improved patient survival in GC patients with high levels of FOXP3+ T cells.

The strength of this current study lies not only in its simultaneous use of multiple markers to quantify T cells subsets in IM tissues but also in its use of spatial metrics to define levels of possible paracrine and physical interaction between both T cell pairs and T cell-epithelial cell pairs. An intercellular distance of 40µm was chosen to represent the maximum effective range of cytokine penetration from a producing cell to a target cell based on previous work done by Thurley et al 2015 [392] and Oyler-Yaniv et al 2017 [393]. Previously Feng et al 2017 [394] investigated the spatial relationship between FOXP3 and CD8 T cells in HPV^- oral squamous cell cancer at 20µm, 30µm and 45µm and identified a significant relationship with reduced overall survival, which was well within the cytokine range of 30-150µm shown by Oyler-Yaniv et al 2017 [393]. However the exact intercellular distance is unlikely to be an absolute factor as cytokine diffusion and consumption as well as consumption cell cytokine receptor density are affected by the local niche cell density and the consumption cell activation state but relative quantitative differences between tissue types contain most likely vital information regarding physical/paracrine levels of cell-cell interaction. As multiple T cell functions such as activation, regulation and cytotoxic activity are also dependent on physical interaction, the exact levels of physically adjacent T cell pairs and T cell-epithelial pairs were also calculated based on 2D attributes and morphology within a region of interest.

Both types of spatial cellular analysis showed overall levels of T cell proximal interactivity reflected T cell density within a tissue type. However single cell analysis showed that CD4, FOXP3 and CD8 T cells targeted the epithelium significantly more in incomplete IM than in complete IM. The latter was richer in inter-glandular lymphoid aggregates whereas the former was characterised more by single T cells roaming the inter-glandular spaces. These lymphoid aggregates were quite different than the tertiary lymphoid structures which occur in the gastric *lamina propria* following *H.* pylori infection and have segregated T cell and B cell compartments [511, 512], as they were mainly composed of T cells and only a small number of other types of cells. This specific difference in T cell localisation between IM subtypes requires further investigation in order to fully comprehend its potential role with respect to progression risk.

Macrophages have been shown to have the ability to influence the type of T cell response that occurs in CG following *H. pylori* infection through the release of BAFF driving a Th17 response [201]. However the current study is the first so far to investigate the relationship between macrophages and T cells in IM. Total T cell and macrophage density were positively correlated

in both CG and incomplete IM but less so in complete IM suggesting important differences in the relationship between these two immune cell types within these tissue types. T cell and macrophage subsets had mostly positive correlations although complete IM in the IM-GC cohort showed a negative correlations both between CD68+CD163+IRF8+ macrophages and DN T cells and between CD68+CD206+IRF8+ macrophages and FOXP3 T cells. Among same immune cell comparisons incomplete IM in IM+GC patients stood out by having positive correlations across all T cell subsets suggesting the presence of a highly coordinated T cell immune response.

Correlation network analysis of normalised touch cell pair data confirmed the heterogeneous relationship between T cells and macrophages in gastric premalignant lesions and showed two clear patterns: 1) CD4, CD8 and FOXP3 T cells located physically adjacent to epithelial cells clustered away from T cell-T cell touch cell pairs with incomplete IM being the most polarised tissue type and 2) progression from IM-GC to IM+GC was accompanied with the introduction of epithelial cell-macrophage touch cell pairs clustering together with epithelial cell-T cell touch cell pairs suggesting that in this latter cohort, T cells interacting with epithelial cells, possibly through the epithelial basal membrane, are more exposed to macrophages and their associated chemokines/cytokines. Given the key role of macrophages as antigen presentation cells and potential drivers of inflammation within the context of *H. pylori* infection [204], it is difficult to comment on why their presence would be associated with the temporally most advanced IM tissues. However it is possible that the M2 CD68+CD163+CD206+ macrophages located directly adjacent to the epithelium are actually suppressing or preventing cytotoxic T cell activity. Such macrophage activity on CD8+ T cells has been previously described in a mouse model of lung squamous cell carcinoma [513].

In an attempt to gain greater insight into how T cell content varies between stomach sites and between points in time, two Progressors patients with available multi-site/time point samples were used as case studies. These two cases were also used to characterise the evolution of the T cell landscape from IM to HGD and to determine whether genomic changes are reflected in changes of the local T cell content. Overall contrasting findings were obtained from patents P1 and P2. In the former T cell populations fluctuated considerably across space and time whereas in the latter relatively homogeneous T cell profiles were detected.

In patient P1 two samples with HGD from the same site separated by only 78 days showed a significant increase in both FOXP3 and CD8 T cell content. Although CD8 T cells were similar in density with adjacent CG, FOXP3 were greatly increase in HGD at the latter time point. The importance of this was confirmed using nearest neighbour analysis which showed a remarkable

increase of FOXP3 T cells around CD8 T cells in the distance range of 10-40µm in HGD compared to adjacent CG. By contrast in patient P2 no difference was observed in total T cell nor in CD8 T cell content when compared to LGD nor to adjacent CG. It is difficult to explain the differences observed between patients P1 and P2 although histologically the latter contained IM glands interspersed through the HGD glands which may have influenced the overall T cell response.

Overall these findings suggest that immune-regulation through the effect of regulatory T cells on CD8 T cells may play a key role in a fraction of patients that have already progressed to HGD. However the data acquired from these two patients has too few data points to derive general conclusions. Previously Guo et al 2019 [239] showed that LGD and particularly HGD was characterised by reduced levels of CD8+ cells but unfortunately this study did not investigate FOXP3 making a comparison with the current study not possible.

A comparison of T cell data with available genomic data from patients P1 and P2 suggested that large scale genomic events are not necessary for direct changes in the T cell landscape to occur. HGD in patient P1 did not show any specific changes between the two time points characterised thus a similar genomic state resulted in two very different levels of T cell subset infiltration. Also HGD in patient P2 which was characterised by many chromosomal losses did not seem to show any differences in T cell content compared to CG, IM and LGD tissues that most likely did not have these losses. However these differences or indeed the lack of differences may be explained by the genomic data being derived from frozen tissue and the T cell data from adjacent FFPE tissue. Alternatively it is likely that there are multiple molecular subtypes of HGD that remain to be characterised, each with its own unique immune response, similar to the GC molecular subtypes as defined by the TCGA and also by the Asian Cancer Research Group [42, 43].

6.4.2 Technical limitations

As the current study used the same samples and the same methodology as the macrophage study described in Chapter 5, it had similar potential limitations (§5.4.2) including:

a) The samples characterised originated from a relatively small number of patients.

b) Tissue degradation due to the use of the 3 day OPAL™ IHC method that involves multiple antigen retrieval steps.

c) Limitations of the inForm software with regards to accurately cell phenotyping rare cell types (in this case mainly DN T cells).

d) Patient bias in the findings from the Progressors' cohort as all 20 tissue samples originated from only 2 patients (case studies).

e) T cell and genomic data comparison in the Progressors patients was carried out from adjacent and not the same tissue thus may have suffered from bias due to tissue heterogeneity.

Overall this study showed that there are four main subsets of T cells in gastric premalignant lesions. It also showed that the complete subtype of IM is highly rich in T cell infiltrates, particularly of CD4 and DN T cells. By contrast incomplete IM is characterised by low T cell content and particularly low numbers of CD8 and DN T cells. Spatial analysis showed that the levels of T cells in proximity of epithelial cells and of each other mirrored the quantitative differences which suggested the possibility of reduced immune-surveillance in incomplete IM as a possible mechanism to explain the increased risk of progression associated with subtype. If early abnormal cells, particularly if these occur in the stem cell compartment which is continuously dividing in the IM gland [514], are not quickly and efficiently eliminated by T cells with cytotoxic capacity or other immune cells, then they may divide and form early dysplastic glands that could lead to future gastric tumours in the presence of additional mutational/chromosomal events.

Single cell spatial analysis showed differences in T cell targeting of epithelial and other T cells between IM subtypes and integration with the macrophage data obtained from serial sections in Chapter 5 suggested fundamental differences in immune response. The seemingly well organised T cell and macrophage response in incomplete IM was dissimilar to the inflammation rich but rather more chaotic microenvironment in complete IM. Finally using two case studies, the local T cell content was shown to fluctuate considerably across time and space and HGD in at least one patient showed a large infiltration of FOXP3 T cells. This suggested that immune regulation through regulatory T cells may play an important role in HGD progression to GC, whereas this is not likely the case in IM progression to dysplasia as both IM subtypes showed similar levels of FOXP3 T cells to CG. Finally characterising the immunological status of premalignant lesions and gaining insight into the exact mechanisms of progression should lead to better patient stratification and ultimately the prevention of GC.

Chapter 7 Characterising the potential of CD10 and Das1 as biomarkers for the complete and incomplete subtypes of intestinal metaplasia

7.1 Introduction

The risk of progression from IM to GC has been previously described [85, 89-91, 93]. In 2003, Boussioutas et al published a landmark study [406] that showed premalignant lesions (CG and IM) can be distinguished from each other by their expression profiles. In 2017, Companioni et al showed that incomplete IM, which is associated with a higher risk of progression [89, 91], over-expressed more oncogenic genes and molecular processes than complete IM [388]. More recently, Zhang et al 2019 [515] carried out a single cell transcriptomic study on a small number of chronic atrophic gastritis (AG), IM and early gastric cancer (EGC) tissues and identified a pre-goblet cell marker (HES6) that defined early stage metaplasia and a panel of EGC-specific signatures. However there is still some dispute among pathologists regarding the patient's benefit from subtyping IM, as shown by the absence of recommendation guidelines not only in Australia but also in the UK for IM subtype-dependent patient surveillance. The subtyping of IM tissue can be affected from inter-pathologist variation [516] and can be quite tedious as IM glands of differing subtypes are interspersed in a two and three dimensional manner making it particularly difficult for the pathologist to arrive to a final diagnosis [105].

The development of highly sensitive and specific biomarkers could lead to a reduced time burden for pathologists in subtyping IM from an H&E stained section or even completely remove the need for an experienced pathologist by developing a reliable combination of biomarkers that could be applied on an automated platform. Additionally such biomarkers could be used to facilitate subtyping in order to better assist with prediction to progression.

Based on current literature and using the findings from chapter 4 as a guide, two markers were selected as candidates to distinguish complete and incomplete IM at a single gland level. The *MME* gene was previously shown to be highly differentially expressed in complete IM compared to incomplete IM (section §4.13.10) and encodes CD10, a membrane-associated neutral peptidase. CD10 is found on the brush border of the small intestine, it identifies normal small intestinal mucosa with 100% specificity and is absent in the colon [420]. Additionally, strong CD10 staining has been shown previously on a subset of IM glands including complete IM glands with only weak or absence of staining in incomplete IM [414, 415]. However, so far, no study has tried to determine the utility of CD10 as a biomarker selective for complete IM.

Das-1 is a monoclonal antibody (7E12H12, IgM isotype) which binds colon epithelial protein (CEP). Previous work has shown that Das-1 reacts with Barrett's epithelium (intestinal

metaplasia at the oesophagus) as well as gastric IM [517, 518] but not with normal stomach, duodenum, jejunum, ileum, liver or pancreas tissue [519]. In addition others have shown that this antibody has significantly higher reactivity ($p<0.0001$) to IM in IM+GC patients (IM patients with concurrent gastric cancer or "late" IM) than in IM-GC patients (IM patients without concurrent gastric cancer or "early" IM) and virtually no positive staining in chronic gastritis (CG-GC, no concurrent gastric cancer) [518]. More in depth analysis by these authors showed that mixed and incomplete IM in the IM+GC cohort stained positive in 100% of cases whereas complete IM stained positive in 82% of cases. By contrast incomplete IM in the IM-GC cohort was positive in 75% cases but mixed and complete IM stained positive only in 43% and 10% of cases respectively [518]. Earlier findings in this current study (§4.3.7) showed the IM+GC samples were shown to be enriched in expression of genes associated with inflammation and GC including *MYC* and *E2F1* due to a possible field cancerisation effect. Thus Das1 staining may provide useful information not only with regards to IM subtype but also with regards to possible risk of progression.

7.2 Hypothesis and aims

Hypothesis: "CD10 and Das1 have clinical utility as biomarkers to detect complete and incomplete intestinal metaplasia".

The main aims of this study were to:

1. Determine the sensitivity and specificity of CD10 and Das1 for identifying complete and incomplete IM respectively at the single gland level.
2. Assess whether using a combined model would improve the ability to detect either IM subtypes at the single gland level.
3. Identify whether Das1 is associated with incomplete IM at the whole section level.
4. Identify whether Das1 is associated with progression, irrespective of IM subtype.
5. Characterise the relationship between Das1 and macrophage/T cell subsets.

7.3 Results

7.3.1 Validation of CD10 and Das1 as biomarkers of intestinal metaplasia subtypes

When subtyping of IM is required for clinical diagnosis, pathologists will invariably assess the entire tissue section and report on the predominant subtype. However in order to improve on this, the ability of the anti-CD10 and Das1 antibodies to identify single complete and incomplete IM glands respectively was investigated in this study. A subset of the IM tissue samples used in

Chapters 5 and 6 and representing the IM-GC, IM+GC and Progressors cohorts were used for this (Table 7.1).

Table 7.1 Clinical details of IM-GC, Progressors and IM+GC patients with intestinal metaplastic tissue used to characterise CD10 and Das1 staining

Parameters	IM-GC (n)[1]	Progressors (n)[1,2]	IM+GC (n)[1]
Gender			
Male	4[3]	2	4
Female	3	0	3
Age			
Male	69 (59-86)[4]	64 (60-68)[4]	72.5 (63-85)[4]
Female	70 (44-77)[4]	-	75 (51-83)[4]
Tumour Pathology			
Intestinal	-	-	3
Diffuse	-	-	4
T stage			
T1	-	-	2
T2	-	-	2
T3	-	-	2
Unspecified	-	-	1
Total n^0 of glands characterised			
CD10 study	96	75	44
Das1 study	81	93	49

[1]Samples were selected with the criteria that they contained the upper part of glands near the surface. Multiple areas per sample containing either complete or incomplete IM glands or both were characterised where possible; [2]Cohort consisted of two patients (P1 and P2) with tissue taken from multiple stomach sites and characterised (for P1 n=11 and for P2 n=7) across multiple time points (multiple hospital visits, for P1 n=4 and P2 n=4); [3]two biopsy samples acquired on different time points (hospital visits) were characterised from a single patient; [4]Median value and range.

The anti-CD10 monoclonal antibody (56C6) used in this study has been previously well characterised [420, 520] and was utilised as part of the OPAL™ T cell panel described in Table 2.9. Das1 staining was carried out on serial sections to those used for the macrophage and T cell studies (Chapters 5 and 6) and to an additional section stained by H&E allowing direct comparison of the same glands (§2.6.2). Initial validation of CD10 and Das1 antibodies was accomplished using the appropriate positive controls, small intestine and colon tissue respectively (Table 2.2 and Figure 7.1).

Subtyping of individual IM glands was carried out by in-house research pathologist Dr Catherine Mitchell after review of the H&E slides and was predominantly based on the assessment of the upper (luminal) region of the glands. This was because the lower regions often lack a brush border, which was the principal criterion together with gland morphology for classifying complete IM. Glands which lacked a brush border and with differing morphology such as irregular sized mucin droplets and variable degree of disorganised architecture were classified as incomplete [137].

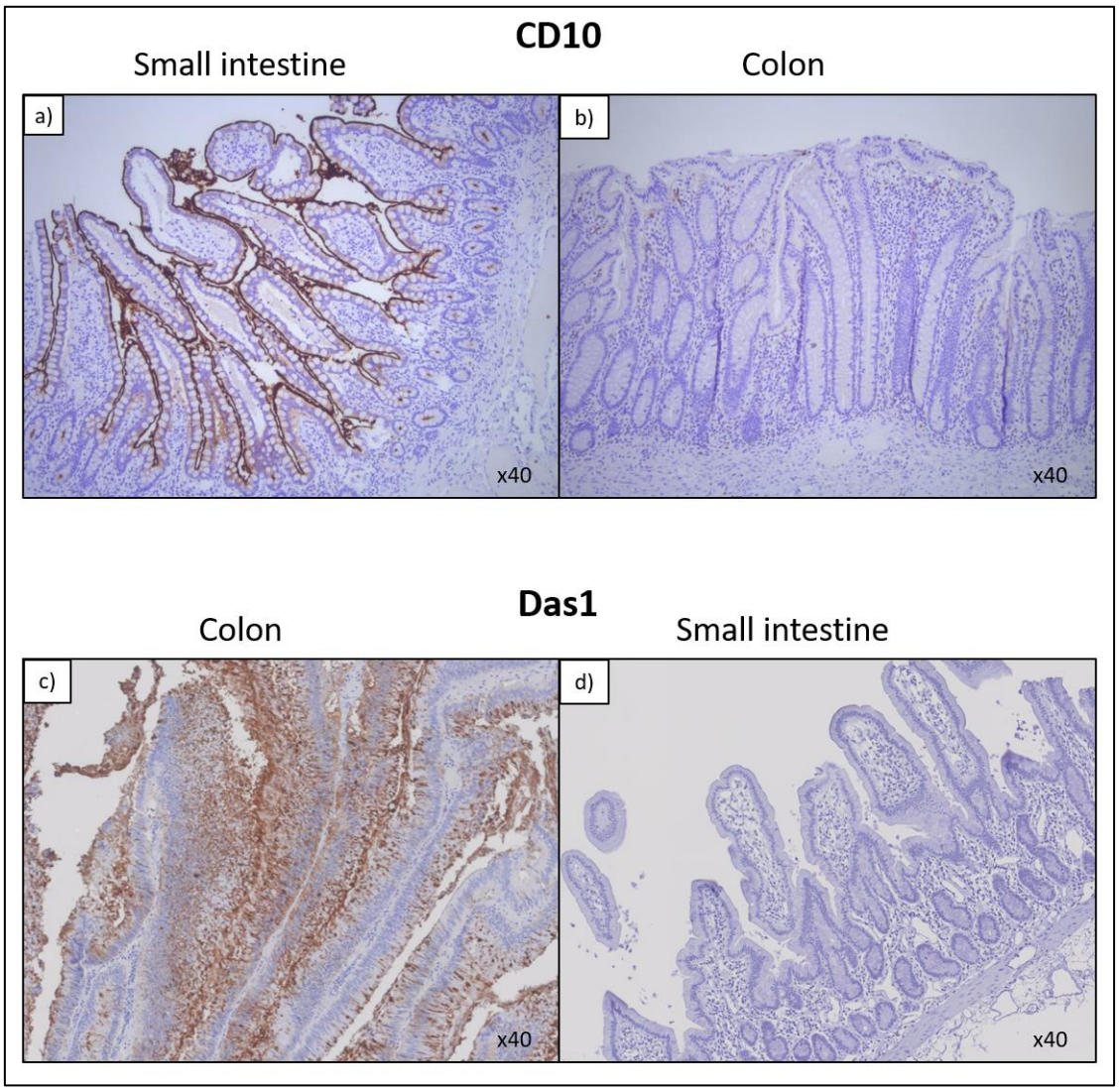


Figure 7.1 Representative staining of anti-CD10 and Das1 staining on small intestine and colon positive control tissues

CD10 staining on a) small intestine tissue and (b) colon tissue; Das1 staining on c) colon and d) small intestine tissues. Images a) and b) were kindly provided by in-house research pathologist Dr Catherine Mitchell and images c) and d) were obtained using the VS120 digital slide scanner.

The single IM glands assessed by the in-house research pathologist were then located on matched scanned images of serial tissue sections which were stained with CD10 and Das1 and scored blindly and independently by two experienced researchers (AB and RB) (§2.6.2-3, Figures 7.2 and 7.3). Data was then pooled and concordance between independent scoring of CD10/Das1 staining with the pathologist's review of H&E stained glands was determined.

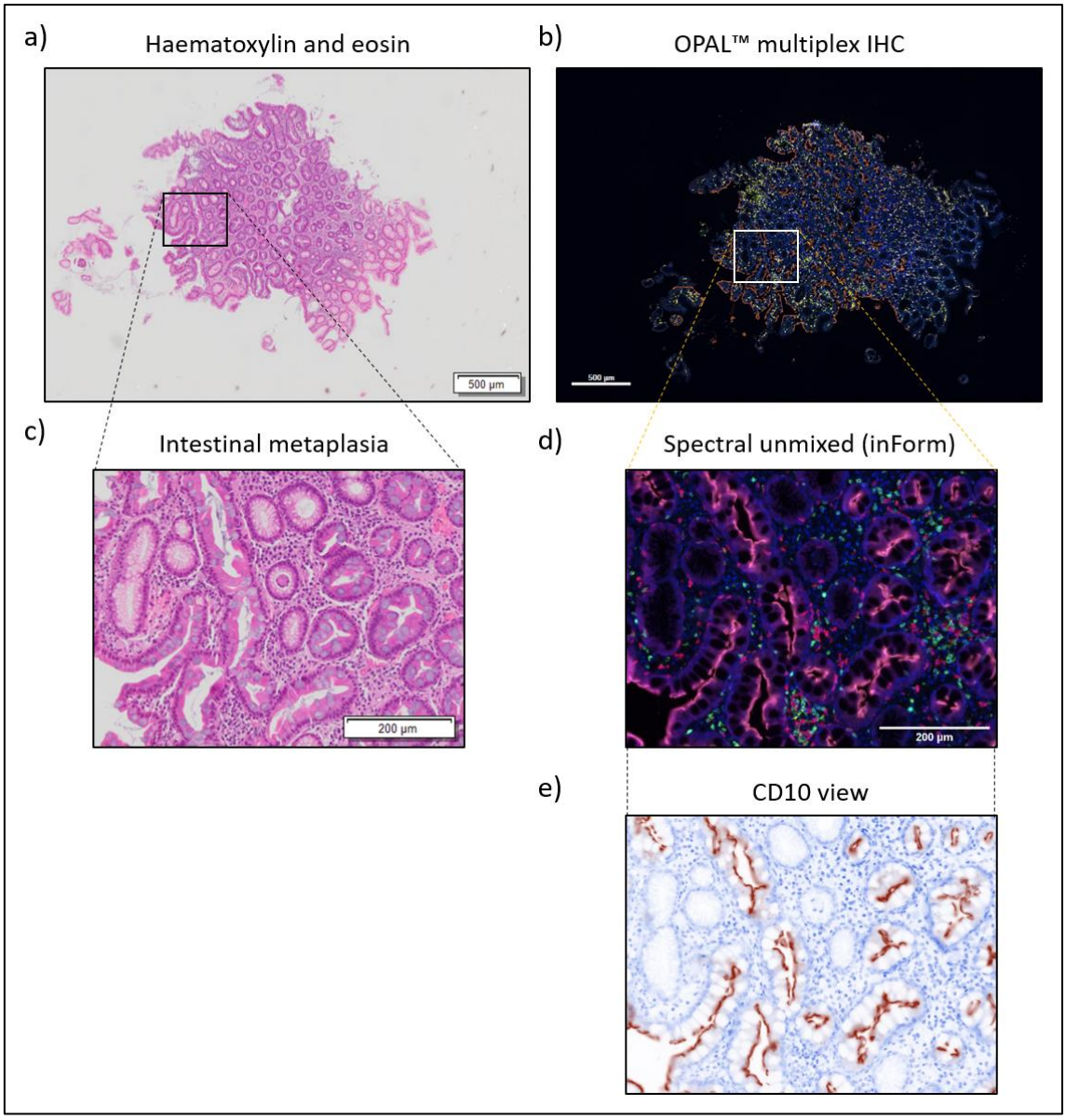


Figure 7.2 Serial sections of biopsy tissue stained with haematoxylin and eosin and with the OPAL™ multiplex IHC T cell panel showing complete intestinal metaplasia with brush border and the presence of CD10

Serial FFPE sections at 4µm thickness were used for a) H&E staining and b) OPAL™ multiplex IHC T cell panel staining (Chapter 6); c) inset of H&E stained section showing IM, d) matched spectrally unmixed image using inForm from the multiplexed IHC scanned slide and e) pseudo-pathology view for CD10 used for single gland scoring. Scale bars: 500µm for a) and b), 200µm for c) and d).

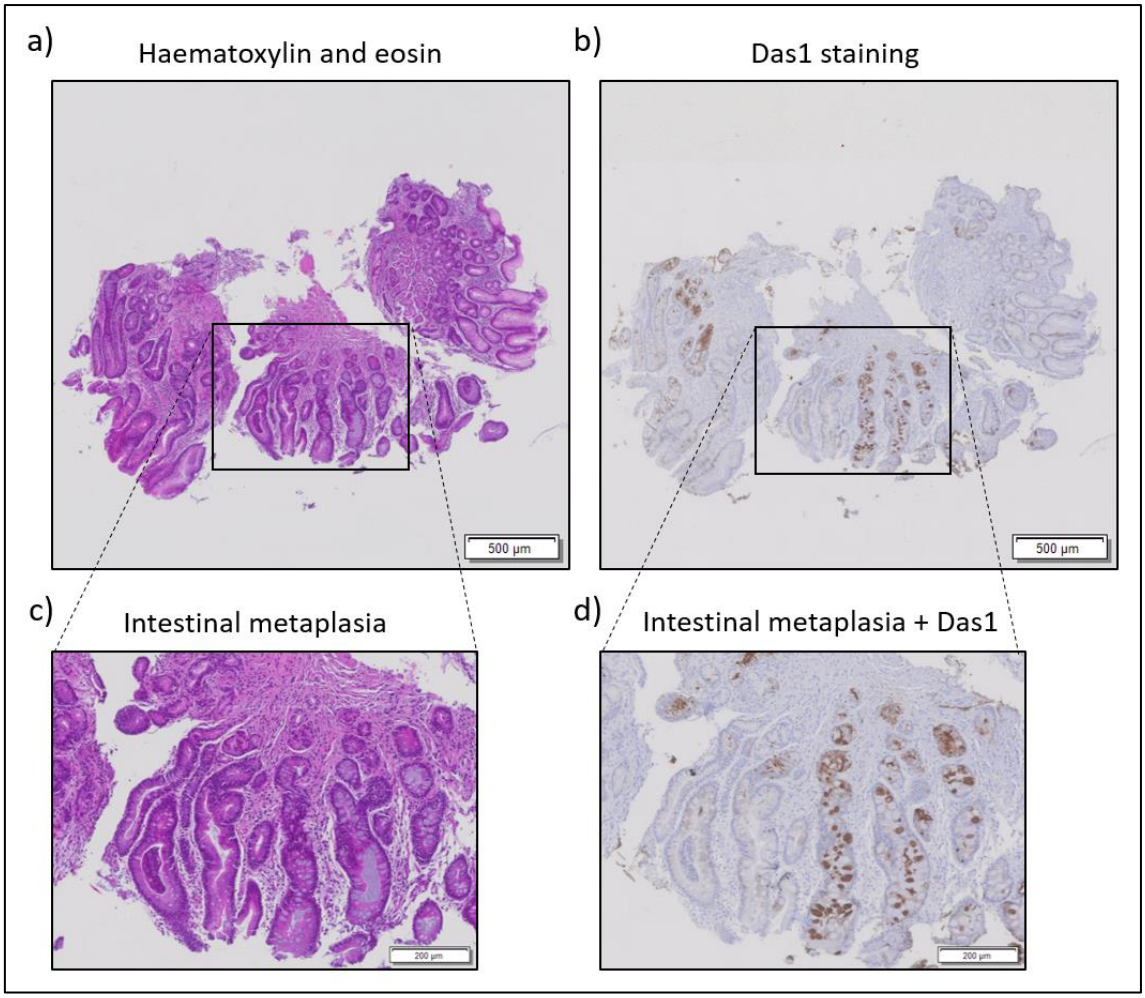


Figure 7.3 Serial sections of biopsy tissue stained with haematoxylin and eosin and with Das1 antibody showing incomplete intestinal metaplasia
Serial FFPE sections 4µm thick used for a) H&E staining and b) Das1 staining with DAB as chromogen; c) inset of H&E stained section with IM and d) inset of Das1 stained section. Scale bars: 500µm for a) and b), 200µm for c) and d).

7.3.2 CD10 has very high sensitivity and specificity for identifying complete intestinal metaplasia glands

Analysis at a single gland level which included all IM samples (IM-GC, the Progressors and the IM+GC cohorts showed that CD10 had both a high sensitivity of 91.06% and a high specificity of 97.83% for detecting complete IM glands (Table 7.2).

Further stratification of the samples based on cohorts which represented varying risk of progression to GC (where IM-GC is lowest risk, Progressors are potentially intermediate risk and IM+GC is highest risk), CD10 had an increasing sensitivity for detecting complete IM glands, from the IM-GC to the Progressors and then to the IM+GC patients with 87.5%, 91.9% and 100.0% respectively. The reverse trend was observed for specificity, with 100.0% in the IM-GC cohort, 97.4% in the Progressors cohort and 95.5% in the IM+GC cohort.

Overall the high sensitivity, specificity and AUROC (range: 0.938 to 0.977) of CD10 for identifying complete IM glands observed across all three patient cohorts suggested that this anti-CD10 monoclonal antibody is able to detect complete IM with high accuracy making it an ideal biomarker for this subtype (AUROC >0.9).

Table 7.2 Sensitivity and specificity of CD10 for individual complete intestinal metaplastic glands

Cohort	IM gland subtype	Total # glands	CD10+ve glands	CD10-ve glands	Sensitivity (95% CI)[1]	Specificity (95% CI)[1]	AUROC[2]
All cohorts							
	Complete	123	112	11	91.1%	97.8%	0.944
	Incomplete	92	2	90	(84.6%-95.5%)	(92.4%-99.7%)	
1.IM-GC							
	Complete	64	56	8	87.5%	100.0%	0.938
	Incomplete	32	0	32	(76.9%-94.5%)	(89.1%-100.0%)	
2.Progressors							
	Complete	37	34	3	91.9%	97.4%	0.946
	Incomplete	38	1	37	(78.1%-98.3%)	(86.2%-99.9%)	
3.IM+GC							
	Complete	22	22	0	100.0%	95.5%	0.977
	Incomplete	22	1	21	(84.6%-100.0%)	(77.2%-99.9%)	

[1]Confidence intervals for sensitivity and specificity are Clopper-Pearson confidence intervals; [2]Area Under Receiver Operating Characteristic.

7.3.3 Das1 has low sensitivity but high specificity for identifying incomplete intestinal metaplasia glands

To determine the suitability of Das1 as a biomarker to identify incomplete IM which has been associated with a higher risk of progression [89, 91], the overall sensitivity and specificity of Das1 for single incomplete IM glands was first calculated using a pooled analysis of data collected across all three patient cohorts, similar to the CD10 analysis. In this instance Das1 had a low sensitivity of 29.2% but a high specificity of 91.3% for incomplete IM glands in all cohorts when combined (Table 7.3).

After separation of the cohorts based on potential risk for progression to GC, Das1 had a similar low sensitivity across all three cohorts (between 28.0% and 32.0%) but high specificity (83.7% to 98.3%). The high specificity of Das1 for incomplete IM glands suggested that this antibody would give few false positives but the low sensitivity would result in a large number of false negatives thus making it overall a low quality biomarker. This conclusion was further supported by the low AUROC values in all three cohorts (range: 0.559 to 0.635).

Table 7.3 Sensitivity and specificity of Das1 for individual incomplete intestinal metaplastic glands

Cohort	IM gland subtype	Total # glands	Das1+ve glands	Das1-ve glands	Sensitivity (95% CI)[1]	Specificity (95% CI)[1]	AUROC[2]
All cohorts							
	Complete	127	11	116	29.2%	91.3%	0.603
	Incomplete	96	28	68	(20.3%-39.3%)	(85.0%-95.6%)	
1.IM-GC							
	Complete	60	1	59	28.6%	98.3%	0.635
	Incomplete	21	6	15	(11.3%-52.2%)	(91.1%-100.0%)	
2.Progressors							
	Complete	43	7	36	28.0%	83.7%	0.559
	Incomplete	50	14	36	(16.2%-42.5%)	(69.3%-93.2%)	
3.IM+GC							
	Complete	24	3	21	32.0%	87.5%	0.598
	Incomplete	25	8	17	(15.0%-53.5%)	(67.6%-97.3%)	

[1]Confidence intervals for sensitivity and specificity are Clopper-Pearson confidence intervals; [2]Area Under Receiver Operating Characteristic.

7.3.4 Logistic regression modelling of combined CD10 and Das1 staining

To further assess the biomarker potential of CD10 and to determine whether Das1 staining could be used in combination with CD10 to obtain an even better outcome for identifying single complete IM glands, logistic regression modelling was carried out with CD10 staining on its own and with CD10 + Das1 staining combined. All single subtyped glands which had both CD10 and Das1 staining status available (n=185) across all three cohorts were used together with the glm function in R.

In the model with CD10 on its own, a highly significant positive association with complete IM glands was observed as expected (Table 7.4). In the combined model, CD10 again had a positive association but Das1 had a negative association with complete IM glands. Both associations were statistically significant but the much lower p value for CD10 suggested a much stronger association. Overall the Akaike information criterion (AIC), commonly used to assess relative quality of statistical methods [521], decreased only marginally when Das1 staining status was added to the model suggesting a small improvement to the model. This was further confirmed by the small increase in AUROC observed in the combined model (Figure 7.4). Overall the addition of Das1 offered a significant but limited improvement.

Table 7.4 Logistic regression models comparing CD10 with combined CD10 + Das1 staining for complete intestinal metaplastic glands

Biomarker model	Coefficient[1]	p value	AIC
CD10	+6.28	1.4e-14	71.1
CD10 + Das1	+6.72 -3.09	3.8e-10 0.018	65.7

[1]Coefficient shows direction and relative change per unit increase.

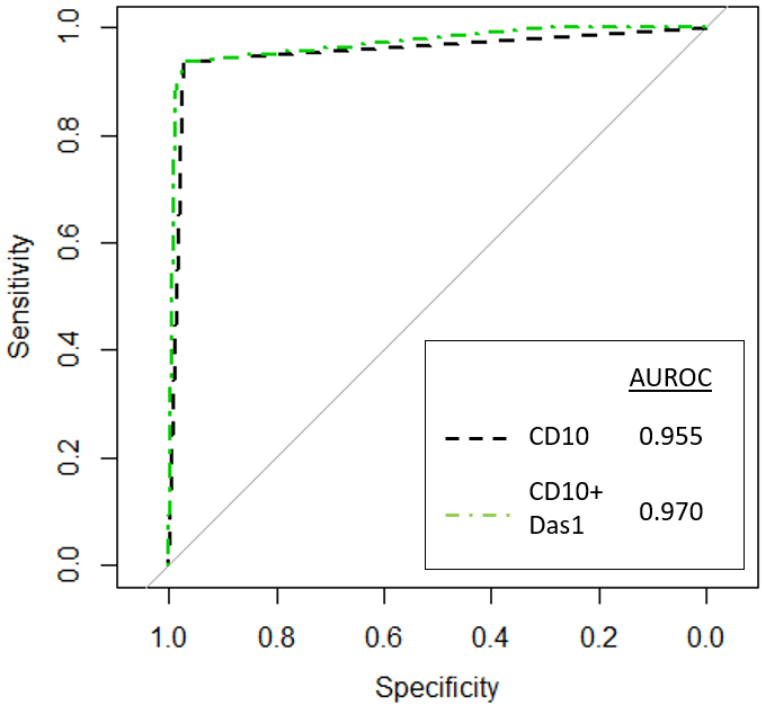


Figure 7.4 Receiver Operating Characteristic (ROC) curve and Area Under Receiver Operating Characteristic (AUROC) for CD10 and CD10 combined with Das1 staining using logistic regression

Logistic regression carried out using all single IM glands with known CD10 and Das1 staining status (n=185) across all three cohorts (IM-GC, Progressors and IM+GC). Modelling and plotting carried out using glm function and pROC package in R.

7.3.5 Das1 staining is associated with incomplete intestinal metaplasia in the IM-GC cohort

Das1 staining was often observed in the lower parts of IM glands (Figure 7.5). Given that the single gland analysis was restricted to the top half of the glands this could explain to a certain degree the overall low number of IM glands with positive staining. Thus to determine whether Das1 staining across all parts of IM glands was associated with the incomplete IM subtype, regions of interest (ROIs) similar in size and location to those used for the OPAL™ IHC macrophage and T cell studies (Chapters 5 and 6) were digitally quantified for positive staining

(§2.6.3, cellSens Dimension software) for all patients in the IM-GC and IM+GC cohorts (Table 5.1 for patient details, Figure 7.6). For each ROI, the fraction (percentage in pixels) of positive staining was calculated. Epithelial cells both in the upper and lower part of glands stained positive but no staining was observed on stromal and immune cells.

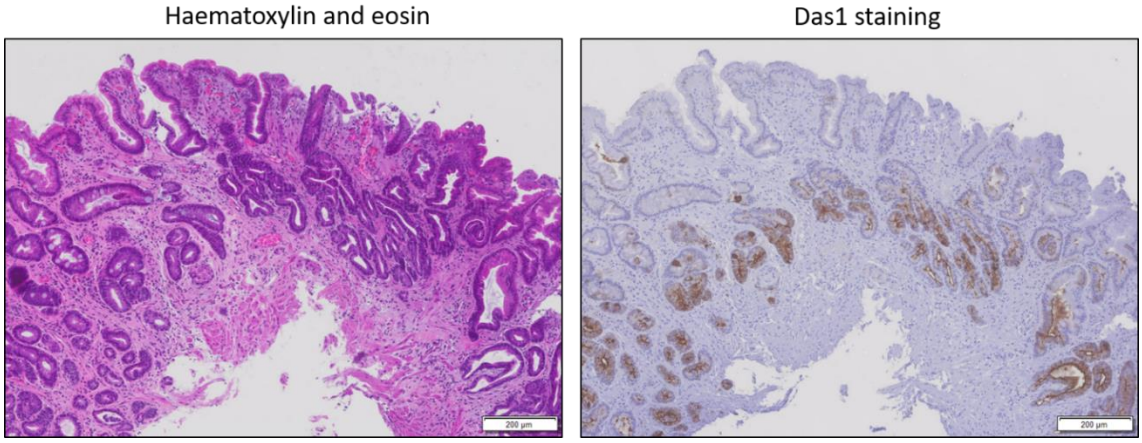


Figure 7.5 Das1 staining in the lower part of incomplete intestinal metaplasia glands
Das1 IHC staining with DAB used as chromogen. Scale bar: 200µm.

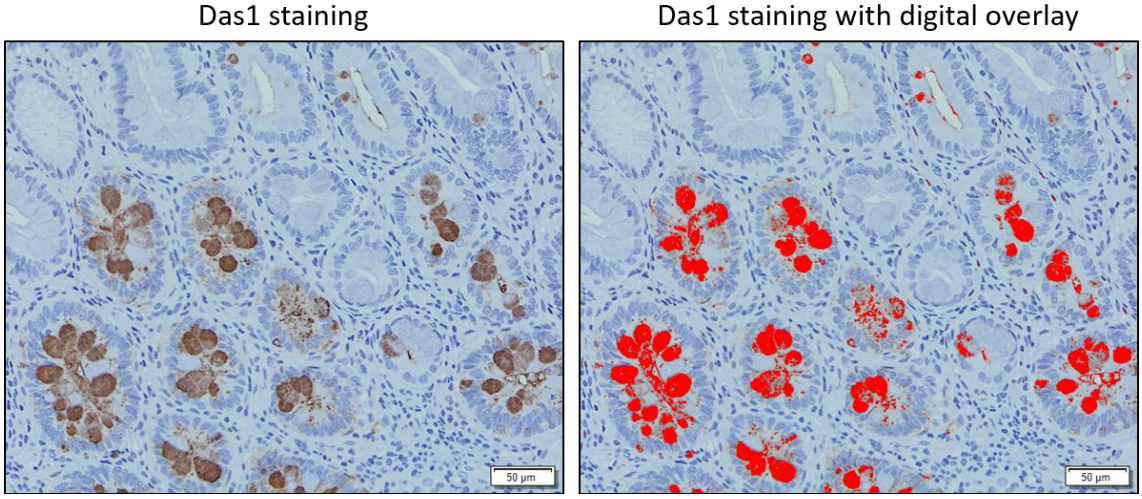


Figure 7.6 Digital quantification of Das1 staining on intestinal metaplasia glands using an overlay
Digital quantification carried out using the cellSens Dimension software (Olympus) as described in section §2.6.3. Scale bar: 50µm.

IM subtyping of whole tissue sections was done as described in section §2.5.1 and Figure 2.3. Briefly IM containing 0% to 40% brush border was defined as “incomplete IM”, IM containing 40% to 60% brush border was defined as “mixed IM” and IM containing 60% to 100% brush border as “complete IM”. For whole section analysis of Das1 staining the “mixed” and “incomplete” IM samples were pooled together and referred simply as incomplete IM similar to Chapters 5 and 6. Where appropriate (see analysis by ROI) Das1 staining was also analysed using all three predefined subtypes of IM (“complete”, “mixed” and “incomplete”) to remove any possible bias (§2.6.4).

In areas with chronic gastritis (CG-GC, control tissue) in the IM-GC cohort, there was little to no Das1 staining. In complete IM (cIM-GC) there was very occasional staining, but significantly more than in CG-GC (p=0.01, Figure 7.7). Incomplete IM (iIM-GC) was characterised by significantly more Das1 staining than complete IM (p=0.009) irrespective of percentage of incomplete IM glands (40%-60% iIM-GC vs cIM-GC: p=0.028 and >60% iIM-GC vs cIM-GC: p=0.0058).

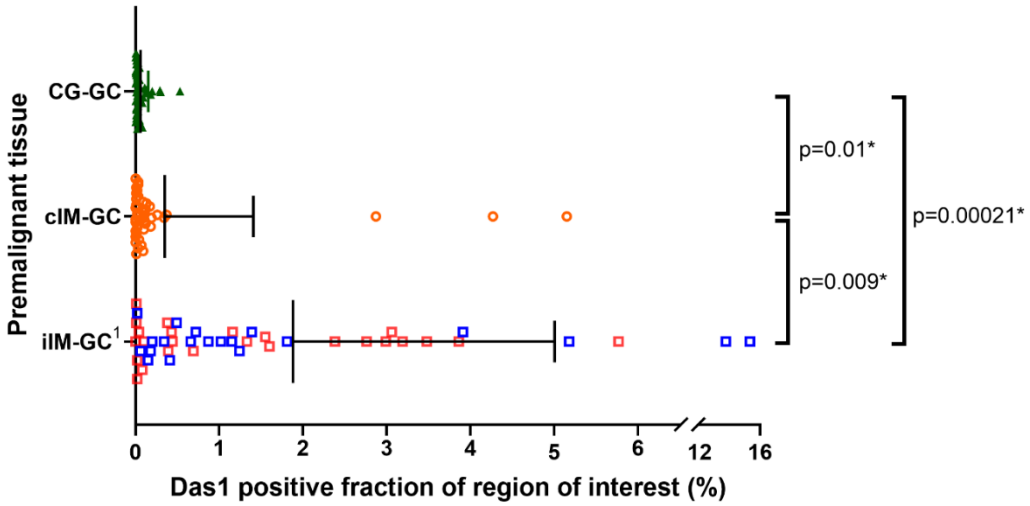


Figure 7.7 Das1 staining by region of interest in the IM-GC samples
Das1 staining digitally quantified for all samples in the IM-GC cohort (CG-GC=14, cIM-GC=10, iIM-GC=11). Each symbol represents data from a single ROI and multiple ROIs were assessed per sample. [1]Blue square data from tissue with >60% incomplete IM, red square data from tissue with 40%-60% incomplete IM (see section §2.5.1 for more details on IM subtyping). Data presented as mean + S.D. *All statistical analysis done using glm function in R (See section §2.6.5).

There were three ROIs in the cIM-GC cohort, all belonging to the same tissue sample (Figure 7.8), that stood out with particularly high Das1 staining fraction (2.87%-5.15%). All three ROIs were found to be outliers as determined using the ROUT method (GraphPad Prism). Interestingly this was the only cIM-GC sample that differed in subtype diagnosis between the original H&E section following patient gastroscopy (incomplete IM) and a second H&E section cut prior to the commencement of this current study (complete IM, consensus subtype obtained by in-house research pathologists Dr Catherine Mitchell and Dr Stephen Lade as described in §2.5.1 and used in Chapters 5 and 6). The most likely explanation is that the gland content of IM rich areas changes in a two and three dimensionally manner thus sections cut from a FFPE block may be rich in one subtype at one level but those cut at another level may be rich in the opposite subtype or contain a mixture of both IM subtype glands.

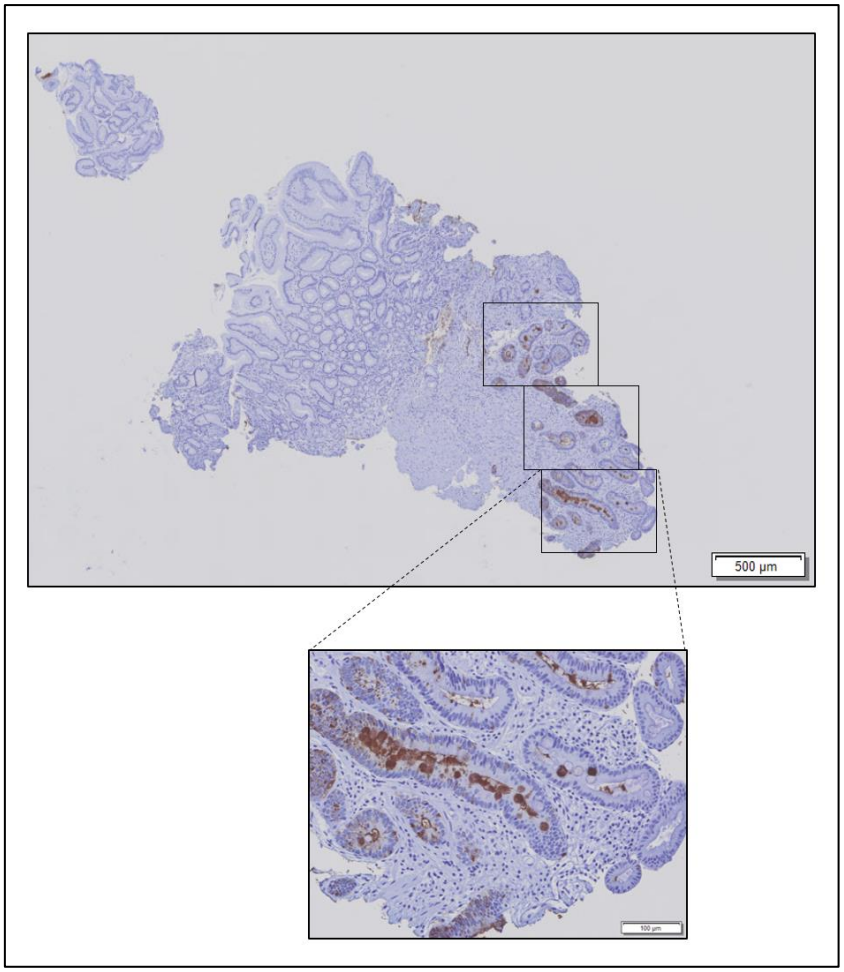


Figure 7.8 Das1 stains positive a case of intestinal metaplasia with differing diagnosis
Das1 staining with inset of a case initially diagnosed with incomplete IM following gastroscopy but then diagnosed as complete IM by the in-house research pathologist Dr Catherine Mitchell prior to commencement of study. Two and three dimensional variation in IM gland subtype is the most likely explanation.

Overall positive Das1 staining was specifically observed in IM when compared to CG in IM-GC samples. Among IM subtypes, Das1 stained significantly more incomplete IM regions. Also Das1 stained positive the only complete IM tissue sample that originally had received an incomplete IM diagnosis.

7.3.6 Whole section Das1 staining is higher in IM-GC patients with incomplete intestinal metaplasia

Having established that Das1 is associated with regions rich in incomplete IM glands, the next logical step was to determine whether a single patient's biopsy could provide useful information regarding IM status as this could have more clinical relevance. For this analysis the previous sample that showed differing IM subtype between sections was grouped with the incomplete IM tissues (most histologically advanced IM subtype analysis). Whole section Das1 staining (combined data from all ROIs within a single section) in complete IM was overall barely present

and did not show a significant difference with CG (Figure 7.9). By contrast incomplete IM at the whole section level had a significantly higher positive fraction for Das1 compared to both CG and complete IM (p=0.00014 and p=0.0018 respectively). Overall Das1 staining across a whole section showed a clear association with incomplete IM suggesting a possible utility for this antibody as a risk biomarker in a clinical setting.

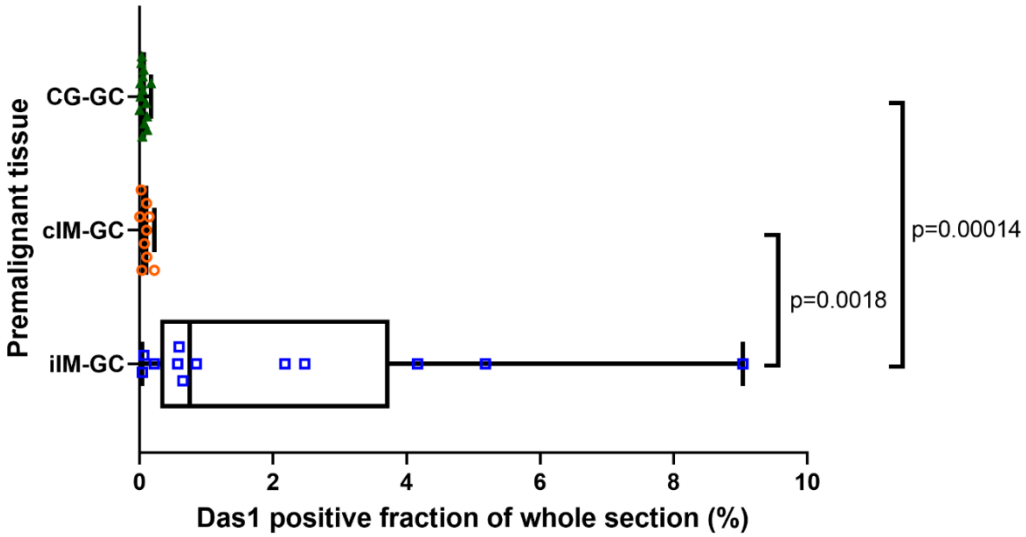


Figure 7.9 Analysis of Das1 staining across whole section in IM-GC samples
Total section area containing either and/or CG (n=14), complete IM (n=9) and incomplete IM (n=12) were analysed for fraction positive for Das1 staining. Most histologically advanced IM subtype used as final subtype (see text for more details). Each symbol represents data from a single biopsy section originating from multiple ROIs. Statistical analysis carried out using unpaired t test and Mann-Whitney test where appropriate.

7.3.7 Das1 staining is associated with incomplete intestinal metaplasia tissue in the IM+GC cohort

To quantify Das1 staining in ROIs of premalignant tissues from IM+GC patients, the same method was used as above (§7.3.5). Complete IM showed significant more staining than CG (p=0.0028, Figure 7.10). Incomplete IM showed a higher percentage of stained area per ROI compared to both CG and complete IM (p=1.7e-05 and p=0.0016 respectively).

Next, an analysis of Das1 staining across the entire tissue section was performed using the most histologically advanced IM subtype method as before. Minimal positive staining was observed in CG but there was an increasing trend in complete IM which did not reach significance (Figure 7.11). Again, incomplete IM was characterised by a higher positive area for Das1 staining per section when compared to both CG and complete IM (p=5.7e-06 and p=0.0048 respectively).

Collectively the data presented in sections §7.3.5-§7.3.7 suggested a significant positive association between the Das1 monoclonal antibody and incomplete IM in both the IM-GC and IM+GC cohorts.

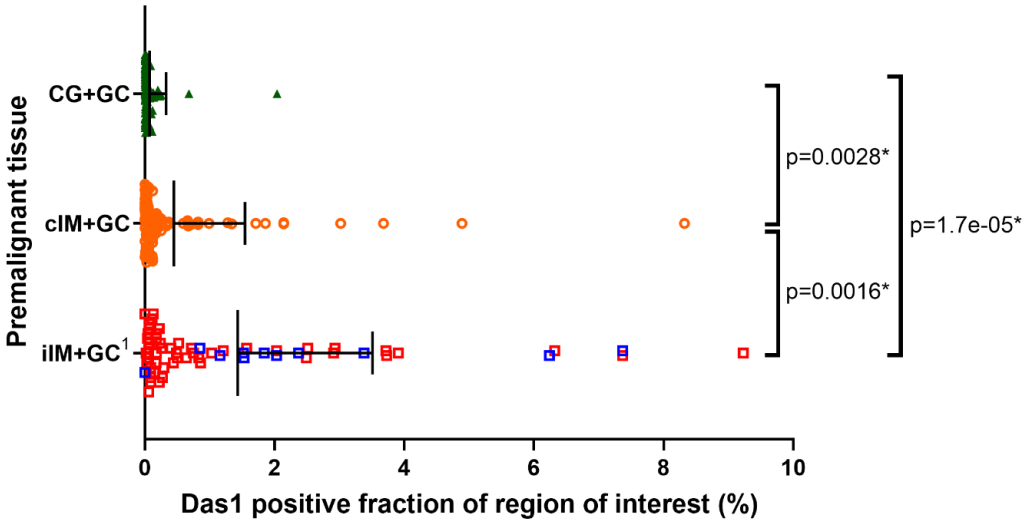


Figure 7.10 Das1 staining by region of interest in the IM+GC samples
Das1 staining digitally quantified for all samples in the IM+GC cohort (CG+GC=11, cIM+GC=10, iIM+GC=7). Each symbol represents data from a single ROI with multiple ROIs per sample. [1]Blue square data from tissue with >60% incomplete IM, red square data from tissue with 40%-60% incomplete IM (see section §2.5.1 for more details on IM subtyping). Data presented as mean + S.D. *All statistical analysis done using glm function in R (See section §2.6.5).

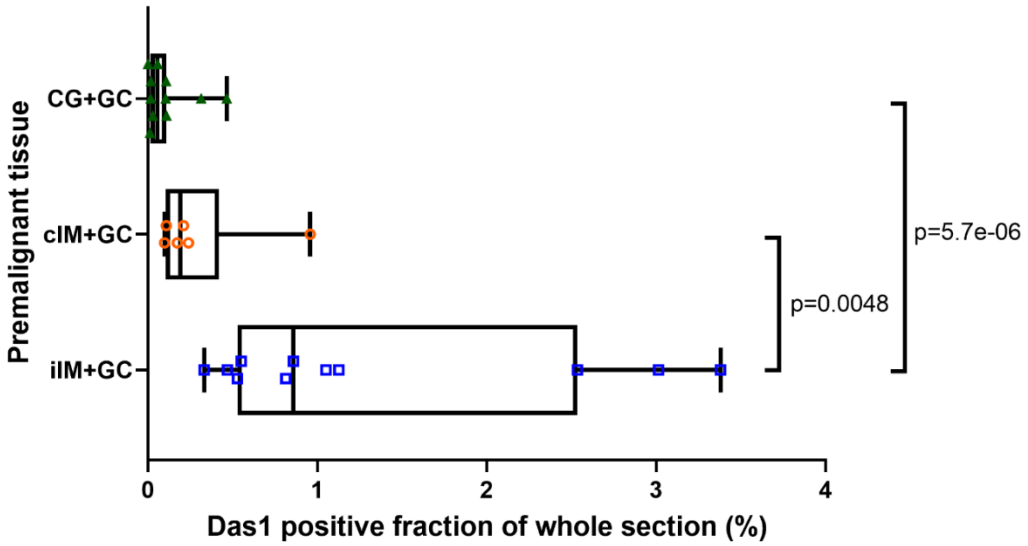


Figure 7.11 Analysis of Das1 staining across whole section in IM+GC samples
Total section area containing either and/or CG (n=11), complete IM (n=6) and incomplete IM (n=11) were analysed for fraction positive for Das1 staining. Most histologically advanced IM subtype used as final subtype (see text for more details). Each symbol represents data from a single gastrectomy tissue section originating from multiple ROIs. Statistical analysis carried out using Mann-Whitney test.

7.3.8 Das1 staining is higher in complete intestinal metaplasia tissues of IM+GC patients

To establish whether Das1 staining assessed on whole sections was associated with temporally more progressed premalignant lesions, tissues with CG and differing IM subtypes were compared between the IM-GC and the IM+GC cohorts. There was no significant difference between CG-GC and CG+GC and between iIM-GC and iIM+GC samples (Figure 7.12). However, complete IM tissues in IM+GC samples did show a significant increase in Das1 staining when compared to those in IM-GC samples. Overall these findings suggest that Das1 staining is more associated with "late" complete IM (IM+GC cohort) but does not change between "early" and "late" incomplete IM.

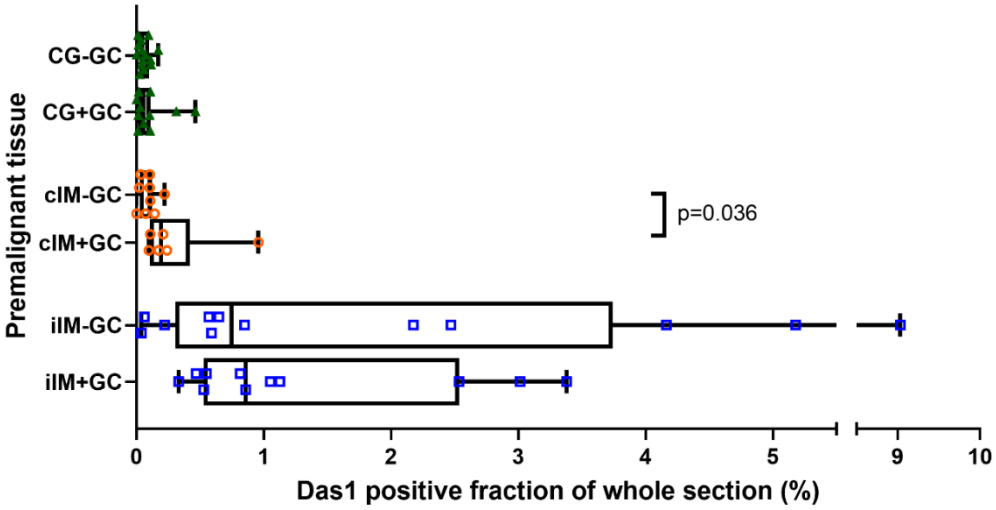


Figure 7.12 Comparison of Das1 staining per section between IM-GC and IM+GC cohorts
Total section area was analysed for fraction positive for Das1 staining as before. Most histologically advanced IM subtype used as final subtype. Each symbol represents data from a single tissue sample. Statistical analysis carried out using Mann-Whitney test.

7.3.9 Das1 staining associated with CD68+IRF8+ and CD68+CD163+IRF8+ macrophages in incomplete intestinal metaplasia in IM-GC patients

Given the previous findings in Chapters 5 and 6 which showed significant differences in both macrophage and T cell content between IM subtypes and the Das1 findings in this chapter, it was logical to compare immune cell subset density and Das1 positive staining to determine whether there was a relationship between epithelial Das1 status and immune response. For this analysis, only data from incomplete IM ROIs was used in order to identify potential relationships between macrophage, T cell and Das1 positive epithelium. The samples were grouped and analysed on the basis of the most advanced histology subtype as before.

In the incomplete IM samples of the IM-GC cohort, a weak positive correlation was identified only between Das1 staining and CD4 T cell density (Pearson's coefficient r=0.31, p=0.046). By

contrast both CD68+IRF8+ (M1 macrophages) and CD68+CD163+IRF8+ macrophages (M1/2 macrophages) were strongly correlated with Das1 staining in IM-GC (r=0.52 with p=0.0017 and r=0.79 with p=3.5e-08 respectively) (Figure 7.13). A similar analysis carried out for the incomplete IM subtype in the IM+GC samples, did not show a significant difference between any of the macrophage nor the T cell subsets and Das1 staining.

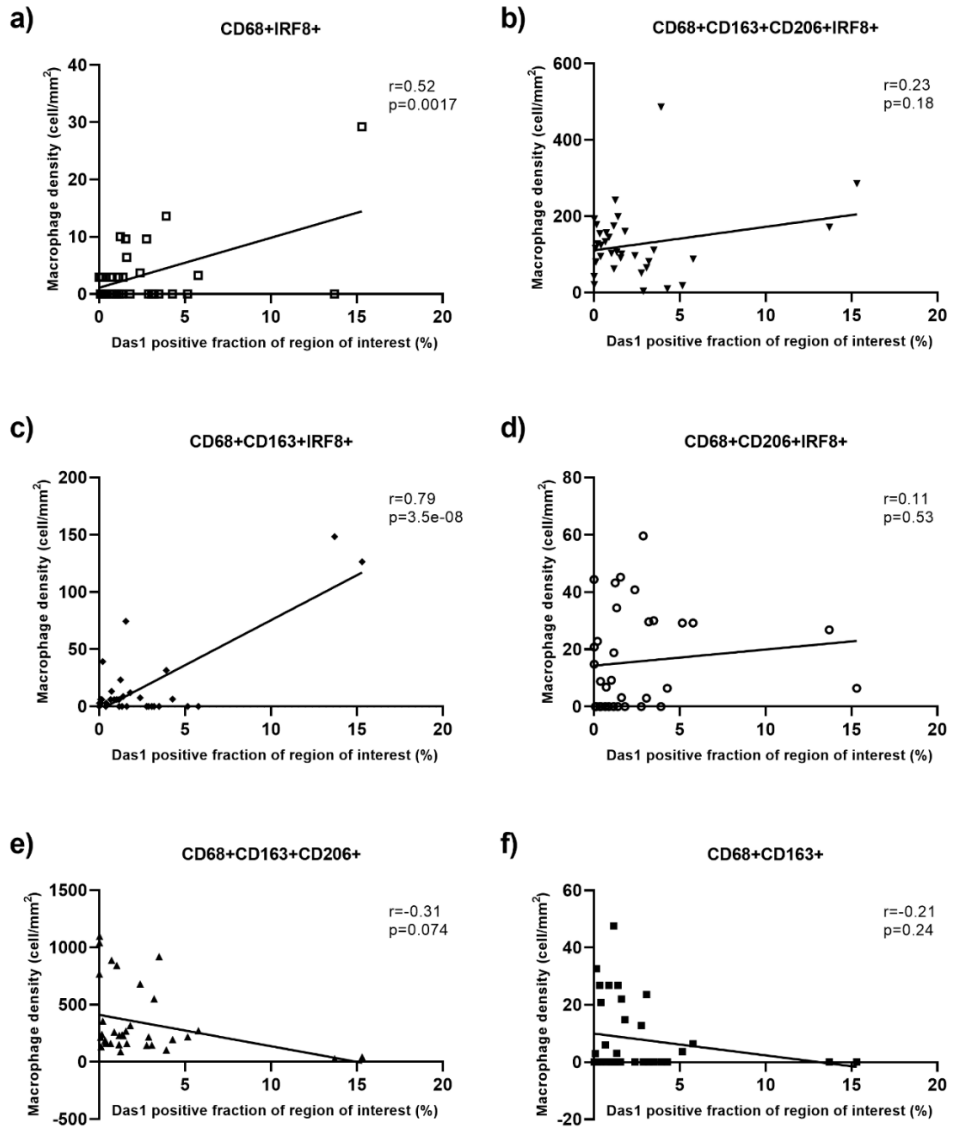


Figure 7.13 The relationship between Das1 staining and macrophage subset density in incomplete intestinal metaplasia of IM-GC samples

Scatter graphs showing the correlation between Das1 positive fraction per region of interest in incomplete IM tissue samples (n=11) and individual macrophage subset density, including a) CD68+IRF8+ macrophages, b) CD68+CD163+CD206+IRF8+ macrophages, c) CD68+CD163+IRF8+ macrophages, d) CD68+CD206+IRF8+ macrophages, e) CD68+CD163+CD206+ macrophages and f) CD68+CD163+ macrophages. Each symbol represents data from a single ROI. Multiple ROIs per tissue sample. Macrophage density data from Chapter 5. Most histologically advanced IM subtype used as final subtype. Pearson's correlation coefficient r shown with statistical significance calculated in GraphPad Prism.

7.4 Summary and discussion

The following is a summary of the main findings of this chapter into the potential suitability of two biomarkers for reliably and accurately subtyping intestinal metaplasia from tissue samples:

1. The monoclonal anti-CD10 antibody (56C6) had very high sensitivity and specificity for single complete intestinal metaplasia glands in all three patients cohorts investigated (IM-GC, Progressors and IM+GC).
2. The monoclonal antibody Das1 (7E12H12) that stains colon epithelial protein had a low sensitivity but high specificity for incomplete intestinal metaplasia glands in all three patients cohorts investigated (IM-GC, Progressors and IM+GC).
3. A combined logistic regression model of CD10 with Das1 on pooled cohort data showed a significant but marginal improvement for identifying single complete intestinal metaplasia glands.
4. Das1 staining was present both at the upper and lower part of intestinal metaplasia glands and was associated with incomplete intestinal metaplasia as analysed across regions rich in intestinal metaplasia and by whole section.
5. Complete intestinal metaplasia in IM+GC samples showed a significant increase in Das1 staining when compared to IM-GC samples.
6. Das1 staining was associated with increasing density of CD68+IRF8+ and of CD68+CD163+IRF8+ macrophages in incomplete intestinal metaplasia of IM-GC patients.

7.4.1 Discussion

IM is a key premalignant lesion in the Correa model (§1.2.1, [64]) and is associated with progression to GC (§1.2.2, [85, 94]). It can be classified into two subtypes, the complete which is small intestinal-like and the incomplete which is more colon-like (§1.3.2, [130]). The latter subtype of IM has been associated with an increased risk of progression to GC in multiple studies [89, 91]. In the current study using tissue samples from patients belonging to three cohorts that likely represent different stages of temporal progression in IM, single glands were characterised for subtype and investigated for the expression of CD10 and CEP (Das1). CD10 showed increasing sensitivity for the detection of complete IM glands starting at 87.5% in IM-GC and reaching up to 100.0% in IM+GC patients. CD10 staining was also characterised by a decreasing specificity for complete IM glands starting at 100.0% in IM-GC down to 95.5% in IM+GC patients. The overall AUROC for CD10 diagnosis of complete IM glands across all three cohorts was 0.944, suggesting that CD10 is an outstanding biomarker (AUROC>0.9) for complete IM.

CEP detection by the Das1 antibody showed similar low sensitivity across all three cohorts (up to 32%) but did have high to very high specificity for incomplete IM glands, particularly in the IM-GC cohort (above 98%) which is clinically the most relevant. Its low sensitivity suggested that it is unlikely to be useful as a biomarker in a clinical setting on its own. Its overall AUROC across all three cohorts was relatively low at 0.603. However a logistic regression model combining CD10 and Das1 staining did show an overall improvement compared to CD10 on its own for complete IM glands. In this model Das1 was significantly associated in a negative manner with complete IM glands.

The suitability of CD10 as a biomarker for complete IM needs to be discussed in the overall context of IM subtyping and biomarker development. Traditionally IM subtyping is done using ABPAS and HID-AB staining but more recently this has been replaced with H&E staining [138], making it relatively more difficult as IM glands tend to exist in a clear polarised state (complete and incomplete IM) but occasionally also in a hybrid state (half complete/half incomplete IM gland, half gastric/half IM gland). Although superior in combination with ABPAS staining [522], HID-AB staining is not carried out anymore in most modern labs as the diamine salt used is toxic [523].

Subtyping of IM is determined qualitatively by a pathologist and this process is affected by both intra-observer and inter-observer variation [516]. Generally inter-observer agreement tends to be lower between general pathologists than between experienced gastrointestinal pathologists [105]. To some extent a precise definition and refined criteria can also reduce both intra- and inter-observer variations, as was shown recently by Kim et al 2018 [524] when grading extent of intestinal metaplasia. In that study, inter-observer agreement was improved significantly through the process of definition and grading consensus between 5 pathologists (baseline versus final: κ=0.56 versus κ=0.68, p=0.006). Overall intra-observer agreement was between good and excellent with κ=0.64-0.86.

Indeed this is where a simple IHC based biomarker such as CD10 can facilitate the process of IM subtyping and reduce intra- and inter-observer variability simultaneously. Its strength lies in its easy to assess negative versus positive staining status, its reproducibility and as a result its relatively reduced requirements of expertise as a general pathologist is likely to give a similar subtype as an experienced gastrointestinal pathologist. Used in combination with a pan-IM marker such as MUC2 which stains goblet cells, CD10 could be further developed into an automated diagnostic test for subtyping IM. Overall the clinical use of CD10 as part of the management guidelines for gastric premalignant lesions could lead to better patient

stratification with improved targeted surveillance of IM patients. Ultimately detection of neoplasia at its earliest possible time point, either in the form of high grade dysplasia or early gastric cancer (EGC) could lead to better quality of life for patients and reduced cost associated with GC treatment.

The relatively low AUROC of Das1 for incomplete IM glands in the current study suggests it would be only of limited use in a clinical setting. However a key inclusion criterion for this study was that subtyping would only involve the upper part of the IM gland which if positive for a brush border would be diagnosed as complete IM. This criterion was optimal for the CD10 part of the study. Subtyping of the lower part (base of) of the IM gland was not considered reliable as it is believed to contain the stem cell compartment and does not always express a brush border (personal discussion with in-house research pathologist Dr Catherine Mitchell prior to study, [514, 525]). Overall this inclusion criterion did not benefit the study of Das1 as a potential biomarker for incomplete IM glands as this antibody often stained the lower part of IM glands and less the upper part.

To investigate the utility of Das1 for identifying incomplete IM in a more optimal setting, multiple regions of interest per tissue sample available from the IM-GC and IM+GC cohorts were characterised using a digitally computer-assisted method [526, 527] to quantify staining in both upper and lower part of IM glands. Indeed Das1 stained significantly larger areas of IM glands in ROIs subtyped as incomplete IM than as complete IM in both cohorts. When analysed by whole section, Das1 staining was again shown to be more associated with incomplete IM in both the IM-GC and IM+GC cohorts thus confirming the findings of others [518, 528]. Finally Das1 was shown to have potential as a progression risk biomarker as IM+GC patients with complete IM showed significant more staining than IM-GC patients.

Previously, Forne et al 2009 [529] showed increased expression of Das1 in IM tissue from IM+GC patients compared to IM-GC patients ($p=0.004$) but concluded that its low presence in the latter excluded it from being useful in a clinical setting. Given that Das1 has been shown to stain both IM glands and adjacent matched gastric cancer tissues, this would suggest that IM glands with high Das1 staining are at the far end of the progression risk spectrum irrespective of subtype [518, 529, 530].

A biologically relevant question that arose during this study regarded the possible relationship between epithelial Das1 status and local immune cells. Das1 staining was mostly very low in complete IM but varied quantitatively in a highly localised manner in incomplete IM suggesting

that this marker was possibly identifying inter-glandular differences that could play an important role in the relationship between the epithelium and the immune microenvironment and its likelihood of progression to gastric cancer. In incomplete IM, Das1 positive staining had a weak positive correlation only with CD4 T cells in the IM-GC samples. By contrast when the relationship between macrophage subset densities and Das1 staining was analysed, a clear positive correlation with both CD68+IRF8+ (M1) and CD68+CD163+IRF8+ (M1/2) subsets was observed.

In Chapter 5, detailed characterisation of the macrophage landscape had shown M2 subsets likely offer the highest level of protection against progression (higher in complete IM) and M1/2 subsets likely offer the lowest level of protection (higher in incomplete IM). Interestingly macrophages positive for CD163 have been previously shown to promote progression to spasmolytic polypeptide expressing metaplasia (SPEM) [207]. Additionally IRF8 expression is induced by IFNγ, which was shown in a transgenic mouse model (expression of IFNγ under the control of the stomach specific H+/K+ ATPase β promoter) to have the capacity to also lead to SPEM and then to dysplasia [531]. Thus it is likely that a local intestinal metaplastic microenvironment with prominent inflammation due at least in part to IFNγ might lead to a higher risk of progression. Further investigation will be required to determine proliferation and apoptosis rates as well as overall levels of genetic instability of epithelial cells positive for Das1.

7.4.2 Technical limitations

This study included a targeted single gland approach to determine the suitability of CD10 and Das1 as biomarkers for subtyping IM. A detailed analysis of Das1 staining on IM tissue from all IM-GC and IM+GC patients previously characterised in Chapters 5 and 6 was also carried out. However the current study did have a small number of potential limitations including:

a) A limited number of tissue samples with appropriate gland orientation from patients across three different cohorts thus introducing patient bias when analysing data by cohort. However this “weakness” was counterbalanced to some extent by the similarity in sensitivity and specificity observed for both markers across cohorts. Overall the “all cohort” analyses provided the most likely accurate results, originating from a total of 18 tissue samples with 215 and 223 individual glands subtyped and scored for CD10 and Das1 staining respectively.

b) The use of the top part of IM glands for characterisation had an important effect on the Das1 single gland assessment as a biomarker for incomplete IM. To adjust for this, analyses by ROI and by whole tissue section were carried out which also allowed for an expanded use of patient

samples. It is important to note that the identification of individual IM glands is much easier at the upper part than at the bottom part as these are often pushed together which makes it rather difficult to assess whether individual glands are being viewed or a single gland with multiple bases.

Overall single gland analysis of CD10 staining showed it has the potential to be an outstanding biomarker for the complete subtype of IM. This biomarker could be used to facilitate patient stratification and improve targeted surveillance. By contrast the Das1 antibody did not seem to have a high enough sensitivity for incomplete IM on a single gland level to be considered a reliable biomarker, at least not in the current setting with the use of only the upper part of the gland as an inclusion criterion. However Das1 was shown to be significantly associated with incomplete IM on a whole section level with the added potential of detecting high risk IM lesions irrespective of subtype.

The Das1 antibody was recently cross-validated as a biomarker in a multi-centre study to identify high risk mucinous pancreatic cystic lesions with relatively high sensitivity and specificity (88% and 99% respectively with AUC=0.965, [532]) thus further investigation within the field of gastric precancerous IM lesions might help determine its optimal use in a clinical setting. An association between Das1 positive incomplete IM glands and IRF8+ macrophages was also reported, suggesting a possible role of epithelial-macrophage crosstalk in progression to GC.

Chapter 8 Developing an intestinal metaplasia organoid model

8.1 Introduction

Gastric carcinogenesis is a process that occurs in an environment of persistent inflammation, mainly triggered by *H. pylori* infection, over a long period of time. This may be driven by a number of initiating factors including EBV infection or other environmental factors such as smoking and high salt diet [42, 283-285, 533-535]. The previous chapters in this thesis provided evidence to suggest that changes not only to the genomic profile of epithelial cells but also to the immune microenvironment likely play a key role in progression to gastric cancer. In order to prove causality it is necessary to have appropriate systems in place to model the disease process. The GC animal models described in section §1.6 have been used to characterise multiple aspects of this but so far no animal model has managed to fully replicate human intestinal metaplasia (IM) and define its role in gastric carcinogenesis.

The Cdx1 and Cdx2 transgenic mice previously described (§1.6.2, [154, 322]) replicate histologically human IM but showed a significant key molecular difference. The Cdx2 mice described by Mutoh et al 2002 [154] did not express Cdx1 and the Cdx1 mice described by Mutoh et al 2004 [322] did not express Cdx2, both of which are key markers of human IM [324, 536-538]. However the Cdx2 mice did progress to GC over a period of 100 weeks [306]. Overall, animal models have greatly enriched our understanding of some of the molecular mechanisms in GC (critically reviewed in [287, 539]) but they are generally associated with long term duration and high cost.

Since 2000, three dimensional (3D) cell culture models termed organoids have gained considerable popularity with the number of yearly publications indexed in Pubmed increasing from approximately 50 (2000) to over 1000 in 2015 [540]. Some of the advantages associated with organoids include their ability to replicate the cellular complexity and physiology of the tissue of origin, their genetic stability with time, the relatively ease of manipulation and their long-term growth capacity [360, 361, 363, 541]. However certain disadvantages have also been reported which are mainly associated with reproducibility, culture heterogeneity, the contamination of target cells for example tumour cells with normal cells and the absence of stromal and immune cells in culture such as fibroblasts and T cells [363, 542].

Although detailed protocols describing the derivation and growth of both normal and tumour gastrointestinal organoids from human tissue have been published [365, 370, 541, 543, 544] no defined methodology for growing organoids from gastric intestinal metaplastic tissue has been

described to date. The development of an IM organoid model is challenging and would have to address and overcome fundamental issues related to the isolation of intestinal-like glands/cells from gastric mucosal tissue, the growth of IM organoids in a background rich in contaminating normal gastric organoids and the identification of optimal growth and differentiation conditions. An IM organoid model could be used to study the key genomic and epigenetic changes required for gastric carcinogenesis, IM subtype transition from the complete to the incomplete subtype and its association with greater risk of progression as well as the role of immune cells in malignant transformation.

8.2 Aims

The overall objective of this study was to develop an IM organoid model. The study's main aims were:

1. To establish protocols for the derivation of gastrointestinal organoid cultures from human biopsies with long term growth capacity.
2. To develop methods for the characterisation of IM organoids.
3. To characterise gastrointestinal organoids, including IM organoids, using IHC and quantify expression levels of key gastrointestinal genes.
4. To investigate the role of niche growth factors medium on gastrointestinal organoid proliferation and differentiation.
5. To enrich for IM organoids by using an intestinal stem cell marker and Fluorescence-Activated Cell Sorting (FACS).
6. To create a human gastrointestinal organoid biobank.

8.3 Results

8.3.1 Clinical details of patient samples

Patient samples were acquired as part of the ongoing screening and surveillance program (S2P) established by our laboratory (see §2.2.2) and used to set up organoid cultures as described in section §2.7.1. Overall, tissue samples from 27 consenting participants (15 males and 12 females) were obtained for this study (Table 8.1). Figure 8.1 shows an overview of the key aspects of this project.

Table 8.1 Clinical details of patient cohort used for gastrointestinal organoid study

Patient and biopsy characteristics	Patients (n)
Gender	
Male	15
Female	12
Age	
Male	70 (28-85)[1]
Female	63 (41-82)[1]
Fresh biopsies for organoids	
Pilot study[2]	
Gastric	
without IM	4
targeting IM	8
with dysplasia	4
Small intestine	3
Main study[3]	
Gastric	
unspecified targeting IM	10
antrum without IM	6
antrum targeting IM	15
body targeting IM	10
Small intestine	22

[1]Median age and range; [2]Pilot study used mainly single biopsies to try and establish organoid cultures; [3]Main study used pooled biopsies (3-5) to establish organoid cultures. Targeting of IM tissue was done during gastroscopy by gastroenterologist AB.

8.3.2 Pilot study to determine feasibility of project

The feasibility of gastroscopy biopsies to establish organoid cultures was first assessed by carrying out a pilot study. Sixteen gastric and 3 small intestinal samples from 6 patients were utilised, initially with single biopsies (first 4 patients) and then with pooled biopsies from the last 2 patients as starting material. Tissue was collected in cold basal medium (section §2.7.1) and processed the same day or within 24hrs. To isolate the glands/stem cells from the gastric mucosa, the tissue was minced using 2 scalpel blades followed by use of the enzyme digestion method which consisted of an incubation step at 37^{o}C in a solution containing Collagenase IV (75U/ml), Dispase (125µg/ml), Hyaluronidase (20µg/ml) and DNAse I (0.1µg/ml) as described in section §2.7.1. After filtration through a 70µm filter, single or clumps of cells were mixed with matrigel, plated and organoid growth medium (OGM) was added, to allow colony formation and growth. Based on growth media previously used to grow normal gastric and Barrett's oesophagus epithelial organoids [365, 366], OGM was freshly made weekly and contained in-house produced conditioned media of Noggin, Wnt3A and R-Spondin 1 (§2.7.12, Table 2.10).

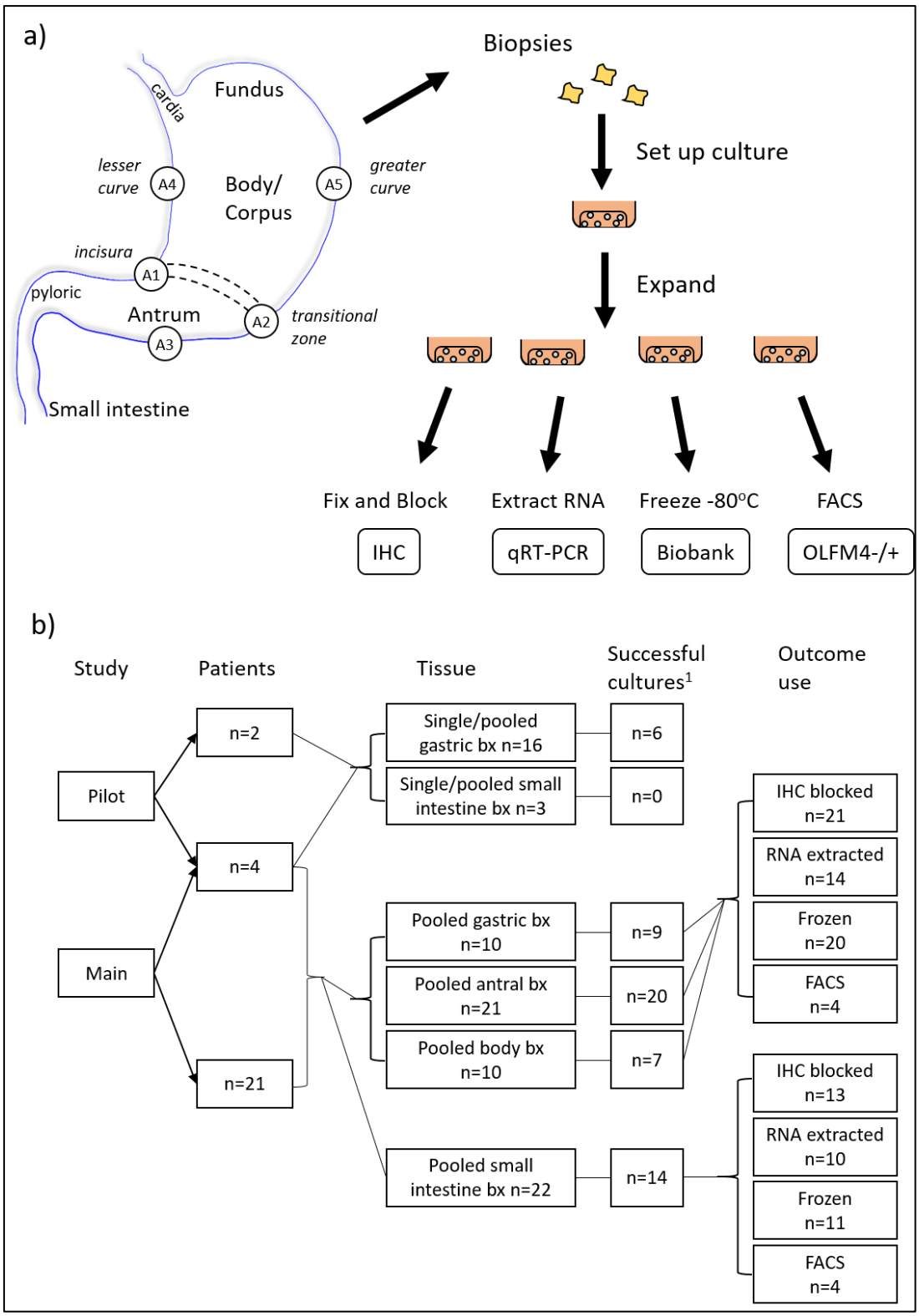


Figure 8.1 Schematic representation including tissue details of workflow for establishing, growing and characterising gastrointestinal organoids

[1]Defined by organoid formation and growth for more than 7 days; a) shows general workflow for gastric and small intestinal tissue used for establishing, growing and characterising organoids and b) shows patient numbers, tissue details with single and pooled biopsies used as starting material for the pilot and main studies and outcome uses. Biopsies collected using the updated Sydney protocol with A1-A3 including the incisura considered as antrum and A4-A5 considered as body.

To assess overall tissue viability and colony formation/growth, a broad range of samples were used in these initial experiments including normal gastric tissue, targeted IM tissue, dysplastic tissue and duodenal tissue (Figure 8.2). Cultures were expanded using a mixture of physical and enzymatic (with recombinant TrypLE™ enzyme) passaging methods. Although organoids grew well in a small number of cases (Figure 8.3), overall the yield, size and longevity of the established cultures was low and numbers were insufficient for any downstream applications, including characterisation. This suggested that protocols were not optimal.

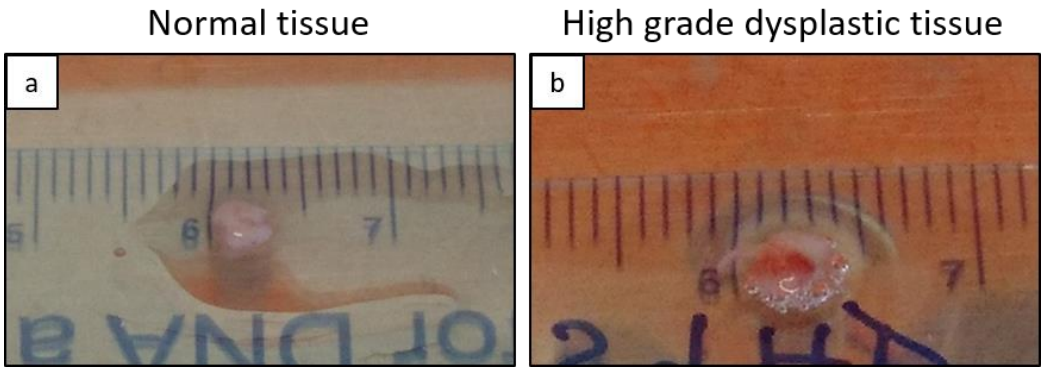


Figure 8.2 Human tissue samples used to set up organoid cultures
Examples of normal (a) and high grade dysplastic (b) tissue used from two separate patients in the pilot study to set up initial organoid cultures.



Figure 8.3 Human organoids grow successfully from a single gastric biopsy but have limited longevity
Organoid cultures established from a single patient biopsy (grew up to ~35 days). Scale bar: 400µm.

8.3.3 Establishing parameters for growing organoids using a porcine model

In order to further optimise organoid establishment conditions a porcine model was employed. This had the advantage of providing significant amounts of starting material for troubleshooting issues that could not be solved with the highly valuable, but limited in availability, human tissue. Additionally the domestic pig shares many similarities genetically, anatomically and physiologically with humans thus making it an excellent model for study. Porcine tissue from stomach, small intestine and colon was obtained from the Diamond Valley Pork abattoir in Laverton and stored in freezing media at -80°C in 1cm^2 sized pieces.

Porcine organoids grew from gastric, small intestine and colon tissue types although the latter was less efficient (only a small number of organoids grew long term) (Figure 8.4). The abundant amount of starting material allowed multiple combinations of isolation methods and growth media to be investigated so that optimal growth and culture conditions could be determined (Table 8.2). Two different isolation methods were trialled, the enzyme digestion method and the chelation buffer method that uses EDTA and physical pressure on the tissue to release glands/crypts (detailed description in §2.7.1, [366, 370]). Gastric and small intestine organoids successfully formed using either isolation method, but the latter in combination with the chelation buffer method were somewhat less efficient (Figures 8.5). Colon organoids did not grow well using either isolation method with only a small number of organoids growing long term.

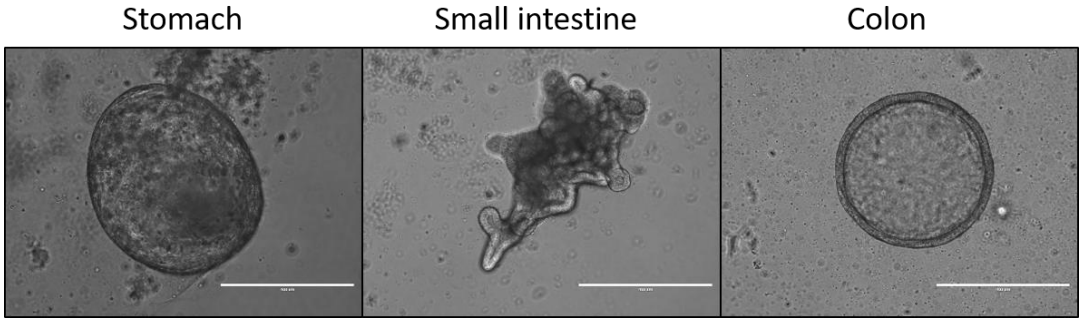


Figure 8.4 Gastric, small intestine and colon organoids grow from porcine tissue
Images of porcine gastric organoid shown from day 18, small intestinal organoid from day 11 and colon organoid from day 17. Scale bar: 400µm.

Table 8.2 Isolation methods and growth media used to identify optimal conditions for establishing and growing porcine organoids

Tissue	Isolation method	Growth medium	
		WRNEFGSTNi[1]	WRNE_GSTNi[2]
Stomach	Enzyme digestion	✓	✓
	Chelation buffer	✓	✓
Small intestine	Enzyme digestion	✓	✓
	Chelation buffer	✓	✓
Colon	Enzyme digestion	✓	✓
	Chelation buffer	✓	✓

[1]The organoid growth medium (OGM) used with in-house produced Wnt3A, RSpondin-1 and Noggin conditioned media as described in Table 2.5; [2]OGM without FGF10, a gastric niche factor, but with N2 supplement added, previously used to grow intestinal and Barrett's epithelium organoids [365]. See text for more details.

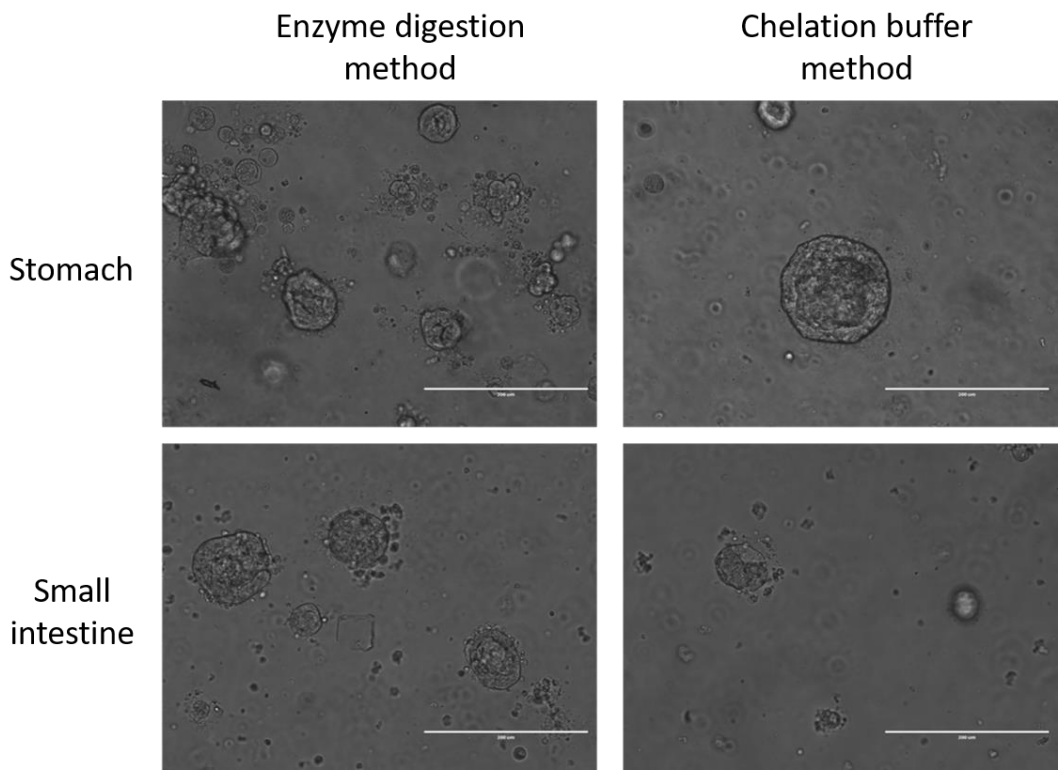


Figure 8.5 Early porcine organoid cultures (day 6) grown from gastric and small intestinal tissue using both the enzyme digestion and the chelation buffer isolation methods
Organoid cultures established from gastric and small intestine porcine tissue on day 6 using either the enzyme digestion method or the chelation buffer method. Scale bar: 200µm.

The role of FGF10 in the organoid growth medium, a niche factor previously shown to play an important role in growing long term human gastric and Barrett's epithelium organoids, [365, 366] was also explored. Gastric and small intestine organoids successfully formed both in the presence and absence of FGF10 but overall, small intestine organoids were slower to form compared to gastric organoids (Figure 8.6). Colon organoids did not grow well using either growth media.

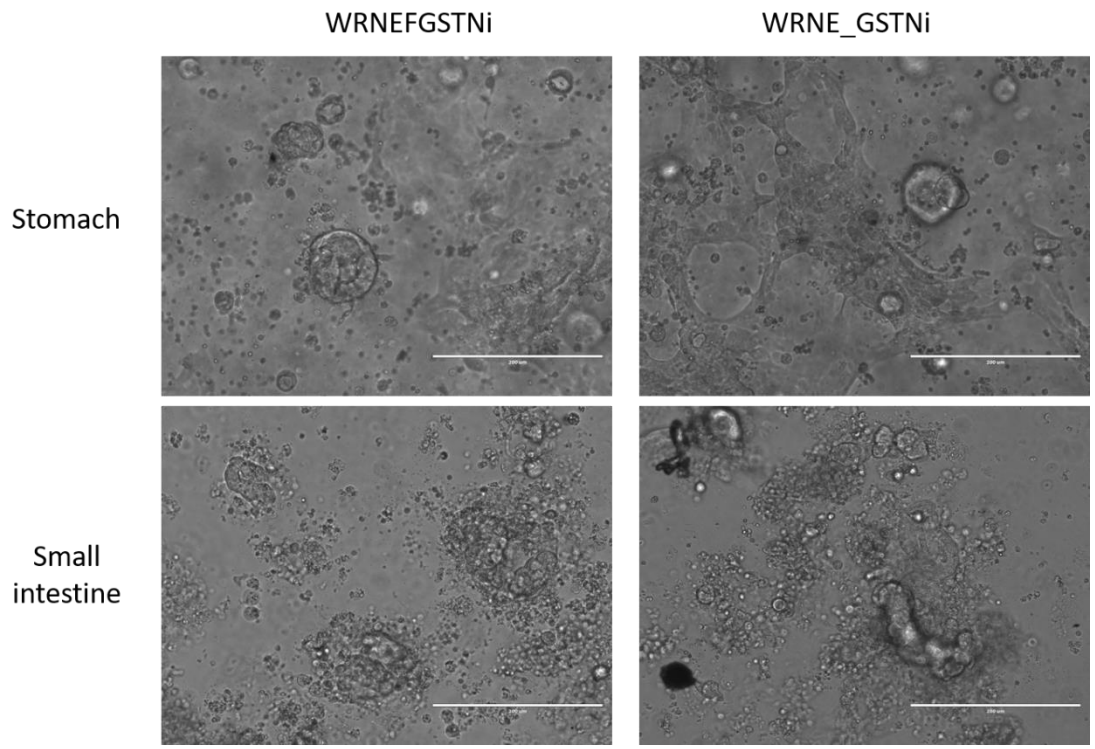


Figure 8.6 Early porcine organoid cultures (day 4) derived from gastric and small intestinal tissue in the presence and absence of FGF10 in the growth medium
Organoid cultures grown from gastric and small intestine porcine tissue on day 4 in organoid growth medium (OGM) with FGF10 (WRNEFGSTNi) and without FGF10 (WRNE_GSTNi). OGM consisted of WRNEFGSTNi where W=Wnt3A, R=RSpondin-1, N=Noggin, E=human EGF, F=FGF10, G=gastrin, S=p38 MAPK inhibitor SB202190, T=TGFβ inhibitor A-83-01, Ni=nicotinamide. Scale bar: 200µm.

Overall, these experiments suggested that with the use of adequate amount of starting material, porcine gastric and small intestine organoid cultures grew successfully, irrespective of isolation method and the presence or absence of FGF10. Thus to address the possible role of starting material on colony formation and growth, differing amounts of previously cryopreserved porcine small intestinal tissue were cut into biopsy size pieces (estimated size ~0.1cm^2) and used to replicate the technical limitations associated with setting up organoid cultures from single human biopsies (Figure 8.7). The use of a single piece of tissue yielded limited success, the combining of 2-3 pieces of tissue produced small numbers of viable organoid cultures and four to five tissue pieces gave excellent organoid formation and growth.

Lastly the viability of reanimating previously cryopreserved porcine organoids which were stored at -80°C (see sections §2.7.6-7 for complete details) was assessed using small intestinal organoids. Organoids cultures started to grow within 1-2 days after resuspension and fresh plating with matrigel (§2.7.1), and grew at least for 14 days after which the experiment was terminated (Figure 8.8).

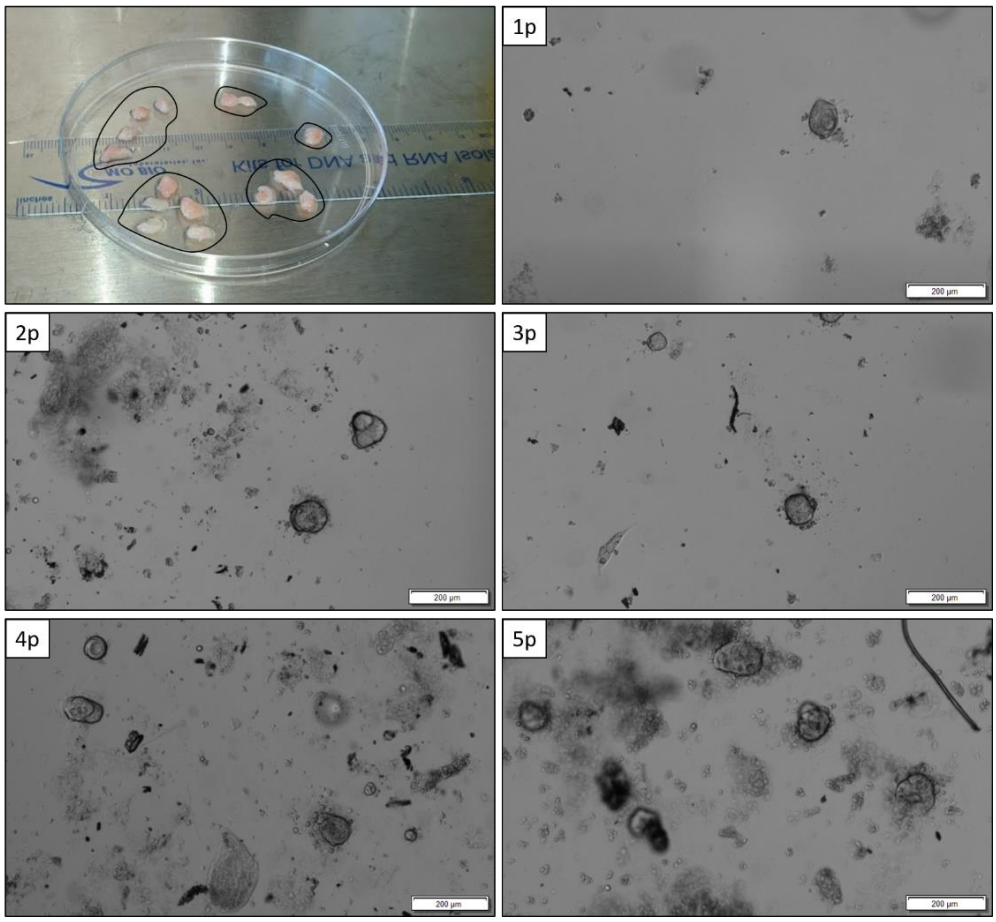


Figure 8.7 Effect of starting amount of tissue in organoid colony formation and growth (day 6) Previously cryopreserved small intestinal tissue was used to set up organoid cultures with differing amount of starting material to replicate the amount of human tissue obtained during collection at endoscopy (1 piece, 2 pieces, 3 pieces, 4 pieces and 5 pieces). Scale bar: 200µm.

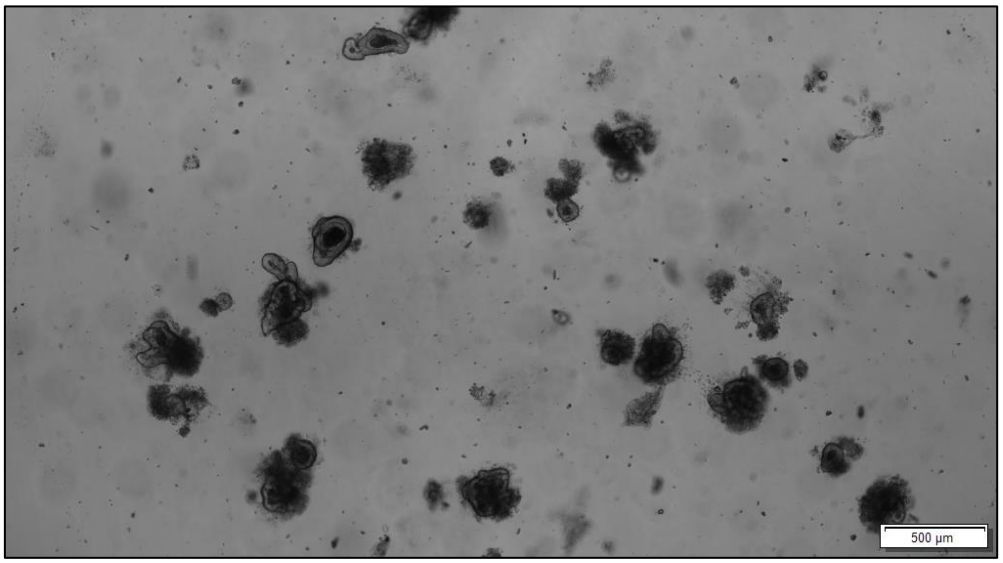


Figure 8.8 Porcine organoids grow from previously frozen small intestinal organoid cultures Previously frozen small intestinal organoid cultures were thawed and used to established new cultures (day 2). Scale bar: 500µm.

8.3.4 Growing human gastrointestinal organoids

Having determined the requirements for sufficient starting material, an adapted protocol was used to establish human organoid cultures. Multiple biopsies (2-4) from the whole stomach or from a single anatomical region of a patient (antrum or body) were pooled together and processed using the chelation buffer method for gastric tissue and a modified protocol that uses repeated vigorous pipetting to release crypts as described by Fujii et al 2015 [397] for small intestinal tissue (§2.7.1). The chelation buffer method, used to grow normal human gastric organoids [366, 370, 545] was preferred over the enzyme digestion method, which is often used to grow gastric tumour organoids [541, 543], as the latter could not be further optimised for use in this study with human non-malignant biopsies. For the small intestine a combination of vigorous pipetting together with a low concentration of EDTA (2.5mM) was used to release the intestinal crypts before plating (§2.7.1, [397, 546].

Gastrointestinal organoids began to form within hours of plating and were, in most cases, grown for a total of 3 to 4 months with a maximum of 6 months before being frozen down (Figure 8.9). Initially OGM was used but this was superseded by the commercially available IntestiCult™ organoid growth medium (STEMCELL Technologies) which gave better colony formation, growth and proliferation results.

8.3.5 Establishing parameters for characterising organoids using the porcine model

Having established working protocols for the establishment of human organoid cultures from both gastric and small intestinal biopsies, porcine tissue was used to establish methods for downstream characterisation. The relationship between organoid number input and RNA yield was investigated. Different numbers of actively growing small intestinal organoids (size range: 200µm-400µm) were lysed and the amount of RNA extracted was quantified (NanoDrop™ 2000, Thermo Scientific™). The amount of RNA extracted was directly proportional to the number of actively growing organoids, and the numbers suggested that to extract sufficient RNA for downstream applications such as quantitative Real Time PCR (qRT-PCR; ~1µg) large numbers of organoids from multiple wells would be required (Figure 8.10).

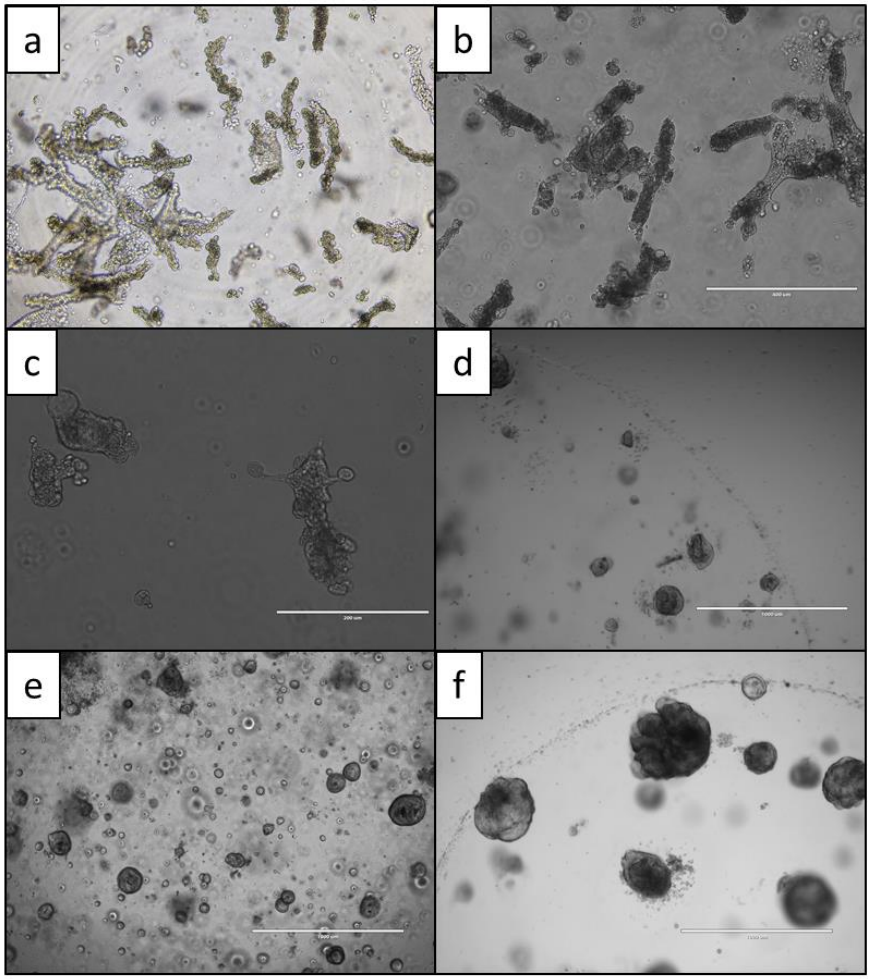


Figure 8.9 Chelation buffer method for organoid derivation from human pooled gastric biopsies

a) the biopsy tissue is washed repeatedly, incubated with a chelating buffer containing 10mM EDTA and whole gastric glands are physically released by applying gentle pressure with a glass slide; b) and c) enclosed glandular structures and initiation of organoid formation occurs within hours of plating; organoids are expanded by trypsinisation using TrypLE™, shown at day 7 (d) and day 31 (e) post passage respectively; f) gastric organoids grow larger mostly with loss of spheroid shape with time (day 60). Scale bars: b) 400µm, c) 200µm, d), e) and f) 1000µm.

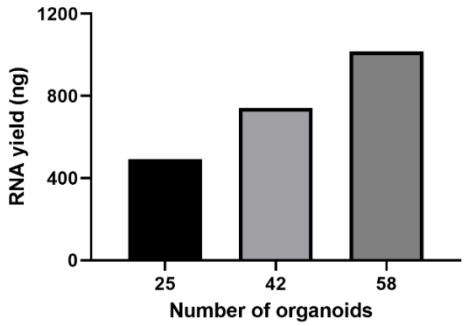


Figure 8.10 RNA yield is proportional to the starting number of actively growing porcine organoids

RNA extracted using Qiagen's RNeasy Mini Kit and quantified using NanoDrop™ (Thermo Scientific™). Organoids were manually counted prior to extraction, all of which were in the size range of 200µm-400µm.

Next, a protocol was developed to prepare formalin fixed paraffin embedded blocks from organoids for downstream immunohistochemistry (IHC). Organoids were liberated from matrigel, fixed in 4% paraformaldehyde and suspended in histogel to maintain structure. They were then embedded in paraffin (see §2.7.11 for complete description). The ability of the blocking method to retain structure and cellular integrity was tested by performing IHC for CDX2. Porcine CDX2 protein has a 96.2% homology to human CDX2 [547] and initial staining with anti-CDX2 antibody showed high levels of expression in porcine small intestinal organoids (Figure 8.11). CD10 expression at the luminal side of an organoid (inner side) was also detected, suggesting the presence of a brush border (Figure 8.11). However not all porcine derived small intestinal organoids expressed CD10.

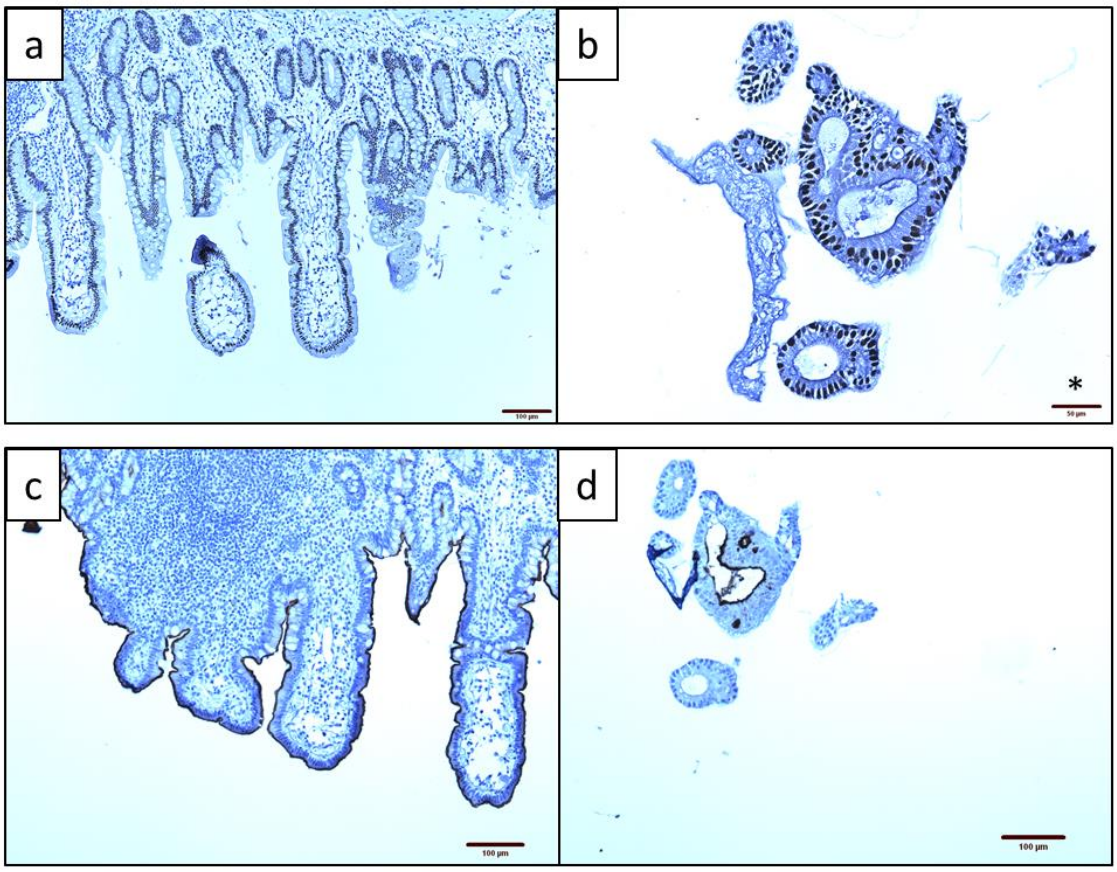


Figure 8.11 Porcine small intestinal organoids stain positive with anti-CDX2 and anti-CD10 antibodies
Images a) and b) show human small intestine and porcine small intestinal organoids stained with anti-CDX2 antibody. Images c) and d) show human small intestine and porcine small intestinal organoids stained with anti-CD10 antibody. Scale bars: *50 µm and 100µm.

8.3.6 Characterising human gastrointestinal organoids by morphology and immunohistochemistry

Despite the distinct appearances of porcine gastric (transparent spheroidal) and small intestinal (budding shapes) organoids, this phenomenon was not replicated in the human setting and the

two types were unable to be distinguished phenotypically. Although human gastric (both antral and body) organoids were predominantly transparent spheroids and human small intestinal tissues tended to have a more opaque and folded shape, there was too much morphological overlap to distinguish them (Figure 8.12). As a consequence using morphology alone would not allow the identification of intestinal metaplastic ("small intestinal-like") organoids in an organoid culture grown from gastric tissue.

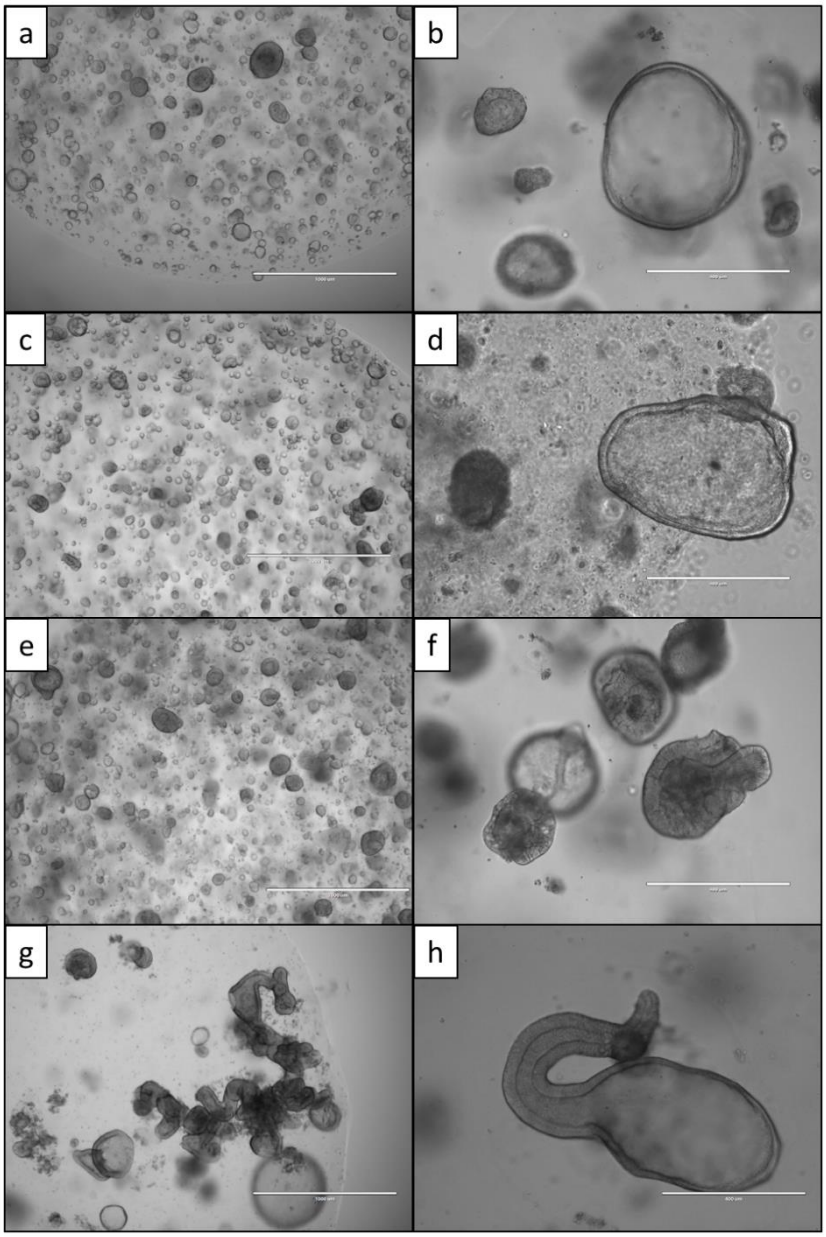


Figure 8.12 Morphology does not allow differentiation between human gastric and small intestinal organoids

Antral (a and b) and body (c and d) organoids tended to have translucent spheroidal shapes but folded opaque organoids were also present. Small intestinal (e and f) organoid populations were enriched for the latter but contained substantial numbers of the former as well. Occasionally, in a small number of patients, certain gastric organoids had "unusual" shapes (g and h). Scale bars for a, c, e and g: 1000µm and scale bars for b, d, f and h: 400µm.

Since morphology was not a suitable method of identifying IM organoids the next logical approach was to develop an IHC method that could be used to sample a population and reliably differentiate between organoids of gastric and intestinal metaplasia origin. A set of antibodies specific for certain gastrointestinal cell types were identified (MUC5AC for gastric surface mucous cells, MUC6 for gastric neck mucous cells, CDX2 for small intestinal epithelial cells, TFF3 for goblet cells and CD10 for brush border) and optimised for IHC on human tissue and organoid FFPE sections (Appendix L and Figure 8.13). MUC5AC and CDX2 were defined as core markers for identifying and differentiating normal gastric (MUC5AC+ and CDX2-) and normal small intestine (MUC5AC- and CDX2+) organoids based on their known expression in tissue.

Initial staining showed that normal gastric organoids expressed high levels of MUC5AC, particularly at the luminal surface (Figure 8.14). Interestingly some individual cells in small intestinal organoids also expressed this marker even though it is normally not found in the small intestine (Figure 8.14). Most but not all cells of small intestinal organoids were positive for CDX2 and all cells of normal gastric organoids were negative for CDX2.

Staining with MUC5AC and CDX2 on all available FFPE blocked gastric organoids from patients in the main study (n=20, Appendix M) revealed 6 cases with cultures that contained CDX2+ organoids (2x gastric unspecified location, 3x antral and 1x incisura). CDX2 staining was patchy but organoids with greater than 50% cells staining positive were considered to be of IM origin (Figure 8.15). Further characterisation using IHC showed that these IM organoids were also predominantly MUC5AC+ and TFF3+, lacked complete goblet cell formation (assessed visually on H&E and ABPAS stained sections) and were mainly CD10- (Figure 8.16). Their staining pattern was not always the same as matched IM tissue from the same patient (Figure 8.16). Overall these findings suggested that the current isolation and growth conditions allowed IM organoid growth, but only with limited differentiation.

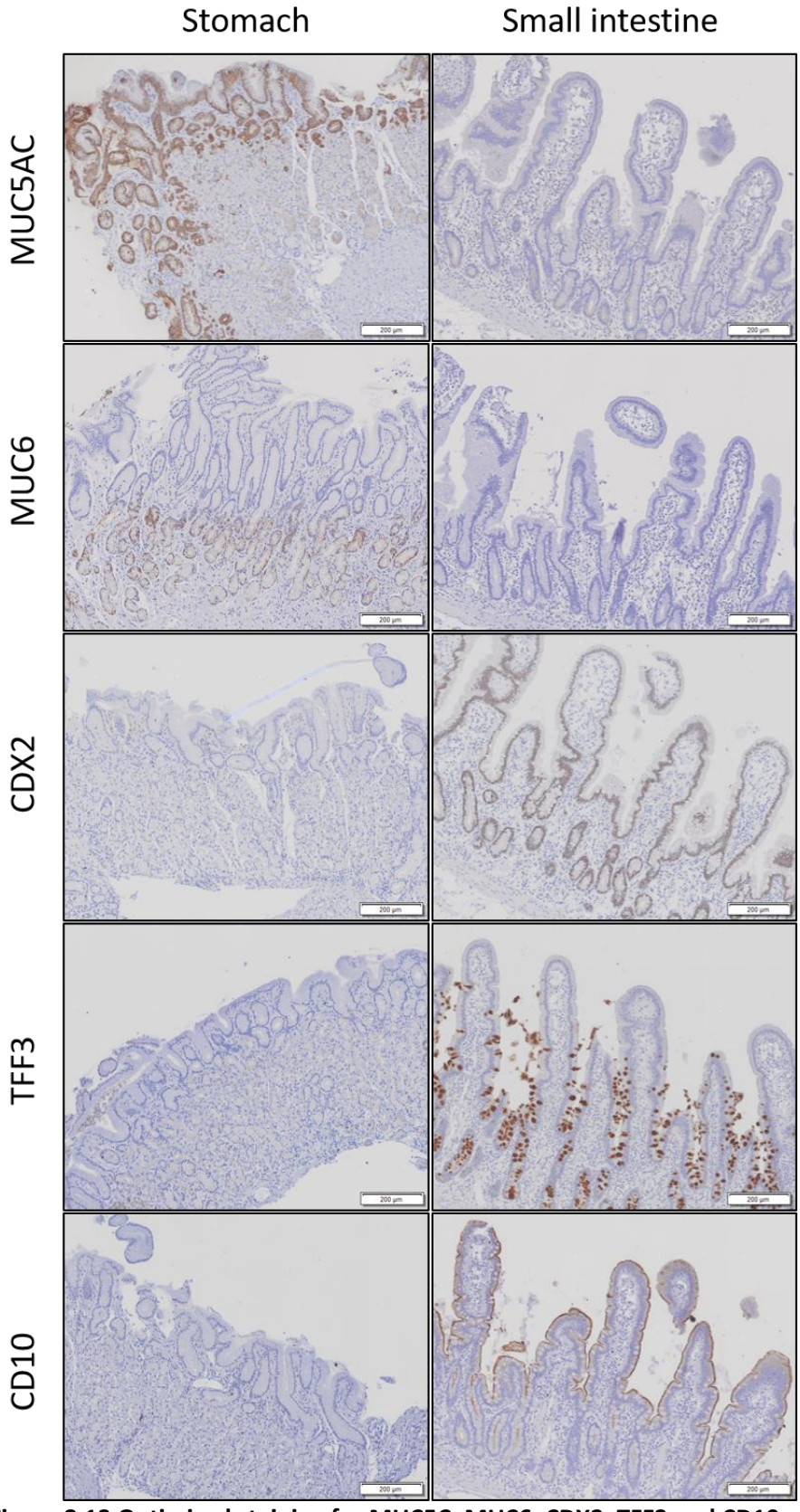


Figure 8.13 Optimised staining for MUC5C, MUC6, CDX2, TFF3 and CD10 antibodies on gastric and small intestinal tissue

Images of optimised antibody staining conditions for anti-MUC5AC (gastric surface mucous cells), anti-MUC6 (gastric neck mucous cells), anti-CDX2 (small intestinal epithelial cells), anti-TFF3 (goblet cells) and anti-CD10 (brush border). Scale bar: 200µm.

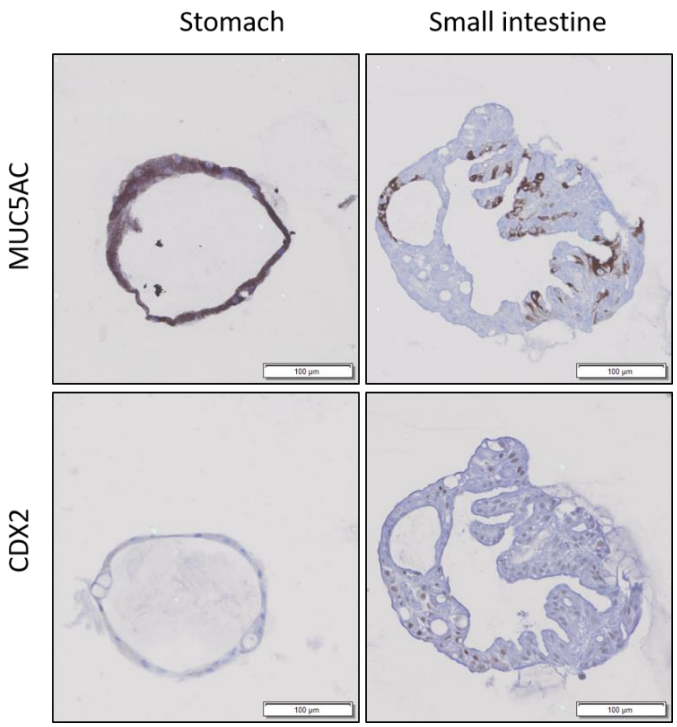


Figure 8.14 MUC5AC and CDX2 staining of gastric and small intestinal organoids
Gastric organoids were positive for MUC5AC but negative for CDX2. Small intestinal organoids were mainly CDX2 positive with occasional cells positive also for MUC5AC. Scale bar: 100µm.

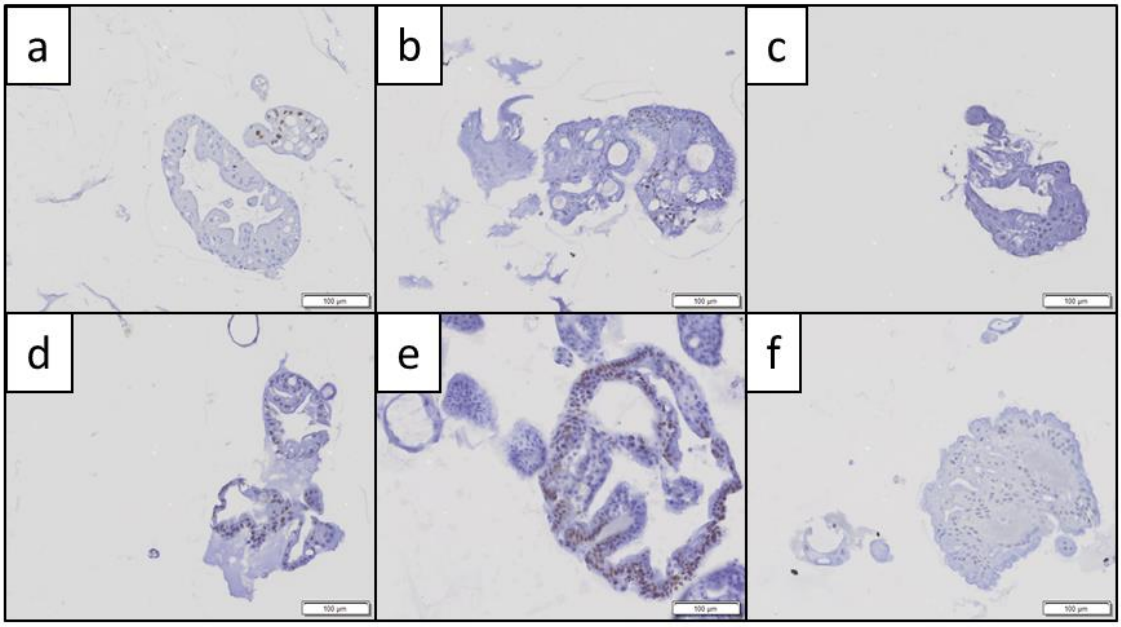


Figure 8.15 Identification of gastric derived intestinal metaplasia organoids using CDX2 staining
a) and b) CDX2 staining of organoids derived from gastric biopsies targeting IM from patients G4 and G5 respectively; c), d) and e) CDX2 staining of organoid cultures grown from antral biopsies targeting IM from patients G10, G15 and G25 respectively; f) CDX2 staining of organoids grown from incisura biopsies targeting IM from patients G24. Overall levels of CDX2 expression varied between organoids from the same patient and between cells within a single organoid. See Appendix M for details of patient samples. Scale bar: 100µm.

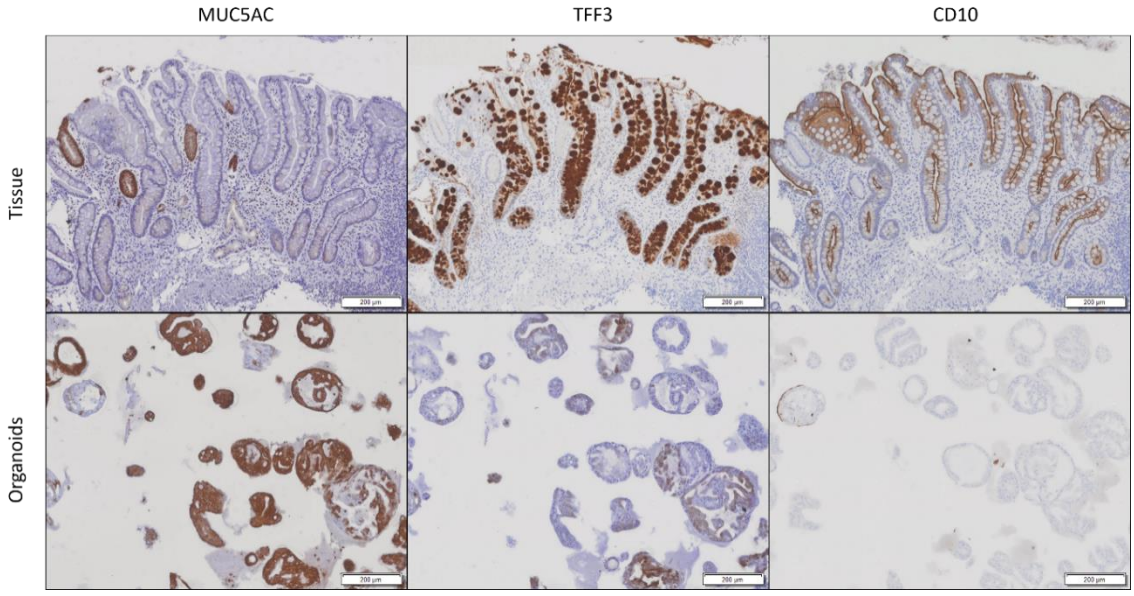


Figure 8.16 Intestinal metaplastic organoids do not fully replicate expression pattern for MUC5AC, TFF3 and CD10 markers on tissue of origin in patient G25
Matched tissue sample from patient G25 does not express MUC5AC unlike the majority of IM organoids, does express TFF3 which is only partially expressed on IM organoids without full formation of goblet cells and also expresses CD10 which is rarely present on IM organoids (top left organoid is positive for CD10). Scale bar: 200µm.

8.3.7 Characterising gastrointestinal organoids using quantitative Real Time PCR

To further characterise gastrointestinal organoids, RNA extraction followed by qRT-PCR was carried out on a subset of samples with available IHC data. Antral and body organoid populations grown in IntestiCult™, previously shown to be CDX2- by IHC and defined as normal gastric organoids, were screened for TFF1 (marker for gastric surface mucous cells), TFF2 (marker for gastric neck mucous cells) and VIL1 (marker for small intestinal brush border) expression (Figure 8.17). As a control small intestinal organoids from the same patient were used. Both antral and body organoids expressed TFF1 and TFF2 but lacked VIL1 expression. By contrast, small intestinal organoids expressed no TFF1 and TFF2 but a considerable amount of VIL1 as expected.

To determine whether IM organoids could be identified using qRT-PCR and validate the previous IHC findings, clonal body organoids and antral organoids both previously shown to be CDX2- (IHC) were compared with an antral organoid culture that predominantly contained CDX2+ organoids (IHC) (patient G15, Figure 8.15d) and a small intestine culture as a control (Figure 8.18). The cloning of organoids involved physically picking a single organoid with a pipette tip within a sterile environment, breaking it into fragments and expanding the resulting fragments into long term organoid cultures and served here as an additional control for qRT-PCR. As an additional method organoid cloning was developed so that individual organoids of interest could be expanded and investigated, including possible IM organoids.

Overall the three body clonal populations derived from three independent organoids from patient G8 showed a very similar expression profile: low in TFF1, high in TFF2, no VIL1 or CDX2 (Figure 8.18). The two antral populations from patients G9 and G23 also showed a high degree of similarity: high in TFF1 and TFF2, very low in VIL1 and CDX2 virtually absent. Finally the previously defined IM organoid culture using IHC from patient G15 differed considerably from the other antral cultures and was more similar to the small intestinal control: low in TFF1 and TFF2, high in VIL1 with some CDX2 expression (Figure 8.18).

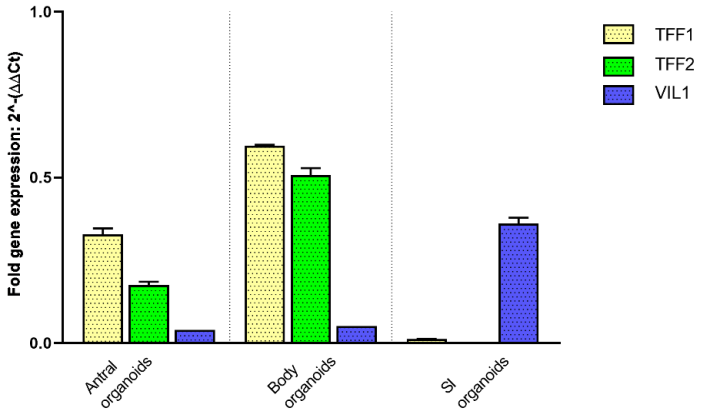


Figure 8.17 Antral, body and small intestinal (SI) organoids characterised for expression of TFF1, TFF2 and VIL1 using qRT-PCR
Gastric markers (TFF1 and TFF2 were normalised to expression in gastric tissue control and SI marker (VIL1) was normalised to a small intestine tissue control. All organoid cultures were from the same patient and grown in IntestiCult™. Mean with + SD shown from three technical replicates of a single experiment.

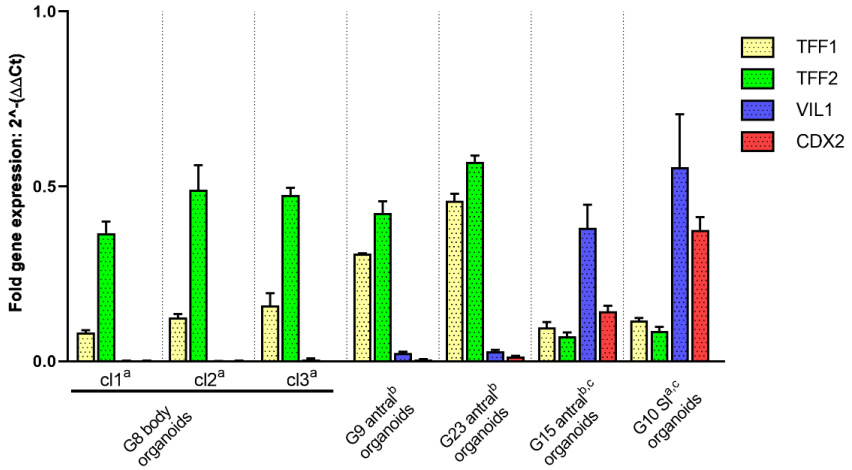


Figure 8.18 Characterisation of clonal body, antral and small intestinal (SI) organoids for expression of TFF1, TFF2, VIL1 and CDX2
[a]Organoid cultures grown in OGM; [b]Organoid cultures grown in IntestiCult™; [c]Cultures previously shown to contain CDX2+ organoids using IHC, all other cultures were CDX2- by IHC. Clonal organoid cultures were created by physically picking a single organoid with a pipette tip within a sterile environment, breaking it into fragments and expanding the resulting fragments into long term organoid cultures. Mean with + SD shown from three technical replicates of a single experiment.

8.3.8 Investigating the role of niche factors in gastrointestinal organoid proliferation and differentiation

A series of three experimental approaches (Table 8.3) were taken to investigate the role of niche factors in (i) gastrointestinal organoid proliferation and differentiation and (ii) their ability to selectively enrich for IM organoids in a population derived from gastric tissue. These experiments involved manipulating the culture media and conditions under which the organoids were maintained and were based on published and optimised protocols which describe the differentiation of gastrointestinal epithelial organoids [365, 366].

For all experiments small intestinal organoids were used as a positive control for IM organoids. This was based on the assumption that growth conditions giving small intestinal organoids a proliferative advantage over gastric organoids could be used to enrich cultures for IM organoids. In addition these experiments could provide additional insight into the optimal conditions for IM organoid differentiation (Table 8.3).

Table 8.3 Experimental plan to investigate the effect of niche factors on the proliferation and differentiation of gastrointestinal organoids

	Experiment 1	Experiment 2	Experiment 3
Objective	Short term effect of niche factors on differentiation	Long term effect of niche factors on proliferation and differentiation	Short term effect of changes to IC on differentiation
Tissue of origin	-Antrum -Small intestine	-Antrum -Body -Small intestine	-Antrum -Small intestine
Growth media	• IC[1] • WRNEFGSTNi[2] • _RNEFGSTNi • WRNEFGST_ • WRNEFG_TNi • WRNEFG_T_	• IC[1] • WRNEFGSTNi[2] • _RNEFGSTNi • WRNE_GSTNi • WRNEF_STNi • _RNE_GSTNi • _RNEF_STNi • WRNE__STNi • _RNE__STNi	• IC[1] • IC[A][3]
Duration	6 days	34-45 days	11 days

[1]IC: IntestiCult™ consisting of human components A and B; [2]Organoid growth medium OGM was made up from WRNEFGSTNi where W=Wnt3A, R=R-Spondin 1, N=Noggin, E=human EGF, F=FGF10, G=gastrin, S= p38 MAPK inhibitor SB202190, T= TGFβ inhibitor A-83-01, Ni=nicotinamide; [3]IntestiCult™ consisting of only human component A.

The first set of experiments aimed to determine the effects of growth media components on organoid differentiation. Cultures were initially grown and expanded in IntestiCult™ (IC) and then transferred to OGM in the presence/absence of the three niche factors Wnt3A, nicotinamide and p38 MAPK inhibitor SB202190 for a period of 6 days (Table 8.3, Experiment 1). This duration was selected to allow enough time for differentiation to occur as described in Sato

et al 2011 [365]. A morphological comparison of the cultures at 6 days indicated no differentiation was observed between the basic IC and OGM conditions (Figure 8.19). Unexpectedly the removal of Wnt3A did not seem to drive organoid differentiation (as defined by smaller size, opaqueness and folded shape with budding structures) in antral nor in small intestinal organoids (Figure 8.19i and 8.19u respectively). The removal of nicotinamide and/or SB202190 resulted in larger translucent spheroidal organoids in both antral and small intestinal cultures which was in contrast to the expected greater level of differentiation (Figure 8.19j-l and 8.19v-x respectively).

The second experimental approach involved establishing long term cultures of normal antral, body (all CDX2- as determined by IHC) and small intestinal organoids to identify niche factors that may be vital for normal proliferation/differentiation in normal gastric organoids but not for small intestinal organoids (Table 8.3, Experiment 2). As before, cultures were initially grown and expanded in IC and then transferred to customised growth media: OGM (WRNEFGSTNi), _RNEFGSTNi, WRNE_GSTNi, WRNEF_STNi, _RNE_GSTNi, _RNEF_STNi, WRNE__STNi and _RNE__STNi. The niche factors FGF10 and gastrin were chosen as they have previously been shown to have little effect on small intestinal organoid growth [365] but are required for gastric organoid cultures to grow long term [366].

The use of IC and OGM (WRNEFGSTNi) did not result in differences in growth, proliferation and morphological differentiation among all three organoid cultures with differing tissue origin (Figure 8.20). The removal of Wnt3A (_RNEFGSTNi) in antral cultures did not have a deleterious effect nor did it lead to differentiated organoid shapes. In contrast, removal of Wnt3A in body organoid cultures lead to smaller, opaque and folded like organoids and then to organoid death, irrespective of the presence or absence of FGF10 and gastrin (_RNEFGSTNi, _RNE_GSTNi, _RNEF_STNi and _RNE__STNi). Interestingly, small intestinal organoids reached large sizes (>3mm) in the absence of Wnt3A (_RNEFGSTNi, _RNE_GSTNi, _RNEF_STNi and _RNE__STNi) with the fusion of multiple organoids observed, possibly due to the restriction of space in the matrigel dome. The removal of FGF10 or gastrin or both (WRNE_GSTNi, WRNEF_STNi and WRNE__STNi) did not seem to affect antral and body organoid proliferation nor differentiation state. In contrast, removal of these two niche factors lead to very large spheroidal small intestinal organoids, suggesting a preference for proliferation over differentiation.

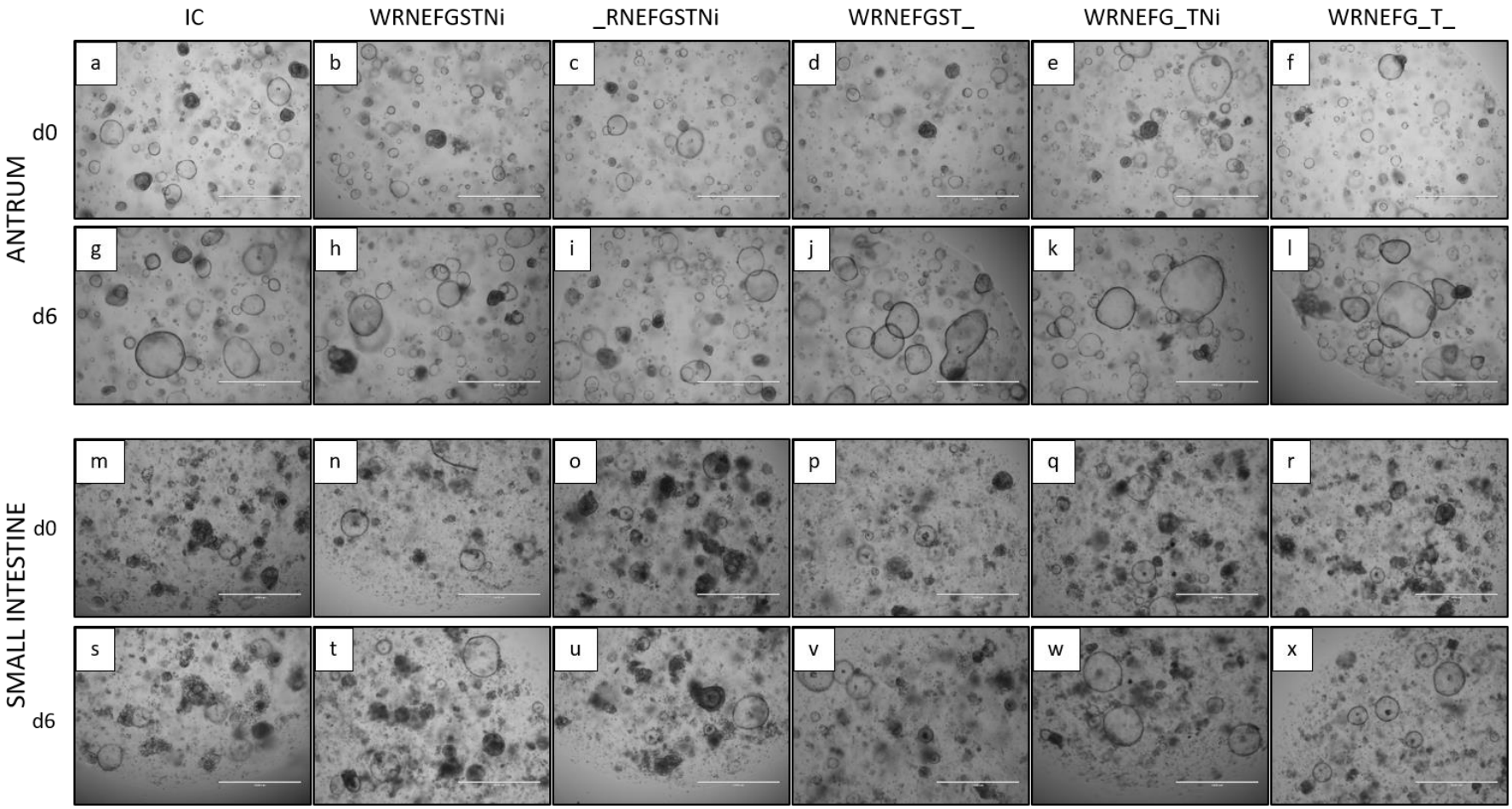


Figure 8.19 Experiment 1: Investigating the effect of removing the niche factors Wnt3A, nicotinamide and p38 MAPK inhibitor SB202190 on antral and small intestinal organoid cultures (Table 8.3)

Organoid cultures from antral and small intestinal biopsies were initially cultured in IntestiCult™ (IC) and then exposed to different growth media to assess the effect of removing Wnt3A, nicotinamide (Ni), p38 MAPK inhibitor SB202190 (S) or a combination of both Ni and S on organoid differentiation state. Scale bar: 1000µm.

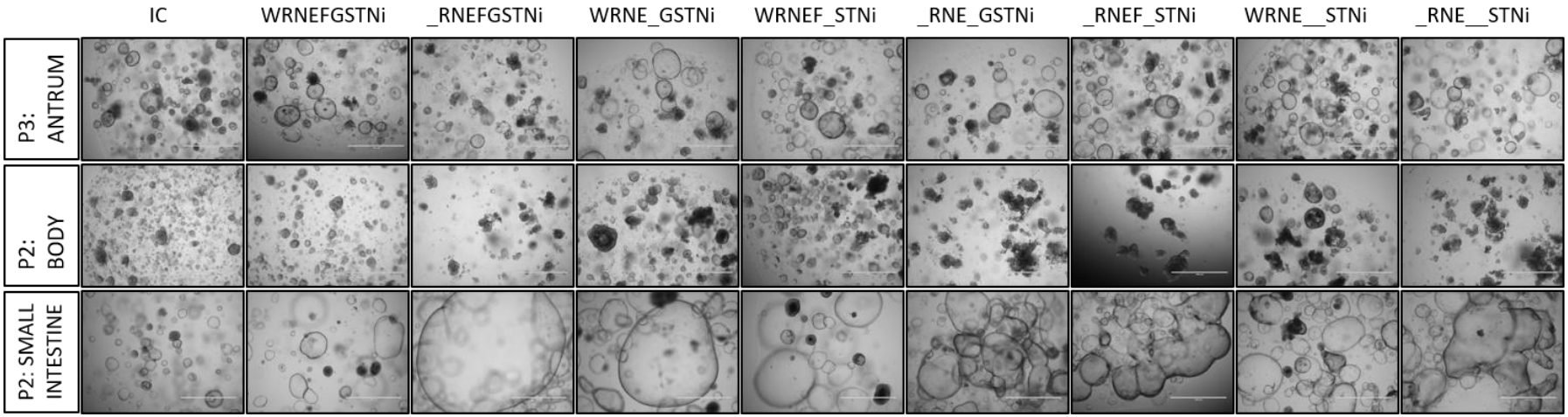


Figure 8.20 Experiment 2: The contribution of different niche factors on antral, body and small intestine organoids (Table 8.3)
Organoid cultures from antral, body and small intestinal biopsies from the same patient were initially cultured in IntestiCult™ (IC) and then exposed long term (34-45 days) to customised growth media to assess the effect of niche factors. Images of body and small intestinal organoids taken after second round of passaging (P2) and for antrum taken after third round of passaging (P3). Note the small number of dark opaque body organoids present in growth media without Wnt3A and the large sized small intestinal organoids in all conditions except for IC and OGM (WRNEFGSTNi). Scale bar: 1000µm.

The possible effect of customised growth media on antral, body and small intestinal organoid differentiation was quantified using strength and pattern of MUC5AC and CDX2 IHC staining as metrics (Table 8.4). All antral and body organoid cultures showed high levels of MUC5AC staining with whole organoid staining pattern suggesting the presence of differentiated gastric surface mucous-like cells as found in the upper part of normal gastric glands. Additionally, all antral and body organoids were CDX2-. The absence of Wnt3A in small intestine organoid cultures resulted in patches of cells instead of single cells being positive for MUC5AC staining but with no difference observed overall in CDX2 staining.

Table 8.4 Immunohistochemistry using MUC5AC and CDX2 to characterise differentiation of gastrointestinal organoids grown in customised growth media (Experiment 2)

Organoids/ growth media	MUC5AC		CDX2	
	Strength[1]	Pattern[2]	Strength[1]	Pattern[2]
Antrum				
IC	3	3	0	0
WRNEFGSTNi	3	3	0	0
_RNEFGSTNi	3	3	0	0
WRNE_GSTNi	3	3	0	0
WRNEF_STNi	3	3	0	0
_RNE_GSTNi	3	3	0	0
_RNEF_STNi	3	3	0	0
WRNE__STNi	3	3	0	0
_RNE__STNi	3	3	0	0
Body				
IC	3	3	0	0
WRNEFGSTNi	3	3	0	0
_RNEFGSTNi	3	3	0	0
WRNE_GSTNi	3	3	0	0
WRNEF_STNi	3	3	0	0
_RNE_GSTNi	3	3	0	0
_RNEF_STNi	3	3	0	0
WRNE__STNi	3	3	0	0
_RNE__STNi	3	3	0	0
Small intestine				
IC	2	1	2	2
WRNEFGSTNi	1	1	2	2
_RNEFGSTNi	2	2	2	3
WRNE_GSTNi	2	1	2	3
WRNEF_STNi	2	1	2	2
_RNE_GSTNi	3	2	3	3
_RNEF_STNi	3	2	2	3
WRNE__STNi	2	1	2	3
_RNE__STNi	3	2	2	2

[1]Strength of staining was quantified manually ranging from no staining (0), weakly positive (1), moderately positive (2) and highly positive (3). [2]Pattern of staining was quantified manually from no staining (0), single cells (1), patches of positive cells (2) and whole organoid positive staining (3).

To gain further insight into differentiation states of organoid cultures grown in customised growth media, RNA was extracted and TFF1, TFF2 and VIL1 expression was quantified using qRT-PCR as before. Previous IHC and qRT-PCR of antral and body cultures of this patient indicated a lack of IM organoids (CDX2- and VIL1- respectively). Antral organoids grown in IC medium expressed moderate levels of TFF1 and TFF2 but only low levels of VIL1 as before (Figure 8.21). However when grown in OGM in the absence of Wnt3A, VIL1 expression was greatly increased. Indeed the simultaneous removal of all three niche factors (Wnt3A, FGF10 and gastrin) resulted in lower levels of TFF1, TFF2 and higher VIL1 expression suggesting a certain degree of plasticity in gene expression under these conditions.

Body organoids grown in IC expressed high to very high levels (even above the gastric reference tissue) of TFF1 and TFF2 but negligible amounts of VIL1 (Figure 8.21). Organoids grown in OGM (WRNEFGSTNi) produced similar levels of TFF1 but much less TFF2. The removal of FGF10 or gastrin led to a considerable increase in TFF1 expression and a minor increase in TFF2 expression. The removal of both FGF10 and gastrin produced similar results as complete OGM. No data was available from body organoid cultures grown in the absence of Wnt3A as these quickly showed signs of morphological differentiation and could not be further expanded to acquire sufficient RNA for downstream applications.

Small intestinal organoid populations showed virtually no TFF1 nor TFF2 expression under any growth medium condition (Figure 8.21). Organoids grown in IC expressed more than twice the amount of VIL1 when compared to OGM (WRNEFGSTNi). The absence of Wnt3A was associated with a trend of increased VIL1 expression suggesting a greater state of differentiation. Finally the selective removal of FGF10 and gastrin did not produced a clear pattern of change in VIL1 expression.

The third experimental approach explored the requirements for organoid differentiation of antral and small intestinal organoids by establishing cultures from the same patient. One set of cultures received IC and another set received IC[A] (IntestiCult™ containing only human component A) as recommended by the manufacturer's protocol to achieve small intestinal differentiation (STEMCELL Technologies) (Table 8.3, Experiment 3). Over a period of 11 days and 1 round of passaging, no effect was observed either on proliferation nor on morphological differentiation in small intestinal organoids with IC[A] medium (Figure 8.22). By contrast antral organoids, became more folded and opaque with reduced proliferation in the same amount of time suggesting partial organoid differentiation.

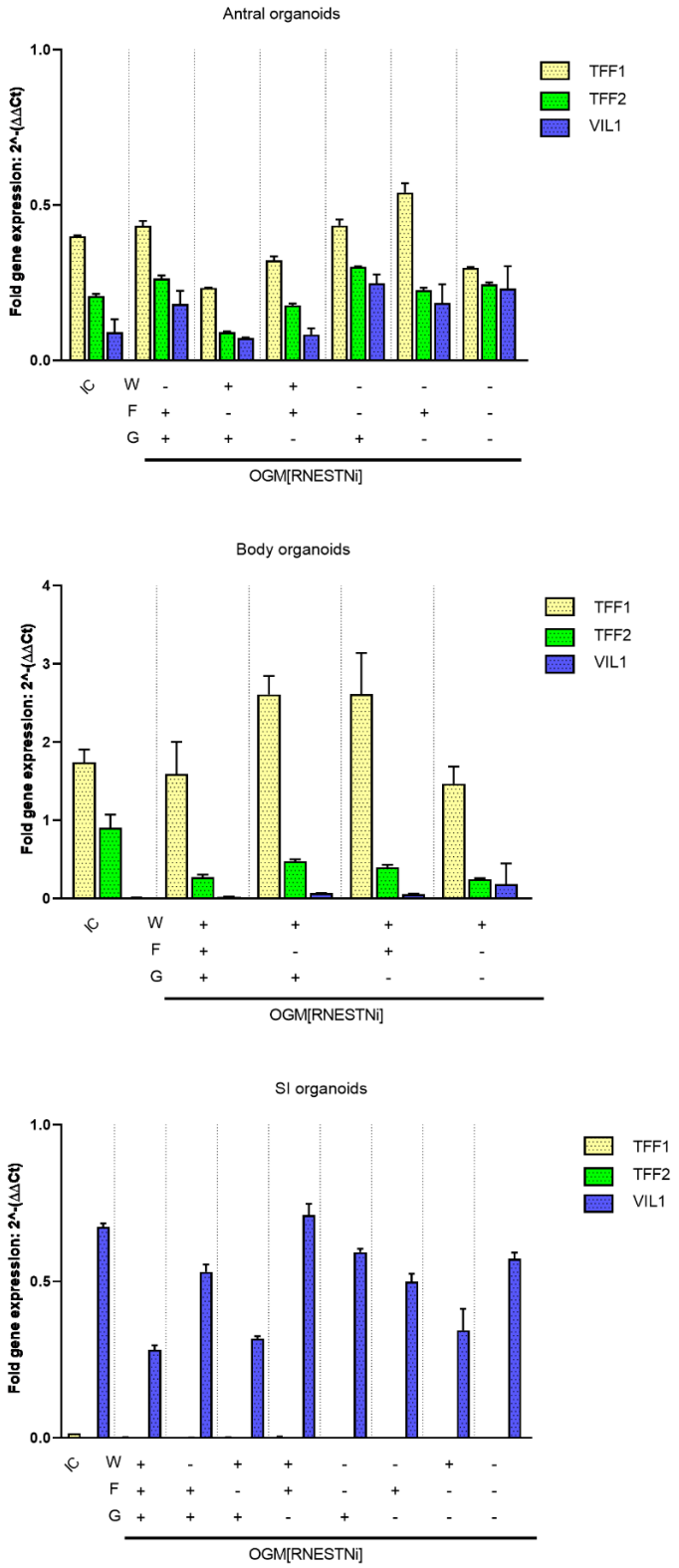


Figure 8.21 Experiment 2: The effect of niche factors on gene expression of antral, body and small intestinal organoids

The expression levels of TFF1, TFF2 and VIL1 in antral, body and small intestinal organoids grown in customised growth media were quantified using qRT-PCR as before. No data available for body organoids grown in the absence of Wnt3A. Mean with + SD shown from three technical replicates of a single experiment.

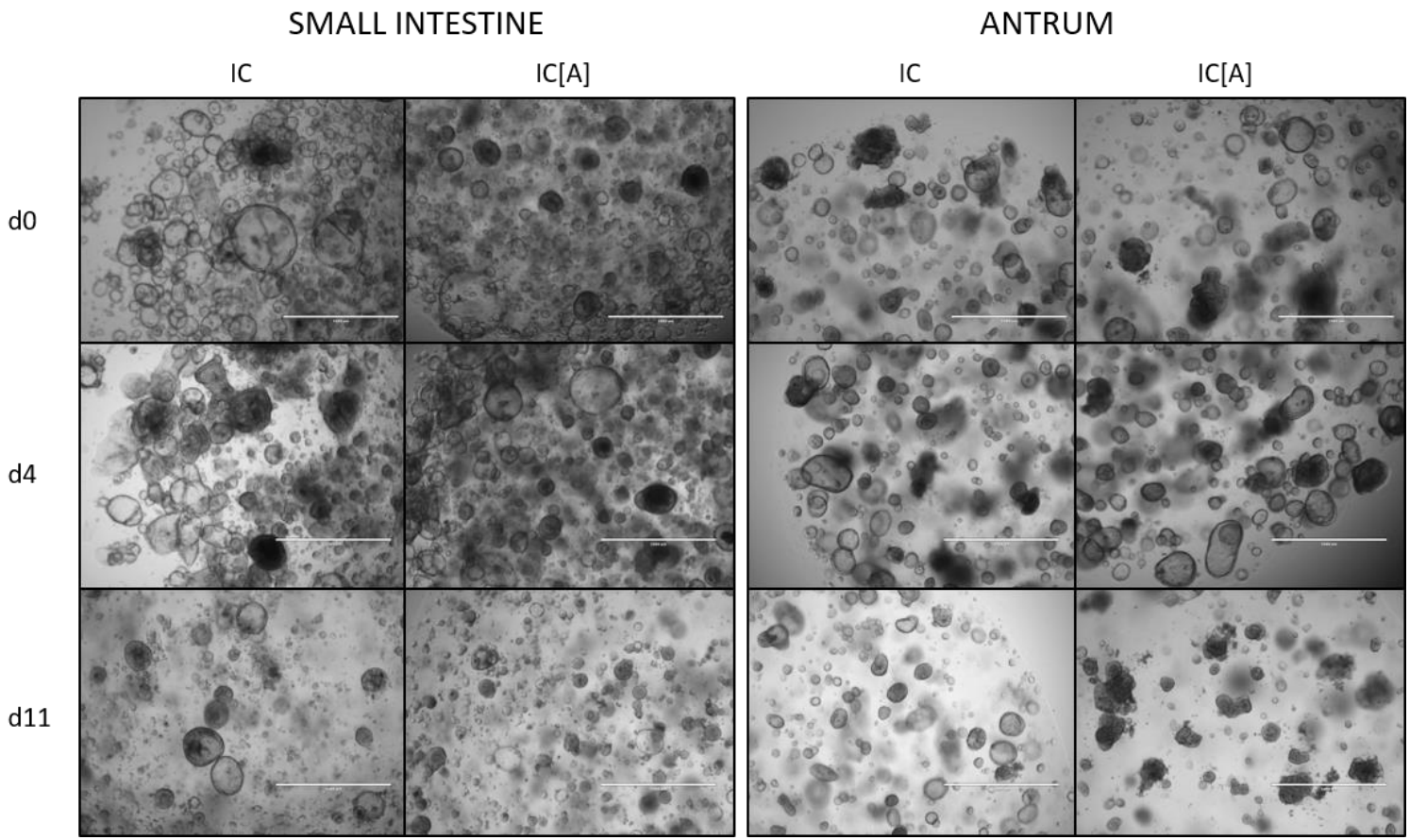


Figure 8.22 Experiment 3: The effect of IntestiCult™ with and without human component B on antral and small intestinal organoids
Organoids were initially grown and expanded using IntestiCult™ (IC) and then set up in parallel cultures without human component B (IC[A]). Dark opaque semi-folded organoids were observed after 11 days with reduced proliferation in the antral cultures with IC[A] medium. Scale bar: 1000µm.

Overall the customised growth media experiments showed that nicotinamide and SB202190 may play a role in suppression of organoid growth/proliferation in antral and small intestinal cultures and that removal of Wnt3A results in a) no visible differences in antral organoids (morphology/IHC) but alteration of gene expression profiles, b) rapid body organoid differentiation (morphology) and cessation of proliferation and c) extreme growth of small intestinal organoids. Additionally when comparing body and small intestine organoids grown in IC and OGM, a substantial reduction in TFF2 and VIL1 expression was detected respectively suggesting a reduction in differentiation towards the lower part of the gastric gland in the former and the brush border in the latter. Finally removal of human component B from IntestiCult™ results in antral organoid undergoing differentiation-like changes morphologically but has no effect on small intestinal organoids. With respect to enriching IM organoids in gastric cultures, removing Wnt3A from expanded antral and body cultures followed by IHC for CDX2 could possibly be used to select and validate the presence of IM organoids.

8.3.9 Growing organoids from cell sorted cells using the intestinal stem cell marker OLFM4

In addition to experiments which involved modification of the growth media, a FACS based selection to enrich for IM organoids was explored. Based on a literature review of gastrointestinal stem cell markers, Olfactomedin 4 (OLFM4) was chosen as a candidate for use in FACS [548]. As a proof of principle, immunohistochemistry was used to show OLFM4 expression was absent in gastric glands but present in IM glands and small intestinal crypts (Figure 8.23). In both IM glands and small intestinal crypts, OLFM4 was highly expressed in the lower part of the gland/crypt respectively.

Using this cell surface marker, the ultimate aim was to cell sort single IM organoid stem cells and grow organoids from this enriched population. To achieve this and to determine whether organoids could actually grow from single OLFM4+ cells, small intestinal organoids were initially used to develop and optimise a FACS protocol. In this optimised protocol, pooled small intestinal biopsies were processed using the vigorous pipetting method to release crypts containing stem cells and organoid cultures were established. Pooled organoid cultures were liberated from matrigel and digested to single cells (45min incubation with TrypLE at 37^{o}C), stained with an anti-OLFM4 antibody, cell sorted using FACS, and seeded in matrigel with IntestiCult™ media (Figure 8.24).

FACS using OLFM4 was then carried out on small intestinal and gastric origin organoids (from antral/incisura and body biopsies with and without targeting of IM) to assess the ability of

organoids to grow from single cells and whether OLFM4+ cells contained exclusively a stem cell population in these organoid populations.

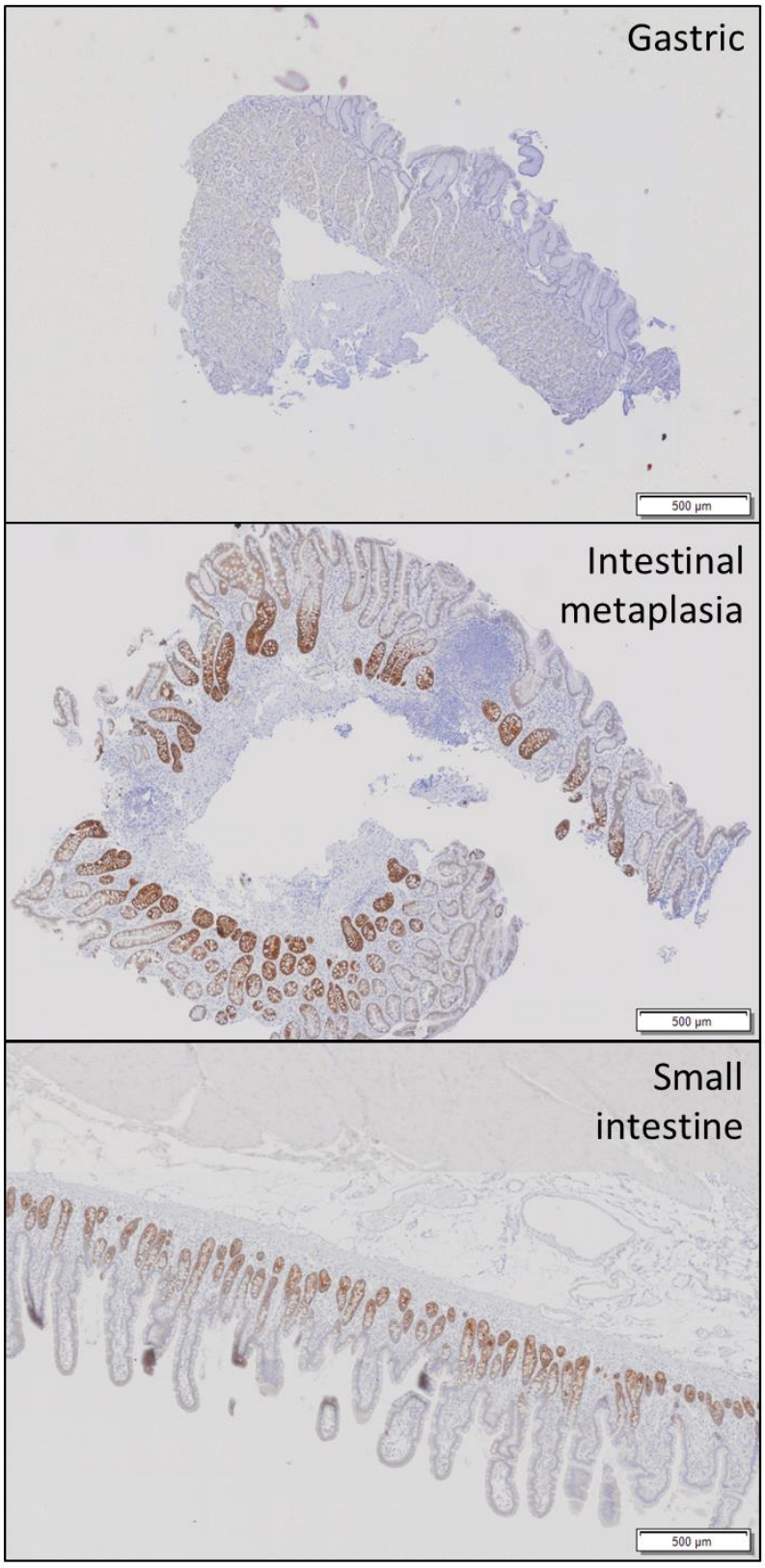


Figure 8.23 OLFM4 staining of gastric, intestinal metaplastic and small intestinal tissue
OLFM4 expression is absent in gastric glands but present in intestinal metaplasia and in small intestine. Scale bar: 500µm.

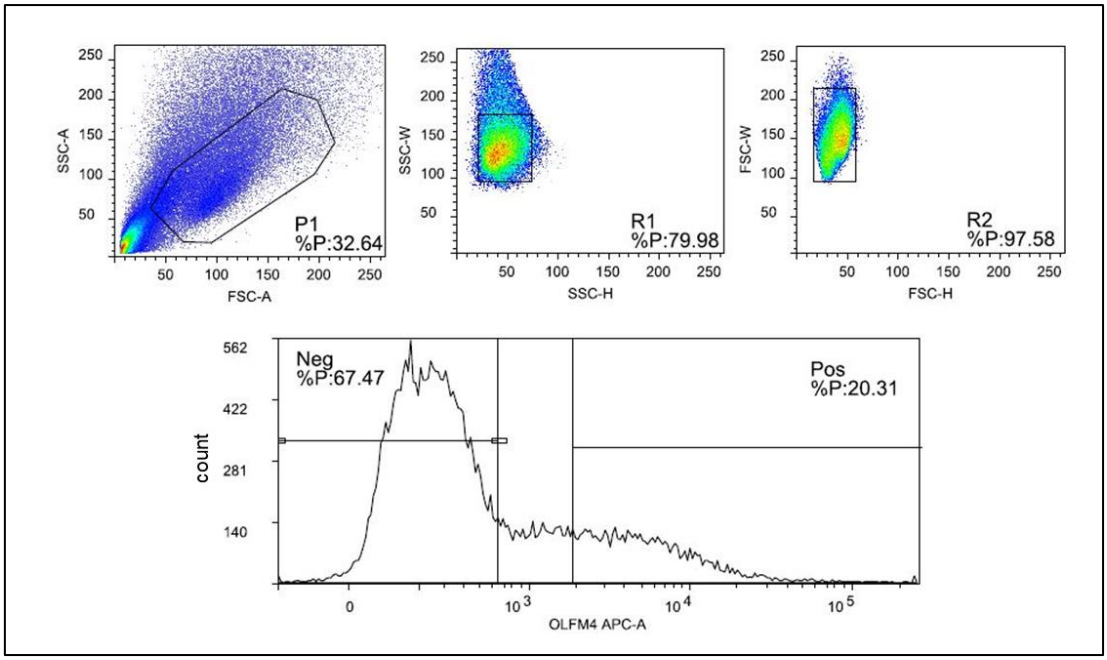


Figure 8.24 FACS plots showing gating strategy to obtain single OLM4- and OLFM4+ cells from gastrointestinal organoids

Organoids were digested to single cells with TrypLE™ (45min at 37°C), stained with anti-OLFM4 primary antibody (clone GW112) followed by staining with a rat anti-mouse IgG1 secondary antibody conjugated to APC and sorted with the BD FACSAria™ Fusion cell sorter. Debris, dead cells and doublets were removed based on physical characteristics (see forward and side scatter graphs, top row) and cells negative/positive for OLFM4 were selected based on fluorescence and sorted. Example shown from small intestinal organoid cells (patient G22).

Overall the percentage of OLFM4+ cells differed considerably between patients and tissue types. For small intestinal organoids, OLFM4+ cells ranged from 20.1% to 77.0% and for gastric origin organoids, OLFM4+ cells ranged from 9.8% to 64.7%. Organoid growth was mainly observed from OLFM4- cells in all organoid cultures except in one patient where organoids grew from both OLFM4+ and OLFM4- cells from antral biopsies targeting IM (patient G19) (Figure 8.25). These grew at a similar rate. OLFM4 sorted single organoid cells grown from incisura tissue with targeted IM from patient G24 and previously shown to contain a small CDX2+ population (IHC) did not show any difference in their ability to form organoids when compared to other gastric origin organoid cultures (Figure 8.25).

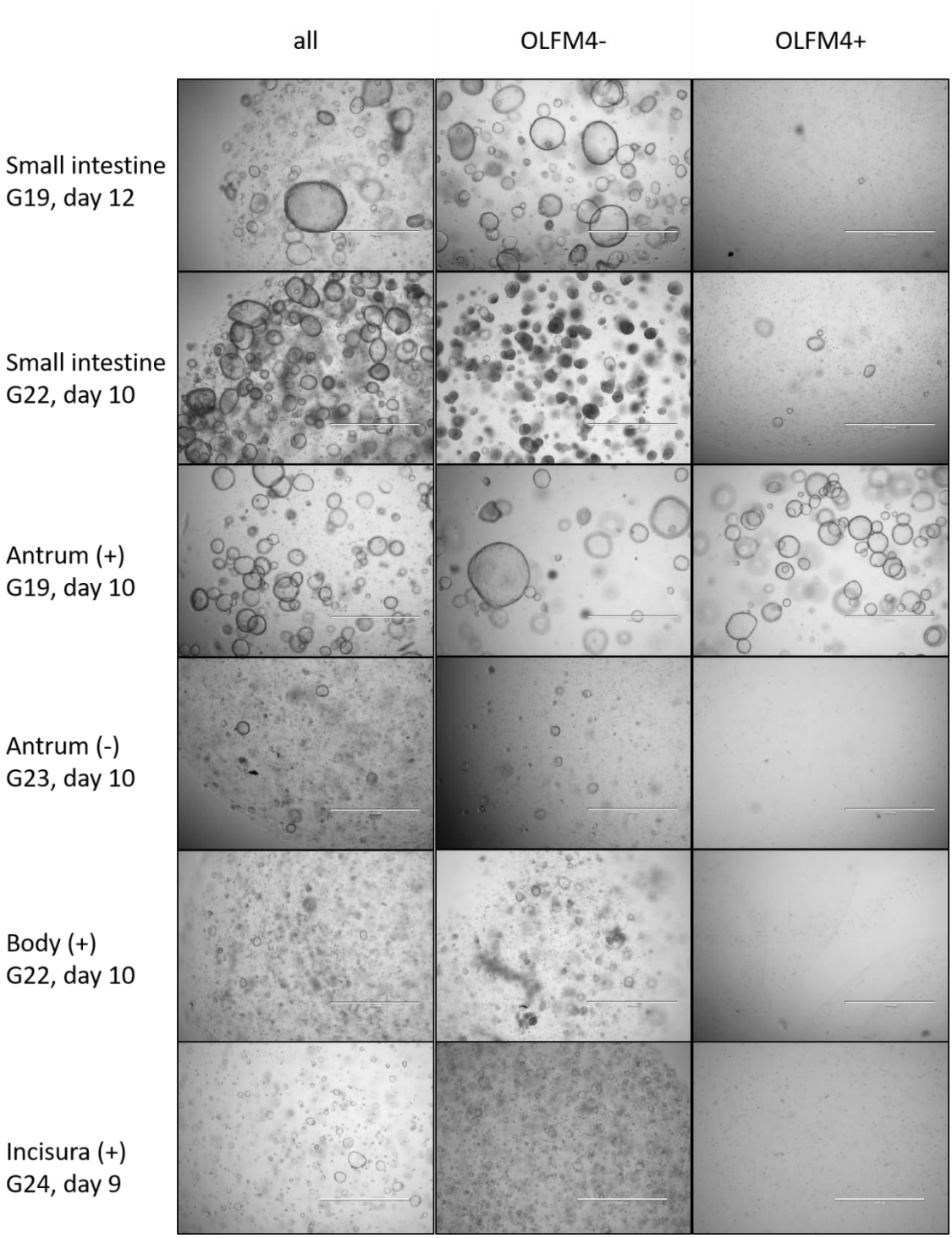


Figure 8.25 Fluorescence-activated cell sorting of gastrointestinal organoids using stem cell marker OLFM4 results in organoid formation mainly in the negatively sorted fraction

Tissue of origin, patient ID and number of days post-FACS shown. Rate of organoid formation and growth differed between tissues and patients. (-) represents biopsies of origin not targeting IM and (+) represents biopsies of origin targeting IM. The incisura (+) organoid culture from patient G24 had previously been shown to contain a small number of CDX2+ organoids (IM organoids). Scale bar: 1000μm.

To assess levels of OLFM4 in IM organoids, FFPE sections of organoid cultures previously shown to contain CDX2+ organoids (§8.3.6 and Figure 8.15) were stained using IHC for OLFM4. The staining pattern differed between patients (Figure 8.26) suggesting that this marker was inconclusive for detecting IM organoid stem cells.

Overall, these findings showed that gastrointestinal organoids could grow after being digested to a single cell level and undergoing FACS sorting. In general the OLFM4- fraction was more likely to form organoids and not the OLFM4+ fraction. Also it remained unclear why organoids grew from targeted IM antral tissue organoids expressing OLFM4. This method was not able to discriminate enough between small intestinal/intestinal metaplastic and gastric stem cells suggesting this was not a feasible method for enrichment of IM organoids.

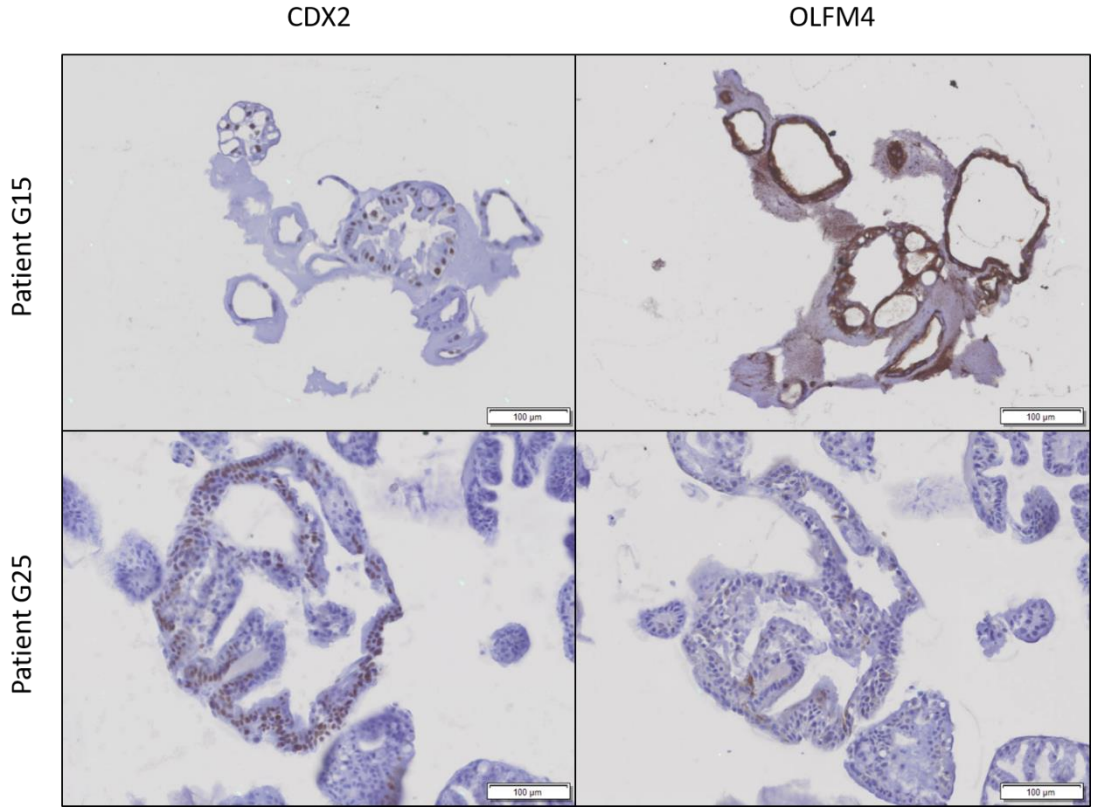


Figure 8.26 Intestinal metaplastic organoids from patients G10 and G25 show differing OLFM4 staining
Scale bar: 100µm.

8.3.10 Creation of an organoid biobank

To preserve human gastrointestinal organoids including IM organoids for future work including karyotyping, DNA sequencing, immune cell co-cultures and genomic manipulation using CRISPR-Cas9, an organoid biobank was created from patients (n=25) of the main study (Appendix M). Where possible, once the organoid cultures from each patient were established, they were passaged and expanded over multiple wells. These were used to (i) generate FFPE blocks, (ii) extract RNA and (iii) cryopreserve and store in liquid nitrogen for long term storage (Figure 8.1). Although additional optimisation may be required the same methodology described in section §2.7.7 and used to produce viable porcine organoids from previously frozen cultures (§8.3.3) could be used to reanimate cryopreserved organoid cultures from the biobank for future experimentation.

8.4 Summary and discussion

The following is a summary of the main outcomes of this study:

1. Human and porcine tissue was used to establish initial gastrointestinal organoid growth and characterisation parameters.
2. Protocols were developed for establishing, expanding, freezing down and characterising antral, body, intestinal metaplastic and small intestinal organoid cultures from human gastroscopy biopsies.
3. Gastrointestinal organoids including intestinal metaplastic organoids were characterised using immunohistochemistry and quantitative RT-PCR.
4. The role of niche factors in organoid proliferation and differentiation was investigated.
5. The utility of the intestinal specific stem cell marker OLFM4 to enrich for IM organoids was tested.
6. A gastrointestinal organoid biobank was created from 25 patients.

8.4.1 Discussion

Initial experiments to grow organoid cultures from a variety of human gastric tissue presented multiple technical challenges. Challenging areas like the amount of starting tissue material, the best tissue treatment method to release gastric glands/stem cells, organoid culture expansion, and freezing and thawing tissue/organoids back into culture were investigated using porcine tissue that was easily amenable to multiple experiments. Downstream methods were also established for fixing and embedding organoids into paraffin blocks and RNA extraction.

Methodology was continuously optimised which led to the successful development of human gastrointestinal organoid cultures starting with as little as 2-3 pooled biopsies. Previous studies used 1cm^2 of normal gastric tissue and 5 small intestinal biopsies to set up organoid cultures [365, 366, 370]. However gastric cancer organoid cultures have been successfully established from both gastroscopy biopsies and gastrectomy tissue [549]. The application of gentle pressure on gastroscopy biopsy tissue to release gastric glands containing stem cells (chelation buffer method) is more successful whereas enzymatic digestion of solid gastrectomy tumour tissue is more suitable to release cancer stem cells (see [549] for discussion, [550]). Efficient isolation of viable stem cells is of paramount importance for setting up organoid cultures, as EUS guided fine-needle biopsy sampling of a primary mass has been shown to provide enough starting material for setting up pancreatic cancer organoids [551].

Once the methodology for organoid plating, expanding and freezing organoids had reached an acceptable success rate, the focus of the project turned onto characterising protein and gene expression levels of the organoid cultures which had been developed and stored within our biobank (n=25). Using IHC, it was shown that the majority of patient samples produced organoids that were positive for MUC5AC, a marker associated with gastric surface mucous cells and negative for CDX2, a marker normally expressed by small intestine, colon and intestinal metaplasia epithelial cells. Only 6/25 patients yielded organoids populations which expressed CDX2+ (with mostly patchy staining) with small intestinal organoids used as a control for this marker. Interestingly most IM organoids and some small intestine organoids expressed MUC5AC.

The relatively low frequency of IM positive organoid cultures derived from the 25 patients was rather surprising as 22 of these had evidence of IM in adjacently collected biopsies acquired at the same time for pathology/research purposes. This low frequency might have been due to one or a combination of the following reasons: 1) sampling issues between biopsies taken for organoid cultures and those taken adjacent and used for detecting the presence/absence of IM, 2) the relative amount of IM glands in tissues used for diagnosis but also in biopsies used directly for setting up cultures (as established by taking a slice of the biopsy prior to setting up the culture) was often very small, 3) the isolation method for releasing IM glands from the gastric mucosa was suboptimal and 4) the growth conditions used for growing and expanding IM cultures were suboptimal. It is likely that the large number of contaminating normal gastric organoids in the sample resulted in lower levels of IM organoid detection.

IM organoids were further characterised using TFF3, a protein normally found in goblet cells of IM, the small intestine and the colon, and CD10, a protein found in the brush border of the small intestine (enterocytes, goblet cells and other epithelial cells) and the complete subtype of IM (Chapter 7). TFF3 expression was detected in some IM organoids and small intestinal organoids but fully differentiated goblet cells were absent (visually also assessed with ABPAS staining) suggesting a semi-differentiated pre-goblet state. Previously goblet formation in small intestinal and colon organoids was achieved through the use of the Notch γ-secretase inhibitors DAPT and DZP [365, 552]. Patchy CD10 expression was detected only in a small number of IM organoids, similar to organoids from small intestine origin. Overall these IHC findings suggested that IM organoids existed in culture in a semi-differentiated state and did not fully recapitulate the cell types observed in IM tissue.

qRT-PCR was used to characterise antral, body, IM and small intestine organoids for their expression of TFF1 (gastric surface mucous cells, similar to MUC5AC), TFF2 (gastric neck mucous cells), VIL1 (brush border of small intestine and IM) and CDX2 (epithelial cells in small intestine, colon and IM). Both antral and body organoids expressed TFF1 and TFF2 as expected with little or no VIL1 and CDX2 expression. IM and small intestinal organoids were low in TFF1 and TFF2 expression but expressed higher levels of VIL1 and CDX2. Interestingly, small intestinal organoids expressed more than twice the amount of CDX2 mRNA compared to IM organoids. Overall these results suggested that this 4 gene panel could be used to differentiate between normal gastric and intestinal metaplastic organoids when cultured with the IntestiCult™ growth medium.

The role of several niche factors was investigated in detail to identify potential conditions that could promote selective IM organoid enrichment. First the roles of nicotinamide, a molecule essential for ATP production, and the p38 MAPK inhibitor SB202190 (which prevents overall organoid differentiation, [553]) were assessed. Previously nicotinamide was shown to be essential for long term growth in small intestinal organoid cultures but together with SB202190 to strongly inhibit goblet (shown by PAS staining) and enteroendocrine cell differentiation (defined by synaptophysin IHC staining) [365]. By contrast nicotinamide was shown to promote initial gastric body organoid formation but to limit the lifespan of cultures and prevent the differentiation of MUC5AC producing gastric mucous cells [366]. To a limited extent the latter was confirmed in this study by the qRT-PCR data that showed low TFF1 expression in three clonal body organoid cultures grown in OGM containing nicotinamide but not by IHC using an anti-MUC5AC antibody (highly positive). Surprisingly removal of nicotinamide or SB202190 or both in antral and small intestinal cultures resulted in larger spheroidal organoids suggesting less

differentiation instead of more as organoid growth and proliferation are generally inversely proportional to organoid differentiation.

The effect of removing Wnt3A was assessed first in short term and then in long term cultures. Wnt signalling plays a vital role in early development, maintenance and regeneration of stem cells [554, 555]. Although not crucial for the formation and growth of mouse small intestinal organoids to form and grow, Wnt3A has been shown to be vital for human organoids, both of small intestinal and gastric origin [365, 556]. In previous studies short term removal of Wnt3 in small intestinal cultures resulted in mature enterocyte differentiation (defined by alkaline phosphatase IHC staining) and in gastric body cultures to more cystic-like organoids and upregulation of MUC5AC, TFF1 and TFF2 [365, 366]. In this current study removal of Wnt3A for 6 days did not result in substantial phenotypic changes in either antral or small intestinal organoids.

Removal of Wnt3A over a prolonged period of time resulted in the formation of very large cyst-like small intestinal organoids in conjunction with a doubling of VIL1 expression suggesting an increase in enterocyte maturation but no overall change in CDX2 staining intensity/pattern was observed using IHC. Interestingly IHC staining with MUC5AC, a protein not found normally in small intestinal tissue, showed an increase in intensity. Removal of Wnt3A in antral organoid cultures did not result in phenotypic changes nor in changes of MUC5AC staining intensity but an increase in TFF1, TFF2 and VIL1 gene expression (a gene not expressed in normal antrum) was detected. Interestingly this plasticity in the expression of a gene normally associated with the small intestine was not replicated at the protein level as CDX2 was not detected. In body organoids removal of Wnt3A quickly lead to a more differentiated morphological state (smaller, opaque and folded shaped) and a cessation of proliferation, a phenomenon previously described by Bartfeld et al 2015 [366]. However, no change was observed in MUC5AC (high positive) and CDX2 (negative) protein status.

The role of FGF10, a multifunctional mesenchymal-epithelial signalling growth factor [557], and gastrin, a peptide hormone released in the antrum/duodenum which stimulates acid production by oxyntic parietal cells [558], in organoid proliferation and differentiation was next investigated. In antral organoids, removal of FGF10 lead to lower TFF1 and TFF2 expression but absence of gastrin did not seem to have an effect overall. When either was removed in the absence of Wnt3A, TFF1 and VIL1 expression increased but when all three factors were removed TFF1 expression decreased but VIL1 expression remained high suggesting a limited growth medium-induced intestinalisation, although all organoids did remain negative for CDX2 protein.

In body organoids, removal of either FGF10 or gastrin resulted in higher expression of TFF1 suggesting greater differentiation towards the upper part of gastric glands but removal of both returned TFF1 expression back to baseline. In small intestinal organoids, removal of gastrin lead to doubling of VIL1 expression but removal of both FGF10 and gastrin resulted in baseline expression. However additional removal of Wnt3A resulted in increased VIL1 expression suggesting that Wnt3A is the main factor involved in VIL1 associated enterocyte differentiation.

Overall the niche factor part of this study produced some interesting findings with regards to antral organoid plasticity at the gene expression level, but likely not at the protein level. Particularly important was the different response to variable growth media seen between antral and body organoids, suggesting that enriching IM organoids from biopsies of differing gastric origins may require tissue adapted strategies. Integrating all current findings and using small intestinal organoids as a model for IM organoids the following strategy could be used to obtain IM enriched cultures: a) expansion of antral derived organoids in IntestiCult™, b) test for the presence of VIL1/CDX2 mRNA and protein and c) if present even at low frequency, IM organoids could be enriched using Wnt3A free OGM for several rounds of expansion and then re-evaluated for CDX2 positivity with IHC and increased cyst-like morphology. For body biopsies believed to contain IM glands (less frequent), the same strategy could be used to eliminate body organoids through differentiation and lack of proliferation without the need for validation with IHC. However this tissue adapted strategy for selecting and expanding enriched IM organoid cultures was not carried out due to the time restrictions associated with completion of my PhD.

As part of an effort to enrich for IM organoids without the need for multiple rounds of growth medium-induced enrichment, a protocol was developed that allowed single dissociated organoid cells to be cell sorted using an established intestinal stem cell marker, OLFM4. OLFM4 has been previously shown to be a robust marker for intestinal Lgr5-positive stem cells for which currently no reliable commercial antibody exists for the human version [548]. OLFM4 was also shown to be both a target gene and a negative regulator of the Wnt/β-catenin pathway and to interact with Frizzled-7 and -10 [559]. In gastric cancer upregulation of OLFM4 was associated with the intestinal subtype but not the diffuse subtype [560]. Previously high levels of OLFM4 were shown with IHC and RNA *in situ* hybridisation in IM glands but only occasionally with low levels in antral or body gastric glands [514, 560, 561].

In this current study OLFM4 was shown to strongly stain the bottom part of intestinal metaplastic and small intestinal glands/crypts thus the stem cell compartment but to be absent in antral tissue. Different patients exhibited considerable heterogeneity with respect to the

OLFM4+ fraction in organoid cultures between tissue types, from being only a minor population to being the predominant population in both small intestinal and gastric cultures. However successful organoid formation and growth was mainly seen in the OLFM4- fraction. In fact biopsy tissue from antral biopsies of a single patient produced organoids from both OLFM4- and OLFM4+ cells suggesting that this marker is not likely a strong differentiator in gastrointestinal organoids grown under this conditions in IntestiCult™ growth medium. This was further confirmed by differing levels of OLFM4 protein expression in IM organoids. It is currently difficult to speculate why an established intestinal stem cell marker did not select at least for small intestinal organoid stem cells grown in human small intestine optimised growth medium but as previously mentioned reproducibility of organoid research has been a rate limiting step in organoid modelling of disease [363].

8.4.2 Technical limitations

The current study consisted of a systematic approach to identify the best possible conditions for isolating and growing human gastrointestinal organoids starting from as little as 2-3 gastroscopy biopsies. Its ultimate aim was to grow and characterise IM organoids. However this study did have a small number of potential limitations including:

a) The relatively small amount of human starting material for optimising protocols. Patient heterogeneity combined with limited biopsies per patient did not allow for the direct comparison of multiple protocols in the same person.

b) The relatively small amounts of IM glands per gastric biopsy, even in targeted IM tissue. From a pathology perspective, even a single IM gland is considered sufficient for a positive diagnosis. However for organoid experiments, selecting and enriching low frequency IM organoids from a majority of normal gastric glands remained highly challenging.

c) The high cost associated with organoid culture reagents. To a certain extent these were resolved with optimised protocols and the in-house production of conditioned media for Wnt3A, R-Spondin 1 and Noggin.

Overall this project produced a series of optimised protocols for successfully isolating and propagating gastric, IM and small intestinal organoids from gastroscopy biopsies. Also methodology was developed for characterising organoids in bulk populations. IM organoids were identified and characterised for the first time and several possible avenues for further enrichment were investigated. Customised growth media possibly in combination with FACS using a yet to be determined IM specific stem cell marker could lead in future studies to pure

IM organoid cultures. Finally an organoid biobank was created that will provide material for such future studies.

Chapter 9 Discussion and future directions

Gastric cancer (GC) remains the fifth most common and third most lethal type of cancer globally [1, 2]. Patients with GC are usually asymptomatic and tend to present at an advanced stage [4, 5]. As a consequence the 5 year overall survival rate is very low, between 20-30%, in most countries, with the exception of countries such as Japan and South Korea which have a general population screening program (~62% and ~76% respectively) [6, 7, 562, 563]. In Australia and New Zealand such a screening program is not economically viable due to the relatively low prevalence of GC (combined age standardised incidence rate of 6.4 and 2.9 per 100 000 population for males and females, respectively in 2018, §1.1.2) [2]. To improve early detection and treatment, it is therefore important that patients at risk of progression are stratified and targeted surveillance is carried out. Patients with early GC (EGC) have a 5yr survival rate greater than 90% [62, 63].

Multiple risk factors have been associated with GC including *H. pylori* infection, male gender, older age, smoking and a high salt diet as well as others (summarised in [28]). For the intestinal type of GC (IGC) as classified by the Lauren classification system, the Correa model with defined premalignant stages has also been used to stratify patients at risk of progression [64, 103, 104]. For the other main Lauren type of GC, the diffuse type (DGC), the Correa model is not believed to play an important role although this has only been investigated in a limited number of studies so far [77-80]. One of the stages associated with the Correa model, intestinal metaplasia (IM), is believed to be a key breaking point for a subset of patients as *H. pylori* eradication treatment does not prevent them from progressing to GC [124]. IM, a lesion defined by the replacement of stomach epithelial cells by epithelial cells normally found in the intestine, has been repeatedly associated with an increased risk of GC [94].

9.1 Intestinal metaplasia is associated with diffuse gastric cancer

The first aim of the current study was to address the gap in existing knowledge with respect to the relationship between IM and DGC. This was done by investigating both spatial histological relationships and molecular profiling with IGC as a baseline, and mixed GC (MGC), which are tumours consisting of roughly equal amounts of the intestinal and the diffuse type, as an additional comparator where possible.

When evaluating GC cases and their adjacent non-tumour histology, and comparing this with tissue distant from the tumour (found at least 2cm away), a trend between DGC and adjacent IM was found but this did not reach significance, possibly because of the relatively small number

of cases investigated (§3.3.2). By comparison a highly significant association was identified between both IGC and MGC with adjacent IM. An earlier type of premalignant lesion, chronic gastritis (CG), was identified more frequently distant than adjacent to tumour for both DGC and IGC. In more than 90% of DGC, IGC and MGC patients, CG was present distant from tumour suggesting that the majority of these GC patients exhibited signs of pan-gastritis.

The current IM findings are consistent with previous histological studies that have shown an association of IM with DGC, though consistently at lower levels than with IGC [31, 398]. In the current study, IM adjacent to DGC tumour was found in ~40% of cases compared with 55% in Lauren's original study and 50% in Matsukura's study [398].

Analysis of clinicopathological details of DGC patients with and without adjacent IM showed an association between patients with IM and older age as well as a trend with *H. pylori* infection (§3.3.3). These findings suggest that DGC tumours that are directly associated with IM likely follow a unique path to reach malignancy within a greater time frame, comparable to that of the majority of IGC tumours which are associated with *H. pylori* infection and older age [38, 564, 565]. A recent publication by Shin et al 2019 [566] also showed DGC tumours surrounded by either severe atrophic gastritis (AG) or IM occurred mostly in older patients. A hypothesis proposed by the authors was that with time a DGC tumour may grow progressively towards areas rich in IM. However this is unlikely to be the correct explanation as DGC tumours surrounded by IM were not associated with a more advanced T or N stage in the current study. Shin et al suggested that IM (and AG) may play a role in weakening the epithelial mechanical barrier against the sporadic spread of DGC cells and thus promoting local spreading. Interestingly the current study showed IM to be associated with a lower N stage in IGC patients, suggesting the role of surrounding IM on tumour spread may differ depending on tumour subtype.

To further investigate the role of premalignant lesions in diffuse gastric carcinogenesis, the molecular relationship between both CG and IM and both DGC and IGC was investigated (§4.3.4). This part of the study was based on the seminal work by Boussioutas et al 2003 [406] which showed using DNA microarrays from a similar set of CG, IM, DGC and IGC samples that each premalignant and malignant lesion had a defined gene expression profile. In the current study, gene expression profiles from Affymetrix microarrays of CG and IM (both from tissue taken at least 2cm away from concurrent GC) were compared with those from IGC and DGC tissues. Overall a shared gene signature consisting of 91 genes and mainly associated with gastrointestinal epithelial function and tissue homeostasis was shown to be under-expressed in

the GC tissues. By contrast a gene signature consisting of genes associated mainly with stromal and developmental processes was shown to be commonly over-expressed in both GC types. These shared gene signatures suggest a potential common origin for both types of GC. If the majority of IGC tumours originate sequentially through each histological step described by the Correa model, then some DGC tumours may also travel through at least the same steps of CG and IM.

Pathway analysis using ssGSEA with IM samples as a reference tissue showed some of the key differences but also some of the common features that separate and yet unite the intestinal and the diffuse subtypes of GC (§4.3.5). As previously described by Boussioutas et al [406], IGC tumours were much more enriched in pathways associated with cell division and proliferation whereas DGC tumours were more enriched in pathways associated with epithelial mesenchymal transition, Notch and TGFβ signalling. However pathways enriched in one GC type were mostly also enriched in another, the level of enrichment being the key difference (Figure 4.5). Interestingly both tumour types showed an enrichment in extracellular matrix related pathways, suggesting not only a potential common path to tumour initiation but also to tumour progression through remodelling of the microenvironment. There is some evidence to suggest that certain diffuse gastric cancers (signet ring cell carcinomas) exhibit histological plasticity with progression, as a greater degree of intestinalisation has been observed with increasing depth of invasion [567].

The exact mechanism of how DGC or IGC tumours form still remains to be elucidated but previous studies have suggested the following: a) IM is derived clonally from gastric mucosa [568], b) IM glands undergo fission to form clonal patches [493, 568], c) dysplastic glands are genetically related to IM glands, d) entire dysplastic fields can share a single foundation mutation [493] and e) high grade dysplastic lesions (HGD) share many key genomic changes with GC tissue [411, 450, 569, 570]. A recent study by Rokutan et al 2019 [570] showed that *APC* mutations were present in all low grade dysplastic (LGD) cases investigated (12/12) but only in just half of HGD cases (7/13) suggesting the likelihood of an alternative path to HGD other than linear evolution from LGD as previously thought. Furthermore *APC* and *TP53* mutations tended to be mutually exclusive and the latter occurred only in HGD (4/13). Interestingly the majority of minute GC cases studied had *TP53* mutations (11/15) suggesting this event to be a critical point in the process of irreversible carcinogenesis (see also [571]). Finally mixed gastric cancers have been shown to have similar chromosomal aberrations in both their diffuse and intestinal components suggesting clonal evolutionary divergence from a single abnormal cell [572].

Although histologically a single entity, it is likely that DGC tumours differ molecularly in their mechanism of carcinogenesis [407]. This heterogeneity in diffuse gastric carcinogenesis was suggested by the molecular classification of the TCGA study [42]where the genomically stable subtype (GS) was enriched in DGC (~74%) but histologically defined DGC tumours were also classified within the molecular subgroups of EBV, MSI and CIN.

Overall IM may have a dual role in its relationship with DGC. In a subset of DGC cases, it may simply be a paramalignant lesion ("an indicator of tissue instability") whereas in another subset of DGC tumours, it may act as a precursor lesion. Further molecular support of IM transformation leading to DGC has been shown by the expression of intestine and IM specific markers such as CDX1, CDX2, CDH17 and OLFM4 not only in IGC but also in a proportion of DGC cases [155, 573, 574].

Finally this study also set a question about the process of carcinogenesis in IGC at the gastro-oesophageal junction (GOJ). Multiple studies have shown the absence of an association between GC and *H. pylori* infection at the GOJ in low incidence countries which mirrors the absence of IM adjacent to IGC at the GOJ shown in the current study [77, 78, 400, 403]. However several other studies have clearly shown the presence of IM in cardia tissue including in the mucosa adjacent to cardia gastric adenocarcinoma [575, 576] suggesting the possibility of multiple pathways leading to IGC formation at the cardia/GOJ, one of which may not follow all of the histological steps associated with the Correa model.

9.2 The complete and incomplete subtypes of intestinal metaplasia differ at the molecular level

IM is histologically classified into the complete ("small intestine-like") and incomplete ("colon-like") subtypes [130]. An increasing number of studies have shown that the incomplete subtype is associated with a greater risk of progression to GC [89, 91, 94, 137, 138]. Additionally incomplete IM was found to be more prevalent in IM tissue from GC patients (IM+GC) than in IM tissue from non-cancer patients (IM-GC) [571] suggesting it is the more advanced subtype. Previous publications on characterising differences between complete and incomplete IM have mainly used immunohistochemistry (IHC) and focused on mucin profiles (MUC1, MUC2, MUC5 and MUC6) [131, 158], the expression of defining gastrointestinal transcription factors such as CDX1, CDX2 and SOX2 [155, 158, 577] and the presence/absence of brush border enzymes [398, 414, 415]. Furthermore a single molecular study based on Affymetrix microarray technology using a small number of samples has also been described [388].

The second aim of my thesis was to address the existing knowledge gap with respect to molecular profiles of the complete and incomplete subtypes in order to try and elucidate the molecular changes that are conferring the greater degree of risk associated with the latter. To achieve this, existing in-lab Affymetrix microarray data obtained using RNA extracted from frozen macro-dissected IM tissue [259] in a non-cancer setting (IM-GC patients) was re-analysed (§4.3.8). The macro-dissected tissue lacked a histology defined subtype due to its origin, and a novel method based on the relative expression level of key small intestinal, particularly of the brush border, and colon genes was used to classify samples as complete and incomplete IM. The majority of the corresponding gene products such as CD10 and sucrase isomaltase have previously also been described in IM studies [398, 414, 415] and any samples that showed a mixed gene expression profile were classified as mixed IM.

Molecular subtyping of IM samples into categories normally associated with histological subtypes has not been done before, but pathway analysis using ssGSEA with GO Cellular Component/Biological Processes confirmed its potential as the complete IM samples were enriched in brush border, digestion and metabolic pathways normally seen in the small intestine (§4.3.9). Furthermore differential gene expression showed complete IM to be highly enriched in expression not only of multiple genes associated with the small intestine brush border but also of several genes associated with glucose and fructose metabolic functions normally seen in mature small intestinal enterocytes (§4.3.10) [578]. Although mucosal tissue architecture differs between the stomach and the small intestine, complete IM glands seem to replicate functionally small intestinal crypts to a considerable degree.

Molecular characterisation of incomplete IM samples showed little functional pathway enrichment but multiple overexpressed genes associated with both the colon and GC were detected including *HOXA10* and *HOXA13*. Overexpressed in several cancer types including oral squamous cell carcinoma and prostate cancer, HOXA10 is a key regulator of embryonic morphogenesis and differentiation and has been shown to enhance cell proliferation and reduce apoptosis in GC possibly through interaction with BCL2 and activation of JAK1/STAT3 signalling, suggesting a potential key oncogenic role in incomplete IM [426, 579-582]. HOXA13 was shown to be upregulated in more advanced GC stages and associated with cell proliferation/invasion and an epithelial-mesenchymal transition phenotype suggesting it may play an important role in IM transformation to malignancy [583, 584]. The overall enrichment in GC associated genes including *CLDN1*, *CDH3, CEACAM5* and *CEACAM6* suggests that incomplete IM is “primed” for

transformation requiring only a small set of genomic changes to push it through to a dysplastic or even directly to a malignant neoplastic stage.

An additional interesting finding of this study resulted from the molecular comparison of IM patients without (IM-GC) and with concurrent GC (IM+GC). Traditionally the characterisation and the search for molecular markers that can be used to differentiate between normal/premalignant and gastric tumour samples has been based on adjacent to tumour samples ([406, 407, 490, 585], reviewed in [454]). Although these adjacent to tumour samples may be free of tumour cells and histologically be similar to normal or premalignant lesions to those in non-cancer patients, they can harbour molecular alterations that cause them to be in an "intermediate state" towards malignancy [451-453, 586, 587]. This is a result of field cancerisation as first described by Slaughter et al 1953 [412, 588]. However these tissues adjacent to tumour samples provide an opportunity to assess the first steps of carcinogenesis, with respect to changes to the epithelium and the surrounding microenvironment, when compared to equivalent samples of non-cancer patients [589]. This process was described as "temporal progression" in the current study with IM+GC samples being a more "advanced" type of IM due to the possible accumulation of more "genomic events" and changes to the microenvironment compared to IM-GC samples.

Gene expression profiling between macro-dissected IM-GC and IM+GC samples seemed to confirm this effect of temporal progression as processes associated with the epithelium but also with the immune microenvironment, particularly with regards to T cell activity, were enriched in the latter samples (§4.3.7). IM+GC samples showed high expression of two key transcription factors *MYC* and *SOX9* that have been previously associated with gastric carcinogenesis. SOX9 is normally expressed in the intestine, in stem/progenitor cells and Paneth cells, and is a transcriptional target of the Wnt signalling pathway [590]. In normal gastric body mucosa, SOX9 is weakly expressed around the neck/isthmus epithelium and in IM moderate expression has been detected at the bottom of the gland with increasing expression in dysplasia and then gastric carcinoma [591-593]. *MYC* overexpression may play an important role both in progression from IM to dysplasia as well as in GC progression [127, 162, 594, 595]. The present study showed a significant trend using the Jonckheere-Terpstra test [382] of increased expression of genes associated with 8q24 (chromosomal band of *MYC* gene) from normal tissue to IGC tissue which is in line with previous findings that show chromosomal copy gain of 8q in IM to be associated with higher risk of progression [127].

Overall the increased expression of *SOX9* and *MYC* but also of other genes associated with cancer such as *KMT2C* (epigenetic regulator) [596], *SMOC2* (wound healing) [597] and *PDZK1IP1* (inflammation) [598] in IM+GC samples seemed to confirm the potential of these samples to be used as a surrogate "temporal" model to identify cellular and molecular processes in IM associated with progression to dysplasia/cancer.

9.3 Macrophage and T cell landscapes differ between complete and incomplete intestinal metaplasia

The third aim of the current study was to address the existing gap in knowledge with respect to the immune landscape in IM and its possible role in progression. It is well established that IM arises in the setting of chronic inflammation (as shown also in §4.3.2). Therefore it was encouraging that the initial bioinformatic analysis, based on gene expression analysis of premalignant lesions in IM+GC patients, suggested that both CG and IM were enriched in M2 macrophages, mast cells, plasma cells, CD8 T cells and CD4 resting memory T cells (§4.3.3). In addition, comparing gene expression profiles of complete and incomplete IM in IM-GC patients showed a significant difference in T cell markers and cytokine/chemokines suggesting higher levels of inflammation and greater infiltration of CD8 and innate like T cells (§4.3.12-14) in the former. These findings were further corroborated using multiplex immunohistochemistry (IHC). Tissue samples with CG, complete IM and incomplete IM from patient cohorts with (IM+GC) and without GC (IM-GC) were used to construct a putative histo-temporal model with increasing risk of progression based on histology and the presence/absence of concurrent GC in patients (Figure 9.1).

In keeping with recent findings in GC from our laboratory and others [198, 490], the macrophage landscape in premalignant tissues was equally heterogeneous in both the IM-GC and IM+GC cohorts and consisted mainly of six subsets (§5.3.3). These subsets were characterised according to the co-localisation of M1 (IRF8) and M2 (CD163 and CD206) markers into 3 subgroups: M1, M1/2 and M2. These 3 macrophage subgroups most likely form part of a spectrum (Figure 5.29), with the novel M1/2 subgroup functionally in between the M1 and M2 polarised states described using *in vitro* experiments [194, 472, 478, 479, 599]. Overall total macrophage density was reduced in incomplete IM, M2 macrophages and in particular CD163+CD206+ macrophages were the predominant subgroup in IM-GC samples and the transition from IM-GC to IM+GC was characterised by a decrease in M2 and an increase in M1/2 macrophages with a final overall ratio approaching 1:1.

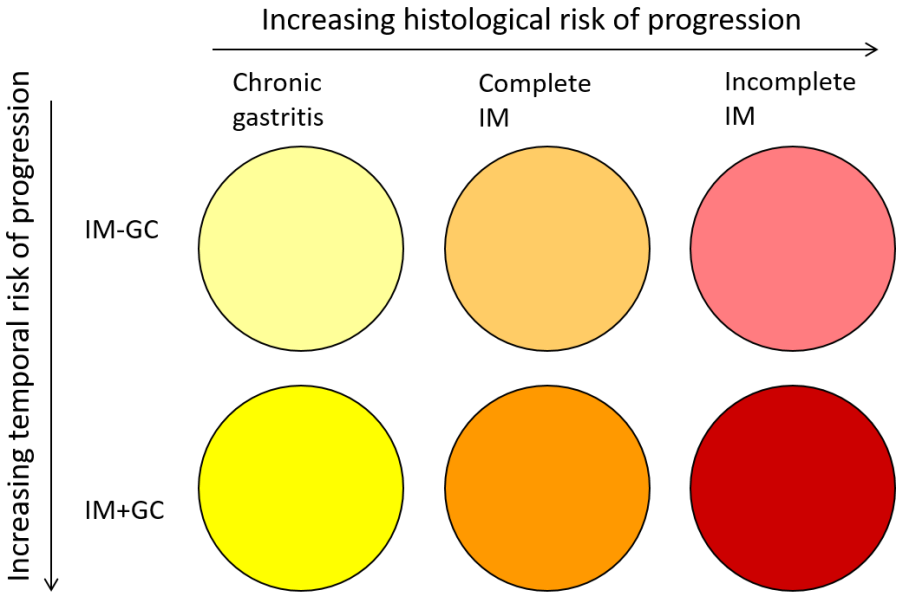


Figure 9.1 Histo-temporal model of increasing risk of progression using Correa premalignant lesions from patients with (IM+GC) and without concurrent gastric cancer (IM-GC)
Premalignant lesions in the IM-GC cohort defined as "early" and in the IM+GC cohort as "late", likely with accumulated genomic/epigenomic alterations and other pro-malignancy changes in the surrounding microenvironment as described in more detail in §9.2. Intestinal metaplasia subtypes based on the Jass and Filipe classification [130].

Incomplete IM in IM-GC patients had particularly high levels of CD163+CD206+IRF8+ macrophages but lower numbers of CD163+CD206+ macrophages which suggested that expression of IRF8 was a key differentiator in macrophages between IM subtypes. IRF8 is known to be induced in the presence of IFNγ and regulates expression of IFNα and IFNβ thus the prevalent T cell response in incomplete IM is likely to be more Th1-like than in complete IM [600]. This was further supported by the over-expression of the *IL18* gene in incomplete IM (§4.3.12) which is associated with a Th1 response [459].

The transition from IM-GC to IM+GC showed a reduction in total macrophage population only in the incomplete subtype and this was due to a lower density of M2 macrophages suggesting that loss of macrophages and phenotype switching from M2 to M1/2 are the two most important macrophage factors associated with progression risk in IM. Cellular spatial analyses showed that the difference in macrophage densities was reflected in the number immediately adjacent and within a functional paracrine radius (40µm) between macrophage subsets but also between macrophages and epithelial cells (§5.3.10-12).

Using the histo-temporal model described in Figure 9.1 and integrating both the quantitative and spatial findings of the current study, it becomes apparent that M2 macrophages provide the highest level of protection, M1/2 macrophages provide an intermediate level of protection and low numbers of total macrophages offer the lowest level of protection against progression.

Given that a key function of macrophages involves the phagocytosis of bacteria, dead cells but also of cancer cells, it suggests that lower numbers of macrophages in incomplete IM tissues result in reduced macrophage "patrolling" of the epithelium [601, 602]. Also, given that another key function of macrophages involves the presentation of antigen to T cells, it is most likely that fewer macrophages result in reduced effectiveness of the local T cell response [603, 604]. The reduced level of protection offered by M1/2 macrophages may be in part explained by the possible differences in amount of reactive nitrogen species (RNS) between IM subtypes. RNS are derived from nitric oxide and superoxide produced by the enzymatic activity of nitric oxide synthase 2 (NOS2) and NADPH oxidase (NOX1). NOS2 expression by macrophages is induced by IFNγ [605] thus based on the relative abundance of IRF8+ macrophages in incomplete IM tissues, it suggests that epithelial cells are more exposed to RNS leading to greater genomic and epigenomic instability in this tissue type.

The analysis of total T cell population in both IM-GC and IM+GC cohorts reflected closely that of total macrophage population, including a reduction in the transition from IM-GC to IM+GC for incomplete IM. This suggested an overall coordinated reduced innate and adaptive immunity in this tissue type. Initially this reduction was due to lower levels in CD8 and DN T cells but in the IM+GC cohort CD4 T cells were also highly reduced in incomplete IM. For complete IM the transition of the T cell landscape from IM-GC to IM+GC tissues was characterised by an even greater density of CD4 and DN T cells suggesting that hyper T cell inflammation may be a risk factor in this subtype of IM (role of inflammation in $gp130^{F/F}$ mouse model of GC described in [242]). Spatial analyses showed that T cell targeting of the epithelium differed between tissue types (§6.3.11) but that overall differences in spatial characteristics reflected differences in T cell subset densities (§6.3.9-10). Finally spatial correlation network analysis showed that the distribution of macrophage subsets and T cells changes in the transition from IM-GC to IM+GC but that generally complete IM is characterised by the formation of lymphoid aggregates interspersed between glands whereas incomplete IM has clear polarised areas of glandular epithelium with T cell interaction separated from areas rich in T cell-T cell interaction (§6.3.12-14).

In an effort to dissect the role of topographical and temporal aspects of IM progression and to characterise the immune landscape in dysplasia, multiple samples of two Progressors case studies were characterised including low and high grade dysplasia (LGD and HGD respectively). The changes in macrophage and T cell populations between sites and between time points suggested that immune cell infiltration is highly dynamic and varies significantly by site, implying

that the immune system may play a role in site-associated risk of progression such as IM in the Maggenstrasse [134]. In one patient HGD was characterised by a strong increase in both FOXP3 and CD8 T cells including a remarkable increase in FOXP3 T cells neighbouring CD8 T cells within their functional space. Interestingly the macrophage landscape in HGD between the two Progressors patients differed considerably. In one patient progression was associated with a sudden increase in M1 and M1/2 macrophages whereas M2 macrophage density plummeted. By contrast in the other patient a significant increase in M2 macrophages was associated with a complete collapse of M1 and M1/2 macrophage populations. However both patients showed a strong increase in CD163+IRF8-/+ macrophages in the absence of CD206 suggesting that CD163+ macrophages irrespective of IRF8 expression may play an important role in progression at that stage.

It is difficult to compare the findings of such detailed characterisation of the innate and adaptive immune system in multiple gastric premalignant lesions as no such previous study has been carried out. However with respect to macrophage profile in human CG tissue, the current study's findings showed some similarities but also some differences with those previously published [205, 469]. CG was characterised by a M1 but also M2 macrophage presence, and in the same study atrophic gastritis (AG) was characterised by an augmented M1 but stable M2 macrophage response as measured using real-time PCR with multiple markers including iNOS (NOS2) and CXCL11 (both M1 markers), and CCL17, CCL18 and CD206 (all M2 markers) [205]. Overall this would suggest that the long term process of gastric carcinogenesis is associated with a changing macrophage landscape and that AG may share certain similarities with the incomplete subtype of IM (a more pro-inflammatory M1-like environment).

Modelling with SPEM mice has shown that macrophages play an important role in the process of metaplasia overall and that CD163+ cells are over-represented in IM [207]. However CD163 as a marker on its own does not certify the presence of macrophages nor, as suggested, of the M2 subtype [482, 606]. The reduction of CD4+ and FOXP3+ cells has been described previously in IM but without any information on CD3 status and IM subtype [236].

By integrating immunological data acquired through both gene expression and immunohistochemistry, it is possible to form a picture of the immune landscape in IM and beyond. Incomplete IM is characterised by a reduction of CD8 T cells suggesting reduced cytotoxicity as both conventional cytotoxic T cells and innate like T cell subsets expressing CD8 have cytolytic capabilities [502, 506-508, 607]. The reduced numbers of DN T cells in this tissue type further confirms the reduction of innate like T cell presence, possibly of MAIT cells and γδ

T cells in the microenvironment. This quantitative difference in T cell density was previously suggested by the over-expression of *CCL25* (both in our samples and the validation cohort [388]) and *CCL5* in complete IM tissues. The former finding was particularly significant as it is normally expressed in the epithelium of the small intestine and not the colon thus providing evidence of the ability of complete IM to replicate the immune microenvironment of the small intestine. Reduced inflammation in incomplete IM was also suggested by lower gene expression of multiple pro-inflammatory cytokine receptor molecules such as IL6R, IL7R and IL11RA. However other differences in cytokine profile between complete and incomplete IM are more difficult to assess. IL18 which has both pro-inflammatory (Th1 responses) and immune-regulatory properties was overexpressed in incomplete IM yet one of its receptor components IL18RAP was also overexpressed in complete IM [436]. Both pro- and anti-tumourgenic properties of IL18 have been reported in previous studies including a possible role in GC tumour growth and the evasion of the anti-tumour immune response either directly or through the generation of myeloid derived suppressor cells (MDSC) [608-610]. However inhibition/modulation of IL18 activity may be occurring as IL37 (this study) and IL18BP (validation cohort), both of which inhibit IL18 signalling [610, 611], were overexpressed in complete IM. Finally it is likely that the interplay between epithelial-derived IL18 and immune cell-derived IL6, IL7, IL11 and IL17 (by Th17, MAIT cells, γδ T cells) results in a polarised immune spectrum driving inflammation in complete IM and immune regulation in incomplete IM. The lack of quantitative FOXP3 T cell differences between IM subtypes suggests that this immune regulation is at least in part cytokine driven and not by regulatory T cell and it affects overall tissue infiltration of specific T cell and macrophage subsets.

Having characterised the cytokine, the chemokine, the quantitative and the spatial immune profiles of complete and incomplete IM, it is also important to discuss the prevailing local context of the immune response in order to gain further insight into how these differences may be key in progression to dysplasia/cancer. The formation of both complete and incomplete IM occurs in an unnaturally high gastric pH due to loss of parietal cells that usually secrete hydrochloric acid (achlorhydria) [75, 612]. Following infection, *H. pylori* burden remains high during CG but starts to decrease with AG and continues to decrease throughout IM, dysplasia and then GC [613]. However other cellular insults may occur due to changes in the local microbiome as the sterilising effect of gastric acid has been weakened. Microbial dysbiosis has been described in GC including changes to bacterial richness and diversity, although its exact role in gastric carcinogenesis has not yet been established [613, 614]. *H. pylori* infection itself leads to changes in the gastric microbiota and gradual reduction of *H. pylori* burden results in

increasing dysbiosis [613, 615-617]. The exact effect of changes in abundance and types of microbial populations on the gastric mucosal immune system are not yet known but a positive correlation was shown between regulatory T cells and plasmacytoid dendritic cells with several bacterial taxa in GC patients [618]. Thus dysbiosis may play an important role in the formation of the immune landscape in IM.

It is also crucial to keep in mind that dysbiosis most likely results in increased levels of cellular stress on IM epithelial cells as well as stem cells at the bottom of the gland. Stem cells replicate to produce progenitor cells which in turn replicate and differentiate into the varying cell populations that make up the IM glandular epithelium. In addition stem cells replicate to renew their own population and thus carry the long term accumulation of potentially deleterious genomic and epigenomic changes. Overall the incurred molecular and cellular instability due to *H. pylori* infection, long term inflammation with accompanying local release of multiple DNA damaging agents including reactive oxygen and nitrogen species (ROS and RNS) together with further stress produced by dysbiosis over a period of time spanning multiple decades likely results in early abnormal stem cells which have the potential to form LGD or directly HGD or even early cancerous cells, if they are not eliminated rapidly by the immune system. The rate of formation of early abnormal cells must be less or equal to the rate of elimination to prevent progression. Although the process of immune surveillance and evasion has been studied more extensively in the context of cancer [619, 620], few studies have looked at the immune changes that occur in premalignant lesions and their role in tumour initiation [621-623]. A recent key study using multiple stages of lung squamous cell carcinogenesis including metaplasia and dysplasia with increasing severity showed that immune activation and suppression occur at the pre-invasive stages of cancer development [624]. Thus it is likely that the high progression risk associated with gastric incomplete IM is not only due to stem cell genomic/epigenomic instability but also due to reduced immune-surveillance. It is reasonable to hypothesize that the reduction in CD8 and DN T cells together with macrophages known to act as antigen presenting cells may lead to reduced abnormal cell killing capacity which gradually becomes worse as incomplete IM develops over time. When lesions reach the more advanced stages of HGD, increased Treg infiltration leads to higher levels of immune-suppression together with a potential key role for macrophages expressing CD163 in the absence of CD206. The CD163 marker has traditionally been a key marker in tumour-associated macrophage (TAM) studies and is normally associated with poor prognosis [481, 625].

In short, my findings suggest the Correa model is encapsulated by a long term dysregulated immune response to *H. pylori* infection, followed by epithelial changes that eventually lead to intestinalisation and a reduction of effective immune-surveillance in the incomplete subtype of IM (Figure 6.20) results in progression to low or high grade dysplasia, which in context of immune-suppression leaves the door open for abnormal cells to reach a malignant stage.

9.4 Determining the biomarker potential of anti-CD10 and Das1 antibodies for subtyping complete and incomplete intestinal metaplasia

Risk factors associated with progression to GC include gender, age, family history of GC, *H. pylori* status, diet, lifestyle choices and the presence of premalignant lesions such as AG and IM but also topography (IM at the body) and extent (multifocal IM). However as mentioned previously, multiple studies have also shown an association between incomplete IM and a higher risk of progression to GC, but this has not filtered through to the current Victoria "Upper gastrointestinal endoscopy categorisation guidelines for adults" (2018). The main reason for this is that the distinction between the complete and incomplete subtypes of IM is still considered a "subjective matter" by pathologists [140]. Overall inter-observer agreement has been shown to be lower between general pathologists than between experienced gastrointestinal pathologists [105].

The fourth aim of the current study was to address the existing gap in reliable biomarkers for subtyping IM with future potential for clinical use. Based on a combination of published literature and the gene expression findings described in section §4.3.10, CD10 and Das1 [518, 626] were chosen as candidate biomarkers for defining complete and the incomplete subtypes of IM, respectively. Characterisation of staining at the single gland level was chosen as the most accurate metric to accomplish this objective. Gene expression profiling had shown that the *MME* gene that encodes CD10 was highly overexpressed in complete IM (§4.3.10).

Immunohistochemistry of IM tissue with an anti-CD10 antibody was used to validate these initial findings. For this study the upper part of individual IM glands was used for subtyping as the brush border associated with the complete subtype of IM is more visible there. Across three different patient cohorts potentially representing separate stages of temporal progression in IM, CD10 was shown to have high to very high sensitivity and specificity for the identification of individual complete IM glands (§7.3.2). An average AUROC value of above 0.94 makes this an outstanding biomarker [627, 628] for complete IM overall. Having a very high specificity for complete IM means lack of staining can also be used to identify incomplete IM thus making it a universal biomarker for IM subtyping. Furthermore in the presence of a general IM marker such

as MUC2 for goblet cells, precise quantification of IM subtype prevalence on a tissue section will be possible even for non-gastrointestinal pathologists. This could be particularly useful given that not all hospitals/institutes, including those that are part of rural and regional healthcare services ([629], https://www.betterhealth.vic.gov.au/ accessed 19/06/2020) have a specialised gastrointestinal pathologist at their disposal.

The Das1 antibody was chosen for this study as it normally stains the colonic epithelial protein found in the colon and had previously been shown to be associated with the incomplete subtype of IM [518]. Studies investigating the relationship of Das1 staining with IM and dysplasia/gastric cancer in the same patient had also described a consistent positive correlation between IM glands positive for Das1 and distant dysplastic/tumour areas as well as increasing staining in both dysplasia and cancer compared to IM [518, 528-530]. Overall this data suggested that Das1 may have dual biomarker potential: 1) as a biomarker for the incomplete subtype of IM and 2) as a biomarker delineating risk of progression irrespective of IM subtype. As a biomarker for incomplete IM glands, Das1 was shown to be of limited value, with a low sensitivity but a high specificity and an average AUROC of 0.60 across all three cohorts studied (§7.3.3). However across total biopsy area, Das1 staining was shown to be more associated with incomplete IM in both the IM-GC and IM+GC cohorts thus confirming previous findings (§7.3.5-7) [518, 528]. Finally Das1 was shown to have potential utility as a progression risk biomarker as IM+GC patients with complete IM showed significant more staining than IM-GC patients (§7.3.8). In combination with a serial anti-CD10 stained section, Das1 could thus be used to identify those patients with complete IM which are most likely to progress to the incomplete subtype or to neoplasia. The molecular mechanism for this possible subtype transition remains to be elucidated although it is commonly believed to be a required event for progression to dysplasia [630-632].

The combined use of CD10 and Das1 in a logistic regression model for subtyping complete IM glands showed a small increase in AUROC (0.955 vs 0.970) suggesting an additional added value of using Das1 in a clinical setting (§7.3.4). Thus if sufficient tissue is available, both markers could be used to subtype IM. First CD10 staining could be used to define areas with complete (+ve staining) and incomplete IM (-ve staining) glands and their relative abundance. A defined percentage of relative abundance of incomplete IM glands for a pathologist to diagnose IM tissue as incomplete IM does not exist currently ([134], personal discussion with in-house research pathologist Dr Catherine Mitchell), thus this is an area that would benefit additionally from the use of CD10. Then Das1 staining could be used first to eliminate any possible areas with

uncertain subtype, particularly for tissue sections rich in the lower part of IM glands (reduced presence of brush border) and second to determine whether the tissue contains complete IM glands at greater risk of progression (+ve staining). However further research is required into the mechanistic relationship between Das1 and IM gland progression to dysplasia to confirm its clinical utility.

To facilitate the process of subtyping IM and assessing risk associated with progression, the combined use of CD10 and Das1 on an automated platform could be developed. Alternatively if relative abundance of subtype is shown to be key for assessing risk of progression, the combined use of CD10 and a pan IM marker such as MUC2 on an automated platform could also be developed. Furthermore, given there are established clinical algorithms of risk with OLGIM [104], future multifactorial risk assessment of patients with IM could include the integration of OLGIM stage with CD10/Das1 status to further improve patient stratification.

Finally the use of any new biomarker needs to be assessed in the context of what is available to local pathologists before a final decision is taken with respect to its future use. Currently most pathologists in the state of Victoria use haematoxylin and eosin stained sections to determine IM subtype, and as mentioned previously IM subtype is not part of the prevailing guidelines. The use of immunohistochemistry with an anti-CD10 antibody would initially lead to an increase of cost but ultimately its introduction in the guidelines would produce clinical benefits to patients as it would allow a greater level of precision with regards to targeted surveillance for those patients at greater risk of progression to GC. Costs associated with GC treatment would be reduced and patient quality of life would increase.

Having previously determined a possible role for the immune microenvironment in progression to GC, the relationship between Das1 positive incomplete IM glands and macrophage subset infiltration was investigated using serial sections. Given that Das1 stains a colon epithelial protein, and previous gene expression profiling had shown that incomplete IM is associated with high expression of both colon and GC associated genes (§4.3.10), the aim of this investigation was to assess the potential crosstalk between high risk glands and macrophages. A significant positive correlation between Das1 staining and two IRF8 expressing macrophage subsets in IM-GC patients was observed, suggesting that epithelial Das1 status may have an effect on the local attraction of specific macrophages. The presence of IRF8 on these macrophage subsets suggests that a pro-inflammatory microenvironment is associated with greater risk of progression which needs to be further investigated.

9.5 Intestinal metaplasia organoids can be grown from gastroscopy biopsies

One of the major deficits in studying gastric carcinogenesis is a lack of human specific models. As mentioned in the Chapter 1 (§1.6.1-2) there are multiple animal models of GC but none fully recapitulate the human condition. Thus the fifth aim of the current study was to address this existing gap by developing appropriate methodology that would allow the growth of intestinal metaplastic organoids from human gastroscopy biopsies. To achieve this would require to go beyond the currently used protocols that invariably use gastrectomy tissue to grow normal gastric organoids [366, 633].

The first and most important technical issue addressed was that of limited starting material. By using first a porcine model and then multiple biopsies from individual patients, optimised protocols were developed for each stage of this study including gland isolation, initial organoid colony formation, growth, expansion, freezing and thawing of organoid cultures (§8.3.2-4). Published protocols for downstream characterisation of organoid cultures including blocking/immunohistochemistry and qRT-PCR were successfully modified for use in this setting (§8.3.5) [634, 635]. The key role of organoid growth medium was investigated by using a combination of the in-house customisable organoid growth medium and the commercially available IntestiCult™ growth medium. The latter gave better overall proliferation rates but the former allowed the gradual manipulation of niche factor content in the growth medium.

Having established the essential protocols, human gastric and small intestine (as a positive control for IM) organoids were characterised using tissue specific immunohistochemistry markers. Normal gastric organoids were MUC5AC positive, irrespective of origin (antral or body), suggesting differentiation similar to the upper part of a gastric gland (§8.3.6). Most, but not all, small intestine organoids contained cells positive for CDX2 suggesting that although this marker was useful, it could in theory produce false negatives and miss true IM organoids (§8.3.6). In the small intestine, CDX2 is mostly expressed in the villi and in differentiated cells with only low levels of staining in the crypt [416, 636]. It is possible that small intestinal organoids contained a substantial number of stem cell-like cells which lacked CDX2 expression, likely as a result of the growth medium used that included Wnt3a. In intestinal crypts Wnt3A and Wnt agonist R-Spondin 1 control crypt proliferation *in vivo*, and in organoid populations R-Spondin 1 and Wnt3 maintain cell proliferation and keep the majority of cells in an undifferentiated semi-stem cell like state [364, 637-639].

Overall IM organoids defined as CDX2+ organoids by immunohistochemistry grown from gastric biopsies were successfully grown from six patients (§8.3.6). Further characterisation with

immunohistochemistry showed that they were mainly positive for MUC5AC, partially positive for TFF3 and mostly negative for CD10. Overall they did not fully recapitulate the characteristics of the parent tissue. This was also observed for small intestine organoids which on numerous occasions contained MUC5AC positive cells, a gastric marker not normally expressed in small intestine tissue. This suggested the possibility of suboptimal growth conditions or specific growth media effects that require further investigation. Finally qRT-PCR was used to validate the presence of *CDX2* but also of *VIL1* mRNA in both small intestinal and IM organoids (§8.3.7).

This study confirmed some of the findings associated with previous studies on gastrointestinal organoids including body organoid differentiation following removal of Wnt3A (§8.3.8) [366]. However some unexpected results were also observed and in particular two sets of results in the growth media manipulation experiments stood out. Firstly after an initial few rounds of passaging/expansion grown in IntestiCult™ growth medium, antral organoids were able to grow and proliferate over an extended period of time without signs of morphological differentiation in Wnt3A-free growth medium. The removal of Wnt3A in human organoid growth media is generally associated with increased differentiation irrespective of organoid type and tissue of origin and levels of organoid differentiation are inversely proportional to their ability to proliferate [362, 365, 366, 640]. This novel finding suggests that human antral organoids may have the capacity to produce their own Wnt3A, similar to the Wnt niche-independent growth capacity in gastric cancer organoids [542]. Technically this could be tested by collecting the media and doing a TOP-flash assay, a luciferase reporter assay commonly used to monitor levels of Wnt activity in growth media [637, 641]. However due to time restrictions associated with completion of my PhD, I could not perform these experiments.

The second surprising result observed was that of the unrestrained growth and proliferation rate in small intestinal organoids with Wnt3A-free media. Although Wnt-free media has been used to grow mouse small intestinal organoids as these constitutively express their own Wnt, no previous study to my knowledge has described human small intestinal growth in the absence of Wnt (and Notch) modulating compounds such as CHIR99021, a glycogen synthase kinase 3β, and valproic acid, a histone deacetylase inhibitor [640, 642].

An additional interesting finding of the current study was the partial growth medium-associated plasticity observed in both antral and small intestinal organoid populations. Antral organoids grown in the absence of Wnt3A with or without FGF10 and gastrin showed an increasing hybrid gastric-intestinal gene expression profile (expression of TFF1 and TFF2 but also of VIL1) but not at the protein level as they remained CDX2 negative. Small intestinal organoids showed some

MUC5AC protein expression but no TFF1 or TFF2 expression in any combination of Wnt3A, FGF10 and gastrin suggesting a limited but stable gastric-intestinal phenotype. Tissue plasticity has been previously modelled using mouse Cdx2^{null} small intestinal organoids. Such organoids were shown to depend on gastric culture conditions (requirement of Wnt3A, FGF10 and gastrin) and were associated with loss of intestinal (*Olfm4*, *Villin*, *Cdx1*, *Muc13* and *Lyz1*) and gain of stomach markers (*Muc6*, *Gli*, and *$H^{+/}K^{+}$ ATPase*) [643]. Interestingly Cdx2^{+} expressing gastric organoids remained gastric-like with only very limited levels of intestinalisation (little expression of *Tff3* and *Muc2*) suggesting ectopic expression of Cdx2 is not enough in mice to drive intestinalisation of the gastric epithelium.

The use of a FACS based strategy with the intestinal specific stem cell marker OLFM4 designed to enrich for IM organoids in a mixed IM/gastric population did not produce the expected results. Although immunohistochemistry with the same OLFM4 antibody showed this marker was expressed in the lower part of the small intestinal crypt and IM glands where the stem cell compartment resides in these two tissue types, organoids grew mainly from OLFM4- cells. OLFM4 was absent in gastric glands and organoids grew from both antral and body OLFM4- cells as expected. Overall these results suggest that although OLFM4 is indeed a potential stem marker in the small intestine and IM, its expression increases in non-stem cells within gastrointestinal organoids and decreases in those cells with the capability to regrow into whole organoids from a single cell. Thus it does not seem to be optimal for selecting single cells from IM organoids with the ability to regrow in a background of normal gastric organoid cells.

9.6 Future directions

The work described in this thesis has provided a number of new areas that require investigation in the field of gastric carcinogenesis. In order to confirm the clonal origins of diffuse and intestinal gastric tumours and identify whether intestinal metaplasia has a premalignant role in either or both, whole genome sequencing of intestinal metaplasia immediately adjacent to both gastric tumour types should be carried out. This work could be extended to include mixed gastric tumours by sequencing intestinal metaplasia immediately adjacent of both the intestinal and diffuse areas of the tumour. Sequencing of adjacent chronic and atrophic gastritis as well as low and grade dysplastic tissue would complement such a study and allow the identification of the main genomic pathways to gastric cancer. A similar study using 23 paired samples provided insights in the clonal architecture of Barrett's oesophagus and oesophageal adenocarcinoma [644].

Additional single cell transcriptome and methylome studies could be used to develop a molecular classification system of gastric premalignant lesions. Already a single cell transcriptomic study based on a small number of chronic and atrophic gastritis, intestinal metaplasia and early gastric cancer tissues characterised the early stages of goblet cells and identified potential biomarkers of early gastric cancer cells [515]. Unfortunately this study only used samples representing the incomplete intestinal metaplasia subtype thus it is not possible to use the produced data to compare differences between intestinal metaplasia subtypes. However single cell transcriptome data could also be used to gain further insight into the immune cell landscape of intestinal metaplasia subtypes. Indeed an integrated multi-omics and immunity Pre Cancer Atlas for all cancer types with premalignant stages was recently proposed [645].

The immune microenvironment in intestinal metaplasia could be further investigated quantitatively and spatially by using multiplex immunohistochemistry with the aid of MAIT cell and γδ T cell specific antibodies to determine the prevalence of these T cell types in intestinal metaplasia. These antibodies together with equipment and reagents for 9-marker OPAL™ multiplex immunohistochemistry are already used at the Peter MacCallum Cancer Centre for similar projects. As intestinal metaplasia occurs in the context of chronic inflammation, levels of T cell activation and exhaustion should also be investigated. Additional characterisation of T cell and macrophage subsets could be carried out by using flow cytometry on fresh biopsy samples that would allow an even greater number of markers to be used. Other immune cell types present in intestinal metaplasia tissues could be identified and characterised using both multiplex immunohistochemistry and flow cytometry from biopsy tissue.

To gain insight into the mechanistic role of T cells and macrophages in intestinal metaplasia, cells from fresh biopsies could be expanded *in vitro* and characterised. Such studies would also benefit from immune co-cultures with intestinal metaplasia-derived organoids to identify immune cell-epithelial cell interactions. *In vitro* manipulation of immune cell responses to intestinal metaplasia organoids could be modulated with the use of cytokines and other molecules known to play an important role in immune responses. The development of intestinal metaplasia subtype specific organoid cultures could be used to enhance our understanding of the role of the immune microenvironment in gastric carcinogenesis.

Data from this thesis could be used to further develop optimal growth media for selective enrichment and characterisation of intestinal metaplasia organoids. For example the observed enrichment of glucose and fructose associated pathways in complete intestinal metaplasia could

be used to create a customised growth medium that would give a selective organoid growth advantage against normal gastric organoids. Other methods that could be used to enrich for intestinal metaplasia organoids include mass spectrometry of culture supernatants to detect metabolites and identify key metabolic differences between normal gastric and intestinal metaplasia organoids followed by customised growth conditions. Alternatively morphology based machine learning could be the used to identify intestinal metaplasia organoids in culture. Cultures with increased probability of containing intestinal organoids could be cloned either manually or using serial dilution.

With the help of single cell transcriptomic data, novel stem cell markers in intestinal metaplasia could be identified that are absent in antral and body glands and used to grow intestinal metaplasia organoids from single cells. The use of intestinal metaplasia organoids to study gastric carcinogenesis could involve sequential genomic changes to gain greater understanding, similar to organoid modelling of colon carcinogenesis by Matano et al 2015 [368] and Drost et al 2015 [367]. Using lentiviral transduction and/or CRISPR-Cas9 editing the over-expression and knock out of key genes associated with gastric carcinogenesis such as MYC and TP53 could be achieved [646]. Such genetically engineered organoids could be inserted into mouse models in order to validate their carcinogenic potential [360, 368, 646]. In addition to the study of carcinogenesis, intestinal metaplasia organoids could be used as a model to test for potential drug treatments that prevent the development of gastric cancer altogether.

To advance the field of intestinal metaplasia patient stratification and targeted surveillance, multi-centre prospective studies could be used to validate CD10 not only as a reliable biomarker for complete intestinal metaplasia but also as a potential low risk intestinal metaplasia marker. Conversely, CD10 negative intestinal metaplasia could then become an established marker for high risk without a need to discuss whether subtyping of IM is a subjective exercise and thus included in the management guidelines of gastric epithelial precancerous lesions. The development of an automated platform for CD10 staining together with a pan IM marker would allow the relative quantification of CD10 positive intestinal metaplasia tissue thus further facilitating the process of intestinal metaplasia subtype diagnosis. Prospective studies could also be used to assess the relationship between progression risk and Das1 staining. Such studies would also incorporate immune cell markers to determine the progression risk factor associated with the presence or absence of certain immune cells such as CD8 T cells in patients with intestinal metaplasia. Future biomarker studies could also include HOXA10, HOXA13 and CLDN1 as potential candidates for incomplete intestinal metaplasia.

9.7 Conclusions

The main objective of this thesis was to identify and characterise the cellular and molecular changes in intestinal metaplasia associated with progression to gastric cancer. The progress described by this thesis in this field is visually summarised in Figure 9.2 and includes the following:

1) Both histologically and molecularly, diffuse gastric cancer was shown to be potentially associated with intestinal metaplasia, at least in a proportion of cases. This suggests that the process of gastric carcinogenesis is heterogeneous, as has been indicated by multiple molecular classification studies of gastric cancer and in particular the TCGA study [42-44].

2) Gene expression profiling showed that the complete and the incomplete subtypes of intestinal metaplasia differ substantially in both epithelial and the immune cell components. Complete intestinal metaplasia was associated with genes highly expressed in the small intestine. Interestingly, incomplete intestinal metaplasia was shown to be associated not only with genes highly expressed in the colon but also in gastric cancer thus making it molecularly closer to a state of malignancy.

3) The use of multiplex immunohistochemistry confirmed these initial findings and showed evidence suggesting that a suboptimal T cell and pro-inflammatory macrophage response leads to reduced immune-surveillance in incomplete intestinal metaplasia. This reduced immune-surveillance may play a key role in further progression of this subtype of intestinal metaplasia to dysplasia and gastric cancer.

4) Histologically similar tissues from patients with and without gastric cancer were shown to be significantly different using both gene expression profiling and multiplex immunohistochemistry confirming previous studies into the possible effect of field cancerisation [451-453].

5) CD10 was shown to be an outstanding biomarker for complete intestinal metaplasia and Das1 was shown to have potential as an additional risk associated biomarker. A logistic regression model using both biomarkers showed an overall AUROC of 0.970 for the complete subtype of intestinal metaplasia.

6) The logistics pathway for growing and characterising intestinal metaplasia organoids from patients using limited biopsy material was established. Differentiation conditions were investigated in detail and a protocol for selecting and growing organoids from single FACS sorted cells was developed using the small intestine stem cell marker OLFM4.

Overall future research in this field should aim to increase our core understanding of the mechanisms involved in gastric carcinogenesis thus enabling precision prevention of gastric cancer by improving patient stratification and targeted surveillance. The vision of a gastric cancer-free world would not only save a large amount of human suffering but also be financially a better place to live in as medical costs associated with treating this disease would substantially decrease.

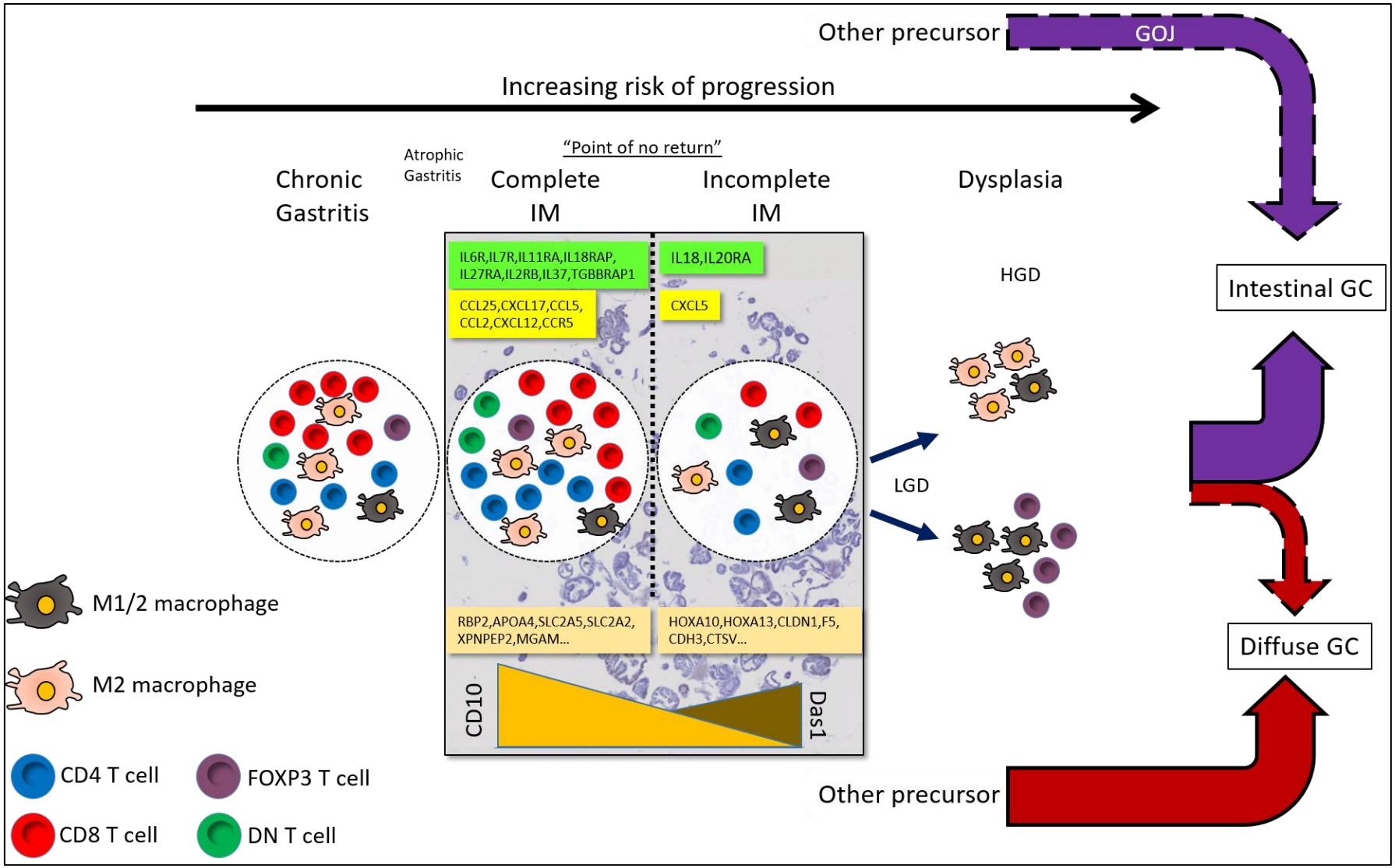


Figure 9.2 Schematic summary of the key findings described in this thesis with respect to intestinal metaplasia and progression to gastric cancer

The process of gastric carcinogenesis is likely more heterogeneous than previously thought with increasing evidence of intestinal metaplasia as a possible premalignant lesion for a fraction of the diffuse subtype of gastric cancers and an unknown precursor at the gastro-oesophageal junction for the intestinal subtype in a low incidence setting such as Australia. Incomplete intestinal metaplasia (IM) is characterised by a significant decrease in inflammation associated cytokines and chemokines, T cell and macrophage subset populations suggesting that reduced immune-surveillance may play a key role in progression. M2 macrophages (CD68+CD163+ and CD68+CD163+CD206+) may have a protective role whereas M1/2 macrophages (CD68+CD163+IRF8+, CD68+CD206+IRF8+ and CD68+CD163+CD206+IRF8+) displaying a combination of M1 and M2 markers may be associated with higher risk. High grade dysplasia (HGD) is characterised by varying macrophage subset populations and immune-regulation by FOXP3 T cells may play a key role in progression to cancer in at least a subgroup of HGD patients. Complete intestinal metaplasia is highly positive for the brush border marker CD10 and incomplete intestinal metaplasia is associated with Das1 staining for the colon epithelial protein. To avoid confusion previously described Das1 staining in dysplastic and gastric cancer tissue is not shown [518, 528]. Finally optimised conditions for establishing and characterising intestinal metaplastic organoids from gastroscopy biopsies were developed.

References

1. Balakrishnan M, George R, Sharma A, Graham DY. Changing Trends in Stomach Cancer Throughout the World. Curr Gastroenterol Rep. 2017;19(8):36.

2. Bray F, Ferlay J, Soerjomataram I, Siegel RL, Torre LA, Jemal A. Global cancer statistics 2018: GLOBOCAN estimates of incidence and mortality worldwide for 36 cancers in 185 countries. CA Cancer J Clin. 2018;68(6):394-424.

3. Ferlay J, Soerjomataram I, Dikshit R, Eser S, Mathers C, Rebelo M, et al. Cancer incidence and mortality worldwide: sources, methods and major patterns in GLOBOCAN 2012. Int J Cancer. 2015;136(5):E359-86.

4. Layke JC, Lopez PP. Gastric cancer: diagnosis and treatment options. Am Fam Physician. 2004;69(5):1133-40.

5. Maconi G, Manes G, Porro GB. Role of symptoms in diagnosis and outcome of gastric cancer. World J Gastroenterol. 2008;14(8):1149-55.

6. Matsuda T, Ajiki W, Marugame T, Ioka A, Tsukuma H, Sobue T, et al. Population-based survival of cancer patients diagnosed between 1993 and 1999 in Japan: a chronological and international comparative study. Jpn J Clin Oncol. 2011;41(1):40-51.

7. Jung KW, Won YJ, Kong HJ, Lee ES. Cancer Statistics in Korea: Incidence, Mortality, Survival, and Prevalence in 2016. Cancer Res Treat. 2019;51(2):417-30.

8. Vogelaar IP, van der Post RS, Bisseling TM, van Krieken JHJ, Ligtenberg MJ, Hoogerbrugge N. Familial gastric cancer: detection of a hereditary cause helps to understand its etiology. Hered Cancer Clin Pract. 2012;10(1):18.

9. Juarez-Salcedo LM, Sokol L, Chavez JC, Dalia S. Primary Gastric Lymphoma, Epidemiology, Clinical Diagnosis, and Treatment. Cancer Control. 2018;25(1):1073274818778256.

10. Masciari S, Dewanwala A, Stoffel EM, Lauwers GY, Zheng H, Achatz MI, et al. Gastric cancer in individuals with Li-Fraumeni syndrome. Genet Med. 2011;13(7):651-7.

11. Capelle LG, Van Grieken NC, Lingsma HF, Steyerberg EW, Klokman WJ, Bruno MJ, et al. Risk and epidemiological time trends of gastric cancer in Lynch syndrome carriers in the Netherlands. Gastroenterology. 2010;138(2):487-92.

12. van Lier MG, Westerman AM, Wagner A, Looman CW, Wilson JH, de Rooij FW, et al. High cancer risk and increased mortality in patients with Peutz-Jeghers syndrome. Gut. 2011;60(2):141-7.

13. Warren JR, Marshall B. Unidentified curved bacilli on gastric epithelium in active chronic gastritis. Lancet. 1983;1(8336):1273-5.

14. Parsonnet J, Friedman GD, Vandersteen DP, Chang Y, Vogelman JH, Orentreich N, et al. Helicobacter pylori infection and the risk of gastric carcinoma. N Engl J Med. 1991;325(16):1127-31.

15. Aromaa A, Kosunen TU, Knekt P, Maatela J, Teppo L, Heinonen OP, et al. Circulating anti-Helicobacter pylori immunoglobulin A antibodies and low serum pepsinogen I level are associated with increased risk of gastric cancer. Am J Epidemiol. 1996;144(2):142-9.

16. Ando T, Goto Y, Maeda O, Watanabe O, Ishiguro K, Goto H. Causal role of Helicobacter pylori infection in gastric cancer. World J Gastroenterol. 2006;12(2):181-6.

17. de Martel C, Ferlay J, Franceschi S, Vignat J, Bray F, Forman D, et al. Global burden of cancers attributable to infections in 2008: a review and synthetic analysis. The Lancet Oncology. 2012;13(6):607-15.

18. IARC. IARC monographs on the evaluation of carcinogenic risks to humans. France: World Health Organisation; 1994.

19. Hooi JKY, Lai WY, Ng WK, Suen MMY, Underwood FE, Tanyingoh D, et al. Global Prevalence of Helicobacter pylori Infection: Systematic Review and Meta-Analysis. Gastroenterology. 2017;153(2):420-9.

20. Windsor HM, Abioye-Kuteyi EA, Leber JM, Morrow SD, Bulsara MK, Marshall BJ. Prevalence of Helicobacter pylori in Indigenous Western Australians: comparison between urban and remote rural populations. Med J Aust. 2005;182(5):210-3.

21. Feldman RA, Eccersley AJ, Hardie JM. Epidemiology of Helicobacter pylori: acquisition, transmission, population prevalence and disease-to-infection ratio. Br Med Bull. 1998;54(1):39-53.

22. Dooley CP, Cohen H, Fitzgibbons PL, Bauer M, Appleman MD, Perez-Perez GI, et al. Prevalence of Helicobacter pylori infection and histologic gastritis in asymptomatic persons. N Engl J Med. 1989;321(23):1562-6.

23. Asaka M, Kimura T, Kudo M, Takeda H, Mitani S, Miyazaki T, et al. Relationship of Helicobacter pylori to serum pepsinogens in an asymptomatic Japanese population. Gastroenterology. 1992;102(3):760-6.

24. Zamani M, Ebrahimtabar F, Zamani V, Miller WH, Alizadeh-Navaei R, Shokri-Shirvani J, et al. Systematic review with meta-analysis: the worldwide prevalence of Helicobacter pylori infection. Aliment Pharmacol Ther. 2018;47(7):868-76.

25. Gonzalez CA, Pera G, Agudo A, Palli D, Krogh V, Vineis P, et al. Smoking and the risk of gastric cancer in the European Prospective Investigation Into Cancer and Nutrition (EPIC). Int J Cancer. 2003;107(4):629-34.

26. Praud D, Rota M, Pelucchi C, Bertuccio P, Rosso T, Galeone C, et al. Cigarette smoking and gastric cancer in the Stomach Cancer Pooling (StoP) Project. Eur J Cancer Prev. 2018;27(2):124-33.

27. Ma K, Baloch Z, He TT, Xia X. Alcohol Consumption and Gastric Cancer Risk: A Meta-Analysis. Med Sci Monit. 2017;23:238-46.

28. Koulis A, Buckle A, Boussioutas A. Premalignant lesions and gastric cancer: Current understanding. World J Gastrointest Oncol. 2019;11(9):665-78.

29. Mao Y, Yang W, Qi Q, Yu F, Wang T, Zhang H, et al. Blood groups A and AB are associated with increased gastric cancer risk: evidence from a large genetic study and systematic review. BMC Cancer. 2019;19(1):164.

30. Gupta S, Tao L, Murphy JD, Camargo MC, Oren E, Valasek MA, et al. Race/Ethnicity-, Socioeconomic Status-, and Anatomic Subsite-Specific Risks for Gastric Cancer. Gastroenterology. 2019;156(1):59-62 e4.

31. Lauren P. The Two Histological Main Types of Gastric Carcinoma: Diffuse and So-Called Intestinal-Type Carcinoma. An Attempt at a Histo-Clinical Classification. Acta Pathol Microbiol Scand. 1965;64:31-49.

32. Ming SC. Gastric carcinoma. A pathobiological classification. Cancer. 1977;39(6):2475-85.

33. Goseki N, Takizawa T, Koike M. Differences in the mode of the extension of gastric cancer classified by histological type: new histological classification of gastric carcinoma. Gut. 1992;33(5):606-12.

34. Berlth F, Bollschweiler E, Drebber U, Hoelscher AH, Moenig S. Pathohistological classification systems in gastric cancer: diagnostic relevance and prognostic value. World J Gastroenterol. 2014;20(19):5679-84.

35. Hu B, El Hajj N, Sittler S, Lammert N, Barnes R, Meloni-Ehrig A. Gastric cancer: Classification, histology and application of molecular pathology. J Gastrointest Oncol. 2012;3(3):251-61.

36. Howson CP, Hiyama T, Wynder EL. The decline in gastric cancer: epidemiology of an unplanned triumph. Epidemiol Rev. 1986;8:1-27.

37. Liu L, Wang ZW, Ji J, Zhang JN, Yan M, Zhang J, et al. A cohort study and meta-analysis between histopathological classification and prognosis of gastric carcinoma. Anticancer Agents Med Chem. 2013;13(2):227-34.

38. Chen YC, Fang WL, Wang RF, Liu CA, Yang MH, Lo SS, et al. Clinicopathological Variation of Lauren Classification in Gastric Cancer. Pathol Oncol Res. 2016;22(1):197-202.

39. Pattison S, Mann GB, Crosthwaite G, Lade S, Mitchell C, Leong T, et al. Predictors of outcome after surgery for gastric cancer in a Western cohort. ANZ J Surg. 2016;86(6):469-74.

40. Deng N, Goh LK, Wang H, Das K, Tao J, Tan IB, et al. A comprehensive survey of genomic alterations in gastric cancer reveals systematic patterns of molecular exclusivity and co-occurrence among distinct therapeutic targets. Gut. 2012;61(5):673-84.

41. Wang K, Yuen ST, Xu J, Lee SP, Yan HH, Shi ST, et al. Whole-genome sequencing and comprehensive molecular profiling identify new driver mutations in gastric cancer. Nat Genet. 2014;46(6):573-82.

42. Cancer Genome Atlas Research N. Comprehensive molecular characterization of gastric adenocarcinoma. Nature. 2014;513(7517):202-9.

43. Cristescu R, Lee J, Nebozhyn M, Kim KM, Ting JC, Wong SS, et al. Molecular analysis of gastric cancer identifies subtypes associated with distinct clinical outcomes. Nat Med. 2015;21(5):449-56.

44. Wang Q, Liu G, Hu C. Molecular Classification of Gastric Adenocarcinoma. Gastroenterology Res. 2019;12(6):275-82.

45. Smyth EC, Verheij M, Allum W, Cunningham D, Cervantes A, Arnold D, et al. Gastric cancer: ESMO Clinical Practice Guidelines for diagnosis, treatment and follow-up. Ann Oncol. 2016;27(suppl 5):v38-v49.

46. Hatta W, Gotoda T, Koike T, Masamune A. History and future perspectives in Japanese guidelines for endoscopic resection of early gastric cancer. Dig Endosc. 2020;32(2):180-90.

47. Sano T, Aiko T. New Japanese classifications and treatment guidelines for gastric cancer: revision concepts and major revised points. Gastric Cancer. 2011;14(2):97-100.

48. Washington K. 7th edition of the AJCC cancer staging manual: stomach. Ann Surg Oncol. 2010;17(12):3077-9.

49. Catalano F, Trecca A, Rodella L, Lombardo F, Tomezzoli A, Battista S, et al. The modern treatment of early gastric cancer: our experience in an Italian cohort. Surg Endosc. 2009;23(7):1581-6.

50. Choi AH, Nelson RA, Merchant SJ, Kim JY, Chao J, Kim J. Rates of lymph node metastasis and survival in T1a gastric adenocarcinoma in Western populations. Gastrointest Endosc. 2016;83(6):1184-92 e1.

51. Smalley SR, Benedetti JK, Haller DG, Hundahl SA, Estes NC, Ajani JA, et al. Updated analysis of SWOG-directed intergroup study 0116: a phase III trial of adjuvant radiochemotherapy versus observation after curative gastric cancer resection. J Clin Oncol. 2012;30(19):2327-33.

52. Zhang N, Fei Q, Gu J, Yin L, He X. Progress of preoperative and postoperative radiotherapy in gastric cancer. World J Surg Oncol. 2018;16(1):187.

53. Cunningham D, Starling N, Rao S, Iveson T, Nicolson M, Coxon F, et al. Capecitabine and oxaliplatin for advanced esophagogastric cancer. N Engl J Med. 2008;358(1):36-46.

54. Ychou M, Boige V, Pignon JP, Conroy T, Bouche O, Lebreton G, et al. Perioperative chemotherapy compared with surgery alone for resectable gastroesophageal adenocarcinoma: an FNCLCC and FFCD multicenter phase III trial. J Clin Oncol. 2011;29(13):1715-21.

55. Marrelli D, Polom K, de Manzoni G, Morgagni P, Baiocchi GL, Roviello F. Multimodal treatment of gastric cancer in the west: Where are we going? World J Gastroenterol. 2015;21(26):7954-69.

56. Noh SH, Park SR, Yang H-K, Chung HC, Chung I-J, Kim S-W, et al. Adjuvant capecitabine plus oxaliplatin for gastric cancer after D2 gastrectomy (CLASSIC): 5-year follow-up of an open-label, randomised phase 3 trial. The Lancet Oncology. 2014;15(12):1389-96.

57. Selim JH, Shaheen S, Sheu WC, Hsueh CT. Targeted and novel therapy in advanced gastric cancer. Exp Hematol Oncol. 2019;8:25.

58. Mitani S, Kawakami H. Emerging Targeted Therapies for HER2 Positive Gastric Cancer That Can Overcome Trastuzumab Resistance. Cancers (Basel). 2020;12(2).

59. Muro K, Chung HC, Shankaran V, Geva R, Catenacci D, Gupta S, et al. Pembrolizumab for patients with PD-L1-positive advanced gastric cancer (KEYNOTE-012): a multicentre, open-label, phase 1b trial. The Lancet Oncology. 2016;17(6):717-26.

60. Brar G, Shah MA. The role of pembrolizumab in the treatment of PD-L1 expressing gastric and gastroesophageal junction adenocarcinoma. Therap Adv Gastroenterol. 2019;12:1756284819869767.

61. Koumarianou A, Krivan S, Machairas N, Ntavatzikos A, Pantazis N, Schizas D, et al. Ten-year survival outcomes of patients with potentially resectable gastric cancer: impact of clinicopathologic and treatment-related risk factors. Ann Gastroenterol. 2019;32(1):99-106.

62. Park JM, Kim YH. Current approaches to gastric cancer in Korea. Gastrointest Cancer Res. 2008;2(3):137-44.

63. Isobe Y, Nashimoto A, Akazawa K, Oda I, Hayashi K, Miyashiro I, et al. Gastric cancer treatment in Japan: 2008 annual report of the JGCA nationwide registry. Gastric Cancer. 2011;14(4):301-16.

64. Correa P, Haenszel W, Cuello C, Tannenbaum S, Archer M. A model for gastric cancer epidemiology. Lancet. 1975;2(7924):58-60.

65. Correa P. Human gastric carcinogenesis: a multistep and multifactorial process--First American Cancer Society Award Lecture on Cancer Epidemiology and Prevention. Cancer Res. 1992;52(24):6735-40.

66. Sobala GM, Crabtree JE, Dixon MF, Schorah CJ, Taylor JD, Rathbone BJ, et al. Acute Helicobacter pylori infection: clinical features, local and systemic immune response, gastric mucosal histology, and gastric juice ascorbic acid concentrations. Gut. 1991;32(11):1415-8.

67. Watari J, Chen N, Amenta PS, Fukui H, Oshima T, Tomita T, et al. Helicobacter pylori associated chronic gastritis, clinical syndromes, precancerous lesions, and pathogenesis of gastric cancer development. World J Gastroenterol. 2014;20(18):5461-73.

68. Ihamaki T, Kekki M, Sipponen P, Siurala M. The sequelae and course of chronic gastritis during a 30- to 34-year bioptic follow-up study. Scand J Gastroenterol. 1985;20(4):485-91.

69. Valle J, Kekki M, Sipponen P, Ihamaki T, Siurala M. Long-term course and consequences of Helicobacter pylori gastritis. Results of a 32-year follow-up study. Scand J Gastroenterol. 1996;31(6):546-50.

70. Sipponen P, Maaroos HI. Chronic gastritis. Scand J Gastroenterol. 2015;50(6):657-67.

71. Kuipers EJ, Uyterlinde AM, Pena AS, Roosendaal R, Pals G, Nelis GF, et al. Long-term sequelae of Helicobacter pylori gastritis. Lancet. 1995;345(8964):1525-8.

72. Adamu MA, Weck MN, Gao L, Brenner H. Incidence of chronic atrophic gastritis: systematic review and meta-analysis of follow-up studies. Eur J Epidemiol. 2010;25(7):439-48.

73. Holleczek B, Schottker B, Brenner H. Helicobacter pylori infection, chronic atrophic gastritis and risk of stomach and esophagus cancer: results from the prospective population-based ESTHER cohort study. Int J Cancer. 2019.

74. Watt PC, Sloan JM, Donaldson JD, Patterson CC, Kennedy TL. Relationship between histology and gastric juice pH and nitrite in the stomach after operation for duodenal ulcer. Gut. 1984;25(3):246-52.

75. Sung J, Kim N, Lee J, Hwang YJ, Kim HW, Chung JW, et al. Associations among Gastric Juice pH, Atrophic Gastritis, Intestinal Metaplasia and Helicobacter pylori Infection. Gut Liver. 2018;12(2):158-64.

76. Rugge M, Correa P, Dixon MF, Hattori T, Leandro G, Lewin K, et al. Gastric dysplasia: the Padova international classification. Am J Surg Pathol. 2000;24(2):167-76.

77. Talley NJ, Zinsmeister AR, Weaver A, DiMagno EP, Carpenter HA, Perez-Perez GI, et al. Gastric adenocarcinoma and Helicobacter pylori infection. J Natl Cancer Inst. 1991;83(23):1734-9.

78. Nomura AM, Kolonel LN, Miki K, Stemmermann GN, Wilkens LR, Goodman MT, et al. Helicobacter pylori, pepsinogen, and gastric adenocarcinoma in Hawaii. J Infect Dis. 2005;191(12):2075-81.

79. Cho SJ, Choi IJ, Kim CG, Lee JY, Kook MC, Seong MW, et al. Helicobacter pylori Seropositivity Is Associated with Gastric Cancer Regardless of Tumor Subtype in Korea. Gut Liver. 2010;4(4):466-74.

80. Yun CY, Kim N, Lee J, Lee JY, Hwang YJ, Lee HS, et al. Usefulness of OLGA and OLGIM system not only for intestinal type but also for diffuse type of gastric cancer, and no interaction among the gastric cancer risk factors. Helicobacter. 2018;23(6):e12542.

81. Li D, Bautista MC, Jiang SF, Daryani P, Brackett M, Armstrong MA, et al. Risks and Predictors of Gastric Adenocarcinoma in Patients with Gastric Intestinal Metaplasia and Dysplasia: A Population-Based Study. Am J Gastroenterol. 2016;111(8):1104-13.

82. Srivastava A, Lauwers GY. Gastric epithelial dysplasia: the Western perspective. Dig Liver Dis. 2008;40(8):641-9.

83. Sung JK. Diagnosis and management of gastric dysplasia. Korean J Intern Med. 2016;31(2):201-9.

84. de Vries AC, van Grieken NC, Looman CW, Casparie MK, de Vries E, Meijer GA, et al. Gastric cancer risk in patients with premalignant gastric lesions: a nationwide cohort study in the Netherlands. Gastroenterology. 2008;134(4):945-52.

85. Song H, Ekheden IG, Zheng Z, Ericsson J, Nyren O, Ye W. Incidence of gastric cancer among patients with gastric precancerous lesions: observational cohort study in a low risk Western population. BMJ. 2015;351:h3867.

86. Inoue M, Tajima K, Matsuura A, Suzuki T, Nakamura T, Ohashi K, et al. Severity of chronic atrophic gastritis and subsequent gastric cancer occurrence: a 10-year prospective cohort study in Japan. Cancer Lett. 2000;161(1):105-12.

87. Tava F, Luinetti O, Ghigna MR, Alvisi C, Perego M, Trespi E, et al. Type or extension of intestinal metaplasia and immature/atypical "indefinite-for-dysplasia" lesions as predictors of gastric neoplasia. Hum Pathol. 2006;37(11):1489-97.

88. Gonzalez CA, Pardo ML, Liso JM, Alonso P, Bonet C, Garcia RM, et al. Gastric cancer occurrence in preneoplastic lesions: a long-term follow-up in a high-risk area in Spain. Int J Cancer. 2010;127(11):2654-60.

89. Gonzalez CA, Sanz-Anquela JM, Companioni O, Bonet C, Berdasco M, Lopez C, et al. Incomplete type of intestinal metaplasia has the highest risk to progress to gastric cancer: results of the Spanish follow-up multicenter study. J Gastroenterol Hepatol. 2016;31(5):953-8.

90. Reddy KM, Chang JI, Shi JM, Wu BU. Risk of Gastric Cancer Among Patients With Intestinal Metaplasia of the Stomach in a US Integrated Health Care System. Clin Gastroenterol Hepatol. 2016;14(10):1420-5.

91. Pittayanon R, Rerknimitr R, Klaikaew N, Sanpavat A, Chaithongrat S, Mahachai V, et al. The risk of gastric cancer in patients with gastric intestinal metaplasia in 5-year follow-up. Aliment Pharmacol Ther. 2017;46(1):40-5.

92. Spence AD, Cardwell CR, McMenamin UC, Hicks BM, Johnston BT, Murray LJ, et al. Adenocarcinoma risk in gastric atrophy and intestinal metaplasia: a systematic review. BMC Gastroenterol. 2017;17(1):157.

93. den Hollander WJ, Holster IL, den Hoed CM, Capelle LG, Tang TJ, Anten MP, et al. Surveillance of premalignant gastric lesions: a multicentre prospective cohort study from low incidence regions. Gut. 2018.

94. Shao L, Li P, Ye J, Chen J, Han Y, Cai J, et al. Risk of gastric cancer among patients with gastric intestinal metaplasia. Int J Cancer. 2018.

95. Akbari M, Tabrizi R, Kardeh S, Lankarani KB. Gastric cancer in patients with gastric atrophy and intestinal metaplasia: A systematic review and meta-analysis. PLoS One. 2019;14(7):e0219865.

96. Vannella L, Lahner E, Osborn J, Annibale B. Systematic review: gastric cancer incidence in pernicious anaemia. Aliment Pharmacol Ther. 2013;37(4):375-82.

97. Lindenbaum J, Rosenberg IH, Wilson PW, Stabler SP, Allen RH. Prevalence of cobalamin deficiency in the Framingham elderly population. Am J Clin Nutr. 1994;60(1):2-11.

98. Murphy G, Dawsey SM, Engels EA, Ricker W, Parsons R, Etemadi A, et al. Cancer Risk After Pernicious Anemia in the US Elderly Population. Clin Gastroenterol Hepatol. 2015;13(13):2282-9 e1-4.

99. Field J, Biondo MA, Murphy K, Alderuccio F, Toh BH. Experimental autoimmune gastritis: mouse models of human organ-specific autoimmune disease. Int Rev Immunol. 2005;24(1-2):93-110.

100. Lahner E, Annibale B. Pernicious anemia: new insights from a gastroenterological point of view. World J Gastroenterol. 2009;15(41):5121-8.

101. Price AB. The Sydney System: histological division. J Gastroenterol Hepatol. 1991;6(3):209-22.

102. Dixon MF, Genta RM, Yardley JH, Correa P. Classification and grading of gastritis. The updated Sydney System. International Workshop on the Histopathology of Gastritis, Houston 1994. Am J Surg Pathol. 1996;20(10):1161-81.

103. Rugge M, Correa P, Di Mario F, El-Omar E, Fiocca R, Geboes K, et al. OLGA staging for gastritis: a tutorial. Dig Liver Dis. 2008;40(8):650-8.

104. Capelle LG, de Vries AC, Haringsma J, Ter Borg F, de Vries RA, Bruno MJ, et al. The staging of gastritis with the OLGA system by using intestinal metaplasia as an accurate alternative for atrophic gastritis. Gastrointest Endosc. 2010;71(7):1150-8.

105. Isajevs S, Liepniece-Karele I, Janciauskas D, Moisejevs G, Putnins V, Funka K, et al. Gastritis staging: interobserver agreement by applying OLGA and OLGIM systems. Virchows Arch. 2014;464(4):403-7.

106. Rugge M, de Boni M, Pennelli G, de Bona M, Giacomelli L, Fassan M, et al. Gastritis OLGA-staging and gastric cancer risk: a twelve-year clinico-pathological follow-up study. Aliment Pharmacol Ther. 2010;31(10):1104-11.

107. Cho SJ, Choi IJ, Kook MC, Nam BH, Kim CG, Lee JY, et al. Staging of intestinal- and diffuse-type gastric cancers with the OLGA and OLGIM staging systems. Aliment Pharmacol Ther. 2013;38(10):1292-302.

108. Zhou Y, Li HY, Zhang JJ, Chen XY, Ge ZZ, Li XB. Operative link on gastritis assessment stage is an appropriate predictor of early gastric cancer. World J Gastroenterol. 2016;22(13):3670-8.

109. Mera RM, Bravo LE, Camargo MC, Bravo JC, Delgado AG, Romero-Gallo J, et al. Dynamics of Helicobacter pylori infection as a determinant of progression of gastric precancerous lesions: 16-year follow-up of an eradication trial. Gut. 2018;67(7):1239-46.

110. Rugge M, Genta RM, Fassan M, Valentini E, Coati I, Guzzinati S, et al. OLGA Gastritis Staging for the Prediction of Gastric Cancer Risk: A Long-term Follow-up Study of 7436 Patients. Am J Gastroenterol. 2018;113(11):1621-8.

111. Yue H, Shan L, Bin L. The significance of OLGA and OLGIM staging systems in the risk assessment of gastric cancer: a systematic review and meta-analysis. Gastric Cancer. 2018.

112. Rokkas T, Rokka A, Portincasa P. A systematic review and meta-analysis of the role of Helicobacter pylori eradication in preventing gastric cancer. Ann Gastroenterol. 2017;30(4):414-23.

113. Abdul Aal GM, Dajani AI, Nounou M, Awad S, Abdul Rasheed Z, Gautam S, et al. Resolution of gastritis induced by Helicobacter pylori 4-5 weeks after successful eradication of infection using a triple therapy regimen of pantoprazole, amoxycillin and clarithromycin for one week. Digestion. 1999;60(3):286-97.

114. Arkkila PE, Seppala K, Farkkila MA, Veijola L, Sipponen P. Helicobacter pylori eradication in the healing of atrophic gastritis: a one-year prospective study. Scand J Gastroenterol. 2006;41(7):782-90.

115. El-Omar EM. Mechanisms of increased acid secretion after eradication of Helicobacter pylori infection. Gut. 2006;55(2):144-6.

116. Machado AM, Figueiredo C, Seruca R, Rasmussen LJ. Helicobacter pylori infection generates genetic instability in gastric cells. Biochim Biophys Acta. 2010;1806(1):58-65.

117. Kodama M, Murakami K, Okimoto T, Sato R, Uchida M, Abe T, et al. Ten-year prospective follow-up of histological changes at five points on the gastric mucosa as recommended by the updated Sydney system after Helicobacter pylori eradication. J Gastroenterol. 2012;47(4):394-403.

118. White JR, Winter JA, Robinson K. Differential inflammatory response to Helicobacter pylori infection: etiology and clinical outcomes. J Inflamm Res. 2015;8:137-47.

119. Kawai T, Moriyasu F, Tsuchida A. Key Issues Associated with Helicobacter pylori Eradication. Digestion. 2016;93(1):19-23.

120. Li L, Zhou X, Xiao S, Ye F, Zhang G. The Effect of Helicobacter pylori Eradication on the Gastrointestinal Microbiota in Patients with Duodenal Ulcer. J Gastrointestin Liver Dis. 2016;25(2):139-46.

121. Hwang YJ, Kim N, Lee HS, Lee JB, Choi YJ, Yoon H, et al. Reversibility of atrophic gastritis and intestinal metaplasia after Helicobacter pylori eradication - a prospective study for up to 10 years. Aliment Pharmacol Ther. 2018;47(3):380-90.

122. Yanagi H, Tsuda A, Matsushima M, Takahashi S, Ozawa G, Koga Y, et al. Changes in the gut microbiota composition and the plasma ghrelin level in patients with Helicobacter pylori-infected patients with eradication therapy. BMJ Open Gastroenterol. 2017;4(1):e000182.

123. Kodama M, Murakami K, Okimoto T, Abe T, Nakagawa Y, Mizukami K, et al. Helicobacter pylori eradication improves gastric atrophy and intestinal metaplasia in long-term observation. Digestion. 2012;85(2):126-30.

124. Chen HN, Wang Z, Li X, Zhou ZG. Helicobacter pylori eradication cannot reduce the risk of gastric cancer in patients with intestinal metaplasia and dysplasia: evidence from a meta-analysis. Gastric Cancer. 2016;19(1):166-75.

125. Shichijo S, Hirata Y, Niikura R, Hayakawa Y, Yamada A, Ushiku T, et al. Histologic intestinal metaplasia and endoscopic atrophy are predictors of gastric cancer development after Helicobacter pylori eradication. Gastrointest Endosc. 2016;84(4):618-24.

126. de Vries AC, Kuipers EJ, Rauws EA. Helicobacter pylori eradication and gastric cancer: when is the horse out of the barn? Am J Gastroenterol. 2009;104(6):1342-5.

127. Huang KK, Ramnarayanan K, Zhu F, Srivastava S, Xu C, Tan ALK, et al. Genomic and Epigenomic Profiling of High-Risk Intestinal Metaplasia Reveals Molecular Determinants of Progression to Gastric Cancer. Cancer Cell. 2018;33(1):137-50 e5.

128. Zullo A, Hassan C, Romiti A, Giusto M, Guerriero C, Lorenzetti R, et al. Follow-up of intestinal metaplasia in the stomach: When, how and why. World J Gastrointest Oncol. 2012;4(3):30-6.

129. Marques-Silva L, Areia M, Elvas L, Dinis-Ribeiro M. Prevalence of gastric precancerous conditions: a systematic review and meta-analysis. Eur J Gastroenterol Hepatol. 2014;26(4):378-87.

130. Jass JR, Filipe MI. A variant of intestinal metaplasia associated with gastric carcinoma: a histochemical study. Histopathology. 1979;3(3):191-9.

131. Reis CA, David L, Correa P, Carneiro F, de Bolos C, Garcia E, et al. Intestinal metaplasia of human stomach displays distinct patterns of mucin (MUC1, MUC2, MUC5AC, and MUC6) expression. Cancer Res. 1999;59(5):1003-7.

132. Teixeira A, David L, Reis CA, Costa J, Sobrinho-Simoes M. Expression of mucins (MUC1, MUC2, MUC5AC, and MUC6) and type 1 Lewis antigens in cases with and without Helicobacter pylori colonization in metaplastic glands of the human stomach. J Pathol. 2002;197(1):37-43.

133. Ikeda Y, Nishikura K, Watanabe H, Watanabe G, Ajioka Y, Hatakeyama K. Histopathological differences in the development of small intestinal metaplasia between antrum and body of stomach. Pathol Res Pract. 2005;201(7):487-96.

134. Cassaro M, Rugge M, Gutierrez O, Leandro G, Graham DY, Genta RM. Topographic patterns of intestinal metaplasia and gastric cancer. Am J Gastroenterol. 2000;95(6):1431-8.

135. Peleteiro B, Lunet N, Figueiredo C, Carneiro F, David L, Barros H. Smoking, Helicobacter pylori virulence, and type of intestinal metaplasia in Portuguese males. Cancer Epidemiol Biomarkers Prev. 2007;16(2):322-6.

136. Solcia E, Luinetti O, Villani L, Quilici P, Klersy C, Fiocca R. Intestinal metaplasia: types, mechanisms of origin, and role in gastric cancer histogenesis. In: Hunt RH, Tytgat GNJ, editors. *Helicobacter pylori*: Kluwer Academic Publishers; 2000. p. 249-54.

137. Filipe MI, Potet F, Bogomoletz WV, Dawson PA, Fabiani B, Chauveinc P, et al. Incomplete sulphomucin-secreting intestinal metaplasia for gastric cancer. Preliminary data from a prospective study from three centres. Gut. 1985;26(12):1319-26.

138. Gonzalez CA, Sanz-Anquela JM, Gisbert JP, Correa P. Utility of subtyping intestinal metaplasia as marker of gastric cancer risk. A review of the evidence. Int J Cancer. 2013;133(5):1023-32.

139. Dinis-Ribeiro M, Lopes C, da Costa-Pereira A, Guilherme M, Barbosa J, Lomba-Viana H, et al. A follow up model for patients with atrophic chronic gastritis and intestinal metaplasia. J Clin Pathol. 2004;57(2):177-82.

140. Banks M, Graham D, Jansen M, Gotoda T, Coda S, di Pietro M, et al. British Society of Gastroenterology guidelines on the diagnosis and management of patients at risk of gastric adenocarcinoma. Gut. 2019;68(9):1545-75.

141. Pimentel-Nunes P, Libanio D, Marcos-Pinto R, Areia M, Leja M, Esposito G, et al. Management of epithelial precancerous conditions and lesions in the stomach (MAPS II): European Society of Gastrointestinal Endoscopy (ESGE), European Helicobacter and Microbiota Study Group (EHMSG), European Society of Pathology (ESP), and Sociedade Portuguesa de Endoscopia Digestiva (SPED) guideline update 2019. Endoscopy. 2019;51(4):365-88.

142. Giroux V, Rustgi AK. Metaplasia: tissue injury adaptation and a precursor to the dysplasia-cancer sequence. Nat Rev Cancer. 2017;17(10):594-604.

143. Algood HM, Cover TL. Helicobacter pylori persistence: an overview of interactions between H. pylori and host immune defenses. Clin Microbiol Rev. 2006;19(4):597-613.

144. Hatakeyama M. Structure and function of Helicobacter pylori CagA, the first-identified bacterial protein involved in human cancer. Proc Jpn Acad Ser B Phys Biol Sci. 2017;93(4):196-219.

145. Maekita T, Nakazawa K, Mihara M, Nakajima T, Yanaoka K, Iguchi M, et al. High levels of aberrant DNA methylation in Helicobacter pylori-infected gastric mucosae and its possible association with gastric cancer risk. Clin Cancer Res. 2006;12(3 Pt 1):989-95.

146. Muhammad JS, Eladl MA, Khoder G. Helicobacter pylori-induced DNA Methylation as an Epigenetic Modulator of Gastric Cancer: Recent Outcomes and Future Direction. Pathogens. 2019;8(1).

147. de Jonge PJ, van Blankenstein M, Looman CW, Casparie MK, Meijer GA, Kuipers EJ. Risk of malignant progression in patients with Barrett's oesophagus: a Dutch nationwide cohort study. Gut. 2010;59(8):1030-6.

148. Hvid-Jensen F, Pedersen L, Drewes AM, Sorensen HT, Funch-Jensen P. Incidence of adenocarcinoma among patients with Barrett's esophagus. N Engl J Med. 2011;365(15):1375-83.

149. Sobala GM, O'Connor HJ, Dewar EP, King RF, Axon AT, Dixon MF. Bile reflux and intestinal metaplasia in gastric mucosa. J Clin Pathol. 1993;46(3):235-40.

150. Matsuhisa T, Arakawa T, Watanabe T, Tokutomi T, Sakurai K, Okamura S, et al. Relation between bile acid reflux into the stomach and the risk of atrophic gastritis and intestinal metaplasia: a multicenter study of 2283 cases. Dig Endosc. 2013;25(5):519-25.

151. Asonuma S, Imatani A, Asano N, Oikawa T, Konishi H, Iijima K, et al. Helicobacter pylori induces gastric mucosal intestinal metaplasia through the inhibition of interleukin-4-mediated HMG box protein Sox2 expression. Am J Physiol Gastrointest Liver Physiol. 2009;297(2):G312-22.

152. Asano N, Imatani A, Watanabe T, Fushiya J, Kondo Y, Jin X, et al. Cdx2 Expression and Intestinal Metaplasia Induced by H. pylori Infection of Gastric Cells Is Regulated by NOD1-Mediated Innate Immune Responses. Cancer Res. 2016;76(5):1135-45.

153. Yuan T, Ni Z, Han C, Min Y, Sun N, Liu C, et al. SOX2 interferes with the function of CDX2 in bile acid-induced gastric intestinal metaplasia. Cancer Cell Int. 2019;19:24.

154. Mutoh H, Hakamata Y, Sato K, Eda A, Yanaka I, Honda S, et al. Conversion of gastric mucosa to intestinal metaplasia in Cdx2-expressing transgenic mice. Biochem Biophys Res Commun. 2002;294(2):470-9.

155. Almeida R, Silva E, Santos-Silva F, Silberg DG, Wang J, De Bolos C, et al. Expression of intestine-specific transcription factors, CDX1 and CDX2, in intestinal metaplasia and gastric carcinomas. J Pathol. 2003;199(1):36-40.

156. Carrasco-Garcia E, Santos JC, Garcia I, Brianti M, Garcia-Puga M, Pedrazzoli J, Jr., et al. Paradoxical role of SOX2 in gastric cancer. Am J Cancer Res. 2016;6(4):701-13.

157. Camilo V, Barros R, Sousa S, Magalhaes AM, Lopes T, Mario Santos A, et al. Helicobacter pylori and the BMP pathway regulate CDX2 and SOX2 expression in gastric cells. Carcinogenesis. 2012;33(10):1985-92.

158. Camilo V, Garrido M, Valente P, Ricardo S, Amaral AL, Barros R, et al. Differentiation reprogramming in gastric intestinal metaplasia and dysplasia: role of SOX2 and CDX2. Histopathology. 2015;66(3):343-50.

159. Calcagno DQ, Leal MF, Demachki S, Araujo MT, Freitas FW, Oliveira e Souza D, et al. MYC in gastric carcinoma and intestinal metaplasia of young adults. Cancer Genet Cytogenet. 2010;202(1):63-6.

160. de Souza CR, Leal MF, Calcagno DQ, Costa Sozinho EK, Borges Bdo N, Montenegro RC, et al. MYC deregulation in gastric cancer and its clinicopathological implications. PLoS One. 2013;8(5):e64420.

161. Khaleghian M, Jahanzad I, Shakoori A, Emami Razavi A, Azimi C. Association Between Amplification and Expression of C-MYC Gene and Clinicopathological Characteristics of Stomach Cancer. Iran Red Crescent Med J. 2016;18(2):e21221.

162. Choi W, Kim J, Park J, Lee DH, Hwang D, Kim JH, et al. YAP/TAZ Initiates Gastric Tumorigenesis via Upregulation of MYC. Cancer Res. 2018;78(12):3306-20.

163. Hamamoto T, Yokozaki H, Semba S, Yasui W, Yunotani S, Miyazaki K, et al. Altered microsatellites in incomplete-type intestinal metaplasia adjacent to primary gastric cancers. J Clin Pathol. 1997;50(10):841-6.

164. Kobayashi K, Okamoto T, Takayama S, Akiyama M, Ohno T, Yamada H. Genetic instability in intestinal metaplasia is a frequent event leading to well-differentiated early adenocarcinoma of the stomach. Eur J Cancer. 2000;36(9):1113-9.

165. Leung WK, Kim JJ, Kim JG, Graham DY, Sepulveda AR. Microsatellite Instability in Gastric Intestinal Metaplasia in Patients with and without Gastric Cancer. The American Journal of Pathology. 2000;156(2):537-43.

166. Guo Y, Huang A, Hu C, Zhou Y, Zhang X, Czajkowsky DM, et al. Complex clonal mosaicism within microdissected intestinal metaplastic glands without concurrent gastric cancer. J Med Genet. 2016;53(9):643-6.

167. Liu P, Zhang XY, Shao Y, Zhang DF. Microsatellite instability in gastric cancer and pre-cancerous lesions. World J Gastroenterol. 2005;11(31):4904-7.

168. Song H, Ekheden IG, Ploner A, Ericsson J, Nyren O, Ye W. Family history of gastric mucosal abnormality and the risk of gastric cancer: a population-based observational study. Int J Epidemiol. 2017.

169. Genta RM, Sonnenberg A. Characteristics of the gastric mucosa in patients with intestinal metaplasia. Am J Surg Pathol. 2015;39(5):700-4.

170. Yamaguchi H, Goldenring JR, Kaminishi M, Lee JR. Identification of spasmolytic polypeptide expressing metaplasia (SPEM) in remnant gastric cancer and surveillance postgastrectomy biopsies. Dig Dis Sci. 2002;47(3):573-8.

171. Halldorsdottir AM, Sigurdardottrir M, Jonasson JG, Oddsdottir M, Magnusson J, Lee JR, et al. Spasmolytic polypeptide-expressing metaplasia (SPEM) associated with gastric cancer in Iceland. Dig Dis Sci. 2003;48(3):431-41.

172. Wang TC, Goldenring JR, Dangler C, Ito S, Mueller A, Jeon WK, et al. Mice lacking secretory phospholipase A2 show altered apoptosis and differentiation with Helicobacter felis infection. Gastroenterology. 1998;114(4):675-89.

173. Schmidt PH, Lee JR, Joshi V, Playford RJ, Poulsom R, Wright NA, et al. Identification of a metaplastic cell lineage associated with human gastric adenocarcinoma. Lab Invest. 1999;79(6):639-46.

174. Hoffmann W. TFF2, a MUC6-binding lectin stabilizing the gastric mucus barrier and more (Review). Int J Oncol. 2015;47(3):806-16.

175. Nam KT, Lee HJ, Sousa JF, Weis VG, O'Neal RL, Finke PE, et al. Mature chief cells are cryptic progenitors for metaplasia in the stomach. Gastroenterology. 2010;139(6):2028-37 e9.

176. Petersen CP, Mills JC, Goldenring JR. Murine Models of Gastric Corpus Preneoplasia. Cell Mol Gastroenterol Hepatol. 2017;3(1):11-26.

177. Weis VG, Petersen CP, Weis JA, Meyer AR, Choi E, Mills JC, et al. Maturity and age influence chief cell ability to transdifferentiate into metaplasia. Am J Physiol Gastrointest Liver Physiol. 2017;312(1):G67-G76.

178. Hibdon ES, Samuelson LC. Cellular Plasticity in the Stomach: Insights Into the Cellular Origin of Gastric Metaplasia. Gastroenterology. 2018;154(4):801-3.

179. Hayakawa Y, Ariyama H, Stancikova J, Sakitani K, Asfaha S, Renz BW, et al. Mist1 Expressing Gastric Stem Cells Maintain the Normal and Neoplastic Gastric Epithelium and Are Supported by a Perivascular Stem Cell Niche. Cancer Cell. 2015;28(6):800-14.

180. Hayakawa Y, Fox JG, Wang TC. Isthmus Stem Cells Are the Origins of Metaplasia in the Gastric Corpus. Cell Mol Gastroenterol Hepatol. 2017;4(1):89-94.

181. Rugge M, Genta RM, Di Mario F, El-Omar EM, El-Serag HB, Fassan M, et al. Gastric Cancer as Preventable Disease. Clin Gastroenterol Hepatol. 2017;15(12):1833-43.

182. Peleteiro B, Lunet N, Carrilho C, Duraes C, Machado JC, La Vecchia C, et al. Association between cytokine gene polymorphisms and gastric precancerous lesions: systematic review and meta-analysis. Cancer Epidemiol Biomarkers Prev. 2010;19(3):762-76.

183. Myung DS, Lee WS, Park YL, Kim N, Oh HH, Kim MY, et al. Association between interleukin-18 gene polymorphism and Helicobacter pylori infection in the Korean population. Sci Rep. 2015;5:11535.

184. Negovan A, Iancu M, Fulop E, Banescu C. Helicobacter pylori and cytokine gene variants as predictors of premalignant gastric lesions. World J Gastroenterol. 2019;25(30):4105-24.

185. Rudnicka K, Backert S, Chmiela M. Genetic Polymorphisms in Inflammatory and Other Regulators in Gastric Cancer: Risks and Clinical Consequences. In: Backert S, editor. Molecular Mechanisms of Inflammation: Induction, Resolution and Escape by Helicobacter pylori. Cham: Springer International Publishing; 2019. p. 53-76.

186. Sanjabi S, Zenewicz LA, Kamanaka M, Flavell RA. Anti-inflammatory and pro-inflammatory roles of TGF-beta, IL-10, and IL-22 in immunity and autoimmunity. Curr Opin Pharmacol. 2009;9(4):447-53.

187. Wojdasiewicz P, Poniatowski LA, Szukiewicz D. The role of inflammatory and anti-inflammatory cytokines in the pathogenesis of osteoarthritis. Mediators Inflamm. 2014;2014:561459.

188. Algood HMS. T Cell Cytokines Impact Epithelial Cell Responses during Helicobacter pylori Infection. J Immunol. 2020;204(6):1421-8.

189. Shachar I, Karin N. The dual roles of inflammatory cytokines and chemokines in the regulation of autoimmune diseases and their clinical implications. J Leukoc Biol. 2013;93(1):51-61.

190. Landskron G, De la Fuente M, Thuwajit P, Thuwajit C, Hermoso MA. Chronic inflammation and cytokines in the tumor microenvironment. J Immunol Res. 2014;2014:149185.

191. Algood HM, Gallo-Romero J, Wilson KT, Peek RM, Jr., Cover TL. Host response to Helicobacter pylori infection before initiation of the adaptive immune response. FEMS Immunol Med Microbiol. 2007;51(3):577-86.

192. Chung HW, Lim JB. Role of the tumor microenvironment in the pathogenesis of gastric carcinoma. World J Gastroenterol. 2014;20(7):1667-80.

193. Fu H, Ma Y, Yang M, Zhang C, Huang H, Xia Y, et al. Persisting and Increasing Neutrophil Infiltration Associates with Gastric Carcinogenesis and E-cadherin Downregulation. Sci Rep. 2016;6:29762.

194. Sica A, Mantovani A. Macrophage plasticity and polarization: in vivo veritas. J Clin Invest. 2012;122(3):787-95.

195. Martinez FO, Gordon S. The M1 and M2 paradigm of macrophage activation: time for reassessment. F1000Prime Rep. 2014;6:13.

196. Mantovani A, Marchesi F, Malesci A, Laghi L, Allavena P. Tumour-associated macrophages as treatment targets in oncology. Nature Reviews Clinical Oncology. 2017.

197. Malyshev I, Malyshev Y. Current Concept and Update of the Macrophage Plasticity Concept: Intracellular Mechanisms of Reprogramming and M3 Macrophage "Switch" Phenotype. Biomed Res Int. 2015;2015:341308.

198. Huang YK, Wang M, Sun Y, Di Costanzo N, Mitchell C, Achuthan A, et al. Macrophage spatial heterogeneity in gastric cancer defined by multiplex immunohistochemistry. Nat Commun. 2019;10(1):3928.

199. Dzierzanowska-Fangrat K, Michalkiewicz J, Cielecka-Kuszyk J, Nowak M, Celinska-Cedro D, Rozynek E, et al. Enhanced gastric IL-18 mRNA expression in Helicobacter pylori-infected children is associated with macrophage infiltration, IL-8, and IL-1 beta mRNA expression. Eur J Gastroenterol Hepatol. 2008;20(4):314-9.

200. Horvath DJ, Jr., Washington MK, Cope VA, Algood HM. IL-23 Contributes to Control of Chronic Helicobacter Pylori Infection and the Development of T Helper Responses in a Mouse Model. Front Immunol. 2012;3:56.

201. Munari F, Fassan M, Capitani N, Codolo G, Vila-Caballer M, Pizzi M, et al. Cytokine BAFF released by Helicobacter pylori-infected macrophages triggers the Th17 response in human chronic gastritis. J Immunol. 2014;193(11):5584-94.

202. Fehlings M, Drobbe L, Moos V, Renner Viveros P, Hagen J, Beigier-Bompadre M, et al. Comparative analysis of the interaction of Helicobacter pylori with human dendritic cells, macrophages, and monocytes. Infect Immun. 2012;80(8):2724-34.

203. Ieni A, Barresi V, Rigoli L, Fedele F, Tuccari G, Caruso RA. Morphological and Cellular Features of Innate Immune Reaction in Helicobacter pylori Gastritis: A Brief Review. Int J Mol Sci. 2016;17(1).

204. Kaparakis M, Walduck AK, Price JD, Pedersen JS, van Rooijen N, Pearse MJ, et al. Macrophages are mediators of gastritis in acute Helicobacter pylori infection in C57BL/6 mice. Infect Immun. 2008;76(5):2235-9.

205. Quiding-Jarbrink M, Raghavan S, Sundquist M. Enhanced M1 macrophage polarization in human helicobacter pylori-associated atrophic gastritis and in vaccinated mice. PLoS One. 2010;5(11):e15018.

206. Hou J, Wang X, Zhang M, Wang M, Gao P, Jiang Y. Circulating CD14(+)CD163(+)CD209(+) M2-like monocytes are associated with the severity of infection in Helicobacter pylori-positive patients. Mol Immunol. 2019;108:13-22.

207. Petersen CP, Weis VG, Nam KT, Sousa JF, Fingleton B, Goldenring JR. Macrophages promote progression of spasmolytic polypeptide-expressing metaplasia after acute loss of parietal cells. Gastroenterology. 2014;146(7):1727-38 e8.

208. Shiu J, Blanchard TG. Dendritic cell function in the host response to Helicobacter pylori infection of the gastric mucosa. Pathog Dis. 2013;67(1):46-53.

209. Mitchell P, Germain C, Fiori PL, Khamri W, Foster GR, Ghosh S, et al. Chronic exposure to Helicobacter pylori impairs dendritic cell function and inhibits Th1 development. Infect Immun. 2007;75(2):810-9.

210. Aceti A, Celestino D, Caferro M, Casale V, Citarda F, Conti EM, et al. Basophil-bound and serum immunoglobulin E directed against Helicobacter pylori in patients with chronic gastritis. Gastroenterology. 1991;101(1):131-7.

211. Nakajima S, Bamba N, Hattori T. Histological aspects and role of mast cells in Helicobacter pylori-infected gastritis. Aliment Pharmacol Ther. 2004;20 Suppl 1:165-70.

212. de Paulis A, Prevete N, Fiorentino I, Walls AF, Curto M, Petraroli A, et al. Basophils infiltrate human gastric mucosa at sites of Helicobacter pylori infection, and exhibit chemotaxis in response to H. pylori-derived peptide Hp(2-20). J Immunol. 2004;172(12):7734-43.

213. Piazuelo MB, Camargo MC, Mera RM, Delgado AG, Peek RM, Jr., Correa H, et al. Eosinophils and mast cells in chronic gastritis: possible implications in carcinogenesis. Hum Pathol. 2008;39(9):1360-9.

214. Caruso RA, Parisi A, Crisafulli C, Bonanno A, Lucian R, Branca G, et al. Intraepithelial infiltration by mast cells in human Helicobacter pylori active gastritis. Ultrastruct Pathol. 2011;35(6):251-5.

215. Prevete N, Rossi FW, Rivellese F, Lamacchia D, Pelosi C, Lobasso A, et al. Helicobacter pylori HP(2-20) induces eosinophil activation and accumulation in superficial gastric mucosa and stimulates VEGF-alpha and TGF-beta release by interacting with formyl-peptide receptors. Int J Immunopathol Pharmacol. 2013;26(3):647-62.

216. Hafsi N, Voland P, Schwendy S, Rad R, Reindl W, Gerhard M, et al. Human dendritic cells respond to Helicobacter pylori, promoting NK cell and Th1-effector responses in vitro. J Immunol. 2004;173(2):1249-57.

217. Yun CH, Lundgren A, Azem J, Sjoling A, Holmgren J, Svennerholm AM, et al. Natural killer cells and Helicobacter pylori infection: bacterial antigens and interleukin-12 act synergistically to induce gamma interferon production. Infect Immun. 2005;73(3):1482-90.

218. Betten A, Bylund J, Christophe T, Boulay F, Romero A, Hellstrand K, et al. A proinflammatory peptide from Helicobacter pylori activates monocytes to induce lymphocyte dysfunction and apoptosis. J Clin Invest. 2001;108(8):1221-8.

219. Rudnicka K, Wlodarczyk M, Moran AP, Rechcinski T, Miszczyk E, Matusiak A, et al. Helicobacter pylori antigens as potential modulators of lymphocytes' cytotoxic activity. Microbiol Immunol. 2012;56(1):62-75.

220. Chen J, Yang J, Jiang J, Zhuang Y, He W. Function and subsets of dendritic cells and natural killer cells were decreased in gastric cancer. Int J Clin Exp Pathol. 2014;7(11):8304-11.

221. Peng LS, Zhang JY, Teng YS, Zhao YL, Wang TT, Mao FY, et al. Tumor-Associated Monocytes/Macrophages Impair NK-Cell Function via TGFbeta1 in Human Gastric Cancer. Cancer Immunol Res. 2017;5(3):248-56.

222. Du Y, Wei Y. Therapeutic Potential of Natural Killer Cells in Gastric Cancer. Front Immunol. 2018;9:3095.

223. Bronstein-Sitton N. Expression of the T Cell Antigen Receptor Chain following Activation Is Controlled at Distinct Checkpoints. 1999.

224. Omilusik KD. The origins of memory T cells. 2017.

225. Eaton KA, Ringler SR, Danon SJ. Murine splenocytes induce severe gastritis and delayed-type hypersensitivity and suppress bacterial colonization in Helicobacter pylori-infected SCID mice. Infect Immun. 1999;67(9):4594-602.

226. Peterson RA, 2nd, Hoepf T, Eaton KA. Adoptive transfer of splenocytes in SCID mice implicates CD4+ T cells in apoptosis and epithelial proliferation associated with Helicobacter pylori-induced gastritis. Comp Med. 2003;53(5):498-509.

227. Eaton KA, Mefford M, Thevenot T. The role of T cell subsets and cytokines in the pathogenesis of Helicobacter pylori gastritis in mice. J Immunol. 2001;166(12):7456-61.

228. Guiney DG, Hasegawa P, Cole SP. Helicobacter pylori preferentially induces interleukin 12 (IL-12) rather than IL-6 or IL-10 in human dendritic cells. Infect Immun. 2003;71(7):4163-6.

229. Gray BM, Fontaine CA, Poe SA, Eaton KA. Complex T cell interactions contribute to Helicobacter pylori gastritis in mice. Infect Immun. 2013;81(3):740-52.

230. Dixon B, Hossain R, Patel RV, Algood HMS. Th17 Cells in Helicobacter pylori Infection: a Dichotomy of Help and Harm. Infect Immun. 2019;87(11).

231. Bagheri N, Azadegan-Dehkordi F, Rahimian G, Rafieian-Kopaei M, Shirzad H. Role of Regulatory T-cells in Different Clinical Expressions of Helicobacter pylori Infection. Arch Med Res. 2016;47(4):245-54.

232. Wu YY, Hsieh CT, Tsay GJ, Kao JT, Chiu YM, Shieh DC, et al. Recruitment of CCR6(+) Foxp3(+) regulatory gastric infiltrating lymphocytes in Helicobacter pylori gastritis. Helicobacter. 2019;24(1):e12550.

233. Serrano C, Wright SW, Bimczok D, Shaffer CL, Cover TL, Venegas A, et al. Downregulated Th17 responses are associated with reduced gastritis in Helicobacter pylori-infected children. Mucosal Immunol. 2013;6(5):950-9.

234. Gil JH, Seo JW, Cho MS, Ahn JH, Sung HY. Role of Treg and TH17 cells of the gastric mucosa in children with Helicobacter pylori gastritis. J Pediatr Gastroenterol Nutr. 2014;58(2):245-51.

235. Larussa T, Leone I, Suraci E, Imeneo M, Luzza F. Helicobacter pylori and T Helper Cells: Mechanisms of Immune Escape and Tolerance. J Immunol Res. 2015;2015:981328.

236. Cheng HH, Tseng GY, Yang HB, Wang HJ, Lin HJ, Wang WC. Increased numbers of Foxp3-positive regulatory T cells in gastritis, peptic ulcer and gastric adenocarcinoma. World J Gastroenterol. 2012;18(1):34-43.

237. Vinagre R, Vinagre IDF, Vilar ESA, Fecury AA, Martins LC. Helicobacter Pylori Infection and Immune Profile of Patients with Different Gastroduodenal Diseases. Arq Gastroenterol. 2018;55(2):122-7.

238. Tan MP, Pedersen J, Zhan Y, Lew AM, Pearse MJ, Wijburg OL, et al. CD8+ T cells are associated with severe gastritis in Helicobacter pylori-infected mice in the absence of CD4+ T cells. Infect Immun. 2008;76(3):1289-97.

239. Guo L, Liu Z, Zhang Y, Quan Q, Huang L, Xu Y, et al. Association of increased B7 protein expression by infiltrating immune cells with progression of gastric carcinogenesis. Medicine (Baltimore). 2019;98(8):e14663.

240. Ying L, Yan F, Meng Q, Yuan X, Yu L, Williams BRG, et al. Understanding immune phenotypes in human gastric disease tissues by multiplexed immunohistochemistry. J Transl Med. 2017;15(1):206.

241. Bhattacharya M. Understanding B Lymphocyte Development: A Long Way to Go. Lymphocytes2019.

242. Hill DG, Yu L, Gao H, Balic JJ, West A, Oshima H, et al. Hyperactive gp130/STAT3-driven gastric tumourigenesis promotes submucosal tertiary lymphoid structure development. Int J Cancer. 2018.

243. Brus I, Siegel H, Yamaguchi N, Jerzy Glass GB. Immunoglobulins IgA and IgG in gastric mucosa of patients with atrophic gastritis and pernicious anemia. Scand J Gastroenterol. 1968;3(1):43-57.

244. Mattsson A, Tinnert A, Hamlet A, Lonroth H, Bolin I, Svennerholm AM. Specific antibodies in sera and gastric aspirates of symptomatic and asymptomatic Helicobacter pylori-infected subjects. Clin Diagn Lab Immunol. 1998;5(3):288-93.

245. Tosi MF, Czinn SJ. Opsonic activity of specific human IgG against Helicobacter pylori. J Infect Dis. 1990;162(1):156-62.

246. Ioachim HL, Hajdu C, Giancotti FR, Dorsett B. Lymphoid proliferations and lymphomas associated with gastric metaplasia, dysplasia, and carcinoma. Hum Pathol. 1999;30(7):833-42.

247. Nguyen TL, Khurana SS, Bellone CJ, Capoccia BJ, Sagartz JE, Kesman RA, Jr., et al. Autoimmune gastritis mediated by CD4+ T cells promotes the development of gastric cancer. Cancer Res. 2013;73(7):2117-26.

248. Hanahan D, Weinberg RA. The hallmarks of cancer. Cell. 2000;100(1):57-70.

249. Hanahan D, Weinberg RA. Hallmarks of cancer: the next generation. Cell. 2011;144(5):646-74.

250. Hinshaw DC, Shevde LA. The Tumor Microenvironment Innately Modulates Cancer Progression. Cancer Res. 2019;79(18):4557-66.

251. Zhuang Y, Peng LS, Zhao YL, Shi Y, Mao XH, Chen W, et al. CD8(+) T cells that produce interleukin-17 regulate myeloid-derived suppressor cells and are associated with survival time of patients with gastric cancer. Gastroenterology. 2012;143(4):951-62 e8.

252. Ma GF, Miao Q, Zeng XQ, Luo TC, Ma LL, Liu YM, et al. Transforming growth factor-beta1 and -beta2 in gastric precancer and cancer and roles in tumor-cell interactions with peripheral blood mononuclear cells in vitro. PLoS One. 2013;8(1):e54249.

253. Shen Z, Kauttu T, Cao J, Seppanen H, Vainionpaa S, Ye Y, et al. Macrophage coculture enhanced invasion of gastric cancer cells via TGF-beta and BMP pathways. Scand J Gastroenterol. 2013;48(4):466-72.

254. Kim JW, Nam KH, Ahn SH, Park DJ, Kim HH, Kim SH, et al. Prognostic implications of immunosuppressive protein expression in tumors as well as immune cell infiltration within the tumor microenvironment in gastric cancer. Gastric Cancer. 2016;19(1):42-52.

255. Thompson ED, Zahurak M, Murphy A, Cornish T, Cuka N, Abdelfatah E, et al. Patterns of PD-L1 expression and CD8 T cell infiltration in gastric adenocarcinomas and associated immune stroma. Gut. 2017;66(5):794-801.

256. Xiang Z, Zhou ZJ, Xia GK, Zhang XH, Wei ZW, Zhu JT, et al. A positive crosstalk between CXCR4 and CXCR2 promotes gastric cancer metastasis. Oncogene. 2017;36(36):5122-33.

257. Yang W, Lai Z, Li Y, Mu J, Yang M, Xie J, et al. Immune signature profiling identified prognostic factors for gastric cancer. Chin J Cancer Res. 2019;31(3):463-70.

258. Wang M, Huang YK, Kong JC, Sun Y, Tantalo DG, Yeang HXA, et al. High-dimensional analyses reveal a distinct role of T-cell subsets in the immune microenvironment of gastric cancer. Clin Transl Immunology. 2020;9(5):e1127.

259. Busuttil RA, George J, Tothill RW, Ioculano K, Kowalczyk A, Mitchell C, et al. A signature predicting poor prognosis in gastric and ovarian cancer represents a coordinated macrophage and stromal response. Clin Cancer Res. 2014;20(10):2761-72.

260. Ohno S, Inagawa H, Dhar DK, Fujii T, Ueda S, Tachibana M, et al. The degree of macrophage infiltration into the cancer cell nest is a significant predictor of survival in gastric cancer patients. Anticancer Res. 2003;23(6D):5015-22.

261. Liu JY, Peng CW, Yang GF, Hu WQ, Yang XJ, Huang CQ, et al. Distribution pattern of tumor associated macrophages predicts the prognosis of gastric cancer. Oncotarget. 2017;8(54):92757-69.

262. Shankaran V, Ikeda H, Bruce AT, White JM, Swanson PE, Old LJ, et al. IFNgamma and lymphocytes prevent primary tumour development and shape tumour immunogenicity. Nature. 2001;410(6832):1107-11.

263. Dunn GP, Old LJ, Schreiber RD. The immunobiology of cancer immunosurveillance and immunoediting. Immunity. 2004;21(2):137-48.

264. Galon J, Costes A, Sanchez-Cabo F, Kirilovsky A, Mlecnik B, Lagorce-Pages C, et al. Type, density, and location of immune cells within human colorectal tumors predict clinical outcome. Science. 2006;313(5795):1960-4.

265. Piersma SJ, Jordanova ES, van Poelgeest MI, Kwappenberg KM, van der Hulst JM, Drijfhout JW, et al. High number of intraepithelial CD8+ tumor-infiltrating lymphocytes is associated with the absence of lymph node metastases in patients with large early-stage cervical cancer. Cancer Res. 2007;67(1):354-61.

266. Kmiecik J, Poli A, Brons NH, Waha A, Eide GE, Enger PO, et al. Elevated CD3+ and CD8+ tumor-infiltrating immune cells correlate with prolonged survival in glioblastoma patients despite integrated immunosuppressive mechanisms in the tumor microenvironment and at the systemic level. J Neuroimmunol. 2013;264(1-2):71-83.

267. Liu K, Yang K, Wu B, Chen H, Chen X, Chen X, et al. Tumor-Infiltrating Immune Cells Are Associated With Prognosis of Gastric Cancer. Medicine. 2015;94(39):e1631.

268. Fridman WH, Pages F, Sautes-Fridman C, Galon J. The immune contexture in human tumours: impact on clinical outcome. Nat Rev Cancer. 2012;12(4):298-306.

269. Nishikawa H, Sakaguchi S. Regulatory T cells in cancer immunotherapy. Curr Opin Immunol. 2014;27:1-7.

270. Togashi Y, Shitara K, Nishikawa H. Regulatory T cells in cancer immunosuppression - implications for anticancer therapy. Nat Rev Clin Oncol. 2019;16(6):356-71.

271. Shimizu J, Yamazaki S, Sakaguchi S. Induction of tumor immunity by removing CD25+CD4+ T cells: a common basis between tumor immunity and autoimmunity. J Immunol. 1999;163(10):5211-8.

272. Kim JY, Kim WG, Kwon CH, Park DY. Differences in immune contextures among different molecular subtypes of gastric cancer and their prognostic impact. Gastric Cancer. 2019;22(6):1164-75.

273. Kim Y, Kim YW, Choi IJ, Cho JY, Kim JH, Kwon JW, et al. Cost comparison between surgical treatments and endoscopic submucosal dissection in patients with early gastric cancer in Korea. Gut Liver. 2015;9(2):174-80.

274. Huang YK, Yu JC, Kang WM, Ma ZQ, Ye X, Tian SB, et al. Significance of Serum Pepsinogens as a Biomarker for Gastric Cancer and Atrophic Gastritis Screening: A Systematic Review and Meta-Analysis. PLoS One. 2015;10(11):e0142080.

275. Tong Y, Wu Y, Song Z, Yu Y, Yu X. The potential value of serum pepsinogen for the diagnosis of atrophic gastritis among the health check-up populations in China: a diagnostic clinical research. BMC Gastroenterol. 2017;17(1):88.

276. Ishigami S, Natsugoe S, Hokita S, Che X, Tokuda K, Nakajo A, et al. Clinical importance of preoperative carcinoembryonic antigen and carbohydrate antigen 19-9 levels in gastric cancer. J Clin Gastroenterol. 2001;32(1):41-4.

277. Yin LK, Sun XQ, Mou DZ. Value of Combined Detection of Serum CEA, CA72-4, CA19-9 and TSGF in the Diagnosis of Gastric Cancer. Asian Pac J Cancer Prev. 2015;16(9):3867-70.

278. Ye DM, Xu G, Ma W, Li Y, Luo W, Xiao Y, et al. Significant function and research progress of biomarkers in gastric cancer. Oncol Lett. 2020;19(1):17-29.

279. Companioni Napoles O, Tsao AC, Sanz-Anquela JM, Sala N, Bonet C, Pardo ML, et al. SCHLAFEN 5 expression correlates with intestinal metaplasia that progresses to gastric cancer. J Gastroenterol. 2017;52(1):39-49.

280. Zhao H, Yang X, Zhou Y, Zhang W, Wang Y, Wen J, et al. Potential role of aquaporin 3 in gastric intestinal metaplasia. Oncotarget. 2015;6(36):38926-33.

281. Zhao H, Wen J, Dong X, He R, Gao C, Zhang W, et al. Identification of AQP3 and CD24 as biomarkers for carcinogenesis of gastric intestinal metaplasia. Oncotarget. 2017;8(38):63382-91.

282. Jaggupilli A, Elkord E. Significance of CD44 and CD24 as cancer stem cell markers: an enduring ambiguity. Clin Dev Immunol. 2012;2012:708036.

283. Fox JG, Wang TC. Inflammation, atrophy, and gastric cancer. J Clin Invest. 2007;117(1):60-9.

284. Tu S, Bhagat G, Cui G, Takaishi S, Kurt-Jones EA, Rickman B, et al. Overexpression of interleukin-1beta induces gastric inflammation and cancer and mobilizes myeloid-derived suppressor cells in mice. Cancer Cell. 2008;14(5):408-19.

285. Merchant JL, Ding L. Hedgehog Signaling Links Chronic Inflammation to Gastric Cancer Precursor Lesions. Cell Mol Gastroenterol Hepatol. 2017;3(2):201-10.

286. Tsukamoto T, Mizoshita T, Tatematsu M. Animal models of stomach carcinogenesis. Toxicol Pathol. 2007;35(5):636-48.

287. Hayakawa Y, Fox JG, Gonda T, Worthley DL, Muthupalani S, Wang TC. Mouse models of gastric cancer. Cancers (Basel). 2013;5(1):92-130.

288. Jiang Y, Yu Y. Transgenic and gene knockout mice in gastric cancer research. Oncotarget. 2017;8(2):3696-710.

289. Poh AR, O'Donoghue RJ, Ernst M, Putoczki TL. Mouse models for gastric cancer: Matching models to biological questions. J Gastroenterol Hepatol. 2016;31(7):1257-72.

290. Sato T. Histopathologic structure of adenocarcinomas induced in glandular stomach of rat by N-methyl-N'-nitro-N-nitrosoguanidine. Tohoku J Exp Med. 1971;105(3):201-21.

291. Peng C, Li NS, Hu Y, Lu NH. Impact factors that modulate gastric cancer risk in Helicobacter pylori-infected rodent models. Helicobacter. 2019;24(4):e12580.

292. Shimizu N, Inada K, Nakanishi H, Tsukamoto T, Ikehara Y, Kaminishi M, et al. Helicobacter pylori infection enhances glandular stomach carcinogenesis in Mongolian gerbils treated with chemical carcinogens. Carcinogenesis. 1999;20(4):669-76.

293. Nakamura Y, Sakagami T, Yamamoto N, Yokota Y, Koizuka H, Hori K, et al. Helicobacter pylori does not promote N-methyl-N-nitrosourea-induced gastric carcinogenesis in SPF C57BL/6 mice. Jpn J Cancer Res. 2002;93(2):111-6.

294. Tatematsu M, Yamamoto M, Shimizu N, Yoshikawa A, Fukami H, Kaminishi M, et al. Induction of glandular stomach cancers in Helicobacter pylori-sensitive Mongolian gerbils treated with N-methyl-N-nitrosourea and N-methyl-N'-nitro-N-nitrosoguanidine in drinking water. Jpn J Cancer Res. 1998;89(2):97-104.

295. Han SU, Kim YB, Joo HJ, Hahm KB, Lee WH, Cho YK, et al. Helicobacter pylori infection promotes gastric carcinogenesis in a mice model. J Gastroenterol Hepatol. 2002;17(3):253-61.

296. Jiao S, Wang H, Shi Z, Dong A, Zhang W, Song X, et al. A peptide mimicking VGLL4 function acts as a YAP antagonist therapy against gastric cancer. Cancer Cell. 2014;25(2):166-80.

297. Ernst M, Najdovska M, Grail D, Lundgren-May T, Buchert M, Tye H, et al. STAT3 and STAT1 mediate IL-11-dependent and inflammation-associated gastric tumorigenesis in gp130 receptor mutant mice. J Clin Invest. 2008;118(5):1727-38.

298. O'Reilly LA, Putoczki TL, Mielke LA, Low JT, Lin A, Preaudet A, et al. Loss of NF-kappaB1 Causes Gastric Cancer with Aberrant Inflammation and Expression of Immune Checkpoint Regulators in a STAT-1-Dependent Manner. Immunity. 2018;48(3):570-83 e8.

299. Watanabe T, Tada M, Nagai H, Sasaki S, Nakao M. Helicobacter pylori infection induces gastric cancer in mongolian gerbils. Gastroenterology. 1998;115(3):642-8.

300. Elfvin A, Bolin I, Von Bothmer C, Stolte M, Watanabe H, Fandriks L, et al. Helicobacter pylori induces gastritis and intestinal metaplasia but no gastric adenocarcinoma in Mongolian gerbils. Scand J Gastroenterol. 2005;40(11):1313-20.

301. Kanda N, Seno H, Kawada M, Sawabu T, Uenoyoma Y, Nakajima T, et al. Involvement of cyclooxygenase-2 in gastric mucosal hypertrophy in gastrin transgenic mice. Am J Physiol Gastrointest Liver Physiol. 2006;290(3):G519-27.

302. Andersson P, McGuire J, Rubio C, Gradin K, Whitelaw ML, Pettersson S, et al. A constitutively active dioxin/aryl hydrocarbon receptor induces stomach tumors. Proc Natl Acad Sci U S A. 2002;99(15):9990-5.

303. Thompson J, Epting T, Schwarzkopf G, Singhofen A, Eades-Perner AM, van Der Putten H, et al. A transgenic mouse line that develops early-onset invasive gastric carcinoma provides a model for carcinoembryonic antigen-targeted tumor therapy. Int J Cancer. 2000;86(6):863-9.

304. Shimada S, Mimata A, Sekine M, Mogushi K, Akiyama Y, Fukamachi H, et al. Synergistic tumour suppressor activity of E-cadherin and p53 in a conditional mouse model for metastatic diffuse-type gastric cancer. Gut. 2012;61(3):344-53.

305. Humar B, Blair V, Charlton A, More H, Martin I, Guilford P. E-cadherin deficiency initiates gastric signet-ring cell carcinoma in mice and man. Cancer Res. 2009;69(5):2050-6.

306. Mutoh H, Sakurai S, Satoh K, Tamada K, Kita H, Osawa H, et al. Development of gastric carcinoma from intestinal metaplasia in Cdx2-transgenic mice. Cancer Res. 2004;64(21):7740-7.

307. Zavros Y, Eaton KA, Kang W, Rathinavelu S, Katukuri V, Kao JY, et al. Chronic gastritis in the hypochlorhydric gastrin-deficient mouse progresses to adenocarcinoma. Oncogene. 2005;24(14):2354-66.

308. Hahn JN, Falck VG, Jirik FR. Smad4 deficiency in T cells leads to the Th17-associated development of premalignant gastroduodenal lesions in mice. J Clin Invest. 2011;121(10):4030-42.

309. Fox JG, Wang TC, Rogers AB, Poutahidis T, Ge Z, Taylor N, et al. Host and microbial constituents influence Helicobacter pylori-induced cancer in a murine model of hypergastrinemia. Gastroenterology. 2003;124(7):1879-90.

310. Okumura T, Ericksen RE, Takaishi S, Wang SS, Dubeykovskiy Z, Shibata W, et al. K-ras mutation targeted to gastric tissue progenitor cells results in chronic inflammation, an altered microenvironment, and progression to intraepithelial neoplasia. Cancer Res. 2010;70(21):8435-45.

311. Ito K, Chuang LS, Ito T, Chang TL, Fukamachi H, Salto-Tellez M, et al. Loss of Runx3 is a key event in inducing precancerous state of the stomach. Gastroenterology. 2011;140(5):1536-46 e8.

312. Barker N, Huch M, Kujala P, van de Wetering M, Snippert HJ, van Es JH, et al. Lgr5(+ve) stem cells drive self-renewal in the stomach and build long-lived gastric units in vitro. Cell Stem Cell. 2010;6(1):25-36.

313. Koike K, Hinrichs SH, Isselbacher KJ, Jay G. Transgenic mouse model for human gastric carcinoma. Proc Natl Acad Sci U S A. 1989;86(14):5615-9.

314. Tsuzuki T, Egashira A, Igarashi H, Iwakuma T, Nakatsuru Y, Tominaga Y, et al. Spontaneous tumorigenesis in mice defective in the MTH1 gene encoding 8-oxo-dGTPase. Proc Natl Acad Sci U S A. 2001;98(20):11456-61.

315. Nam KT, O'Neal R, Lee YS, Lee YC, Coffey RJ, Goldenring JR. Gastric tumor development in Smad3-deficient mice initiates from forestomach/glandular transition zone along the lesser curvature. Lab Invest. 2012;92(6):883-95.

316. Takaku K, Miyoshi H, Matsunaga A, Oshima M, Sasaki N, Taketo MM. Gastric and duodenal polyps in Smad4 (Dpc4) knockout mice. Cancer Res. 1999;59(24):6113-7.

317. Lefebvre O, Chenard MP, Masson R, Linares J, Dierich A, LeMeur M, et al. Gastric mucosa abnormalities and tumorigenesis in mice lacking the pS2 trefoil protein. Science. 1996;274(5285):259-62.

318. Oshima H, Matsunaga A, Fujimura T, Tsukamoto T, Taketo MM, Oshima M. Carcinogenesis in mouse stomach by simultaneous activation of the Wnt signaling and prostaglandin E2 pathway. Gastroenterology. 2006;131(4):1086-95.

319. Li Q, Jia Z, Wang L, Kong X, Li Q, Guo K, et al. Disruption of Klf4 in villin-positive gastric progenitor cells promotes formation and progression of tumors of the antrum in mice. Gastroenterology. 2012;142(3):531-42.

320. Liu W, Pan HF, Wang Q, Zhao ZM. The application of transgenic and gene knockout mice in the study of gastric precancerous lesions. Pathol Res Pract. 2018;214(12):1929-39.

321. Silberg DG, Sullivan J, Kang E, Swain GP, Moffett J, Sund NJ, et al. Cdx2 ectopic expression induces gastric intestinal metaplasia in transgenic mice. Gastroenterology. 2002;122(3):689-96.

322. Mutoh H, Sakurai S, Satoh K, Osawa H, Hakamata Y, Takeuchi T, et al. Cdx1 induced intestinal metaplasia in the transgenic mouse stomach: comparative study with Cdx2 transgenic mice. Gut. 2004;53(10):1416-23.

323. Mizoshita T, Inada K, Tsukamoto T, Kodera Y, Yamamura Y, Hirai T, et al. Expression of Cdx1 and Cdx2 mRNAs and relevance of this expression to differentiation in human gastrointestinal mucosa--with special emphasis on participation in intestinal metaplasia of the human stomach. Gastric Cancer. 2001;4(4):185-91.

324. Eda A, Osawa H, Yanaka I, Satoh K, Mutoh H, Kihira K, et al. Expression of homeobox gene CDX2 precedes that of CDX1 during the progression of intestinal metaplasia. J Gastroenterol. 2002;37(2):94-100.

325. Satoh K, Mutoh H, Eda A, Yanaka I, Osawa H, Honda S, et al. Aberrant expression of CDX2 in the gastric mucosa with and without intestinal metaplasia: effect of eradication of Helicobacter pylori. Helicobacter. 2002;7(3):192-8.

326. Goldenring JR. Pyloric metaplasia, pseudopyloric metaplasia, ulcer-associated cell lineage and spasmolytic polypeptide-expressing metaplasia: reparative lineages in the gastrointestinal mucosa. J Pathol. 2018;245(2):132-7.

327. Tomita H, Takaishi S, Menheniott TR, Yang X, Shibata W, Jin G, et al. Inhibition of gastric carcinogenesis by the hormone gastrin is mediated by suppression of TFF1 epigenetic silencing. Gastroenterology. 2011;140(3):879-91.

328. Wang TC, Dangler CA, Chen D, Goldenring JR, Koh T, Raychowdhury R, et al. Synergistic interaction between hypergastrinemia and Helicobacter infection in a mouse model of gastric cancer. Gastroenterology. 2000;118(1):36-47.

329. Spicer Z, Miller ML, Andringa A, Riddle TM, Duffy JJ, Doetschman T, et al. Stomachs of mice lacking the gastric H,K-ATPase alpha -subunit have achlorhydria, abnormal parietal cells, and ciliated metaplasia. J Biol Chem. 2000;275(28):21555-65.

330. Judd LM, Andringa A, Rubio CA, Spicer Z, Shull GE, Miller ML. Gastric achlorhydria in H/K-ATPase-deficient (Atp4a(-/-)) mice causes severe hyperplasia, mucocystic metaplasia and upregulation of growth factors. J Gastroenterol Hepatol. 2005;20(8):1266-78.

331. Scarff KL, Judd LM, Toh BH, Gleeson PA, Van Driel IR. Gastric H(+),K(+)-adenosine triphosphatase beta subunit is required for normal function, development, and membrane structure of mouse parietal cells. Gastroenterology. 1999;117(3):605-18.

332. Franic TV, Judd LM, Robinson D, Barrett SP, Scarff KL, Gleeson PA, et al. Regulation of gastric epithelial cell development revealed in H(+)/K(+)-ATPase beta-subunit- and gastrin-deficient mice. Am J Physiol Gastrointest Liver Physiol. 2001;281(6):G1502-11.

333. Li Q, Karam SM, Gordon JI. Simian virus 40 T antigen-induced amplification of pre-parietal cells in transgenic mice. Effects on other gastric epithelial cell lineages and evidence for a p53-independent apoptotic mechanism that operates in a committed progenitor. J Biol Chem. 1995;270(26):15777-88.

334. Li Q, Karam SM, Gordon JI. Diphtheria toxin-mediated ablation of parietal cells in the stomach of transgenic mice. J Biol Chem. 1996;271(7):3671-6.

335. Ogawa M, Nomura S, Varro A, Wang TC, Goldenring JR. Altered metaplastic response of waved-2 EGF receptor mutant mice to acute oxyntic atrophy. Am J Physiol Gastrointest Liver Physiol. 2006;290(4):G793-804.

336. Gut MO, Parkkila S, Vernerova Z, Rohde E, Zavada J, Hocker M, et al. Gastric hyperplasia in mice with targeted disruption of the carbonic anhydrase gene Car9. Gastroenterology. 2002;123(6):1889-903.

337. Nagata A, Ito M, Iwata N, Kuno J, Takano H, Minowa O, et al. G protein-coupled cholecystokinin-B/gastrin receptors are responsible for physiological cell growth of the stomach mucosa in vivo. Proc Natl Acad Sci U S A. 1996;93(21):11825-30.

338. Langhans N, Rindi G, Chiu M, Rehfeld JF, Ardman B, Beinborn M, et al. Abnormal gastric histology and decreased acid production in cholecystokinin-B/gastrin receptor-deficient mice. Gastroenterology. 1997;112(1):280-6.

339. Schultheis PJ, Clarke LL, Meneton P, Harline M, Boivin GP, Stemmermann G, et al. Targeted disruption of the murine Na+/H+ exchanger isoform 2 gene causes reduced viability of gastric parietal cells and loss of net acid secretion. J Clin Invest. 1998;101(6):1243-53.

340. Brembeck FH, Schreiber FS, Deramaudt TB, Craig L, Rhoades B, Swain G, et al. The mutant K-ras oncogene causes pancreatic periductal lymphocytic infiltration and gastric mucous neck cell hyperplasia in transgenic mice. Cancer Res. 2003;63(9):2005-9.

341. Choi E, Hendley AM, Bailey JM, Leach SD, Goldenring JR. Expression of Activated Ras in Gastric Chief Cells of Mice Leads to the Full Spectrum of Metaplastic Lineage Transitions. Gastroenterology. 2016;150(4):918-30 e13.

342. Tu SP, Quante M, Bhagat G, Takaishi S, Cui G, Yang XD, et al. IFN-gamma inhibits gastric carcinogenesis by inducing epithelial cell autophagy and T-cell apoptosis. Cancer Res. 2011;71(12):4247-59.

343. Tatematsu M, Yamamoto M, Iwata H, Fukami H, Yuasa H, Tezuka N, et al. Induction of glandular stomach cancers in C3H mice treated with N-methyl-N-nitrosourea in the drinking water. Jpn J Cancer Res. 1993;84(12):1258-64.

344. Yamamoto M, Furihata C, Ogiu T, Tsukamoto T, Inada K, Hirano K, et al. Independent variation in susceptibilities of six different mouse strains to induction of pepsinogen-altered pyloric glands and gastric tumor intestinalization by N-methyl-N-nitrosourea. Cancer Lett. 2002;179(2):121-32.

345. Nomura S, Yamaguchi H, Ogawa M, Wang TC, Lee JR, Goldenring JR. Alterations in gastric mucosal lineages induced by acute oxyntic atrophy in wild-type and gastrin-deficient mice. Am J Physiol Gastrointest Liver Physiol. 2005;288(2):G362-75.

346. Cantorna MT, Balish E. Inability of human clinical strains of Helicobacter pylori to colonize the alimentary tract of germfree rodents. Can J Microbiol. 1990;36(4):237-41.

347. De Groote D, Van Doorn LJ, Van den Bulck K, Vandamme P, Vieth M, Stolte M, et al. Detection of non-pylori Helicobacter species in "Helicobacter heilmannii"-infected humans. Helicobacter. 2005;10(5):398-406.

348. Van den Bulck K, Decostere A, Baele M, Driessen A, Debongnie JC, Burette A, et al. Identification of non-Helicobacter pylori spiral organisms in gastric samples from humans, dogs, and cats. J Clin Microbiol. 2005;43(5):2256-60.

349. Yoshizawa N, Takenaka Y, Yamaguchi H, Tetsuya T, Tanaka H, Tatematsu M, et al. Emergence of spasmolytic polypeptide-expressing metaplasia in Mongolian gerbils infected with Helicobacter pylori. Lab Invest. 2007;87(12):1265-76.

350. Park JG, Frucht H, LaRocca RV, Bliss DP, Jr., Kurita Y, Chen TR, et al. Characteristics of cell lines established from human gastric carcinoma. Cancer Res. 1990;50(9):2773-80.

351. Vollmers HP, Stulle K, Dammrich J, Pfaff M, Papadopoulos T, Betz C, et al. Characterization of four new gastric cancer cell lines. Virchows Arch B Cell Pathol Incl Mol Pathol. 1993;63(6):335-43.

352. Ku JL, Kim KH, Choi JS, Kim SH, Shin YK, Chang HJ, et al. Establishment and characterization of six human gastric carcinoma cell lines, including one naturally infected with Epstein-Barr virus. Cell Oncol (Dordr). 2012;35(2):127-36.

353. Busuttil RA, Liu DS, Di Costanzo N, Schroder J, Mitchell C, Boussioutas A. An orthotopic mouse model of gastric cancer invasion and metastasis. Sci Rep. 2018;8(1):825.

354. Palanca-Wessels MC, Barrett MT, Galipeau PC, Rohrer KL, Reid BJ, Rabinovitch PS. Genetic analysis of long-term Barrett's esophagus epithelial cultures exhibiting cytogenetic and ploidy abnormalities. Gastroenterology. 1998;114(2):295-304.

355. Palanca-Wessels MC, Klingelhutz A, Reid BJ, Norwood TH, Opheim KE, Paulson TG, et al. Extended lifespan of Barrett's esophagus epithelium transduced with the human telomerase catalytic subunit: a useful in vitro model. Carcinogenesis. 2003;24(7):1183-90.

356. Chen BJ, Zeng S, Xie R, Hu CJ, Wang SM, Wu YY, et al. hTERT promotes gastric intestinal metaplasia by upregulating CDX2 via NF-kappaB signaling pathway. Oncotarget. 2017;8(16):26969-78.

357. Naito S, Inoue S, Kinjo M, Tanaka K. Thromboplastic and fibrinolytic activities of cultured human gastric cancer cell lines. Gan. 1983;74(2):240-7.

358. Cekanova M, Rathore K. Animal models and therapeutic molecular targets of cancer: utility and limitations. Drug Des Devel Ther. 2014;8:1911-21.

359. Kemp CJ. Animal Models of Chemical Carcinogenesis: Driving Breakthroughs in Cancer Research for 100 Years. Cold Spring Harb Protoc. 2015;2015(10):865-74.

360. Clevers H. Modeling Development and Disease with Organoids. Cell. 2016;165(7):1586-97.

361. Dedhia PH, Bertaux-Skeirik N, Zavros Y, Spence JR. Organoid Models of Human Gastrointestinal Development and Disease. Gastroenterology. 2016;150(5):1098-112.

362. Fatehullah A, Tan SH, Barker N. Organoids as an in vitro model of human development and disease. Nat Cell Biol. 2016;18(3):246-54.

363. Huch M, Knoblich JA, Lutolf MP, Martinez-Arias A. The hope and the hype of organoid research. Development. 2017;144(6):938-41.

364. Sato T, Vries RG, Snippert HJ, van de Wetering M, Barker N, Stange DE, et al. Single Lgr5 stem cells build crypt-villus structures in vitro without a mesenchymal niche. Nature. 2009;459(7244):262-5.

365. Sato T, Stange DE, Ferrante M, Vries RG, Van Es JH, Van den Brink S, et al. Long-term expansion of epithelial organoids from human colon, adenoma, adenocarcinoma, and Barrett's epithelium. Gastroenterology. 2011;141(5):1762-72.

366. Bartfeld S, Bayram T, van de Wetering M, Huch M, Begthel H, Kujala P, et al. In vitro expansion of human gastric epithelial stem cells and their responses to bacterial infection. Gastroenterology. 2015;148(1):126-36 e6.

367. Drost J, van Jaarsveld RH, Ponsioen B, Zimberlin C, van Boxtel R, Buijs A, et al. Sequential cancer mutations in cultured human intestinal stem cells. Nature. 2015;521(7550):43-7.

368. Matano M, Date S, Shimokawa M, Takano A, Fujii M, Ohta Y, et al. Modeling colorectal cancer using CRISPR-Cas9-mediated engineering of human intestinal organoids. Nat Med. 2015;21(3):256-62.

369. Li X, Nadauld L, Ootani A, Corney DC, Pai RK, Gevaert O, et al. Oncogenic transformation of diverse gastrointestinal tissues in primary organoid culture. Nat Med. 2014;20(7):769-77.

370. Bartfeld S, Clevers H. Organoids as Model for Infectious Diseases: Culture of Human and Murine Stomach Organoids and Microinjection of Helicobacter Pylori. J Vis Exp. 2015(105).

371. Bertaux-Skeirik N, Feng R, Schumacher MA, Li J, Mahe MM, Engevik AC, et al. CD44 plays a functional role in Helicobacter pylori-induced epithelial cell proliferation. PLoS Pathog. 2015;11(2):e1004663.

372. Schlaermann P, Toelle B, Berger H, Schmidt SC, Glanemann M, Ordemann J, et al. A novel human gastric primary cell culture system for modelling Helicobacter pylori infection in vitro. Gut. 2016;65(2):202-13.

373. McCracken KW, Cata EM, Crawford CM, Sinagoga KL, Schumacher M, Rockich BE, et al. Modelling human development and disease in pluripotent stem-cell-derived gastric organoids. Nature. 2014;516(7531):400-4.

374. Neal JT, Li X, Zhu J, Giangarra V, Grzeskowiak CL, Ju J, et al. Organoid Modeling of the Tumor Immune Microenvironment. Cell. 2018;175(7):1972-88 e16.

375. Ootani A, Li X, Sangiorgi E, Ho QT, Ueno H, Toda S, et al. Sustained in vitro intestinal epithelial culture within a Wnt-dependent stem cell niche. Nat Med. 2009;15(6):701-6.

376. Ashok A, Choudhury D, Fang Y, Hunziker W. Towards manufacturing of human organoids. Biotechnol Adv. 2020;39:107460.

377. Ye W, Luo C, Li C, Huang J, Liu F. Organoids to study immune functions, immunological diseases and immunotherapy. Cancer Lett. 2020;477:31-40.

378. Mariette C, Piessen G, Briez N, Gronnier C, Triboulet JP. Oesophagogastric junction adenocarcinoma: which therapeutic approach? The Lancet Oncology. 2011;12(3):296-305.

379. Benjamini Y, Hochberg A. Controlling the false discovery rate: a practical and powerful approach to multiple testing. Journal of the Royal Statistical Society, Series B. 1995;57(1):289-300.

380. Irizarry RA, Hobbs B, Collin F, Beazer-Barclay YD, Antonellis KJ, Scherf U, et al. Exploration, normalization, and summaries of high density oligonucleotide array probe level data. Biostatistics. 2003;4(2):249-64.

381. Ritchie ME, Phipson B, Wu D, Hu Y, Law CW, Shi W, et al. limma powers differential expression analyses for RNA-sequencing and microarray studies. Nucleic Acids Res. 2015;43(7):e47.

382. Terpstra TJ. The asymptotic normality and consistency of kendall's test against trend, when ties are present in one ranking. Indagationes Mathematicae (Proceedings). 1952;55:327-33.

383. Shannon P, Markiel A, Ozier O, Baliga NS, Wang JT, Ramage D, et al. Cytoscape: a software environment for integrated models of biomolecular interaction networks. Genome Res. 2003;13(11):2498-504.

384. Bindea G, Mlecnik B, Hackl H, Charoentong P, Tosolini M, Kirilovsky A, et al. ClueGO: a Cytoscape plug-in to decipher functionally grouped gene ontology and pathway annotation networks. Bioinformatics. 2009;25(8):1091-3.

385. Raudvere U, Kolberg L, Kuzmin I, Arak T, Adler P, Peterson H, et al. g:Profiler: a web server for functional enrichment analysis and conversions of gene lists (2019 update). Nucleic Acids Res. 2019;47(W1):W191-W8.

386. Holm S. A Simple Sequentially Rejective Multiple Test Procedure. Scandinavian Journal of Statistics. 1979;6(2):65-70.

387. Barbie DA, Tamayo P, Boehm JS, Kim SY, Moody SE, Dunn IF, et al. Systematic RNA interference reveals that oncogenic KRAS-driven cancers require TBK1. Nature. 2009;462(7269):108-12.

388. Companioni O, Sanz-Anquela JM, Pardo ML, Puigdecanet E, Nonell L, Garcia N, et al. Gene expression study and pathway analysis of histological subtypes of intestinal metaplasia that progress to gastric cancer. PLoS One. 2017;12(4):e0176043.

389. Newman AM, Liu CL, Green MR, Gentles AJ, Feng W, Xu Y, et al. Robust enumeration of cell subsets from tissue expression profiles. Nat Methods. 2015;12(5):453-7.

390. Stack EC, Wang C, Roman KA, Hoyt CC. Multiplexed immunohistochemistry, imaging, and quantitation: a review, with an assessment of Tyramide signal amplification, multispectral imaging and multiplex analysis. Methods. 2014;70(1):46-58.

391. Kent SJ. phenoptr: inForm Helper Functions. R package version 0.2.7.: https://akoyabio.github.io/phenoptr/; 2020.

392. Thurley K, Gerecht D, Friedmann E, Hofer T. Three-Dimensional Gradients of Cytokine Signaling between T Cells. PLoS Comput Biol. 2015;11(4):e1004206.

393. Oyler-Yaniv A, Oyler-Yaniv J, Whitlock BM, Liu Z, Germain RN, Huse M, et al. A Tunable Diffusion-Consumption Mechanism of Cytokine Propagation Enables Plasticity in Cell-to-Cell Communication in the Immune System. Immunity. 2017;46(4):609-20.

394. Feng Z, Bethmann D, Kappler M, Ballesteros-Merino C, Eckert A, Bell RB, et al. Multiparametric immune profiling in HPV- oral squamous cell cancer. JCI Insight. 2017;2(14).

395. Carstens JL, Correa de Sampaio P, Yang D, Barua S, Wang H, Rao A, et al. Spatial computation of intratumoral T cells correlates with survival of patients with pancreatic cancer. Nat Commun. 2017;8:15095.

396. Clopper CJ, Pearson ES. The Use of Confidence or Fiducial Limits Illustrated in the Case of the Binomial. Biometrika. 1934;26(4):404-13.

397. Fujii M, Matano M, Nanki K, Sato T. Efficient genetic engineering of human intestinal organoids using electroporation. Nat Protoc. 2015;10(10):1474-85.

398. Matsukura N, Suzuki K, Kawachi T, Aoyagi M, Sugimura T, Kitaoka H, et al. Distribution of marker enzymes and mucin in intestinal metaplasia in human stomach and relation to complete and incomplete types of intestinal metaplasia to minute gastric carcinomas. J Natl Cancer Inst. 1980;65(2):231-40.

399. Correa P. A human model of gastric carcinogenesis. Cancer Res. 1988;48(13):3554-60.

400. Kamangar F, Dawsey SM, Blaser MJ, Perez-Perez GI, Pietinen P, Newschaffer CJ, et al. Opposing risks of gastric cardia and noncardia gastric adenocarcinomas associated with Helicobacter pylori seropositivity. J Natl Cancer Inst. 2006;98(20):1445-52.

401. Limburg P, Qiao Y, Mark S, Wang G, Perez-Perez G, Blaser M, et al. Helicobacter pylori seropositivity and subsite-specific gastric cancer risks in Linxian, China. J Natl Cancer Inst. 2001;93(3):226-33.

402. Kamangar F, Qiao YL, Blaser MJ, Sun XD, Katki H, Fan JH, et al. Helicobacter pylori and oesophageal and gastric cancers in a prospective study in China. Br J Cancer. 2007;96(1):172-6.

403. Cavaleiro-Pinto M, Peleteiro B, Lunet N, Barros H. Helicobacter pylori infection and gastric cardia cancer: systematic review and meta-analysis. Cancer Causes Control. 2011;22(3):375-87.

404. Islami F, Kamangar F. Helicobacter pylori and esophageal cancer risk: a meta-analysis. Cancer Prev Res (Phila). 2008;1(5):329-38.

405. Son T, Hyung WJ, Lee JH, Kim YM, Kim HI, An JY, et al. Clinical implication of an insufficient number of examined lymph nodes after curative resection for gastric cancer. Cancer. 2012;118(19):4687-93.

406. Boussioutas A, Li H, Liu J, Waring P, Lade S, Holloway AJ, et al. Distinctive patterns of gene expression in premalignant gastric mucosa and gastric cancer. Cancer Res. 2003;63(10):2569-77.

407. Chen X, Leung SY, Yuen ST, Chu KM, Ji J, Li R, et al. Variation in gene expression patterns in human gastric cancers. Mol Biol Cell. 2003;14(8):3208-15.

408. Gentles AJ, Newman AM, Liu CL, Bratman SV, Feng W, Kim D, et al. The prognostic landscape of genes and infiltrating immune cells across human cancers. Nat Med. 2015;21(8):938-45.

409. Calcagno DQ, Leal MF, Assumpcao PP, Smith MA, Burbano RR. MYC and gastric adenocarcinoma carcinogenesis. World J Gastroenterol. 2008;14(39):5962-8.

410. Jin DH, Park SE, Lee J, Kim KM, Kim S, Kim DH, et al. Copy Number Gains at 8q24 and 20q11-q13 in Gastric Cancer Are More Common in Intestinal-Type than Diffuse-Type. PLoS One. 2015;10(9):e0137657.

411. Busuttil RA, Boussioutas A, Di Costanzo N, Mitchell C. Manuscript in preparation. 2020.

412. Slaughter DP, Southwick HW, Smejkal W. Field cancerization in oral stratified squamous epithelium; clinical implications of multicentric origin. Cancer. 1953;6(5):963-8.

413. Grotzinger C, Kneifel J, Patschan D, Schnoy N, Anagnostopoulos I, Faiss S, et al. LI-cadherin: a marker of gastric metaplasia and neoplasia. Gut. 2001;49(1):73-81.

414. Niwa T, Ikehara Y, Nakanishi H, Tanaka H, Inada K, Tsukamoto T, et al. Mixed gastric- and intestinal-type metaplasia is formed by cells with dual intestinal and gastric differentiation. J Histochem Cytochem. 2005;53(1):75-85.

415. Shin N, Park DY. Pathologic Diagnosis of Gastric Intestinal Metaplasia. The Korean Journal of Helicobacter and Upper Gastrointestinal Research. 2013;13(2):84.

416. Silberg DG, Swain GP, Suh ER, Traber PG. Cdx1 and cdx2 expression during intestinal development. Gastroenterology. 2000;119(4):961-71.

417. Liu Q, Teh M, Ito K, Shah N, Ito Y, Yeoh KG. CDX2 expression is progressively decreased in human gastric intestinal metaplasia, dysplasia and cancer. Mod Pathol. 2007;20(12):1286-97.

418. Galand G. Brush border membrane sucrase-isomaltase, maltase-glucoamylase and trehalase in mammals. Comparative development, effects of glucocorticoids, molecular mechanisms, and phylogenetic implications. Comp Biochem Physiol B. 1989;94(1):1-11.

419. Friederich E, Vancompernolle K, Louvard D, Vandekerckhove J. Villin function in the organization of the actin cytoskeleton. Correlation of in vivo effects to its biochemical activities in vitro. J Biol Chem. 1999;274(38):26751-60.

420. Lloyd JM, Owens SR. CD10 immunohistochemistry stains enteric mucosa, but negative staining is unreliable in the setting of active enteritis. Mod Pathol. 2011;24(12):1627-32.

421. Podolsky DK, Lynch-Devaney K, Stow JL, Oates P, Murgue B, De-Beaumont M, et al. Identification of human intestinal trefoil factor. Goblet cell-specific expression of a peptide targeted for apical secretion. J Biol Chem. 1993;268(16):12230.

422. Moehle C, Ackermann N, Langmann T, Aslanidis C, Kel A, Kel-Margoulis O, et al. Aberrant intestinal expression and allelic variants of mucin genes associated with inflammatory bowel disease. J Mol Med (Berl). 2006;84(12):1055-66.

423. Pelaseyed T, Bergstrom JH, Gustafsson JK, Ermund A, Birchenough GM, Schutte A, et al. The mucus and mucins of the goblet cells and enterocytes provide the first defense line of the gastrointestinal tract and interact with the immune system. Immunol Rev. 2014;260(1):8-20.

424. Svensson M, Agace WW. Role of CCL25/CCR9 in immune homeostasis and disease. Expert Rev Clin Immunol. 2006;2(5):759-73.

425. Walz A, Schmutz P, Mueller C, Schnyder-Candrian S. Regulation and function of the CXC chemokine ENA-78 in monocytes and its role in disease. J Leukoc Biol. 1997;62(5):604-11.

426. Chen W, Wu G, Zhu Y, Zhang W, Zhang H, Zhou Y, et al. HOXA10 deteriorates gastric cancer through activating JAK1/STAT3 signaling pathway. Cancer Manag Res. 2019;11:6625-35.

427. Qin Z, Chen Z, Weng J, Li S, Rong Z, Zhou C. Elevated HOXA13 expression promotes the proliferation and metastasis of gastric cancer partly via activating Erk1/2. Onco Targets Ther. 2019;12:1803-13.

428. Hu B, Fan H, Lv X, Chen S, Shao Z. Prognostic significance of CXCL5 expression in cancer patients: a meta-analysis. Cancer Cell Int. 2018;18:68.

429. Eftang LL, Esbensen Y, Tannaes TM, Blom GP, Bukholm IR, Bukholm G. Up-regulation of CLDN1 in gastric cancer is correlated with reduced survival. BMC Cancer. 2013;13:586.

430. Hibi K, Kitamura YH, Mizukami H, Goto T, Sakuraba K, Sakata M, et al. Frequent CDH3 demethylation in advanced gastric carcinoma. Anticancer Res. 2009;29(10):3945-7.

431. Zhou J, Fan X, Chen N, Zhou F, Dong J, Nie Y, et al. Identification of CEACAM5 as a Biomarker for Prewarning and Prognosis in Gastric Cancer. J Histochem Cytochem. 2015;63(12):922-30.

432. Ru GQ, Han Y, Wang W, Chen Y, Wang HJ, Xu WJ, et al. CEACAM6 is a prognostic biomarker and potential therapeutic target for gastric carcinoma. Oncotarget. 2017;8(48):83673-83.

433. Matsuoka T, Yashiro M. Biomarkers of gastric cancer: Current topics and future perspective. World J Gastroenterol. 2018;24(26):2818-32.

434. Fergusson JR, Smith KE, Fleming VM, Rajoriya N, Newell EW, Simmons R, et al. CD161 defines a transcriptional and functional phenotype across distinct human T cell lineages. Cell Rep. 2014;9(3):1075-88.

435. Schwartz AM, Putlyaeva LV, Covich M, Klepikova AV, Akulich KA, Vorontsov IE, et al. Early B-cell factor 1 (EBF1) is critical for transcriptional control of SLAMF1 gene in human B cells. Biochim Biophys Acta. 2016;1859(10):1259-68.

436. Dinarello CA, Novick D, Kim S, Kaplanski G. Interleukin-18 and IL-18 binding protein. Front Immunol. 2013;4:289.

437. Yang GF, Deng CS, Xiong YY, Gong LL, Wang BC, Luo J. Expression of nuclear factor-kappa B and target genes in gastric precancerous lesions and adenocarcinoma: association with Helicobactor pylori cagA (+) infection. World J Gastroenterol. 2004;10(4):491-6.

438. Huang L, Wu RL, Xu AM. Epithelial-mesenchymal transition in gastric cancer. Am J Transl Res. 2015;7(11):2141-58.

439. Tanabe S, Aoyagi K, Yokozaki H, Sasaki H. Regulated genes in mesenchymal stem cells and gastric cancer. World J Stem Cells. 2015;7(1):208-22.

440. Qian C, Liu F, Ye B, Zhang X, Liang Y, Yao J. Notch4 promotes gastric cancer growth through activation of Wnt1/beta-catenin signaling. Mol Cell Biochem. 2015;401(1-2):165-74.

441. Yao Y, Ni Y, Zhang J, Wang H, Shao S. The role of Notch signaling in gastric carcinoma: molecular pathogenesis and novel therapeutic targets. Oncotarget. 2017;8(32):53839-53.

442. Seidlitz T, Chen YT, Uhlemann H, Scholch S, Kochall S, Merker SR, et al. Mouse Models of Human Gastric Cancer Subtypes With Stomach-Specific CreERT2-Mediated Pathway Alterations. Gastroenterology. 2019;157(6):1599-614 e2.

443. Liang L, Fang JY, Xu J. Gastric cancer and gene copy number variation: emerging cancer drivers for targeted therapy. Oncogene. 2016;35(12):1475-82.

444. Yamashita S, Kishino T, Takahashi T, Shimazu T, Charvat H, Kakugawa Y, et al. Genetic and epigenetic alterations in normal tissues have differential impacts on cancer risk among tissues. Proc Natl Acad Sci U S A. 2018.

445. Kress TR, Sabo A, Amati B. MYC: connecting selective transcriptional control to global RNA production. Nat Rev Cancer. 2015;15(10):593-607.

446. Stine ZE, Walton ZE, Altman BJ, Hsieh AL, Dang CV. MYC, Metabolism, and Cancer. Cancer Discov. 2015;5(10):1024-39.

447. Kokkola A, Monni O, Puolakkainen P, Nordling S, Haapiainen R, Kivilaakso E, et al. Presence of high-level DNA copy number gains in gastric carcinoma and severely dysplastic adenomas but not in moderately dysplastic adenomas. Cancer Genet Cytogenet. 1998;107(1):32-6.

448. van Dekken H, Alers JC, Riegman PHJ, Rosenberg C, Tilanus HW, Vissers K. Molecular Cytogenetic Evaluation of Gastric Cardia Adenocarcinoma and Precursor Lesions. The American Journal of Pathology. 2001;158(6):1961-7.

449. Weiss MM, Kuipers EJ, Postma C, Snijders AM, Stolte M, Vieth M, et al. Genome wide array comparative genomic hybridisation analysis of premalignant lesions of the stomach. Mol Pathol. 2003;56(5):293-8.

450. Buffart TE, Carvalho B, Mons T, Reis RM, Moutinho C, Silva P, et al. DNA copy number profiles of gastric cancer precursor lesions. BMC Genomics. 2007;8:345.

451. Heaphy CM, Bisoffi M, Fordyce CA, Haaland CM, Hines WC, Joste NE, et al. Telomere DNA content and allelic imbalance demonstrate field cancerization in histologically normal tissue adjacent to breast tumors. Int J Cancer. 2006;119(1):108-16.

452. Heaphy CM, Griffith JK, Bisoffi M. Mammary field cancerization: molecular evidence and clinical importance. Breast Cancer Res Treat. 2009;118(2):229-39.

453. Aran D, Camarda R, Odegaard J, Paik H, Oskotsky B, Krings G, et al. Comprehensive analysis of normal adjacent to tumor transcriptomes. Nat Commun. 2017;8(1):1077.

454. de Assumpcao PP, Khayat AS, Thomaz Araujo TM, Barra WF, Ishak G, Cruz Ramos AMP, et al. Traps and trumps from adjacent-to-tumor samples in gastric cancer research. Chin J Cancer Res. 2018;30(5):564-7.

455. Fishilevich S, Nudel R, Rappaport N, Hadar R, Plaschkes I, Iny Stein T, et al. GeneHancer: genome-wide integration of enhancers and target genes in GeneCards. Database (Oxford). 2017;2017.

456. Siveke JT, Hamann A. T helper 1 and T helper 2 cells respond differentially to chemokines. J Immunol. 1998;160(2):550-4.

457. Campbell DJ, Butcher EC. Intestinal attraction: CCL25 functions in effector lymphocyte recruitment to the small intestine. Journal of Clinical Investigation. 2002;110(8):1079-81.

458. Nakanishi K. Unique Action of Interleukin-18 on T Cells and Other Immune Cells. Front Immunol. 2018;9:763.

459. Yoshimoto T, Takeda K, Tanaka T, Ohkusu K, Kashiwamura S, Okamura H, et al. IL-12 up-regulates IL-18 receptor expression on T cells, Th1 cells, and B cells: synergism with IL-18 for IFN-gamma production. J Immunol. 1998;161(7):3400-7.

460. Hitzler I, Sayi A, Kohler E, Engler DB, Koch KN, Hardt WD, et al. Caspase-1 has both proinflammatory and regulatory properties in Helicobacter infections, which are differentially mediated by its substrates IL-1beta and IL-18. J Immunol. 2012;188(8):3594-602.

461. Harrison OJ, Srinivasan N, Pott J, Schiering C, Krausgruber T, Ilott NE, et al. Epithelial-derived IL-18 regulates Th17 cell differentiation and Foxp3(+) Treg cell function in the intestine. Mucosal Immunol. 2015;8(6):1226-36.

462. Koltsova EK, Ley K. The mysterious ways of the chemokine CXCL5. Immunity. 2010;33(1):7-9.

463. Zhou SL, Dai Z, Zhou ZJ, Wang XY, Yang GH, Wang Z, et al. Overexpression of CXCL5 mediates neutrophil infiltration and indicates poor prognosis for hepatocellular carcinoma. Hepatology. 2012;56(6):2242-54.

464. Mantovani A, Sica A, Sozzani S, Allavena P, Vecchi A, Locati M. The chemokine system in diverse forms of macrophage activation and polarization. Trends Immunol. 2004;25(12):677-86.

465. Duluc D, Delneste Y, Tan F, Moles MP, Grimaud L, Lenoir J, et al. Tumor-associated leukemia inhibitory factor and IL-6 skew monocyte differentiation into tumor-associated macrophage-like cells. Blood. 2007;110(13):4319-30.

466. Murray PJ, Allen JE, Biswas SK, Fisher EA, Gilroy DW, Goerdt S, et al. Macrophage activation and polarization: nomenclature and experimental guidelines. Immunity. 2014;41(1):14-20.

467. Lundgren A, Suri-Payer E, Enarsson K, Svennerholm AM, Lundin BS. Helicobacter pylori-specific CD4+ CD25high regulatory T cells suppress memory T-cell responses to H. pylori in infected individuals. Infect Immun. 2003;71(4):1755-62.

468. Rad R, Brenner L, Bauer S, Schwendy S, Layland L, da Costa CP, et al. CD25+/Foxp3+ T cells regulate gastric inflammation and Helicobacter pylori colonization in vivo. Gastroenterology. 2006;131(2):525-37.

469. Cherdantseva LA, Potapova OV, Sharkova TV, Belyaeva YY, Shkurupiy VA. Association of Helicobacter pylori and iNOS production by macrophages and lymphocytes in the gastric mucosa in chronic gastritis. J Immunol Res. 2014;2014:762514.

470. D'Souza C, Pediongco T, Wang H, Scheerlinck JY, Kostenko L, Esterbauer R, et al. Mucosal-Associated Invariant T Cells Augment Immunopathology and Gastritis in Chronic Helicobacter pylori Infection. J Immunol. 2018;200(5):1901-16.

471. Liu Z. Prevalence of programmed death-1 ligand-1 (PD-L1) and infiltrating lymphocytes in human gastric carcinogenesis. 2017.

472. Roszer T. Understanding the Mysterious M2 Macrophage through Activation Markers and Effector Mechanisms. Mediators Inflamm. 2015;2015:816460.

473. Gunthner R, Anders HJ. Interferon-regulatory factors determine macrophage phenotype polarization. Mediators Inflamm. 2013;2013:731023.

474. Dong H, Zhu G, Tamada K, Chen L. B7-H1, a third member of the B7 family, co-stimulates T-cell proliferation and interleukin-10 secretion. Nat Med. 1999;5(12):1365-9.

475. Hirayama D, Iida T, Nakase H. The Phagocytic Function of Macrophage-Enforcing Innate Immunity and Tissue Homeostasis. Int J Mol Sci. 2017;19(1).

476. Betjes MG, Haks MC, Tuk CW, Beelen RH. Monoclonal antibody EBM11 (anti-CD68) discriminates between dendritic cells and macrophages after short-term culture. Immunobiology. 1991;183(1-2):79-87.

477. Chistiakov DA, Killingsworth MC, Myasoedova VA, Orekhov AN, Bobryshev YV. CD68/macrosialin: not just a histochemical marker. Lab Invest. 2017;97(1):4-13.

478. Buechler C, Ritter M, Orso E, Langmann T, Klucken J, Schmitz G. Regulation of scavenger receptor CD163 expression in human monocytes and macrophages by pro- and antiinflammatory stimuli. J Leukoc Biol. 2000;67(1):97-103.

479. Soldano S, Pizzorni C, Paolino S, Trombetta AC, Montagna P, Brizzolara R, et al. Alternatively Activated (M2) Macrophage Phenotype Is Inducible by Endothelin-1 in Cultured Human Macrophages. PLoS One. 2016;11(11):e0166433.

480. Shiraishi D, Fujiwara Y, Horlad H, Saito Y, Iriki T, Tsuboki J, et al. CD163 Is Required for Protumoral Activation of Macrophages in Human and Murine Sarcoma. Cancer Res. 2018;78(12):3255-66.

481. Park JY, Sung JY, Lee J, Park YK, Kim YW, Kim GY, et al. Polarized CD163+ tumor-associated macrophages are associated with increased angiogenesis and CXCL12 expression in gastric cancer. Clin Res Hepatol Gastroenterol. 2016;40(3):357-65.

482. Barros MH, Hauck F, Dreyer JH, Kempkes B, Niedobitek G. Macrophage polarisation: an immunohistochemical approach for identifying M1 and M2 macrophages. PLoS One. 2013;8(11):e80908.

483. Aron-Wisnewsky J, Tordjman J, Poitou C, Darakhshan F, Hugol D, Basdevant A, et al. Human adipose tissue macrophages: m1 and m2 cell surface markers in subcutaneous and omental depots and after weight loss. J Clin Endocrinol Metab. 2009;94(11):4619-23.

484. Svensson-Arvelund J, Mehta RB, Lindau R, Mirrasekhian E, Rodriguez-Martinez H, Berg G, et al. The human fetal placenta promotes tolerance against the semiallogeneic fetus by inducing regulatory T cells and homeostatic M2 macrophages. J Immunol. 2015;194(4):1534-44.

485. Tamura T, Kurotaki D, Koizumi S. Regulation of myelopoiesis by the transcription factor IRF8. Int J Hematol. 2015;101(4):342-51.

486. Twum DY, Colligan SH, Hoffend NC, Katsuta E, Cortes Gomez E, Hensen ML, et al. IFN regulatory factor-8 expression in macrophages governs an antimetastatic program. JCI Insight. 2019;4(3).

487. Jablonski KA, Amici SA, Webb LM, Ruiz-Rosado Jde D, Popovich PG, Partida-Sanchez S, et al. Novel Markers to Delineate Murine M1 and M2 Macrophages. PLoS One. 2015;10(12):e0145342.

488. Buscher K, Ehinger E, Gupta P, Pramod AB, Wolf D, Tweet G, et al. Natural variation of macrophage activation as disease-relevant phenotype predictive of inflammation and cancer survival. Nat Commun. 2017;8:16041.

489. Orecchioni M, Ghosheh Y, Pramod AB, Ley K. Macrophage Polarization: Different Gene Signatures in M1(LPS+) vs. Classically and M2(LPS-) vs. Alternatively Activated Macrophages. Front Immunol. 2019;10:1084.

490. Sathe A, Grimes SM, Lau BT, Chen J, Suarez C, Huang RJ, et al. Single cell genomic characterization reveals the cellular reprogramming of the gastric tumor microenvironment. Clin Cancer Res. 2020.

491. L. Ferreira V, H.L. Borba H, de F. Bonetti A, P. Leonart L, Pontarolo R. Cytokines and Interferons: Types and Functions. Autoantibodies and Cytokines2019.

492. Kwak Y, Seo AN, Lee HE, Lee HS. Tumor immune response and immunotherapy in gastric cancer. J Pathol Transl Med. 2020;54(1):20-33.

493. Gutierrez-Gonzalez L, Graham TA, Rodriguez-Justo M, Leedham SJ, Novelli MR, Gay LJ, et al. The clonal origins of dysplasia from intestinal metaplasia in the human stomach. Gastroenterology. 2011;140(4):1251-60 e1-6.

494. Toth ZE, Mezey E. Simultaneous visualization of multiple antigens with tyramide signal amplification using antibodies from the same species. J Histochem Cytochem. 2007;55(6):545-54.

495. Mantegazza AR, Magalhaes JG, Amigorena S, Marks MS. Presentation of phagocytosed antigens by MHC class I and II. Traffic. 2013;14(2):135-52.

496. Roberts CA, Dickinson AK, Taams LS. The Interplay Between Monocytes/Macrophages and CD4(+) T Cell Subsets in Rheumatoid Arthritis. Front Immunol. 2015;6:571.

497. Jenne DE, Tschopp J. Granzymes, a family of serine proteases released from granules of cytolytic T lymphocytes upon T cell receptor stimulation. Immunol Rev. 1988;103:53-71.

498. Spira A, Disis ML, Schiller JT, Vilar E, Rebbeck TR, Bejar R, et al. Leveraging premalignant biology for immune-based cancer prevention. Proc Natl Acad Sci U S A. 2016;113(39):10750-8.

499. Liu X, Xu D, Huang C, Guo Y, Wang S, Zhu C, et al. Regulatory T cells and M2 macrophages present diverse prognostic value in gastric cancer patients with different clinicopathologic characteristics and chemotherapy strategies. J Transl Med. 2019;17(1):192.

500. Treiner E, Duban L, Bahram S, Radosavljevic M, Wanner V, Tilloy F, et al. Selection of evolutionarily conserved mucosal-associated invariant T cells by MR1. Nature. 2003;422(6928):164-9.

501. Nielsen MM, Witherden DA, Havran WL. gammadelta T cells in homeostasis and host defence of epithelial barrier tissues. Nat Rev Immunol. 2017;17(12):733-45.

502. Booth JS, Salerno-Goncalves R, Blanchard TG, Patil SA, Kader HA, Safta AM, et al. Mucosal-Associated Invariant T Cells in the Human Gastric Mucosa and Blood: Role in Helicobacter pylori Infection. Front Immunol. 2015;6:466.

503. Futagami S, Hiratsuka T, Suzuki K, Kusunoki M, Wada K, Miyake K, et al. gammadelta T cells increase with gastric mucosal interleukin (IL)-7, IL-1beta, and Helicobacter pylori urease specific immunoglobulin levels via CCR2 upregulation in Helicobacter pylori gastritis. J Gastroenterol Hepatol. 2006;21(1 Pt 1):32-40.

504. Chen TE, Xu XM, Liu P, Liang SY, Lv WX. Elucidating the function and tolerance mechanism of gamma delta (gamma delta) T cells in a Helicobacter pylori infection model. Genet Mol Res. 2015;14(3):10543-52.

505. Casetti R, Agrati C, Wallace M, Sacchi A, Martini F, Martino A, et al. Cutting edge: TGF-beta1 and IL-15 Induce FOXP3+ gammadelta regulatory T cells in the presence of antigen stimulation. J Immunol. 2009;183(6):3574-7.

506. Le Bourhis L, Dusseaux M, Bohineust A, Bessoles S, Martin E, Premel V, et al. MAIT cells detect and efficiently lyse bacterially-infected epithelial cells. PLoS Pathog. 2013;9(10):e1003681.

507. Gherardin NA, McCluskey J, Rossjohn J, Godfrey DI. The Diverse Family of MR1-Restricted T Cells. J Immunol. 2018;201(10):2862-71.

508. Raverdeau M, Cunningham SP, Harmon C, Lynch L. gammadelta T cells in cancer: a small population of lymphocytes with big implications. Clin Transl Immunology. 2019;8(10):e01080.

509. Park SL, Buzzai A, Rautela J, Hor JL, Hochheiser K, Effern M, et al. Tissue-resident memory CD8(+) T cells promote melanoma-immune equilibrium in skin. Nature. 2019;565(7739):366-71.

510. Li Z, Li D, Tsun A, Li B. FOXP3+ regulatory T cells and their functional regulation. Cell Mol Immunol. 2015;12(5):558-65.

511. Winter S, Loddenkemper C, Aebischer A, Rabel K, Hoffmann K, Meyer TF, et al. The chemokine receptor CXCR5 is pivotal for ectopic mucosa-associated lymphoid tissue neogenesis in chronic Helicobacter pylori-induced inflammation. J Mol Med (Berl). 2010;88(11):1169-80.

512. Pipi E, Nayar S, Gardner DH, Colafrancesco S, Smith C, Barone F. Tertiary Lymphoid Structures: Autoimmunity Goes Local. Front Immunol. 2018;9:1952.

513. Peranzoni E, Lemoine J, Vimeux L, Feuillet V, Barrin S, Kantari-Mimoun C, et al. Macrophages impede CD8 T cells from reaching tumor cells and limit the efficacy of anti-PD-1 treatment. Proc Natl Acad Sci U S A. 2018;115(17):E4041-E50.

514. Jang BG, Lee BL, Kim WH. Intestinal Stem Cell Markers in the Intestinal Metaplasia of Stomach and Barrett's Esophagus. PLoS One. 2015;10(5):e0127300.

515. Zhang P, Yang M, Zhang Y, Xiao S, Lai X, Tan A, et al. Dissecting the Single-Cell Transcriptome Network Underlying Gastric Premalignant Lesions and Early Gastric Cancer. Cell Rep. 2019;27(6):1934-47 e5.

516. Svanholm H, Starklint H, Gundersen HJ, Fabricius J, Barlebo H, Olsen S. Reproducibility of histomorphologic diagnoses with special reference to the kappa statistic. APMIS. 1989;97(8):689-98.

517. Griffel LH, Amenta PS, Das KM. Use of a novel monoclonal antibody in diagnosis of Barrett's esophagus. Dig Dis Sci. 2000;45(1):40-8.

518. Mirza ZK, Das KK, Slate J, Mapitigama RN, Amenta PS, Griffel LH, et al. Gastric intestinal metaplasia as detected by a monoclonal antibody is highly associated with gastric adenocarcinoma. Gut. 2003;52(6):807-12.

519. Das KM, Sakamaki S, Vecchi M, Diamond B. The production and characterization of monoclonal antibodies to a human colonic antigen associated with ulcerative colitis: cellular localization of the antigen by using the monoclonal antibody. J Immunol. 1987;139(1):77-84.

520. Kaufmann O, Flath B, Spath-Schwalbe E, Possinger K, Dietel M. Immunohistochemical detection of CD10 with monoclonal antibody 56C6 on paraffin sections. Am J Clin Pathol. 1999;111(1):117-22.

521. Cavanaugh JE, Neath AA. The Akaike information criterion: Background, derivation, properties, application, interpretation, and refinements. Wiley Interdisciplinary Reviews: Computational Statistics. 2019;11(3).

522. Quan S, Lin J, Jiang Z, He X, Sun C, Lin Z, et al. AB-PAS as a potential alternative for the diagnosis of intestinal metaplasia. Biomedical Research. 2017;28(10):4726-9.

523. Survana SK, Layton CB, J. D. Bancroft’s Theory and Practice of Histological Techniques. 7th ed: Churchill Livingstone Elsevier; 2013.

524. Kim SS, Kook MC, Shin OR, Kim HS, Bae HI, Seo AN, et al. Factors to improve the interobserver agreement for gastric atrophy and intestinal metaplasia: consensus of definition and criteria. Histopathology. 2018;72(5):838-45.

525. Jang BG, Lee BL, Kim WH. Distribution of LGR5+ cells and associated implications during the early stage of gastric tumorigenesis. PLoS One. 2013;8(12):e82390.

526. Kokolakis G, Panagis L, Stathopoulos E, Giannikaki E, Tosca A, Kruger-Krasagakis S. From the protein to the graph: how to quantify immunohistochemistry staining of the skin using digital imaging. J Immunol Methods. 2008;331(1-2):140-6.

527. Jensen EC. Quantitative analysis of histological staining and fluorescence using ImageJ. Anat Rec (Hoboken). 2013;296(3):378-81.

528. Watari J, Das KK, Amenta PS, Tanabe H, Tanaka A, Geng X, et al. Effect of eradication of Helicobacter pylori on the histology and cellular phenotype of gastric intestinal metaplasia. Clin Gastroenterol Hepatol. 2008;6(4):409-17.

529. Forne M, Fernandez-Banares F, Gonzalez-Minguez C, Casalots J, Poblet-Mas N, Garcia-Gil LJ, et al. Lack of clinical usefulness of Das-1 monoclonal antibody and mucin expression as risk markers of gastric carcinoma in patients with gastric intestinal metaplasia. Am J Clin Pathol. 2009;131(1):99-105.

530. Feng XS, Wang YF, Hao SG, Ru Y, Gao SG, Wang LD. Expression of Das-1, Ki67 and sulfuric proteins in gastric cardia adenocarcinoma and intestinal metaplasia lesions. Exp Ther Med. 2013;5(6):1555-8.

531. Syu LJ, El-Zaatari M, Eaton KA, Liu Z, Tetarbe M, Keeley TM, et al. Transgenic expression of interferon-gamma in mouse stomach leads to inflammation, metaplasia, and dysplasia. Am J Pathol. 2012;181(6):2114-25.

532. Das KK, Geng X, Brown JW, Morales-Oyarvide V, Huynh T, Pergolini I, et al. Cross Validation of the Monoclonal Antibody Das-1 in Identification of High-Risk Mucinous Pancreatic Cystic Lesions. Gastroenterology. 2019;157(3):720-30 e2.

533. Yeh JM, Hur C, Schrag D, Kuntz KM, Ezzati M, Stout N, et al. Contribution of H. pylori and smoking trends to US incidence of intestinal-type noncardia gastric adenocarcinoma: a microsimulation model. PLoS Med. 2013;10(5):e1001451.

534. Buckland G, Travier N, Huerta JM, Bueno-de-Mesquita HB, Siersema PD, Skeie G, et al. Healthy lifestyle index and risk of gastric adenocarcinoma in the EPIC cohort study. Int J Cancer. 2015;137(3):598-606.

535. Moore A, Hikri E, Goshen-Lago T, Barkan T, Morgenstern S, Brook E, et al. Young-onset gastric cancer and Epstein-Barr Virus (EBV) - a major player in the pathogenesis? BMC Cancer. 2020;20(1):34.

536. Silberg DG, Furth EE, Taylor JK, Schuck T, Chiou T, Traber PG. CDX1 protein expression in normal, metaplastic, and neoplastic human alimentary tract epithelium. Gastroenterology. 1997;113(2):478-86.

537. Tsukamoto T, Inada K, Tanaka H, Mizoshita T, Mihara M, Ushijima T, et al. Down-regulation of a gastric transcription factor, Sox2, and ectopic expression of intestinal homeobox genes, Cdx1 and Cdx2: inverse correlation during progression from gastric/intestinal-mixed to complete intestinal metaplasia. Journal of Cancer Research and Clinical Oncology. 2004;130(3):135-45.

538. Lee BH, Kim N, Lee HS, Kang JM, Park HK, Jo HJ, et al. The Role of CDX2 in Intestinal Metaplasia Evaluated Using Immunohistochemistry. Gut Liver. 2012;6(1):71-7.

539. Ding L, El Zaatari M, Merchant JL. Recapitulating Human Gastric Cancer Pathogenesis: Experimental Models of Gastric Cancer. Adv Exp Med Biol. 2016;908:441-78.

540. Simian M, Bissell MJ. Organoids: A historical perspective of thinking in three dimensions. J Cell Biol. 2017;216(1):31-40.

541. Steele NG, Chakrabarti J, Wang J, Biesiada J, Holokai L, Chang J, et al. An Organoid-Based Preclinical Model of Human Gastric Cancer. Cell Mol Gastroenterol Hepatol. 2019;7(1):161-84.

542. Nanki K, Toshimitsu K, Takano A, Fujii M, Shimokawa M, Ohta Y, et al. Divergent Routes toward Wnt and R-spondin Niche Independency during Human Gastric Carcinogenesis. Cell. 2018;174(4):856-69 e17.

543. Seidlitz T, Merker SR, Rothe A, Zakrzewski F, von Neubeck C, Grutzmann K, et al. Human gastric cancer modelling using organoids. Gut. 2018.

544. Yan HHN, Siu HC, Law S, Ho SL, Yue SSK, Tsui WY, et al. A Comprehensive Human Gastric Cancer Organoid Biobank Captures Tumor Subtype Heterogeneity and Enables Therapeutic Screening. Cell Stem Cell. 2018;23(6):882-97 e11.

545. Mahe MM, Aihara E, Schumacher MA, Zavros Y, Montrose MH, Helmrath MA, et al. Establishment of Gastrointestinal Epithelial Organoids. Curr Protoc Mouse Biol. 2013;3(4):217-40.

546. Sugimoto S, Sato T. Establishment of 3D Intestinal Organoid Cultures from Intestinal Stem Cells. Methods Mol Biol. 2017;1612:97-105.

547. Li XG, Xu GF, Zhai ZY, Gao CQ, Yan HC, Xi QY, et al. CDX2 increases SLC7A7 expression and proliferation of pig intestinal epithelial cells. Oncotarget. 2016;7(21):30597-609.

548. van der Flier LG, Haegebarth A, Stange DE, van de Wetering M, Clevers H. OLFM4 is a robust marker for stem cells in human intestine and marks a subset of colorectal cancer cells. Gastroenterology. 2009;137(1):15-7.

549. Gao M, Lin M, Rao M, Thompson H, Hirai K, Choi M, et al. Development of Patient-Derived Gastric Cancer Organoids from Endoscopic Biopsies and Surgical Tissues. Ann Surg Oncol. 2018.

550. Boj SF, Hwang CI, Baker LA, Chio, II, Engle DD, Corbo V, et al. Organoid models of human and mouse ductal pancreatic cancer. Cell. 2015;160(1-2):324-38.

551. Tiriac H, Bucobo JC, Tzimas D, Grewel S, Lacomb JF, Rowehl LM, et al. Successful creation of pancreatic cancer organoids by means of EUS-guided fine-needle biopsy sampling for personalized cancer treatment. Gastrointest Endosc. 2018;87(6):1474-80.

552. Kishida K, Pearce SC, Yu S, Gao N, Ferraris RP. Nutrient sensing by absorptive and secretory progenies of small intestinal stem cells. Am J Physiol Gastrointest Liver Physiol. 2017;312(6):G592-G605.

553. Holmberg FE, Seidelin JB, Yin X, Mead BE, Tong Z, Li Y, et al. Culturing human intestinal stem cells for regenerative applications in the treatment of inflammatory bowel disease. EMBO Mol Med. 2017;9(5):558-70.

554. Logan CY, Nusse R. The Wnt signaling pathway in development and disease. Annu Rev Cell Dev Biol. 2004;20:781-810.

555. ten Berge D, Kurek D, Blauwkamp T, Koole W, Maas A, Eroglu E, et al. Embryonic stem cells require Wnt proteins to prevent differentiation to epiblast stem cells. Nat Cell Biol. 2011;13(9):1070-5.

556. Sato T, van Es JH, Snippert HJ, Stange DE, Vries RG, van den Born M, et al. Paneth cells constitute the niche for Lgr5 stem cells in intestinal crypts. Nature. 2011;469(7330):415-8.

557. Watson J, Francavilla C. Regulation of FGF10 Signaling in Development and Disease. Front Genet. 2018;9:500.

558. Dimaline R, Varro A. Novel roles of gastrin. J Physiol. 2014;592(14):2951-8.

559. Liu W, Li H, Hong SH, Piszczek GP, Chen W, Rodgers GP. Olfactomedin 4 deletion induces colon adenocarcinoma in Apc(Min/+) mice. Oncogene. 2016;35(40):5237-47.

560. Liu W, Zhu J, Cao L, Rodgers GP. Expression of hGC-1 is correlated with differentiation of gastric carcinoma. Histopathology. 2007;51(2):157-65.

561. Jang BG, Lee BL, Kim WH. Olfactomedin-related proteins 4 (OLFM4) expression is involved in early gastric carcinogenesis and of prognostic significance in advanced gastric cancer. Virchows Archiv. 2015;467(3):285-94.

562. Jim MA, Pinheiro PS, Carreira H, Espey DK, Wiggins CL, Weir HK. Stomach cancer survival in the United States by race and stage (2001-2009): Findings from the CONCORD-2 study. Cancer. 2017;123 Suppl 24:4994-5013.

563. Rawla P, Barsouk A. Epidemiology of gastric cancer: global trends, risk factors and prevention. Prz Gastroenterol. 2019;14(1):26-38.

564. Parsonnet J, Vandersteen D, Goates J, Sibley RK, Pritikin J, Chang Y. Helicobacter pylori infection in intestinal- and diffuse-type gastric adenocarcinomas. J Natl Cancer Inst. 1991;83(9):640-3.

565. Endo S, Ohkusa T, Saito Y, Fujiki K, Okayasu I, Sato C. Detection of Helicobacter pylori infection in early stage gastric cancer. A comparison between intestinal- and diffuse-type gastric adenocarcinomas. Cancer. 1995;75(9):2203-8.

566. Shin SY, Kim JH, Chun J, Yoon YH, Park H. Chronic atrophic gastritis and intestinal metaplasia surrounding diffuse-type gastric cancer: Are they just bystanders in the process of carcinogenesis? PLoS One. 2019;14(12):e0226427.

567. Yamachika T, Inada K, Fujimitsu Y, Nakamura S, Yamamura Y, Kitou T, et al. Intestinalization of gastric signet ring cell carcinomas with progression. Virchows Arch. 1997;431(2):103-10.

568. McDonald SA, Greaves LC, Gutierrez-Gonzalez L, Rodriguez-Justo M, Deheragoda M, Leedham SJ, et al. Mechanisms of field cancerization in the human stomach: the expansion and spread of mutated gastric stem cells. Gastroenterology. 2008;134(2):500-10.

569. Waddingham W, Graham D, Banks M, Jansen M. The evolving role of endoscopy in the diagnosis of premalignant gastric lesions. F1000Res. 2018;7.

570. Rokutan H, Abe H, Nakamura H, Ushiku T, Arakawa E, Hosoda F, et al. Initial and crucial genetic events in intestinal-type gastric intramucosal neoplasia. J Pathol. 2018.

571. Busuttil RA, Zapparoli GV, Haupt S, Fennell C, Wong SQ, Pang JM, et al. Role of p53 in the progression of gastric cancer. Oncotarget. 2014;5(23):12016-26.

572. Carvalho B, Buffart TE, Reis RM, Mons T, Moutinho C, Silva P, et al. Mixed gastric carcinomas show similar chromosomal aberrations in both their diffuse and glandular components. Cell Oncol. 2006;28(5-6):283-94.

573. Lee HJ, Nam KT, Park HS, Kim MA, Lafleur BJ, Aburatani H, et al. Gene expression profiling of metaplastic lineages identifies CDH17 as a prognostic marker in early stage gastric cancer. Gastroenterology. 2010;139(1):213-25 e3.

574. Panarelli NC, Yantiss RK, Yeh MM, Liu Y, Chen YT. Tissue-specific cadherin CDH17 is a useful marker of gastrointestinal adenocarcinomas with higher sensitivity than CDX2. Am J Clin Pathol. 2012;138(2):211-22.

575. Ruol A, Parenti A, Zaninotto G, Merigliano S, Costantini M, Cagol M, et al. Intestinal metaplasia is the probable common precursor of adenocarcinoma in barrett esophagus and adenocarcinoma of the gastric cardia. Cancer. 2000;88(11):2520-8.

576. Siddiki HA, Lam-Himlin DM, Kahn A, Bandres MV, Burdick GE, Crowell MD, et al. Intestinal metaplasia of the gastric cardia: findings in patients with versus without Barrett's esophagus. Gastrointest Endosc. 2018.

577. Barros R, Freund JN, David L, Almeida R. Gastric intestinal metaplasia revisited: function and regulation of CDX2. Trends Mol Med. 2012;18(9):555-63.

578. Merino B, Fernandez-Diaz CM, Cozar-Castellano I, Perdomo G. Intestinal Fructose and Glucose Metabolism in Health and Disease. Nutrients. 2019;12(1).

579. Yamatoji M, Kasamatsu A, Yamano Y, Sakuma K, Ogoshi K, Iyoda M, et al. State of homeobox A10 expression as a putative prognostic marker for oral squamous cell carcinoma. Oncol Rep. 2010;23(1):61-7.

580. Shah CA, Wang H, Bei L, Platanias LC, Eklund EA. HoxA10 regulates transcription of the gene encoding transforming growth factor beta2 (TGFbeta2) in myeloid cells. J Biol Chem. 2011;286(4):3161-76.

581. Li B, Cao X, Weng C, Wu Y, Fang X, Zhang X, et al. HoxA10 induces proliferation in human prostate carcinoma PC-3 cell line. Cell Biochem Biophys. 2014;70(2):1363-8.

582. Song C, Han Y, Luo H, Qin Z, Chen Z, Liu Y, et al. HOXA10 induces BCL2 expression, inhibits apoptosis, and promotes cell proliferation in gastric cancer. Cancer Med. 2019;8(12):5651-61.

583. Han Y, Tu WW, Wen YG, Li DP, Qiu GQ, Tang HM, et al. Identification and validation that up-expression of HOXA13 is a novel independent prognostic marker of a worse outcome in gastric cancer based on immunohistochemistry. Med Oncol. 2013;30(2):564.

584. He YX, Song XH, Zhao ZY, Zhao H. HOXA13 upregulation in gastric cancer is associated with enhanced cancer cell invasion and epithelial-to-mesenchymal transition. Eur Rev Med Pharmacol Sci. 2017;21(2):258-65.

585. Zhang W, Liu S, Zhan H, Yan Z, Zhang G. Transcriptome sequencing identifies key pathways and genes involved in gastric adenocarcinoma. Mol Med Rep. 2018;18(4):3673-82.

586. Assumpcao MB, Moreira FC, Hamoy IG, Magalhaes L, Vidal A, Pereira A, et al. High-Throughput miRNA Sequencing Reveals a Field Effect in Gastric Cancer and Suggests an Epigenetic Network Mechanism. Bioinform Biol Insights. 2015;9:111-7.

587. Baba Y, Ishimoto T, Kurashige J, Iwatsuki M, Sakamoto Y, Yoshida N, et al. Epigenetic field cancerization in gastrointestinal cancers. Cancer Lett. 2016;375(2):360-6.

588. Dakubo GD. Danely P.Slaughters Field Cancerization Concept of Carcinogenesis: The Path Forward to Early Cancer Detection and Chemoprevention. Cell & Developmental Biology. 2015;04(02).

589. Dakubo GD, Jakupciak JP, Birch-Machin MA, Parr RL. Clinical implications and utility of field cancerization. Cancer Cell Int. 2007;7:2.

590. Bastide P, Darido C, Pannequin J, Kist R, Robine S, Marty-Double C, et al. Sox9 regulates cell proliferation and is required for Paneth cell differentiation in the intestinal epithelium. J Cell Biol. 2007;178(4):635-48.

591. Zhou CJ, Guo JQ, Zhu KX, Zhang QH, Pan CR, Xu WH, et al. Elevated expression of SOX9 is related with the progression of gastric carcinoma. Diagn Cytopathol. 2011;39(2):105-9.

592. Sashikawa Kimura M, Mutoh H, Sugano K. SOX9 is expressed in normal stomach, intestinal metaplasia, and gastric carcinoma in humans. J Gastroenterol. 2011;46(11):1292-9.

593. Mesquita P, Freire AF, Lopes N, Gomes R, Azevedo D, Barros R, et al. Expression and Clinical Relevance of SOX9 in Gastric Cancer. Dis Markers. 2019;2019:8267021.

594. Zhang L, Hou Y, Ashktorab H, Gao L, Xu Y, Wu K, et al. The impact of C-MYC gene expression on gastric cancer cell. Mol Cell Biochem. 2010;344(1-2):125-35.

595. George S, Lucero Y, Torres JP, Lagomarcino AJ, O'Ryan M. Gastric Damage and Cancer-Associated Biomarkers in Helicobacter pylori-Infected Children. Frontiers in Microbiology. 2020;11.

596. Gala K, Li Q, Sinha A, Razavi P, Dorso M, Sanchez-Vega F, et al. KMT2C mediates the estrogen dependence of breast cancer through regulation of ERalpha enhancer function. Oncogene. 2018;37(34):4692-710.

597. Su JR, Kuai JH, Li YQ. Smoc2 potentiates proliferation of hepatocellular carcinoma cells via promotion of cell cycle progression. World J Gastroenterol. 2016;22(45):10053-63.

598. Garcia-Heredia JM, Carnero A. Dr. Jekyll and Mr. Hyde: MAP17's up-regulation, a crosspoint in cancer and inflammatory diseases. Mol Cancer. 2018;17(1):80.

599. Chistiakov DA, Myasoedova VA, Revin VV, Orekhov AN, Bobryshev YV. The impact of interferon-regulatory factors to macrophage differentiation and polarization into M1 and M2. Immunobiology. 2018;223(1):101-11.

600. Weisz A, Marx P, Sharf R, Appella E, Driggers PH, Ozato K, et al. Human interferon consensus sequence binding protein is a negative regulator of enhancer elements common to interferon-inducible genes. J Biol Chem. 1992;267(35):25589-96.

601. Epelman S, Lavine KJ, Randolph GJ. Origin and functions of tissue macrophages. Immunity. 2014;41(1):21-35.

602. Lavin Y, Merad M. Macrophages: gatekeepers of tissue integrity. Cancer Immunol Res. 2013;1(4):201-9.

603. Unanue ER. Antigen-presenting function of the macrophage. Annu Rev Immunol. 1984;2:395-428.

604. Henry F, Bretaudeau L, Barbieux I, Meflah K, Gregoire M. Induction of antigen presentation by macrophages after phagocytosis of tumour apoptotic cells. Res Immunol. 1998;149(7-8):673-9.

605. Blanchette J, Jaramillo M, Olivier M. Signalling events involved in interferon-gamma-inducible macrophage nitric oxide generation. Immunology. 2003;108(4):513-22.

606. Maniecki MB, Moller HJ, Moestrup SK, Moller BK. CD163 positive subsets of blood dendritic cells: the scavenging macrophage receptors CD163 and CD91 are coexpressed on human dendritic cells and monocytes. Immunobiology. 2006;211(6-8):407-17.

607. Zhang N, Bevan MJ. CD8(+) T cells: foot soldiers of the immune system. Immunity. 2011;35(2):161-8.

608. Lim HX, Hong HJ, Cho D, Kim TS. IL-18 enhances immunosuppressive responses by promoting differentiation into monocytic myeloid-derived suppressor cells. J Immunol. 2014;193(11):5453-60.

609. Deswaerte V, Nguyen P, West A, Browning AF, Yu L, Ruwanpura SM, et al. Inflammasome Adaptor ASC Suppresses Apoptosis of Gastric Cancer Cells by an IL18-Mediated Inflammation-Independent Mechanism. Cancer Res. 2018;78(5):1293-307.

610. Baker KJ, Houston A, Brint E. IL-1 Family Members in Cancer; Two Sides to Every Story. Front Immunol. 2019;10:1197.

611. Jia H, Liu J, Han B. Reviews of Interleukin-37: Functions, Receptors, and Roles in Diseases. Biomed Res Int. 2018;2018:3058640.

612. Tosetti C, Stanghellini V, Tucci A, Poli L, Salvioli B, Biasco G, et al. Gastric emptying and dyspeptic symptoms in patients with nonautoimmune fundic atrophic gastritis. Dig Dis Sci. 2000;45(2):252-7.

613. Ferreira RM, Pereira-Marques J, Pinto-Ribeiro I, Costa JL, Carneiro F, Machado JC, et al. Gastric microbial community profiling reveals a dysbiotic cancer-associated microbiota. Gut. 2018;67(2):226-36.

614. Liu X, Shao L, Liu X, Ji F, Mei Y, Cheng Y, et al. Alterations of gastric mucosal microbiota across different stomach microhabitats in a cohort of 276 patients with gastric cancer. EBioMedicine. 2019;40:336-48.

615. Aviles-Jimenez F, Vazquez-Jimenez F, Medrano-Guzman R, Mantilla A, Torres J. Stomach microbiota composition varies between patients with non-atrophic gastritis and patients with intestinal type of gastric cancer. Sci Rep. 2014;4:4202.

616. Coker OO, Dai Z, Nie Y, Zhao G, Cao L, Nakatsu G, et al. Mucosal microbiome dysbiosis in gastric carcinogenesis. Gut. 2018;67(6):1024-32.

617. Guo Y, Zhang Y, Gerhard M, Gao JJ, Mejias-Luque R, Zhang L, et al. Effect of Helicobacter pylori on gastrointestinal microbiota: a population-based study in Linqu, a high-risk area of gastric cancer. Gut. 2019.

618. Ling Z, Shao L, Liu X, Cheng Y, Yan C, Mei Y, et al. Regulatory T Cells and Plasmacytoid Dendritic Cells Within the Tumor Microenvironment in Gastric Cancer Are Correlated With Gastric Microbiota Dysbiosis: A Preliminary Study. Front Immunol. 2019;10:533.

619. Dhodapkar MV, Krasovsky J, Olson K. T cells from the tumor microenvironment of patients with progressive myeloma can generate strong, tumor-specific cytolytic responses to autologous, tumor-loaded dendritic cells. Proc Natl Acad Sci U S A. 2002;99(20):13009-13.

620. Vesely MD, Schreiber RD. Cancer immunoediting: antigens, mechanisms, and implications to cancer immunotherapy. Ann N Y Acad Sci. 2013;1284:1-5.

621. Ohman J, Magnusson B, Telemo E, Jontell M, Hasseus B. Langerhans cells and T cells sense cell dysplasia in oral leukoplakias and oral squamous cell carcinomas--evidence for immunosurveillance. Scand J Immunol. 2012;76(1):39-48.

622. Ohman J, Mowjood R, Larsson L, Kovacs A, Magnusson B, Kjeller G, et al. Presence of CD3-positive T-cells in oral premalignant leukoplakia indicates prevention of cancer transformation. Anticancer Res. 2015;35(1):311-7.

623. Johnson SD, De Costa AM, Young MR. Effect of the premalignant and tumor microenvironment on immune cell cytokine production in head and neck cancer. Cancers (Basel). 2014;6(2):756-70.

624. Mascaux C, Angelova M, Vasaturo A, Beane J, Hijazi K, Anthoine G, et al. Immune evasion before tumour invasion in early lung squamous carcinogenesis. Nature. 2019;571(7766):570-5.

625. Komohara Y, Jinushi M, Takeya M. Clinical significance of macrophage heterogeneity in human malignant tumors. Cancer Sci. 2014;105(1):1-8.

626. Das KM, Prasad I, Garla S, Amenta PS. Detection of a shared colon epithelial epitope on Barrett epithelium by a novel monoclonal antibody. Ann Intern Med. 1994;120(9):753-6.

627. Hosmer DW, Lemeshow S. Applied Logistic Regression, 2nd Ed. Chapter 5. 2nd Edition ed. New York: John Wiley and Sons; 2000. p. pp. 160-4.

628. Mandrekar JN. Receiver operating characteristic curve in diagnostic test assessment. J Thorac Oncol. 2010;5(9):1315-6.

629. Hughes-Anderson W, Rankin SL, House J, Aitken J, Heath D, House AK. Open access endoscopy in rural and remote Western Australia: does it work? ANZ J Surg. 2002;72(10):699-703.

630. Gutierrez-Gonzalez L, Wright NA. Biology of intestinal metaplasia in 2008: more than a simple phenotypic alteration. Dig Liver Dis. 2008;40(7):510-22.

631. Busuttil RA, Boussioutas A. Intestinal metaplasia: a premalignant lesion involved in gastric carcinogenesis. J Gastroenterol Hepatol. 2009;24(2):193-201.

632. Correa P, Piazuelo MB, Wilson KT. Pathology of gastric intestinal metaplasia: clinical implications. Am J Gastroenterol. 2010;105(3):493-8.

633. Bertaux-Skeirik N, Centeno J, Gao J, Gabre J, Zavros Y. Oncogenic Transformation of Human-Derived Gastric Organoids. Methods Mol Biol. 2016.

634. Huch M, Gehart H, van Boxtel R, Hamer K, Blokzijl F, Verstegen MM, et al. Long-term culture of genome-stable bipotent stem cells from adult human liver. Cell. 2015;160(1-2):299-312.

635. Broutier L, Andersson-Rolf A, Hindley CJ, Boj SF, Clevers H, Koo BK, et al. Culture and establishment of self-renewing human and mouse adult liver and pancreas 3D organoids and their genetic manipulation. Nat Protoc. 2016;11(9):1724-43.

636. Mallo GV, Rechreche H, Frigerio JM, Rocha D, Zweibaum A, Lacasa M, et al. Molecular cloning, sequencing and expression of the mRNA encoding human Cdx1 and Cdx2 homeobox. Down-regulation of Cdx1 and Cdx2 mRNA expression during colorectal carcinogenesis. Int J Cancer. 1997;74(1):35-44.

637. Korinek V, Barker N, Morin PJ, van Wichen D, de Weger R, Kinzler KW, et al. Constitutive transcriptional activation by a beta-catenin-Tcf complex in APC-/- colon carcinoma. Science. 1997;275(5307):1784-7.

638. Hoffman J, Kuhnert F, Davis CR, Kuo CJ. Wnts as essential growth factors for the adult small intestine and colon. Cell Cycle. 2004;3(5):554-7.

639. Kim KA, Kakitani M, Zhao J, Oshima T, Tang T, Binnerts M, et al. Mitogenic influence of human R-spondin1 on the intestinal epithelium. Science. 2005;309(5738):1256-9.

640. Kretzschmar K, Clevers H. Organoids: Modeling Development and the Stem Cell Niche in a Dish. Dev Cell. 2016;38(6):590-600.

641. Molenaar M, van de Wetering M, Oosterwegel M, Peterson-Maduro J, Godsave S, Korinek V, et al. XTcf-3 transcription factor mediates beta-catenin-induced axis formation in Xenopus embryos. Cell. 1996;86(3):391-9.

642. Yin X, Farin HF, van Es JH, Clevers H, Langer R, Karp JM. Niche-independent high-purity cultures of Lgr5+ intestinal stem cells and their progeny. Nat Methods. 2014;11(1):106-12.

643. Simmini S, Bialecka M, Huch M, Kester L, van de Wetering M, Sato T, et al. Transformation of intestinal stem cells into gastric stem cells on loss of transcription factor Cdx2. Nat Commun. 2014;5:5728.

644. Ross-Innes CS, Becq J, Warren A, Cheetham RK, Northen H, O'Donovan M, et al. Whole-genome sequencing provides new insights into the clonal architecture of Barrett's esophagus and esophageal adenocarcinoma. Nat Genet. 2015;47(9):1038-46.

645. Spira A, Yurgelun MB, Alexandrov L, Rao A, Bejar R, Polyak K, et al. Precancer Atlas to Drive Precision Prevention Trials. Cancer Res. 2017;77(7):1510-41.

646. Fujii M, Clevers H, Sato T. Modeling Human Digestive Diseases with CRISPR-Cas9-modified Organoids. Gastroenterology. 2018.

APPENDICES

Appendix A

World Journal of Gastrointestinal Oncology

Submit a Manuscript: https://www.f6publishing.com

World J Gastrointest Oncol 2019 September 15; 11(9): 665-678

DOI: 10.4251/wjgo.v11.i9.665

ISSN 1948-5204 (online)

REVIEW

Premalignant lesions and gastric cancer: Current understanding

Athanasios Koulis, Andrew Buckle, Alex Boussioutas

ORCID number: Athanasios Koulis (0000-0003-0939-8839); Andrew Buckle (0000-0002-2180-0555); Alex Boussioutas (0000-0002-8109-6897).

Author contributions: All authors equally contributed to this paper with conception, literature review and analysis, drafting and critical revision and editing, and final approval of the final version.

Conflict-of-interest statement: No potential conflicts of interest.

Open-Access: This article is an open-access article which was selected by an in-house editor and fully peer-reviewed by external reviewers. It is distributed in accordance with the Creative Commons Attribution Non Commercial (CC BY-NC 4.0) license, which permits others to distribute, remix, adapt, build upon this work non-commercially, and license their derivative works on different terms, provided the original work is properly cited and the use is non-commercial. See: http://creativecommons.org/licenses/by-nc/4.0/

Manuscript source: Invited manuscript

Received: February 25, 2019
Peer-review started: February 26, 2019
First decision: May 24, 2019
Revised: May 29, 2019
Accepted: August 20, 2019
Article in press: August 21, 2019
Published online: September 15, 2019

P-Reviewer: De Silva AP, Gassler N, Park WS

Athanasios Koulis, Andrew Buckle, Alex Boussioutas, Upper Gastrointestinal Translational Laboratory, Peter MacCallum Cancer Centre, Melbourne 3000, Australia

Athanasios Koulis, Andrew Buckle, Alex Boussioutas, the Sir Peter MacCallum Department of Surgical Oncology, the University of Melbourne, Melbourne 3010, Australia

Alex Boussioutas, Department of Medicine, Royal Melbourne Hospital, University of Melbourne, Parkville, 3050, Australia

Corresponding author: Alex Boussioutas, MBBS, PhD, FRACP, Upper Gastrointestinal Translational Laboratory, Peter MacCallum Cancer Centre, Locked Bag 1, A'Beckett Street, Victoria 8006, Australia. alex.boussioutas@petermac.org
Telephone: +61-3-85595000

Abstract

Over the last two decades there has been a broad paradigm shift in our understanding of gastric cancer (GC) and its premalignant states from gross histological models to increasingly precise molecular descriptions. In this review we reflect upon the historic approaches to describing premalignant lesions and GC, highlight the current molecular landscape and how this could inform future risk assessment prevention strategies.

Key words: *Helicobacter pylori*; Correa cascade; Atrophic gastritis; Intestinal metaplasia; Point of no return; Dysplasia; Stem cells; Gastric cancer

©The Author(s) 2019. Published by Baishideng Publishing Group Inc. All rights reserved.

Core tip: Despite recent advances in our understanding of the molecular and cellular events involved in gastric cancer, little is known about how gastric premalignant lesions actually lead to this usually lethal disease (5 years survival about 20% in most Western countries). It is still not clear whether some or all of these lesions are directly involved in the process of gastric carcinogenesis or whether they are simply bystanders. In this review, we attempt to shed some light into how our current understanding of premalignant lesions may be used to improve patient stratification and lead to better overall patient survival rates.

Citation: Koulis A, Buckle A, Boussioutas A. Premalignant lesions and gastric cancer: Current understanding. *World J Gastrointest Oncol* 2019; 11(9): 665-678
URL: https://www.wjgnet.com/1948-5204/full/v11/i9/665.htm
DOI: https://dx.doi.org/10.4251/wjgo.v11.i9.665

S-Editor: Ma YJ
L-Editor: Filipodia
E-Editor: Qi LL

INTRODUCTION

Gastric cancer (GC) is the fifth most common cancer worldwide and third highest cause of cancer-related death. In 2012, 950000 individuals were diagnosed with the disease and 723000 died. High incidence areas are Eastern Asia, particularly China, Japan and South Korea, Eastern Europe, Central and South America. Low incidence areas are Australia and New Zealand, North America, Western Europe, South Central Asia and most parts of Africa[1]. Risk factors for GC include male sex, age, high salt intake, including salt preserved foods, smoked or dried meat and fish, pickled food, low intake of fresh fruit and vegetables, smoking, radiation exposure, low levels of physical activity, obesity and low socioeconomic status[2-15].

HISTOLOGICAL AND MOLECULAR CLASSIFICATIONS OF GC

The majority of GC are adenocarcinomas and these can be subdivided by the Lauren histopathology system into intestinal and diffuse subtypes[16]. The intestinal subtype of GC (IGC) is characterised by tumour cells that form gland-like structures whereas the diffuse subtype (DGC) has single or groups of tumour cells that are poorly differentiated or undifferentiated infiltrating the gastric wall. GC with components of both DGC and IGC are referred to as mixed. Given all three subtypes are adenocarcinomas this raises questions regarding the pre-malignant pathways and aetiologies of each. Given they arise from the same gastric inflammatory milieu are they a spectrum of the same disease with overlapping molecular identities or do they represent unique entities with disparate causes and premalignant pathways?

The Cancer Genome Atlas (TCGA) Research Network published a landmark study into molecular classification of established GC in 2014. The study performed integrative genomic and epigenomic analysis of 295 gastric adenocarcinomas and reported on four major subclasses based on somatic copy number, mutation analysis, methylation and gene expression status. These were named: Epstein Barr virus positive, microsatellite unstable (MSI), genomically stable (GS) and chromosomal unstable subtypes[17]. While there was significant overlap regarding the molecular signatures between the IGC, DGC and mixed types consistent with common aspects of oncogenesis, 75% of the DGCs were of the GS subclass suggesting a divergent pathway. The TCGA analysis also demonstrates the potential limitation of histological systems such as the Lauren classification, with cellular phenotypes often not reflecting the heterogeneous nature of complex underlying molecular changes.

There are a number of inherited genetic conditions that predispose to GC such as somatic mismatch repair mutations in Lynch Syndrome and CDH1 mutations in Hereditary Diffuse GC. Although these are of interest in elucidating the molecular pathways of oncogenesis, discussion of these conditions is largely outside the scope of this review.

THE CORREA CASCADE

Chronic gastric inflammation

In 1975 Correa *et al*[18] described a stepwise progression of conditions within the stomach that were thought to result in GC. This was one of the first considerations of premalignant conditions in this disease and it was later found to be initiated by *Helicobacter pylori* (*H. pylori*). The initial step in the Correa cascade is the development of Chronic gastritis (ChG). *H. pylori* represents the archetypal cause of ChG, with infected patients in some studies having a greater than 10-fold higher chance of developing GC[19]. The effects of *H. pylori* on the gastric epithelium have been extensively studied, with one of the most important pathogenic factors being cytotoxin-associated gene A protein (CagA) positive strains. Virtually all of East Asian strains and 60% of Western strains of *H. pylori* strains are $cagA^+$, with infected patients developing more distinct inflammation, gastric ulceration and higher risk of GC[20-22]. Bacterial CagA protein interacts with a series of host epithelial proteins including ASPP2, RUNX3, PI3K, SHP2 and E-cadherin, resulting in the degradation and inactivation of p53 and RUNX3, deregulation of the PI3K-AKT, Ras-ERK and Wnt pathways and disruption of adherens junctions[23]. CagA has also been shown to alter DNA methylation patterns further deregulating normal epithelial gene expression patterns[24]. Intestinal metaplasia (IM) samples show higher levels of methylation than Atrophic gastritis (AG) samples, suggesting that DNA methylation pattern changes may play a vital role in the Correa model of IGC[24,25].

Autoimmune gastritis and atrophic gastritis

Autoimmune gastritis is a common aetiology of ChG, which results in activation of the adaptive immune system against parietal cells and intrinsic factor, leading to the destruction of the oxyntic gastric mucosa. As with other forms of chronic inflammation, autoimmune gastritis is a risk factor for GC through progression to intestinal metaplasia[26]. In a meta-analysis the overall relative risk of GC in patients with autoimmune gastritis was 6.8 (95%CI: 2.6–18.1)[27].

ChG leads to AG which refers to the atrophy and loss of gastric mucosal glands. Loss of specialised cells has significant implications on gastric function, with hypochlorhyria being one of the most recognised. In this state the loss of peptic acid production and raised gastric pH has implications on nutrient absorption (such as iron) and has significant implications on the gastric microbiome[28]. There has been considerable interest in the relationship between the gastric microbiome and GC, with a recent study uncovering dysbiosis of bacterial taxa along the Correa cascade[29]. At this stage it is uncertain if this dysbiosis represents a pre-malignant factor contributing to carcinogenesis in its own right, or simply a reflection of the change in the gastric microenvironment.

A key risk factor of chronic inflammation is the release of large amounts of reactive oxygen and nitrogen free species (ROS and NOS respectively), which are associated with DNA damage and increased mutation rates. Previous studies have shown that ROS and NOS released by inflammatory and epithelial cells can cause oxidative and nitrative DNA damage including the production of 8-oxo-7,8-dihydro-2′-deoxyguanosine (8-oxodG), a known mutagen and 8-nitroguanine[30,31]. The latter is formed by inducible nitric oxide synthase iNOS. Gene expression of iNOS is regulated by the NF-κB and STAT pathways among others[32]. These changes can result in DNA mutations thus promoting cellular changes and carcinogenesis.

GASTRIC STEM CELLS AND IM

In normal gastric epithelium stem cell populations give rise to nascent epithelial cells that mature and differentiate as they migrate to the apex of the gland[33]. Gastric and intestinal stem cells share an endodermal lineage, and through the process of chronic inflammation gastric stem cells may reprogram, producing metaplastic intestinal-type epithelium that replaces the normal gastric mucosa[34]. The continuing chronic inflammatory process results in further accumulation of genetic lesions in stem cells, ultimately resulting in dysplasia and cancer. As such IM can be thought of as a marker of stem cell stress and damage, with multiple inflammatory aetiologies converging to histologically identical metaplastic change. There have been multiple gastric stem cell populations characterised including $Lgr5^+$ stem cells in the adult antrum and the neonatal corpus and antrum, $Mist1^+$ stem cells found in the isthmus region of the corpus glands and $Troy^+$ stem cells that are thought to reside in the base of the corpus glands[33,35,36]. The role each of these plays in oncogenesis is an area of ongoing research. However, it is notable that different regions of the stomach have different stems cells and based on epidemiological evidence histological and molecular subgroups are found in different anatomic distributions suggesting a possible predetermined pathway for conversion to specific GC subgroups. For instance, TCGA found different anatomic distribution of molecular subgroups of GC with MSI being more likely to occur in the gastric corpus and antrum but rarely in the cardia[17].

IM

IM is usually found incidentally in patients undergoing upper endoscopy and is usually asymptomatic. While IM is defined by intestinal differentiation it is molecularly heterogeneous but can be histologically categorised as complete or incomplete subtypes (Figure 1). Complete IM (type I) resembles the small intestine epithelium with goblet cells, Paneth cells, eosinophilic enterocytes and a brush border[37]. It is associated with loss of markers of gastric mucin (MUC1, MUC5AC, MUC6) and expression of the intestinal sialic mucin, MUC2[38]. Incomplete IM more closely resembles the large intestine epithelium, lacking absorptive cells, but with columnar cells resembling gastric foveolar cells. It does not have a brush border and maintains expression of gastric mucin markers (MUC1, MUC5AC, MUC6) usually together with gain of MUC2[38]. Incomplete IM is further subdivided into Type II IM, with cells expressing a mixture of neutral mucins and intestinal sialomucins and Type III IM, with cells expressing sulfomucins[37]. In practice histopathological classification between complete and incomplete IM is often not mutually exclusive, with segments of tissue containing elements of both subtypes. The distinction between complete and

incomplete IM is clinically important as it appears incomplete harbours a higher risk of progression to cancer[39-42].

In the context of long-term *H. pylori* infection, IM possibly develops as an adaptive and protective lesion[43]. There has been extensive work into determining how *H. pylori* infection leads to IM with a number of genes implicated including SOX2 and CDX2. SOX2 is a transcription factor involved in gastric differentiation which negatively regulates intestinal differentiation, whereas CDX2 is a key intestinal transcription factor involved in establishing and maintaining IM[44]. SOX2 and CDX2 seem to be inversely regulated by *H. pylori*[45]. Complete IM has been shown to be predominantly SOX2 negative (93%) and incomplete IM mainly SOX2 positive (85%)[46]. Moreover CDX2 expression has been shown to be also induced in part through an NF-κB dependent mechanism following *H. pylori* infection[47].

Duodeno-gastric reflux is another proposed gastric insult contributing to ChG and IM formation, analogous to gastroesophageal acid reflux in Barrett's oesophagus[48]. There has been an association of increased incidence of IM after exposure to bile acids reported in a large-scale study involving a total of 2283 patients[49]. In this context the development of IM may represent a protective mechanism, with a metaplasia to an intestinal phenotype more capable of resisting the effects of bile than the normal gastric mucosa.

Risk factors in IM

H. pylori is a significant risk factor in the establishment of IM, however there are other clinical and environmental exposures that have been shown to be important risk factors for IM progression to GC. In a large-scale US study (n = 810821 patients) IM was more common in men, was more prevalent with increasing age and East Asian ancestry. This suggests IM may occur due to environmental exposures but in the context of hereditary risk[50]. Hereditary risk is relevant in GC even excluding major genetic syndromes with several studies showing intestinal-type GC is associated with a strong family history of GC[51-53]. With respect to premalignant lesions, it was shown that among siblings with a family history of any precancerous change there is an increase in risk of subsequent non-cardia GC with a hazard ratio of 2.5 compared with siblings of index persons with "normal or minor mucosal changes"[54]. The availability of siblings' precancerous data to the clinician could be useful in assessing a patient's risk of progressing to GC.

Once established, the degree of IM has been shown to be related to the risk of progression to cancer. Extensive IM with IM in the corpus, incomplete IM and IM located along the Maggenstrasse (along the lesser curve of the stomach) have been shown to increase the risk of progression towards cancer[40,42,55,56]. In one study of microsatellite instability (MSI), this molecular finding was enriched in GC and adjacent IM suggesting this may be an early event in MSI subtype GCs. It is notable that microsatellite unstable IM was of incomplete type in this study[57] which provides further evidence for the potential unique molecular pathways that begin in the premalignant context.

OLGA AND OLGIM

Both the Operative Link on Gastritis Assessment (OLGA) and on Gastric Intestinal Metaplasia (OLGIM) are based on histological assessment of random biopsies taken from designated areas of the stomach according to the Sydney protocol[58-60]. At least four sites are sampled from the stomach during upper gastroscopy (two antral and two corpus). Both OLGA and OLGIM are scoring standards used to grade and stage chronic gastric inflammation, gastric atrophy and intestinal metaplasia. They provide information with regards to topography and extent of atrophic gastritis and intestinal metaplasia, the latter being easier to assess and more consistent. Initially reported by Rugge *et al*[61,62] 2010 and 2011 for both OLGA and OLGIM and more recently by the meta-analysis carried out by Yue *et al*[63] 2018 OLGA and OLGIM stages Type III/IV are consistently associated with increased risk of progression to GC. These findings suggest that high risk patients with OLGA/OLGIM stages type III/IV would benefit from close and frequent monitoring to detect neoplastic lesions at the earliest possible stage.

POINT OF NO RETURN

The Correa cascade is often referred to as a linear progression, however in the majority of patients there may be little to no change along the Cascade cascade over

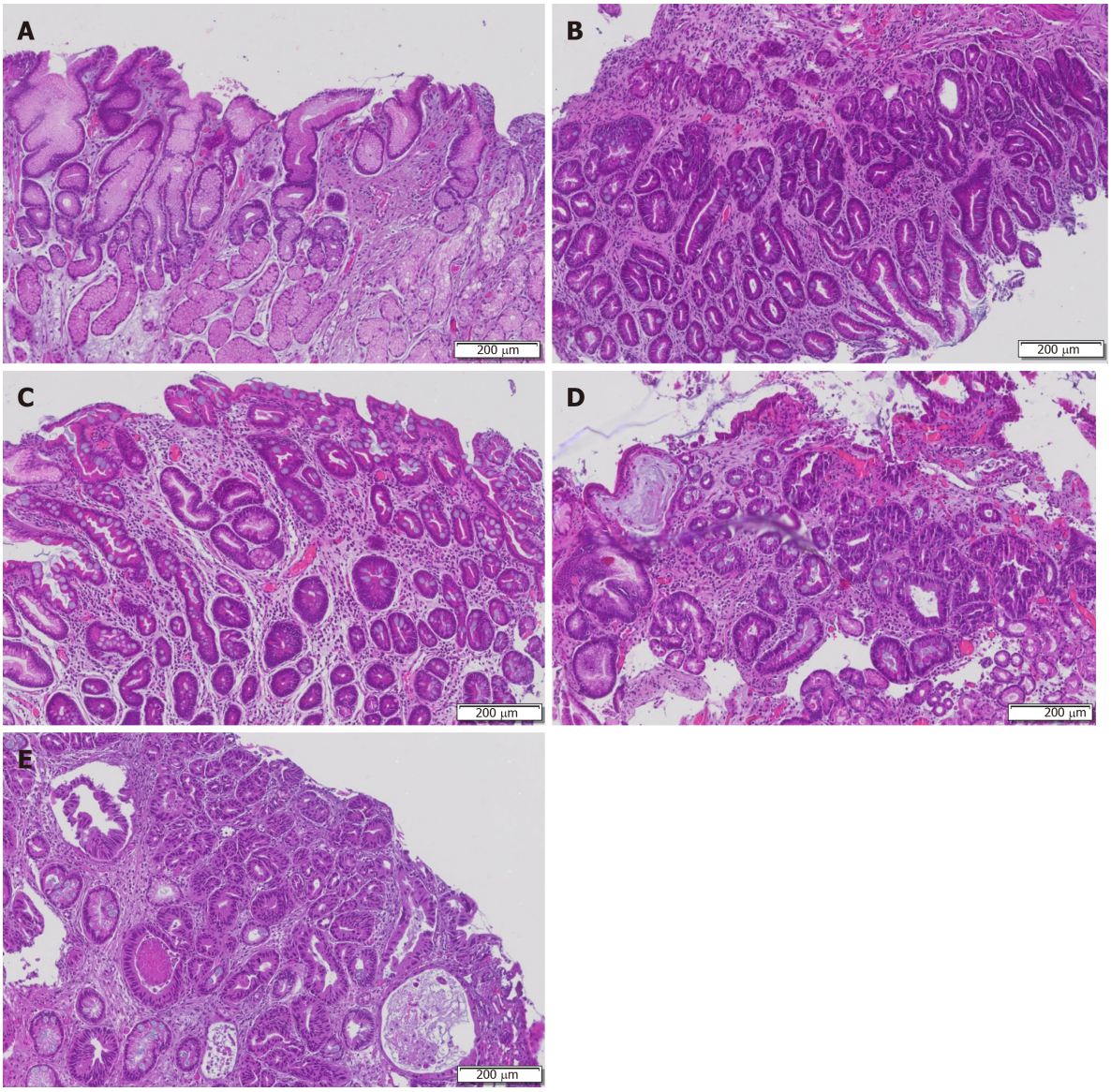


Figure 1 Complete or incomplete subtypes. A: Chronic gastritis with mucosal atrophy and lymphocytic infiltrate (asterix); B: Incomplete intestinal metaplasia resembling the colonic-type epithelium with irregular mucin droplets (arrowheads) and absence of a brush border; C: Complete intestinal metaplasia resembling the small intestinal epithelium with goblet cells alternating with eosinophilic enterocytes, brush border and Paneth cells; D: Low-grade dysplasia characterized by crowded glands with columnar cells and preserved polarity and pseudostratified nuclei; E: High-grade dysplasia with cuboidal cells, mitotic activity, prominent nucleoi, and high nuclear-cytoplasmia ratio.

many years. In other patients it can be a dynamic process with regression and/or progression of lesions, perhaps even rapid progression bypassing some of the putative stages. It is clearly evident that *H. pylori* infection and chronic inflammation in selected individuals causes progression of the cascade and it has been observed that successful eradication of *H. pylori* can lead to regression of histological features. There has been speculation that there is a point at which eradication is less effective at causing regression and indeed does not change the risk of progression in certain individuals. This has been referred as the "point of no return". *H. pylori* eradication results in complete resolution of histological inflammation and regression of atrophy in AG patients, with greater improvement seen in corpus AG compared to antral AG patients[64]. Unfortunately, the same effect is not seen in IM patients[64-67]. Once IM is established, eradication is only partially successful at reducing the risk of progression to GC. This suggests that IM may be the "point of no return" where genetic damage to gastric stem cells becomes irreversible. Although there is much evidence to support a point of no return, there has been evidence of regression from IM to AG or ChG in some cohorts[40,68]. A graphical summary of some of the larger IM progression studies is shown in Figure 2[40,68-73].

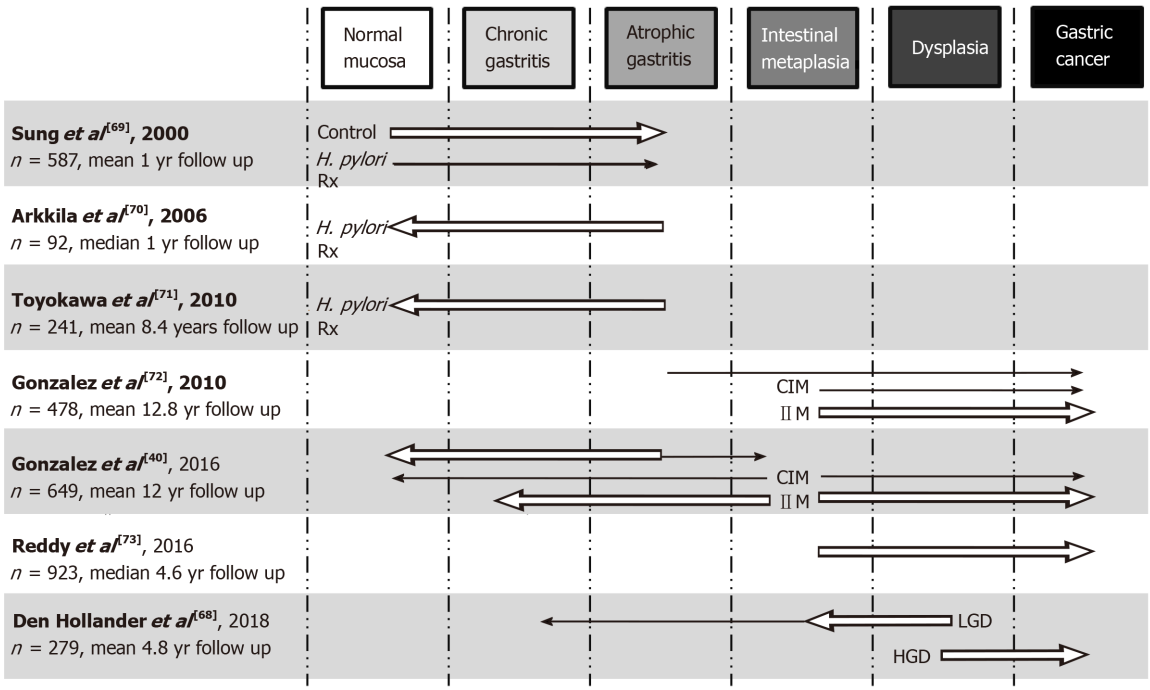


Figure 2 Graphical representation of selected large studies investigating progression/regression of premalignant gastric lesions across the stages of the Correa cascade. Arrows represent the direction of effect findings, with the size of the arrow the strength of effect (not to scale between cohorts and only major findings of trials represented). *H. pylori* Rx: *Helicobacter pylori* antibiotic therapy; CIM: Complete IM; IIM: Incomplete IM; LGD: Low-grade dysplasia; HGD: High-grade dysplasia; IM: Intestinal metaplasia.

SPASMOLYTIC PEPTIDE EXPRESSING METAPLASIA

Work from animal models of GC has introduced the concept of Spasmolytic peptide expressing metaplasia (SPEM). This is a cell lineage shown to be strongly associated with chronic gastritis in the fundus and gastric adenocarcinoma in animals[74]. It is often thought as an alternative metaplastic lineage to IM. SPEM is morphologically similar to Brunner's glands of the duodenum and expresses the trefoil spasmolytic polypeptide (SP or TFF2)[75]. It has been hypothesised that SPEM is an alternative precursor to GC and is associated with increased risk compared to IM[76]. Although SPEM is not a defined stage in the Correa cascade, it has been useful for studying the process of metaplasia formation in mice. To avoid confusion, SPEM is identified in the corpus and the fundus but not in the antrum as its characteristics are very similar to those of the deep antral and pyloric glands which also express TFF2. In mice infected with *Helicobacter felis*, SPEM develops after 6 to 12 mo of infection in the presence of active inflammation. First parietal cells are lost (oxyntic atrophy) and then the normal gastric lineages are replaced with metaplastic cells[77]. In two acute drug-induced SPEM models, with DMP-777 protonophore (abrogated inflammation) and L635 (prominent inflammation) as well as with *H. felis* infection in mice (chronic inflammation), it is suggested SPEM arises from the transdifferentiation of chief cells[77,78]. However more recently a study by Kinoshita *et al*[79] suggested that SPEM is the result of a regenerative process initiated by neck progenitor cells after chief cell loss. In another mouse model, SPEM in INS-GAS mice progressed to dysplasia after 1 year[80]. Following *H. pylori*-infection, Mongolian gerbils progressively develop ChG, followed by loss of parietal cells and metaplasia[81]. After 1 year of infection, SPEM is observed and mixed glands expressing both SPEM and IM are also seen. In humans there is growing evidence that suggests SPEM can either progress directly to dysplasia or become IM in the presence of continuous chronic inflammation[82]. These animal systems have been useful in studying the natural history of these lesions but it remains to be seen whether they are reliable models of the human condition.

THE ROLE OF THE IMMUNE MICROENVIRONMENT

We have continually reiterated the role of chronic inflammation in the development of

GC. In the context of a chronically inflamed microenvironment, there is some evidence that IM may arise due to the actions of specific immune cells. Using the murine model of L635-induced SPEM and following administration of clodronate, it was shown that macrophages are involved in the development of acute SPEM[83]. These macrophages were predominantly of the M2 subset (alternatively activated) and in the same study M2 macrophages were also shown to be increased in human SPEM and IM. Another prevalent immune cell in IM is neutrophils which were shown to be approximately 9-fold enriched compared to normal gastric tissue[84]. GC tissues were roughly 24 times enriched in neutrophils compared to normal gastric tissue. Thus macrophages and neutrophils may be vital immune cells required in the gastric microenvironment for SPEM and IM to develop and then to progress to GC. The role of the immune system in the process of gastric carcinogenesis has not yet been fully investigated.

CELLULAR AND MOLECULAR PATHWAYS OF PROGRESSION

IM progression to dysplasia and subsequently cancer occurs infrequently and the molecular mechanisms responsible for this progression are still not well understood. There are a number of challenges with studying this paradigm in view of the long duration over which these conditions progress, thus limiting prospective studies. This is compounded by the low rates of progression from each of the Correa stages and the potential confounder of tissue sampling when undertaking endoscopic follow up. Although the exact genomic or epigenomic pathways for IM progression to dysplasia are still being investigated, it is possible to postulate how certain events are necessary for progression by combining available data from a small number of key studies. It is known that: (1) IM is clonally derived from within the gastric mucosa[34,85]; (2) Gastric and IM glands divide by fission to form clonal patches[34,85,86]; (3) Over time, different gastric stem cells with accumulated genomic events (somatic mutations/chromosomal copy number gains and/or losses) can give rise to unique IM glands; (4) Further genomic changes may drive IM glands to proliferate or persist over a long period of time; (5) Dysplastic glands are formed that are genetically related to IM glands; entire dysplastic fields can share a foundation mutation[86] from which multiple subclones can result; and (6) This event can happen simultaneously in multiple regions of the stomach leading to an increased risk of GC developing across several locations and therefore providing a field cancerization effect.

To better understand how this process may unfold, studies on gastric adenoma (GA) and Barrett's oesophagus (BO) progression to GC and oesophageal adenocarcinoma (OAC), respectively, can be used as examples. In a recent study of gastric adenoma and paired GC from the same patients were used to determine clonal evolution. Clonal structure analyses showed that most GA/GC pairs exhibit parallel evolution with early divergence instead of a linear sequence of GA to GC progression[87]. Additionally, a small number of GC cases were clonally unrelated from paired GA suggesting the synchronous evolution of multiple clones that may progress to GC. BO is a premalignant intestinal metaplastic lesion that's often associated with gastro-oesophageal disease and predisposes patients to develop OAC[88]. Although exact values differ between studies, two population-based BO follow-up studies showed that the annual risk of progression of BO is 0.12%-0.14%[89,90]. BO has a higher mutation load (6.76 SNVs/Mb) than gastric IM but still lower than OAC (10.02 SNVs/Mb) and was shown to be polyclonal[91]. In one patient with BO, high grade dysplasia was shown to arise from multiple clones suggesting that the severity of intestinal metaplasia (a result of clonal expansion and cumulative molecular aberrations) may also play a key role in synchronous progression to GC[91].

Overall a holistic molecular approach is needed to elucidate the crucial events of how premalignant lesions actually cross the bridge to malignancy, a so-called "Pre-Cancer Genome Atlas"[92]. Using whole genome MBD-seq and RRBS analyses Kim *et al* showed that hypermethylation of gastrointestinal hormone receptors may play a key role in early gastric carcinogenesis[93]. Both gastrin and gastric acid secretion are thought to play important roles in cell differentiation and may play a part in creating a permissive environment or even directly involved in the process of carcinogenesis. A good summary review on the potential cellular and molecular pathways of gastric carcinogenesis was written by Rivas-Ortiz which added useful insight to this area[94]. It is very likely that GC is the result of multiple events co-occurring over time and space leading to various subtypes of GC (see TCGA molecular subtypes). If this is true, then it is also likely that differing sets of pre-cancerous events contribute to gastric carcinogenesis. Although some events may overlap across all GC subtypes *e.g.*,

chronic gastritis, others may be specific for a particular GC subtype *e.g.*, the breakdown of cellular mechanisms that keep diploidy intact leading to the chromosomal instability subtype.

HIGH RISK GENOMIC AND EPIGENOMIC ALTERATIONS IN IM

The median time for gastric intestinal metaplasia to progress to GC has been estimated to be 6.1 years, in contrast to low grade dysplasia which is only 2.6 years[95]. A recent study of genomic and epigenomic profiling of IM showed that IM has a low mutational burden compared to non-hypermutated GC (2.6 *vs* 6.9 mutations/Mb) and harbour recurrent mutations in certain tumour suppressor genes like FBXW7 (6/108 IM cases) but less in others, specifically TP53 and ARID1A (2/108 and 3/108 IM cases)[96]. However the presence of low frequency TP53 mutations in IM patients is in contrast to previous work within our group that showed an absence of TP53 mutations in IM samples paired with GC samples from the same patients[97]. A second finding of our study was that overexpression of p53 protein using immunohistochemistry has limited correlation to TP53 mutations. In the Huang *et al*[96] 2018 study, patients that progressed to dysplasia and GC had previously chromosome 8q amplifications and shortened telomeres. Interestingly, patients with IM that regressed had normal epigenomic patterns. DNA methylation profiling showed that the majority of IM patients in the high methylation group had relatively high mutational load, frequent chromosomal copy number variations and FBXW7 mutations and occurred mainly in the antrum.

LOW AND HIGH-GRADE DYSPLASIA DIFFER IN MUTATIONAL PATTERNS

The Padova classification was developed in 2000 to standardise histopathological reporting, which identifies five main categories for dysplastic lesions: (1) Negative for dysplasia; (2) Indefinite for dysplasia; (3) Non-invasive neoplasia; (4) Suspicious for invasive carcinoma; and (5) Invasive adenocarcinoma[98]. In practice, pathologists use categories 1 and 2 and subdivide category 3 as low (LGD) and high grade (HGD), the latter being associated with a higher risk of progression. A recent study using targeted deep DNA sequencing of 67 GC-related genes detected APC mutations in all LGD and also in some HGD cases[99]. However, APC and TP53 appeared to be mutually exclusive, the latter being present only in HGD and diminutive intramucosal GC (diameter < 10 mm). Analysis of tumor variant allele frequency suggested TP53 mutation is the initial event in TP53-mutated intramucosal GC. Importantly, this study suggested that linear evolution of LGD to HGD is rare and that early mutational events determine the evolution of dysplastic lesions. Early APC mutations lead to LGD whereas TP53 mutations lead to HGD which, following other genomic aberrations, subsequently evolve into early GC.

THE CORREA CASCADE AND DIFFUSE GC

Although there is considerable evidence of IM progressing to dysplasia and then to IGC, it is still debated whether any of the premalignant lesions that are part of the Correa cascade actually play a role in diffuse gastric carcinogenesis. In a prospective Japanese study, a proportion of patients that developed DGC had pangastritis (9/13), moderate to severe atrophy (9/13 and 1/13 respectively) and IM (8/13) at base line[100], suggesting a significant association between IM and DGC development[100]. A more recent study in South Korea showed that OLGA and OLGIM may have clinical utility in patients at risk of developing DGC[101]. Multivariate logistic regression analysis showed family history of GC, *H. pylori* infection, and OLGA/OLGIM stages III/IV were independent risk factors for both IGC and DGC[101]. Thus, atrophy and particularly IM likely play a dual role in gastric carcinogenesis dependent on context. If the right conditions are met, cellular and molecular changes within the stem cell compartment of these lesions lead to GC; if not, their presence creates a permissive environment for progression to GC to occur, possibly through hypochlorhydria and dysbiosis, and is also an indicator of increased patient progression risk. DGC may be the result of an "alternative" route to carcinogenesis, where a CDH1 mutation within the glandular stem cell compartment of a gastric gland or atrophic gland or even a

metaplastic gland/crypt produces a parent tumour cell.

Neuroendocrine cell dedifferentiation: An alternative route to GC?

An alternative paradigm to the stem cell theory as the tumour cell of origin has been gaining ground in recent years. In certain circumstances mature neuroendocrine cells may dedifferentiate, accumulate mutations and other genomic events and become tumour cells themselves[102]. Neuroendocrine tumours are the most likely results of such an event but also gastric adenocarcinomas. The enterochromafin like cell (ECL) is the main neuroendocrine cell in the oxyntic stomach, it produces and releases histamine and has gastrin receptors. Although the exact molecular and cellular mechanisms of this pathway to GC are not known, it is thought that loss of parietal cells and atrophy precedes cellular dedifferentiation of ECL cells. Thus, this pathway to GC may not fully follow the Correa cascade, going directly from an atrophic state to a hyperplastic, then dysplastic and then to either a neuroendocrine tumour or a gastric adenocarcinoma.

CONCLUSION

Our understanding of the molecular basis of GC and its premalignant lesions is accumulating rapidly, providing useful insights into the natural history of the disease (Figure 3). Knowledge remains lacking in many domains however, including the relationship between premalignant lesions and TCGA subtypes of GC. It could be the molecular changes characterising the TCGA GC subtypes represent disparate insults predisposing to initiation of the Correa cascade. Alternatively, the subtypes could represent accumulated "hits" following initiation with *H. pylori* infection. Insights into this pathway would stratify those at risk as well as inform prognosis and surveillance guidelines.

The observation that IM appears a relative point of no return along the Correa cascade, with only a small fraction of patients progressing to dysplasia and GC raises questions of the molecular determinants of progression. In the first study of its type, Huang *et al* laid the foundation for understanding this process, following an IM cohort for a minimum of 5 years and describing the molecular changes associated with progression in a large Chinese cohort. Validation of these findings in alternative cohorts is required for its use clinically.

In high-risk populations screening and surveillance has been successful in the early detection of GCs and improvements in 5-year survivals. However further work is required in low-risk populations to make strong evidence-based decisions regarding clinical screening or surveillance. In those known to have IM the risk factors discussed above should prompt the clinician to carefully consider surveillance including incomplete IM, dysplasia, extensive IM involving the corpus, male gender and those from high-risk ethnicities. The addition of molecular data such as TP53 mutation data, methylation patterns and chromosome 8 status would further improve risk-assessment algorithms, however larger population-based data is required for this to be accurate and practical.

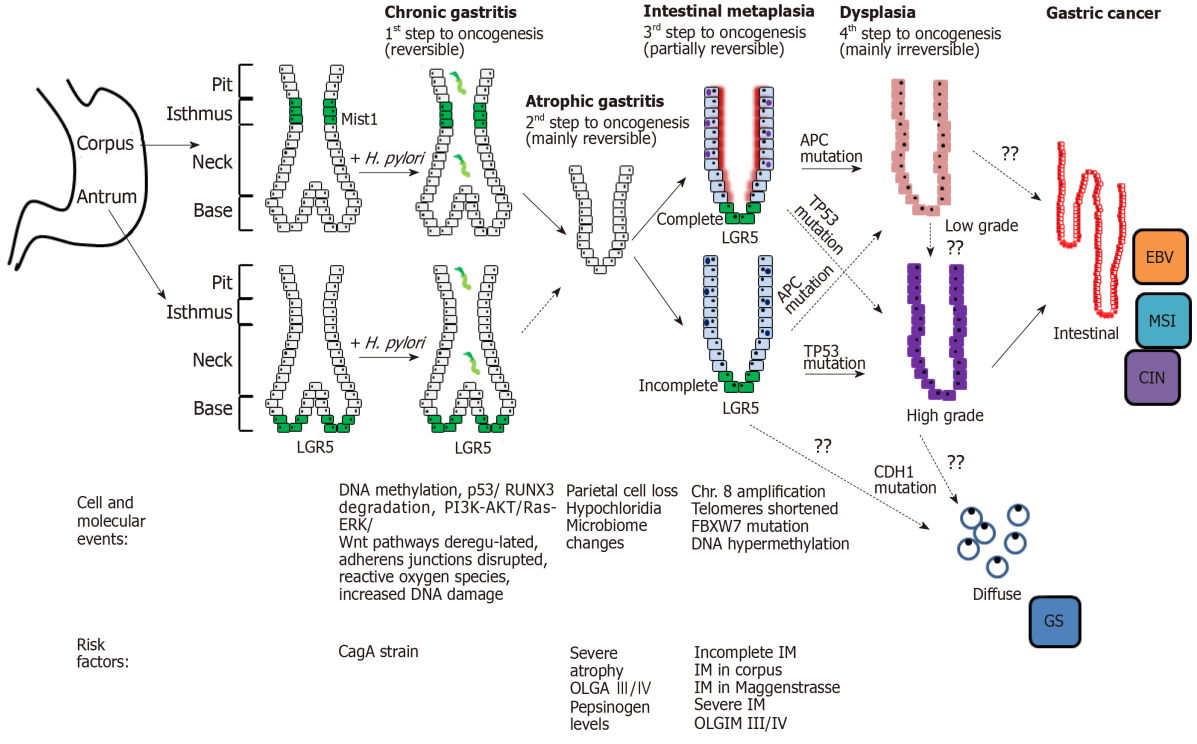


Figure 3 Summary of the cellular and molecular events associated with progression to cancer.*H. pylori*: *Helicobacter pylori*; EBV: Epstein Barr virus positive; MSI: Microsatellite unstable; CagA: Cytotoxin-associated gene A protein; IM: Intestinal metaplasia; GS: Genomically stable.

REFERENCES

1 **Ferlay J**, Soerjomataram I, Dikshit R, Eser S, Mathers C, Rebelo M, Parkin DM, Forman D, Bray F. Cancer incidence and mortality worldwide: sources, methods and major patterns in GLOBOCAN 2012. *Int J Cancer* 2015; **136**: E359-E386 [PMID: 25220842 DOI: 10.1002/ijc.29210]

2 **Joossens JV**, Hill MJ, Elliott P, Stamler R, Lesaffre E, Dyer A, Nichols R, Kesteloot H. Dietary salt, nitrate and stomach cancer mortality in 24 countries. European Cancer Prevention (ECP) and the INTERSALT Cooperative Research Group. *Int J Epidemiol* 1996; **25**: 494-504 [PMID: 8671549 DOI: 10.1093/ije/25.3.494]

3 **Haenszel W**, Kurihara M, Segi M, Lee RK. Stomach cancer among Japanese in Hawaii. *J Natl Cancer Inst* 1972; **49**: 969-988 [PMID: 4678140 DOI: 10.1093/jnci/49.4.969]

4 **Strumylaite L**, Zickute J, Dudzevicius J, Dregval L. Salt-preserved foods and risk of gastric cancer. *Medicina (Kaunas)* 2006; **42**: 164-170 [PMID: 16528133]

5 **Lin SH**, Li YH, Leung K, Huang CY, Wang XR. Salt processed food and gastric cancer in a Chinese population. *Asian Pac J Cancer Prev* 2014; **15**: 5293-5298 [PMID: 25040991 DOI: 10.7314/APJCP.2014.15.13.5293]

6 **Ren JS**, Kamangar F, Forman D, Islami F. Pickled food and risk of gastric cancer--a systematic review and meta-analysis of English and Chinese literature. *Cancer Epidemiol Biomarkers Prev* 2012; **21**: 905-915 [PMID: 22499775 DOI: 10.1158/1055-9965.EPI-12-0202]

7 **Tsugane S**, Sasazuki S. Diet and the risk of gastric cancer: review of epidemiological evidence. *Gastric Cancer* 2007; **10**: 75-83 [PMID: 17577615 DOI: 10.1007/s10120-007-0420-0]

8 **Jenab M**, Riboli E, Ferrari P, Sabate J, Slimani N, Norat T, Friesen M, Tjønneland A, Olsen A, Overvad K, Boutron-Ruault MC, Clavel-Chapelon F, Touvier M, Boeing H, Schulz M, Linseisen J, Nagel G, Trichopoulou A, Naska A, Oikonomou E, Krogh V, Panico S, Masala G, Sacerdote C, Tumino R, Peeters PH, Numans ME, Bueno-de-Mesquita HB, Büchner FL, Lund E, Pera G, Sanchez CN, Sánchez MJ, Arriola L, Barricarte A, Quirós JR, Hallmans G, Stenling R, Berglund G, Bingham S, Khaw KT, Key T, Allen N, Carneiro F, Mahlke U, Del Giudice G, Palli D, Kaaks R, Gonzalez CA. Plasma and dietary vitamin C levels and risk of gastric cancer in the European Prospective Investigation into Cancer and Nutrition (EPIC-EURGAST). *Carcinogenesis* 2006; **27**: 2250-2257 [PMID: 16774936 DOI: 10.1093/carcin/bgl096]

9 **González CA**, Pera G, Agudo A, Palli D, Krogh V, Vineis P, Tumino R, Panico S, Berglund G, Simán H, Nyrén O, Agren A, Martinez C, Dorronsoro M, Barricarte A, Tormo MJ, Quiros JR, Allen N, Bingham S, Day N, Miller A, Nagel G, Boeing H, Overvad K, Tjonneland A, Bueno-De-Mesquita HB, Boshuizen HC, Peeters P, Numans M, Clavel-Chapelon F, Helen I, Agapitos E, Lund E, Fahey M, Saracci R, Kaaks R, Riboli E. Smoking and the risk of gastric cancer in the European Prospective Investigation Into Cancer and Nutrition (EPIC). *Int J Cancer* 2003; **107**: 629-634 [PMID: 14520702 DOI: 10.1002/ijc.11426]

10 **Praud D**, Rota M, Pelucchi C, Bertuccio P, Rosso T, Galeone C, Zhang ZF, Matsuo K, Ito H, Hu J, Johnson KC, Yu GP, Palli D, Ferraroni M, Muscat J, Lunet N, Peleteiro B, Malekzadeh R, Ye W, Song H, Zaridze D, Maximovitch D, Aragonés N, Castaño-Vinyals G, Vioque J, Navarrete-Muñoz EM, Pakseresht M, Pourfarzi F, Wolk A, Orsini N, Bellavia A, Håkansson N, Mu L, Pastorino R, Kurtz RC, Derakhshan MH, Lagiou A, Lagiou P, Boffetta P, Boccia S, Negri E, La Vecchia C. Cigarette smoking and gastric cancer in the Stomach Cancer Pooling (StoP) Project. *Eur J Cancer Prev* 2018; **27**: 124-133 [PMID:

27560662 DOI: 10.1097/CEJ.0000000000000290]
11 **Han MA**, Kim YW, Choi IJ, Oh MG, Kim CG, Lee JY, Cho SJ, Eom BW, Yoon HM, Ryu KW. Association of smoking history with cancer recurrence and survival in stage III-IV male gastric cancer patients. *Cancer Epidemiol Biomarkers Prev* 2013; **22**: 1805-1812 [PMID: 23904463 DOI: 10.1158/1055-9965.EPI-13-0385]
12 **Preston DL**, Ron E, Tokuoka S, Funamoto S, Nishi N, Soda M, Mabuchi K, Kodama K. Solid cancer incidence in atomic bomb survivors: 1958-1998. *Radiat Res* 2007; **168**: 1-64 [PMID: 17722996 DOI: 10.1667/RR0763.1]
13 **Abioye AI**, Odesanya MO, Abioye AI, Ibrahim NA. Physical activity and risk of gastric cancer: a meta-analysis of observational studies. *Br J Sports Med* 2015; **49**: 224-229 [PMID: 24434186 DOI: 10.1136/bjsports-2013-092778]
14 **O'Doherty MG**, Freedman ND, Hollenbeck AR, Schatzkin A, Abnet CC. A prospective cohort study of obesity and risk of oesophageal and gastric adenocarcinoma in the NIH-AARP Diet and Health Study. *Gut* 2012; **61**: 1261-1268 [PMID: 22174193 DOI: 10.1136/gutjnl-2011-300551]
15 **Uthman OA**, Jadidi E, Moradi T. Socioeconomic position and incidence of gastric cancer: a systematic review and meta-analysis. *J Epidemiol Community Health* 2013; **67**: 854-860 [PMID: 23929615 DOI: 10.1136/jech-2012-201108]
16 **Lauren P**. The Two Histological Main Types Of Gastric Carcinoma: Diffuse and So-Called Intestinal-Type Carcinoma. An Attempt at A Histo-Clinical Classification. *Acta Pathol Microbiol Scand* 1965; **64**: 31-49 [PMID: 14320675 DOI: 10.1111/apm.1965.64.1.31]
17 **Cancer Genome Atlas Research Network**. Comprehensive molecular characterization of gastric adenocarcinoma. *Nature* 2014; **513**: 202-209 [PMID: 25079317 DOI: 10.1038/nature13480]
18 **Correa P**, Haenszel W, Cuello C, Tannenbaum S, Archer M. A model for gastric cancer epidemiology. *Lancet* 1975; **2**: 58-60 [PMID: 49653 DOI: 10.1016/S0140-6736(75)90498-5]
19 **Kim N**, Park RY, Cho SI, Lim SH, Lee KH, Lee W, Kang HM, Lee HS, Jung HC, Song IS. Helicobacter pylori infection and development of gastric cancer in Korea: long-term follow-up. *J Clin Gastroenterol* 2008; **42**: 448-454 [PMID: 18344895 DOI: 10.1097/MCG.0b013e318046eac3]
20 **Blaser MJ**, Perez-Perez GI, Kleanthous H, Cover TL, Peek RM, Chyou PH, Stemmermann GN, Nomura A. Infection with Helicobacter pylori strains possessing cagA is associated with an increased risk of developing adenocarcinoma of the stomach. *Cancer Res* 1995; **55**: 2111-2115 [PMID: 7743510 DOI: 10.1002/1097-0142(19950515)75:10<2623::AID-CNCR2820751033>3.0.CO]
21 **Wroblewski LE**, Peek RM, Wilson KT. Helicobacter pylori and gastric cancer: factors that modulate disease risk. *Clin Microbiol Rev* 2010; **23**: 713-739 [PMID: 20930071 DOI: 10.1128/CMR.00011-10]
22 **Murata-Kamiya N**. Pathophysiological functions of the CagA oncoprotein during infection by Helicobacter pylori. *Microbes Infect* 2011; **13**: 799-807 [PMID: 21477660 DOI: 10.1016/j.micinf.2011.03.011]
23 **Hatakeyama M**. Structure and function of Helicobacter pylori CagA, the first-identified bacterial protein involved in human cancer. *Proc Jpn Acad Ser B Phys Biol Sci* 2017; **93**: 196-219 [PMID: 28413197 DOI: 10.2183/pjab.93.013]
24 **Na HK**, Woo JH. Helicobacter pylori Induces Hypermethylation of CpG Islands Through Upregulation of DNA Methyltransferase: Possible Involvement of Reactive Oxygen/Nitrogen Species. *J Cancer Prev* 2014; **19**: 259-264 [PMID: 25574460 DOI: 10.15430/JCP.2014.19.4.259]
25 **Schneider BG**, Piazuelo MB, Sicinschi LA, Mera R, Peng DF, Roa JC, Romero-Gallo J, Delgado AG, de Sablet T, Bravo LE, Wilson KT, El-Rifai W, Peek RM, Correa P. Virulence of infecting Helicobacter pylori strains and intensity of mononuclear cell infiltration are associated with levels of DNA hypermethylation in gastric mucosae. *Epigenetics* 2013; **8**: 1153-1161 [PMID: 24128875 DOI: 10.4161/epi.26072]
26 **Coati I**, Fassan M, Farinati F, Graham DY, Genta RM, Rugge M. Autoimmune gastritis: Pathologist's viewpoint. *World J Gastroenterol* 2015; **21**: 12179-12189 [PMID: 26576102 DOI: 10.3748/wjg.v21.i42.12179]
27 **Vannella L**, Lahner E, Osborn J, Annibale B. Systematic review: gastric cancer incidence in pernicious anaemia. *Aliment Pharmacol Ther* 2013; **37**: 375-382 [PMID: 23216458 DOI: 10.1111/apt.12177]
28 **Parsons BN**, Ijaz UZ, D'Amore R, Burkitt MD, Eccles R, Lenzi L, Duckworth CA, Moore AR, Tiszlavicz L, Varro A, Hall N, Pritchard DM. Comparison of the human gastric microbiota in hypochlorhydric states arising as a result of Helicobacter pylori-induced atrophic gastritis, autoimmune atrophic gastritis and proton pump inhibitor use. *PLoS Pathog* 2017; **13**: e1006653 [PMID: 29095917 DOI: 10.1371/journal.ppat.1006653]
29 **Coker OO**, Dai Z, Nie Y, Zhao G, Cao L, Nakatsu G, Wu WK, Wong SH, Chen Z, Sung JJY, Yu J. Mucosal microbiome dysbiosis in gastric carcinogenesis. *Gut* 2018; **67**: 1024-1032 [PMID: 28765474 DOI: 10.1136/gutjnl-2017-314281]
30 **Kawanishi S**, Hiraku Y, Oikawa S. Mechanism of guanine-specific DNA damage by oxidative stress and its role in carcinogenesis and aging. *Mutat Res* 2001; **488**: 65-76 [PMID: 11223405 DOI: 10.1016/S1383-5742(00)00059-4]
31 **Hussain SP**, Harris CC. Inflammation and cancer: an ancient link with novel potentials. *Int J Cancer* 2007; **121**: 2373-2380 [PMID: 17893866 DOI: 10.1002/ijc.23173]
32 **Jaiswal M**, LaRusso NF, Gores GJ. Nitric oxide in gastrointestinal epithelial cell carcinogenesis: linking inflammation to oncogenesis. *Am J Physiol Gastrointest Liver Physiol* 2001; **281**: G626-G634 [PMID: 11518674 DOI: 10.1152/ajpgi.2001.281.3.G626]
33 **Barker N**, Huch M, Kujala P, van de Wetering M, Snippert HJ, van Es JH, Sato T, Stange DE, Begthel H, van den Born M, Danenberg E, van den Brink S, Korving J, Abo A, Peters PJ, Wright N, Poulsom R, Clevers H. Lgr5(+ve) stem cells drive self-renewal in the stomach and build long-lived gastric units in vitro. *Cell Stem Cell* 2010; **6**: 25-36 [PMID: 20085740 DOI: 10.1016/j.stem.2009.11.013]
34 **Waddingham W**, Graham D, Banks M, Jansen M. The evolving role of endoscopy in the diagnosis of premalignant gastric lesions. *F1000Res* 2018; **7** [PMID: 29946429 DOI: 10.12688/f1000research.12087.1]
35 **Hayakawa Y**, Ariyama H, Stancikova J, Sakitani K, Asfaha S, Renz BW, Dubeykovskaya ZA, Shibata W, Wang H, Westphalen CB, Chen X, Takemoto Y, Kim W, Khurana SS, Tailor Y, Nagar K, Tomita H, Hara A, Sepulveda AR, Setlik W, Gershon MD, Saha S, Ding L, Shen Z, Fox JG, Friedman RA, Konieczny SF, Worthley DL, Korinek V, Wang TC. Mist1 Expressing Gastric Stem Cells Maintain the Normal and Neoplastic Gastric Epithelium and Are Supported by a Perivascular Stem Cell Niche. *Cancer Cell* 2015; **28**: 800-814 [PMID: 26585400 DOI: 10.1016/j.ccell.2015.10.003]
36 **Stange DE**, Koo BK, Huch M, Sibbel G, Basak O, Lyubimova A, Kujala P, Bartfeld S, Koster J, Geahlen

JH, Peters PJ, van Es JH, van de Wetering M, Mills JC, Clevers H. Differentiated Troy+ chief cells act as reserve stem cells to generate all lineages of the stomach epithelium. *Cell* 2013; **155**: 357-368 [PMID: 24120136 DOI: 10.1016/j.cell.2013.09.008]

37 **Jass JR**, Filipe MI. A variant of intestinal metaplasia associated with gastric carcinoma: a histochemical study. *Histopathology* 1979; **3**: 191-199 [PMID: 468122 DOI: 10.1111/j.1365-2559.1979.tb02996.x]

38 **Reis CA**, David L, Correa P, Carneiro F, de Bolós C, Garcia E, Mandel U, Clausen H, Sobrinho-Simões M. Intestinal metaplasia of human stomach displays distinct patterns of mucin (MUC1, MUC2, MUC5AC, and MUC6) expression. *Cancer Res* 1999; **59**: 1003-1007 [PMID: 10070955]

39 **González CA**, Sanz-Anquela JM, Gisbert JP, Correa P. Utility of subtyping intestinal metaplasia as marker of gastric cancer risk. A review of the evidence. *Int J Cancer* 2013; **133**: 1023-1032 [PMID: 23280711 DOI: 10.1002/ijc.28003]

40 **González CA**, Sanz-Anquela JM, Companioni O, Bonet C, Berdasco M, López C, Mendoza J, Martín-Arranz MD, Rey E, Poves E, Espinosa L, Barrio J, Torres MÁ, Cuatrecasas M, Elizalde I, Bujanda L, Garmendia M, Ferrández Á, Muñoz G, Andreu V, Paules MJ, Lario S, Ramírez MJ, Barkun A. Study group, Gisbert JP. Incomplete type of intestinal metaplasia has the highest risk to progress to gastric cancer: results of the Spanish follow-up multicenter study. *J Gastroenterol Hepatol* 2016; **31**: 953-958 [PMID: 26630310 DOI: 10.1111/jgh.13249]

41 **Pittayanon R**, Rerknimitr R, Klaikaew N, Sanpavat A, Chaithongrat S, Mahachai V, Kullavanijaya P, Barkun A. The risk of gastric cancer in patients with gastric intestinal metaplasia in 5-year follow-up. *Aliment Pharmacol Ther* 2017; **46**: 40-45 [PMID: 28449219 DOI: 10.1111/apt.14082]

42 **Shao L**, Li P, Ye J, Chen J, Han Y, Cai J, Lu X. Risk of gastric cancer among patients with gastric intestinal metaplasia. *Int J Cancer* 2018 [PMID: 29707766 DOI: 10.1002/ijc.31571]

43 **Giroux V**, Rustgi AK. Metaplasia: tissue injury adaptation and a precursor to the dysplasia-cancer sequence. *Nat Rev Cancer* 2017; **17**: 594-604 [PMID: 28860646 DOI: 10.1038/nrc.2017.68]

44 **Mutoh H**, Sakurai S, Satoh K, Tamada K, Kita H, Osawa H, Tomiyama T, Sato Y, Yamamoto H, Isoda N, Yoshida T, Ido K, Sugano K. Development of gastric carcinoma from intestinal metaplasia in Cdx2-transgenic mice. *Cancer Res* 2004; **64**: 7740-7747 [PMID: 15520178 DOI: 10.1158/0008-5472.CAN-04-1617]

45 **Camilo V**, Barros R, Sousa S, Magalhães AM, Lopes T, Mário Santos A, Pereira T, Figueiredo C, David L, Almeida R. Helicobacter pylori and the BMP pathway regulate CDX2 and SOX2 expression in gastric cells. *Carcinogenesis* 2012; **33**: 1985-1992 [PMID: 22791809 DOI: 10.1093/carcin/bgs233]

46 **Camilo V**, Garrido M, Valente P, Ricardo S, Amaral AL, Barros R, Chaves P, Carneiro F, David L, Almeida R. Differentiation reprogramming in gastric intestinal metaplasia and dysplasia: role of SOX2 and CDX2. *Histopathology* 2015; **66**: 343-350 [PMID: 25196071 DOI: 10.1111/his.12544]

47 **Asano N**, Imatani A, Watanabe T, Fushiya J, Kondo Y, Jin X, Ara N, Uno K, Iijima K, Koike T, Strober W, Shimosegawa T. Cdx2 Expression and Intestinal Metaplasia Induced by H. pylori Infection of Gastric Cells Is Regulated by NOD1-Mediated Innate Immune Responses. *Cancer Res* 2016; **76**: 1135-1145 [PMID: 26759244 DOI: 10.1158/0008-5472.CAN-15-2272]

48 **Sobala GM**, O'Connor HJ, Dewar EP, King RF, Axon AT, Dixon MF. Bile reflux and intestinal metaplasia in gastric mucosa. *J Clin Pathol* 1993; **46**: 235-240 [PMID: 8463417 DOI: 10.1136/jcp.46.3.235]

49 **Matsuhisa T**, Arakawa T, Watanabe T, Tokutomi T, Sakurai K, Okamura S, Chono S, Kamada T, Sugiyama A, Fujimura Y, Matsuzawa K, Ito M, Yasuda M, Ota H, Haruma K. Relation between bile acid reflux into the stomach and the risk of atrophic gastritis and intestinal metaplasia: a multicenter study of 2283 cases. *Dig Endosc* 2013; **25**: 519-525 [PMID: 23363381 DOI: 10.1111/den.12030]

50 **Genta RM**, Sonnenberg A. Characteristics of the gastric mucosa in patients with intestinal metaplasia. *Am J Surg Pathol* 2015; **39**: 700-704 [PMID: 25602799 DOI: 10.1097/PAS.0000000000000384]

51 **Lissowska J**, Groves FD, Sobin LH, Fraumeni JF, Nasierowska-Guttmejer A, Radziszewski J, Regula J, Hsing AW, Zatonski W, Blot WJ, Chow WH. Family history and risk of stomach cancer in Warsaw, Poland. *Eur J Cancer Prev* 1999; **8**: 223-227 [PMID: 10443951 DOI: 10.1097/00008469-199906000-00010]

52 **Eto K**, Ohyama S, Yamaguchi T, Wada T, Suzuki Y, Mitsumori N, Kashiwagi H, Anazawa S, Yanaga K, Urashima M. Familial clustering in subgroups of gastric cancer stratified by histology, age group and location. *Eur J Surg Oncol* 2006; **32**: 743-748 [PMID: 16762526 DOI: 10.1016/j.ejso.2006.04.005]

53 **Shin CM**, Kim N, Lee HS, Lee DH, Kim JS, Jung HC, Song IS. Intrafamilial aggregation of gastric cancer: a comprehensive approach including environmental factors, Helicobacter pylori virulence, and genetic susceptibility. *Eur J Gastroenterol Hepatol* 2011; **23**: 411-417 [PMID: 21502924 DOI: 10.1097/MEG.0b013e328343b7f5]

54 **Song H**, Ekheden IG, Ploner A, Ericsson J, Nyren O, Ye W. Family history of gastric mucosal abnormality and the risk of gastric cancer: a population-based observational study. *Int J Epidemiol* 2018; **47**: 440-449 [PMID: 29161426 DOI: 10.1093/ije/dyx238]

55 **Cassaro M**, Rugge M, Gutierrez O, Leandro G, Graham DY, Genta RM. Topographic patterns of intestinal metaplasia and gastric cancer. *Am J Gastroenterol* 2000; **95**: 1431-1438 [PMID: 10894575 DOI: 10.1111/j.1572-0241.2000.02074.x]

56 **Sakitani K**, Hirata Y, Watabe H, Yamada A, Sugimoto T, Yamaji Y, Yoshida H, Maeda S, Omata M, Koike K. Gastric cancer risk according to the distribution of intestinal metaplasia and neutrophil infiltration. *J Gastroenterol Hepatol* 2011; **26**: 1570-1575 [PMID: 21575058 DOI: 10.1111/j.1440-1746.2011.06767.x]

57 **Hamamoto T**, Yokozaki H, Semba S, Yasui W, Yunotani S, Miyazaki K, Tahara E. Altered microsatellites in incomplete-type intestinal metaplasia adjacent to primary gastric cancers. *J Clin Pathol* 1997; **50**: 841-846 [PMID: 9462267 DOI: 10.1136/jcp.50.10.841]

58 **Dixon MF**, Genta RM, Yardley JH, Correa P. Classification and grading of gastritis. The updated Sydney System. International Workshop on the Histopathology of Gastritis, Houston 1994. *Am J Surg Pathol* 1996; **20**: 1161-1181 [PMID: 8827022 DOI: 10.1097/00000478-199610000-00001]

59 **Rugge M**, Correa P, Di Mario F, El-Omar E, Fiocca R, Geboes K, Genta RM, Graham DY, Hattori T, Malfertheiner P, Nakajima S, Sipponen P, Sung J, Weinstein W, Vieth M. OLGA staging for gastritis: a tutorial. *Dig Liver Dis* 2008; **40**: 650-658 [PMID: 18424244 DOI: 10.1016/j.dld.2008.02.030]

60 **Capelle LG**, de Vries AC, Haringsma J, Ter Borg F, de Vries RA, Bruno MJ, van Dekken H, Meijer J, van Grieken NC, Kuipers EJ. The staging of gastritis with the OLGA system by using intestinal metaplasia as an accurate alternative for atrophic gastritis. *Gastrointest Endosc* 2010; **71**: 1150-1158 [PMID: 20381801 DOI: 10.1016/j.gie.2009.12.029]

61 **Rugge M**, de Boni M, Pennelli G, de Bona M, Giacomelli L, Fassan M, Basso D, Plebani M, Graham DY. Gastritis OLGA-staging and gastric cancer risk: a twelve-year clinico-pathological follow-up study. *Aliment Pharmacol Ther* 2010; **31**: 1104-1111 [PMID: 20180784 DOI: 10.1111/j.1365-2036.2010.04277.x]

62 **Rugge M**, Fassan M, Pizzi M, Farinati F, Sturniolo GC, Plebani M, Graham DY. Operative link for gastritis assessment vs operative link on intestinal metaplasia assessment. *World J Gastroenterol* 2011; **17**: 4596-4601 [PMID: 22147965 DOI: 10.3748/wjg.v17.i41.4596]

63 **Yue H**, Shan L, Bin L. The significance of OLGA and OLGIM staging systems in the risk assessment of gastric cancer: a systematic review and meta-analysis. *Gastric Cancer* 2018; **21**: 579-587 [PMID: 29460004 DOI: 10.1007/s10120-018-0812-3]

64 **Rokkas T**, Pistiolas D, Sechopoulos P, Robotis I, Margantinis G. The long-term impact of Helicobacter pylori eradication on gastric histology: a systematic review and meta-analysis. *Helicobacter* 2007; **12** Suppl 2: 32-38 [PMID: 17991174 DOI: 10.1111/j.1523-5378.2007.00563.x]

65 **Wang J**, Xu L, Shi R, Huang X, Li SW, Huang Z, Zhang G. Gastric atrophy and intestinal metaplasia before and after Helicobacter pylori eradication: a meta-analysis. *Digestion* 2011; **83**: 253-260 [PMID: 21282951 DOI: 10.1159/000280318]

66 **Shin CM**, Kim N, Chang H, Kim JS, Lee DH, Jung HC. Follow-Up Study on CDX1 and CDX2 mRNA Expression in Noncancerous Gastric Mucosae After Helicobacter pylori Eradication. *Dig Dis Sci* 2016; **61**: 1051-1059 [PMID: 26841784 DOI: 10.1007/s10620-016-4048-y]

67 **Chen HN**, Wang Z, Li X, Zhou ZG. Helicobacter pylori eradication cannot reduce the risk of gastric cancer in patients with intestinal metaplasia and dysplasia: evidence from a meta-analysis. *Gastric Cancer* 2016; **19**: 166-175 [PMID: 25609452 DOI: 10.1007/s10120-015-0462-7]

68 **den Hollander WJ**, Holster IL, den Hoed CM, Capelle LG, Tang TJ, Anten MP, Prytz-Berset I, Witteman EM, Ter Borg F, Hartog GD, Bruno MJ, Peppelenbosch MP, Lesterhuis W, Doukas M, Kuipers EJ, Spaander MCW. Surveillance of premalignant gastric lesions: a multicentre prospective cohort study from low incidence regions. *Gut* 2019; **68**: 585-593 [PMID: 29875257 DOI: 10.1136/gutjnl-2017-314498]

69 **Sung JJ**, Lin SR, Ching JY, Zhou LY, To KF, Wang RT, Leung WK, Ng EK, Lau JY, Lee YT, Yeung CK, Chao W, Chung SC. Atrophy and intestinal metaplasia one year after cure of H. pylori infection: a prospective, randomized study. *Gastroenterology* 2000; **119**: 7-14 [PMID: 10889149 DOI: 10.1053/gast.2000.8550]

70 **Arkkila PE**, Seppälä K, Färkkilä MA, Veijola L, Sipponen P. Helicobacter pylori eradication in the healing of atrophic gastritis: a one-year prospective study. *Scand J Gastroenterol* 2006; **41**: 782-790 [PMID: 16785190 DOI: 10.1080/00365520500463175]

71 **Toyokawa T**, Suwaki K, Miyake Y, Nakatsu M, Ando M. Eradication of Helicobacter pylori infection improved gastric mucosal atrophy and prevented progression of intestinal metaplasia, especially in the elderly population: a long-term prospective cohort study. *J Gastroenterol Hepatol* 2010; **25**: 544-547 [PMID: 19817964 DOI: 10.1111/j.1440-1746.2009.05995.x]

72 **González CA**, Pardo ML, Liso JM, Alonso P, Bonet C, Garcia RM, Sala N, Capella G, Sanz-Anquela JM. Gastric cancer occurrence in preneoplastic lesions: a long-term follow-up in a high-risk area in Spain. *Int J Cancer* 2010; **127**: 2654-2660 [PMID: 20178099 DOI: 10.1002/ijc.25273]

73 **Reddy KM**, Chang JI, Shi JM, Wu BU. Risk of Gastric Cancer Among Patients With Intestinal Metaplasia of the Stomach in a US Integrated Health Care System. *Clin Gastroenterol Hepatol* 2016; **14**: 1420-1425 [PMID: 27317852 DOI: 10.1016/j.cgh.2016.05.045]

74 **Schmidt PH**, Lee JR, Joshi V, Playford RJ, Poulsom R, Wright NA, Goldenring JR. Identification of a metaplastic cell lineage associated with human gastric adenocarcinoma. *Lab Invest* 1999; **79**: 639-646 [PMID: 10378506 DOI: 10.1121/1.424682]

75 **Wang TC**, Goldenring JR, Dangler C, Ito S, Mueller A, Jeon WK, Koh TJ, Fox JG. Mice lacking secretory phospholipase A2 show altered apoptosis and differentiation with Helicobacter felis infection. *Gastroenterology* 1998; **114**: 675-689 [PMID: 9516388 DOI: 10.1016/S0016-5085(98)70581-5]

76 **Halldórsdóttir AM**, Sigurdardóttrir M, Jónasson JG, Oddsdóttir M, Magnússon J, Lee JR, Goldenring JR. Spasmolytic polypeptide-expressing metaplasia (SPEM) associated with gastric cancer in Iceland. *Dig Dis Sci* 2003; **48**: 431-441 [PMID: 12757153 DOI: 10.1023/A:1022564027468]

77 **Nam KT**, Lee HJ, Sousa JF, Weis VG, O'Neal RL, Finke PE, Romero-Gallo J, Shi G, Mills JC, Peek RM, Konieczny SF, Goldenring JR. Mature chief cells are cryptic progenitors for metaplasia in the stomach. *Gastroenterology* 2010; **139**: 2028-2037.e9 [PMID: 20854822 DOI: 10.1053/j.gastro.2010.09.005]

78 **Weis VG**, Petersen CP, Weis JA, Meyer AR, Choi E, Mills JC, Goldenring JR. Maturity and age influence chief cell ability to transdifferentiate into metaplasia. *Am J Physiol Gastrointest Liver Physiol* 2017; **312**: G67-G76 [PMID: 27881402 DOI: 10.1152/ajpgi.00326.2016]

79 **Kinoshita H**, Hayakawa Y, Niu Z, Konishi M, Hata M, Tsuboi M, Hayata Y, Hikiba Y, Ihara S, Nakagawa H, Hirata Y, Wang TC, Koike K. Mature gastric chief cells are not required for the development of metaplasia. *Am J Physiol Gastrointest Liver Physiol* 2018; **314**: G583-G596 [PMID: 29345968 DOI: 10.1152/ajpgi.00351.2017]

80 **Wang TC**, Dangler CA, Chen D, Goldenring JR, Koh T, Raychowdhury R, Coffey RJ, Ito S, Varro A, Dockray GJ, Fox JG. Synergistic interaction between hypergastrinemia and Helicobacter infection in a mouse model of gastric cancer. *Gastroenterology* 2000; **118**: 36-47 [PMID: 10611152 DOI: 10.1016/S0016-5085(00)70412-4]

81 **Shimizu T**, Choi E, Petersen CP, Noto JM, Romero-Gallo J, Piazuelo MB, Washington MK, Peek RM, Goldenring JR. Characterization of progressive metaplasia in the gastric corpus mucosa of Mongolian gerbils infected with Helicobacter pylori. *J Pathol* 2016; **239**: 399-410 [PMID: 27125972 DOI: 10.1002/path.4735]

82 **Goldenring JR**, Nam KT, Wang TC, Mills JC, Wright NA. Spasmolytic polypeptide-expressing metaplasia and intestinal metaplasia: time for reevaluation of metaplasias and the origins of gastric cancer. *Gastroenterology* 2010; **138**: 2207-2210, 2210.e1 [PMID: 20450866 DOI: 10.1053/j.gastro.2010.04.023]

83 **Petersen CP**, Weis VG, Nam KT, Sousa JF, Fingleton B, Goldenring JR. Macrophages promote progression of spasmolytic polypeptide-expressing metaplasia after acute loss of parietal cells. *Gastroenterology* 2014; **146**: 1727-38.e8 [PMID: 24534633 DOI: 10.1053/j.gastro.2014.02.007]

84 **Fu H**, Ma Y, Yang M, Zhang C, Huang H, Xia Y, Lu L, Jin W, Cui D. Persisting and Increasing Neutrophil Infiltration Associates with Gastric Carcinogenesis and E-cadherin Downregulation. *Sci Rep* 2016; **6**: 29762 [PMID: 27412620 DOI: 10.1038/srep29762]

85 **McDonald SA**, Greaves LC, Gutierrez-Gonzalez L, Rodriguez-Justo M, Deheragoda M, Leedham SJ, Taylor RW, Lee CY, Preston SL, Lovell M, Hunt T, Elia G, Oukrif D, Harrison R, Novelli MR, Mitchell I,

Stoker DL, Turnbull DM, Jankowski JA, Wright NA. Mechanisms of field cancerization in the human stomach: the expansion and spread of mutated gastric stem cells. *Gastroenterology* 2008; **134**: 500-510 [PMID: 18242216 DOI: 10.1053/j.gastro.2007.11.035]

86 **Gutierrez-Gonzalez L**, Graham TA, Rodriguez-Justo M, Leedham SJ, Novelli MR, Gay LJ, Ventayol-Garcia T, Green A, Mitchell I, Stoker DL, Preston SL, Bamba S, Yamada E, Kishi Y, Harrison R, Jankowski JA, Wright NA, McDonald SA. The clonal origins of dysplasia from intestinal metaplasia in the human stomach. *Gastroenterology* 2011; **140**: 1251-1260.e1-6 [PMID: 21223968 DOI: 10.1053/j.gastro.2010.12.051]

87 **Jung SH**, Kim SY, An CH, Lee SH, Jung ES, Park HC, Kim MS, Chung YJ, Lee SH. Clonal Structures of Regionally Synchronous Gastric Adenomas and Carcinomas. *Clin Cancer Res* 2018; **24**: 4715-4725 [PMID: 29945994 DOI: 10.1158/1078-0432.CCR-18-0345]

88 **Schoofs N**, Bisschops R, Prenen H. Progression of Barrett's esophagus toward esophageal adenocarcinoma: an overview. *Ann Gastroenterol* 2017; **30**: 1-6 [PMID: 28042232 DOI: 10.20524/aog.2016.0091]

89 **de Jonge PJ**, van Blankenstein M, Looman CW, Casparie MK, Meijer GA, Kuipers EJ. Risk of malignant progression in patients with Barrett's oesophagus: a Dutch nationwide cohort study. *Gut* 2010; **59**: 1030-1036 [PMID: 20639249 DOI: 10.1136/gut.2009.176701]

90 **Hvid-Jensen F**, Pedersen L, Drewes AM, Sørensen HT, Funch-Jensen P. Incidence of adenocarcinoma among patients with Barrett's esophagus. *N Engl J Med* 2011; **365**: 1375-1383 [PMID: 21995385 DOI: 10.1056/NEJMoa1103042]

91 **Ross-Innes CS**, Becq J, Warren A, Cheetham RK, Northen H, O'Donovan M, Malhotra S, di Pietro M, Ivakhno S, He M, Weaver JMJ, Lynch AG, Kingsbury Z, Ross M, Humphray S, Bentley D, Fitzgerald RC. Whole-genome sequencing provides new insights into the clonal architecture of Barrett's esophagus and esophageal adenocarcinoma. *Nat Genet* 2015; **47**: 1038-1046 [PMID: 26192915 DOI: 10.1038/ng.3357]

92 **Campbell JD**, Mazzilli SA, Reid ME, Dhillon SS, Platero S, Beane J, Spira AE. The Case for a Pre-Cancer Genome Atlas (PCGA). *Cancer Prev Res (Phila)* 2016; **9**: 119-124 [PMID: 26839336 DOI: 10.1158/1940-6207.CAPR-16-0024]

93 **Kim HJ**, Kang TW, Haam K, Kim M, Kim SK, Kim SY, Lee SI, Song KS, Jeong HY, Kim YS. Whole genome MBD-seq and RRBS analyses reveal that hypermethylation of gastrointestinal hormone receptors is associated with gastric carcinogenesis. *Exp Mol Med* 2018; **50**: 156 [PMID: 30510283 DOI: 10.1038/s12276-018-0179-x]

94 **Rivas-Ortiz CI**, Lopez-Vidal Y, Arredondo-Hernandez LJR, Castillo-Rojas G. Genetic Alterations in Gastric Cancer Associated with Helicobacter pylori Infection. *Front Med (Lausanne)* 2017; **4**: 47 [PMID: 28512631 DOI: 10.3389/fmed.2017.00047]

95 **Li D**, Bautista MC, Jiang SF, Daryani P, Brackett M, Armstrong MA, Hung YY, Postlethwaite D, Ladabaum U. Risks and Predictors of Gastric Adenocarcinoma in Patients with Gastric Intestinal Metaplasia and Dysplasia: A Population-Based Study. *Am J Gastroenterol* 2016; **111**: 1104-1113 [PMID: 27185078 DOI: 10.1038/ajg.2016.188]

96 **Huang KK**, Ramnarayanan K, Zhu F, Srivastava S, Xu C, Tan ALK, Lee M, Tay S, Das K, Xing M, Fatehullah A, Alkaff SMF, Lim TKH, Lee J, Ho KY, Rozen SG, Teh BT, Barker N, Chia CK, Khor C, Ooi CJ, Fock KM, So J, Lim WC, Ling KL, Ang TL, Wong A, Rao J, Rajnakova A, Lim LG, Yap WM, Teh M, Yeoh KG, Tan P. Genomic and Epigenomic Profiling of High-Risk Intestinal Metaplasia Reveals Molecular Determinants of Progression to Gastric Cancer. *Cancer Cell* 2018; **33**: 137-150.e5 [PMID: 29290541 DOI: 10.1016/j.ccell.2017.11.018]

97 **Busuttil RA**, Zapparoli GV, Haupt S, Fennell C, Wong SQ, Pang JM, Takeno EA, Mitchell C, Di Costanzo N, Fox S, Haupt Y, Dobrovic A, Boussioutas A. Role of p53 in the progression of gastric cancer. *Oncotarget* 2014; **5**: 12016-12026 [PMID: 25427447 DOI: 10.18632/oncotarget.2434]

98 **Rugge M**, Correa P, Dixon MF, Hattori T, Leandro G, Lewin K, Riddell RH, Sipponen P, Watanabe H. Gastric dysplasia: the Padova international classification. *Am J Surg Pathol* 2000; **24**: 167-176 [PMID: 10680883 DOI: 10.1097/00000478-200002000-00001]

99 **Rokutan H**, Abe H, Nakamura H, Ushiku T, Arakawa E, Hosoda F, Yachida S, Tsuji Y, Fujishiro M, Koike K, Totoki Y, Fukayama M, Shibata T. Initial and crucial genetic events in intestinal-type gastric intramucosal neoplasia. *J Pathol* 2019; **247**: 494-504 [PMID: 30474112 DOI: 10.1002/path.5208]

100 **Uemura N**, Okamoto S, Yamamoto S, Matsumura N, Yamaguchi S, Yamakido M, Taniyama K, Sasaki N, Schlemper RJ. Helicobacter pylori infection and the development of gastric cancer. *N Engl J Med* 2001; **345**: 784-789 [PMID: 11556297 DOI: 10.1056/NEJMoa001999]

101 **Yun CY**, Kim N, Lee J, Lee JY, Hwang YJ, Lee HS, Yoon H, Shin CM, Park YS, Kim JW, Lee DH. Usefulness of OLGA and OLGIM system not only for intestinal type but also for diffuse type of gastric cancer, and no interaction among the gastric cancer risk factors. *Helicobacter* 2018; **23**: e12542 [PMID: 30303591 DOI: 10.1111/hel.12542]

102 **Waldum HL**, Öberg K, Sørdal ØF, Sandvik AK, Gustafsson BI, Mjønes P, Fossmark R. Not only stem cells, but also mature cells, particularly neuroendocrine cells, may develop into tumours: time for a paradigm shift. *Therap Adv Gastroenterol* 2018; **11**: 1756284818775054 [PMID: 29872453 DOI: 10.1177/1756284818775054]

Appendix B

Production of R-Spondin 1 and Wnt3A conditioned media (Dr Rita Busuttil)

The HEK293T-hu-RSPO1-Fc R-Spondin 1 secreting cell line was cultured in DMEM + 10% FCS + 1% Anti-Anti + Zeocin at 500µg/ml. Cells were seeded and when ~70% confluent, harvest medium (ADMEM/F12 + 1% Anti-Anti + 10mM HEPES + 1x GlutaMAX) was added to the flask. Conditioned media was collected after 7 days, centrifuged at 500g for 5min, filtered through a 0.22µm filter and stored at -20°C for up to 6 months.

The L-cell Wnt3A secreting cell line was cultured in DMEM + 10% FCS + 1% Anti/Anti and 400µg/ml of G418. $1.5x10^6$ cells were seeded per T175 flask in 20ml of media and when cells reached ~70% confluency, harvest medium (DMEM + 10% FCS + 1% Anti-Anti) was added to the flask. After 7 days conditioned media was collected, centrifuged at 500g for 5min, filtered through a 0.22µm filter and stored at 4°C for up to 6 months.

Appendix C

Anatomical distribution of Lauren gastric cancer types with adjacent chronic gastritis (CG) and/or intestinal metaplasia (IM)

CG/IM adjacent to	**Anatomical location**		
Lauren GC type	Antrum	Body	GOJ
CG adjacent to			
IGC (n=95)	23	48	24
DGC (n=56)	8	41	7
MGC (n=33)	7	22	4
AdNOS (n=13)	3	2	8
IM adjacent to			
IGC (n=75)	25	44	6
DGC (n=28)	4	20	4
MGC (n=25)	6	18	1
AdNOS (n=2)	1	0	1

Appendix D

Top 10 genes by log2 fold change differentially expressed in CG+GC and in IM+GC samples compared to IGC samples

Symbol	Function	logFC	AveExpr	adj.P.Val	Symbol	Function	logFC	AveExpr	adj.P.Val
High in CG+GC					High in IGC				
ATP4B	Gastric acid secretion	-5.49	8.69	3.30E-08	*OLFM4*	Anti-apoptotic	3.33	9.36	4.31E-04
GIF	Cobalamin binding	-5.17	9.44	3.23E-07	*INHBA*	Cell differentiation	3.31	7.61	1.51E-09
ATP4A	Gastric acid secretion	-5.12	8.32	3.46E-09	*SPP1*	ECM	3.24	8.16	4.49E-07
AQP4	Water channel activity	-4.72	5.43	1.28E-09	*CDH17*	Cell adhesion	3.21	7.86	6.55E-06
GKN2	Epithelial integrity	-4.64	10.44	7.58E-07	*CLDN1*	Cell junction	3.03	6.75	7.90E-11
CHIA	Chitinase activity	-4.46	6.96	1.00E-07	*CLDN7*	Cell adhesion	2.91	8.23	1.99E-11
KCNJ16	Potassium channel activity	-4.36	6.57	2.14E-10	*CLDN3*	Cell junction	2.85	6.41	1.68E-06
ESRRG	Nuclear hormone receptor	-4.21	7.01	2.36E-09	*IGF2BP3*	RNA synthesis/metabolism	2.79	5.66	1.95E-07
MFSD4A	Glucose transporter activity	-4.18	8.69	7.43E-09	*DMBT1*	Calcium-dependent protein binding	2.76	9.31	9.02E-05
KCNE2	Potassium channel activity	-4.12	8.28	8.90E-11	*CHI3L1*	Chitinase activity	2.76	6.80	1.26E-07
High in IM+GC					High in IGC				
GKN2	Epithelial integrity	4.10	10.3	6.50E-05	*INHBA*	Cell differentiation	-3.30	7.64	2.69E-07
CLCA1	Goblet cell mucin production	3.94	6.89	3.64E-06	*SPP1*	ECM	-2.68	8.36	6.93E-05
DEFA5	Antimicrobial activity	3.84	6.90	7.15E-05	*COL11A1*	ECM	-2.48	5.3	2.64E-04
GKN1	Epithelial integrity	3.67	11.3	1.85E-04	*CST1*	Cysteine Proteinase inhibitor	-2.44	6.57	1.81E-04
ALDOB	Fructose metabolism	3.53	7.87	2.10E-05	*CXCL8*	Inflammation	-2.40	7.17	2.94E-04
KRT20	Epithelial integrity	3.34	9.00	9.90E-05	*IGF2BP3*	RNA synthesis/metabolism	-2.37	5.81	9.06E-05
TMPRSS15	Activation of proenzymes	3.29	5.12	5.81E-05	*COL8A1*	ECM	-2.35	7.21	4.67E-05
SST	Reduces gastric acid secretion	3.10	7.50	5.23E-05	*DUXAP10*	Pseudogene	-2.25	6.14	1.36E-04
ADH1B	Alcohol metabolism	3.06	7.32	6.03E-06	*SULF1*	Cell signalling	-2.22	7.95	3.70E-05
SOSTDC1	BMP antagonist	2.98	7.18	1.29E-05	*CTHRC1*	Tissue repair	-2.20	8.99	2.43E-05

Affymetrix array data of CG+GC (n=22) and IM+GC (n=23) samples compared with IGC samples (n=50), first by normalising using the RMA algorithm and then using differential gene expression with the limma package in R; differentially expressed genes were defined as log2 fold change >1.2 with adjusted $p<0.05$ using the Benjamini-Hochberg method for multiple test correction; genes with log2 normalised average expression of less than 5 were excluded.

Appendix E

Top 10 genes by log2 fold change differentially expressed in CG+GC and in IM+GC samples compared to DGC samples

Symbol	Function	logFC	AveExpr	adj.P.Val	Symbol	Function	logFC	AveExpr	adj.P.Val
High in CG+GC					High in DGC				
ATP4B	Gastric acid secretion	-5.47	9.03	9.60E-08	*INHBA*	Cell differentiation	4.15	7.86	3.98E-16
GIF	Cobalamin binding	-5.19	9.71	3.58E-07	*COL8A1*	ECM	4.02	7.81	7.33E-15
ATP4A	Gastric acid secretion	-5.03	8.61	1.22E-08	*SFRP4*	Cell growth/differentiation	4.01	7.62	4.16E-11
AQP4	Water channel activity	-4.76	5.65	6.98E-10	*THBS4*	ECM	3.37	8.10	4.22E-09
CHIA	Chitinase activity	-4.71	7.05	1.42E-08	*FNDC1*	ECM	3.23	5.46	8.80E-11
KCNJ16	Potassium channel activity	-4.38	6.80	6.67E-10	*SPP1*	ECM	3.18	7.78	6.00E-08
ESRRG	Nuclear hormone receptor	-4.28	7.16	3.22E-09	*THBS2*	Cell adhesion	3.10	8.27	6.07E-12
MFSD4A	Glucose transporter activity	-4.06	8.94	1.94E-08	*WISP1*	ECM/cell survival	3.09	5.59	5.43E-14
KCNE2	Potassium channel activity	-4.04	8.47	1.17E-09	*SULF1*	Cell signalling	3.07	8.07	7.01E-12
GKN2	Epithelial integrity	-3.78	11.25	6.72E-05	*ANPEP*	Aminopeptidase activity	2.97	7.46	3.67E-05
High in IM+GC					High in DGC				
REG3A	Cell proliferation/antimicrobial	3.87	9.41	4.67E-05	*INHBA*	Cell differentiation	-4.14	7.93	2.25E-14
ALDOB	Fructose metabolism	3.64	7.99	3.42E-06	*COL8A1*	ECM	-3.94	7.91	6.03E-13
DEFA5	Antimicrobial activity	3.41	7.55	2.76E-04	*SFRP4*	Cell growth/differentiation	-3.83	7.68	1.40E-09
CLCA1	Goblet cell mucin production	3.38	7.63	3.56E-04	*FNDC1*	ECM	-3.12	5.6	2.72E-09
TMPRSS15	Activation of proenzymes	3.37	5.19	1.07E-04	*THBS4*	ECM	-3.10	8.25	6.32E-07
GKN2	Epithelial integrity	3.20	11.1	1.91E-03	*ASPN*	ECM	-3.02	7.13	8.32E-11
SI	Carbohydrate digestion	3.19	7.04	1.35E-03	*SULF1*	Cell signalling	-2.97	8.20	1.72E-10
APOB	Chylomicron related activity	3.13	6.30	7.03E-05	*CTHRC1*	Tissue repair	-2.86	9.24	6.39E-11
C6orf58	Early liver development	2.96	7.83	2.46E-03	*COL10A1*	Extracellular matrix	-2.84	5.61	8.59E-07
ATP4B	Gastric acid secretion	2.95	8.00	1.06E-02	*WISP1*	ECM/cell survival	-2.83	5.79	6.54E-12

Affymetrix array data of CG+GC (n=22) and IM+GC (n=23) samples compared with DGC samples (n=38), first by normalising using the RMA algorithm and then using differential gene expression with the limma package in R; differentially expressed genes were defined as log2 fold change >1.2 with adjusted $p<0.05$ using the Benjamini-Hochberg method for multiple test correction; genes with log2 normalised average expression of less than 5 were excluded.

Appendix F

List of all immune related genes used to characterise bcIM-GC and biIM-GC samples

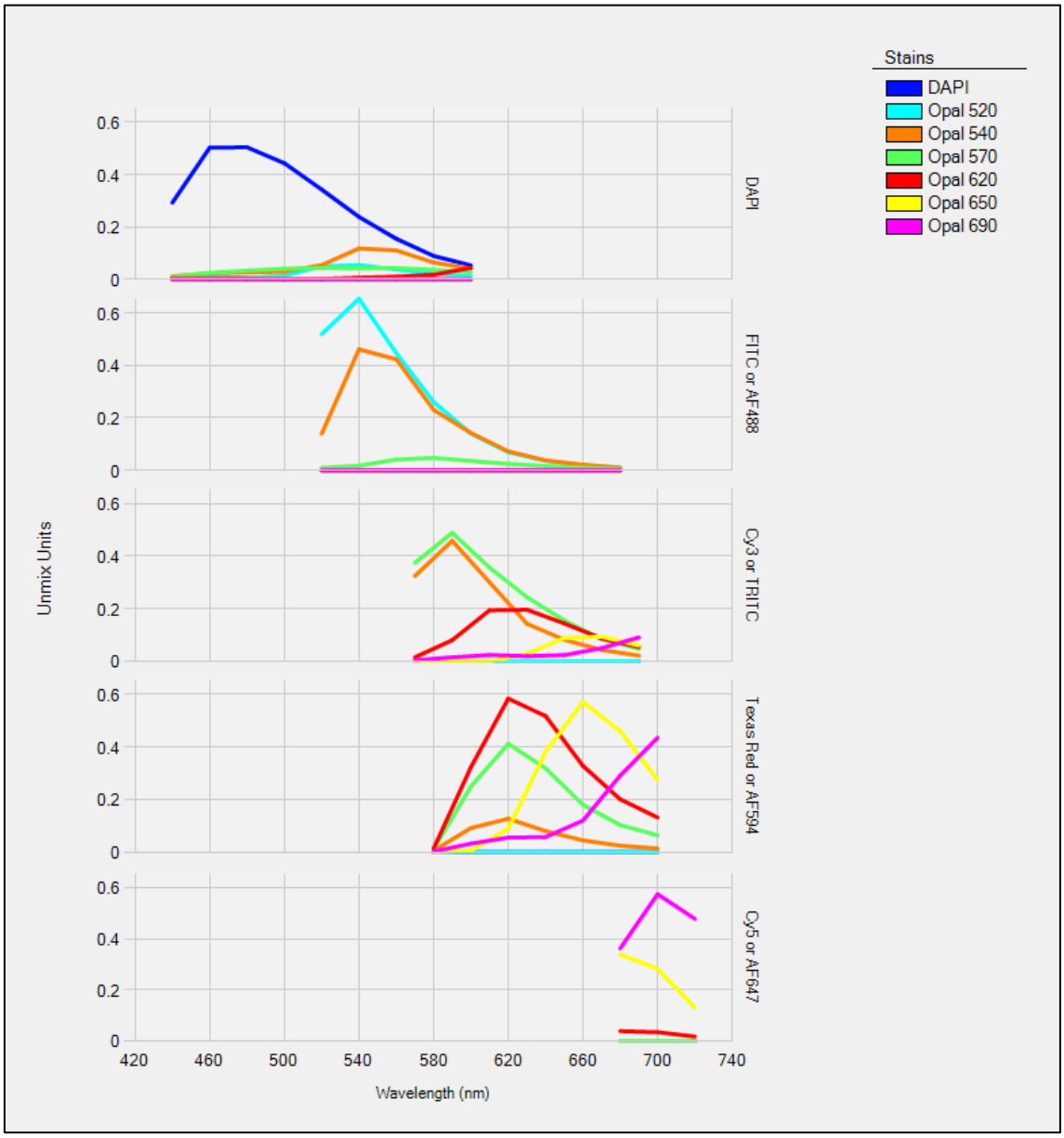
Type/name of gene						
CD genes	*CD33*	*CD8B*	*IL1A*	*IL37*	**TFGβ genes**	*CCR7*
CD101	*CD34*	*CD9*	*IL1B*	*IL3RA*	*TGFA*	*CCR8*
CD109	*CD36*	*CD93*	*IL1F10*	*IL4*	*TGFB1*	*CCR9*
CD14	*CD37*	*CD96*	*IL1R1*	*IL4I1*	*TGFB1I1*	*CCRL2*
CD151	*CD38*	*CD99*	*IL1R2*	*IL4R*	*TGFB2*	**CXCL genes**
CD160	*CD3D*	*CD99L2*	*IL1RAP*	*IL5*	*TGFB3*	*CXCL1*
CD163	*CD3E*	*CD99P1*	*IL1RAPL1*	*IL5RA*	*TGFBI*	*CXCL10*
CD163L1	*CD3EAP*	**IL genes**	*IL1RAPL2*	*IL6*	*TGFBR1*	*CXCL11*
CD164	*CD3G*	*IL10*	*IL1RL1*	*IL6R*	*TGFBR2*	*CXCL12*
CD177	*CD4*	*IL10RA*	*IL1RL2*	*IL6R-AS1*	*TGFBR3*	*CXCL13*
CD180	*CD40*	*IL10RB*	*IL1RN*	*IL6ST*	*TGFBRAP1*	*CXCL14*
CD19	*CD40LG*	*IL10RB-DT*	*IL2*	*IL7*	**CCL genes**	*CXCL16*
CD1A	*CD44*	*IL11*	*IL20*	*IL7R*	*CCL1*	*CXCL17*
CD1B	*CD46*	*IL11RA*	*IL20RA*	*IL9*	*CCL11*	*CXCL2*
CD1C	*CD47*	*IL12A*	*IL20RB*	*IL9R*	*CCL13*	*CXCL3*
CD1D	*CD48*	*IL12A-AS1*	*IL21*	**IFN genes**	*CCL16*	*CXCL5*
CD1E	*CD5*	*IL12B*	*IL21R*	*IFNA1*	*CCL17*	*CXCL6*
CD2	*CD52*	*IL12RB1*	*IL21R-AS1*	*IFNA10*	*CCL18*	*CXCL8*
CD200	*CD53*	*IL12RB2*	*IL22*	*IFNA14*	*CCL19*	*CXCL9*
CD200R1	*CD55*	*IL13*	*IL22RA1*	*IFNA16*	*CCL2*	**CXCR genes**
CD207	*CD58*	*IL13RA1*	*IL22RA2*	*IFNA17*	*CCL20*	*CXCR1*
CD209	*CD59*	*IL13RA2*	*IL23A*	*IFNA2*	*CCL21*	*CXCR2*
CD22	*CD5L*	*IL15*	*IL23R*	*IFNA21*	*CCL22*	*CXCR3*
CD226	*CD6*	*IL15RA*	*IL24*	*IFNA4*	*CCL23*	*CXCR4*
CD24	*CD63*	*IL16*	*IL25*	*IFNA5*	*CCL24*	*CXCR5*
CD244	*CD69*	*IL17A*	*IL26*	*IFNA7*	*CCL25*	*CXCR6*
CD247	*CD7*	*IL17B*	*IL27*	*IFNA8*	*CCL26*	**Other**
CD248	*CD70*	*IL17C*	*IL27RA*	*IFNAR1*	*CCL27*	*FOXP3*
CD27	*CD72*	*IL17D*	*IL2RA*	*IFNAR2*	*CCL28*	*KLRB1*
CD274	*CD74*	*IL17F*	*IL2RB*	*IFNB1*	*CCL4*	
CD276	*CD79A*	*IL17RA*	*IL2RG*	*IFNE*	*CCL5*	
CD28	*CD79B*	*IL17RB*	*IL3*	*IFNG*	*CCL7*	
CD2AP	*CD80*	*IL17RC*	*IL31RA*	*IFNGR1*	*CCL8*	
CD2BP2	*CD81*	*IL17RD*	*IL32*	*IFNGR2*	**CCR genes**	
CD300A	*CD81-AS1*	*IL17RE*	*IL33*	*IFNK*	*CCR10*	
CD300C	*CD82*	*IL18*	*IL34*	*IFNL1*	*CCR2*	
CD300LB	*CD83*	*IL18BP*	*IL36A*	*IFNL2*	*CCR3*	
CD300LF	*CD84*	*IL18R1*	*IL36B*	*IFNLR1*	*CCR4*	
CD300LG	*CD86*	*IL18RAP*	*IL36G*	*IFNW1*	*CCR5*	
CD320	*CD8A*	*IL19*	*IL36RN*		*CCR6*	

Appendix G

Core transcriptional signature of KLRB1 (CD161)-associated upregulated genes from Ferguson et al 2014 [434]

ABCA2	*COL5A1*	*GFPT2*	*LATS2*	*PIK3AP1*	*SLC7A5*
ABCB1	*COL5A3*	*GPR65*	*LONRF3*	*PLCB1*	*SLCO3A1*
ACTN4	*COLQ*	*GPR68*	*LTB4R*	*PLEKHG3*	*SMAD3*
ADCY9	*CREB3L2*	*GTF3C1*	*LTK*	*PLXNC1*	*SMAD7*
ADRB2	*CTNNA1*	*GZMA*	*MAFF*	*PODXL*	*SNAI3*
AGPAT4	*CTSH*	*GZMK*	*MAP3K5*	*PRDM1*	*SYNE2*
ALCAM	*CXCR6*	*IFI44*	*MAP3K8*	*PRDM8*	*SYTL2*
ARNTL	*CXXC5*	*IFNGR1*	*MATK*	*PRF1*	*THBS1*
AUTS2	*CYB561*	*IGFBP4*	*ME1*	*PTGDS*	*TLE1*
B4GALT1	*CYFIP1*	*IL12RB2*	*METRNL*	*PTPRM*	*TNF*
CACNA2D2	*DENND3*	*IL15*	*MICALCL*	*RAB11FIP1*	*TNFRSF18*
CACNA2D4	*DUSP5*	*IL18R1*	*MYO1D*	*RASD1*	*TNFSF14*
CAMTA1	*EIF2C4*	*IL18RAP*	*MYO1F*	*RHBDF2*	*TPM2*
CAPN12	*ELOVL4*	*IL23R*	*NADK*	*RORA*	*VCL*
CCR2	*ELOVL6*	*IRAK2*	*NBEAL2*	*RORC*	*VLDLR*
CD58	*ERN1*	*JSRP1*	*NETO2*	*RPPH1*	*WNT1*
CD72	*FAM43A*	*KIAA1539*	*NPC1*	*SESN1*	*YPEL1*
CERK	*FAS*	*KIF5C*	*PBX4*	*SIPA1L2*	*ZBTB16*
CFH	*FOSL2*	*KLRB1*	*PERP*	*SLAMF1*	*ZDHHC14*
CLCF1	*GALM*	*KLRG1*	*PHACTR2*	*SLC1A5*	
CLIC5	*GBP5*	*LAG3*	*PHLDA1*	*SLC2A8*	

Appendix H



Spectral library used to unmix high resolution (x20) images of multiplexed OPAL™ IHC stained sections with the macrophage panel

Spectral library created from high resolution images of single primary antibody stains on control tissue, each with a unique fluorophore (§2.5.2, Tables 2.2, 2.3 and 2.9). The spectral library was used in inForm to unmix high resolution multiplex images obtained using the VECTRA microscope. OPAL™ 520: PDL1, OPAL™ 540: CD163, OPAL™ 570: CD68, OPAL™ 620: CD206, OPAL™ 650: IRF8 and OPAL™ 690: AE1AE3.

Appendix I

Main unique chromosomal changes and single nucleotide variants determined by whole exome sequencing in patient P1 from frozen intestinal metaplastic and high grade dysplastic tissue, obtained at different sites and time points (Busuttil et al 2020 [411])

Time point and site		Main unique events			
		Chromosomal gain	Chromosomal loss	Loss of heterozygosity	Number of unique single nucleotide variants (genes)
t1					
A3					
	IM	7A, 8A, 18A	-	-	115 (including in PHOX2B, KIT, IL6ST)
	HGD	7A, 8A	-	6p	-
A4					
	IM	7B, 8A, 8B, 13A	-	-	111+5
	HGD	7B, 8A, 8B, 13A	-	-	111+5
t2					
A3					
	HGD	7A, 8A, 8B[1]	13B	17 (TP53)	274 (including in SYK, TP53)
t3					
A3					
	IM	-	-	-	168
	HGD	7A, 8A, 8B[1]	13B	17 (TP53)	274 (including in SYK, TP53)
t4					
A1					
	IM	8B	3q	-	5+133 (including EZH2, CDH11)
A3					
	IM1	-	-	-	109 (including MAP2K1)
	IM2	-	-	-	174
A4					
	IM	9, 13B	-	-	-

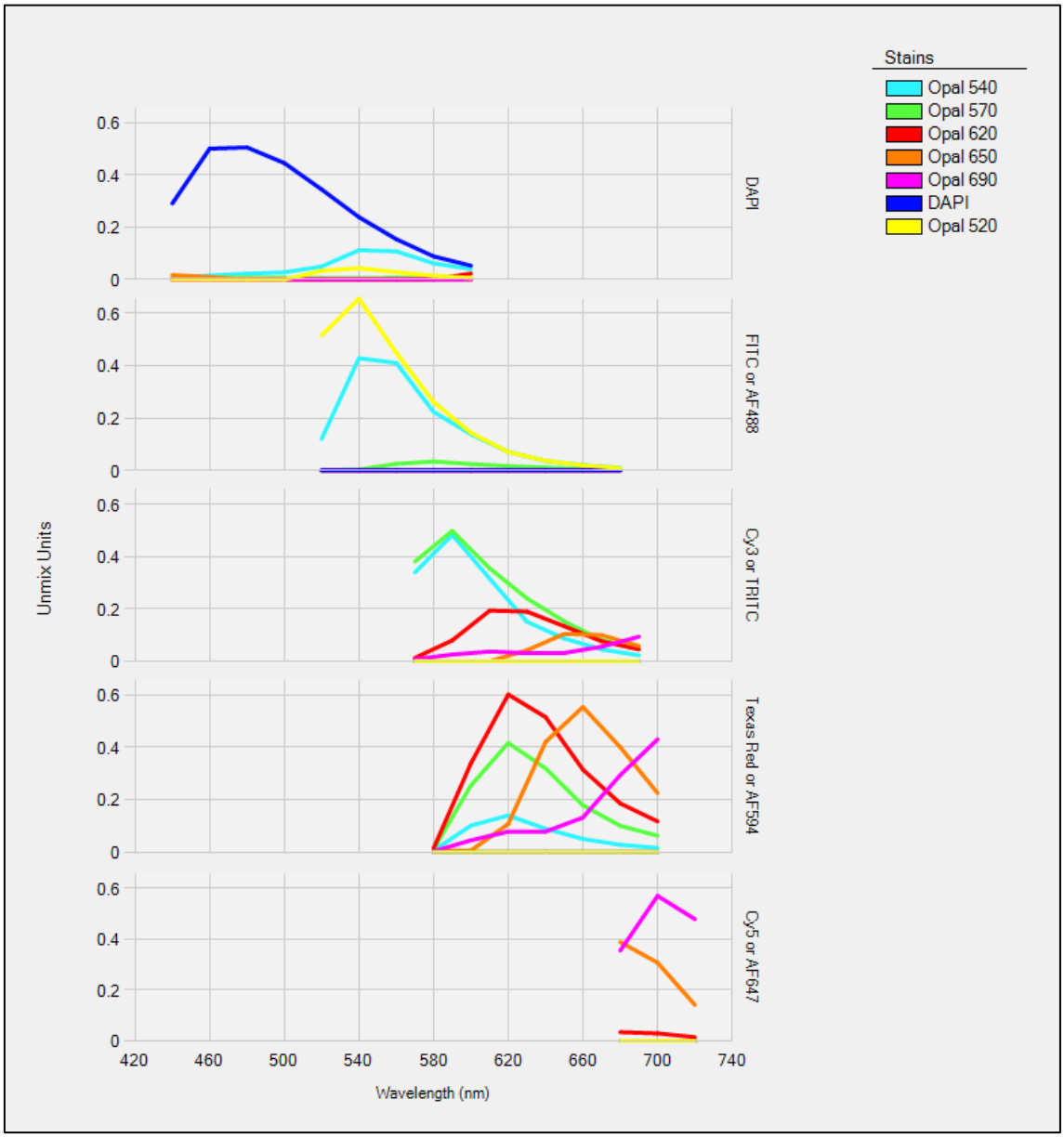
[1]These samples had multiple other chromosomal events similar to the chromosomal instability gastric cancer subtype as described in the TCGA study (TCGA 2014 [42]).

Appendix J

Main unique chromosomal changes and single nucleotide variants determined by whole exome sequencing in patient P2 from frozen intestinal metaplastic and high grade dysplastic tissue, obtained at different sites and time points (Busuttil et al 2020 [411])

Time point and site		Main unique events			
		Chromosomal gain	Chromosomal loss	Loss of heterozygosity	Number of unique single nucleotide variants (genes)
t1					
A2					
	IM	7, 8, 10, 13	14, 17p, 19, 21	18, 20	11+88+45 (including EBF1, TP53)
	HGD	8, 10, 13	1p, 5, 12, 14, 17p, 19, 21	10, 18, 20	79+88+45 (including EBF1, TP53)
A3					
	IM1	8	-	-	11+173
	IM2	-	-	-	55
t2					
A1					
	IM	-	-	-	58
A2					
	IM	20	-	-	35
	HGD	8, 10, 13	1p, 4, 5, 7, 11, 12, 14, 15, 16, 17p, 19, 21, 22	2, 10, 18, 20	79+88+45+41 (including EBF1, TP53)
A3					
	IM	6	-	-	37
A4					
	IM	2, 20	-		35

Appendix K



Spectral library used to unmix high resolution (x20) images of multiplexed OPAL™ IHC stained sections with the T cell panel

Spectral library created from high resolution images of single primary antibody stains on control tissue, each with a unique fluorophore (§2.5.1, Tables 2.2, 2.3 and 2.9). The spectral library was used in inForm to unmix high resolution multiplex images obtained using the VECTRA microscope. OPAL™ 520: CD4, OPAL™ 540: FOXP3, OPAL™ 570: CD3, OPAL™ 620: CD8, OPAL™ 650: CD10 and OPAL™ 690: AE1AE3.

Appendix L

Antibodies used for characterisation of human gastrointestinal organoids

Antibody (clone)	Species	Dilution	Control tissue	Target	Supplier
CD10 (56C6)	Mouse	1/50	Small intestine	Brush border	Abcam
CDX2 (EPR2764Y)	Rabbit	1/200	Small intestine	Epithelial cells	Cell Marque
MUC5AC (MRQ-19)	Mouse	1/1000	Stomach	Surface mucous cells	Cell Marque
MUC6 (CLH5)	Mouse	1/200	Stomach	Neck mucous cells	Novus Biologicals
OLFM4 (GW112)	Mouse	1/4000	Small intestine	Stem cells	Sino Biological Inc.
TFF3 (415909)	Mouse	1/50	Small intestine	Goblet cells	BioScientific

Appendix M

Clinical and experimental details of all patients from main organoid study/organoid biobank

PatientID	Visit #	Sex	Age	Tissue (target IM)	# days in culture	IHC block	RNA extracted	Frozen
G1	1	F	41	G (+IM)	75	✓	-	✓
				SI	9	-	-	-
G2	1	M	85	G (+IM)	126	✓	-	✓
				SI	7	-	-	-
G3	1	M	57	G (+IM)	7	-	-	-
				SI	7	-	-	-
G4	1	F	62	G (+IM)	53	✓	-	✓
				SI	7		-	-
G5	1	F	74	G (+IM)	137	✓	-	-
				SI	7	-	-	-
G6	1	F	50	G (+IM)	83	-	-	✓
				SI	7	-	-	-
G7	1	M	28	G (+IM)	14	-	-	-
				SI	6	-	-	-
G8	1	M	57	G (body+IM)	130	✓	-	✓
				SI	7	-	-	-
G9	1	F	83	G (+IM)	48	-	-	-
	2		84	G (antrum+IM)	26	-	-	-
				G (antrum-IM)	77	✓	✓	✓
G10	1	F	64	G (+IM)	68	✓	-	✓
				SI	117	✓	✓	✓
G11	1	M	70	G (+IM)	97	✓	✓	✓
				SI	130	✓	✓	✓
G12	1	M	67	G (antrum+IM)	131	✓	✓	-
				G (antral scar)	7	-	-	-
				SI	131	✓	✓	
G13	1	M	71	G (antrum+IM)	141	-	-	✓
				G (body+IM)	132	✓	✓	✓
				SI	111	✓	✓	✓
G14	1	F	80	G (antrum+IM)	90	-	-	-
				G (body+IM)	7	-	-	-
				SI	90	✓	-	-
G15	1	F	77	G (antrum+IM)	104	✓	✓	✓
				G (body+IM)	26	-	-	-
				SI	111	✓	✓	✓
G16	1	M	65	G (antrum+IM)	104	✓	✓	✓
				SI	102	✓	✓	✓
G17	1	F	57	G (antrum+IM)	91	✓	✓	✓
				G (body+IM)	110	✓	✓	✓
				SI[1]	130	✓	✓	✓
G18	1	M	66	G (antrum+IM)	104	-	-	-
				SI[1]	91	✓		✓
G19	1	F	73	G (antrum+IM)[1]	179	✓	✓	✓
				G (body+IM)	7	-	-	-
				SI[1]	109	✓	✓	✓
G20	1	M	74	G (antrum+IM)	105	✓	✓	✓
				G (body+IM)	7	-	-	-
G21	1	M	81	G (antrum+IM)	20	-	-	-
				G (antrum-IM)	78	-	-	-
				G (body+IM)	50	✓	-	✓
				SI	42	✓	-	✓
G22	1	F	61	G (antrum+IM)	50	-	-	-
				G (antrum-IM)	43	-	-	-
				G (body+IM)[1]	124	-	✓	✓
				SI[1]	89	✓	✓	✓
G23	1	F	44	G (antrum-IM)[1]	124	✓	✓	✓
				G (body+IM)	71	-	✓	-
G24	1	M	76	G (antrum+IM)	36	-	-	-
				G (incisura+IM)[1]	187	✓	-	-
G25	1	M	57	G (antrum+IM)	53	✓	-	-
				G (antrum-IM)	99	✓	✓	✓
				SI	110	✓	✓	✓

G=gastric, SI=small intestine; +IM: biopsies taken targeting IM tissue during gastroscopy; -IM: biopsies taken targeting tissue that did not contain IM during gastroscopy; [1]Used in OLFM4 FACS experiments (Section §8.3.9)